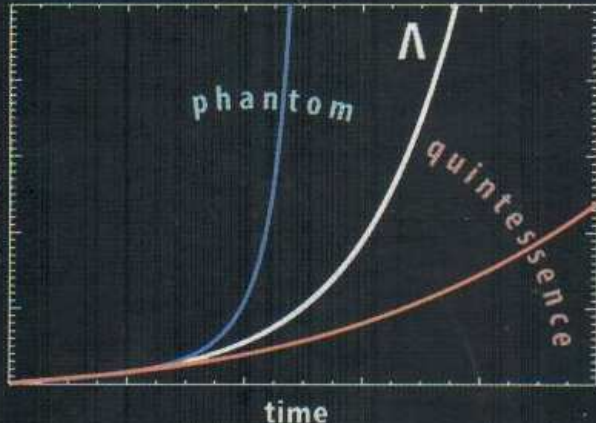


arXiv:1502.04177v1 [astro-ph.CO] 14 Feb 2015

# DARK ENERGY AND DARK MATTER IN THE UNIVERSE

**1**  
VOLUME

## OBSERVATIONAL EVIDENCE AND THEORETICAL MODELS



**Dark energy and dark matter in the Universe**  
**in three volumes**

B. Novosyadlyj, V. Pelykh, Yu. Shtanov, A. Zhuk

**DARK ENERGY:**  
**OBSERVATIONAL EVIDENCE**  
**AND THEORETICAL MODELS**

**Volume 1**

Editor V. Shulga

---

PROJECT  
«UKRAINIAN SCIENTIFIC BOOK  
IN A FOREIGN LANGUAGE»

---

KYIV · AKADEMPERIODYKA · 2013

NATIONAL ACADEMY OF SCIENCES OF UKRAINE  
BOGOLYUBOV INSTITUTE FOR THEORETICAL PHYSICS  
PIDSTRYHACH INSTITUTE FOR APPLIED PROBLEMS  
OF MECHANICS AND MATHEMATICS  
RADIOASTRONOMICAL INSTITUTE  
IVAN FRANKO NATIONAL UNIVERSITY OF LVIV  
MECHNIKOV NATIONAL UNIVERSITY OF ODESSA

---

НАЦІОНАЛЬНА АКАДЕМІЯ НАУК УКРАЇНИ  
ІНСТИТУТ ТЕОРЕТИЧНОЇ ФІЗИКИ ім. М.М. БОГОЛЮБОВА  
ІНСТИТУТ ПРИКЛАДНИХ ПРОБЛЕМ МЕХАНІКИ  
І МАТЕМАТИКИ ім. Я.С. ПІДСТРИГАЧА  
РАДІОАСТРОНОМІЧНИЙ ІНСТИТУТ  
ЛЬВІВСЬКИЙ НАЦІОНАЛЬНИЙ УНІВЕРСИТЕТ імені ІВАНА ФРАНКА  
ОДЕСЬКИЙ НАЦІОНАЛЬНИЙ УНІВЕРСИТЕТ імені І.І. МЕЧНИКОВА

UDK 524.8+539  
BBK 22.6+22.3  
D20

**Reviewers:**

*S.I. VILCHYNSKIY*, Dr. Sc., Professor, Head of Department of Quantum Field Theory at Taras Shevchenko National University of Kyiv  
*O.B. ZASLAVSKII*, Dr. Sc., Senior researcher, Leading researcher at V.N. Karazin Kharkiv National University

*Approved for publication by the Scientific Council of the Bogolyubov Institute for Theoretical Physics and Pidstryhach Institute for Applied Problems of Mechanics and Mathematics of the National Academy of Sciences of Ukraine*

*Publication was made possible by a State contract promoting the production of scientific printed material*

**Dark energy and dark matter in the Universe: in three D20 volumes / Editor V. Shulga. — Vol. 1. Dark energy: observational evidence and theoretical models / Novosyadlyj B., Pelykh V., Shtanov Yu., Zhuk A. — K. : Akadempriodyka, 2013. — 380 p.**

ISBN 978-966-360-239-4

ISBN 978-966-360-240-0 (vol. 1)

The book elucidates the current state of the dark energy problem and presents the results of the authors, who work in this area. It describes the observational evidence for the existence of dark energy, the methods and results of constraining of its parameters, modeling of dark energy by scalar fields, the space-times with extra spatial dimensions, especially Kaluza—Klein models, the braneworld models with a single extra dimension as well as the problems of positive definition of gravitational energy in General Relativity, energy conditions and consequences of their violation in the presence of dark energy.

This monograph is intended for science professionals, educators and graduate students, specializing in general relativity, cosmology, field theory and particle physics.

**UDC 524.8+539  
BBK 22.6+22.3**

ISBN 978-966-360-239-4  
ISBN 978-966-360-240-0 (vol. 1)

© Novosyadlyj B., Pelykh V.,  
Shtanov Yu., Zhuk A., 2013  
© Akadempriodyka, design, 2013



---

# CONTENTS

---

	FOREWORD OF THE EDITOR.....	9
	ACKNOWLEDGMENTS.....	11
<b>1</b>	<b>Observational evidence for dark energy</b>	
CHAPTER	1.1. Introduction.....	13
	1.2. Dynamics of expansion of the homogeneous isotropic multicomponent Universe.....	16
	1.3. The luminosity distance — redshift relation and SNe Ia evidence for dark energy.....	22
	1.4. The angular diameter distance — redshift relation and acoustic peak tests.....	30
	1.4.1. CMB acoustic peaks.....	30
	1.4.2. Baryon acoustic oscillations.....	38
	1.4.3. X-ray gas fraction in clusters.....	42
	1.5. Evidence for dark energy from study of large scale structure.....	45
	1.5.1. Linear power spectrum of matter density perturbations	45
	1.6. Angular power spectrum of CMB temperature fluctua- tions.....	55
	1.6.1. Integrated Sachs—Wolfe effect.....	55
	1.6.2. Weak gravitational lensing of CMB.....	60
	1.7. Age of the Universe.....	62
	1.8. Constraints on dark energy parameters from combined data.....	64
	1.9. Summary.....	70
<b>2</b>	<b>Scalar field models of dark energy</b>	
CHAPTER	2.1. Introduction.....	72
	2.2. Cosmological constant as vacuum energy: ideas and problems.....	73
	2.3. Scalar fields as dark energy.....	74

2.4. Scalar perturbations of the scalar field and other components .....	77
2.5. Specifying the scalar-field models of dark energy .....	82
2.5.1. Lagrangian .....	83
2.5.2. Potential .....	83
2.5.3. EoS parameter .....	86
2.5.4. The effective sound speed .....	97
2.6. Quintessential scalar fields with barotropic EoS .....	100
2.6.1. Classical scalar field .....	100
2.6.2. Tachyonic scalar field .....	103
2.6.3. Quintessential scalar fields in the phase plane .....	105
2.6.4. Best-fit parameters of QSF .....	107
2.7. Phantom scalar fields with barotropic EoS .....	113
2.7.1. Gravitation instability of PSF and large scale structure formation .....	119
2.7.2. Best-fit parameters of PSF .....	122
2.8. Distinguishing of scalar field models of dark energy ...	123
2.9. Summary .....	130

### 3 CHAPTER

#### Kaluza—Klein models

3.1. Introduction .....	133
3.2. Dimensional reduction, stable compactification, gravitational excitons, effective cosmological constant .....	136
3.2.1. General setup .....	136
3.2.2. Stable compactification with minimal scalar fields ...	140
3.2.3. Perfect fluid: no-go theorem .....	142
3.2.4. Conventional cosmology from multidimensional models .....	145
3.3. Abelian gauge fields in KK models, dimensional reduction .....	152
3.4. Gravitational excitons and their cosmological and astrophysical implications. Dark matter from extra dimensions	155
3.4.1. Effective equation of motion for gravexcitons .....	156
3.4.2. Light and ultra-light gravexcitons: $m_\psi \leq 10^{-2}$ GeV	158
3.4.3. Heavy gravexcitons: $m_\psi \geq 10^{-2}$ GeV .....	160
3.4.4. Variation of the fine-structure constant .....	163
3.4.5. Lorentz invariance violation .....	165
3.5. Dark energy in curvature-non-linear $f(R)$ multidimensional cosmological models .....	170
3.5.1. Internal space stabilization for pure geometrical $f(R)$ models .....	171
3.5.2. Dark energy in $f(R)$ models with form fields .....	177
3.6. $Sp$ -branes. Dynamical dark energy from extra dimensions .....	183

---

	3.6.1. Dark energy in pure geometrical $S_p$ -brane model with hyperbolic internal space . . . . .	187
	3.7. Problematic aspects of Kaluza—Klein models . . . . .	192
	3.7.1. Equations of state in general case . . . . .	195
	3.7.2. Latent solitons . . . . .	197
	3.7.3. Experimental restrictions on the equations of state of a multidimensional perfect fluid . . . . .	199
	3.8. Summary . . . . .	203
<b>4</b>	<b>Braneworld models</b>	
CHAPTER	4.1. Introduction . . . . .	206
	4.2. General setup and notation . . . . .	208
	4.3. Cosmological solutions . . . . .	211
	4.4. Vacuum and static branes . . . . .	214
	4.5. Properties of braneworld gravity . . . . .	218
	4.6. Phantom property of braneworld dark energy . . . . .	224
	4.7. Disappearing dark energy . . . . .	232
	4.8. Cosmic mimicry . . . . .	235
	4.9. Loitering . . . . .	242
	4.9.1. Loitering Universe . . . . .	242
	4.9.2. Loitering in braneworld models . . . . .	243
	4.9.3. The parameter space in loitering models . . . . .	250
	4.9.4. Inflation in braneworld models with loitering . . . . .	252
	4.10. Quiescent singularities . . . . .	254
	4.10.1. Homogeneous case . . . . .	254
	4.10.2. Inhomogeneous case . . . . .	258
	4.11. Asymmetric branes . . . . .	262
	4.11.1. Induced cosmological constant on the brane . . . . .	264
	4.11.2. Cosmic mimicry . . . . .	265
	4.11.3. Phantom branes . . . . .	267
	4.11.4. Disappearing dark energy . . . . .	269
	4.11.5. Quiescent singularities . . . . .	271
	4.11.6. Stability issues . . . . .	272
	4.12. Gravitational instability on the brane . . . . .	272
	4.12.1. Scalar cosmological perturbations on the brane . . . . .	273
	4.12.2. Simplified boundary conditions for scalar perturbations . . . . .	275
	4.12.3. Scalar perturbations in the DGP model . . . . .	279
	4.12.4. Scalar perturbations in the mimicry model . . . . .	283
	4.13. Perturbations of the bulk . . . . .	288
	4.13.1. General system of equations . . . . .	288
	4.13.2. Perturbations on the flat background bulk geometry . . . . .	292
	4.13.3. Quasi-static approximation . . . . .	295
	4.14. Summary . . . . .	296

<b>5</b>	<b>Energy in general relativity</b>	
CHAPTER	<b>in view of spinor and tensor methods</b>	
	<b>5.1. Introduction</b> .....	302
	<b>5.2. Connection between spinor and tensor methods in the positive energy problem</b> .....	304
	<b>5.2.1. Sen—Witten equation in Petrov type <math>N</math> space-time</b>	305
	<b>5.2.2. Nodal surfaces of selfadjoint elliptic second order equations</b> .....	305
	<b>5.2.3. The solutions of Sen—Witten equation have no zeros</b>	306
	<b>5.2.4. Sen—Witten equations and SOF</b> .....	308
	<b>5.2.5. Conclusion</b> .....	310
	<b>5.3. Nodal points of elliptic equations and system of equations</b> .....	311
	<b>5.3.1. Conditions for the absence of nodal points</b> .....	313
	<b>5.3.2. The conditions of nodal points absence for the solutions of Sen—Witten equation</b> .....	317
	<b>5.3.3. Towards Sen—Witten equation, special orthonormal frame and preferred time variables</b> .....	318
	<b>5.4. Sen—Witten orthonormal three-frame and gravitational energy quasilocalization</b> .....	321
	<b>5.4.1. Direct link between the 4-covariant spinor 3-form and the Einstein Hamiltonian</b> .....	323
	<b>5.4.2. In which cases the conditions of Theorem 4 are fulfilled?</b> .....	329
	<b>5.5. Summary</b> .....	331
	<b>APPENDIX A. Friedmann equations for the multicomponent scalar-field model</b>	333
	<b>APPENDIX B. Mathematical details of the braneworld model</b>	336
	<b>B.1. Variational problem in the presence of the brane</b> .....	336
	<b>B.2. Graphical representation of the brane evolutiong</b> .....	338
	<b>B.3. Background cosmological solution in the bulk</b> .....	339
	<b>B.4. Scalar perturbation of the bulk metric</b> .....	340
	<b>BIBLIOGRAPHY</b> .....	341
	<b>INDEX</b> .....	374
	<b>ABOUT THE AUTHORS</b> .....	378





---

## FOREWORD OF THE EDITOR

---

Current science of the extraterrestrial world, based on observations and physical theories, during the last decades has collected many independent types of evidence to certify that about 95 % of the energy-mass content of our Universe is dark and invisible, and its physical nature is unknown. There are also many arguments that it is composed of two ingredients: dark matter, which facilitates clustering of the baryonic matter, and dark energy, which is almost uniform and is responsible for the accelerated expansion of the Universe. Scientific teams of physicists, astrophysicists and cosmologists all over the world endeavor to unveil these mysterious components, which today dominate in the average density of the Universe and determine the physical properties and evolution of our Universe. This task becomes extremely important for the elaboration of particle physics beyond the Standard Model.

In 2007, the programme of the National Academy of Sciences of Ukraine “Investigations of the structure and composition of the Universe, hidden mass and dark energy (Cosmomicrophysics)” was initiated, aimed at consolidating the efforts of different scientific teams in several research institutes and universities working in the field of astroparticle physics and theory of gravity and investigating the dark components of the Universe. The results of six-year activity in the framework of this programme will be presented in the three-volume edition “Dark energy and dark matter in the Universe”. The present book is the first of the volume series and is devoted to the problem of dark energy. It describes the current state of the problem of dark energy as well as the contribution of the authors to this issue. Their investigation in this area was supported in part by the Cosmomicrophysics programme during the last six years, but the book also contains their previous results obtained in the framework of the state projects in their respective institutions as well as other projects and grants which are mentioned in the acknowledgments. The first and second chapters of the book are written by Bohdan

Novosyadlyj, the third one by Alexander Zhuk, the fourth one by Yuri Shtanov and the fifth one by Volodymyr Pelykh.

This monography is dedicated to the memory of our colleagues and friends Peter Fomin (1930–2011), Anatolij Minakov (1949–2012) and Victor Vakulik (1953–2012), distinguished Ukrainian physicists who had passed away when this book was being written. Peter Fomin made significant contributions to the quantum field theory and quantum cosmology; he is the author of the idea of quantum birth of the Universe. Anatolij Minakov laid the foundations for the application of the theory of gravitational lensing to the interpretation of gravitational lens systems and estimation of dark matter abundance. Victor Vakulik was an unsurpassed specialist in computer simulation and a brilliant interpreter of astrophysical observational data.

V. SHULGA

A handwritten signature in blue ink, appearing to read 'Shulga', with a horizontal line extending to the right.



---

## ACKNOWLEDGMENTS

---

We are grateful to the National Academy of Sciences of Ukraine for financial support of the research program “Investigations of the structure and composition of the Universe, hidden mass and dark energy (Cosmomicrophysics)”, within which this monograph is written. We are thankful to the editor of this monograph academician Valerij Shulga for the suggestion of its writing, participation in the formation of its content and organization of its publication. We also thank academician Yaroslav Yatskiv for his generous support of this project. We also appreciate helpful and highly professional assistance from the staff of the academic publisher “Akademperiodyka”.

We are deeply grateful to our co-authors for productive long-term collaboration, the results of which form the basis of the monograph. Among them: Stepan Apunevych, Viktor Baukh, Valdir Bezerra, Ulrich Bleyer, Alexey Chopovsky, Luis Crispino, Ruth Durrer, Maxim Eingorn, Seyed Hossein Fakhr, Peter Fomin, Stephan Gottlöber, Uwe Günther, Vladimir Ivashchuk, Tinatin Kahniashvili, Uwe Kasper, Svetlana Kriskiv, Yuriy Kulinich, Vladimir Lukash, Orival de Medeiros, Vitaly Melnikov, Paulo Moniz, Martin Rainer, Carlos Romero, Varun Sahni, Tamerlan Saidov, Olga Sergijenko, Arman Shafieloo, Alexey Starobinsky, Alexey Toporensky, Petr Tretyakov, Ricardo Valdarnini, Alexander Viznyuk.

Last but not least, we thank our families for their unconditional and devoted support and understanding.

Our research was supported by the university and institution projects of the Ministry of Education and Science and National Academy of Sciences of Ukraine as well as by grants from the SCOPES programme financed by the Swiss National Science Foundation, the Tomalla Foundation, the DAAD programme of Germany, the Brazilian sponsoring agency CAPES, the Abdus Salam ICTP, the SISSA, the Ministry of Science and Technology of India, the IUCAA (India) and the Theory Division of the CERN visitor programs.

*B. NOVOSYADLYJ,  
V. PELYKH, Yu. SHTANOV, A. ZHUK*

Lviv — Kyiv — Odessa

*To the memory  
of prominent Ukrainian scientists,  
our colleagues and friends  
Peter Fomin, Anatolij Minakov  
and Victor Vakulik*

# 1

## CHAPTER

---

# OBSERVATIONAL EVIDENCE FOR DARK ENERGY

---

### 1.1. Introduction

The term “dark energy” has appeared in the titles and abstracts of scientific papers in 1998 after announcements about discovery of the accelerated expansion the Universe, made by two teams practically simultaneously — Supernova Cosmology Project [1,2] and High-Z Supernova Search [3,4]. The first application of this term in the conventional now meaning we have found in the papers [5–7], one year before M. Turner and M. White called this essence “smooth component” [8] and P. Steinhardt “quintessence” [9]. Up to now the number of papers devoted to this subject has amounted to more than ten thousands and continues to grow in about two thousands per year during last years (Fig. 1), that signifies the actuality of dark energy problem and its importance for fundamental physics, astrophysics and cosmology.

Dark energy stands for the wide spectrum of new physical substances capable to provide the accelerated expansion of the Universe. But not only that. It must be noted, that cosmology was looking for such essence for years. Indeed, measurements of peculiar velocities of galaxies carried out in the second half of 80s and first half of 90s showed, that total matter density (baryons and cold dark matter, CDM) of our Universe is  $0.4 \pm 0.1$  of critical one [10]. On the other hand, all measurements of the Hubble constant showed, that it is larger than  $60 \text{ km/s} \cdot \text{Mpc}$  [11]. It meant, that the age of the maximally open Universe does not exceed 13 billion years, while the age of oldest stars in the globular clusters was estimated to be  $13.5 \pm 2$  billion years [12]. So, open models of the Universe have not enough margin of safety, but models with cosmological constant have: even at the upper limit of

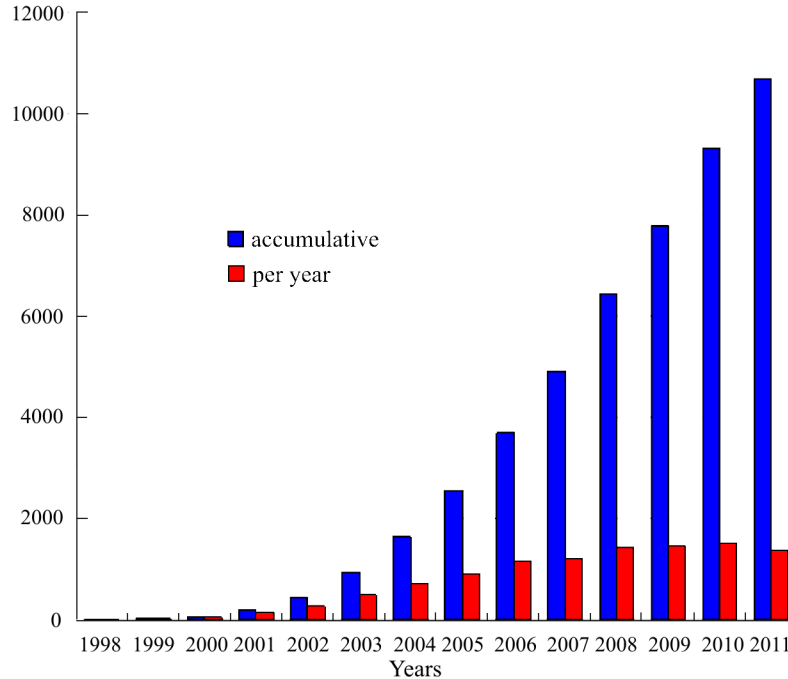


**Fig. 1.1.** Number of papers (accumulative and per year) in SAO/NASA Astrophysics Data System with key words “dark energy” in title or abstract

Hubble constant estimation —  $85 \text{ km/s} \cdot \text{Mpc}$  — the age of the Universe is about 14 billion years. The matter dominated model with low 3-space curvature was ruled out by these data at high confidential level.

Other indications of the presence of unusual component in our Universe came from the study of large scale structure formation. Bahcall et al. [13] have revealed the massive rich clusters of galaxies at redshifts  $z > 0.5$ , such early appearance of them in the COBE normalized [14, 15] hierarchical scenarios of large scale structure formation is possible if growth factor of density perturbations is lower than one in the standard CDM model (SCDM) with density dominated by cold dark matter and zero 3-space curvature. It is such in open CDM (OCDM) and CDM with cosmological constant ( $\Lambda$ CDM) models. The last ones had higher margin of safety than former. The measurements of power spectra of matter density perturbations [16], X-ray cluster temperature function [17] and galaxy bulk flows [18] also preferred  $\Lambda$ CDM model [19, 20]. But the science lacked for the direct test for such model — determination of deceleration parameter  $q_0$ , which is positive in the matter dominated models (decelerated expansion) and negative in the  $\Lambda$  dominated ones (accelerated expansion). Its early estimations, listed in review [21], were very rough,  $-1.3 \leq q_0 \leq 1.6$ , and gave no possibility to constraint the

models. Improving this test became the key task for Hubble Space Telescope (HST) and largest ground-based telescopes installed in 90s. And this problem was successfully solved using Type Ia supernovae (SNe Ia) as standard candles for magnitude-redshift relation.

The 1998 became the prominent year for cosmology. The High-Z Supernova Search team on the base of spectral and photometric investigations of 16 high-redshift and 34 nearby SNe Ia claimed [3] that deceleration parameter  $q_0 < 0$  at confidential levels from 99.5% ( $2.8\sigma$ ) to 99.9% ( $3.9\sigma$ ) for  $q_0 = \Omega_m/2 - \Omega_\Lambda$ . These authors found also that more uncertain estimate for its value is  $q_0 = -1 \pm 0.4$ . The Supernova Cosmology Project team during ten-year observations had discovered 42 SNe Ia at redshifts between 0.18 and 0.83 which were photometrically and spectroscopically investigated carefully. After complete analysis of the data the team claimed [2] that cosmological constant is non-zero and positive with the confidence of 99%, including the identified systematic uncertainties. They obtained the relation which approximates the joint probability distribution of matter and cosmological constant density parameters:  $0.8\Omega_m + 0.6\Omega_\Lambda \approx -0.2 \pm 0.1$ . It means that deceleration parameter  $q_0 \approx -5\Omega_m/6 - 1/3 \pm 1/6$  and is surely negative. So, the accelerated expansion of the Universe was strongly preferred by magnitude-redshift data for SNe Ia. But for assurance other proofs based on the other observations should be realized. The large scale structure evidence had not enough stringency yet, since different scenarios then were under discussions — its forming from adiabatic or iso-curvature primordial perturbations, topological defects, cosmological strings or other seeds. In the last two years of XX century the precise measurements of cosmic microwave background (CMB) temperature anisotropy realized in the BOOMERanG [22] and MAXIMA [23] stratospheric experiments revealed the acoustic peaks in its angular power spectrum predicted by scenario of large scale structure formation from adiabatic primordial perturbations. So, the large scale structure data jointly with CMB anisotropy have become the powerful test for dark energy models. During the first decade of XXI century the numerous data proving the existence of dark energy have been obtained. For the discovery of the accelerating expansion of the Universe through observations of distant supernovae Saul Perlmutter, Adam G. Riess and Brian P. Schmidt were honored with the Nobel Prize in Physics for 2011.

On the other hand theorists have proposed many candidates for dark energy which well match the observational data [24–44]. So, the important problem of nowadays cosmology is developing of key tests for distinguishing between different models of dark energy and constraining the values of their parameters. The state-of-art observational evidence for dark energy and constraints on its parameters are discussed in this chapter.

## 1.2. Dynamics of expansion of the homogeneous isotropic multicomponent Universe

The base of cosmology as physical science is General Relativity founded by Albert Einstein [45]. He was also the first who in 1917 introduced the new essence, cosmological constant [46], which acts against gravitation attraction<sup>1</sup> and now is considered as the simplest candidate for dark energy. The other fundamental conceptual base of standard cosmology is the cosmological principle which states that on the large scales the Universe is homogeneous and isotropic. The geometric properties of such Universe define the general form of space-time line element as

$$ds^2 = g_{\mu\nu} dx^\mu dx^\nu = a^2(\eta) (-d\eta^2 + dr^2 + \chi^2(r)(d\vartheta^2 + \sin^2\vartheta d\varphi^2)), \quad (1.1)$$

where  $g_{\mu\nu}$  is a metric tensor,  $\eta$  is the conformal time defined by relation  $c dt = a(\eta)d\eta$ ,  $a(\eta)$  is the scale factor,  $r, \vartheta, \varphi$  are spherical coordinates in 3-space with a curvature  $K$  and

$$\chi(r) = \begin{cases} \frac{1}{\sqrt{K}} \sin \sqrt{K}r, & K > 0 \text{ (spherical 3-space),} \\ r, & K = 0 \text{ (flat 3-space),} \\ \frac{1}{\sqrt{|K|}} \sinh \sqrt{|K|}r, & K < 0 \text{ (hyperspherical 3-space).} \end{cases} \quad (1.2)$$

Here and below the Greek indices ( $\nu, \mu, \dots$ ) run from 0 to 3 and the Latin ones ( $i, j, \dots$ ) run from 1 to 3. Henceforth we put  $c = 1$ , so the time variable  $t \equiv x_0$  as well as conformal time  $\eta$  have the dimension of a length. We follow also usual convention that terms with the same upper and lower indices are summed over. The space-time with metric (1.1) is called Friedmann–Robertson–Walker (FRW) one in memoriam of the first investigations of homogeneous and isotropic solutions of Einstein’s equations by A. Friedman in 1922 [47] and distance-redshift relation in the expanding Universe<sup>2</sup> by H. Robertson in 1928 [49] and A. Walker in 1933 [50].

Today we know that our Universe is filled with matter-energy and fields, which can be classified as relativistic component (cosmic background radiation and relic neutrino), non-relativistic one (baryon and dark matter) and dark energy of unknown nature which accelerates its expansion. Each of them can be described by energy-momentum tensor of perfect fluid

$$T_{\mu\nu N} = (\rho_N + p_N) u_{\mu N} u_{\nu N} + p_N g_{\mu\nu}, \quad (1.3)$$

---

<sup>1</sup> A. Einstein introduced it in order to realize a static universe in the framework of General Relativity, but after discussion with A. Friedmann and discovery of expansion of the Universe by E. Hubble he abandoned this idea.

<sup>2</sup> Physical properties of the non-stationary Universe with FRW metric were first analyzed by G. Lemaitre in 1927 [48]



that is consequence of symmetry of FRW space-time. Here  $\rho_N$  is energy density and  $p_N$  is pressure, which are defined as time- and space-like eigenvalues of  $T_{\mu N}^{\nu}$  correspondingly,  $u_N^{\mu} = (-a, 0, 0, 0)$  is four-velocity of the fluid in comoving coordinates, and  $N$  stands for relativistic ( $r$ ), matter ( $m$ ) or dark energy ( $de$ ) components. The space-time metric (1.1) and energy-momentum tensors (1.3) of each component are used for analysis of expansion dynamics, physical phenomena and distant-redshift relations of homogeneous isotropic Universe, called also cosmological background. In the theory of large scale structure formation they have more general forms, that will be discussed later.

Assuming that the interaction between all components is only gravitational, each of them should satisfy the differential energy-momentum conservation law separately:

$$T_{\mu;\nu N}^{\nu} = 0. \quad (1.4)$$

Hereafter “;” denotes the covariant derivative with respect to the coordinate with given index in the space with metric  $g_{ij}$ . In the homogeneous Universe the density  $\rho_N$  and pressure  $p_N$  of perfect fluid are functions of time only, so the equation of state (EoS) can be presented in the simple form

$$p_N(\eta) = w_N(\eta)\rho_N(\eta), \quad (1.5)$$

where  $w_N$  is called EoS parameter, it can be constant or time-variable, that depends on physical properties of the component ( $N$ ).

In the space-time (1.1) the differential energy-momentum conservation law (1.4) gives

$$\dot{\rho}_N = -3\frac{\dot{a}}{a}\rho_N(1 + w_N), \quad (1.6)$$

here and below a dot denotes the derivative with respect to the conformal time,  $\dot{\phantom{x}} \equiv d/d\eta$ .

For the non-relativistic matter  $w_m = 0$  and for the relativistic one  $w_r = 1/3$ . For these cases the equation (1.6) can be easily integrated to obtain the time dependences of density of these components in the form

$$\rho_m = \rho_m^{(0)}(a_0/a)^3, \quad \rho_r = \rho_r^{(0)}(a_0/a)^4, \quad (1.7)$$

where index “0” in parentheses and without them denotes the current values of corresponding variables. The EoS parameter of dark energy is unknown and can be constant or time-variable. In the general case the integral of equation (1.6) for dark energy is as follows

$$\rho_{de} = \rho_{de}^{(0)}(a_0/a)^{3(1+\tilde{w}_{de})}, \quad (1.8)$$

where  $\tilde{w}_{de} = w_{de}$  for the constant EoS parameter  $w_{de}$  and

$$\tilde{w}_{de} = \frac{1}{\ln(a/a_0)} \int_{a_0}^a w_{de} d \ln a \quad (1.9)$$

for the time-variable one.

In this chapter we consider mainly the dark energy with constant EoS parameter  $w_{de}$ . The case  $w_{de} = -1$  corresponds to the well studied  $\Lambda$ CDM model with  $\rho_{de} = \rho_\Lambda = \text{const}$ . When  $w_{de} > -1$  the density of DE monotonically decreases with time (often called quintessence), in the opposite case ( $w_{de} < -1$ ) it increases. Since in the last case the density starts from zero at  $a = 0$  it is dubbed “phantom” [51].

The Einstein equations relate the Ricci tensor  $R_{\mu\nu}$  to the total energy-momentum tensor of all components as follows

$$R_{\mu\nu} - \frac{1}{2}g_{\mu\nu}R = 8\pi G \sum_N T_{\mu\nu N}, \quad (1.10)$$

where  $R \equiv g^{\alpha\beta}R_{\alpha\beta}$  is scalar curvature of space-time. For the space-time with metric (1.1) they become

$$\left(\frac{\dot{a}}{a}\right)^2 + K = \frac{8\pi G}{3}a^2 \sum_N \rho_N, \quad (1.11)$$

$$\frac{\ddot{a}}{a} - \left(\frac{\dot{a}}{a}\right)^2 = -\frac{4\pi G}{3}a^2 \sum_N \rho_N(1 + 3w_N), \quad (1.12)$$

which can be integrated for  $a(\eta)$  when right-hand sides (r.h.s.) are defined.

The first term in left-hand side (l.h.s.) of (1.11) is the rate of expansion and in l.h.s. of (1.12) is acceleration ( $d^2a/dt^2$ ). So, the dynamics of cosmic expansion is determined by specifying the properties of matter-energy components of the Universe.

It is convenient to introduce the dimensionless parameters of matter density  $\Omega_m$ , radiation density  $\Omega_r$ , dark energy density  $\Omega_{de}$  and curvature of 3-space  $\Omega_K$  as follows

$$\begin{aligned} \Omega_m &\equiv \left(\frac{8\pi G\rho_m a^2}{3(\dot{a}/a)^2}\right)_{\eta_0}, & \Omega_r &\equiv \left(\frac{8\pi G\rho_r a^2}{3(\dot{a}/a)^2}\right)_{\eta_0}, \\ \Omega_{de} &\equiv \left(\frac{8\pi G\rho_{de} a^2}{3(\dot{a}/a)^2}\right)_{\eta_0}, & \Omega_K &\equiv \left(\frac{-K}{(\dot{a}/a)^2}\right)_{\eta_0}. \end{aligned} \quad (1.13)$$

The density parameter of relativistic component  $\Omega_r$  at current epoch is the sum of photon and neutrino ones and equals

$$\Omega_r = 4.17 \cdot 10^{-5} \left(\frac{1 + \rho_\nu/\rho_\gamma}{1.6813}\right) \left(\frac{T_0}{2.726}\right)^4 \approx 4.17 \cdot 10^{-5} h^{-2}. \quad (1.14)$$

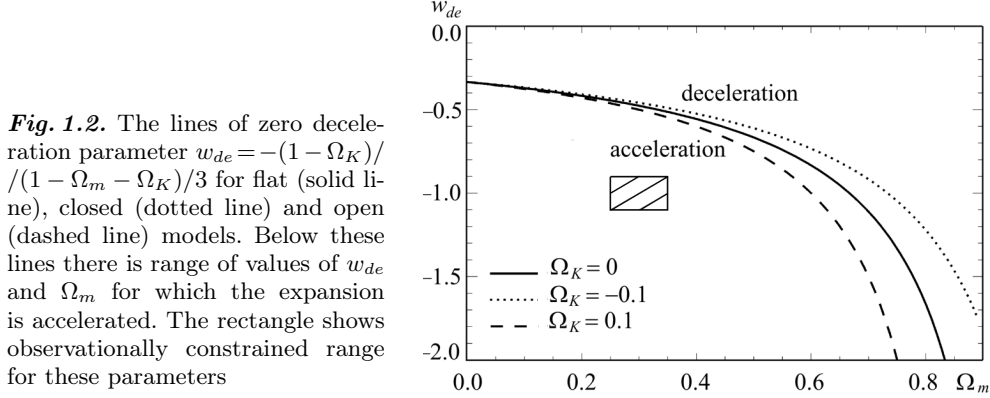


**Fig. 1.2.** The lines of zero deceleration parameter  $w_{de} = -(1 - \Omega_K) / (1 - \Omega_m - \Omega_K) / 3$  for flat (solid line), closed (dotted line) and open (dashed line) models. Below these lines there is range of values of  $w_{de}$  and  $\Omega_m$  for which the expansion is accelerated. The rectangle shows observationally constrained range for these parameters

The equations (1.11), (1.12) in this notation become

$$H = H_0 \left( \Omega_r \frac{a_0^4}{a^4} + \Omega_m \frac{a_0^3}{a^3} + \Omega_K \frac{a_0^2}{a^2} + \Omega_{de} \left( \frac{a_0}{a} \right)^{3(1+w_{de})} \right)^{1/2}, \quad (1.15)$$

$$q = \frac{H_0^2}{H^2} \left( \Omega_r \frac{a_0^4}{a^4} + \frac{1}{2} \Omega_m \frac{a_0^3}{a^3} + \frac{1}{2} (1 + 3w_{de}) \Omega_{de} \left( \frac{a_0}{a} \right)^{3(1+w_{de})} \right), \quad (1.16)$$

where  $H \equiv a^{-1} da/dt = a^{-2} da/d\eta = \dot{a}/a^2$  is Hubble parameter at any time  $\eta$  and  $q \equiv -(a\ddot{a}/\dot{a}^2 - 1)$  is deceleration parameter.

At the current epoch  $\eta = \eta_0$  the Friedmann equations (1.15), (1.16) are simplified to the form

$$\Omega_r + \Omega_m + \Omega_K + \Omega_{de} = 1, \quad (1.17)$$

$$q_0 = \Omega_r + \frac{1}{2} \Omega_m + \frac{1}{2} (1 + 3w_{de}) \Omega_{de}. \quad (1.18)$$

If the Universe is filled only with matter and radiation then deceleration parameter is always positive ( $d^2a/dt^2 < 0$ ) for any curvature, as one can see from (1.16)–(1.18). And when only third component with

$$w_{de} < -\frac{1}{3} \frac{1 - \Omega_K}{1 - \Omega_m - \Omega_K} \quad (1.19)$$

is present then deceleration parameter  $q_0$  at current epoch could be negative ( $d^2a/dt^2 > 0$ ). In the last expression we omit  $\Omega_r$ , since it is substantively lower than  $\Omega_m$ . In Fig. 1.2 the ranges of values of parameters for which expansion of the Universe is accelerated are shown.

If the dark energy is cosmological constant  $\Lambda$ , for which  $w_{de} = -1$  and  $\Omega_\Lambda \equiv \Lambda/3H_0^2$ , then the accelerated expansion of the Universe will take place under condition  $\Omega_m < 2(1 - \Omega_K)/3$ . In the models with vanishing curvature (standard  $\Lambda$ CDM ones) matter density parameter must be lower than 0.66. The dependence of deceleration parameter  $q_0$  on  $\Omega_m$  for different  $\Omega_K$  and  $w_{de}$  at current epoch is shown in Fig. 1.3.

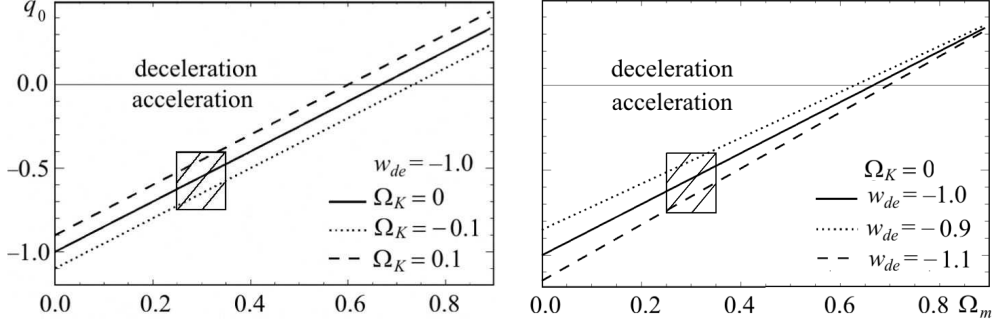


**Fig. 1.3.** The dependence of current value of deceleration parameter on  $\Omega_m$  for different  $\Omega_K$  (left panel) and different  $w_{de}$  (right one). The rectangles show observational constraints on  $q_0$  and  $\Omega_m$  from [2]

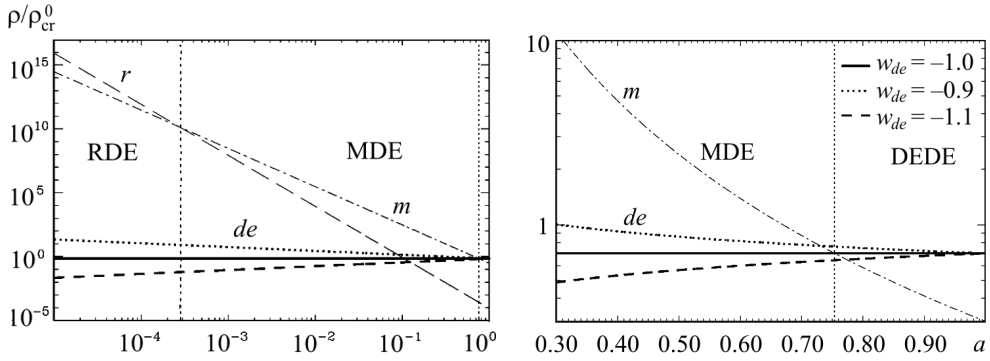


**Fig. 1.4.** The evolution of energy density of relativistic ( $r$ ), matter ( $m$ ) and dark energy  $w = \text{const}$  ( $de$ ) components. RDE – radiation dominated epoch, MDE – matter dominated epoch and DEDE – dark energy dominated epoch. In the left panel the plot is in log-log scale from early epoch to current one, in the right panel the plot is in norm-log scale and illustrates the late epoch. All lines correspond to model with  $\Omega_m = 0.3$  and  $\Omega_{de} = 0.7$ . The MDE-DEDE crossing line is shown for  $\Lambda$ -model ( $w_{de} = -1$ )

The dynamics of expansion of the multicomponent Universe is different in different epochs, that follows from equations (1.15), (1.16). Really, for  $w_{de}$ , which satisfies condition (1.19), the dynamical history can be divided into three periods (Fig. 1.4):

**radiation dominated** (RD) epoch, when  $\rho_r \gg \rho_m \gg \rho_{de}$  and  $q = 1$ ; it was at  $a \ll a_{eq}^{(r-m)}$ , where  $a_{eq}^{(r-m)} = 4.17 \cdot 10^{-5} \Omega_m^{-1} h^{-2}$  is scale factor at radiation-matter equality;

**matter dominated** (MD) epoch, when  $\rho_m \gg \rho_r$  and  $\rho_m \gg \rho_{de}$ ; then  $q = 0.5$ ; it was at  $a_{eq}^{(r-m)} \ll a \ll a_{eq}^{(m-de)}$ , where  $a_{eq}^{(m-de)} = (\Omega_m / \Omega_{de})^{-1/3w_{de}}$  is scale factor at matter – dark energy equality;

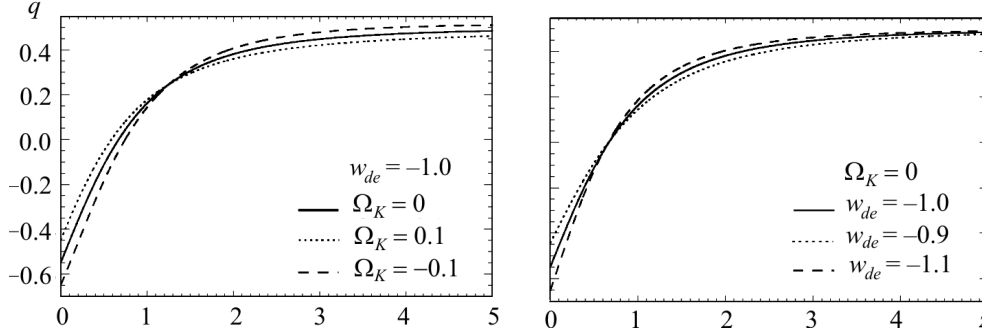


**Fig. 1.5.** The dependence of deceleration parameter  $q$  on  $z$  for cosmological models with different  $\Omega_K$  (left panel) and  $w_{de}$  (right one). Here values of other parameters are:  $\Omega_m = 0.3$ ,  $\Omega_{de} = 1 - \Omega_K - \Omega_m$ ,  $H_0 = 70$  km/s/Mpc

**dark energy dominated** (DED) epoch, when  $\rho_{de} \gg \rho_m \gg \rho_r$  at  $a > a_{eq}^{(m-de)}$ ; it is epoch of accelerated expansion of the Universe. In the case of  $w_{de} = \text{const}$  it will last forever.

In the model with realistic parameters  $\Omega_m = 0.3$ ,  $\Omega_{de} = 0.7$ ,  $h = 0.7$ ,  $w_{de} = -1$  the scale factors (redshifts) related to epoch change-overs (shown in Fig. 1.4) are  $a_{eq}^{(r-m)} = 2.9 \cdot 10^{-4}$  ( $z_{eq}^{(r-m)} = 3500$ ) and  $a_{eq}^{(m-de)} = 0.75$  ( $z_{eq}^{(m-de)} = 0.32$ ).

The measurements of  $q_0$  give the possibility to connect  $\Omega_m$ ,  $\Omega_{de}$  and  $w_{de}$  by relation (1.18), where  $\Omega_r$  can be omitted. In the flat Universe, for which  $\Omega_{de} = 1 - \Omega_m$ , it can be reduced to the relation between  $w_{de}$  and  $\Omega_{de}$ :

$$\Omega_{de} = (2q_0 - 1)/3w_{de}. \quad (1.20)$$

And only for the flat  $\Lambda$ -model we can estimate  $\Omega_\Lambda$  from measurements of  $q_0$ :  $\Omega_\Lambda = (1 - 2q_0)/3$ . For joint estimation of  $w_{de}$  and  $\Omega_{de}$  the measurements of  $q$  at other redshifts are required. For example, if we have estimations of  $q_0$  and redshift  $z_{q=0}$  where decelerated expansion was changed by accelerated one ( $q = 0$ ), then EoS parameter can be estimated from transcendent equation

$$(1 + z_{q=0})^{3w_{de}} = \frac{2q_0 - 1 - 3w_{de}}{(1 + 3w_{de})(2q_0 - 1)}, \quad (1.21)$$

and  $\Omega_{de}$  from equation (1.20). In the general case for estimation of  $\Omega_m$ ,  $\Omega_{de}$  and  $w_{de}$  the form of  $q(z)$  dependence in the range  $0 < z < 5$ , shown in Fig. 1.5, must be measured. It can be done by realization of tests “luminosity distance — redshift” for sources with known luminosities or “angular diameter distance — redshift” for sources with known diameters.

### 1.3. The luminosity distance — redshift relation and SNe Ia evidence for dark energy

The luminosity distance is defined by

$$d_L^2 \equiv \frac{L}{4\pi F}, \quad (1.22)$$

where  $L$  is absolute luminosity of a source and  $F$  is an observed flux. The source is at comoving distance  $r$  and has emitted photons at  $\eta$ , which observer from the Earth detects in the point  $r = 0$  at current moment of time  $\eta_0$ .

Taking into account the redshifting of each photon detected by observer from the Earth and lowering the photons arrival rate, both by the factor  $a(\eta_0)/a(\eta) = 1 + z$ , in the FRW space-time (1.1) the luminosity distance  $d_L$  of a source and its redshift are bound by relation

$$d_L = (1 + z)\chi \left( \int_0^z \frac{dz'}{H(z')} \right), \quad (1.23)$$

where function  $\chi$  is defined by expression (1.2) and  $H(z')$  by equation (1.15). The computed  $d_L(z)$ -dependences for models with different values of  $\Omega_m$ ,  $\Omega_K$ ,  $\Omega_{de}$  and  $w_{de}$  are shown in Fig. 1.6. There also shown for comparison the luminosity distances to high- $z$  SNe Ia derived from their moduli distances and corrected magnitudes presented in Table 5 of [3] and Table 1 of [2] correspondingly<sup>3</sup>. They certainly indicate that models with dark energy are strongly preferred by the SNe Ia observations.

One can see, that models with values of parameters  $\Omega_K$  and  $w_{de}$  from the ranges  $[-0.1, 0.1]$  and  $[-0.9, -1.1]$  correspondingly are only slightly distinguished by  $d_L(z)$  for  $0 \leq z \leq 5$  since it is integral of  $H^{-1}(z)$  over  $z$ . Fig. 1.5 illustrates that the deceleration parameter, which is defined by ratio of the first derivative of  $H(z)$  with respect to redshift  $z$  and  $H(z)$ ,

$$q(z) = \frac{z + 1}{H(z)} \frac{dH(z)}{dz} - 1 \quad (1.24)$$

is more sensitive to value of EoS parameter. One expects, that higher derivatives of  $H(z)$  with respect to redshift  $z$  are also more sensitive to value of EoS parameter. It is convenient to introduce the dimensionless parameters

analogical to the deceleration parameter  $q(t) \equiv -\frac{1}{a(t)H^2(t)} \frac{d^2a(t)}{dt^2}$ :

$$j(t) = \frac{1}{a(t)H^3(t)} \frac{d^3a(t)}{dt^3}, \quad s(t) = \frac{1}{a(t)H^4(t)} \frac{d^4a(t)}{dt^4},$$

<sup>3</sup> These papers contain the most accurate data in 1998–1999 supporting the existence of dark energy and become the base for awarding of Nobel Prize in physics to S. Perlmutter, A. Riess and B. Shmidt in 2011.

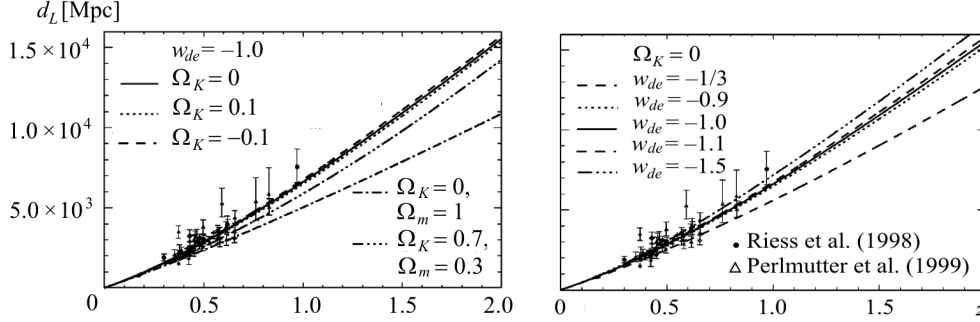


**Fig. 1.6.** Left panel: The dependence of luminosity distance  $d_L$  on redshift for cosmological models with different values of  $\Omega_K, \Omega_\Lambda, \Omega_m$ :  $(0, 0, 1)$ ,  $(0, 0.7, 0.3)$ ,  $(-0.1, 0.8, 0.3)$ ,  $(0.1, 0.6, 0.3)$ ,  $(0.7, 0, 0.3)$ . Right panel: The same for cosmological models with  $\Omega_K = 0$ ,  $\Omega_{de} = 0.7$ ,  $\Omega_m = 0.3$  and different values of  $w_{de}$ . In both panels the luminosity distances to high- $z$  supernovae Ia derived from the data presented in [2, 3] are shown by signs. (It is assumed that  $H_0 = 70$  km/s/Mpc for all calculations here)

dubbed *jerk* and *snap* (see [52, 53] and citing therein), which are represented by second and third derivatives of  $H(z)$  with respect to  $z$  as follows

$$j(z) = q^2(z) + \frac{(z+1)^2}{H(z)} \frac{d^2 H(z)}{dz^2}, \quad (1.25)$$

$$s(z) = -q^3(z) - [4q(z) + 3] \frac{(z+1)^2}{H(z)} \frac{d^2 H(z)}{dz^2} - \frac{(z+1)^3}{H(z)} \frac{d^3 H(z)}{dz^3}. \quad (1.26)$$

They are shown in Fig. 1.7. Indeed, they can be used for accurate determinations of  $w_{de}$  if high-precision measurements of  $d_L$  will be possible, since  $H(z) = \left[ \frac{d}{dz} \left( \frac{d_L}{z+1} \right) \right]^{-1}$  for the flat Universe for example. Unfortunately, the contemporary observational data give the possibility to establish  $q$  at current epoch only, which is the coefficient of second order term in the power series of  $d_L$  on  $z$  in the vicinity of  $z = 0$

$$d_L(z) = \frac{c}{H_0} \left\{ z + \frac{1}{2} [1 - q_0] z^2 - \frac{1}{6} [1 - q_0 - 3q_0^2 + j_0 + \Omega_K] z^3 + \frac{1}{24} [2 - 2q_0 - 15q_0^2 - 15q_0^3 + 5j_0 + 10q_0 j_0 + s_0 + \Omega_K] z^4 + O(z^5) \right\}. \quad (1.27)$$

This expansion of  $d_L$  in  $z$  up to fourth order term<sup>4</sup> approximates the exact expression (1.23) with error  $\leq 1\%$  up to  $z \approx 0.5$  for all models in Fig. 1.6 excluding OMD one with  $\Omega_K = 0.7$ , for which this level of approximation accuracy is overcome at  $z \sim 0.2$ . The including of third order term in the value of  $d_L$  at  $z \sim 0.1$  gives 3–7% of value of second one, the including of fourth

<sup>4</sup> It have been deduced firstly by M. Visser [52]. The term of third order in  $z$  was previously calculated by T. Chiba and T. Nakamura [54], the first two terms are Weinberg's version of Hubble law [55].

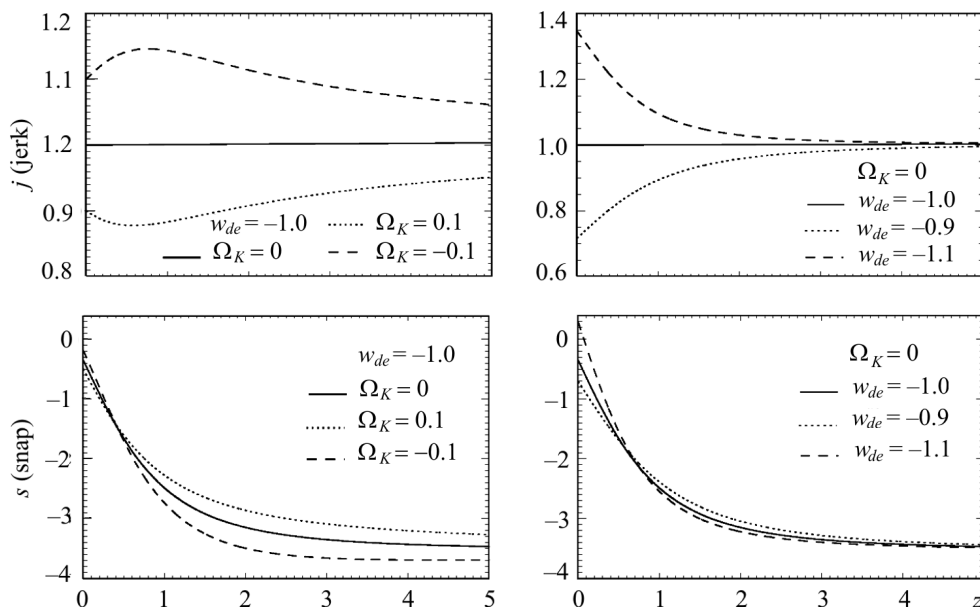


**Fig. 1.7.** The dependence of jerk parameter  $j$  (top panels) and snap parameter  $s$  (bottom panels) on redshift  $z$  for cosmological models with different  $\Omega_K$  (left panel) and  $w_{de}$  (right one). The values of other parameters are the same as in Fig. 1.5

one is at the level of few tenthes of percent, so, their estimation on the base of current data on SNe Ia luminosity distances is impossible. Enough precision of observations for obtaining the information on the variation of  $q(z)$  and  $j(z)$  will be reached at the end of current decade, as it is expected.

The observed flux and absolute luminosity of sources in astrophysics traditionally are presented by visible and absolute magnitudes  $m$  and  $M$ , which are connected to the luminosity distance  $d_L$  by well known relation

$$(m - M) = 5 \log d_L + 25. \quad (1.28)$$

Their difference in the l.h.s. is called distance modulus and is marked by  $\mu$ .

The sources with known luminosity  $L$  or absolute magnitude  $M$  are called standard candles, they give possibility to measure the distances, that is crucial for astrophysics and cosmology. The best standard candles in cosmology are Type Ia supernovae (SNe Ia), which are thermonuclear explosions of near-Chandrasekhar mass carbon-oxygen white dwarfs residing in binary systems. The word “the best” means “the better than any other one”, nothing more. They are not ideal standard candles, since their raw peak brightnesses vary by factor two, this limits their cosmological applications. The key astrophysical development in the cosmological use of SNe Ia was the realization that their luminosities could be further standardized using empirical relationships: SN



Ia light-curve width — SN Ia luminosity [56, 57] and SN Ia color — SN Ia luminosity [58]. Light curves can be described by stretch parameter  $s$ , which stretches or tightens a template of light curve to match an observed one.

The correction of observed peak magnitudes in the most cosmological applications is as follows

$$m_B^{(corr)} = m_B^{(obs)} + \alpha(s - 1) - \beta C^{(obs)}, \quad (1.29)$$

where  $\alpha$  and  $\beta$  are parameters, which must be determined for sample of SNe Ia. As a rule, the magnitudes are measured in the standard B and V bands and the color is their difference,  $C^{(obs)} = m_B^{(obs)} - m_V^{(obs)}$ . For using the measured  $m_B^{(obs)}$  and  $m_V^{(obs)}$  of distant SNe Ia in the cosmological context they must be corrected also for redshifting of their spectral energy distributions as well as extinction along the line of sight. A few methods have been developed for SNe Ia light-curve fitting, which were called the stretch one [59–61], CMAGIC [62], BATM [63],  $\Delta m_{15}$  [64, 65], Spectral Adaptive Light curve Template (SALT) [66] and its improvement SALT2 [67], Multicolor Light Curve Shape (MLCS) [68] and its improvement MLCS2k2 [69], SiFTO [70] etc. They give quite similar results for reasonably large sample of supernovae. The typical precision achieved in SN Ia distance estimations is  $\sim 5\text{--}7\%$  which make them crucial objects for cosmology.

Since 1998 a lot of observational projects for search and rigorous investigations of Type Ia supernovae were realized using the most advanced telescopes of the world. Up to now about thousand SNe Ia at  $0.1 \leq z \leq 1.6$  were discovered and photometrically and spectroscopically investigated carefully. They have been collected by high-redshift surveys including Hubble Space Telescope (HST) [71, 72], SuperNova Legacy Survey (SNLS) [73], Equation of State: SuperErNovae trace Cosmic Expansion (ESSENCE) [74, 75], Super Nova Sloan Digital Sky Survey (SN SDSS) [76, 77] ones. The first unified sample of SNe Ia “Union” (HST + SNLS + ESSENCE) [78] counted 307 selected supernovae, the second one — “Union2” [79] — counts 557 supernovae eligible for cosmological applications. Their luminosity distance moduli, calculated using SALT2 method for light-curve fitting, versus redshifts are shown in the left panel of Fig. 1.8. The best-fit curve corresponds to the model with parameters<sup>5</sup>  $\Omega_{de} = 0.2875$ ,  $w_m = -1.0486$ ,  $h = 0.7013$ , the total  $\chi^2$  for it, calculated as

$$\chi^2 = \sum_{i=1}^{N_{tot}} \frac{(\mu_i - \mu_{bf})^2}{\Delta\mu_i^2}, \quad (1.30)$$

is equal to 542.6 and the standard deviation, called also RMS of the Hubble residuals,  $\sigma = \sqrt{\sum_{i=1}^{N_{tot}} (\mu_i - \mu_{bf})^2 / N_{tot}}$ , is 0.28. Here  $\mu_i$  is luminosity distance

<sup>5</sup> They have been determined for the data [79] using Levenberg–Marquardt method [80] and relations (1.23)–(1.28).

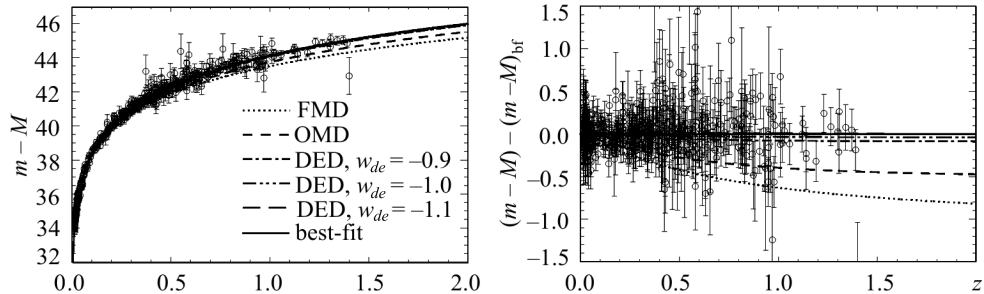


**Fig. 1.8.** Left panel: the distance moduli  $(m-M)(z)$  for 557 SNe Ia from Union2 compilation [79] (signs) and for five models (lines): flat matter dominated (FMD,  $\Omega_m = 1.0$ ), open matter dominated (OMD,  $\Omega_m = 0.3$ ) and dark energy dominated (DED,  $\Omega_m = 0.3$ ,  $\Omega_{de} = 0.7$ ) with  $w_{de} = -0.9$ ,  $w_{de} = -1.0$  and  $w_{de} = -1.1$ . Right panel: the residuals of the distance modulus relative to the best-fit model for SNe Ia data ( $\Omega_m = 0.2875$ ,  $w_{de} = -1.0486$ ,  $h = 0.7013$ ) as well as for other models

modulus of  $i$ th supernova from Union2 sample,  $\Delta\mu_i$  is statistical error of its determination,  $\mu_{bf}$  is the theoretical distance modulus at the redshift of  $i$ th supernova for best-fit model.

The dependences of luminous distance modulus on redshifts in different cosmological models — flat matter dominated (FMD,  $\Omega_m = 1.0$ ), open matter dominated (OMD,  $\Omega_m = 0.3$ ) and three dark energy dominated (DED,  $\Omega_m = 0.3$ ,  $\Omega_{de} = 0.7$ ) with  $w_{de} = -0.9$ ,  $w_{de} = -1.0$  and  $w_{de} = -1.1$  ones are shown in Fig. 1.8 by lines for comparison. The  $\chi^2$ 's for them are 2047, 1182, 569, 547, 544 correspondingly ( $\mu_{mod}$  instead of  $\mu_{bf}$  in formula (1.30)). In the right panel of Fig. 1.8 the residuals of the distance modulus relative to the best-fit curve for SNe Ia data as well as other models are shown. One can see, that SNe Ia luminosity distance — redshift test strongly prefers the dark energy dominated cosmological models. The 68.3%, 95.4% and 99.7% confidence regions of the  $\Omega_m - w_{de}$  plane from SNe Ia alone from Union (dashed contours) and Union2 (shaded contours) compilations are shown in Fig. 1.9. It supports conclusion that cosmological models without dark energy are ruled out at high confidence level. But allowable range for values of EoS parameter is too wide yet ( $-1.4 < w_{de} < -0.75$  at  $1\sigma$  C.L.) for distinguishing the type of dark energy, so, the extensi-

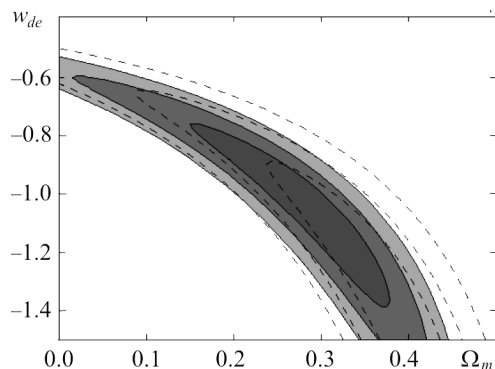


**Fig. 1.9.** 68.3%, 95.4% and 99.7% confidence regions of the  $\Omega_m - w_{de}$  plane from SNe Ia alone from Union (dashed contours) and Union2 (shaded contours) compilations (from [79])

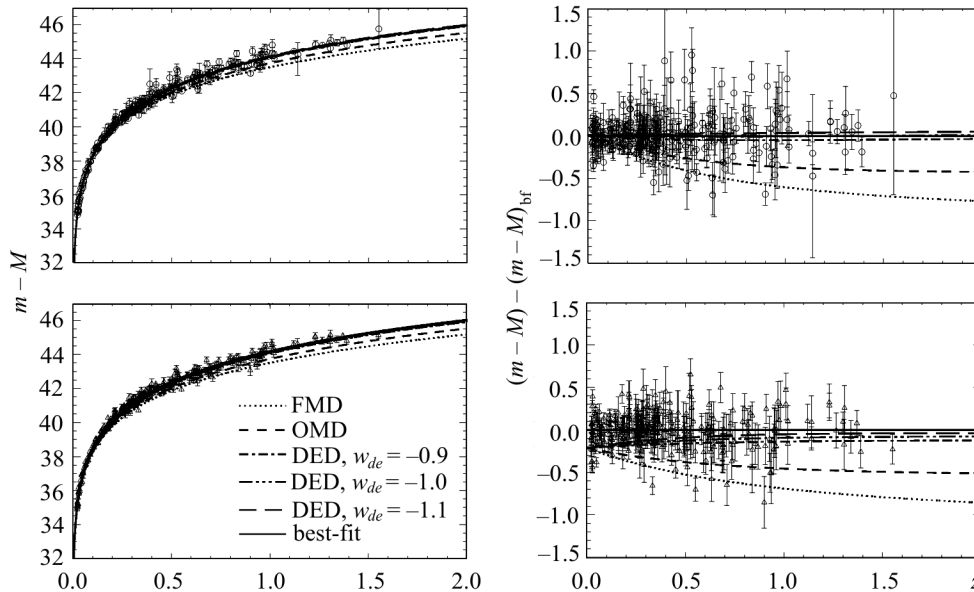


**Fig. 1.10.** Left panel: the distance moduli  $(m-M)(z)$  for 288 SNe Ia from SDSS compilation [77] (signs) and for five models (lines): flat matter dominated (FMD,  $\Omega_m = 1.0$ ), open matter dominated (OMD,  $\Omega_m = 0.3$ ) and dark energy dominated (DED,  $\Omega_m = 0.3$ ,  $\Omega_{de} = 0.7$ ) with  $w_{de} = -0.9$ ,  $w_{de} = -1.0$  and  $w_{de} = -1.1$ . Right panel: the residuals of the distance moduli relative to the best-fit models for SNe Ia data as well as for other models. In the top panels the luminosity distance moduli are calculated using SALT2 light-curve fitting method, in bottom ones — using MLCS2k2 method

on of SNe Ia sample and reducing of identified systematic errors remain crucial problem of SNe Ia observations and astrophysics (see excellent review of M. Sullivan in [81]).

The homogeneous sample of 103 SNe Ia at the redshifts range  $0.04 < z < 0.42$  was selected from SDSS-II SuperNova Survey and combined with SNe Ia from HST, SNLS and ESSENCE surveys in order to reduce the statistical and systematic errors in the estimation of their luminosity distance moduli [77]. In the left panel of Fig. 1.10 the luminosity distance moduli versus redshifts are presented for 288 SNe Ia from this compilation, called SDSS SN one. Two methods for SNe Ia light-curve fitting have been used there — SALT2 (open circles) and MLCS2k2 (open triangles) in order to compare them. The best-fit curve to SDSS SN SALT2 corresponds to the model with parameters  $\Omega_m = 0.323$ ,  $w_{de} = -1.1292$ ,  $h = 0.7046$ , the total  $\chi^2$  for it equals 559.5 and the standard deviation is 0.23, lower than for Union2 SALT2 supernova distance moduli. For the same FMD, OMD and DED ( $w_{de} = -0.9$ ,  $w_{de} = -1.0$ ,  $w_{de} = -1.1$ ) models, shown by lines in Fig. 1.10, the  $\chi^2$ 's are correspondingly 1972, 1626, 560 and 567. In the case of SDSS SN MLCS2k2 supernova distance

moduli the best-fit model has parameters:  $\Omega_m = 0.3205$ ,  $w_{de} = -0.7854$ ,  $h = 0.6344$ . The total  $\chi^2$  for it equals 778.8 and the standard deviation is 0.21, lowest in comparison with Union2 and SDSS SN SALT2 compilations. The  $\chi^2$ 's for FMD, OMD and 3 DED models equal 4170, 2880, 1626, 1500, 1397 correspondingly. So, Union2 and SDSS SN SALT2 compilations are similar, while SDSS SN MLCS2k2 compilation prefer essentially higher  $w_{de}$  and lower  $H_0$ .

Combining the SDSS SN compilation with other cosmological measurements (BAO from SDSS LRG survey and CMB temperature anisotropy from WMAP experiment) Kessler et al. (2009) [77] have found that for spatially flat cosmological model  $w_{de} = -0.96 \pm 0.06(\text{stat}) \pm 0.12(\text{syst})$ ,  $\Omega_m = 0.265 \pm \pm 0.016(\text{stat}) \pm 0.025(\text{syst})$  using the SALT2 and  $w_{de} = -0.76 \pm 0.07(\text{stat}) \pm \pm 0.11(\text{syst})$ ,  $\Omega_m = 0.307 \pm 0.019(\text{stat}) \pm 0.023(\text{syst})$  using MLCS2k2 fitter. So, the  $1\sigma$  confidence contours for  $w_{de}$  and  $\Omega_m$  for the same SN sample using SALT2 and MLCS2k2 fitters overlap only partially. This means, that one of them or both have yet unidentified systematic errors. In the paper [77] the differences between 2 methods of light curve fitting, SALT2 and MLCS2k2, are thoroughly analyzed but convincing arguments for one or the another are not given.

The papers [82–84] present the modern high-quality sample of SNe Ia, based on 3-year SuperNova Legacy Survey (SNLS3) data including other mentioned above supernova samples. It contains 472 selected SNe Ia for cosmological applications with distance moduli determined by updated versions of SALT2 and SiFTO light-curve fitting methods. They use the same phenomenological correction formula (1.29) but differ substantially in their detailed parametrization of observables and in the procedures considered for training and light-curve fitting (see for details § 4.3.1 and § 4.3.2 in [82]). The RMSs of the Hubble residuals are 0.17 for SNLS3 SALT2 supernovae and 0.15 for SNLS3 SiFTO ones, essentially lower then for previous SNe Ia samples of similar completeness. Comparison of SN-only statistical constraints on  $\Omega_m$ ,  $w_{de}$  for SALT2 and SiFTO fitters assuming a flat universe and constant EoS parameter is shown in the left panel of Fig. 1.11. In the right panel of Fig. 1.11 68.3%, 95.4% and 99.7% confidence regions of the  $\Omega_m - w_{de}$  plane from SNe Ia alone (SNLS3 compilation with SALT2 and SiFTO fitters) assuming a flat universe and constant dark energy equation of state are shown. All contours are prolate and convoluted, this indicates some degeneracy of likelihood function. The median line can be approximated roughly by

$$w_{de}^{(SNIa)} \approx -0.651 - 0.122\Omega_m - 5.076\Omega_m^2. \quad (1.31)$$

The best-fit values of  $w_{de}$  and  $\Omega_m$  and their  $1\sigma$  confidential ranges are  $w_{de} = -0.95_{-0.19}^{+0.17}$ ,  $\Omega_m = 0.214_{-0.097}^{+0.072}$  for SALT2 light-curve fitter and  $w_{de} = -0.85_{-0.20}^{+0.14}$ ,  $\Omega_m = 0.173_{-0.098}^{+0.095}$  for SiFTO one [83].

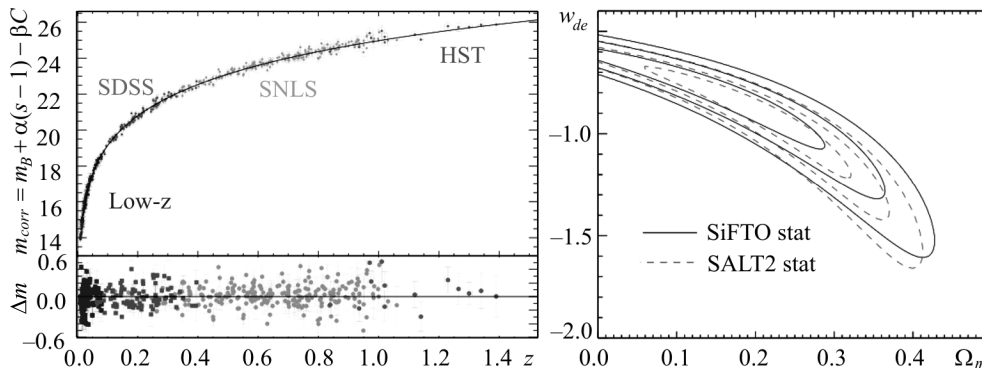


**Fig. 1.11.** Left panel: the distance moduli  $(m - M)(z)$  for 472 selected SNe Ia and residuals from best-fit curve  $\Delta m = m_{corr} - m_{bf}$  (bottom). Right panel: 68.3%, 95.4% and 99.7% confidence regions of the  $\Omega_m - w_{de}$  plane from SNe Ia alone (SNLS3 compilation with SALT2 and SiFTO fitters) assuming a flat universe and constant dark energy equation of state. (From [83])

One can conclude, that luminosity distance — redshift relation for SNe Ia obtained by using SALT2 and SiFTO light-curve fitting methods prefers  $w_{de}$  in the  $1\sigma$  confidential range  $(-1.15, -0.7)$ , while using MLCS2k2 method in the range  $(-0.94, -0.6)$ . Therefore, the  $\Lambda$ -models are not excluded by SNe Ia alone with SALT2 and SiFTO light-curve fitters, while SNe Ia with MLCS2k2 one exclude them at  $1\sigma$  confidential level.

The discussions on advantages of different light-curve fitting methods continue in the literature. In spite of that, one can certainly conclude that data on SNe Ia luminosity distances prefer the dark energy dominated cosmological models. The low accuracy of current determination of  $w_{de}$ , which is important for establishing of the nature of dark energy, does not understate the main conclusion issued from SNe Ia luminosity distance — redshift relation: it requires the cosmic acceleration at  $>99.999\%$  confidential level, including all systematic effects [83].

Other observational evidence for existence of dark energy, based on the luminosity distance — redshift relation, comes from the investigations of gamma-ray bursts (GRBs). Using peak energy — peak luminosity relation for 63 optically identified GRBs Tsutsui et al. (2009) extend the Hubble diagram up to  $z = 5.6$  [85] and show that dark energy dominated models are preferable for these data too. Although constraints from GRBs themselves are not so strong as from SNe Ia they are important argument for existence of dark energy since the other class of objects at higher redshifts supports that.

### 1.4. The angular diameter distance — redshift relation and acoustic peak tests

The objects of known dimensions can be used as “standard rulers” for measuring of angular diameter distances which are defined as follows

$$d_A \equiv \frac{D}{\Theta}, \quad (1.32)$$

where  $D$  is known orthogonal to the line of sight actual size of the object and  $\Theta$  is its measured angular diameter. To relate  $d_A$  with redshift  $z$  of the object astrophysicists use FRW metric (1.1) for space-like interval at the sphere with comoving radius  $\chi(r)$  at the moment  $\eta$  of emitting of photons, which observer from the Earth detects at the current moment of time  $\eta_0$  and measures the angle  $\Theta$  that subtends an object of actual size  $D = a(\eta)\chi(r)\Theta$  ( $d\eta = dr = d\phi = 0$ ). Therefore, the angular diameter distance — redshifts relation becomes as follows

$$d_A = \frac{1}{(1+z)}\chi\left(\int_0^z \frac{dz'}{H(z')}\right), \quad (1.33)$$

where function  $\chi$  is defined by expression (1.2) and  $H(z')$  by equation (1.15). Comparing this relation with (1.23) one can see, that angular diameter distance and luminosity one are related by simple ratio:  $d_A = d_L/(1+z)^2$ .

We know now that all astrophysical objects — galaxies, rich clusters of galaxies and so on — are not “standard rulers” of enough accuracy to be used for testing of cosmological models. Only acoustic peaks in the power spectra of CMB temperature fluctuations and the baryon acoustic oscillations (BAO) in two-point correlation function of matter density space distribution are. Since power spectra and correlation function are statistical measures of fluctuations and the tests based on their features are statistical in their nature too.

#### 1.4.1. CMB acoustic peaks

Mapping of the CMB temperature sky with subdegree angular resolution and  $\Delta T/T \sim 10^{-5}$  sensitivity has revealed the acoustic peaks, predicted by the adiabatic scenario of large scale structure formation. The first such maps of small parts of the sky, obtained in the balloon experiments BOOMERanG [22] and MAXIMA [23], have indicated that positions and amplitudes of acoustic peaks in the angular power spectrum of CMB temperature fluctuations prefer the flat Universe with low matter density, supporting the discovery of dark energy through observations of distant supernova. The all-sky precise measurements of CMB anisotropy in the cosmic experiment WMAP [86, 94, 95] opened up a new opportunity to determine the

cosmological parameters with high precision and provide another independent test for the existence of dark energy.

The theory of CMB anisotropy was initiated by R. Sachs & A. Wolfe [96] and J. Silk [97]. The CMB radiation comes from last scattering surface at which electrons are trapped by hydrogen to form atoms, so-called recombination or decoupling epoch. The thermal photons were tightly coupled to baryons by Thomson and Compton scattering before the decoupling epoch at  $z_{dec} \sim 1000$ , but they could freely move to us after that. So, an adequate calculation of the recombination process is crucial for modeling the power spectrum of CMB temperature fluctuations and polarization. The first analyses of recombination kinetics were carried out by Zeldovich et al. (1968) [98] and Peebles (1968) [99] in 1967. In subsequent papers [100–105] the main processes have been studied using the 3-level approximation of hydrogen and helium atoms.

The most complete analysis of cosmological recombination processes with taking into account the multi-level structure of hydrogen and helium atoms ( $\simeq 300$  levels) and non-equilibrium ionization-recombination kinetics has been performed by S. Seager, D. Sasselov & D. Scott [106]. Also all known plasma thermal processes were taken into account therein. These authors have provided cosmological community with software RECFAST [107] which ensures the accuracy of calculation of number density of electrons  $\sim 1\%$ . However, the researches aimed on improving the calculation of recombination and decoupling of the radiation from baryon plasma are still going on (see recent papers by [108–111] and citing therein). Development of perturbations of number densities of ions and electrons stipulated by scalar mode of cosmological fluctuations and physical processes during recombination epoch have been analyzed by one of the authors of this book [112]. Last improvements of cosmological recombination calculations result into new codes CosmoRec [113] and HyRec [114], which provide the subpercent accuracy of calculation of number density of ionization fractions during and after recombination.

The dependences of relative number density of free electrons  $x_e \equiv n_e/(n_H + n_{He})$  on redshift in the flat matter dominated (FMD) cosmological model ( $\Omega_{cdm} = 0.95$ ,  $\Omega_b = 0.05$ ,  $h = 0.70$ ), open one (OMD) ( $\Omega_{cdm} = 0.25$ ,  $\Omega_b = 0.05$ ,  $h = 0.70$ ) and flat dark energy dominated (DED) one ( $\Omega_\Lambda = 0.70$ ,  $w_{de} = -1$ ,  $\Omega_{cdm} = 0.25$ ,  $\Omega_b = 0.05$ ,  $h = 0.70$ ) computed by RECFAST are shown in Fig. 1.12. The difference between  $x_e(z)$  for DED and OMD does not exceed one percent and between DED and FMD three percents during decoupling epoch and later, so the lines  $x_e(z)$  are superimposed. The dotted line shows visibility function  $d\tau/dze^{-\tau}$  ( $\times 270$ ), peak of which corresponds to the decoupling moment  $z_{dec}$ .

Scalar mode of cosmological perturbations, which provide the large scale structure formation, is also the main source for the CMB temperature anisotropy.

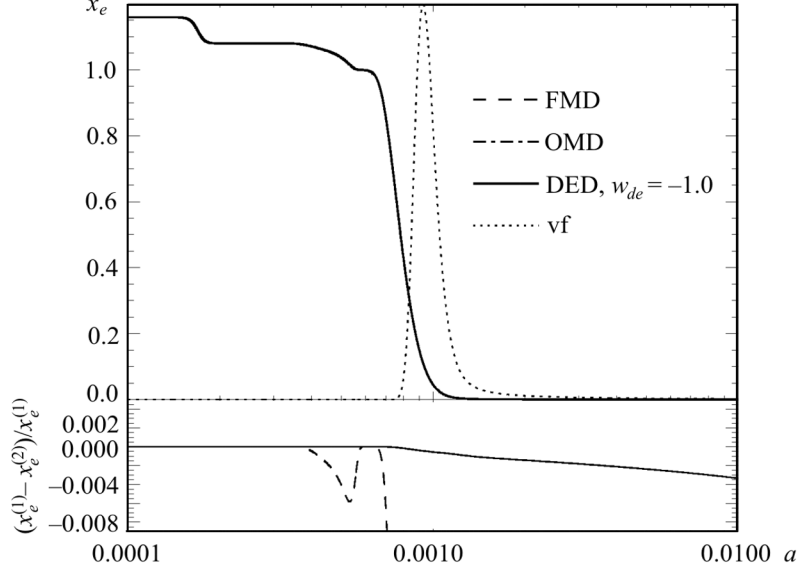


**Fig. 1.12.** Top panel: the dependences of relative number densities of free electrons on redshift in the flat matter dominated (FMD) cosmological model (dashed line;  $\Omega_{cdm} = 0.95$ ,  $\Omega_b = 0.05$ ,  $h = 0.70$ ), open one (OMD) (dash-dotted line;  $\Omega_{cdm} = 0.25$ ,  $\Omega_b = 0.05$ ,  $h = 0.70$ ) and flat dark energy dominated (DED) one (solid line;  $\Omega_\Lambda = 0.70$ ,  $w_{de} = -1$ ,  $\Omega_{cdm} = 0.25$ ,  $\Omega_b = 0.05$ ,  $h = 0.70$ ). Dotted line presents visibility function  $d\tau/dze^{-\tau}$  ( $\times 270$ ). Bottom panel: the relative differences of  $x_e$  are shown by solid line for (DED-OMD)/DED and dashed line for (DED-FMD)/DED

pies. They generate CMB temperature fluctuations which can be written in gauge-invariant form as a sum of four terms — the ordinary Sachs–Wolfe effect, the integrated Sachs–Wolfe term, the Doppler term and the acoustic term [96]:

$$\begin{aligned} \left(\frac{\Delta T}{T_0}\right)(\mathbf{n}) = & (\Phi - \Psi)(\eta_{dec}, r_{dec}, \mathbf{n}) - \int_{\eta_{dec}}^{\eta_0} (\dot{\Phi}(\eta, r, \mathbf{n}) - \dot{\Psi}(\eta, r, \mathbf{n})) d\eta + \\ & + V_i(\eta_{dec}, r_{dec}) n^i + \frac{1}{4} D_\gamma(\eta_{dec}, r_{dec}, \mathbf{n}). \end{aligned} \quad (1.34)$$

Here  $\Phi$  and  $\Psi$  are the Bardeen metric potentials [115],  $V_i$  is the baryon velocity and  $D_\gamma$  is a gauge-invariant variable for the radiation density fluctuations. A dot denotes the partial derivative w.r.t. conformal time  $\eta$ . For perfect fluids and for dust we have  $\Psi = -\Phi$ . In Newtonian limit the Bardeen potentials just reduce to the ordinary Newtonian potential. For adiabatic perturbations  $\frac{1}{4} D_\gamma = \frac{1}{3} \delta_b - \frac{5}{3} \Phi$ , where  $\delta_b$  is the magnitude of baryon matter density perturbations, it corresponds to  $\epsilon_m$  in Bardeen’s notation. The variable  $\eta$  is conformal time,  $r$  is comoving radial coordinate and  $\mathbf{n}$  is direction on the sky



point (or  $\theta$ ,  $\phi$ ) in metric (1.1). In the linear perturbation theory it is convenient to perform the Fourier transformation of all spatially-dependent variables and use the equations for corresponding Fourier amplitudes. It is convenient to present the  $\mathbf{n}$ -dependence of  $\Delta T/T_0(k, \mathbf{n})$  in spherical harmonic series

$$\frac{\Delta T}{T_0}(k, \mathbf{n}) = \sum_{\ell, m} a_{\ell m}(k, \eta_0) Y_{\ell m}(\mathbf{n}), \quad \langle a_{\ell m} a_{\ell' m'}^* \rangle = \delta_{\ell m} \delta_{\ell' m'} C_\ell,$$

$$C_\ell = \frac{2}{\pi} \int_0^\infty dk k^2 \left( \frac{\Delta T}{T_0} \right)_\ell^2.$$

So,  $C_\ell$  is angular power spectrum of temperature fluctuations ( $\ell = \pi/\theta$ ). For its computation in any cosmological model the coupled system of Einstein–Boltzmann equations for evolution of metric, density and velocity perturbations must be solved. The complete system of such equations for multicomponent Universe (radiation, neutrinos, baryons and dark matter) as well as method of their integration firstly were described by Ma & Bertschinger (1995) [116]. These authors also have provided the cosmological community with software COSMICS, which makes accurate calculations of evolution density and velocity perturbations of all components as well as perturbation of metrics in synchronous and conformal-Newtonian gauges. This code was used by number of authors to calculate the transfer function of density perturbations and power spectra of CMB temperature fluctuations and polarization, in particular, by [117, 118] for development of publicly available software CMBFAST. Other improved publicly available cosmological codes which use similar approach are CMBEasy [119], CAMB [120, 121] and CLASS [122–124]. The CAMB code is included in CosmoMC software [125, 126] doing the fast Markov chain Monte Carlo exploration of cosmological parameter space for an input set of data. It is widely used in modern cosmology. We omit here the detailed discussion of theory of CMB anisotropy because of its bulkiness, completeness of its coverage in the cited above papers as well as availability of numerous books ([127, 128] for example) and review papers ([129, 130] for example).

In Fig. 1.13 the binned angular power spectrum of CMB temperature fluctuations obtained on the base of 7-year WMAP observations [93–95] as well as model ones calculated using CAMB code [120, 121] are presented. The solid line shows the CMB power spectrum in the flat  $\Lambda$ CDM model with best-fit parameters (minimal set) which we have determined using the CosmoMC software [131]: baryon matter density in units of critical one  $\Omega_b = 0.046$ , cold dark matter density  $\Omega_{cdm} = 0.234$ , cosmological constant density parameter  $\Omega_\Lambda = 0.72$ , Hubble constant  $H_0 = 70.0$  km/s · Mpc, spectral index of primordial power spectrum of scalar mode  $n_s = 0.97$ , amplitude of primordial spectrum  $A_s = 2.2 \cdot 10^{-9}$  and redshift or reionization  $z_{rei} = 10.5$ . The best-fit  $\Lambda$ CDM

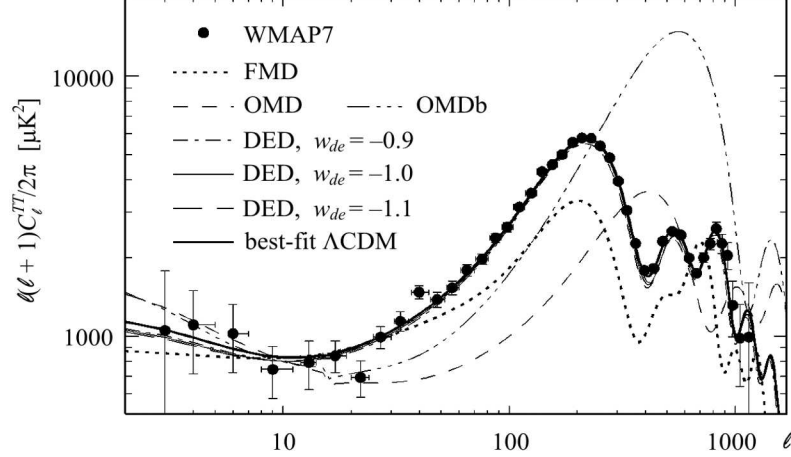


**Fig. 1.13.** The binned power spectra of CMB temperature fluctuations measured in experiment WMAP [93–95] (dots) and predicted by models (lines): flat cold dark matter dominated (FMD,  $\Omega_b = 0.05$ ,  $\Omega_{cdm} = 0.95$ ), open cold dark matter dominated (OMD,  $\Omega_b = 0.05$ ,  $\Omega_{cdm} = 0.25$ ), open baryon matter dominated model (OMDb,  $\Omega_b = 0.3$ ) and flat dark energy dominated (DED,  $\Omega_b = 0.05$ ,  $\Omega_{cdm} = 0.25$ ,  $\Omega_{de} = 0.7$ ) with  $w_{de} = -0.9$ ,  $w_{de} = -1.0$  and  $w_{de} = -1.1$ . The solid line is best-fit  $\Lambda$ CDM model with parameters  $\Omega_b = 0.046$ ,  $\Omega_{cdm} = 0.234$ ,  $\Omega_\Lambda = 0.72$ ,  $H_0 = 70.0$  km/s · Mpc,  $n_s = 0.97$ ,  $A_s = 2.2 \cdot 10^{-9}$  and  $z_{rei} = 10.5$

model power spectrum passes all points of WMAP7 data (thick solid line) ( $\chi_{min}^2 = 44.3$  for  $N_{DoF} = 39$ ). The other model spectra have been calculated for reasonable values of cosmological parameters and normalized to amplitude of 10th spherical harmonic multipole by method proposed in [15]. One can see that all matter dominated models (FMD, OMD, OMDb) strongly contradict the WMAP observational spectrum ( $\chi^2 = 116430, 13879, 66178$  correspondingly), that is visible by the naked eye. Only dark energy dominated models (DED) can match the positions and amplitudes of acoustic peaks in the angular power spectrum of CMB temperature fluctuations (their lines are superimposed with best-fit  $\Lambda$ CDM model one).

To understand the numerical results, presented in Fig. 1.13, let us use some analytic formulas and approximations of simulations which have been developed in the papers [132–137].

A useful fitting formula for  $z_{dec}$  is given by [133]:

$$z_{dec} = \frac{1}{a_{dec}} - 1 = 1048[1 + 0.00124\omega_b^{-0.738}][1 + g_1\omega_m^{g_2}], \quad (1.35)$$

where

$$g_1 = 0.0783\omega_b^{-0.238}[1 + 39.5\omega_b^{0.763}]^{-1}, \quad g_2 = 0.56[1 + 21.1\omega_b^{1.81}]^{-1},$$

$\omega_b \equiv \Omega_b h^2$  and  $\omega_m \equiv \Omega_m h^2$ . In the cosmological model with  $\Omega_{cdm} = 0.25$ ,  $\Omega_b = 0.05$ ,  $h = 0.70$  the redshift of decoupling is  $z_{dec} = 1089$  (peak of visibility function in Fig. 1.12).

The locations of the acoustic peaks in the CMB power spectrum depend on the value of sound horizon at decoupling epoch

$$r_s(z_{dec}) \equiv \frac{1}{1 + z_{dec}} \int_{z_{dec}}^{\infty} \frac{c_s dz}{H(z)} \quad (1.36)$$

and the angular diameter distance to the last scattering surface,  $d_A(z_{dec})$ . Comparing with numerical calculations it was shown (see [134–136] and references therein) that the spherical harmonic which corresponds to the  $m$ -th acoustic peak is well approximated by the relation

$$\ell_{p_m} = (m - \phi_m) \pi \frac{d_A(z_{dec})}{r_s(z_{dec})}, \quad (1.37)$$

where  $\phi_m$  takes into account the shift of  $m$ -th peak from its location in the idealized model which is caused by driving effects from the decay of the gravitational potential. Doran and Lilley (2002) give the accurate analytic approximation in the form

$$\phi_m = \bar{\phi} - \delta\phi_m, \quad (1.38)$$

where  $\bar{\phi}$  is overall phase shift of the spectrum (or the first peak) and  $\delta\phi_m$  is a relative shift of each peak and dip caused by the Doppler shift of the oscillating fluid. For the overall phase shift of the spectrum they found

$$\bar{\phi} = (1.466 - 0.466n_s) a_1 r_*^{a_2}, \quad (1.39)$$

where

$$r_* \equiv \rho_{rad}(z_{dec})/\rho_m(z_{dec}) = \frac{0.0416}{\omega_m} \left( \frac{1 + \rho_\nu/\rho_\gamma}{1.6813} \right) \left( \frac{T_0}{2.726} \right)^4 \left( \frac{z_{dec}}{1000} \right) \quad (1.40)$$

is the ratio of radiation density to matter one at decoupling and

$$a_1 = 0.286 + 0.626\omega_b, \quad a_2 = 0.1786 - 6.308\omega_b + 174.9\omega_b^2 - 1168\omega_b^3$$

are fitting coefficients. Here and below the numbers in the expressions are obtained for a present CMB temperature of  $T_0 = 2.726$  K and the ratio of densities of massless neutrinos and photons  $\rho_\nu/\rho_\gamma = 0.6813$  for three massless neutrino species ( $f_\nu \equiv \rho_\nu/(\rho_\gamma + \rho_\nu) = 0.405$ ). All values can be easily scaled to other values of  $T_0$  and  $f_\nu$ .

The relative shift of the 1st acoustic peak is zero,  $\delta\phi_1 = 0$ . For the 2nd one it is

$$\delta\phi_2 = c_0 - c_1 r_* - c_2/r_*^{c_3} + 0.05(n_s - 1), \quad (1.41)$$

with

$$\begin{aligned} c_0 &= -0.1 + 0.213e^{-52\omega_b}, & c_1 &= 0.015 + 0.063e^{-3500\omega_b^2}, \\ c_2 &= 6 \cdot 10^{-6} + 0.137(\omega_b - 0.07)^2, & c_3 &= 0.8 + 70\omega_b, \end{aligned} \quad (1.42)$$

and for the 3rd peak

$$\delta\phi_3 = 10 - d_1 r_*^{d_2} + 0.08(n_s - 1), \quad (1.43)$$

with  $d_1 = 9.97 + 3.3\omega_b$ ,  $d_2 = 0.0016 + 0.196\omega_b + 2.25 \cdot 10^{-5}\omega_b^{-1}$ .

The sound speed in the pre-recombination plasma is

$$c_s = c/\sqrt{3(1+R)}$$

with

$$R \equiv 3\rho_b/4\rho_\gamma = 30315(T_0/2.726)^{-4}\omega_b a \quad (1.44)$$

and scale factor is well approximated by<sup>6</sup>

$$a(\eta) = a_{eq} \left[ \frac{\eta}{\eta_1} + \left( \frac{\eta}{2\eta_1} \right)^2 \right], \quad (1.45)$$

with

$$a_{eq} = \frac{4.17 \cdot 10^{-5}}{\omega_m} \left( \frac{1 + \frac{\rho_\nu}{\rho_\gamma}}{1.6813} \right) \left( \frac{T_0}{2.726} \right)^4, \quad \eta_1 \equiv \frac{\eta_{eq}}{2(\sqrt{2}-1)} = \frac{c}{H_0} \frac{\sqrt{\Omega_r}}{\Omega_m} \quad (1.46)$$

the integral for sound horizon (1.36) can be reduced to the analytic formula

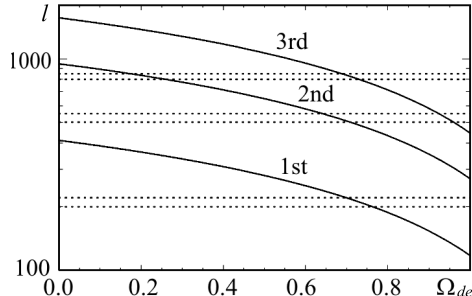
$$r_s(z_{dec}) = \frac{19.9}{\sqrt{\omega_b \omega_m}} \left( \frac{T_0}{2.726} \right)^2 \ln \frac{\sqrt{1+R_{dec}} + \sqrt{R_{dec} + R_{eq}}}{1 + \sqrt{R_{eq}}} \text{ Mpc}. \quad (1.47)$$

The deviation of the acoustic extrema locations calculated using formulas (1.37)–(1.47) from the values obtained by CAMB code is <1% for the first peak, <6% for the second one and <3% for the third one (for DED models and somewhat worse for other ones) in the sufficiently wide range of parameters.

The dependences of locations of the first, second and third acoustic peaks on  $\Omega_{de}$  for models with  $\Omega_m = 0.3$ ,  $\Omega_b = 0.05$ ,  $n_s = -0.97$ ,  $H_0 = 70 \text{ km/s} \cdot \text{Mpc}$  are shown in Fig. 1.14. The  $1\sigma$  ranges for them obtained from the WMAP7 angular power spectrum of CMB temperature fluctuations [93, 95] are shown there too. One can see that only model with  $\Omega_{de} \approx 0.7$  predicts the peak locations which match the observational data. In Table 1.1 the locations of

<sup>6</sup> It is obtained by integration of (1.15) with  $\Omega_K = \Omega_{de} = 0$ , which is allowable since at this epoch  $\Omega_K a^{-2}$ ,  $\Omega_{de} a^{-3(1+w_{de})} \ll \Omega_m a^{-3}$ ,  $\Omega_r a^{-4}$  in the realistic models.

**Fig. 1.14.** Dependences of locations of the 1st, 2nd and 3rd acoustic peaks on  $\Omega_{de}$  for models with  $\Omega_m = 0.3$ ,  $\Omega_b = 0.05$ ,  $n_s = -0.97$ ,  $H_0 = 70\text{km/s}\cdot\text{Mpc}$  (solid lines). The  $1\sigma$  ranges for them obtained from the WMAP7 angular power spectrum of CMB temperature fluctuations [93] are shown by horizontal dotted lines



acoustic peaks are presented for the FMD, OMD and DED models. The FMD and OMD models are ruled out by WMAP7 data while DED ones well agree with them. The weak dependence of peak locations on  $w_{de}$  is recognized too. The DED models with  $w_{de} \approx -1$  are preferable.

As a rule for estimation of the cosmological parameters including dark energy ones all data on CMB anisotropy are used, not only data on peak positions. The form of the power spectrum of CMB temperature fluctuations and its amplitude depend on practically all cosmological parameters, the minimal set of which in the models with dark energy contain eight ones: density parameter of baryons  $\Omega_b$ , density parameter of cold dark matter  $\Omega_{cdm}$ , density parameter of dark energy  $\Omega_{de}$ , EoS parameter of dark energy  $w_{de}$ , Hubble constant  $H_0$ , spectral index of initial matter density power spectrum  $n_s$  (scalar mode), amplitude of initial matter density power spectrum  $A_s$  and reionization optical depth  $\tau_{rei}$ . So, determination of dark energy parameters using CMB anisotropy data has sense jointly with other ones. It can be done by maximization of the likelihood function

$$L(\mathbf{x}; \theta_k) = \exp\left(-\frac{1}{2}(x_i - x_i^{th})C_{ij}(x_j - x_j^{th})\right),$$

where  $\mathbf{x}$  is measured CMB anisotropy data,  $\mathbf{x}^{th}$  is predicted in the model with parameters  $\theta_k$ ,  $C_{ij}$  is covariance matrix. Assuming a flat Universe the number of free parameters is reduced to seven, since  $\Omega_{de} = 1 - \Omega_m$ .

Integrating  $L(\mathbf{x}; \theta_k)$  over  $H_0$ ,  $n_s$ ,  $A_s$ ,  $\tau_{rei}$  and  $\Omega_b$  and  $\Omega_{cdm}$  for fixed their sum  $\Omega_m = \Omega_b + \Omega_{cdm}$  one can obtain 2-dimensional marginalized likelihood

**Table 1.1. Locations of acoustic peaks: observations versus models**

Peaks	WMAP7	FMD	OMD	DED $w_{de} = -0.9$	DED $w_{de} = -1.0$	DED $w_{de} = -1.1$
1st	$210 \pm 10$	201	412	216	218	220
2nd	$526 \pm 24$	426	947	499	504	508
3rd	$825 \pm 25$	764	1563	821	829	836

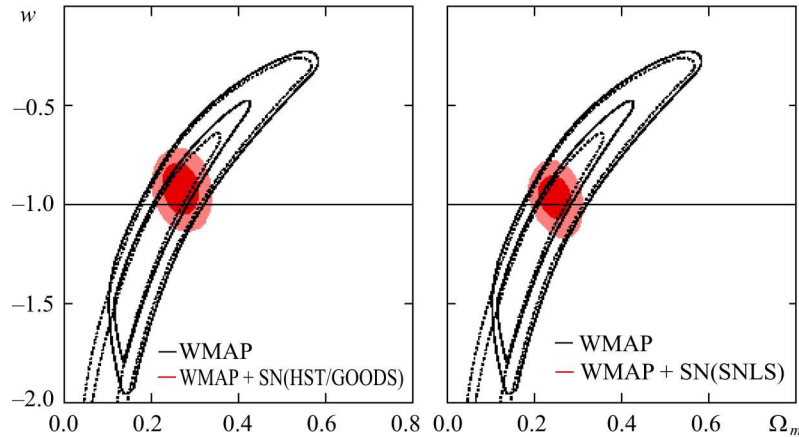


**Fig. 1.15.** The 2D marginalized contours (68% and 95% CL) in the  $\Omega_m - w$  plane for WMAP data only (lines) and WMAP data combined with SN Ia data (shaded regions). The dashed lines show the contours for WMAP data only without prior on  $H_0$  and solid ones with the assumed prior of  $H_0 < 100$  km/s/Mpc. (From [89])

function  $\mathcal{L}(\mathbf{x}; \Omega_m, w_{de})$ . The 2-dimensional marginalized contours (68% and 95% CL) in the  $\Omega_m - w_{de}$  plane for WMAP data [89] are presented in Fig. 1.15. Their prolate and convoluted form indicates some degeneracy in the  $\Omega_m - w_{de}$  plane: the line of maximal likelihood density distribution is

$$w_{de}^{(CMB)} \approx -2.61 + 9.45\Omega_m - 10.45\Omega_m^2. \quad (1.48)$$

It crosses with the similar approximation  $w_{de}^{(SNIa)}$  (Eq. (1.31)) in the point  $\Omega_m = 0.23$ ,  $w_{de} = -0.96$ .

The best-fit values of  $w_{de}$  and  $\Omega_{de}$  and their  $1\sigma$  confidential ranges determined from the WMAP5 data only are  $w_{de} = -1.06^{+0.41}_{-0.42}$ ,  $\Omega_{de} = 0.73^{+0.10}_{-0.11}$ . Limits are significantly improved when WMAP data are combined with SNe Ia data, that is illustrated by shaded contours in Fig. 1.15. In the case of WMAP+SNLS data the best-fit values of dark energy parameters are:  $w_{de} = -0.97 \pm 0.07$  and  $\Omega_{de} = 0.73 \pm 0.03$ .

Therefore, the acoustic peak locations in the angular power spectrum of CMB temperature fluctuations are independent evidence for existence of dark energy or cosmological constant.

### 1.4.2. Baryon acoustic oscillations

Other realization of “angular diameter distance — redshift” test is implemented by extraction of the baryon acoustic oscillations (BAO) from the space distribution of galaxies which is described by two-point correlation function or power spectrum of luminous matter density perturbations.

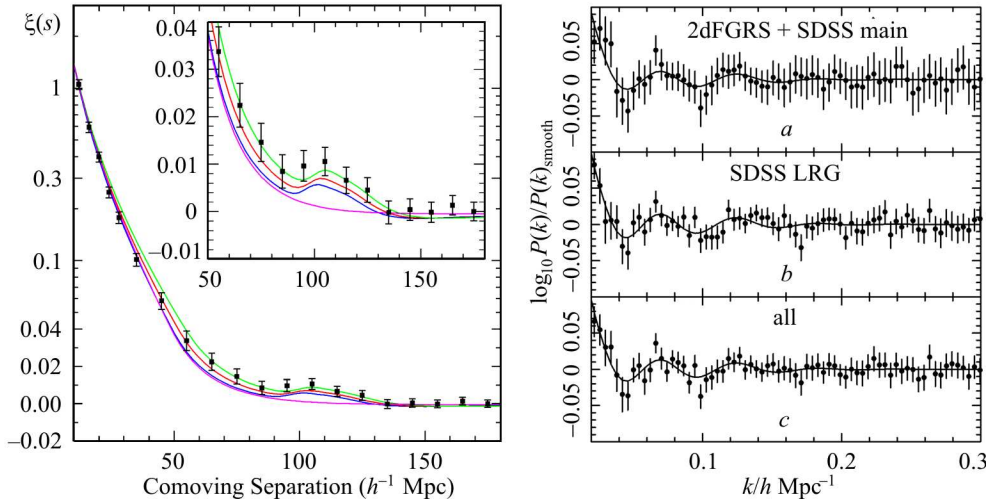


**Fig. 1.16.** Left panel: The space two-point correlation function of the SDSS LRG sample. The models are from top to bottom  $\Omega_m h^2 = 0.12, 0.13, 0.14$ , all with  $\Omega_b h^2 = 0.024$  and  $n = 0.98$  and with a mild non-linear prescription folded in. For a pure CDM model the peak vanishes (lowest line at separation  $< 130 h^{-1} \text{ km/s} \cdot \text{Mpc}$ ). (From [141]). Right panel: BAO in power spectra from the combined SDSS and 2dFGRS main galaxies (a), from the SDSS DR5 LRG sample (b) and the combination of these two samples (c). (From [142])

The idea about modulation of the spectrum of density perturbations by prerecombination acoustic oscillations in the baryonic Universe was announced first by A. Sakharov in 1965 [138]. That is why they are called sometimes in the literature Sakharov oscillations. P.J.E. Peebles was first who has analyzed their manifestation in the autocorrelation function of the mass distribution  $\xi(r)$ , has computed the spike in  $\xi(r)$  at large  $r$  caused by the oscillation of the initial power spectrum of density perturbations [139] and has predicted the possibility of their detection on the base of the galaxy sky surveys. The physics of BAO phenomena, the analysis of numerical modeling as well as useful analytic approximations are presented in the papers [133, 140] and numerous early and recent reviews and textbooks.

The first certain detection of the BAO signal was made by SDSS collaboration [141] in 2005 using the two-point correlation function of luminous red galaxies (left panel of Fig. 1.16). Later, in 2007, they were detected in power spectra obtained from the combined SDSS and 2dFGRS main galaxies samples, from the SDSS DR5 LRG sample and the combination of these two samples [142] (right panel of Fig. 1.16).

The statistically significant bump at  $100 h^{-1} \text{ km/s} \cdot \text{Mpc}$  scale in the redshift-space correlation function or oscillations in the power spectrum of matter density perturbations (Fig. 1.16) is the outcome of acoustic peak shown in Fig. 1.13. It is manifestation of baryon-photon plasma oscillations before

and during cosmological recombination epoch. The main part of CMB radiation comes to Earth from the last scattering surface at  $z_{dec}$  defined by maximum of visibility function (Fig. 1.12), which in the DED-models with best-fit parameters is  $\approx 1090$  (optical depth from current epoch to  $z_{dec}$  caused by Thomson scattering is  $\tau_{dec} \approx 0.7$ ).

The fraction of free electrons at this moment was yet large enough ( $x_e \approx 0.12$ ) and since the ratio of radiation density to baryon matter one then was  $\rho_{rad}(z_{dec})/\rho_b(z_{dec}) \approx 1.7$  the radiation density perturbations drag the baryon matter density ones via Compton and Coulomb interactions. It continues until the rate of Compton scattering between photons and electrons becomes too low to drag baryons. The drag epoch  $z_{drag}$ , defined as the time at which the baryons are released from the Compton drag of the photons in terms of a weighted integral over the Thomson scattering rate, is well approximated by following expression obtained in [140]:

$$z_{drag} = 1291 \frac{\omega_m^{0.251}}{1 + 0.659 \omega_m^{0.828}} [1 + b_1 \omega_b^{b_2}], \quad (1.49)$$

where  $b_1 = 0.313 \omega_m^{-0.419} [1 + 0.607 \omega_m^{0.674}]$  and  $b_2 = 0.238 \omega_m^{0.223}$ . In the models with  $\Omega_b = 0.05$ ,  $\Omega_m = 0.3$  and  $h = 0.7$  it equals 1026. The sound horizon at  $z_{drag}$ , when baryons were released from the Compton drag of photons, plays a crucial role in determination of the location of baryon acoustic oscillations. It can be estimated using expression (1.47), where  $R_{dec}$  must be substituted by  $R_{drag}$ . In the same DED model  $r_s(z_{drag}) = 148$  Mpc in comoving coordinates. It is well approximated by expression

$$r_s(z_{drag}) \approx \frac{44.5 \ln(9.83/\Omega_m h^2)}{\sqrt{1 + 10(\Omega_b h^2)^{3/4}}}, \quad (1.50)$$

presented in [140], where the approximation for the first peak location in  $k$ -space is presented too:

$$k_{BAO} \approx \frac{5\pi}{2r_s} (1 + 0.21\Omega_m h^2). \quad (1.51)$$

In the FMD model it equals 0.083, in the OMD and DED ones with presented above parameters it is 0.055. The linear scales  $\lambda_{BAO} = 2\pi/k_{BAO}$ , which correspond to these wave numbers are 76 and 114 Mpc respectively. But we observe the angular and redshift distributions of galaxies and deduce the linear scales from the angular distance – redshift relation. So, it is possible to measure the following ratios

$$\theta_s(z) = \frac{r_s(z_{drag})}{(1+z)d_A(z)}, \quad \Delta z_s(z) = \frac{r_s(z_{drag})H(z)}{c}, \quad (1.52)$$



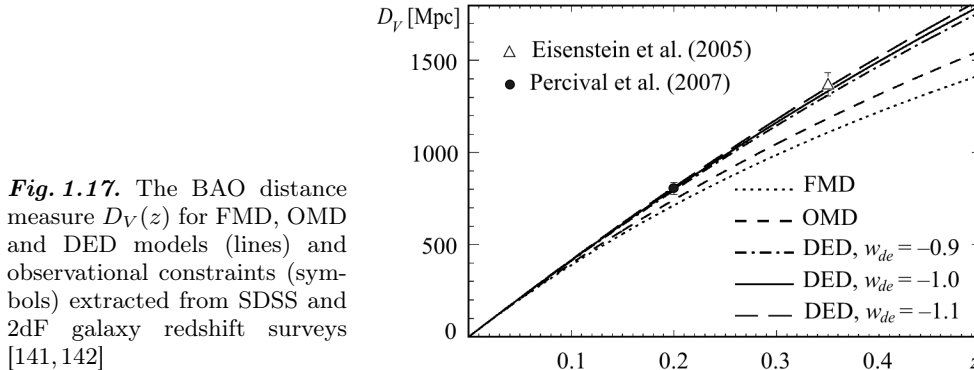


**Fig. 1.17.** The BAO distance measure  $D_V(z)$  for FMD, OMD and DED models (lines) and observational constraints (symbols) extracted from SDSS and 2dF galaxy redshift surveys [141, 142]

where  $\theta_s(z)$  is measured angular size of physical length  $r_s(z_{drag})/(1+z)$ , which lies orthogonal to the line of sight at redshift  $z$ , and  $\Delta z_s(z)$  is  $z$ -extension of the same length when it lies along the light of sight.

Using both measures (1.52) it is possible to obtain a combined distance scale ratio which is related to spherically averaged correlation function or power spectrum:

$$[\theta_s^2(z)\Delta z_s(z)]^{1/3} \equiv \frac{r_s(z_{drag})}{[(1+z)^2 d_A^2(z)c/H(z)]^{1/3}}.$$

In the paper [141] the following measure was introduced

$$D_V(z) = \left[ (1+z)^2 d_A^2(z) \frac{cz}{H(z)} \right]^{1/3}, \quad (1.53)$$

it is the dilation scale as the cube root of the product of the radial dilation times the square of the transverse dilation. Its  $z$ -dependence for FMD, OMD and DED models is presented in Fig. 1.17. The observational constraints for it extracted from the SDSS Luminous Red Galaxies (SDSS LRG) survey [141] and SDSS galaxy samples (Data Release 5) combined with 2dF Galaxy Redshift Survey (2dF GRS) data [142] are presented there too. One can see that they prefer DED models.

In the paper [143] the data release 7 (DR7) of SDSS galaxy survey combined with 2dF GRS data was used for measuring the BAO signal in a series of redshift slices. The relative distance measure  $d_z = r_s(z_{drag})/D_V(z)$  was determined for  $z = 0.2, 0.35$  and showed that DED models best matches these data (Fig. 1.18).

From the likelihood analysis Percival et al. (2010) found that the BAO data alone weakly constraint the dark energy parameters in the plane  $\Omega_m - w_{de}$ , that is shown in Fig. 1.19 by lines. The strong degeneracy of  $\Omega_m - w_{de}$  likelihood distribution function give possibility to constraint the matter density parameter

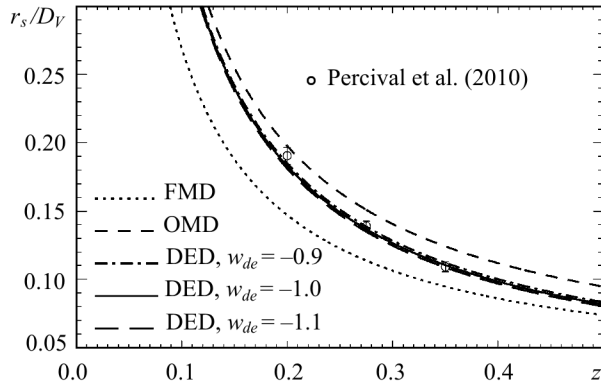


**Fig. 1.18.** The BAO relative distance measure  $r_s(z_{drag})/D_V(z)$  for FMD, OMD and DED models (lines) and observational constraints extracted from SDSS DR7 and 2dF galaxy redshift surveys [143] (symbols)

$\Omega_m$  for fixed EoS parameter  $w_{de}$  according to approximate expression

$$\begin{aligned} \Omega_m \approx & 0.282 + 0.0935(1 + w_{de}) + \\ & + 0.015(1 + w_{de})^2 \pm [0.058 + 0.012(1 + w_{de})]. \end{aligned} \quad (1.54)$$

It crosses with similar approximation  $w_{de}^{(SNIa)}$  (Eq. 1.31) in the point  $\Omega_m \approx \approx 0.275$ ,  $w_{de} \approx -1.06$ . The limits are significantly improved when BAO data are combined with SN Ia or CMB data. Really, BAO data combined with SN Ia ones give the best-fit values and  $1\sigma$  CL as follows  $\Omega_m = 0.29 \pm 0.02$ ,  $w_{de} = -0.97 \pm 0.11$ , and combined with WMAP5 data on CMB anisotropy they give  $\Omega_m = 0.283 \pm 0.026$ ,  $w_{de} = -0.97 \pm 0.17$ .

Therefore, BAO data extracted from different galaxy surveys alone prefer cosmological models with dark energy and combined with CMB anisotropy and SN Ia distance moduli data significantly improve the determination of dark energy parameters.

### 1.4.3. X-ray gas fraction in clusters

Other probe of the accelerated expansion of the Universe based on the “angular diameter distance — redshift” relation is the measurement of the X-ray gas mass fraction,  $f_{gas}$ , in clusters of galaxies situated at different redshifts. This  $f_{gas}$  technique for determination of cosmological parameters was proposed independently by S. Sasaki [144] and U. Pen [145] in 1996. It was improved and tested in papers [146–151] on the base of data of Chandra observatory.

The first certain detection of cosmic acceleration using the  $f_{gas}$  technique was made by Allen et al. in 2004 [149] using Chandra observations of 26 hot ( $kT \gtrsim 5$  keV), X-ray luminous ( $L_{bol} \gtrsim 10^{45} h_{70}^{-2}$  erg/s), dynamically relaxed clusters spanning the redshift range 0.07–0.9. It led to a  $\sim 3\sigma$  detection of the acceleration of expansion of the Universe and the tight constraint on the mean

mass density  $\Omega_m = 0.25 \pm 0.04$  in excellent agreement with independent findings from SN Ia distance moduli, CMB anisotropy and galaxy redshift surveys studies. This constraint originates from the dependence of the  $f_{gas}$  measurements, which are derived from the observed X-ray gas temperature and density profiles, on the assumed distances to the clusters,  $f_{gas} \propto d_A(z)^{1.5}$ . To understand the origin of this dependence, consider a spherical region of observed angular radius  $\theta$  within which the mean gas mass fraction is measured. The physical size,  $R$ , is related to the angle  $\theta$  as  $R = \theta d_A$ . The X-ray luminosity emitted from within this region,  $L_X$ , is related to the detected flux,  $F_X$ , as  $L_X = 4\pi d_L^2 F_X$ , where  $d_L$  is the luminosity distance and  $d_A = d_L/(1+z)^2$

is the angular diameter distance. Since the X-ray emission is primarily due to collisional processes (bremsstrahlung and line emission) and is optically thin, we may also write  $L_X \propto n^2 V$ , where  $n$  is the mean number density of colliding gas particles and  $V$  is the volume of the emitting region, with  $V = 4\pi(\theta d_A)^3/3$ .

Considering the cosmological distance dependences, we see that  $n \propto d_L/d_A^{1.5}$ , and that the observed gas mass within the measurement radius  $M_{gas} \propto nV \propto d_L d_A^{1.5}$ . The total mass,  $M_{tot}$ , determined from the X-ray data under the assumption of hydrostatic equilibrium,  $M_{tot} \propto d_A$ . Thus, the X-ray gas mass fraction measured within angle  $\theta$  is  $f_{gas} = M_{gas}/M_{tot} \propto d_L d_A^{0.5}$ . The expectation from non-radiative hydrodynamical simulations is that for the largest ( $kT \gtrsim 5$  keV), dynamically relaxed clusters and for measurement radii beyond the innermost core ( $r \gtrsim r_{2500}$ , where  $r_{2500}$  is defined by condition  $\rho_{gas}(r \leq r_{2500}; z) \geq 2500\rho_{cr}(z)$ ),  $f_{gas}$  should be approximately constant with redshift. However, possible systematic variation of  $f_{gas}$  with redshift can be accounted for in a straightforward manner, so long as the allowed range of such variation is constrained by numerical simulations or other complementary data.

The rigorous phenomenological expression for  $f_{gas}^{ph}$  used for testing of cosmology by observations is as follows

$$f_{gas}^{ph}(z; \mathbf{P}, \mathbf{Q}) = \frac{KA\gamma b_0(1 + \alpha_b z)}{1 + s_0(1 + \alpha_s z)} \left( \frac{\Omega_b}{\Omega_m} \right) \left[ \frac{d_A^\Lambda(z)}{d_A(z)} \right]^{1.5}, \quad (1.55)$$

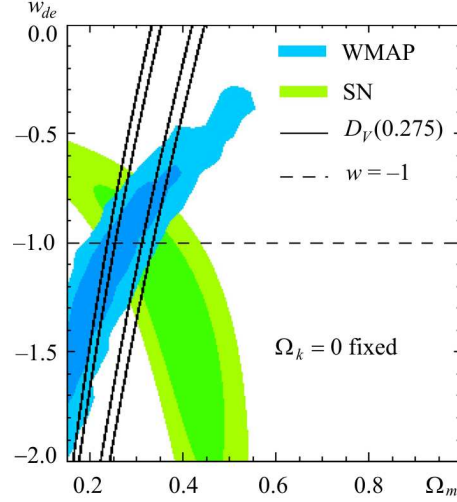


**Fig. 1.19.** The 2D marginalized contours (68% and 95% CL) in the  $\Omega_m - w_{de}$  plane from BAO data (lines), WMAP and Union SN Ia. BAO constraints in  $\Omega_m - w_{de}$  space deduced from the  $r_s/D_V(0.275)$  relation (From [143])

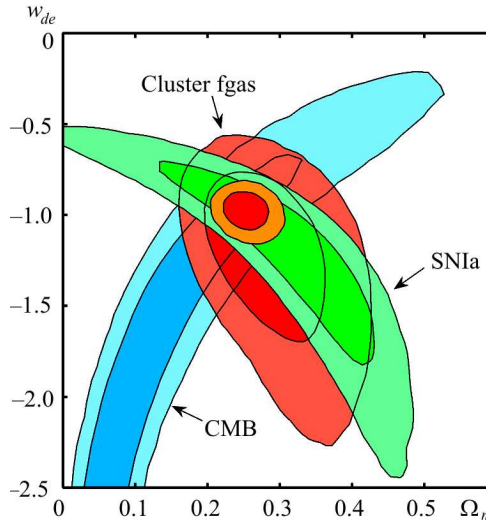
where  $\mathbf{P} = (\Omega_b, \Omega_m, \Omega_{de}, w_{de}, H_0)$  is set of parameters in the cosmological model of interest,  $d_A(z)$  is the angular diameter distance (1.33) computed for it,  $d_A^\Lambda(z)$  is the angular diameter distance computed in the reference spatially-flat  $\Lambda$ CDM model (with  $\Omega_m = 0.3$ ,  $\Omega_{de} = 0.7$ ,  $w_{de} = -1$ ,  $h = 0.7$ ), and  $\mathbf{Q} = (s_0, b_0, \alpha_s, \alpha_b, K, A, \gamma)$  is set of parameters related to modeling the cluster gas mass fraction. The factor  $K$  is a ‘calibration’ constant that parameterizes residual uncertainty in the accuracy of the instrument calibration and X-ray modeling; the factor  $A$  accounts for the change in angle subtended by innermost core of cluster  $r_{2500}$  as the underlying cosmology is varied; the parameter  $\gamma$  models non-thermal pressure support in the clusters; the factor  $b_0(1 + \alpha_b z)$  is the ratio by which the baryon fraction measured at the central part of X-ray clusters is depleted with respect to the universal mean at redshift  $z$ ; the parameter  $s_0(1 + \alpha_s z)$  models the baryonic mass fraction in stars at redshift  $z$ . They are discussed in depth in [151]. Thus, in the general case the approach contains 12 parameters ( $\mathbf{P} + \mathbf{Q}$ ) for determination by matching  $f_{gas}^{ph}$  to  $f_{gas}^{obs}$ . The number of free parameters can be reduced to 8 if the flat Universe is assumed and 4 cluster model parameters  $K, A, \gamma, b_0$  are presented by one combined  $\tilde{K}$ , which is their product [152].

Allen et al. (2008) collected 42 hot, X-ray luminous, dynamically relaxed galaxy clusters spanning the redshift range  $0.05 < z < 1.1$  and measured for them  $f_{gas}^{obs}$  using Chandra data (see for details [151]). Since the angular diameter distance  $d_A(z)$ , and so  $f_{gas}^{ph}$ , depends on the assumed dark energy model, one can compare predicted values of the gas mass fraction with measurements for clusters at redshift  $z_i$  by constructing a  $\chi^2 = \sum_i (f_{gas}^{ph}(z_i) - f_{gas}^{obs}(z_i))^2 / \sigma_i^2$  function ( $\sigma_i$  are the one standard deviation measurement errors and the summation is over the 42 clusters) and constrain parameters of given dark energy models.

For determination of cosmological parameters by  $f_{gas}$  technique the authors of [151, 152] have used a Markov chain Monte Carlo method and priors on baryonic content and Hubble constant. Analyzing the data for all 42 clusters, employing priors  $\Omega_b h^2 = 0.0214 \pm 0.0020$  [153] and  $h = 0.72 \pm 0.08$  [154] Allen et al. (2008) have detected the effects of dark energy at  $\sim 99.99\%$  C.L. with  $\Omega_m = 0.28 \pm 0.06$  and  $w_{de} = -1.14 \pm 0.31$  for a flat cosmology with a constant dark energy equation of state. Practically the same values of the dark energy parameters were obtained independently by Samushia & Ratra (2008). In Fig. 1.20 the two-dimensional  $\Omega_m$ - $w_{de}$  marginalized over rest parameters contours from cluster X-ray gas mass fraction alone as well as combined with CMB anisotropy and SN Ia moduli distances data are presented. The constraints obtained from all three data sets are as follows:  $\Omega_m = 0.253 \pm 0.021$  and  $w_{de} = -0.98 \pm 0.07$ .

So, the measurements of the ratio of baryonic-to-total mass,  $f_{gas}$ , in the largest, dynamically relaxed galaxy clusters clearly detect the effects of dark

**Fig. 1.20.** The 68% and 95% confidence constraints in the  $\Omega_m$ - $w_{de}$  plane obtained from the analysis of the Chandra  $f_{gas}$  data using priors on baryonic content and Hubble constant ( $\Omega_b h^2 = 0.0214 \pm 0.0020$  [153],  $h = 0.72 \pm 0.08$  [154]). Also the independent results obtained from CMB data using a weak uniform prior on  $h$  ( $0.2 < h < 2.0$ ) and SNIa data are shown. The inner contours show the constraint obtained from all three datasets without any external priors (From [151])



energy on the expansion of the Universe and constrain the parameters of dark energy model via its effects on the distance-redshift relation. The  $f_{gas}$  data alone allow the range of dark energy parameters which overlaps with ones constrained by other data (see Fig. 1.20). The accuracy is somewhat less or comparable to that obtained from CMB anisotropy or SNe Ia distance moduli method, but importance of this technique consists in the fact that quite similar cosmological results are obtained from the distance-redshift information for quite different class of source populations.

## 1.5. Evidence for dark energy from study of large scale structure

### 1.5.1. Linear power spectrum of matter density perturbations

The large scale structure of the Universe is formed by the gravitational growth of primordial perturbations generated presumably in the inflation epoch. As it follows from the pioneering work of E. Lifshits [155] the temporal behavior of amplitudes of the Fourier modes

$$\delta(\mathbf{k}, \eta) \equiv \frac{1}{(2\pi)^3} \int e^{-i\mathbf{k}\mathbf{r}} \delta(\mathbf{r}, \eta) d^3r,$$

of density perturbations in the real space

$$\delta(\mathbf{r}, \eta) \equiv (\rho(\mathbf{r}, \eta) - \bar{\rho}(\eta)) / \bar{\rho}(\eta)$$

is result of competition of gravity and pressure gradient, thus, depends on nature of density-dominating component and relation of scale of perturbati-

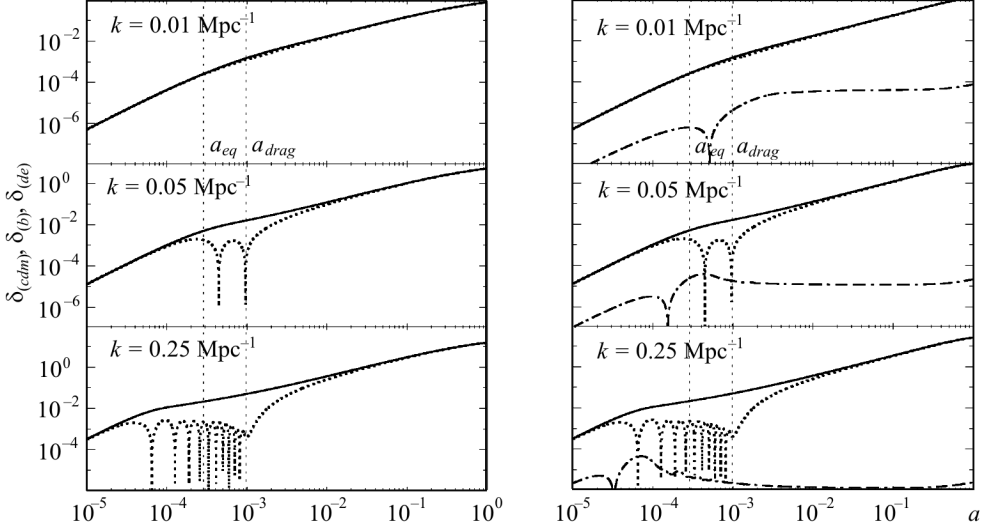


**Fig. 1.21.** Evolution of Fourier amplitudes ( $k = 0.01, 0.05, 0.25 \text{ Mpc}^{-1}$ ) of density perturbations of cold dark matter (solid line), baryonic matter (dotted line) and dark energy (dash-dotted line) computed by CAMB. In the left panel OMD model, in the right DED with  $w_{de} = -0.9$  (parameters are the same as in Fig. 1.13). The vertical thin dotted lines show radiation matter equality moment,  $a_{eq}$ , and the drag one,  $a_{drag}$ , when the baryons are released from the Compton drag of the photons

on to horizon scale. In the case of spatial isotropy the most interesting is dependence of Fourier modes of density perturbations on the module of wave vector  $k \equiv |\mathbf{k}|$ . The amplitudes of superhorizon perturbations ( $k\eta \ll 1$ ) in the synchronous gauge increase as  $\delta(k, \eta) \propto \eta^2$  in RD epoch as well as in MD one. But  $\eta \propto a \propto t^{1/2}$  in RD epoch, and  $\eta \propto a^{1/2} \propto t^{1/3}$  in MD epoch. It means, that starting from the radiation matter equality

$$\eta_{eq} = 2(\sqrt{2} - 1) \frac{c}{H_0} \frac{\sqrt{\Omega_r}}{\Omega_m} = \frac{16.05}{\Omega_m h^2}, \quad (1.56)$$

$$a_{eq} = 1.619 \cdot 10^{-7} \eta_{eq}^2 \Omega_m h^2 = \frac{4.17 \cdot 10^{-5}}{\Omega_m h^2}, \quad (1.57)$$

when  $\bar{\rho}_r(\eta_{eq}) = \bar{\rho}_m(\eta_{eq})$ , the rate of increasing of density perturbations is lower. The wave number that corresponds to the horizon scale at the radiation matter equality is as follows

$$k_{eq} \equiv \eta_{eq}^{-1} = 0.0623 \Omega_m h^2. \quad (1.58)$$

The density perturbations of baryon-photon plasma with scale smaller than horizon scale ( $k > k_{eq}$ ) oscillate with approximately constant amplitudes,  $\delta_b \propto \cos(k\eta/\sqrt{3})$  till  $a_{drag}$ , when the baryons are released from the Compton drag of the photons due to the recombination (dotted line in Fig. 1.21).

The Fourier amplitudes of density perturbations of cold dark matter increased all time, since it is collisionless. But perturbations with wave numbers  $k \gg k_{eq}$  have entered the horizon long before the radiation matter equality, at  $\eta_h = k^{-1} \ll \eta_{eq} = k_{eq}^{-1}$  and oscillations of baryon-photon plasma effectively suppressed the increasing of dark matter perturbations, so that at  $\eta_h \ll \eta \ll \eta_{eq}$  they grow logarithmically [132]:

$$\delta_{cdm} \propto \ln \left( I_2 \frac{a}{a_h} \right), \quad (1.59)$$

where  $a_h \equiv a(\eta_h)$  can be estimated using (1.45)

$$a_h = 2(\sqrt{2} - 1) \frac{k_{eq}}{k} a_{eq} \left( 1 + \frac{(\sqrt{2} - 1)}{2} \left( \frac{k_{eq}}{k} \right)^2 \right) \approx 2(\sqrt{2} - 1) \frac{k_{eq}}{k} a_{eq}. \quad (1.60)$$

and the value of constant  $I_2 = 0.594(1 - 0.631f_\nu + 0.284f_\nu^2)$  depends on neutrino fraction in the relativistic component  $f_\nu \equiv \rho_\nu/\rho_r$  ( $f_\nu = 0.405$  and  $I_2 = 0.47$  for standard model).

In Fig. 1.21 the evolution of density perturbations of cold dark matter and baryonic matter with wave numbers  $k = 0.01, 0.05, 0.25 \text{ Mpc}^{-1}$  is shown from before horizon crossing up to current epoch for OMD (left panel) and DED (right panel) models. For DED models it is shown also the evolution of dark energy density perturbations. In the models with  $w_{de} = \text{const} < -1/3$  their amplitudes are essentially lower than corresponding amplitudes for matter components and they do not leave appreciable fingerprints in the form of matter power spectrum. This figure illustrates also that dark matter is responsible for the formation of galaxies and large scale structure of the Universe.

Therefore, Fourier amplitudes of density perturbations of cold dark matter with  $k \leq k_{eq}$  before radiation matter equality  $a \leq a_{eq}$  increased all time  $\propto a^2$  independently on  $k$ , while perturbations with  $k > k_{eq}$  changed their growth rate to (1.59) at  $a \geq a_h$  and their amplitudes at  $a_{eq}$  depend on  $k$  additionally to the  $k$ -dependence of the primordial power spectrum. The pure crossing horizon effect can be well demonstrated by using transfer function defined as

$$T_{cdm}(k, a_{eq}) = \frac{\delta_{cdm}(k, a_{eq})}{\delta_{cdm}(k_1, a_{eq})} \frac{\delta_{cdm}(k_1, a_1)}{\delta_{cdm}(k, a_1)},$$

where  $k_1 \ll k_h, a_1 \ll a_h$ . Roughly assuming  $\delta_{cdm}(k \leq k_{eq}, a \leq a_{eq}) = \delta_{cdm}(k \geq k_{eq}, a \leq a_h) = B(k)a^2$  and  $\delta_{cdm}(k \geq k_{eq}, a_h \leq a \leq a_{eq}) = B(k)(a_h^2 + \ln(a/a_h))$ , where  $B(k)$  is primordial amplitude, we obtain

$$T_{cdm}(k, a_{eq}) = 1 \text{ for } k \ll k_{eq} \text{ and } T_{cdm}(k, a_{eq}) = \left( \frac{k_{eq}}{k} \right)^2 \left( 1 + \ln \frac{k}{k_{eq}} \right) \text{ for } k \gg k_{eq}.$$

If cold dark matter is dominating matter component then the  $k$ -dependence of transfer function slightly changes after  $\eta_{eq}$ , in the opposite case the other effects must be taken into account (Silk damping [97] and photon Compton drag [133] for baryonic component, collisionless damping for hot or warm dark matter components, etc.) which additionally suppress the initial matter power spectrum<sup>7</sup> at  $k \gg k_{eq}$ . But horizon crossing effect is dominating one at scales related to the observed large scale structure of the Universe and accurately described by the linear theory of cosmological perturbations in multicomponent universe.

If primordial power spectrum of scalar mode perturbations, generated in the early Universe, is power law,  $B^2(k) = Ak^{n_s}$ , then the initial (after recombination) one is

$$\mathcal{P}_m(k, a) \equiv \langle \delta_m(k, a) \delta_m^*(k, a) \rangle = Ak^{n_s} T_m^2(k, a),$$

where  $A$  is normalization constant and  $T_m(k, a_{drag})$  is the transfer function of matter density perturbations  $\delta_m(k, a) = \Omega_b \delta_b(k, a) / \Omega_m + \Omega_{cdm} \delta_{cdm}(k, a) / \Omega_m$  ( $\Omega_m = \Omega_b + \Omega_{cdm}$ ), which takes into account all processes affecting the form of the spectrum up to end of the drag epoch. The initial power spectrum  $\mathcal{P}_m(k, a)$  has peak at some  $k_{max}$  from  $[0, \infty]$  for any  $n_s$  from  $0 < n_s < 4$ , or at  $k_{max} \approx k_{eq}$  for  $n_s \approx 1$ . The exact value of peak position depends on matter density  $\Omega_m$ , dimensionless Hubble parameter  $h$  and spectral index  $n_s$  of primordial power spectrum. Thus, the determination of peak position in the initial power spectrum of matter density perturbations  $\mathcal{P}_m(k, a)$  from observations fixes the matter content for given values of  $h$  and  $n_s$ . If 3-curvature is known or constrained by other observations then these data constrain also the dark energy content. And not only the peak position of  $\mathcal{P}_m(k, a)$  give possibility to do that, but also its inclination and amplitude at any  $k > k_{eq}$  do so. The essence is that amplitude of the matter density perturbations depends also on dynamics of expansion of the Universe.

Indeed, the equation of evolution of matter density perturbations in synchronous gauge at DM – DED epochs (see [130] and citing therein) is as follows

$$\ddot{\delta}_m + \frac{\dot{a}}{a} \dot{\delta}_m + \left( \frac{\ddot{a}}{a} - 2 \frac{\dot{a}^2}{a^2} - K \right) \delta_m = 0, \quad (1.61)$$

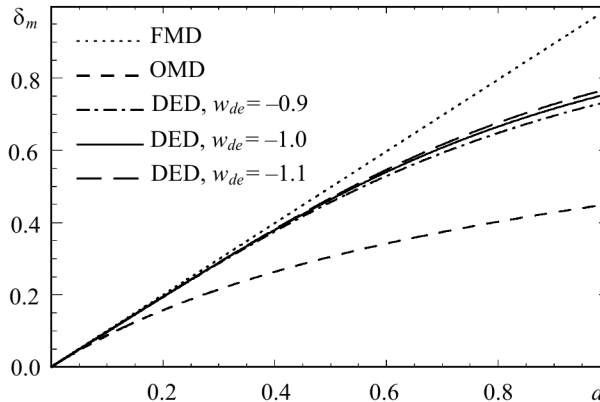
where  $a$  is solution of equation (1.15). It shows that the rate of amplitude growth depends on matter content, parameters of dark energy and curvature, but does not depend on scale of perturbations. So, the form of initial power spectrum is practically the same during the linear stage of evolution of matter density perturbations at DM – DED epochs.

---

<sup>7</sup>The imprint of the baryon acoustic oscillations at Compton drag epoch on the matter power spectrum was discussed shortly in the section 1.4.2.



**Fig. 1.22.** Evolution of matter density perturbations at MD – DED epochs in the FMD, OMD and DED models computed by CAMB for the same parameters as in Fig. 1.13. Amplitudes are arbitrarily normalized to  $10^{-2}$  at  $z = 100$  ( $a = 0.01$ ) – the same for any scale



In Fig. 1.22 it is shown the evolution of matter density perturbations from  $z = 100$  ( $a = 0.01$ ) up to the current epoch ( $z = 0$ ,  $a = 1$ ) for the FMD, OMD and DED models computed by CAMB with the same parameters as in Fig. 1.13. The growth of linear matter density perturbations at this epoch is approximated with about one percent accuracy by simple expression [156]

$$\delta_m(a) \propto \exp \int_0^a \Omega_m^\gamma(a') d \ln a', \quad (1.62)$$

where  $\Omega_m(a) = \Omega_m a^{-3} / (\Omega_m a^{-3} + \Omega_{de} a^{-3(1+w_0)} + \Omega_K a^{-2})$  and  $\gamma$  is growth index which we suppose equals<sup>8</sup> 0.6. In the literature some authors use the value  $D(a) = \delta_m(a)/a$ , dubbed growth factor, which shows how the growth rate of matter density perturbations in the models with dark energy or curvature is retarded in comparison with one in the Einstein – de Sitter model, in which  $\delta_m(a) \propto a$ . Fig. 1.22 illustrates the possibility of distinguishing of these models by studying of matter clustering at different redshifts.

After the cosmological recombination the baryons are released from the Compton drag of the photons and are free to fall inside the dark matter potential wells and starting from  $a \approx 0.01$  ( $z \approx 100$ ) their spectrum catches the dark matter one (see Fig. 1.21). The form of transfer functions for both components

$$T_{(i)}(k, a) = \frac{\delta_{(i)}(k, a)}{\delta_{(i)}(k_1, a)} \frac{\delta_{(i)}(k_1, a_1)}{\delta_{(i)}(k, a_1)}, \quad (1.63)$$

<sup>8</sup> Linder in the paper [156] proposed other best-fit values for growth index:  $\gamma = 0.545 + 0.05(1 + w)$  ( $z = 1$ ), but for  $w = \text{const}$  models the approximation function (1.62) with  $\gamma = 0.6$  fits the lines in Fig. 1.22 with percent accuracy for DED models as well as for OMD ones, while that  $\sim 2\text{--}3\%$ .

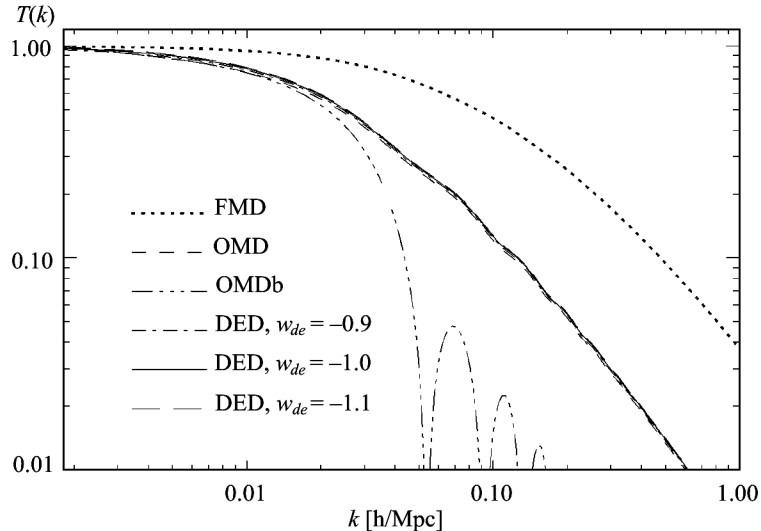


**Fig. 1.23.** Transfer functions of matter density perturbations at current epoch in the FMD, OMD and DED models with the same parameters as in Fig. 1.13 calculated using the CAMB [120]

where  $a \gg 0.01$ ,  $k_1 \ll k_h$ ,  $a_1 \ll a_h$  and (*i*) notes here *cdm* or *b*, after that is invariable<sup>9</sup>.

In Fig. 1.23 the transfer functions of matter density perturbations, defined as

$$T_m(k) = \frac{\Omega_{cdm}}{\Omega_m} T_{cdm}(k, 1) + \frac{\Omega_b}{\Omega_m} T_b(k, 1), \quad (1.64)$$

at current epoch in the FMD, OMD and DED models with the same parameters as in Fig. 1.13 are shown. For comparison it is shown also the transfer function for the open (low matter density) baryonic dominated model with  $\Omega_m = \Omega_b = 0.3$  in which the baryon oscillations in  $k$ -space are frozen acoustic oscillations which they were at the drag epoch. The lines, which mark transfer functions in OMD and DED models with the same values of  $\Omega_{cdm}$  and  $\Omega_b$ , overlap. Contrary, the transfer functions in the models with different  $\Omega_m$  (FMD and OMD or DED models), or models with the same  $\Omega_m$  but different  $\Omega_{cdm}$  and  $\Omega_b$  (OMD and OMDb) are quite different. So, transfer function of matter density perturbations is not sensitive<sup>10</sup> to presence of cosmological constant or dark energy with constant EoS parameter with value from vicinity of –

<sup>9</sup> If the dark matter is warm or some fraction is hot (massive active neutrinos) then the amplitude of density perturbations at scales lower free-streaming one decay [157] (see also [158, 159] and citing therein).

<sup>10</sup> The cases of affect of other dark energy models on the matter transfer functions are discussed in the next section.

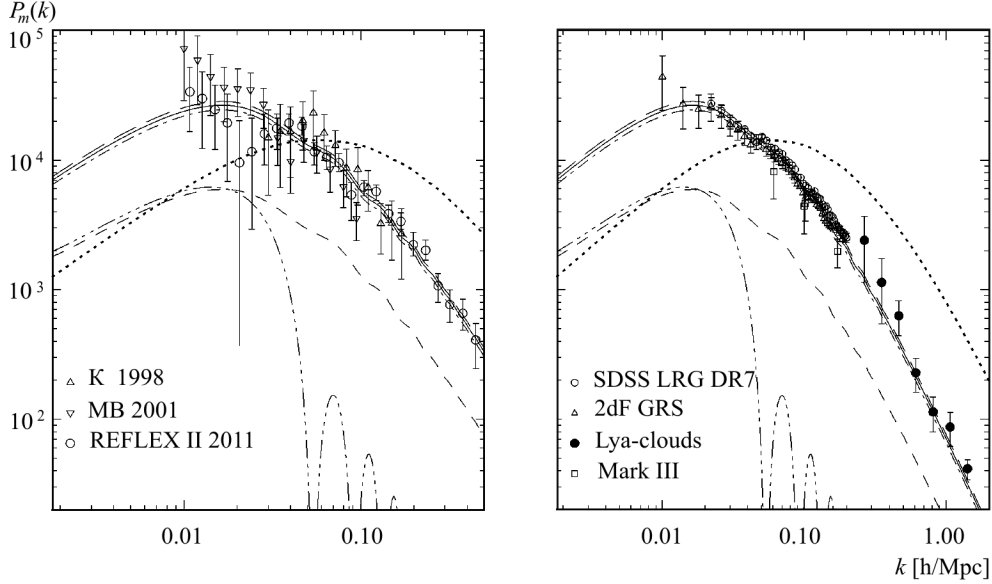


**Fig. 1.24.** The linear power spectra in FMD, OMD, OMDb and DED models, which have been normalized at decoupling epoch to the amplitude of the angular power spectrum of CMB temperature fluctuations [15] obtained in the COBE experiment [14], versus measured ones from the Abell/ACO (R 1998 [160], MB 2001 [161]) and X-ray galaxy cluster catalogue REFLEX II [162] (left panel), galaxy ones (SDSS LRG DR7 [163], 2dF GRS [164]), peculiar velocity field from Mark III catalogue [165, 166] (in units of  $\Omega_m^{1.2} h^{-3} \text{Mpc}^3$ ) and Ly $\alpha$ -clouds along the line of sight to the distant quasars [167] (right panel)

1. It is explained by the essence of transfer function, since it does not take into account the growth factor which depends on expansion dynamics of the Universe (Fig. 1.22).

The characteristic of large scale structure of the Universe, which can be obtained directly from observations, is power spectrum of matter density perturbations

$$P_m(k) = Ak^{n_s} T_m^2(k) \left[ \frac{\delta_m(1)}{\delta_m(a_i)} \right]^2, \quad (1.65)$$

where  $A$  is normalization constant deduced, for example, from CMB anisotropy data and the ratio in the brackets is growth factor of matter density perturbations, which can be calculated numerically or using analytical approximation (1.62). The power spectra for the same models are presented in Fig. 1.24. They are normalized at decoupling epoch to the amplitude at horizon scale deduced from CMB temperature fluctuations [15] (the same normalization as in Fig. 1.13).

The normalized model power spectra are compared with observational ones derived from the Abell/ACO [160, 161] and X-ray galaxy cluster catalogue

REFLEX II [162], galaxy ones SDSS LRG DR7 [163] and 2dF GRS [164], peculiar velocity field from Mark III catalogue [165,166] (in units  $\Omega_m^{1.2}h^{-3}\text{Mpc}^3$ ) and Ly $\alpha$ -clouds along the line of sight to the distant quasars [167]. They are related via bias factor  $b_i$ ,

$$P_i(k) = b_i^2 P_m(k),$$

which depends on classes, scales and luminosities of objects [168] (index “i” marks the class of objects with corresponding catalogue). In the left panel the cluster power spectra are reduced by square bias factor 2.5, 4 and 3.5 for Abell/ACO rich clusters with richness  $R \geq 0$  [160], with richness  $R \geq 1$  [161] and REFLEX II X-ray clusters with  $L_X > 0.015 \cdot 10^{44}$  erg/s correspondingly. The values of bias factors are well explained by the peaks statistics of random Gaussian fields [168]. The figures 14 and 15 in [162] illustrate the dependence of bias factor on luminosity for X-ray clusters. The spectra in the right panel are unbiased. The amplitude of matter power spectrum derived from the Mark III catalogue of peculiar velocities of galaxies [165,166] presented in the units of  $\Omega_m^{1.2}h^{-3}\text{Mpc}^3$ . So, in the OMD model it is biased by the factor  $\sim 14.8$  ( $b_{\text{Mark III}} \approx 3.8$ ), in the DED models it is biased by the factor  $\sim 3.2$  ( $b_{\text{Mark III}} \approx 1.6$ ). The value of bias factor for OMD model is too large for galaxies from the point of view of the statistics of random Gaussian fields [168]. The amplitude of the matter power spectrum measured from the Ly $\alpha$  forest at  $z = 2.5$  is recalculated to  $z = 0$  using (1.62) in the DED model (presented in Fig. 1.24) and is practically unbiased ( $b_{\text{Ly}\alpha} \sim 1$ ). Recalculation to  $z = 0$  in the OMD model gives biased clustering of Ly $\alpha$ -clouds with  $b_{\text{Ly}\alpha} \sim 2.3$  and, contrary, in the FMD model it gives unbiased clustering with  $b_{\text{Ly}\alpha} \sim 0.4-0.6$ . For both models the bias parameters for Ly $\alpha$ -clouds are hard for explanation in the framework of current theory of large scale structure formation. The most accurate measurements of matter power spectrum realized on the base of galaxy redshift surveys SDSS and 2dF. They agree perfectly with form and amplitude of the matter power spectrum in DED models normalized to CMB data. The matter power spectrum of OMD model matches the SDSS LRG7 and 2dF LRG spectra with biasing parameter  $\sim 1.6$ . The both FMD and OMDb models are ruled out by these data at high confidential level. The model spectra at small scale,  $k \geq 0.1$ , are corrected for non-linear evolution of density perturbations in the late epoch using HALOFIT approximation [169].

One can conclude, that the form and amplitude of the linear power spectrum of DED model normalized at early epoch to CMB power spectrum obtained in the COBE or WMAP experiments<sup>11</sup>, evolved according to the theory of linear perturbations through  $\sim 13$  billion years of MD – DED epochs, match well the observational power spectra derived from catalogue of different types of objects at current epoch. Therefore, the data on the power spectra

---

<sup>11</sup> They have close amplitudes at low spherical harmonics.

of space inhomogeneities of different types of objects, which are elements of the large scale structure of the Universe, prefer the models with dark energy dominating by density now.

The linear power spectrum of matter density perturbations is important measurable characteristics of the large scale structure of the Universe but not exclusive. Its moments, defined as

$$\sigma_j^2(R_{ss}) \equiv \frac{1}{2\pi^2} \int_0^\infty P(k) W^2(kR_{ss}) k^{2+2j} dk \quad (j = -1, 0, 1, 2, \dots). \quad (1.66)$$

are measurable too. Here  $W(R_{ss})$  is Fourier transformation of window function of smoothing (averaging) scale  $R_{ss}$ . The Gaussian and Heaviside (top-hat) smoothing are used most often. So, the window functions can be as follows

$$W_G(kR_{ss}) = \exp\left(-\frac{k^2 R_{ss}^2}{2}\right),$$

for the Gaussian smoothing  $f_G(R_{ss}) = \exp(-(r - r')^2/2R_{ss}^2)$  in the real space, or

$$W_H(kR_{ss}) = 3 \frac{\sin(kR_{ss}) - (kR_{ss}) \cos(kR_{ss})}{(kR_{ss})^3}$$

for top-hat one  $f_H(R_{ss}) = \Theta(1 - |r - r'|/R_{ss})$ , where

$$\Theta(x) = \begin{cases} 1, & x \geq 0 \\ 0, & x < 0 \end{cases},$$

is Heaviside step function. The (0)-moment,  $\sigma_0$ , is r.m.s. of matter density perturbation field smoothed by sphere with  $R_{ss}$ :

$$\sigma_0(R_{ss}) = \langle \delta^2(r, R_{ss}) \rangle^{1/2}, \quad (1.67)$$

where

$$\delta(r, R_{ss}) \equiv \frac{3}{R_{ss}^3} \int_0^\infty dr' r'^2 \delta(r') \Theta\left(1 - \frac{|r - r'|}{R_{ss}}\right),$$

The (-1)-moment,  $\sigma_{-1}$ , is connected with r.m.s. of peculiar velocity of galaxies in the sphere with radius  $R_{ss}$ , dubbed *bulk flow*:

$$\sigma_V(R_{ss}) \equiv \langle V^2(R_{ss}) \rangle^{1/2} = H_0 f(1) \sigma_{-1}, \quad (1.68)$$

where  $f(a)$  is the ratio of growth function for amplitude of velocity perturbations  $V(a)$  and analogical growth function for amplitude of density ones  $\delta_m(a)$ . Since, the density perturbations and velocity ones are connected by Euler

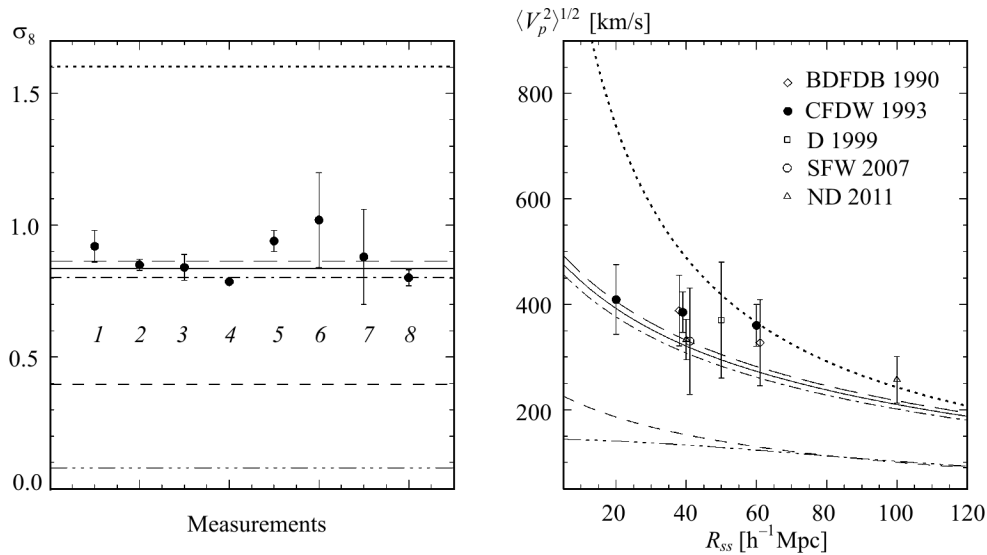


**Fig. 1.25.** Left panel: the r.m.s. of matter density perturbations  $\sigma_8$  computed for the model spectra presented in Fig. 1.24 (horizontal lines). By the dots its values from different measurements are shown: 1 – SDSS and 2dF galaxies catalogues [141, 164, 170], 2 – Ly $\alpha$  forest [171], 3 – Cosmic Shear [172], 4 – cluster of galaxies catalogue [173], 5 – Sunyaev–Zeldovich effect [174], 6 – cosmic flows [175], 7 – CFI++ Tully–Fisher catalogue [176], 8 – CMB angular power spectrum of temperature fluctuations [93, 95]. Right panel: bulk flows for different models and scales. By the signs its values from different measurements are shown: BDFDB 1990 [177], CFDW 1993 [178], D 1999 [179], SFW 2007 [180], ND 2011 [176]

equation  $-ikV = \dot{\delta}_m(a)$ , so, their ratio is  $f(a) = d \ln \delta_m(a) / d \ln a$  and taking into account (1.62)  $f(1) = \Omega_m^{\gamma}$ . The ratio of other two moments,  $\sigma_1$  and  $\sigma_2$ , gives the characteristic scale of peaks in the Gaussian fluctuation field

$$R_* \equiv \sqrt{3} \cdot \frac{\sigma_1}{\sigma_2}. \quad (1.69)$$

Most measurements of r.m.s. of matter density perturbations are related to scale  $8h^{-1}$ Mpc containing the mass of order of rich clusters of galaxies. The recent ones have been carried out on the base of different catalogs and types of objects (galaxies, clusters, cosmic shear, Ly $\alpha$ -clouds, Sunyaev–Zeldovich effect, cosmic flows, CFI++ Tully–Fisher measurements, CMB anisotropy data) and are presented in Fig. 1.25 (left panel). Some recent measurements of the bulk flows at different scales are presented in the right panel of Fig. 1.25. One can see, that all measurements of these moments prefer models with dark energy.

All techniques of obtaining the linear power spectrum of matter density perturbations from the space distributions of any class of objects have sequences of uncertainties, distortions and contaminations which essentially

lower its accuracy and scale extension. It is because the tracers of large scale structure of the Universe are luminous objects or dense absorption clouds of baryonic matter at different distances, stages of nonlinear evolution, chemical compositions, internal structure, dynamics, kinematics and so on. The discreteness of their space distributions, volume and luminosities limitations of their samples complicate their cosmological interpretation too. Most from these problems are absent when linear power spectrum is extracted from CMB anisotropy formed in the early Universe.

## 1.6. Angular power spectrum of CMB temperature fluctuations

### 1.6.1. Integrated Sachs—Wolfe effect

In the subsection 1.4.1 we have discussed briefly the physical effects related to the formation of angular power spectrum of CMB temperature fluctuations caused by scalar mode of cosmological perturbations, main source of CMB anisotropy. We emphasized there the importance of positions of acoustic peaks, measurements of which are realization of “angular diameter distance — redshift” test indicating the presence of dark energy. The positions of troughs can be used for that as well as [136, 137]. The ratios of amplitudes of acoustic peaks and deeps of troughs are sensitive to physical densities of baryons and dark matter [136, 137], that is illustrated by Fig. 1.13.

The amplitude and inclination of the CMB power spectrum at low spherical harmonics ( $\ell \leq 20$ ) is sensitive to the presence of dark energy or space curvature via the late integrated Sachs—Wolfe (ISW) effect<sup>12</sup> [96], which is described by second term in the r.h.s. of expression (1.34). The spherical  $\ell$ -harmonic of Fourier mode of  $\left(\frac{\Delta T}{T_0}\right)_k$ , caused by the late ISW effect, is following:

$$\left(\frac{\Delta T}{T_0}\right)_{k\ell}^{(ISW)} = -(2\ell + 1) \int_1^{a_{dec}} (\Psi'_k - \Phi'_k) j_\ell(kr) da, \quad (1.70)$$

where  $r(a) = \int_1^a (\tilde{a}^2 H(\tilde{a}))^{-1} d\tilde{a}$  is the comoving distance along the line of sight,  $\Psi_k$  and  $\Phi_k$  are amplitudes of Fourier modes of Bardeen metric potentials.

At the MD and DED epochs  $\Psi_k = -\Phi_k$  and the amplitude of  $k$ -mode of gravitational potential changes as

$$(3K - k^2)\Psi_k(a) = \frac{3}{2}H_0^2 \sum_i \Omega_i(a)\delta_i(k; a)/a, \quad (1.71)$$

<sup>12</sup> Producing the additional temperature fluctuations of CMB by decaying of gravitational potential of large scale perturbation at the linear stage of its evolution. At the non-linear stage (formation of galaxy clusters, for example) it is called Rees—Sciama effect [182].

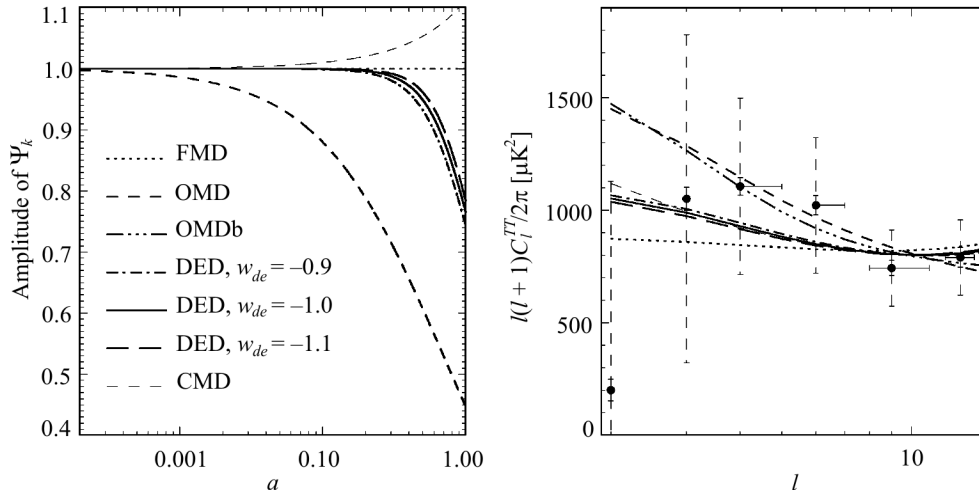


**Fig. 1.26.** Left panel: Evolution of the amplitude of metric perturbation at MD – DED epochs in the FMD, OMD and DED models. The growing gravitational potential in the closed matter dominated model with  $\Omega_m = 1.2$  and  $\Omega_{de} = 0$  (CMD, thin short dash line) is shown for comparison. The lines of OMD and OMDb are overlapped. Right panel: The model angular power spectrum of CMB temperature fluctuations at low spherical harmonics where the late ISW effect gives contribution comparable with ordinary SF effect in the OMD and DED models (lines). The binned power spectrum from WMAP7 measurements [93, 95] is shown by dots. The  $1\sigma$  errors shown by dashed lines are computed from diagonal terms of the Fisher matrix and include the measurement errors and cosmic variance, the errors shown by solid lines are measurements ones only multiplied by 10 for visibility

that follows from Einstein equations for scalar perturbations (see, for example, Eq. 62 in [130]). In the left panel of Fig. 1.26 the evolution of amplitudes of  $\Psi_k(a)$  in FMD, OMD and DED models at MD – DED epochs is shown. There the approximation (1.61) for  $\delta_m(a)$  was used. The late ISW effect gives contribution to  $\Delta T/T$  along the line of sight to the last scattering surface where  $\Psi'_k \neq 0$ . In the FMD model it is absent, since  $\Psi_k$  is constant. Its value at decoupling equals  $\Delta T/T$  caused by ordinary Sachs–Wolfe (OSW) effect (the first term in the r.h.s. of (1.34)). In the OMD and DED models maximal rate of decaying of  $\Psi_k$  is at the current epoch, but taking into account the properties of Bessel functions of  $\ell > 0$  order the main contribution to  $\Delta T/T$  is accumulated at  $0.01 \lesssim z \lesssim 1$  with peak of integral over  $k$  in (1.70) at  $z \sim 0.3–0.4$ , that was shown in our paper [181]. The later property causes the maximal effect of ISW at small  $k$  (large scales) and lowest  $\ell$ . The growing gravitational potential in the closed matter dominated model with  $\Omega_m = 1.2$  and  $\Omega_{de} = 0$  is shown there for complicity. It must be noted here, that  $\Psi'_k \neq 0$  also in the vicinity of the last scattering surface, this is caused by transition of dynamics of expansion from radiation density dominated Universe to matter one and oscillating of baryon-photon plasma at decoupling epoch. So, it gives notable contribution



into  $\Delta T/T$  in the models with low  $\Omega_m$  and at scales close to the horizon scale at decoupling epoch, that corresponds to spherical harmonics  $\sim 100$ . It is dubbed the early ISW effect and is related to the primary anisotropy of CMB.

In the right panel of Fig. 1.26 the model angular power spectra of CMB temperature fluctuations is shown for low spherical harmonics where the late ISW effect gives maximal contribution to  $\Delta T/T$  in the OMD and DED models. In these models the late ISW contributes to the quadrupole component of  $\Delta T/T$  about 20% in the DED models and about 60% in the OMD with  $\Omega_m \approx 0.3$ . So, the negative space curvature causes stronger ISW effect than dark energy for models with similar  $\Omega_m$ . And contrary, the space curvature  $|\Omega_K| \sim 0.2$  gives the ISW contribution comparable to ISW one in the DED models with  $\Omega_{de} \sim 0.7$  (in the figure it is shown for closed model). It causes the degeneracy in the space of parameters  $\Omega_m - \Omega_K - \Omega_{de} - w_{de}$  when CMB data alone are used for determination of cosmological parameters. That is why the prior on zero curvature is applied as rule. The binned power spectrum from WMAP7 measurements [93, 95] is shown by dots. The  $1\sigma$  errors shown by dashed lines are computed from diagonal terms of the Fisher matrix and include the measurement errors and cosmic variance, the errors shown by vertical solid lines are measurement ones multiplied by 10 for visibility. Therefore, CMB anisotropy data in the range of ISW effect are not enough accurate due to unremovable cosmic variance for constraining the dark energy models. But since the contribution of late ISW into  $\Delta T/T$  forms in the range of observable large scale structure of the Universe the cross-correlation between them can be used to detect it and to constraint the dark energy parameters [183–186].

The essence of such approach consist in the fact that CMB anisotropy sky map, presented by  $\left(\frac{\Delta T}{T_0}\right)(\mathbf{n})$  in the form (1.34), contains the ISW contribution from matter density perturbations,  $\delta_m(k; a, \mathbf{n})$  at  $z \lesssim 1$ , which strongly correlate with galaxies space inhomogeneities  $\delta_g(k; a, \mathbf{n}) = b_g(k; a)\delta_m(k; a, \mathbf{n})$ , deduced from the galaxy sky surveys. For the comoving scales  $\gtrsim 100\text{Mpc}$  the bias factor  $b_g$  varies weakly with scale and redshift [142] and the general assumption about its time and scale independence is well-grounded. Other components of (1.34), which are related with perturbations at decoupling epoch, do not correlate with  $\delta_g(k; a, \mathbf{n})$  at current epoch and do not contribute to cross-correlation function (CCF), defined as

$$C^{Tg}(\vartheta) \equiv \left\langle \frac{\Delta T}{T_0}(\mathbf{n}_1)\delta_g(\mathbf{n}_2) \right\rangle \quad (1.72)$$

with the average carried over all the pairs at the same angular distance  $\vartheta = |\mathbf{n}_1 - \mathbf{n}_2|$ .

It is possible to express this value in the harmonic space with the use of the Legendre polynomials  $\mathcal{P}_\ell$ :

$$C^{Tg}(\vartheta) = \sum_{\ell=2}^{\infty} \frac{2\ell+1}{4\pi} C_\ell^{Tg} \mathcal{P}_\ell[\cos(\vartheta)], \quad (1.73)$$

where cross-correlation power spectra are given by

$$C_\ell^{Tg} = \frac{2}{\pi} \int_0^\infty dk k^2 P_m(k) I_\ell^{ISW}(k) I_\ell^g(k). \quad (1.74)$$

The two integrands in the last expression are respectively

$$I_\ell^{ISW}(k) = 2 \int_1^{a_{min}} e^{-\tau(a)} \left( \frac{\delta_m(a)}{a} \right)' j_\ell[kr(a)] da, \quad (1.75)$$

$$I_\ell^g(k) = \int_1^{a_{min}} b_g \mathcal{N}'(a) \delta_m(a) j_\ell[kr(a)] da, \quad (1.76)$$

where  $\Psi_k$  and  $\delta_m(k, z)$  are the Fourier components of the gravitational potential and matter perturbations,  $j_\ell(x)$  are the spherical Bessel functions,  $\mathcal{N}'$  is a selection function of the galaxy survey,  $\delta_m(a)$  is growth function of matter density perturbations at linear stage,  $r(a)$  is the comoving distance along the line of sight,  $\tau(a)$  is the optical depth along the line of sight caused by Thomson scattering by free electrons and  $a_{min}$  corresponds to  $z_{max}$  of the survey.

Applying the (1.72) to the CMB and galaxies sky maps one can obtain the observational CCF which contains the information about parameters of our Universe. They can be constrained by comparison of CCF function computed for the model with given parameters using (1.73)–(1.76).

Such approach has been used by several groups [187–194] to detect the ISW effect using WMAP all sky maps of the CMB temperature fluctuations and several maps of galaxy space distributions. The cross-correlations between  $\frac{\Delta T}{T_0}(\mathbf{n})$  map and individual  $\delta_m(\mathbf{n})$  maps with different galaxy surveys that trace the matter distribution with light from the whole range of the electromagnetic spectrum have been detected at 2–3 $\sigma$  significance. It indicates the rapid slowing down in the growth of amplitude of density perturbations and means the existence of dark energy in the flat Universe. The combination of data from different surveys and redshifts essentially reduces uncertainties and introduces important new constraints [195, 196]. The best surveys available for this purpose include the following: the optical Sloan Digital Sky Survey (SDSS), the infrared 2 Micron All-Sky Survey (2MASS), the X-ray catalogue from the High Energy Astrophysical Observatory (HEAO) and radio galaxy

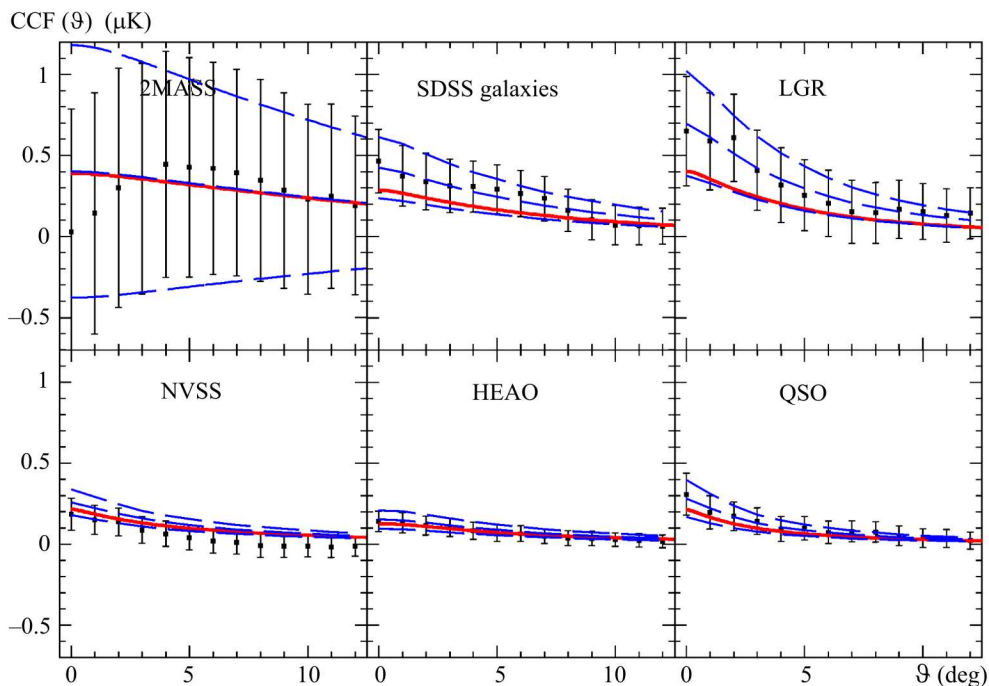


**Fig. 1.27.** Measurements of the CCFs between the WMAP CMB maps and all available galaxy catalogue that trace the matter distribution with light from the whole range of the electromagnetic spectrum (black points), compared with the theory from WMAP best fit cosmology and the galactic bias from the literature (solid lines). Their  $1\sigma$  deviations are shown by dashed lines. The errors are calculated from Monte Carlo simulations of temperature and density fluctuations (From [197])

catalogue from the NRAO VLA Sky Survey (NVSS). The high quality of the SDSS data allows us to extract some further subsamples from it, consisting of Luminous Red Galaxies (LRG) and quasars (QSO) in addition to the main galaxy sample. The results of measurements of the CCFs between WMAP CMB maps and each from these catalogues obtained in [197] are presented in Fig. 1.27. The analysis of auto- and cross-correlations between all catalogues and including the full covariance matrix between all data gave the possibility to authors of [197] to increase the significance of the total combined measurement of ISW effect up to  $4.5\sigma$  and to constraint the  $\Omega_m - w_{de}$  parameter space as it is shown in Fig. 1.28. One can see, that measurement of ISW effect is a good probe for dark energy and independent evidence for its presence in our Universe, like SNe Ia, CMB acoustic peaks and BAOs. Its combination with other detections of dark energy narrows essentially confidence ranges of DE parameters (right panel of Fig. 1.28).

The analysis of the constraining power of future measurements of the ISW effect on models of  $w_{de}(z)$  was carried out in [198]. There it was demonstrated

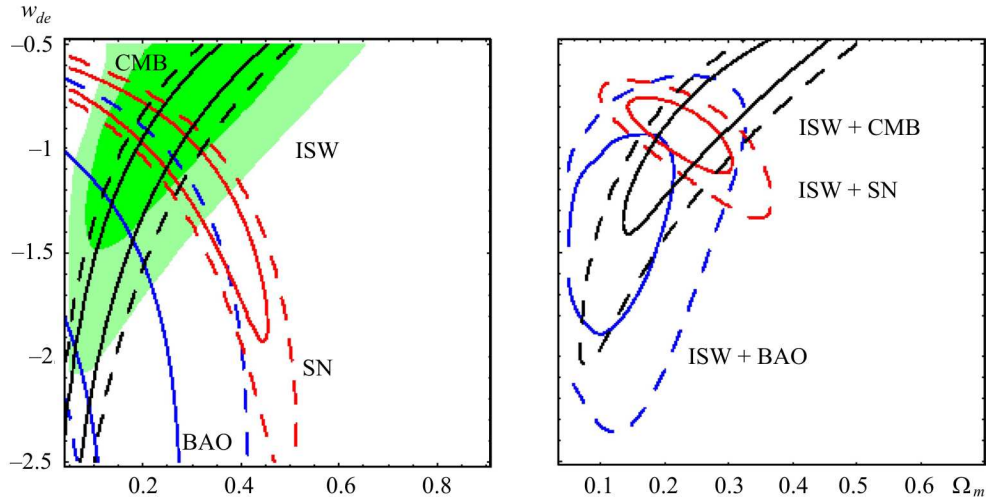


**Fig. 1.28.**  $\Omega_m - w_{de}$  constraints from measurements of the ISW effect (shadow range in the left panel). Constraints from other observations, including CMB, SNe Ia and BAO are shown for comparison. In the right panel the combined likelihoods using the ISW + each one of these other constraints are presented. In the both panels the 1 and 2  $\sigma$  contours are shown by solid and dashed lines respectively (From [197])

that the cross-correlation of Planck CMB data and Large Synoptic Survey Telescope galaxy catalogues will provide important independent constraints on  $w_{de}(z)$  at high  $z$ .

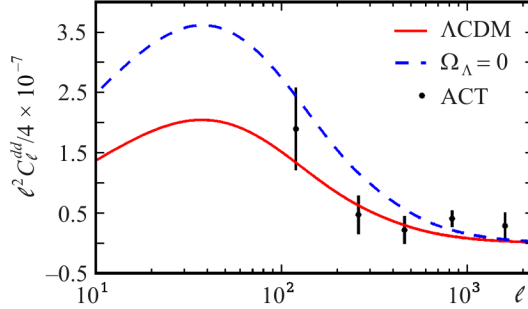
### 1.6.2. Weak gravitational lensing of CMB

The measurements of gravitational lensing of CMB temperature fluctuations by the foreground large scale structure are powerful source of information about the geometry, expansion history and dark components of the Universe (see excellent reviews [199–201] and citing therein). The first detection of lensing signal at  $3.4\sigma$  significance was realized by Smith et al. (2008) [202] from cross-correlation of WMAP data [88,89] with  $\approx 2$  million radio sources founded in the NRAO VLA Sky Survey (NVSS) [203]. In the next year Hirata et al. (2008) [204] for the same data set announced the detection of lensing signal at  $2.1\sigma$  significance. They supported the result by cross-correlation of WMAP3 data with SDSS LRG and quasar samples at  $1.8\sigma$  significance. Combining all three large scale structure samples they stated the detection at  $2.5\sigma$  level. The obtained there cross-correlation amplitude agrees well with one expected for DED model with WMAP cosmological parameters.

Recently, the lensing signal has been detected in CMB alone by Atacama Cosmology Telescope (ACT) [205] at  $4\sigma$  significance. The gravitational lensing remaps the CMB temperature fluctuations on the sky as follows

$$T(\tilde{\mathbf{n}}) = \tilde{T}(\tilde{\mathbf{n}} + \alpha(\tilde{\mathbf{n}})),$$

**Fig. 1.29.** The CMB lensing power spectra detected by Atacama Cosmology Telescope [205] (dots) and computed for two models (lines), which have practically indistinguishable  $TT$  power spectra well matching the WMAP7 one ( $\Lambda$ CDM with  $\Omega_\Lambda = 0.73$ ,  $\Omega_m = 0.27$  and closed MD model with  $\Omega_\Lambda = 0$ ,  $\Omega_m = 1.29$ ) (From [206])



where  $\alpha(\tilde{\mathbf{n}})$  is deflection field and tilde denotes the unlensed quantities. It imprints a distinctive non-Gaussian signature on the pattern of the microwave sky, which can be measured by 4-point correlation function or power spectrum of the convergence field  $\kappa = \frac{1}{2}\nabla\alpha$  in the form

$$(2\pi)^2 \delta(\mathbf{L} - \mathbf{L}') \hat{C}_L^{\kappa\kappa} = |N^\kappa(\mathbf{L})|^2 \int \frac{d^2\ell}{(2\pi)^2} \int \frac{d^2\ell'}{(2\pi)^2} |g(\ell, \mathbf{L})|^2 \times \\ \times \left[ T^*(\ell) T^*(\mathbf{L} - \ell) T(\ell') T(\mathbf{L}' - \ell') - \langle T^*(\ell) T^*(\mathbf{L} - \ell) T(\ell') T(\mathbf{L}' - \ell') \rangle_{\text{Gauss}} \right],$$

where  $\ell, \ell', \mathbf{L}, \mathbf{L}'$  are coordinates in Fourier space in the flat-sky approximation,  $g$  defines the filters that can be used to optimize signal-to-noise,  $N$  is a normalization, and the second term is the Gaussian part of the 4-point correlation function. Subtraction from the full 4-point function its Gaussian part gives the non-Gaussian lensing signal.

The power spectrum of the convergence field extracted from ACT temperature maps in [205] is presented<sup>13</sup> in Fig. 1.29. There are also shown the predicted power spectra of the convergence field for  $\Lambda$ CDM ( $\Omega_\Lambda = 0.73$ ,  $\Omega_m = 0.27$ ) and closed MD ( $\Omega_\Lambda = 0$ ,  $\Omega_m = 1.29$ ) models, which have practically indistinguishable  $TT$  power spectra [206]. They differ only at largest angular scales ( $\ell < 10$ ) due to the ISW effect, but there cosmic variance is too large (see right panel of Fig. 1.26). Strong degeneracy in  $\Omega_m - w_{de}$  parameter space constrained by CMB  $TT$  power spectrum alone is illustrated by prolate and convoluted form of confidence contours in Fig. 1.28. The addition of lensing data should break this degeneracy.

Recently, these data have been used by Sherwin et al. (2011) [206] for constraining the  $\Omega_m - \Omega_\Lambda$  parameter space on the base of WMAP7  $TT$  and ACT lensing power spectra. The results are presented in Fig. 1.30. One can see

<sup>13</sup> For details of pipeline of obtaining the lensing power spectrum from ACT data we refer to the original paper [205].

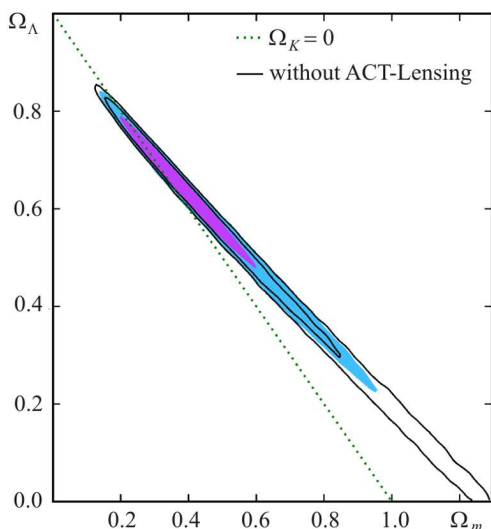


**Fig. 1.30.** Two-dimensional marginalized posterior probability for  $\Omega_m$  and  $\Omega_\Lambda$  (68% and 95% C.L.). Shaded contours are for WMAP + ACT lensing, black lines are for WMAP only (From [206])

that ACT lensing data prefer model with dark energy and serve as one more independent argument for its existence and dominance in density.

In the paper [207] it was shown that combining of expected Planck CMB data with the weak lensing survey of Euclid will give powerful constraints on early dark energy and will be able to break degeneracies in the parameter set inherent to the

various observational channels. So, the current and planned experiments for measurements of gravitational lensing promise to become the crucial data in unveiling the mystery of dark sector of our Universe.

## 1.7. Age of the Universe

We have mentioned at the beginning of this chapter the problem of agreement of the expansion age of the Universe with age of the oldest stars of our galaxy. The estimations of the age of the oldest stars in the globular clusters, obtained in the 90s of last century, are in the range  $13.5 \pm 2$  Gyrs [12, 208–211]. The similar results were obtained using other methods: white dwarf cooling sequence in globular clusters ( $14.5 \pm 1.5$  Gyrs [212],  $12.7 \pm 0.7$  Gyrs [213]) and content of U-238 in the old stars of halo of the Milky Way ( $14.0 \pm 2.4$  Gyrs [214]). The lower limit of such estimations is 11 Gyrs at  $2\sigma$  C.L. [211]. The expansion age of the Universe should be larger. So, what we have here?

The age of the Universe in the general cosmological model with given parameters is as follows:

$$t_0 = \int_0^1 \frac{da}{aH(a)}, \quad (1.77)$$

where  $H(a)$  is given by Eq. (1.15). Since  $\Omega_r \sim 10^{-5}$  and the main contribution to the integral comes from the range  $a > 0.01$ , the radiation term in (1.15) can be neglected. In the Einstein–de Sitter model ( $\Omega_r = \Omega_K = \Omega_{de} = 0$ ,  $\Omega_m = 1$ )

the age of the Universe is defined by current value of Hubble constant

$$t_0 = \frac{2}{3} \frac{1}{H_0}, \quad (1.78)$$

and equals  $9.3 \pm 0.6$  Gyrs for  $H_0 = 70 \pm 4$  km/s · Mpc, that is essentially lower than the age of the oldest stars of our galaxy and, therefore, this model is ruled out by these measurements.

In the open models without dark energy the equation (1.77) is integrated to give

$$t_0 = \frac{H_0^{-1}}{1 - \Omega_m} \left[ 1 + \frac{\Omega_m}{2\sqrt{1 - \Omega_m}} \ln \left( \frac{1 - \sqrt{1 - \Omega_m}}{1 + \sqrt{1 - \Omega_m}} \right) \right]. \quad (1.79)$$

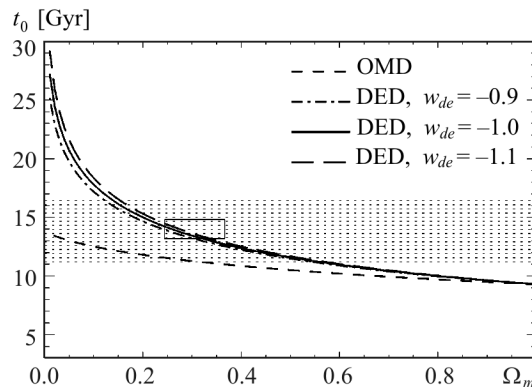
In the limit  $\Omega_m \rightarrow 1$  we recover the value (1.78). In the limit  $\Omega_m \rightarrow 0$  we obtain also finite value:  $t_0 \rightarrow H_0^{-1}$ . For  $H_0 = 70 \pm 4$  km/s · Mpc and  $\Omega_m = 0.3 \pm 0.1$  from (1.79) we obtain  $t_0 = 11.3 \pm 1.2$  Gyrs, that is at lower limits of measurements of age of the oldest stars. These models prefer uncomfortably low  $\Omega_m$ , that contradict its measurements from peculiar velocity of galaxies, for example, and large negative curvature, that contradict data on positions of CMB acoustic peaks.

The equation (1.77) has analytic solution also for flat  $\Lambda$ CDM model:

$$t_0 = \frac{H_0^{-1}}{3\sqrt{1 - \Omega_m}} \ln \left( \frac{1 - \sqrt{1 + \Omega_m}}{1 - \sqrt{1 - \Omega_m}} \right). \quad (1.80)$$

In the limit  $\Omega_m \rightarrow 1$  we obtain the value (1.78) of Einstein–de Sitter model, but in the opposite limit  $\Omega_m \rightarrow 0$  the cosmic age goes to infinity,  $t_0 \rightarrow \infty$ , which makes this model more suitable for agreement with independent measurements of cosmic age (see Fig. 1.31). Really, for the same range of

**Fig. 1.31.** The dependences of age of the Universe on matter density in the models without dark energy (OMD,  $\Omega_{de} = 0$ ) and in the flat models ( $\Omega_K = 0$ ) with dark energy (DED). The dotted strip shows the age of the Universe estimated from the age of oldest white dwarfs, oldest stars of globular clusters and from the content of U-238 in the oldest stars of galaxy halo. The rectangle shows marginalized  $1\sigma$  constraints from combined data (Table 1.2)



parameters ( $H_0 = 70 \pm 4 \text{ km/s} \cdot \text{Mpc}$  and  $\Omega_m = 0.3 \pm 0.1$ ) the age of expansion of the Universe is now in the interval 12–16 Gyrs.

In the models with non- $\Lambda$  dark energy, even in the simplest among them —  $w$ CDM ( $w = \text{const} \neq -1$ ), the integral in (1.77) can be calculated only numerically. The results of calculations for DED and OMD models are shown in Fig. 1.31. Also the measurements of age of the oldest stars are shown there. One can see, that the DED models can explain, in principle, all independent measurements of cosmic age. One can see, that EoS parameter also affects the age of expansion of the Universe which increases with decreasing of  $w_{de}$ . It was used by Krauss & Chaboyer (2003) [211] for constraining of dark energy parameters on the base of estimation of age of globular cluster: for the Hubble key project the best-fit value of Hubble constant they have obtained  $w_{de} < -0.4$  and  $\Omega_m < 0.38$  at  $1\sigma$  C.L.

Therefore, the independent measurements of age of the oldest stars of our galaxy and Hubble constant from distant galaxies are important evidence for existence of dark energy in the Universe.

### 1.8. Constraints on dark energy parameters from combined data

The complex approaches for establishing the most adequate model of the Universe have been started in the 90s of the past century. Using available at that time observational data on large scale structure (galaxies and clusters power spectra, bulk motions, cluster mass and temperature functions, damped Ly- $\alpha$  systems) and COBE CMB anisotropy measurements it was stated at  $1\sigma$  confidence level that  $\Omega_\Lambda > 0$  before indication of dark energy by SN Ia measurements (see our papers [19, 20] and citing therein). Complementation of these data by SN Ia luminous distance measurements and CMB acoustic peaks positions from the ground-based and stratospheric experiments available at the boundary of millennium enhances the confidence level of existence of dark energy to 99.99% [135, 137, 215–224].

Simultaneously with progress in accumulation of cosmological data and increasing their accuracy and quality, the physical interpretations as well as mathematical and computing methods of comparison of theoretical predictions with observations and extracting of the cosmological parameters from them were progressed too. The highly accurate fast codes for estimation of large number of parameters become publicly available (CosmoMC, for example). Together with publications of the results of the digital galaxy sky surveys and the first year WMAP all-sky CMB survey they originates the next level of cosmology investigations, dubbed precision cosmology. It becomes possible to establish the most optimal values of main cosmological parameters at high confidence level, which is very important for investigation of the nature of dark



energy and constraining the classes and number of its models. Since its effect on the predicted values of the characteristics of the Universe (age, dynamics of expansion, large scale structure) is comparable with influence of values of rest cosmological parameters ( $\Omega_K, \Omega_{cdm}, \Omega_b, \Omega_\nu, N_\nu, H_0, A_s, n_s, A_t, n_t, Y_p, \tau$ ), the dark energy parameters must be determined jointly with all other ones. The analysis of Monte Carlo Markov chains is widely used for this puprose, in it two functions

$$\mathcal{L}(\mathbf{x}; \theta_k) = \exp\left(-\frac{1}{2}(x_i - x_i^{th}(\theta_k))C_{ij}(x_j - x_j^{th}(\theta_k))\right), \quad (1.81)$$

and

$$\mathcal{P}(\theta_k; \mathbf{x}) = \frac{L(\mathbf{x}; \theta_k)p(\theta_k)}{g(\mathbf{x})}, \quad (1.82)$$

the likelihood and posterior ones correspondingly are under consideration. Here  $\theta_k$  notes all cosmological parameters,  $\mathbf{x}$  notes all observational values,  $\mathbf{x}^{th}$  notes their model predictions,  $C_{ij}$  is covariance matrix for all observational data,  $p(\theta_k)$  is prior for  $\theta_k$  parameter,  $g(\mathbf{x})$  is probability distribution function of data. If model is correct, the data are normally distributed and do not contain dominating systematic errors then normalized to 1 at maximum dependences of their likelihood and posterior functions on each parameter marginalized over the rest ones coincide.

It was shown ([94, 137, 225] and citing therein) that contribution of tensor mode of cosmological perturbations to CMB temperature fluctuations is negligibly small and, therefore, can be omitted in the problem of determination of dark energy parameters. Also, there it was shown that the value of active neutrino density parameter,  $\Omega_\nu$ , is lower than 0.03 at 95.4 % confidence level. Its best-fit value is close to zero. Such low upper limit for active neutrino density parameter makes it unimportant for dark energy problem. Therefore, two parameters,  $A_t$  and  $\Omega_\nu$  can be assumed to be zero without loss of generality in the problem of determination of dark energy parameters. The spectral index of tensor mode,  $n_t$ , in this case is neglected too. The effective number of neutrino species,  $N_\nu$ , is not crucial parameter too and in our task is commonly assumed to be equal to effective number from standard model of particle physics, 3.04.

The similar situation is with primordial helium parameter  $Y_p$ . Its value defines the number density of free electrons at decoupling epoch as  $n_e = 11.31(1 + z_{dec})(1 - Y_p)\Omega_b h^2$  [226] that influences photon free streaming and suppresses the CMB power spectrum at small angular scale. The change of primordial helium parameter in the range of its 95.4 % limits,  $0.16 < Y_p < 0.46$  [94], causes the variation of amplitude of 2nd, 3d and 4th acoustic peaks in the range 1–2 %. So, without loss of generality one can fix it at standard fiducial value 0.24, which matches well the Big Bang nucleosynthesis (BBN) constraint [227, 228] and incorporates the other measurements of primordial content

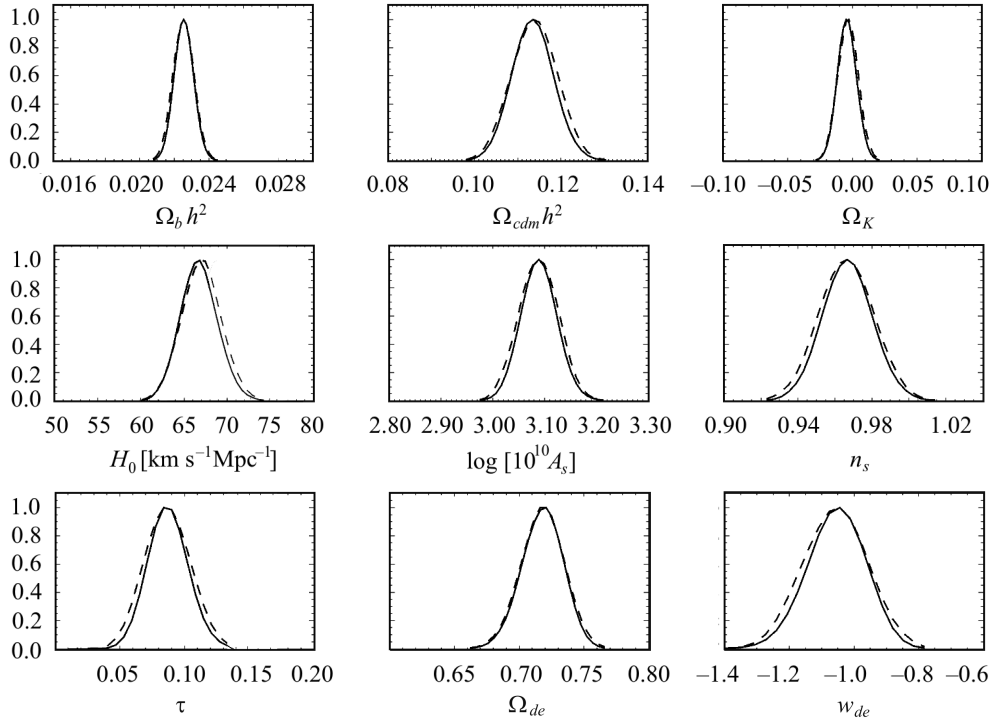


**Fig. 1.32.** Posterior (solid line) and likelihood (dashed line) functions for main cosmological parameters and combined datasets WMAP7 + HST + BBN + SDSS LRG7 + SN SDSS SALT2

of helium [229, 230]. Of course, the exact values of these parameters are very important for physics and cosmology, but they correspond to other problems of current cosmology which are beyond the scope of this book. They become especially actual in the light of forthcoming experiments.

Therefore, in the problem of determination of dark energy parameters at current level there are 7 important cosmological parameters ( $\Omega_K$ ,  $\Omega_{cdm}$ ,  $\Omega_b$ ,  $H_0$ ,  $A_s$ ,  $n_s$ ,  $\tau$ ) apart the dark energy ones  $\Omega_{de}$  and  $w_{de}$  ones. In Figs. 1.32 and 1.33 the marginalized likelihood and posterior functions are presented for main cosmological parameters and current observational data on dynamics of expansion of the Universe (SN SDSS [77], HST [231]), its large scale structure (SDSS LRG7 [163], BAO [143]) and CMB anisotropy (WMAP7 [93–95]). In the first figure SNe Ia from SDSS supernova survey are processed using SALT2 light-curve fitting method, in the second one – MLCS2k2 method. Maxima of functions define the best-fit parameters and limits of 68.3% (95.4%) fraction of area under the curves define  $1\sigma$  ( $2\sigma$ ) confidence limits of optimal values of corresponding parameters. They are presented in Table 1.2 for different assumptions and SNe Ia compilations. One can see, that best-fit values of  $w_{de}$

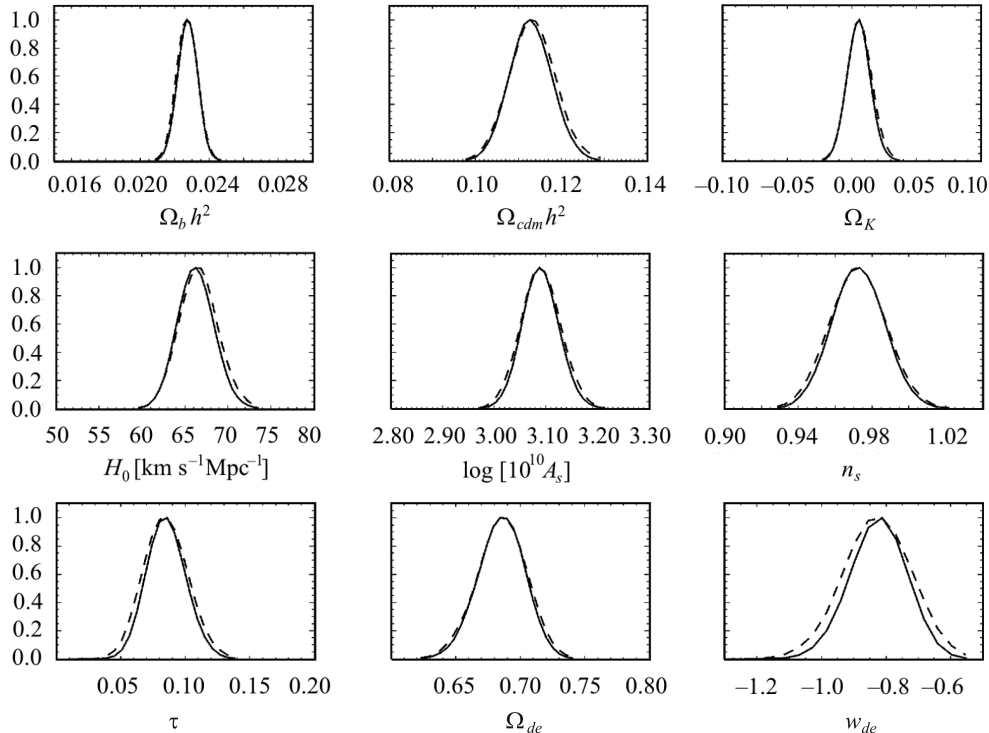


**Fig. 1.33.** Posterior (solid line) and likelihood (dashed line) functions for main cosmological parameters and combined datasets WMAP7 + HST + BBN + SDSS LRG7 + SN SDSS MLCS2k2

are somewhat different for SALT2 and MLCS2k2 light-curve fittings for the same data set: in the first case it is in the phantom range, in the second one in the quintessence one. But confidential limits for both are wide and do not exclude each other. The presented in Fig. 1.32 and 1.33 likelihood and posterior functions, which are practically superimposed and Gaussian, prove that the theory matches well observational data and its parameters are determined surely. One can see, that current data unambiguously prefer the models with low spatial curvature and high dark energy density now. Since the admissible values of curvature parameter are very close to zero and computations of models with non-zero curvature by CAMB are essentially time consuming most researchers fix it equal to zero when determine the dark energy parameters.

The remarkable achievement of current cosmology is visible here too: it is establishing of the existence of dark energy ( $\Omega_{de} > 0$ ) at 99.999% or more confidence level ( $\gtrsim 12\sigma$ ) with its content in the  $1\sigma$  range  $0.64 < \Omega_{de} < 0.76$ . In spite of the relatively small dispersions of parameters shown in Figs. 1.32 and 1.33 and Table 1.2, a large number of dark energy models can “belong”

there yet. Really,  $1\sigma$  range of marginalized likelihood/posterior functions for  $w_{de}$  includes  $\Lambda$ CDM, phantom and quintessence dark energy. Its more accurate and assured determination becomes the key problem of dark energy investigations.

In Figs. 1.9, 1.11, 1.15, 1.19, 1.20, 1.28, 1.30 the  $1$  and  $2\sigma$  contours in  $\Omega_m - w_{de}$  plane of likelihood distribution function marginalized over all rest parameters are presented for the different determinations. One can see, that practically each method shows some degeneracy (see expressions (1.31), (1.48), (1.54)) which makes contours prolate and convoluted. It is caused by integral character of “distant—redshift” relations in the low- $z$  observations or geometrical projections in the high- $z$  ones. For example, the degeneracy in  $\Omega_m - w_{de}$  plane of likelihood distribution function, obtained from CMB data alone, can be understood as follows. The first peak of the CMB temperature power spectrum is connected with the sound horizon at decoupling, when the CMB was last scattered by free electrons. It depends (see equations (1.35)—(1.47)) on  $\Omega_b$ ,  $\Omega_m$ ,  $H_0$ ,  $T_0$  and effective number of relativistic fractions  $N_{\text{eff}}$ . The projecti-

**Table 1.2. The best-fit values for cosmological parameters and the  $1\sigma$  limits from the extremal values of the N-dimensional distribution determined for the  $\Lambda$ CDM and  $w$ CDM models by the MCMC technique from the combined datasets WMAP7 + HST + BBN + SDSS LRG7 + + SN SDSS SALT2 (1) and WMAP7 + HST + BBN + SDSS LRG7 + + SN SDSS MLCS2k2 (2). By the asterisk in brackets the derived parameters are noted. The Hubble constant  $H_0$  is in units  $\text{km s}^{-1} \text{Mpc}^{-1}$**

Parameters	$\Lambda$ CDM	$\Lambda$ CDM	$w$ CDM	$w$ CDM
	1	2	1	2
$\Omega_b h^2$	$0.0225^{+0.0016}_{-0.0013}$	$0.0223^{+0.0016}_{-0.0013}$	$0.0228^{+0.0008}_{-0.0012}$	$0.0226^{+0.0017}_{-0.0014}$
$\Omega_{cdm} h^2$	$0.113^{+0.012}_{-0.012}$	$0.117^{+0.011}_{-0.013}$	$0.115^{+0.010}_{-0.012}$	$0.115^{+0.013}_{-0.014}$
$\Omega_m^{(*)}$	$0.286^{+0.042}_{-0.043}$	$0.319^{+0.047}_{-0.051}$	$0.279^{+0.048}_{-0.033}$	$0.307^{+0.057}_{-0.049}$
$\Omega_K$	$-0.001^{+0.016}_{-0.017}$	$-0.004^{+0.016}_{-0.019}$	$-0.002^{+0.012}_{-0.019}$	$0.006^{+0.026}_{-0.023}$
$H_0$	$68.8^{+6.5}_{-4.9}$	$66.0^{+6.0}_{-5.0}$	$70.2^{+4.3}_{-6.1}$	$66.8^{+5.6}_{-5.9}$
$\log(10^{10} A_s)$	$3.09^{+0.09}_{-0.09}$	$3.09^{+0.08}_{-0.09}$	$3.09^{+0.07}_{-0.08}$	$3.09^{+0.10}_{-0.09}$
$n_s$	$0.970^{+0.034}_{-0.036}$	$0.962^{+0.035}_{-0.033}$	$0.969^{+0.029}_{-0.027}$	$0.973^{+0.039}_{-0.040}$
$\tau$	$0.084^{+0.046}_{-0.033}$	$0.085^{+0.041}_{-0.036}$	$0.085^{+0.034}_{-0.029}$	$0.082^{+0.050}_{-0.034}$
$t_0^{(*)}$	$13.87^{+0.78}_{-0.75}$	$14.04^{+0.77}_{-0.71}$	$13.58^{+0.99}_{-0.58}$	$13.62^{+0.098}_{-0.91}$
$\Omega_{de}^{(*)}$	$0.715^{+0.041}_{-0.037}$	$0.685^{+0.047}_{-0.043}$	$0.723^{+0.032}_{-0.044}$	$0.687^{+0.044}_{-0.052}$
$w_{de}$	-1	-1	$-1.04^{+0.17}_{-0.19}$	$-0.84^{+0.22}_{-0.22}$
$-\log L$	3865.11	3859.24	3865.05	3857.32

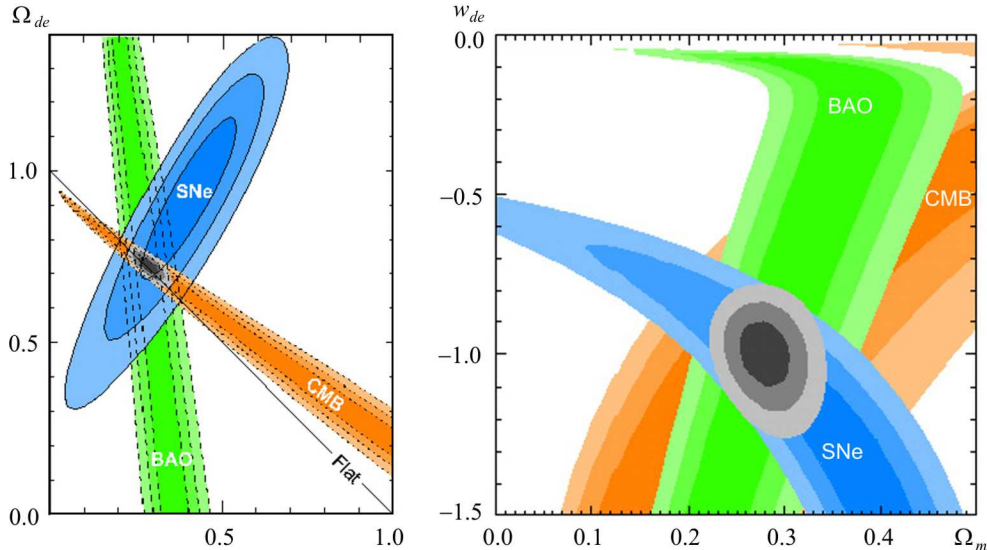


**Fig. 1.34.** Confidence level (68.3%, 95.4% and 99.7%) contours in  $\Omega_m - \Omega_\Lambda$  plane (left panel) and in  $\Omega_m - w_{de}$  plane (right panel) obtained from CMB, BAO and SN data alone as well as their combination (From [78])

on of this sound horizon onto the same degree-scale angle on the sky, as it follows from eqs. (1.33) and (1.37), can be realized in cosmologies with different combinations of  $H_0$ ,  $\Omega_b$ ,  $\Omega_K$ ,  $\Omega_m$ ,  $\Omega_{de}$  and  $w_{de}$ . But when we take into account the position and amplitude of other peaks and troughs, which have different dependences on cosmological parameters, the ranges of possible combination of parameters become narrow. Their dimensions, amounts and forms depend also on accuracy of observational data. So, the models with values of parameters which are inside the contour cannot be surely distinguished using only the measurements of primordial CMB power spectrum. Fortunately, for different techniques of dark energy parameter determination the contours or surfaces of equal likelihood or posterior have different orientations, prolateness and convolution in the parameter space (see Figs. 1.9, 1.11, 1.15, 1.19, 1.20, 1.28, 1.30), that give the possibility to break the degeneracies by using combined datasets for determinations of cosmological parameters. It also narrows the confidence ranges of main cosmological parameters and establishes the concordance model of the Universe.

Fig. 1.34 illustrates breaking of the degeneracies in  $\Omega_{de} - \Omega_m$  and  $w_{de} - \Omega_m$  marginalized likelihood distributions by using the combined dataset for determinations of cosmological parameters. There the Union compilation of SNe Ia [78], 5-year WMAP data [90] and BAO [141] have been used. In the left panel the density parameters  $\Omega_{de}$  and  $\Omega_m$  are constrained by the whole data set for the case of fixed EoS parameter  $w_{de} = -1$  ( $\Lambda$ CDM). The

best-fit values from combined dataset are as follows<sup>14</sup>:  $\Omega_{de} = 0.713 \pm 0.047$ ,  $\Omega_m = 0.285 \pm 0.022$  and  $\Omega_K = -0.009 \pm 0.0098$ . In the right panel the constraints are computed for flat models, there best-fit values of  $w_{de}$  and  $\Omega_m$  are  $-0.969 \pm 0.089$  and  $0.274 \pm 0.020$  correspondingly. These values somewhat differ from ones presented in Table 1.2, where we used the updated observational data (WMAP7 [93–95], SN SDSS [77], HST [231], SDSS LRG7 [163], BAO [143]). The main reason for difference of best-fit values of dark energy parameters consists in different datasets and different light-curve fitting in SNe Ia compilations, SALT method in Union compilation and MLCS2k2 method in SN SDSS one. Also, our  $1\sigma$  ranges are wider, since we present the extremal values of corresponding parameters in N-dimensional distributions.

The main advantage of combined analysis consists in the fact of existence of concordance model, which matches practically all cosmological and astrophysical observational data. This concordance model is dark energy dominated and close to flat  $\Lambda$ CDM one at current epoch. But small departure from standard  $\Lambda$ CDM allows existence of large number of alternative models, which include physical fields, fluids, generalized or modified gravity theories. In this section we analyzed only  $\Lambda$ CDM and  $w$ CDM models as simplest ones and showed the incontrovertible observational evidence for existence of dark energy.

### 1.9. Summary

The state-of-art observational evidence for existence of dark energy and methods of constraining of its parameters were discussed in this chapter. The list of independent indicators of dark energy developed during last decade in observational, data processing and theoretical aspects is as follows:

- luminosity distance — redshift relation for SNe Ia,
- luminosity distance — redshift relation for GRBs,
- angular diameter distance — redshift relation for CMB acoustic peaks,
- angular diameter distance — redshift relation for BAO peaks in matter density perturbations,
- angular diameter distance — redshift relation for X-ray clusters of galaxies,
- formation of the large scale structure of the Universe and its elements,
- cross-correlation of ISW anisotropy of CMB with large scale structure distribution of galaxies,
- weak gravitational lensing of CMB,
- age of the oldest stars of our Galaxy.

We have shown that each of from them prefers the dark energy dominated model for agreement of current physical models of objects with numerous accurate observational data on their luminosities, spectra, sizes, distances, ages

---

<sup>14</sup> Symmetrized errors include statistical and systematical ones (Table 6 in [78]) as root square from sum of their squares.

etc. We suppose that indirect but important argument for dark energy is existence of concordance model, in which all heterogeneous observational data are fitted well simultaneously. The determinations of dark energy parameter  $\Omega_{de}$  from different combinations of observable data give close values:  $\Omega_{de} = 0.69 \pm 0.05$  for WMAP7 + HST + BBN + SDSS LRG7 + SN SDSS MLCS2k2 dataset and  $\Omega_{de} = 0.72 \pm 0.04$  for WMAP7 + HST + BBN + SDSS LRG7 + SN SDSS SALT2 dataset. The EoS parameter is worse determined: its value considerably depends on prior assumptions and combinations of dataset and most determinations give its value in the interval  $(-1.2-0.8)$ . Its best-fit value is in the quintessence range ( $w_{de} = -0.84 \pm 0.22$ ) if dataset contains the SNe Ia distance moduli obtained with MLCS2k2 method of light-curve fitting and is in the phantom range ( $w_{de} = -1.04 \pm 0.18$ ) if used SNe Ia distance moduli are obtained with SALT2 one. Since they are out of  $1\sigma$ -range of each other one can conclude that some inconsistency or tension exists between fitters SALT2 and MLCS2k2.

In the next chapters we will discuss the different physical models of dark energy and their agreement with observational data presented in this chapter.

# 2

## CHAPTER

---

# SCALAR FIELD MODELS OF DARK ENERGY

---

### 2.1. Introduction

In this and next two chapters we analyze the different models of dark energy. Since the explanation of accelerated expansion of the Universe is out of standard models of matter and gravitation the three ways are to find it: the modifying of form of matter, the modifying of gravity, or both. The historical first one is modifying of gravity: Albert Einstein in 1917 [46] added the cosmological constant to the left part of General Relativity equations. But then the empty space is curved, that destroys the main conception of General relativity: the matter-energy causes the space curvature. On the other hand, then the gravity has two fundamental constants,  $G$  and  $\Lambda$ , which through the cosmological values  $H_0$ ,  $\rho_{cr}$  and  $\Omega_\Lambda$  can be expressed as  $G = 3H_0^2/(8\pi\rho_{cr})$  and  $\Lambda = 3H_0^2\Omega_\Lambda$ . Their numbers in units of  $c = 1$  are drastically different,  $G = 10^{13}$  cm/g and  $\Lambda = 10^{-56}$  cm<sup>-2</sup>, that has not found the physical interpretation. That is why physicists prefer to put  $\Lambda$  in the right hand side of General Relativity equations and interpret it as matter-energy component. There it also has not obtained suitable physical interpretation, but lead to the other problems, “fine tuning” and “cosmic coincidence” ones, which have no satisfactory physical explanations too. This is the first reason of existence of large number of alternatives to cosmological constant, in spite of that the cosmological models with  $\Lambda$  well match the observational data on dynamics of expansion and large scale structure of the Universe. The other reason is originated, in our opinion, by successes of inflation and particle physics theories. Indeed, if scalar field or inflaton existed in the very early Universe



and accelerated its expansion, then why cannot something like it exist later or now? Ratra and Peebles (1988) [35] and Wetterich (1988) [36] were first who analyzed the cosmological consequences of presence of scalar fields in the contemporary Universe. The active development of these ideas in the next years after discovery of accelerated expansion of the Universe in 1998 (see [37–44] and citing therein) has led to the current dark energy conception [24–34].

## 2.2. Cosmological constant as vacuum energy: ideas and problems

The physical interpretation of cosmological constant has long history. In 1968 Ya. Zeldovich [232] argued that the energy of zero oscillations of vacuum is Lorentz-invariant  $p_{vac} = -\rho_{vac}c^2$ , i.e. it is equivalent to the  $\Lambda$ -constant  $T_{\mu\nu}^{vac} = \Lambda g_{\mu\nu}$ . The importance of such identification can hardly be underestimated, since the existence of vacuum energy is indisputable in quantum mechanics and field theory, as it causes the observed inevitable natural broadening of spectral lines and Lamb shifts<sup>1</sup>. On the other hand, the General theory of relativity states, that all of existing kinds of energy are the sources of gravitational field and should be included as proper stress-energy tensors in the right-hand side of Einstein equations,  $G_{\mu\nu} = 8\pi G(T_{\mu\nu} + T_{\mu\nu}^{vac})$ . This means that  $\Lambda$ -constant should be introduced in order to take into account the gravitational action of the vacuum.

However, the explanation of numerical value of observable  $\Lambda$ -constant is complicated. Indeed, the value of energy of zero oscillations of vacuum can be estimated as follows [233]:

$$\rho_{vac} \propto \int_0^{k_{cut}} \sqrt{k^2 + m^2} k^2 dk \propto k_{cut}^4, \quad (2.1)$$

where  $k_{cut} \gg m$  is the ultraviolet limit, or the scale of spectrum cut-off, necessary for the finite value of vacuum energy to be obtained<sup>2</sup>. The most plausible scale for the cut-off is the Planck energy scale  $k_{cut} \propto M_{pl}$ , for which the value for the vacuum energy is  $\rho_{vac} \propto M_{pl}^4 \approx 10^{96} \text{ kg/m}^3$ . Such density exceeds the observable value of  $\Lambda$ -constant,  $\rho_{\Lambda} = 8\pi G\Lambda = 1.88 \times 10^{-26} \Omega_{\Lambda} h^2 \text{ kg/m}^3$ , by 123 orders and it is the main problem of such physical interpretation of  $\Lambda$ . Since the appropriate scale for cut-off,  $k_{cut} \propto M_X \approx 10^{-3} \text{ eV}$ , is impossible to obtain in the framework of existing particle physics theories, Zeldovich proposed the idea of ordering of polarized vacuum [232]. This is a vacuum represented as birth and annihilation of the same type pairs

<sup>1</sup> In 1955, Lamb was honored with Nobel prize for the discovery of shift in the structure of energy spectrum of Hydrogen atom. This shift is measured and predicted with accuracy as high as 11 digits. The theoretical prediction is based on the interactions of electrons with zero oscillations of electromagnetic field.

<sup>2</sup> In quantum electrodynamics the arbitrary large value of vacuum energy is eliminated by renormalization, though the absolute value (the finiteness) in this theory is not so fundamental as in the theory of gravitation.

of particle and antiparticle. The ordering implies the zero rest mass for particle-antiparticle pair, so only the energy of their gravitational interaction is left. For the particles of masses  $m$ , separated by the distance  $\lambda = \hbar/(mc)$ , one can evaluate the energy density of gravitation, and hence vacuum energy as  $\rho_{vac}c^2 \approx (Gm^2/\lambda)/\lambda^3 = Gm^6c^4/\hbar^4$ . The estimated value of vacuum energy is appropriate for the mass of pion, it is intermediate value between the mass of proton and electron. The result looks very promising, since the proper order of magnitude for vacuum energy is obtained, but at the same time the result is vague, since it has not found further development in particle physics, hence there is no additional grounding for it. Also the attempts were made to construct the observed value for  $\rho_\Lambda$  from the vacuum energy at Planck scales  $\rho_{vac} \propto 10^{96} \text{ kg/m}^3$  by multiplying by  $e^{-2/\alpha}$  [234], where  $\alpha = e^2/(\hbar c)$  is the fine structure constant, or by  $(M_{SUSY}/M_{pl})^8$  [235], where  $M_{SUSY} \simeq 10^3 \text{ GeV}$  is the energy scale of supersymmetry breaking at electro-weak interaction. Unfortunately, these attempts have failed to find the grounding too.

Another yet unsolved problem of vacuum energy is connected with the circumstances of its emergence. It is quite natural to suppose, that this energy is a remnant of processes taking places in the early Universe. Since the vacuum energy density does not vary during the expansion, at the moment of emergence it was by many orders smaller than the density of any other components of medium. The value of vacuum energy density should be fine-tuned in the early Universe to be of the same order as the matter density now. Moreover, the small variation of the value in the early Universe leads to the crucial consequences for the formation of its large scale structure in future.

So, three unresolved problems arise in the way of interpretation of cosmological constant as vacuum energy: its small value, fine tuning in the early Universe and strange coincidence of the value of its density with the matter density now (see also [236–239]). These problems, on one hand, stipulate us to reconsider our point of view on the nature of vacuum, and, on the other hand, enforce to search the alternative interpretation of  $\Lambda$ -constant. We suppose, that history of  $\Lambda$ -cosmology is not completed, since it is the simplest theory of dark energy from the mathematical point of view, matching well practically all observational data mentioned in the previous chapter.

### 2.3. Scalar fields as dark energy

Other radical alternative of explanation of accelerated expansion of the Universe consists in abandonment of cosmological constant, zeroing of vacuum energy<sup>3</sup> but introducing the scalar field  $\phi(a)$ , which smoothly (does not depend on spatial coordinates in the main order of its

<sup>3</sup>There are many hypothetical mechanism to do that in supersymmetry and string theories of particle physics. It is easier to build the theory which gives zero for energy of averaged vacuum state than such small that corresponds to dark energy density.

value) fills the Universe and satisfies some conditions. The simplest variants of such fields assume the minimal coupling with other matter-energy components of the Universe via gravitation only. Their physical properties are given by two functions: potential  $U(\phi)$  and Lagrangian density

$$\mathcal{L} = \mathcal{F}(X, U(\phi)), \quad (2.2)$$

where  $X \equiv \frac{1}{2}\phi_{;\mu}\phi^{;\mu}$  is kinetic term, which describes the rate of change of the field  $\phi$ . The covariant Euler–Lagrange equation, or variational principle applied to the action

$$S = \int \sqrt{-g}\mathcal{L}(X, U)d^4x, \quad (2.3)$$

gives the field equation of motion in the FRW metric ( $g$  is its determinant), which can be solved jointly with Friedmann equations (1.11)–(1.12). To do so, the energy density and stress or energy-momentum tensor of field must be defined.

The energy-momentum tensor of such field is as follows:

$$T_{\mu\nu} = \mathcal{L}_{,X}\phi_{;\mu}\phi_{;\nu} - g_{\mu\nu}\mathcal{L}. \quad (2.4)$$

It can be rewritten in the form of perfect fluid energy-momentum tensor

$$T_{\mu\nu} = (\rho_{de} + p_{de})u_{\mu}u_{\nu} - g_{\mu\nu}p_{de}$$

with energy density ( $T_0^0$ )

$$\rho_{de} = 2X\mathcal{L}_{,X} - \mathcal{L}, \quad (2.5)$$

pressure ( $T_i^i$ )

$$p_{de} = \mathcal{L} \quad (2.6)$$

and four-velocity  $u_{\mu} \equiv \phi_{;\mu}/\sqrt{2X} = (a, 0, 0, 0)$  in the comoving coordinates. The value of pressure, as a rule, is presented in the Friedmann equations by EoS parameter  $w_{de}$

$$p_{de} = w_{de}\rho_{de}, \quad (2.7)$$

which for the scalar field dark energy model should satisfy the equation

$$w_{de}(a) \equiv \frac{p_{de}(a)}{\rho_{de}(a)} = \frac{\mathcal{L}}{2X\mathcal{L}_{,X} - \mathcal{L}}. \quad (2.8)$$

It is a function of time and determination of character of its variation (monotonous, non-monotonous, increasing, decreasing or oscillating) and its evolution is crucial task for modern cosmology. Determining of the time-dependence of  $w_{de}(a)$  from observations gives evolution of dark energy density according to equations (1.8)–(1.9). This is enough for description of dynamics of expansion of the homogeneous Universe using Friedmann equations (1.11)–(1.12), but insufficient for understanding of field evolution as well as for including the scalar field in theory of the large scale structure formation.

Indeed, applying the Euler–Lagrange equation for action (2.2), or differential energy-momentum conservation law (1.4) for (2.4), we obtain the equation of motion for scalar field in the general form:

$$\left(\ddot{\phi} + 2aH\dot{\phi}\right) \mathcal{L}_{,X} - a^2 \frac{\partial U}{\partial \phi} \mathcal{L}_{,U} + \frac{\ddot{\phi}\dot{\phi}^2 - aH\dot{\phi}^3}{a^2} \mathcal{L}_{,XX} + \frac{\partial U}{\partial \phi} \dot{\phi}^2 \mathcal{L}_{,XU} = 0. \quad (2.9)$$

It can be solved jointly with Friedmann equations (1.11)–(1.12) for the specified functional form of Lagrangian  $\mathcal{L}(X, U)$  and potential  $U(\phi)$ .

On the other hand, Einstein equations and/or differential energy-momentum conservation law indicate, that such scalar field in contrast to vacuum dark energy cannot be perfectly smooth, it is perturbed by gravitational influence of matter-radiation inhomogeneities or has its own ones, generated in the early Universe. The equations for scalar field density and velocity perturbations, as we will see below, contain besides  $w_{de}$  two other values, so called effective sound speed  $c_s^2 = \delta p_{de}/\delta \rho_{de}$  and adiabatic one<sup>4</sup>  $c_a^2 = \dot{p}_{de}/\dot{\rho}_{de}$ . Note that in the case of scalar field dark energy the adiabatic sound speed is not the true velocity of sound propagation. The perturbed scalar field has non-negligible entropy and thus non-adiabatic pressure perturbations. In the dark energy rest frame the total pressure perturbation can be presented as  $\delta p_{de} = c_s^2 \delta \rho_{de}$  and the effective sound speed is defined for given Lagrangian as

$$c_s^2 \equiv \frac{\delta p}{\delta \rho} = \frac{p_{,X}}{\rho_{,X}} = \frac{\mathcal{L}_{,X}}{\mathcal{L}_{,X} + 2X\mathcal{L}_{,XX}}. \quad (2.10)$$

The adiabatic sound speed is not independent quantity, it is related to EoS parameter  $w_{de}$  by the differential equation

$$aw'_{de} = 3(1 + w_{de})(w_{de} - c_a^2). \quad (2.11)$$

It can be calculated for known  $w_{de}(a)$ , or, on contrary, used for solution of equation (2.11) for  $w_{de}(a)$  with defined  $c_a^2$ .

Therefore, in cosmology applications of scalar field models of dark energy the  $\Omega_{de}$ ,  $w_{de}(a)$  and  $c_s^2$  must be given or determined. In the previous chapter it was shown that  $\Omega_{de}$  and  $w_{de} = \text{const}$  are determined firmly by available observational data. The time variable  $w_{de}$  is less constrained and the effective sound speed estimations are very rough now [240–246]. Future observational programs are designed to achieve the 1 percent accuracy of their determination. But even then, as one can see from equations (2.2)–(2.10), the reconstruction or reverse engineering of potential and Lagrangian will be an ambiguous task.

---

<sup>4</sup> The terms “effective sound speed” and “adiabatic sound speed” of dark energy are used in the literature for designation of dark energy intrinsic values which formally correspond to thermodynamical ones.

In the case of functional forms of Lagrangian and potential given ad hoc the EoS parameter  $w_{de}$  and the effective sound speed  $c_s^2$  are defined by (2.8) and (2.10) correspondingly. Friedmann equations (1.11)–(1.12) together with (2.9) form the closed set of equations for determination of the evolution of  $a$  and  $\phi$ . Together with the set of equations for evolution of metric, density and velocity perturbations for all components it gives the possibility to test different scalar fields as dark energy and determine their intrinsic parameters by comparison the model-predicted characteristics of the Universe with observational data. It is one of the ways of intensive investigations of dark energy since its discovery. Another one consists in defining of some functional forms for  $w_{de}(a)$  and  $c_s^2(a)$  and search for the corresponding forms of Lagrangians and potentials. The third one is combined – definition of functional forms of  $w_{de}(a)$  and  $\mathcal{L}(X, U)$ , giving the possibility to calculate  $c_s^2(a)$  and reconstruct  $U(\phi)$ . We will not discuss the advantages and imperfections of different approaches, each of them is useful for its specific aspects, but in the next sections we will use the combined one to analyze the possibility to distinguish different scalar field models of dark energy.

## 2.4. Scalar perturbations of the scalar field and other components

In the subsection 1.5.1 it was shown that the rate of growth of matter density perturbations is sensitive to the value of smoothed density of dark energy ( $\Omega_{de}$ ) and tempo of its change in the past via  $w_{de}$ . It affects strongly the ratio of amplitudes of matter power spectrum at different redshifts. Other possible fingerprints of dark energy in the matter power spectrum are related to the gravitational interplay of density perturbations in both components.

Let us consider the two-component model with matter and dark energy in the terms of their energy densities, pressures and four-velocities. For derivation of the evolution equations for scalar linear perturbations it is convenient to use the conformal Newtonian gauge with space-time metric

$$ds^2 = a^2(\eta)[(1 + 2\Psi(\mathbf{x}, \eta))d\eta^2 - (1 + 2\Phi(\mathbf{x}, \eta))\delta_{\alpha\beta}dx^\alpha dx^\beta],$$

where  $\Psi(\mathbf{x}, \eta)$  and  $\Phi(\mathbf{x}, \eta)$  are gauge-invariant metric perturbations called Bardeen's potentials [115], which in the case of zero proper anisotropy of medium (as for the dust matter and scalar fields) have equal absolute values and opposite signs:  $\Psi(\mathbf{x}, \eta) = -\Phi(\mathbf{x}, \eta)$  [247].

The perturbations in the energy density  $\rho_{de}$ , pressure  $p_{de}$  and the four-velocity  $u_{(de)}^\mu$  of dark energy are defined in the following way:

$$\begin{aligned}\rho_{de}(\eta, \mathbf{x}) &= \bar{\rho}_{de}(\eta) + \delta\rho_{de}(\eta, \mathbf{x}) = \bar{\rho}_{de}(\eta)(1 + \delta_{de}(\eta, \mathbf{x})), \\ p_{de}(\eta, \mathbf{x}) &= \bar{p}_{de}(\eta) + \delta p_{de}(\eta, \mathbf{x}) = \bar{p}_{de}(\eta)(1 + \pi_{de}(\eta, \mathbf{x})), \\ u_{(de)}^\mu &= \bar{u}_{(de)}^\mu + \delta u_{(de)}^\mu,\end{aligned}$$

where  $\bar{\rho}_{de}(\eta)$ ,  $\bar{p}_{de}(\eta)$  and  $\bar{u}_{\mu(de)} = (-a, 0, 0, 0)$  are the unperturbed background values of energy density, pressure and four-velocity in the world with FRW line element (1.1), respectively. Since  $u_{(de)}^{\mu} u_{\mu(de)} = -1$ , it turns out that  $a^{-1} \delta u_{0(de)} = a \delta u_{(de)}^0 = -\Psi$ . In the case of scalar mode of perturbations the spatial part of the four-velocity  $\delta u_{(de)}^i$  can be expressed as a gradient of some scalar function  $V(\eta, \mathbf{x})$

$$\delta u_{(de)}^i = g^{ij} V_{,j}. \quad (2.12)$$

For scalar fields the entropy perturbations are inherent and cause in addition to the adiabatic pressure perturbations, which follow from the variation of (2.7), the non-adiabatic pressure ones  $\delta p_{de}^{(nad)}$ , so the total perturbation is their sum [240–254]:

$$\delta p_{de} = c_a^2 \delta \rho_{de} + \delta p_{de}^{(nad)}.$$

The intrinsic entropy  $\Gamma_{de}$  is defined by non-adiabatic part of pressure as

$$\Gamma_{de} = \pi_{de} - \frac{c_a^2}{w_{de}} \delta_{de},$$

and in the variables of conformal-Newtonian gauge equals [240, 242, 248, 249]

$$\Gamma_{de} = \frac{c_s^2 - c_a^2}{w_{de}} \left( \delta_{de} + 3aH(1 + w_{de}) \frac{V_{de}}{k} \right).$$

So, the relative perturbation of dark energy pressure is

$$\pi_{de} = \frac{c_s^2}{w_{de}} \delta_{de} + 3aH(c_s^2 - c_a^2) \frac{1 + w_{de}}{w_{de}} \frac{V_{de}}{k}. \quad (2.13)$$

In the rest frame of dark energy ( $V_{de} = \delta\phi = 0$ ) it can be presented as

$$\pi_{de} = \frac{c_s^2}{w_{de}} \delta_{de},$$

where the effective (rest-frame) sound speed  $c_s^2$  for the scalar field with given Lagrangian can be calculated according to (2.10).

The perturbations are supposed to be small ( $|\Phi| \sim |\Psi| \sim |\delta_{de}| \sim |\pi_{de}| \sim |V_{de}| \ll 1$ ), henceforth all following equations are linearized with respect to the perturbed variables. In the linear perturbation theory it is convenient to perform the Fourier transformation of all spatially-dependent variables, so the equations are written for the corresponding Fourier amplitudes of the metric ( $\Psi(k, \eta)$ ), dark energy density  $\delta_{de}(k, \eta)$ , pressure  $\pi_{de}(k, \eta)$  and velocity  $V_{de}(k, \eta)$  perturbations (here  $k$  is wave number). These variables are gauge-invariant [115, 130, 247].

Since we suppose the minimal coupling between dark energy and matter, then from the differential conservation law  $T_{\nu;\mu}^{\mu}(de) = 0$  we obtain the equations for evolution of density and velocity perturbations of dark energy:

$$\begin{aligned} & \dot{\delta}_{de} - 3aH(w - c_s^2)\delta_{de} + \\ & + (1 + w_{de}) \left\{ [k^2 + 9a^2H^2(c_s^2 - c_a^2)] \frac{V_{de}}{k} - 3\dot{\Psi} \right\} = 0, \quad (2.14) \\ & \dot{V}_{de} + aH(1 - 3c_s^2)V_{de} - \frac{c_s^2k}{1 + w_{de}}\delta_{de} - k\Psi = 0. \end{aligned}$$

By the same way the equations for evolution of density and velocity perturbations can be obtained of cold dark matter, which is pressureless,  $p_{dm} = \pi_{dm} = 0$ , perfect fluid. So, they can be easily deduced from (2.14) by assuming  $w_{dm} = c_{a(dm)}^2 = c_{s(dm)}^2 = 0$  and re-denoting corresponding values:

$$\dot{\delta}_{dm} + kV_{dm} - 3\dot{\Psi} = 0, \quad (2.15)$$

$$\dot{V}_{dm} + aHV_{dm} - k\Psi = 0. \quad (2.16)$$

The Einstein equations for scalar metric and energy-momentum tensor perturbations,

$$\delta R_{\nu}^{\mu} - \frac{1}{2}\delta_{\nu}^{\mu}\delta R = 4\pi G \left( \delta T_{\nu}^{\mu}(dm) + \delta T_{\nu}^{\mu}(de) \right),$$

where  $\delta R_{\nu}^{\mu}$  and  $\delta R$  are perturbed parts of Ricci tensor and scalar curvature of four-space correspondingly, complete the system of equations (2.14)–(2.16) by equations for evolution of gravitational potential. One of them is as follows:

$$\dot{\Psi} + aH\Psi - \frac{4\pi G a^2}{k} (\rho_{dm}V_{dm} + \rho_{de}(1 + w_{de})V_{de}) = 0, \quad (2.17)$$

The system of 5 linear differential equations (2.14)–(2.17) for 5 unknown functions  $\delta_{de}$ ,  $V_{de}$ ,  $\delta_{dm}$ ,  $V_{dm}$  and  $\Psi$  is closed and can be solved for given initial conditions. In the first and this chapters we assume adiabatic initial conditions for perturbations of dark matter, baryons and relativistic components. At the beginning of matter dominated era, when density of relativistic components vanishes and dark energy is subdominant, in the limit  $\Omega_r$  and  $\Omega_{de} \rightarrow 0$  the growing solution (growth mode) of equations (2.15)–(2.17) is as follows:

$$\Psi = \text{const}, \quad \delta_{dm} = -(2 + k^2\eta^2/6)\Psi, \quad V_{dm} = k\eta\Psi/3$$

(for more details see [130]). Putting some small value  $\Psi_{init}$  at  $\eta_{init} \ll k^{-1}$  we obtain the adiabatic initial conditions for the dark matter component:

$$\delta_{dm}^{init} = -2\Psi_{init}, \quad V_{dm}^{init} = k\eta_{init}\Psi_{init}/3. \quad (2.18)$$

Assuming that dark energy is subdominant in the early Universe and  $w_{de}$ ,  $c_s^2$ ,  $c_a^2$  are constant one can solve the equations (2.14) for  $\Psi = \text{const}$  and for superhorizon scale of perturbations ( $k\eta \ll 1$ ) obtaining the initial conditions for density and velocity perturbations of dark energy:

$$\delta_{de}^{init} = -6 \frac{(1 + w_{de})(c_a^2 - c_s^2)}{(3 - 2c_s^2)(w_{de} - c_s^2)} \Psi_{init}, \quad V_{de}^{init} = k\eta_{init} \Psi_{init} / (3 - 2c_s^2). \quad (2.19)$$

The equations (2.15)–(2.17) with initial conditions (2.18)–(2.19) have been used for analysis of mutual influence of perturbations in two-component Universe with scalar field dark energy with different Lagrangians [131, 255–257]. The same equations (2.15)–(2.17) have been used recently in [246] for analysis of effect of dark energy perturbations on dark matter ones in scalar field models with generalization of kinetic term of classical Lagrangian, but, unfortunately, there the initial conditions for both components are not specified. In these papers it has been shown that scalar fields with evolving  $w_{de}$  and  $c_s^2$  affect distinctly on the power spectrum of matter density perturbations at subhorizon scales.

Therefore, the dark energy perturbations must be included in complete theory of cosmological perturbations which is used for determinations of cosmological parameters from CMB anisotropy and large scale structure data. The Einstein–Boltzmann equations for scalar perturbations in multicomponent Universe (cold dark matter, baryons, photons and neutrinos), in which all important physical processes at different epochs have been taken into account, are presented in the paper [116]. They are the base for publicly available codes CMBFAST [117, 118], CMBEasy [119], CAMB [120, 121] and CLASS [122–124], designed for integration of Einstein–Boltzmann equations and accurate computation of power spectra of CMB anisotropy and matter density perturbations for different cosmologies. The most advanced and widely used in cosmological applications is CAMB code which gives possibility to include also different models of dark energy and is supplied as part of the CosmoMC parameter estimation package. There the Einstein–Boltzmann equations in synchronous gauge are integrated. Since this code will be used below we present here the evolution equations (2.15)–(2.17) and initial conditions (2.18)–(2.19) in synchronous gauge too.

In the synchronous gauge the line element in 4-space with flat 3-space is as follows:

$$ds^2 = g_{\mu\nu} dx^\mu dx^\nu = a^2(\eta)(-d\eta^2 + (\delta_{ij} + h_{ij})dx^i dx^j), \quad (2.20)$$

where  $h_{ij}(\eta, \mathbf{x})$  is metric perturbations. The scalar perturbations of metric  $h_{ij}$  can be decomposed into the trace  $h \equiv h_i^i$  and traceless  $\tilde{h}_{ij}$  components as  $h_{ij} = h\delta_{ij}/3 + \tilde{h}_{ij}$ . As above, the perturbations are supposed to be small



( $h \ll 1$ ), so, all following equations containing  $h$  are linearized with respect to the metric and matter-energy perturbed variables. In the multicomponent fluid each component moves with a small peculiar velocity  $V^i = dx^i/d\eta$ , defined by its intrinsic properties (density, pressure, entropy etc.), gravitational potential  $h$  and initial conditions. At the linear stage of evolution of perturbations the cold dark matter (CDM) component is a pressureless perfect fluid interacting with other components only via gravity. Therefore, the synchronous coordinates are usually defined as comoving to the particles of CDM:  $V_{cdm} = 0$ . The evolution equations for dark energy perturbations can be deduced by the same way as in conformal Newtonian gauge or by gauge transformations  $x_{(con)}^\mu \rightarrow x_{(syn)}^\mu + \xi^\mu$  which transform  $g_{\mu\nu}^{(con)} \rightarrow g_{\mu\nu}^{(syn)}$  keeping  $ds^2$  as invariant.

Both ways lead to the equations for evolution of density and velocity perturbations of dark energy and cold dark matter as well as metric perturbations in synchronous gauge as follows:

$$\begin{aligned} & \dot{\delta}_{de} + 3(c_s^2 - w_{de})aH\delta_{de} + \\ & + (1 + w_{de})\frac{\dot{h}}{2} + (1 + w_{de}) [k^2 + 9a^2H^2(c_s^2 - c_a^2)] \frac{V_{de}}{k} = 0, \end{aligned} \quad (2.21)$$

$$\dot{V}_{de} + aH(1 - 3c_s^2)V_{de} - \frac{c_s^2 k}{1 + w_{de}}\delta_{de} = 0, \quad (2.22)$$

$$\dot{\delta}_{dm} + \frac{\dot{h}}{2} = 0, \quad (2.23)$$

$$V_{dm} = 0, \quad (2.24)$$

$$\begin{aligned} & (aH\dot{h}) - 8\pi Ga^2 [\rho_{dm}a (a^{-1}\delta_{dm}) + \\ & + \rho_{de} (\dot{\delta}_{de} - aH(1 + 3w_{de})\delta_{de} - kV_{de})] = 0. \end{aligned} \quad (2.25)$$

The adiabatic initial conditions for dark matter and subdominant dark energy are:

$$\begin{aligned} \delta_{de}^{init} &= -\frac{(4 - 3c_s^2)(1 + w_{de})}{8 + 6c_s^2 - 12w_{de} + 9c_s^2(w_{de} - c_a^2)} h_{init}, \\ V_{de}^{init} &= -\frac{c_s^2 k \eta_{init}}{8 + 6c_s^2 - 12w_{de} + 9c_s^2(w_{de} - c_a^2)} h_{init}, \\ \delta_{dm}^{init} &= -\frac{1}{2} h_{init}, \\ V_{dm}^{init} &= 0. \end{aligned} \quad (2.26)$$

The character of evolution of scalar field density perturbations depends on the temporal behavior of EoS parameter, adiabatic and effective sound speeds, which can be defined or deduced for specified  $\mathcal{L}(X, U)$  and  $U(\phi)$ .

The evolution of dark energy perturbations can be analyzed also in the terms of perturbations of field variable

$$\phi(\eta, \mathbf{x}) = \bar{\phi}(\eta) + \delta\phi(\eta, \mathbf{x}),$$

where it is supposed that the perturbation amplitude is small,  $|\delta\phi| \ll |\phi|$ , henceforth all following equations can be linearized with respect to  $\delta\phi$  and its derivatives. Substituting it into (2.4), using the differential conservation law  $T_{0(de);\mu}^\mu = 0$  and taking into account (2.9) one can obtain the second order linear differential equation for  $\delta\phi$ , with coefficients comprising  $H$ ,  $w_{de}$ ,  $c_s^2$ ,  $c_a^2$ ,  $\mathcal{L}_{,X}$ ,  $\mathcal{L}_{,U}U_{,\phi}$  etc. and free term with metric perturbations. The density, pressure and velocity perturbations of dark energy, which are necessary to write the free term in equations for metric perturbations (2.17), are related with  $\delta\phi$  by relationships:

$$\delta\rho_{de} = \left(\dot{\bar{\phi}}\delta\dot{\phi} - \Psi\dot{\bar{\phi}}^2\right) \left(\frac{\partial\mathcal{L}}{\partial X} + 2X\frac{\partial^2\mathcal{L}}{\partial X^2}\right) - \left(\frac{\partial\mathcal{L}}{\partial U}\frac{\partial U}{\partial\phi} - 2X\frac{\partial^2\mathcal{L}}{\partial X\partial U}\frac{dU}{d\phi}\right) \delta\phi, \quad (2.27)$$

$$\delta p_{de} = \left(\dot{\bar{\phi}}\delta\dot{\phi} - \Psi\dot{\bar{\phi}}^2\right) \frac{\partial\mathcal{L}}{\partial X} + \frac{\partial\mathcal{L}}{\partial U}\frac{\partial U}{\partial\phi}\delta\phi, \quad (2.28)$$

$$V_{de} = \frac{k\delta\phi}{\dot{\bar{\phi}}}. \quad (2.29)$$

They can be used also for definition of the initial conditions  $\delta\phi_{init}$  and  $\dot{\delta\phi}_{init}$  from (2.19).

Presented in this section evolution equations for homogeneous and perturbed scalar field are used for interpretation of observational data on dynamics of expansion and large scale structure formation in the MD and DED epochs. For interpretation of CMB anisotropy data the equations (2.14) or (2.21)–(2.22) as well as corresponding initial conditions must be included in the Einstein-Boltzmann code, CAMB for example.

## 2.5. Specifying the scalar-field models of dark energy

The scalar field model of dark energy should be specified for cosmological applications by definition of Lagrangian and potential or dependences of EoS parameter and effective sound speed on scale factor (redshift or time). In this section we list some of them, most widely used in the literature.

### 2.5.1. Lagrangian

The Lagrangians used for specifying the scalar field dark energy models are as follows:

canonical or classical Lagrangian [258–268]

$$\mathcal{L} = X - U(\phi), \quad (2.30)$$

non-canonical Dirac-Born-Infeld one [269–278], which is relativistic generalization of classical Lagrangian,

$$\mathcal{L} = -U(\phi)\sqrt{1 - 2X}, \quad (2.31)$$

classical Lagrangian with opposite sign of kinetic term [51, 279–284]

$$\mathcal{L} = -X - U(\phi), \quad (2.32)$$

canonical form of Lagrangian with generalization of kinetic term in the form some function  $F(X)$  [246]

$$\mathcal{L} = F(X) - U(\phi), \quad (2.33)$$

non-canonical form of Lagrangian with non-canonical kinetic term [285–291]

$$\mathcal{L}(\phi, \phi_{;\nu}\phi^{;\nu}, U(\phi)), \quad (2.34)$$

two-field Lagrangians of canonical or non-canonical form with canonical or non-canonical kinetic terms

$$\mathcal{L}(F(\phi, \phi_{;\nu}, \phi_{;\mu}\phi^{;\mu}), U(\phi); F(\psi, \psi_{;\nu}, \psi_{;\mu}\psi^{;\mu}), U(\psi)). \quad (2.35)$$

In the case of the additional coupling of dark energy with other component(s) the Lagrangian contains the additional term(s), describing this non-gravitational interaction(s). The limit of generalization of functional forms of Lagrangians does not exist, it is only restricted by fantasia and technical possibilities of researches.

### 2.5.2. Potential

As it follows from (2.8) and (2.10), for definition of  $w_{de}$  and  $c_s^2$  the potential in Lagrangian must be given too. For different types of Lagrangians the different potentials are studied. The scalar fields with canonical Lagrangian (2.30) have the simplest and best studied equation of motion (2.9),

$$\ddot{\phi} + 2aH\dot{\phi} + a^2\frac{dU}{d\phi} = 0. \quad (2.36)$$

called Klein—Gordon one. They were called by Steinhardt and Caldwell [9, 292] the “quintessence”. The large number of potentials, motivated by particle physics beyond the standard model, have been used to probe the scalar field as dark energy. They should satisfy the condition  $U > a^{-2}\dot{\phi}^2$ , where  $\phi$  is solution of (2.36), in order to have  $w_{de} < -1/3$  near the current epoch. Other conditions for scalar field potentials follows from the requirement that the energy density of the scalar field should be significantly less than that of radiation and dark matter during RD epoch  $U(z < z_{dec}) \ll \rho_\gamma - \dot{\phi}^2/2$ , provide long enough MD epoch to allow galaxies to form which requires  $U(z < 1) \ll \rho_{dm} - \dot{\phi}^2/2$  and accelerate the expansion now, that requires  $U(z \approx 0) \approx 3.3\rho_{dm} - \dot{\phi}^2/2$  now.

We present here the list of some functional forms of potentials, which elucidate the main properties of scalar field models of dark energy with canonical Lagrangian:

the power-law potential, often used in particle physics ([233] and citing therein)

$$U = M^{4-n}\phi^n \quad \text{with } n > 0, \quad (2.37)$$

the power-law tracker potential used in SUSY [293, 294] and supergravity [41, 44] theories

$$U = M^{4+n}\phi^{-n} \quad \text{with } n > 0, \quad (2.38)$$

the polynomial form of potential

$$U = \sum_n a_n \phi^n, \quad (2.39)$$

the exponential potential used for moduli or dilaton fields [295, 296]

$$U = M^4 \exp(-\beta\phi/M_p), \quad (2.40)$$

the exponential tracker field potential

$$U = M^4 \exp(M_p/\phi), \quad (2.41)$$

the combined power-law and exponential tracker potential used also in SUSY [293, 294] and supergravity [41, 44] theories

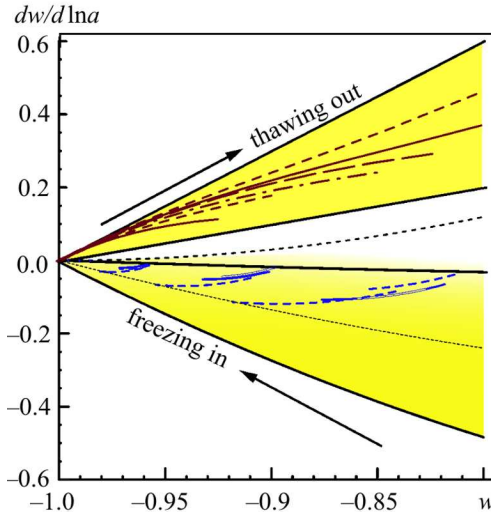
$$U = M^{4+n}\phi^{-n} \exp(\alpha\phi^2/M_p^2), \quad (2.42)$$

the potential used for presenting pseudo-Nambu-Goldstone boson (PNGB) [297] and some type of axions

$$U = M^4 \cos^2(\phi/2f) \dots \quad (2.43)$$

Here  $M_p$  is Planck mass, other values —  $n$ ,  $M$ ,  $a_n$ ,  $\alpha$ ,  $\beta$ ,  $f$  — are parameters of scalar field which need the definition or determination to match the observational data on dynamics of expansion of the Universe.

**Fig. 2.1.** Classes of quintessence scalar fields ( $w_{de}(a) > -1$ ), freezing ( $w'_{de} < 0$ ) and thawing ( $w'_{de} > 0$ ) ones, in the phase plane  $w_{de}(a) - w'_{de}(a)$  [298]. Black solid lines show the boundaries of these classes in the phase space, the short-dashed line shows the boundary between field evolution accelerating and decelerating down the potential (see for details [298]). The solid, dashed, dotted and dash-dotted lines show evolutionary tracks of scalar fields with potentials (2.37)–(2.43). The arrows show the direction of evolution from beginning ( $a = 0$ : right-most points for freezing and left-most points for thawing scalar fields) to current epoch ( $a = 1$ : left-most points for freezing and right-most points for thawing scalar fields) (From [298])



Presented list of potentials is far incomplete but spectrum of scalar field properties for them is wide enough that to allow the possibility to classify them as “freezing models” and “thawing” models [298]. In the class of freezing models the fields were rolling along the potentials in the past, but their movements gradually slow down after the system enters the phase of cosmic acceleration and freeze out at the minimum of potential at finite  $\phi$  or at infinity of field variable when minimum of potential is absent. The EoS parameters  $w_{de}$  of such fields can start from any value  $> -1$  and go to  $-1$  at the freezing stage. On contrary, in the class of thawing models the fields have been frozen by Hubble friction (term  $2aH\dot{\phi}$  in (2.36)) until recently and then start to evolve with increasing  $w_{de}$ . In this models  $w_{de} \approx -1$  at the early epochs and  $-1 < w_{de} < -1/3$  now.

These classes of quintessence scalar fields are separated in the phase plane  $w_{de}(a) - w'_{de}(a)$  (shown in Fig. 2.1). The evolutionary tracks of scalar fields with potentials (2.37)–(2.43) are shown there too. The freezing models with potentials (2.38) and (2.42) are shown there by solid and dashed lines correspondingly. The thawing ones in this figure are represented by potentials (2.37) and (2.43). The evolutionary track for field with potential (2.43) is shown by solid line and for field with potential (2.37) by short-, dot-, and long-dashed ones for  $n = 1, 2, 4$  correspondingly. All scalar fields shown there have at current epoch  $-1 < w_{de} < -0.8$  and  $\Omega_{de} \approx 0.7$ , so, they can be considered as real candidates for the dark energy.

Unfortunately, for Lagrangians other than canonical one we have no such intensive analysis of scalar fields. Maybe in the nearest future this lack will be removed.

### 2.5.3. EoS parameter

Another way of specifying of scalar field model of dark energy consists in assumption about the dependence of EoS parameter  $w_{de}$  on the scale factor  $a$ . It can be made in *ad hoc* manner or by solution of equations that implement the defined field properties.

**Ad hoc setting of  $w_{de}(a)$ .** Traditional approach is to present  $w_{de}$  in the form

$$w_{de}(a) = \sum_n w_n f_n(a),$$

where  $w_n$  is a parameter and  $f_n(a)$  some simple function of scale factor  $a$ . Let us list used in the literature function forms for  $w_{de}(a)$  ordered by the number of their parameters.

i) *One-parametric EoS.* Appears in the models with  $w_{de} = \text{const}$ . They are the simplest and best studied models of dark energy scalar field. This parameter is constrained by majority of observational data, though the accuracy of determination of its best-fit value is too low,  $\sim 15\text{--}25\%$ , while the density parameter  $\Omega_{de}$  is determined with accuracy  $\sim 5\%$  (see Chapter 1). The best-fit value of constant  $w_{de}$  for the most determinations is in the range  $(-1.2, -0.8)$ . In these models  $c_a^2 = w_{de}$ , but  $c_s^2$  must be defined additionally by definition of either Lagrangian or itself in *ad hoc* manner. Similarly to the simplest models the  $w_{de} = \text{const}$ -models are very specific. For example, in the case of scalar field with classical Lagrangian (2.30)

$$X = \frac{1 + w_{de}}{1 - w_{de}} U, \quad U = \frac{1 - w_{de}}{2} \rho_{de}, \quad c_s^2 = 1,$$

in the case of scalar field with Dirac–Born–Infeld one (2.31)

$$X = \frac{1 + w_{de}}{2}, \quad U = \sqrt{-w_{de}} \rho_{de}, \quad c_s^2 = -w_{de},$$

and so on, this can be deduced using equation (2.8). The evolution of energy density and deceleration parameter for  $w$ CDM models with parameters from Table 1.2 are shown in Fig. 2.2. The evolution of deceleration parameters in both models is similar, they differ slightly by value of  $q$  at current epoch  $q_0 = \Omega_m + (1 + 3w_{de})\Omega_{de}$  (in the model with  $w_{de} = -0.84$   $q_0 = -0.4$ , in the models with  $w_{de} = -1.04$   $q_0 = -0.62$ ) and asymptotic value at  $a \rightarrow \infty$ :  $q_\infty = (1 + 3w_{de})/2$  ( $-0.76$  for  $w_{de} = -0.84$  and  $-1.06$  for  $w_{de} = -1.04$ ). The energy density evolution for these models is quite different: it decreases from  $\infty$  at  $a = 0$  to 0 when  $a \rightarrow \infty$  in scalar field model with  $w_{de} = -0.84$  and increases from 0 at  $a = 0$  to  $\infty$  when  $a \rightarrow \infty$  in scalar field model with  $w_{de} = -1.04$ . The first is quintessence scalar field, the second is phantom [51] one.

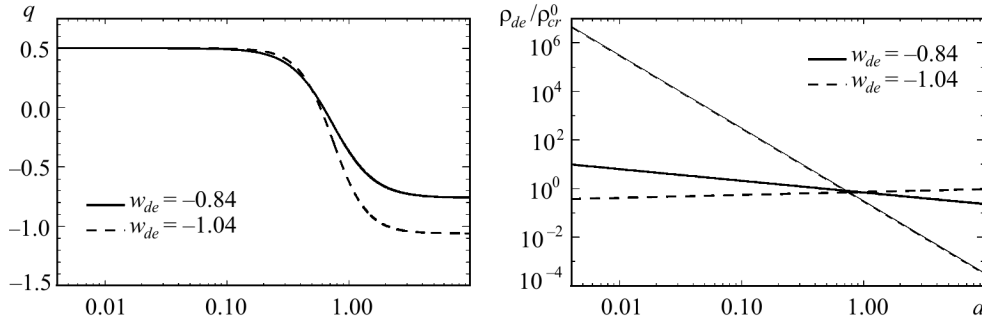


**Fig. 2.2.** The evolution of deceleration parameter  $q$  (left panel) and energy density  $\rho_{de}$  in units of critical one at current moment (right panel) in the models with parameters of  $w$ CDM models from Table 1.2 (dataset 1 – dashed line, dataset 2 – solid line). The dark matter density evolution for both models is shown for comparison by thin lines (superimposed), which go from the upper left to lower right corner

ii) *Two-parametric EoS.* The simplest approximation for time-variable EoS parameter, which is widely used,

$$w_{de}(a) = w_0 + (1 - a)w_a, \quad (2.44)$$

was proposed by Chevallier, Polarski and Linder [299, 300], called in the literature the CPL one. Here,  $w_0$  and  $w_a$  denote the present values of  $w_{de}$  and its first derivative with respect to  $a$  with opposite sign<sup>5</sup> respectively. The determination of them in [94] on the base of WMAP7 + BAO + SN data gives  $w_0 = -0.93 \pm 0.12$ ,  $w_a = -0.41 \pm 0.72$ . The dependence (2.44) with these parameters is shown in Fig. 2.3 (CPL K11) in the range  $0.001 \leq a \leq 10$ . Such dark energy evolves from the field with  $w = w_0 + w_a = -1.34$  at the early epoch ( $a = 0$ ) to  $w = w_0 = -0.93$  at the current one ( $a = 1$ ) which will increase in future. The evolution of deceleration parameter for the same range of  $a$  is shown in Fig. 2.4 (left panel). Its energy density increases from zero to  $\sim 1.25\rho_{de}^{(0)}$  at  $a \approx 0.83$  and decreases asymptotically to

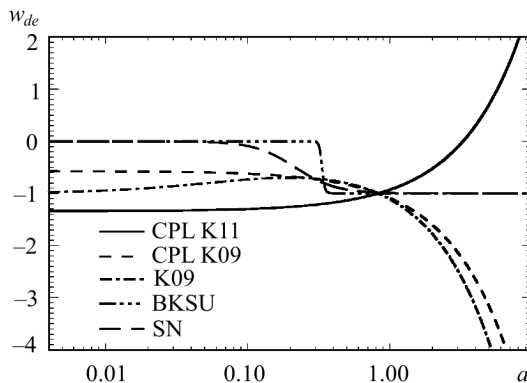


**Fig. 2.3.** Time dependences of EoS parameter for different parametrizations: CPL with parameters determined in [94] (CPL K11), CPL with parameters determined in [91] (CPL K09)

<sup>5</sup> It is first derivative with respect to  $z$  at the current epoch  $z = 0$ .

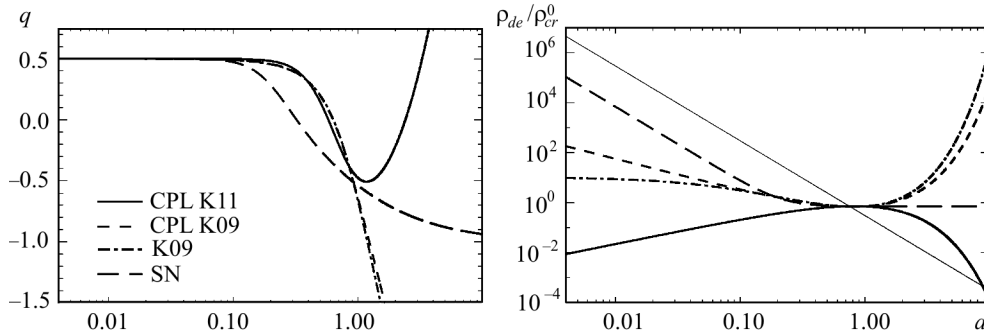


**Fig. 2.4.** The evolution of deceleration parameter  $q$  (left panel) and energy density  $\rho_{de}$  in units of critical one at current moment (right panel) in the models with different parametrizations of EoS parameter: CPL with parameters determined in [94] (CPL K11), CPL with parameters determined in [91] (CPL K09). The dark matter density evolution for all models is shown for comparison by thin lines (superimposed), going from the upper left to lower right corner

zero after that according to (1.8) with effective EoS parameter

$$\tilde{w}_{de} = w_0 + w_a \frac{1 - a + \ln a}{\ln a},$$

which goes to  $+\infty$  or  $-\infty$  depending on sign of  $w_a$  when  $a \rightarrow +\infty$  (Fig. 2.4, right panel).

The previous determination of these parameters by [91] using similar but older datasets gave  $w_0 = -1.09 \pm 0.12$ ,  $w_a = 0.52 \pm 0.46$  (Fig. 2.3, CPL K09). It means that in this case the dark energy evolves from quintessential field with  $w = -0.57$  at the early epoch to the phantom one at current epoch with  $w = -1.09$ . Its density decreases at early epoch, achieves the minimal value of  $\sim 0.83\rho_{de}^{(0)}$  at the same scale factor  $a \approx 0.83$  and grows later. The evolution of deceleration parameter and energy density is shown in Fig. 2.4 by lines marked as CPL K09.

One can see, that  $w_{de}$ ,  $q$  and  $\rho_{de}$  diverge asymptotically at  $a > 1$ , therefore, such models of dark energy are not usable for prediction of future dynamics of expansion of the Universe. It is objection to this parametrization.

Another form of  $w_{de}$  parametrization,

$$w_{de}(a) = w_0 + w_1 z = w_0 + w_1 \frac{1 - a}{a},$$

has been proposed and used in [301] for analysis of possibility to discriminate models with constant and time-varying EoS parameters on the base of SNe data. It has, however, essential disadvantage: it can be used only for low- $z$  cosmology, since it diverges at high  $z$ .



iii) *Three-parametric EoS*. Recently this form has been modified by [91] in order to bring the behavior of dynamical dark energy at early epoch closer to that of  $\Lambda$ -term:

$$w_{de}(a) = \frac{a}{a + a_{trans}} [w_0 + (1 - a)w_a] - \frac{a_{trans}}{a + a_{trans}}, \quad (2.45)$$

This approximation has the additional third parameter  $a_{tran}$  which, however, is weakly constrained by observations. One can see, that at the early epoch when  $a \ll a_{tran}$   $w_{de} \approx -1$  and has explicit asymptotic behavior  $a \rightarrow 0$   $w_{de} \rightarrow -1$ . At  $a \gg a_{trans}$  this parametrization becomes the CPL one. It also has the analytical form of effective equation of state,  $\tilde{w}_{de}(a)$ , which gives the evolution of dark energy density and deceleration parameter:

$$\tilde{w}_{de}(a) = -1 + \frac{1 - a}{\ln a} w_a + \frac{1 + w_0 + (1 + a_{trans})w_a}{\ln a} \ln \frac{a + a_{trans}}{1 + a_{trans}}.$$

The values of parameters in (2.45) have been determined in [91] for  $a_{trans} = 10$  and are as follows:  $w_0 = -1.12 \pm 0.13$ ,  $w_a = 0.70 \pm 0.53$ . The  $a$ -dependences of  $w_{de}$ ,  $q$  and  $\rho_{de}$  with them are presented in Figs. 2.3–2.4. One can see, that this parametrization meets the same objection as CPL one: prediction of future dynamics of expansion of the Universe is doubtful. The other objection is restriction of properties of scalar field in the early Universe: it supposes that scalar field starts from vacuum-like state ( $w_{de}(0) = -1$ ). But establishing of its true origin from observations is important for unveiling of nature of dark energy as well as physics of Very Early Universe and unified theory of particle physics. One more lack is the weak constraint for the third parameter from observational data.

iv) *Four-parametric EoS*. The four-parametric EoS in the form

$$w(z) = w_0 + \frac{(w_f - w_0)}{1 + \exp(\frac{z - z_t}{\Delta})}, \quad z \equiv \frac{1}{a} - 1, \quad (2.46)$$

has been proposed in [302]. Here  $w_0$  is the initial EoS at  $a = 0$  and  $w_f$  is final one at  $a = 1$  when the transition epoch  $a_t$  is in the past ( $a_t < 1$ ) and  $z_t/\Delta \gg 1$ . It has been studied by authors only for the special case of  $w_0 = 0$  (at the beginning the dark energy is dust-like) and transition is sharp ( $z_t/\Delta = 30$ ). Such time dependence of EoS has physical motivation: it appears in the models like vacuum metamorphosis where non-perturbative quantum effects are important at late times [303–305]. It was shown [302] that in such case the CMB and SNe Ia data prefer the model with  $z_t = 2.0^{+2.2}_{-0.76}$  and  $w_f = -1^{+0.2}$  (Fig. 2.3). One can see that the third parameter  $z_t$  is poorly constrained even for fixed  $w_0$  and  $\Delta$ . It is important to constraint all four parameters  $w_0$ ,  $w_f$ ,  $z_t$  and  $\Delta$  jointly, but it looks impossible at current accuracy level of cosmological observations. Disadvantage of this simple four-parametric form of

$w(a)$  is absence of analytic solution of integral (1.9) for  $\tilde{w}_{de}$  and, as consequence, analytic representations for  $\rho_{de}(a)$ ,  $H(a)$  and  $q(a)$ .

The mentioned parametrizations of time dependence of EoS parameter allow the phantom divide crossing ( $w = -1$ ) and extend the variety of properties of dark energy and its possible physical interpretations. The additional degeneracies and uncertainties of parameters related to the early dark energy density and time variations of EoS parameter are inherent for them. And vice versa, the value of EoS  $w_{de}$  as well as of energy density  $\Omega_{de}$  related to the late epoch are determined well as a result of their main impact on the expansion history of the Universe, horizon scale, distance to CMB last scattering surface and scale-independent growth factor of linear matter density perturbations. These values, however, give no possibility to constrain essentially the types of cosmological scalar fields, or, in other words, the forms of their Lagrangians and potentials.

**Some exact solutions of Eq. (2.11).** The cosmological constant or vacuum-like fields as well as  $w_{de} = \text{const}$  dark energy are analyzed at different stages of evolution of the Universe, from Beginning ( $a \ll 1$ ) to current epoch ( $a = 1$ ), and for prediction of its future ( $a \gg 1$ ). In the case of ii)–iv) parametrizations their application at  $a \ll 1$  or  $a \gg 1$  are ambiguous since energy density and pressure of dark energy can acquire there surprising values as a consequence of extension of those parametrizations which are good approximations only at the vicinity of  $a = 1$ . Instead of probing the numberless analytical forms of  $w_{de}(a)$  one can probe the scalar field dark energy models assuming their specific properties. Let us consider the simplest ones.

i) *Constant density*,  $\rho_{de} = \text{const}$ . If the density of dark energy is constant in space and time then we have the well studied model with cosmological constant or vacuum field models,  $\tilde{w}_{de} = -1$ , that follows from Eq. (1.8).

ii) *Constant pressure*,  $p_{de} = \text{const}$ . Such assumption is equivalent to the adiabatic sound speed,  $c_a^2 = \dot{p}_{de}/\dot{\rho}_{de}$ , is zero when  $\dot{\rho}_{de} \neq 0$ . Equation (2.11) in this case has the simple analytic solution

$$w_{de}(a) = \frac{w_0 a^3}{1 + w_0(1 - a^3)}, \quad (2.47)$$

where  $w_0 = w_{de}(a = 1)$  is free parameter. Such one-parametric EoS has interesting asymptotic properties: when  $a \rightarrow 0$  then  $w_{de} \rightarrow 0$ , and when  $a \rightarrow \infty$  then  $w_{de} \rightarrow -1$ . Such dark energy at the Beginning is dust-like and in the future it is similar to vacuum energy field. It is like to the vacuum metamorphosis model, mentioned above, but with gradual transition from dust-like state to vacuum-like one (Fig. 2.5). So, such model has no fine tuning problem. Its other advantage is that the effective EoS parameter (1.9) has exact analytic form:

$$\tilde{w}_{de}(a) = -\frac{1}{3} \frac{\ln(1 + w_0 - w_0 a^3)}{\ln a}$$

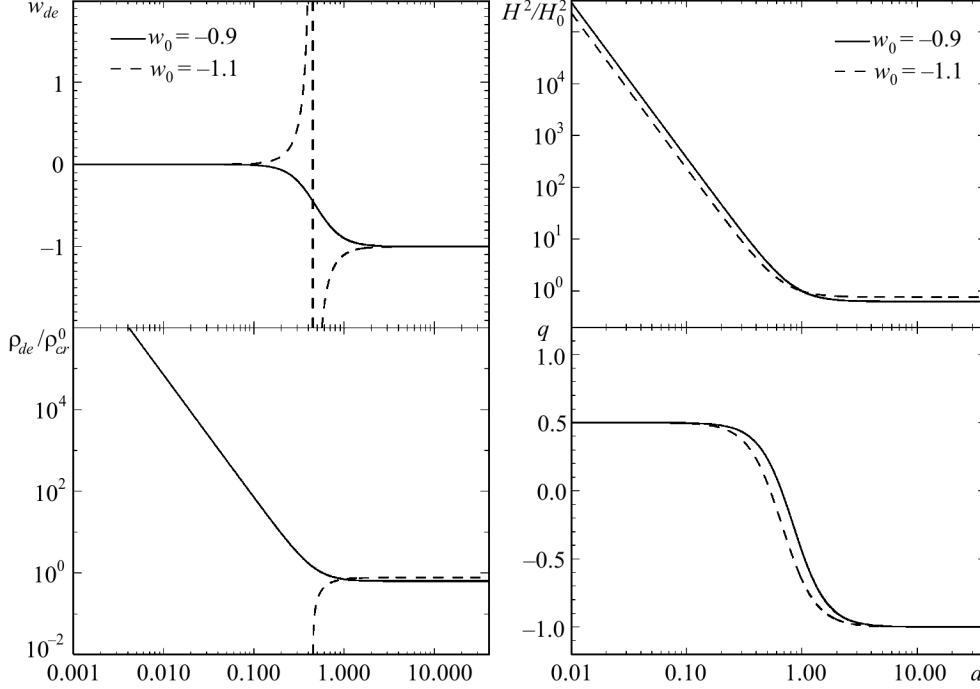


**Fig. 2.5.** Left column: top panel – the dependences of EoS parameter on scale factor for  $p_{de} = \text{const}$  ( $c_a^2 = 0$ ) scalar field with  $w_0 = -0.9$  and  $-1.1$ ; bottom panel – the dependences of dark energy density (in the units of critical one at the current epoch) with EoS parameters from the top panel on scale factor. Right column: The dynamics of expansion of the Universe with  $p_{de} = \text{const}$  scalar field ( $c_a^2 = 0$ ) –  $H^2(a)$  (top panel) and  $q(a)$  (bottom one) for the same  $w_{de}$  as in left panel

and the same asymptotic behavior. The energy density, accordingly, has simple analytic dependence too

$$\rho_{de}(a) = \rho_{de}^{(0)}[(1 + w_0)a^{-3} - w_0].$$

In the range  $w_0 \geq -1$  the EoS parameter  $w_{de}$  is monotonic decreasing function of  $a$ , repulsive property of scalar field increases and the Universe with such dark energy will exponentially expand in far future. If  $w_0 = -1$ , then  $w_{de}(a) = \tilde{w}_{de}(a) = -1$  and we have the vacuum-like field. When  $w_0 < -1$ , the properties of the field become unusual: at  $a_{d2k} = [(1 + w_0)/w_0]^{1/3} < 1$  the EoS parameter has discontinuity of the second kind since energy density of scalar field  $\rho_{de}$  becomes zero (left panel of Fig. 2.5). This discontinuity is not physical, since physical values  $\rho_{de}$  and  $p_{de}$  are smooth continuous functions. In this case  $\rho_{de}$  is negative at  $0 \leq a < a_{d2k}$  and positive later. In spite of  $\rho_{de} \propto a^{-3}$  in the multicomponent medium with matter and radiation all energy conditions are always satisfied and Einstein equations for evolution of the homogeneous Universe have real solutions (see for details Chapter 5). Such dynamics of EoS

parameter is interesting in the scalar field model which supposes negative value of energy density, that will be discussed later. In the right panel the evolution of Hubble parameter  $H(a)$  and deceleration one  $q(a)$  are shown for  $w_0 = -0.9$  and  $-1.1$ . One can see, that dynamical evolution of the Universe filled with  $p_{de} = \text{const}$  DE with  $w_0 = -0.9$  and  $-1.1$  in past and in future is similar though dynamical evolution of fields is quite different.

We have studied this model in [131, 255, 257] for  $w_0 \geq -1$  and shown that it matches all observational data as well as  $\Lambda$ CDM and  $w$ CDM models do. The best-fit parameters of such dark energy are  $\Omega_{de} = 0.72_{-0.05}^{+0.04}$ ,  $w_0 = 0.99_{-0.01}^{+0.03}$ . It was shown also that it is perturbed and causes the appreciable influence on the matter power spectrum at subhorizon scales.

iii) *Barotropic EoS or constant adiabatic sound speed  $c_a^2$* . This assumption is more general than previous one and allows other distinct properties of dark energy favorable for analytic, semianalytic and numerical analysis. In such case the temporal derivative of  $p_{de}(\eta)$  is proportional to the temporal derivative of  $\rho_{de}(\eta)$ . The integral form of this condition is the generalized linear barotropic equation of state

$$p_{de} = c_a^2 \rho_{de} + C, \quad (2.48)$$

where  $C$  is a constant. Cosmological scenarios for the Universe filled with the fluid with such EoS equation<sup>6</sup> have been analyzed in [306, 307]. The solution of the differential equation (2.11) for  $c_a^2 = \text{const}$  is following:

$$w_{de}(a) = \frac{(1 + c_a^2)(1 + w_0)}{1 + w_0 - (w_0 - c_a^2)a^{3(1+c_a^2)}} - 1, \quad (2.49)$$

where the integration constant of (2.11)  $w_0$  is chosen as the current value of  $w_{de}$ . One can easily find that (2.49) gives (2.48) with  $C = \rho_{de}^{(0)}(w_0 - c_a^2)$ , where  $\rho_{de}^{(0)}$  is current density of dark energy. Thus, we have two values  $w_0$  and  $c_a^2$  defining the EoS parameter  $w_{de}$  at any redshift  $z = a^{-1} - 1$ .

The effective EoS parameter  $\tilde{w}_{de}$  is also analytical function of scale factor

$$\tilde{w}_{de}(a) = -1 - \frac{\ln(c_a^2 - w_0 + (1 + w_0)a^{-3(1+c_a^2)}) - \ln(c_a^2 + 1)}{3 \ln a}. \quad (2.50)$$

The differential equation (1.6) with  $w_{de}$  from (2.49) has the analytic solution too:

$$\rho_{de} = \rho_{de}^{(0)} \frac{(1 + w_0)a^{-3(1+c_a^2)} + c_a^2 - w_0}{1 + c_a^2}. \quad (2.51)$$

The expressions (2.48) and (2.51) can be used for finding of the allowable values of  $c_a^2$ . Really, if  $c_a^2 > 0$  then the energy density of scalar field increases

<sup>6</sup> Often called in literature “wet dark fluid”.

with decreasing  $a$  faster than matter density. In the Universe with such scalar field the MD epoch, required for large scale structure formation, is absent. The age of such Universe is lower than age of oldest stars of our galaxy. Besides, at early epoch  $\rho_{de} > \rho_m$  and  $p_{de} > 0$  that changes drastically the transfer function of matter density perturbations. So, the range of values for  $c_a^2 > 0$  must be excluded from consideration. Therefore, the sound range of allowable values of  $c_a^2$  is  $< 0$  and  $w_0 < -1/3$ . Other constraints for  $c_a^2$  and  $w_0$  follow from analysis of dynamics of expansion of the Universe, but their optimal values one can deduce from comparison of computed predictions with all set of observational data, which are mentioned in the Chapter 1.

The dynamical properties of such scalar field depend on the ratio  $c_a^2$  between  $w_0$  as well as on whether they are  $> -1$  or  $< -1$ . If any of them equals  $-1$ , then  $w_{de}(a) = \tilde{w}_{de}(a) = -1$  and we have vacuum-like field again. In the case  $w_0 = c_a^2$  we have the well studied  $w_{de} = \text{const}$  model.

*a) Both  $c_a^2$  and  $w_0 > -1$  (quintessential range).*

The time dependences of barotropic EoS parameter for different values of  $c_a^2 > -1$  are shown in the left top panel of Fig. 2.6. As it follows from (2.49),  $c_a^2$  corresponds to the EoS parameter at the beginning of expansion,  $w_{de}(0) = c_a^2$ .

The dependences of dark energy density on scale factor for the same values of  $c_a^2$  are shown in the left bottom panel of Fig. 2.6. The dynamics of expansion of the homogeneous isotropic Universe, described by  $H(a)$  and  $q(a)$  (Friedmann equations (1.15)–(1.16)), with the same scalar field models is shown in the right panel of Fig. 2.6.

One can see, that in the case  $c_a^2 > w_0$   $w_{de}(a)$  is monotonic decreasing function in the whole range of scale factor variation,  $0 < a < \infty$ , while in the case  $c_a^2 < w_0$   $w_{de}(a)$  has discontinuity of the second kind at  $a_{d2k} = [(1 + w_0)/(w_0 - c_a^2)]^{1/3(1+c_a^2)} > 1$ , where  $\rho_{de}$  becomes zero. After that the energy density of such scalar field acquires negative values and somewhat later  $H$  reaches zero too and the Universe will start to recollapse (right panel of Fig. 2.6). We note here that  $\rho_{de}(a)$  and  $p_{de}(a)$  are smooth continuous functions at any  $a$ .

*b) Both  $c_a^2$  and  $w_0 < -1$  (phantom range).*

As it follows from (2.49), in this case  $c_a^2$  corresponds to the EoS parameter at the scale factor infinity,  $w_{de}(a \rightarrow \infty)$ . But when  $a \rightarrow 0$ , then  $w_{de} \rightarrow -1$  and  $\rho_{de} \rightarrow \rho_{de}^{(0)}(c_a^2 - w_0)/(1 + c_a^2)$ . The energy density increases monotonically with increasing of  $a$ , that follows from (2.51). It is always positive for  $c_a^2 \leq w_0$  and sign-alternating in the case of  $c_a^2 > w_0$ . In the last case the energy density is negative at  $a < a_{d2k}$  and positive at  $a > a_{d2k}$ . When  $\rho_{de}$  becomes zero at  $a = a_{d2k} < 1$  the  $w_{de}(a)$  has discontinuity of the second kind in past, but  $\rho_{de}(a)$  and  $p_{de}(a)$  are smooth continuous functions.

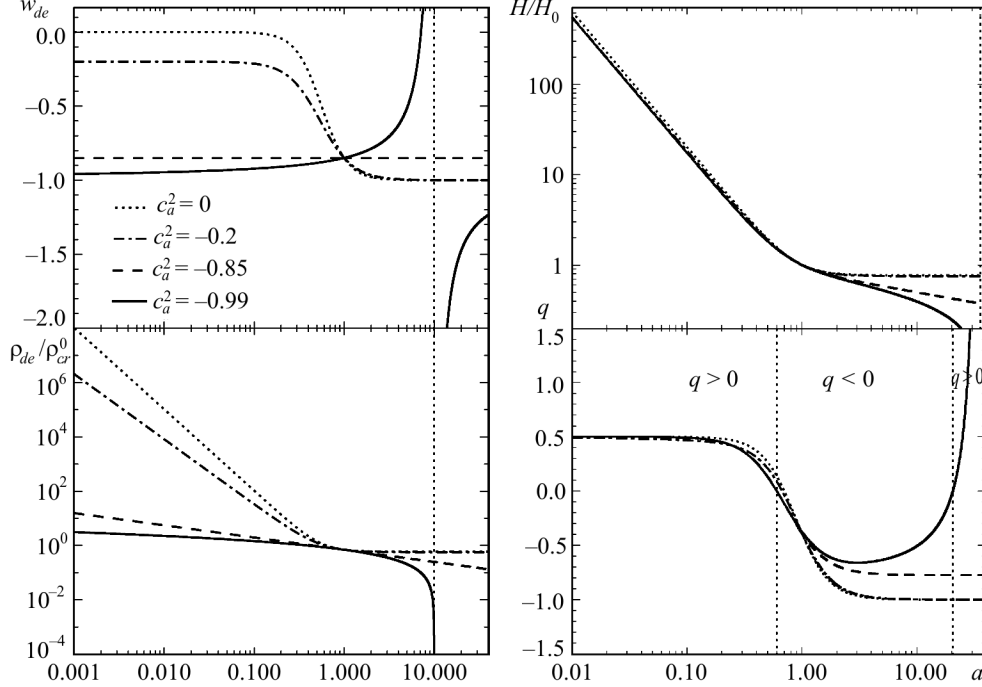


**Fig. 2.6.** Left column: top panel — the dependences of EoS parameter on scale factor for barotropic quintessential scalar field with  $w_0 = -0.85$  and different  $c_a^2$  (0, -0.2, -0.85, -0.99); bottom panel — the dependences of dark energy density (in the units of critical one at the current epoch) with EoS parameters presented in the top panel on scale factor. Right column: The dynamics of expansion of the Universe with barotropic quintessential scalar field —  $H(a)$  (top panel) and  $q(a)$  (bottom one) for the same  $w_{de}$  as in left panel

The dependences of  $w_{de}$ ,  $\rho_{de}$ ,  $H$  and  $q$  on  $a$  for different  $c_a^2$  and  $w_0 = -1.2$  are shown in Fig. 2.7. One can see that in spite of the second kind discontinuity of  $w_{de}$  such scalar field practically does not influence the dynamics of the Universe in the MD and RD epochs (the lines in the right panels of Fig. 2.7 are superimposed at  $a < 0.8$ .)

*c) Phantom divide crossing.*

It happens when  $c_a^2 > -1$  and  $w_0 < -1$  or when  $c_a^2 < -1$  and  $w_0 > -1$ . In both cases the crossing of the line  $w_{de} = -1$  passes as discontinuity of the second kind of  $w_{de}(a)$  at  $a = a_{d2k}$ , which is in the past in the first case, and in the future in the last one. In both cases the physical measurable values  $\rho_{de}(a)$  and  $p_{de}(a)$  are smooth continuous functions, that is shown in the left panel of Fig. 2.8.

So, the scalar field with barotropic EoS is capable to describe the different possible dynamical properties of dark energy (like vacuum energy,  $w = -1$  const fluid, quintessence, phantom, transition from quintessence to phantom

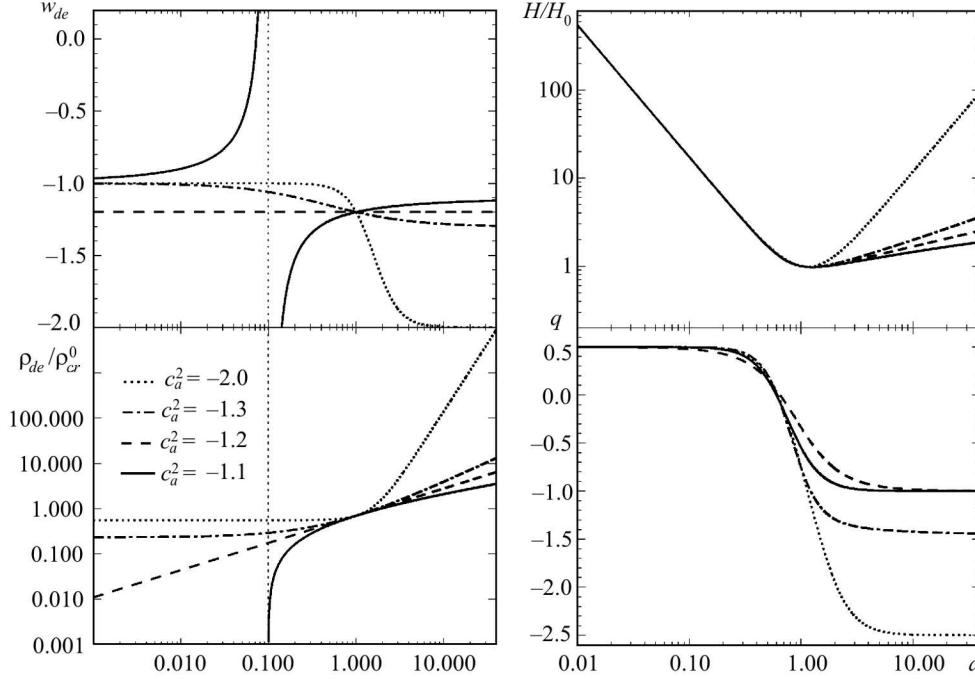


**Fig. 2.7.** Left column: top panel — the dependences of EoS parameter on scale factor for barotropic phantom scalar field with  $w_0 = -1.2$  and different  $c_a^2$  ( $-2.0, -1.3, -1.2, -1.1$ ); bottom panel — the dependences of dark energy density (in the units of critical one at the current epoch) with EoS parameters presented in the top panel on scale factor. Right column: The dynamics of expansion of the Universe with barotropic phantom scalar field —  $H(a)$  (top panel) and  $q(a)$  (bottom one) for the same models as in left panel

and vice-versa), which are defined by two parameters only,  $w_0$  and  $c_a^2$ . Their determination on the base of observations can unveil the dynamical properties of dark energy in our Universe. But such scalar field allows monotonic evolution of energy density which can acquire negative values in the past or future. Its crossing over zero leads to second kind discontinuity of  $w_{de}(a)$ . We have no other arguments against this possibility besides that the null energy condition  $\sum_N \rho_N \geq 0$  must be satisfied always in the past. This condition can be used for establishing of the limits for values of  $w_0$  for any  $c_a^2$ . Since it can be violated in the late DE dominated epoch, the density of relativistic component can be omitted. So, the null energy condition is satisfied when

$$w_0 \geq -\frac{1 + (1 + c_a^2) \frac{\Omega_m}{\Omega_{de}} a^{3c_a^2} + c_a^2 a^{3(1+c_a^2)}}{1 - a^{3(1+c_a^2)}}. \quad (2.52)$$

The right part of inequality as function of  $a$  goes to  $-\infty$  when  $a \rightarrow 0$  or  $a \rightarrow 1$  and has maxima at  $0.5 < a_m < 1$  which we denote by  $w_{0m}$ . The

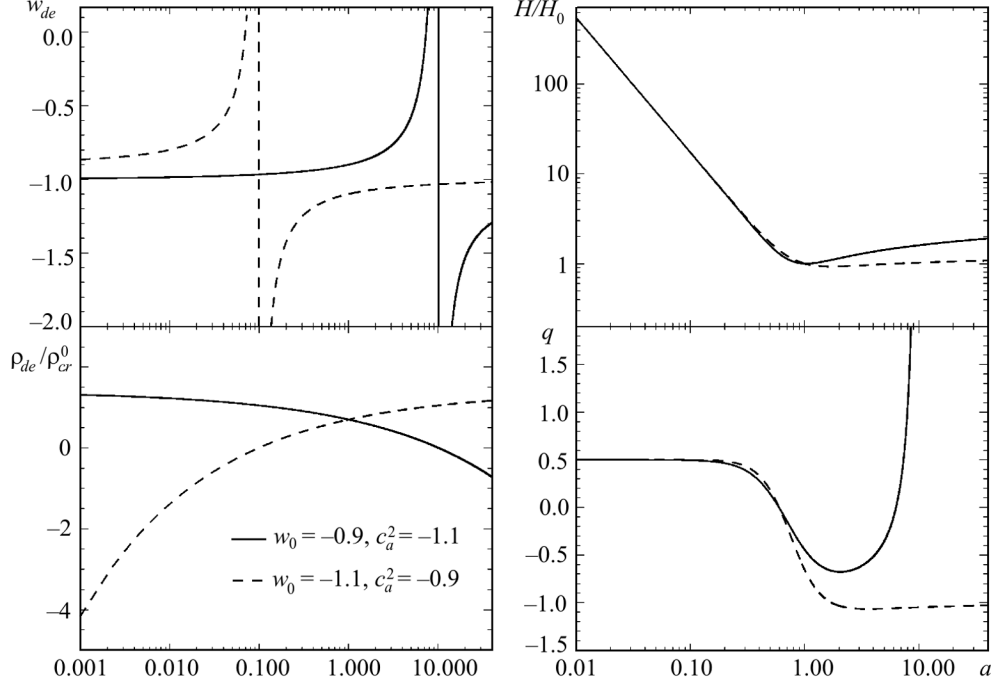


**Fig. 2.8.** Left column: top panel — the dependences of EoS parameter on scale factor for barotropic quintessential scalar field with phantom divide crossing EoS parameter ( $w_0 = -0.9$ ,  $c_a^2 = -1.1$  and  $w_0 = -1.1$ ,  $c_a^2 = -0.9$ ); bottom panel — the dependences of dark energy density (in the units of critical one at the current epoch) with EoS parameters presented in the top panel on scale factor. Right column: The dynamics of expansion of the Universe with barotropic quintessential scalar field —  $H(a)$  (top panel) and  $q(a)$  (bottom one) for the same  $w_{de}$  as in left panel

dependences of  $w_{0m}$  on  $c_a^2$  for different  $\Omega_m/\Omega_{de}$  are shown in Fig. 2.9. One can state that the null energy condition is satisfied in any epoch in the past when  $w_0 \geq w_{0m}$  for given  $c_a^2$  and  $\Omega_m/\Omega_{de}$ . The dependences of  $w_{0m}$  on  $c_a^2$  and  $\Omega_m/\Omega_{de}$ , shown in Fig. 2.9 by solid lines, can be approximated by simple expression

$$\begin{aligned}
 w_{0m} = & -0.9103 - 1.272 \frac{\Omega_m}{\Omega_{de}} + \left( 0.7407 + 1.658 \frac{\Omega_m}{\Omega_{de}} \right) c_a^2 + \\
 & + \left( -0.03778 + 0.08091 \frac{\Omega_m}{\Omega_{de}} \right) c_a^4, \quad (2.53)
 \end{aligned}$$

the accuracy of which is few percents (dashed lines in Fig. 2.9).

Therefore, defining of  $w_{de}(a)$  on the whole time axis and  $\Omega_{de}$  at current epoch governs completely the dynamical properties of homogeneous scalar field and the whole Universe, gives possibility to describe its history, present



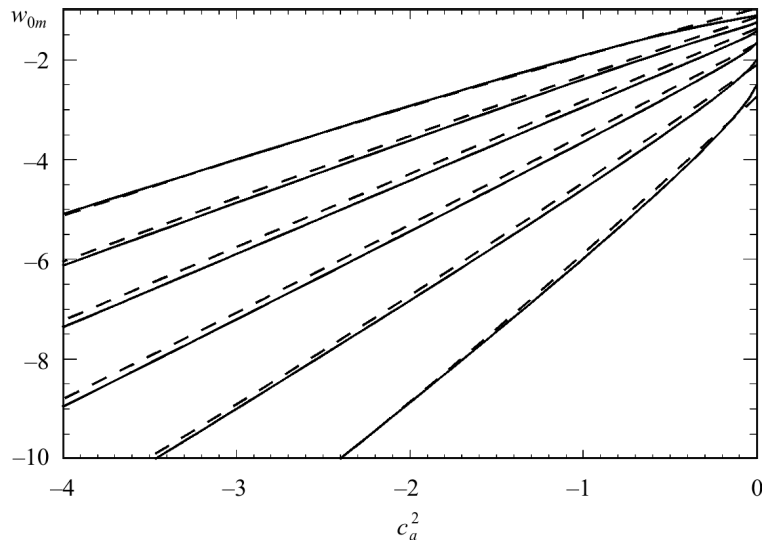


**Fig. 2.9.** Minimal  $w_0$  as the function of  $c_a^2$  for different  $\Omega_m/\Omega_{de}$  (0.1/0.9, 0.2/0.8, 0.3/0.7, 0.4/0.6, 0.5/0.5, 0.6/0.4 from top to bottom). For values above the corresponding lines the null energy condition  $\sum_N \rho_N \geq 0$  is always satisfied in the past. Dashed line shows the analytic approximation (2.53)

and future. But for analysis of gravitational instability of scalar field and its influence on the formation of large scale structure of the Universe the effective sound speed as parameter of equations (2.14) must be defined too.

#### 2.5.4. The effective sound speed

If Lagrangian of scalar field is defined then effective sound speed can be calculated from (2.10). In the opposite case it can be specified apart. First of all we must find the allowable range of its values. Analysis of equations for evolution of scalar field density and velocity perturbations shows that  $c_s^2$  must be positive or zero, since in the opposite case the scalar field is strongly gravitationally unstable and can essentially change the transfer function and power spectrum of matter density perturbations and, even, the angular power spectrum of CMB temperature fluctuations. On the other hand,  $c_s^2$  cannot exceed 1 to retain causality. So, the range of allowable values of  $c_s^2$  is  $[0, 1]$ .

In most of papers the authors assume some value for  $c_s^2$  supposing that it is constant. In Fig. 2.10 the evolution of Fourier amplitude ( $k = 0.05 \text{ Mpc}^{-1}$ ) of linear density perturbations of dark energy with different values of constant effective sound speed  $c_s^2$  and either constant (left panel) or variable (right panel) EoS parameter is shown. It is computed by CAMB for multicomponent Universe in the synchronous gauge comoving to cold dark matter component.

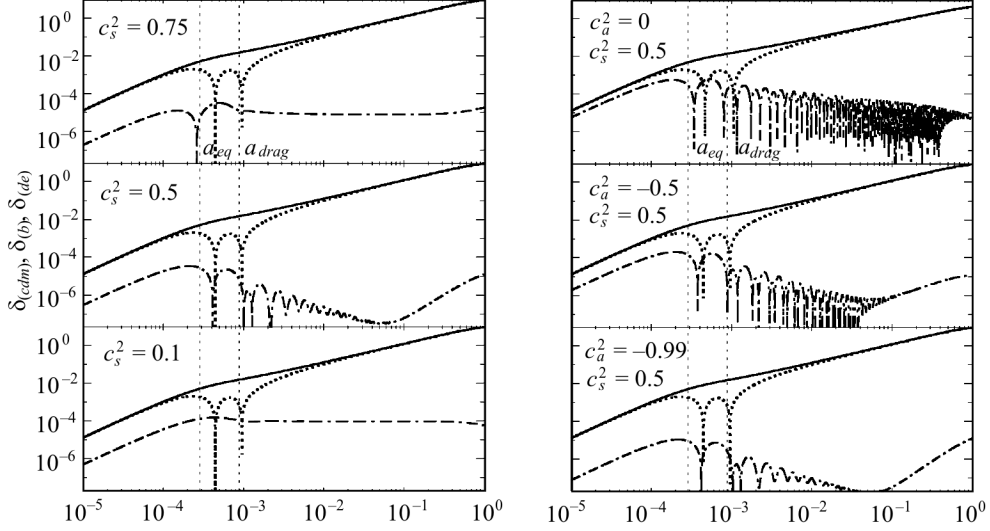


**Fig. 2.10.** Evolution of Fourier amplitude ( $k = 0.05 \text{ Mpc}^{-1}$ ) of density perturbations of cold dark matter (solid line), baryonic matter (dotted line) and dark energy (dash-dotted line) computed by CAMB for models with constant effective sound speed  $c_s^2$ . Left panel: models with constant EoS parameter ( $w_{de} = -0.9$ ) and different  $c_s^2$  (0.75, 0.5, 0.1) from top to bottom); right panel: models with  $w_{de}$  variable according to (2.49) with  $w_0 = -0.9$  and  $c_a^2 = 0, -0.5, -0.99$  (from top to bottom)

The corresponding amplitudes for dark matter and baryonic components are presented there for comparison. A few conclusions can be deduced from their analysis: a) evolution of energy density perturbations of scalar field depends on value of effective sound speed; b) the amplitude increases when scale of perturbation is larger than acoustic horizon scale ( $k^{-1} > c_s t$ ) and decays when it becomes smaller ( $k^{-1} < c_s t$ ); c) practically for any  $0 < c_s^2 \leq 1$  at current epoch the amplitude of energy density perturbations of scalar field is essentially lower than amplitudes of dark matter and baryonic components; d) the value of EoS parameter as well as the character of its time variation changes the evolution of density (right panel of Fig. 2.10) too: for lower initial value of  $w_{de}$  — lower initial amplitude of scalar field density perturbations.

The time-variable effective sound speed was considered too. For example, the authors of [246] have proposed and analyzed the simple analytic dependence in form

$$c_s^2(a) = c_0 + c_1 \left( \frac{a}{1+a} \right)^\gamma, \quad (2.54)$$

which comprehends infinite number of monotonic evolution tracks between 0 to 1, defined by constants  $c_0$ ,  $c_1$  and  $\gamma$ . The first of them equals  $c_s^2$  at the Beginning,  $a = 0$ , the second one is asymptotic value  $c_s^2 \rightarrow c_1$  when  $a \rightarrow \infty$  and  $c_0 = 0$ . The power-law index  $\gamma$  governs the rate of change. The increasing

from 0 to 1 and decreasing from 1 to 0 effective sound speed for three values of  $\gamma = 1, 0.5, 0.1$  is shown in Fig. 2.11. The evolution of density perturbations of scalar field with these effective sound speeds and  $w_{de} = \text{const} = -0.9$  is presented in Fig. 2.12 (left panel for increasing, right panel for decreasing  $c_s^2$ 's). One can see, that increasing or decreasing of  $c_s^2$  as well as their rates influence the time evolution of energy density perturbations of scalar fields.

In all cases considered here the amplitudes of subhorizon density perturbations of scalar fields are essentially lower than corresponding amplitudes of dark matter and baryonic components, that is caused by decaying of perturbations of scalar fields after entering into horizon. At super- and near-horizon scales they are comparable (it depends also on initial conditions for

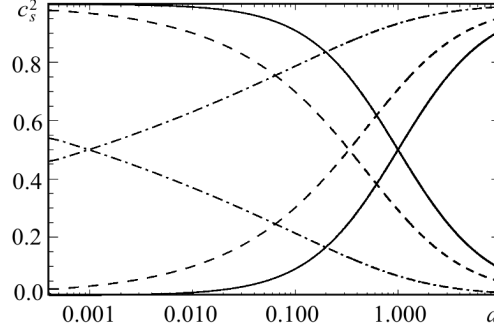


**Fig. 2.11.** Variable effective sound speed  $c_s^2(a)$  defined by (2.54): increasing curves are calculated for  $c_0 = 0, c_1 = 1, \gamma = 1$  (solid line), 0.5 (dashed line), 0.1 (dash-dotted line) and decreasing ones for  $c_0 = 1, c_1 = -1$  and the same  $\gamma$ 's

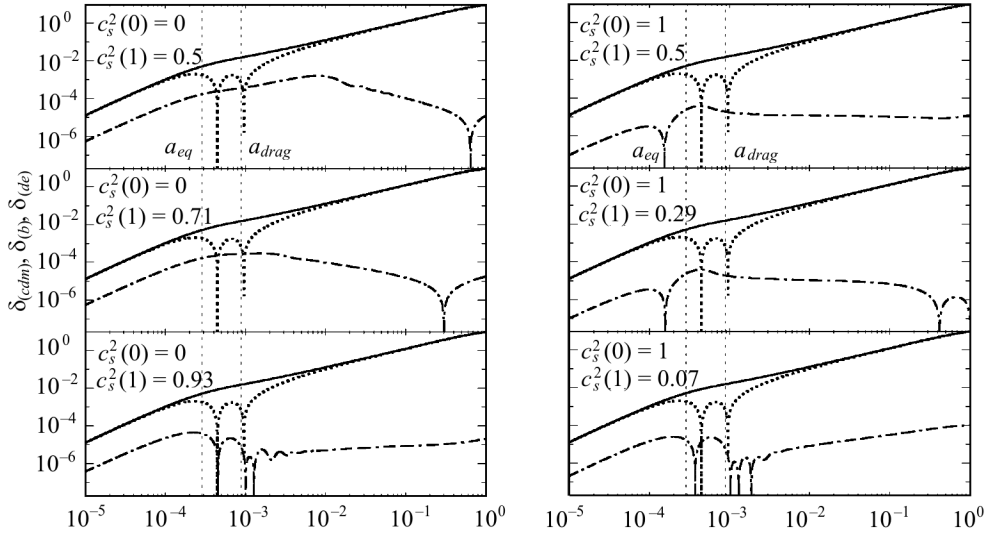


**Fig. 2.12.** Evolution of Fourier amplitude ( $k = 0.05 \text{ Mpc}^{-1}$ ) of density perturbations of cold dark matter (solid line), baryonic matter (dotted line) and dark energy (dash-dotted line) for models with constant EoS parameter ( $w_{de} = -0.9$ ) and variable effective sound speed (2.54). Left panel: models with increasing  $c_s^2$  ( $c_0 = 0, c_1 = 1; \gamma = 1, 0.5, 0.1$  from top to bottom); right panel: models with decreasing  $c_s^2$  ( $c_0 = 1, c_1 = -1; \gamma = 1, 0.5, 0.1$  from top to bottom)

density perturbations in each component) and their gravitational interaction can leave appreciable fingerprints in initial power spectrum of matter density perturbations. The impact of scalar field perturbations on the linear power spectrum of matter density ones is expected to be essentially lower than the growth factor caused by the background dynamics, but it is scale-dependent and can be appreciable for some types of scalar fields. Some of them are studied carefully in [244, 246].

At the end of this subsection we would like to note that specifying of scalar field by defining of  $w_{de}$  and  $c_s^2$  determines completely its dynamical and perturbative properties as of energy component of the Universe but gives no possibility to reconstruct the Lagrangian, potential and field variable unambiguously, that follows from Eq. (2.8) and (2.10). So, we can say nothing about its physical nature and field properties. That is why we prefer the combined approach to specifying of scalar field — its general property and form of Lagrangian. Below we consider the scalar fields with generalized barotropic equations of state and classical, phantom and tachyon Lagrangians and discuss their properties, possibility to match all set of observational data as well as possibility of distinguishing between them.

## 2.6. Quintessential scalar fields with barotropic EoS

In this section we consider the scalar field models of dark energy specified by the barotropic EoS (2.48)–(2.51) and different types of Lagrangians to analyze the evolution of fields, their perturbative properties and influence on the power spectrum of matter density perturbations. We will determine their parameters jointly with minimal set of cosmological parameters using current observational data and discuss the possibility of distinguishing between different types of scalar field models of dark energy. We suppose that the Universe is filled with non-relativistic particles (cold dark matter and baryons), relativistic ones (thermal electromagnetic radiation and massless neutrino) and minimally coupled scalar field as dark energy.

### 2.6.1. Classical scalar field

The scalar field with canonical (classical or Klein–Gordon) Lagrangian

$$L_{clas} = X - U(\phi), \quad (2.55)$$

and positive values of kinetic term  $X$  and potential  $U(\phi)$  is called the classical one. At any time its energy density and pressure are simply linear combinations of  $X$  and  $U$ ,

$$\rho_{clas} = X + U(\phi), \quad P_{clas} = X - U(\phi), \quad (2.56)$$

and EoS parameter  $w_{de} \equiv p_{de}/\rho_{de}$  for such field is the ratio of these combinations,

$$w_{clas} = \frac{X - U}{X + U}. \quad (2.57)$$

One can see, that for positive values of  $X$  and  $U$  the EoS parameter always is  $\geq -1$ . For explanation of accelerated expansion of the Universe at the current epoch ( $q_0 < 0$ ) it must satisfy two conditions:

$$\text{a) } X^{(0)} < U^{(0)}/2, \quad \text{b) } U^{(0)} - 2X^{(0)} > \rho_m^{(0)}/2, \quad (2.58)$$

where index (0) marks the current values of corresponding variables.

Using relations (2.56)–(2.57) and (2.49)–(2.51) the field variable, potential and kinetic term can be presented in terms of density and EoS parameters as follows:

$$\begin{aligned} \phi(a) - \phi_0 &= \pm \sqrt{(1 + w_0)\rho_{de}^{(0)}} \int_1^a \frac{da'}{a'^{(\frac{5}{2} + \frac{3}{2}c_a^2)} H(a')}, \\ U(a) &= \frac{(1 - c_a^2)(1 + w_0)a^{-3(1+c_a^2)} + 2(c_a^2 - w_0)}{2(1 + c_a^2)} \rho_{de}^{(0)}, \\ X(a) &= \frac{1 + w_0}{2} a^{-3(1+c_a^2)} \rho_{de}^{(0)}. \end{aligned} \quad (2.59)$$

One can see that for cosmological model of real Universe ( $H(a) > 0$ ,  $\rho_{de}^{(0)} > 0$ ) the quintessential barotropic scalar field ( $w_0 > -1$ ,  $c_a^2 > -1$ ) has always real values of field variable and potential. Its kinetic term  $X(a)$  is positive for any  $a$ , the potential  $U(a)$  is positive for any  $c_a^2 < 1$  at  $a \leq 1$ . But its sign in the future ( $a \gg 1$ ) depends on relation of values of  $c_a^2$  and  $w_0$ . Indeed, when  $a \rightarrow \infty$  then  $U \rightarrow \frac{c_a^2 - w_0}{1 + c_a^2} \rho_{de}^{(0)}$  and is positive for  $c_a^2 > w_0$  and negative for  $c_a^2 < w_0$ .

The dynamics of expansion of the Universe at late epoch and in the future depends on the density and EoS parameters of scalar field. It is shown in Fig. 2.6. The behavior of field and dynamics of the Universe expansion can be divided into three types, defined by the relation between adiabatic sound speed and EoS parameter or the sign of derivative of EoS parameter with respect to scale factor.

1)  $w' < 0$  ( $c_a^2 > w_0$ ): As it follows from (2.49), in this case  $w_{de}$  decreases monotonically from  $c_a^2$  at the early epoch to  $w_0$  at current one up to  $-1$  at the infinite time. The constant  $C$  in EoS equation (2.48) is negative. The dark energy density and pressure tend asymptotically to  $\rho_{de}^{(\infty)} = \rho_{de}^{(0)}(c_a^2 - w_0)/(1 + c_a^2)$  and  $p_{de}^{(\infty)} = -\rho_{de}^{(\infty)}$ . Therefore, in this case the scalar field rolls down to the

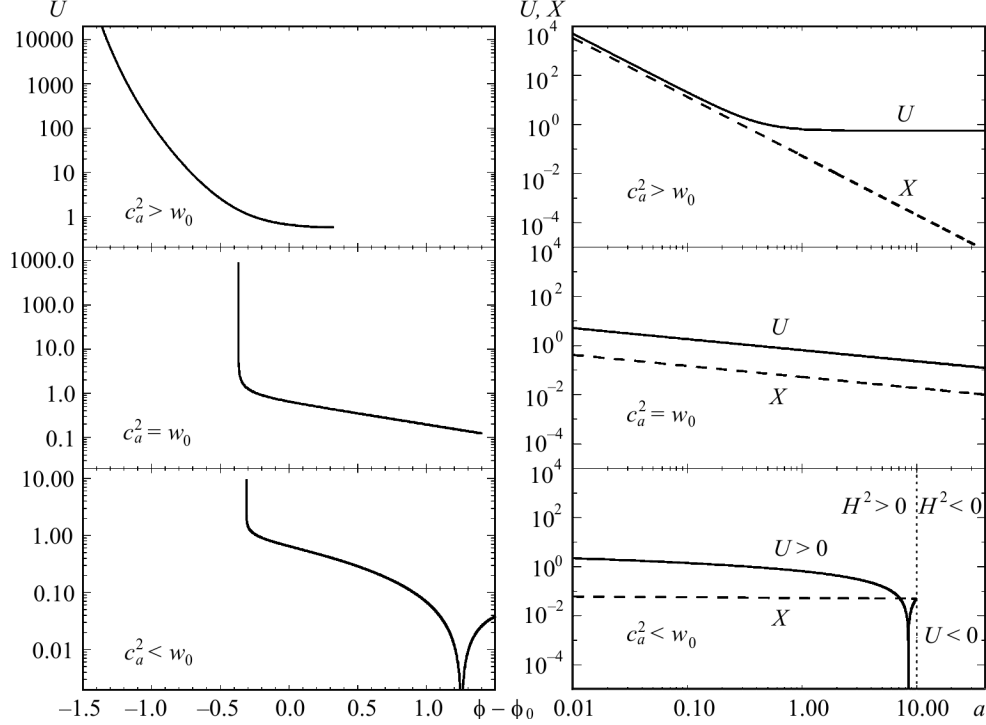


**Fig. 2.13.** Potentials  $U(\phi - \phi_0)$  (left) and dependences of potentials and kinetic terms on scale factor  $a$  (right) for classical scalar field with barotropic EoS. In the top panels  $c_a^2 = -0.2$ , in the middle ones  $c_a^2 = -0.85$  and in the bottom ones  $c_a^2 = -0.99$ , in all panels  $w_0 = -0.85$ . Potential and kinetic term are in the units of current critical energy density,  $3c^2 H_0^2 / 8\pi G$ , the field variable in units of  $\sqrt{3c^2 / 8\pi G}$ . The current epoch in the left panels corresponds to  $\phi - \phi_0 = 0$  and the field evolves from left to right

minimum of potential (see Fig. 2.13) and in far future the Universe will proceed into de Sitter stage of its expansion with  $w_{de}^{(\infty)} = -1$ ,  $q^{(\infty)} = -1$  and  $H^{(\infty)} = \sqrt{\Omega_{de}(c_a^2 - w_0)/(c_a^2 + 1)}H_0$ . So, the scalar field of such type has the following general properties (see relations (2.57)–(2.59) and top panels of Fig. 2.13): a) its kinetic term and potential are always real positive; b) kinetic term is always lower than potential ( $X < U$ ); c) the potential rolls down to minimum ( $U_{min} > 0$ ) at the finite value of the field variable  $\phi_{min}$  (left top panel), which is reached at time infinity (right top panel); d) the kinetic term of such field tends asymptotically to 0, it means that  $\dot{\phi} \rightarrow 0$  and the field “freezes”.

2)  $w' = 0$  ( $c_a^2 = w_0$ ): It corresponds to the well-studied case  $w_{de} = \text{const}$ . In this case  $C = 0$  and we have usual barotropic EoS  $p_{de} = w_0 \rho_{de}$ ,  $\rho_{de} \rightarrow 0$  when  $a \rightarrow \infty$ . So, the Universe in the future will experience the power-law expansion with  $a \propto t^{2/3(1+w_0)}$  and deceleration parameter  $q \rightarrow (1 + 3w_0)/2$ . The scalar field of such type has the following general properties (see relations

(2.57)–(2.59) and middle panels of Fig. 2.13): a) its kinetic term and potential have always real positive values; b) the ratio of potential to kinetic term is constant and large than unity,  $U/X = \text{const} > 1$ ; c) its potential rolls down to minimum  $U_{min} = 0$  at some finite value of the field variable and time infinity; d) the kinetic term of such field tends asymptotically to 0, it means that  $\dot{\phi} \rightarrow 0$  and the field “freezes”.

3)  $w' > 0$  ( $c_a^2 < w_0$ ): The EoS parameter  $w_{de}$  increases monotonically from  $c_a^2$  at the early epoch to  $w_0$  at the current one and still continues to increase after that. The field will satisfy the strong energy condition  $\rho_{de} + 3p_{de} \geq 0$  ( $w_{de} > -1/3$ ) starting from

$$a_{(w=-\frac{1}{3})} = \left[ \frac{(1 + 3c_a^2)(1 + w_0)}{2(c_a^2 - w_0)} \right]^{\frac{1}{3(1+c_a^2)}}$$

and then accelerated expansion of the Universe will be changed by the decelerated one. The EoS parameter will reach 0 in future at

$$a_{(w=0)} = \left[ \frac{c_a^2(1 + w_0)}{c_a^2 - w_0} \right]^{\frac{1}{3(1+c_a^2)}},$$

and 1 at

$$a_{(w=1)} = \left[ \frac{(1 - c_a^2)(1 + w_0)}{2(w_0 - c_a^2)} \right]^{\frac{1}{3(1+c_a^2)}}, \quad (2.60)$$

when potential becomes zero (relation (2.59) and left bottom panel of Fig. 2.13). The scalar field energy density at these  $a$  is positive:  $\rho_{de}(a_{(w=0)}) = \rho_{de}^{(0)}(c_a^2 - w_0)/c_a^2$  and  $\rho_{de}(a_{(w=1)}) = \rho_{de}^{(0)}(c_a^2 - w_0)/(c_a^2 - 1)$  correspondingly. The energy density of scalar field continues decreasing, reaches 0 at

$$a_{(\rho=0)} = \left[ \frac{1 + w_0}{w_0 - c_a^2} \right]^{\frac{1}{3(1+c_a^2)}}$$

and then becomes negative. The EoS parameter at this moment has discontinuity of the second kind (Fig. 2.6). Soon after that, when  $\rho_m + \rho_{de}$  reaches 0, the expansion of the Universe is changed by the contraction since at this moment  $\dot{a} = 0$ ,  $\ddot{a} < 0$ , as it follows from equations (1.15) and (1.16), which have no solution for larger  $a$ . Such behavior can be corrected only slightly by the curvature parameter from the observationally allowable range.

### 2.6.2. Tachyonic scalar field

The scalar field  $\xi$  with Dirac–Born–Infeld Lagrangian

$$L_{tach} = -\tilde{U}(\xi)\sqrt{1 - 2\tilde{X}}, \quad (2.61)$$

and positive values of kinetic term  $0 \leq \tilde{X} \leq 1/2$  and potential  $\tilde{U}(\xi)$  can be another good candidate for quintessential dark energy [269, 270]. Such field is

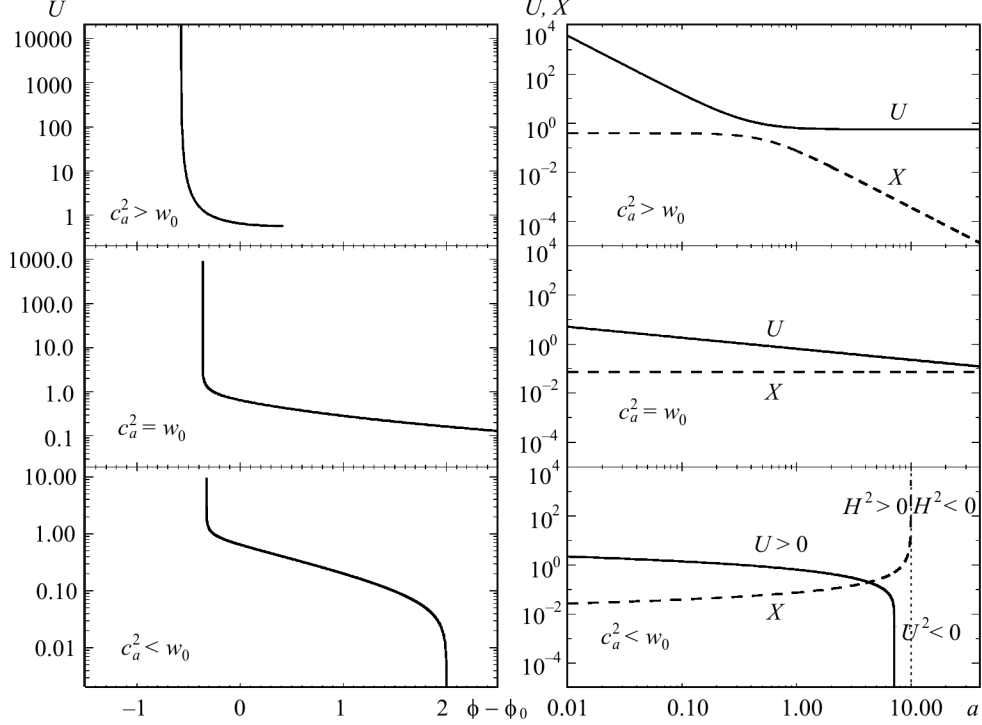


**Fig. 2.14.** Potentials  $U(\phi - \phi_0)$  (left) and dependences of potentials and kinetic terms on scale factor  $a$  (right) for tachyonic scalar field with barotropic EoS. Dark energy parameters and units of variables are the same as in Fig. 2.13

often called in the literature tachyonic one. At any time the energy density and pressure are functions of  $\tilde{X}$  and  $\tilde{U}$ :

$$\rho_{tach} = \frac{\tilde{U}(\xi)}{\sqrt{1 - 2\tilde{X}}}, \quad P_{tach} = -\tilde{U}(\xi)\sqrt{1 - 2\tilde{X}}. \quad (2.62)$$

The EoS parameter  $w_{de} \equiv p_{de}/\rho_{de}$  for this field is following:

$$w_{tach} = 2\tilde{X} - 1. \quad (2.63)$$

One can see, that in the case of tachyonic field the EoS parameter is always  $\geq -1$  for positive values of  $\tilde{X}$  independently on value and sign of  $\tilde{U}$ . For explanation of accelerated expansion of the Universe at the current epoch ( $q_0 < 0$ ) it must satisfy two conditions:

$$\text{a) } \tilde{X}^{(0)} < 1/3, \quad \text{b) } \tilde{U}^{(0)} \frac{1 - 3\tilde{X}^{(0)}}{\sqrt{1 - 2\tilde{X}^{(0)}}} > \rho_m^{(0)}/2, \quad (2.64)$$

where index (0) marks the current values of corresponding variables.



The tachyonic field variable, potential and kinetic term can be presented in terms of dark energy density (2.51) and EoS parameter (2.49) as follows:

$$\begin{aligned}\xi(a) - \xi_0 &= \pm \int_1^a \frac{da' \sqrt{1 + w_{de}(a')}}{a' H(a')}, \\ \tilde{U}(a) &= \rho_{de}(a) \sqrt{-w_{de}(a)}, \\ \tilde{X}(a) &= \frac{1 + w_{de}(a)}{2}.\end{aligned}\tag{2.65}$$

The potentials  $\tilde{U}(\xi - \xi_0)$ , evolution of potentials and kinetic terms for models with decreasing, constant and increasing EoS parameter are shown in Fig. 2.14. One can see that accelerated expansion of the Universe is caused by rolling down of field to minimum of its potential quite similarly as in the case of classical field. Meanwhile, for the same time dependence of  $\rho_{de}$  and  $w_{de}$  (or  $p_{de}$ ) the evolution of  $\tilde{U}$  and  $\tilde{X}$  for tachyonic field differs essentially from corresponding evolution for classical one, that follows from comparison of expressions (2.59) and (2.65) or Fig. 2.13 and 2.14. Moreover, in the case of increasing EoS parameter the potential of tachyonic field at  $a_{w=0}$  becomes imaginary, while one of classical field is real always. Therefore, the same dynamics of expansion of the homogeneous Universe can be provided by different homogeneous scalar fields, classical and tachyonic fields are the example of such model degeneracy. But in the case of these two fields it can be partially broken if cosmological perturbations are taken into account. That will be shown below.

### 2.6.3. Quintessential scalar fields in the phase plane

The general properties of the quintessential scalar field models of dark energy with barotropic EoS can be deduced also from the analysis of their occupation of the  $w_{de} - dw_{de}/d \ln a$  phase plane. From (2.11) and the constraint  $-1 \leq c_a^2 \leq 0$  follows that the scalar field models of dark energy with  $c_a^2 = \text{const}$  occupy the  $w_{de} - dw_{de}/d \ln a$  region limited by the lines  $dw_{de}/d \ln a = 3(1 + w_{de})^2$  and  $dw_{de}/d \ln a = 3w_{de}(1 + w_{de})$  (Fig. 2.15). The last one coincides with the lower limit for freezing scalar field models of dark energy deduced by [298] from the analysis of the simplest particle-physics models of cosmological scalar fields. Below it the scalar fields have too large density at the early epoch that contradicts the data on CMB anisotropy. Above the upper limit there is a range of fields that started as phantom ones, which is excluded for fields with classical Lagrangian as well as tachyonic one considered above.

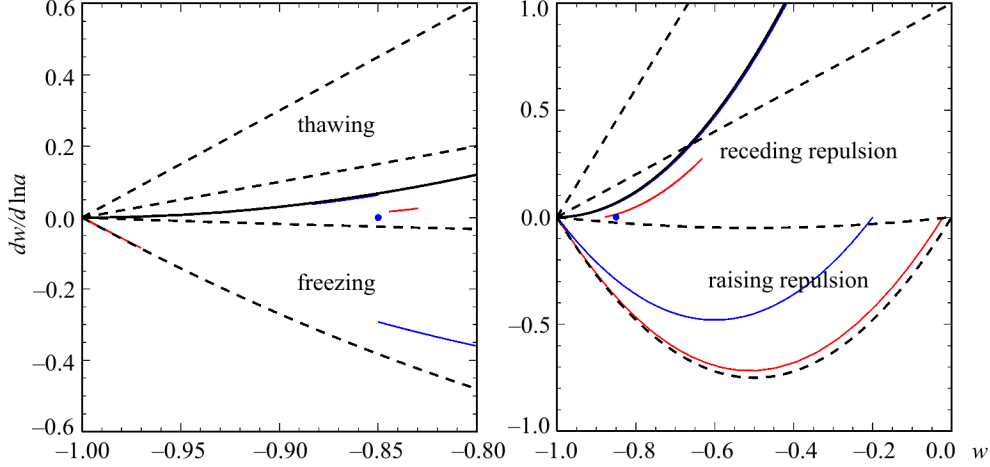


**Fig. 2.15.** The  $w_{de} - dw_{de}/d \ln a$  phase plane for quintessential scalar fields with barotropic EoS as models of dynamical dark energy (solid lines). If  $dw_{de}/d \ln a < 0$  the fields evolve from right to left raising their repulsion properties, if  $dw_{de}/d \ln a > 0$  the fields evolve from left to right receding them. Thick dashed lines show the ranges occupied by the thawing and freezing scalar fields deduced by [298] from the analysis of simplest particle physics scalar field models of dynamical dark energy. In the left panel the phase plane evolution tracks of the scalar fields with barotropic EoS are shown in the range  $0.5 \leq a \leq 1$  ( $0 \leq z \leq 1$ ) and in the same scale as in Fig. 2.1 for easy comparison. In the right panel the phase plane evolution tracks of the scalar fields with barotropic EoS correspond to the range  $0.0001 \leq a \leq 10$  ( $-0.9 \leq z \leq 10000$ ). Thick solid black lines show the limits for such scalar field models: the upper line corresponds to  $c_a^2 = -1$ , the lower one to  $c_a^2 = 0$  (superimposed with the lower limit for freezing scalar fields from [298]). The blue solid lines and dot show the phase tracks of the models shown in Figs. 2.13 and 2.14, the red solid lines show the phase tracks of the best fitting models  $\mathbf{q}_1$  and  $\mathbf{q}_2$  from Table 2.1

The scalar fields which are in the phase plane between the lines  $dw_{de}/d \ln a = 0$  and  $dw_{de}/d \ln a = 3w_{de}(1 + w_{de})$  evolve from right to left in Fig. 2.15 and their repulsion properties are raising with time. They are unlimited in time and  $w_{de}$  for them tends asymptotically to  $-1$ . The scalar fields which are in the phase plane between the lines  $dw_{de}/d \ln a = 0$  and  $dw_{de}/d \ln a = 3(1 + w_{de})^2$  evolve from left to right in Fig. 2.15 and their repulsion properties are receding with time ( $dw_{de}/d \ln a > 0$ ,  $w_{de}$  increases) to change the accelerated expansion by decelerated one and even collapse. They can start in the range below the lower limit for thawing scalar fields, then enter the range of thawing scalar fields limited by [298], cross it and go out of upper limit  $dw_{de}/d \ln a = 3(1 + w_{de})^2$  when  $w_{de} > 0$ . So, the scalar fields with  $dw_{de}/d \ln a > 0$  ( $c_a^2 < w_0$ ) can only partially be called thawing.

We propose to call them “scalar fields receding repulsion”, reflecting their main properties. Symmetrically, the scalar fields with  $dw_{de}/d \ln a < 0$  ( $c_a^2 > w_0$ ), occupying the same range as freezing scalar fields from [298], can be

**Table 2.1. The best-fit values and  $1\sigma$  confidential ranges of parameters of cosmological model with classical and tachyonic QSF determined by the Markov chain Monte Carlo technique using two observational datasets: WMAP7 + HST + BBN + BAO + SN SDSS SALT2 ( $q_1, t_1$ ) and WMAP7 + HST + BBN + BAO + SN SDSS MLCS2k2( $q_2, t_2$ ). The Hubble constant  $H_0$  is in units  $\text{km s}^{-1} \text{Mpc}^{-1}$ . We denote the rescaled energy density of the component  $X$  by  $\omega_X \equiv \Omega_X h^2$**

Parameters	Classical QSF		Tachyonic QSF	
	$q_1$	$q_2$	$t_1$	$t_2$
$\Omega_{de}$	$0.73^{+0.03}_{-0.05}$	$0.70^{+0.04}_{-0.05}$	$0.73^{+0.03}_{-0.04}$	$0.71^{+0.04}_{-0.05}$
$w_0$	$-0.996^{+0.16}_{-0.004}$	$-0.83^{+0.22}_{-0.17}$	$-0.989^{+0.15}_{-0.011}$	$-0.83^{+0.20}_{-0.17}$
$c_a^2$	$-0.022^{+0.022}_{-0.978}$	$-0.88^{+0.88}_{-0.12}$	$-0.48^{+0.48}_{-0.52}$	$-0.97^{+0.96}_{-0.03}$
$10\omega_b$	$0.226^{+0.015}_{-0.015}$	$0.226^{+0.016}_{-0.014}$	$0.226^{+0.014}_{-0.014}$	$0.230^{+0.013}_{-0.017}$
$\omega_{cdm}$	$0.110^{+0.011}_{-0.013}$	$0.108^{+0.016}_{-0.012}$	$0.111^{+0.010}_{-0.016}$	$0.110^{+0.014}_{-0.013}$
$H_0$	$70.2^{+3.5}_{-4.3}$	$66.3^{+4.3}_{-3.7}$	$70.2^{+3.2}_{-4.4}$	$67.1^{+3.7}_{-4.9}$
$n_s$	$0.97^{+0.04}_{-0.04}$	$0.97^{+0.04}_{-0.03}$	$0.97^{+0.04}_{-0.03}$	$0.98^{+0.04}_{-0.04}$
$\log(10^{10} A_s)$	$3.09^{+0.10}_{-0.10}$	$3.07^{+0.11}_{-0.08}$	$3.08^{+0.11}_{-0.08}$	$3.08^{+0.11}_{-0.09}$
$\tau_{rei}$	$0.091^{+0.040}_{-0.041}$	$0.089^{+0.044}_{-0.037}$	$0.087^{+0.043}_{-0.037}$	$0.091^{+0.042}_{-0.040}$
$-\log L$	3865.01	3857.21	3865.09	3857.23

called “scalar fields raising repulsion”. Most of quintessential scalar field models of dark energy filling the phase plane fit well the current observational data and main problem consists now in distinguishing between them.

#### 2.6.4. Best-fit parameters of QSF

Let us estimate the parameters of QSF with barotropic EoS ( $\Omega_{de}, w_0, c_a^2$ ) simultaneously with other cosmological parameters ( $\omega_b, \omega_{cdm}, H_0, n_s, A_s$  and  $\tau_{rei}$ ) using the following datasets: (1) *CMB temperature fluctuations and polarization angular power spectra* from the 7-year WMAP observations (hereafter WMAP7) [93–95]; (2) *Baryon acoustic oscillations* in the space distribution of galaxies from SDSS DR7 (hereafter BAO) [143]; (3) *Hubble constant measurements* from HST (hereafter HST) [231]; (4) *Big Bang Nucleosynthesis prior* on baryon abundance (hereafter BBN) [227,228]; (5) *supernovae Ia luminosity distances* from SDSS compilation (hereafter SN SDSS) [77], determined using SALT2 method of light curve fitting [67] (hereafter SN SDSS SALT2) and MLCS2k2 [69] one (hereafter SN SDSS MLCS2k2).

In order to find the best-fit values of parameters of cosmological model with QSF and their confidence limits we perform the Markov chain Monte Carlo (MCMC) analysis for two combined datasets: WMAP7 + HST + BBN +

+ BAO + SN SDSS SALT2 and WMAP7 + HST + BBN + BAO + SN SDSS MLCS2k2. We use the publicly available package CosmoMC [125, 126] including code CAMB [120, 121] for the calculation of model predictions. This code has been modified to study the dark energy models discussed here. The parameters  $w_0$  and  $c_a^2$  are determined using the priors  $-1 < w_0 < 0$  and  $-1 < c_a^2 < 0$ .

The results of estimations of QSF parameters jointly with the minimal set of cosmological ones for two sets of observational data (WMAP7 + HST + BBN + BAO + SN SDSS SALT2 and WMAP7 + HST + BBN + BAO + SN SDSS MLCS2k2) are presented in Table 2.1. We denoted the sets of best-fit parameters for them as  $\mathbf{q}_1$  and  $\mathbf{q}_2$  for classical QSF and  $\mathbf{t}_1$  and  $\mathbf{t}_2$  for tachyonic QSF accordingly. The  $1\sigma$  confidential limits are determined from the extremal values of the N-dimensional distribution. One can see, that WMAP7 + HST + BBN + BAO + SN SDSS SALT2 dataset prefers the scalar field model of dark energy with decreasing EoS parameter: at the current epoch it is close to  $-1$ , at the early epoch it is  $-0.02$ . The acceleration has changed the sign at  $z \approx 0.75$  and now the deceleration parameter  $q_0$  equals  $-0.59$ . In the future such QSF will approach the  $\Lambda$ CDM model with exponential expansion — late eternal inflation. The dataset WMAP7 + HST + BBN + BAO + SN SDSS MLCS2k2 prefers the scalar field model of dark energy with slowly increasing EoS parameter: it started from the value  $-0.88$  at the early epoch and is  $-0.83$  at current one. In this model the decelerated expansion has been changed by the accelerated one at  $z \approx 0.66$  and at current epoch the deceleration parameter  $q_0$  equals  $-0.38$ . While  $w_{de}$  continues to increase the deceleration parameter reaches the minimal value, begins increasing and becomes positive (start of decelerated expansion) in far future at  $a \approx 20.46$  ( $z \approx -0.95$ ). The turnaround point is at  $a \approx 35.5$ , when Universe will 172.5 Gyrs old. Then the redshifts of galaxies will be changed by blueshifts, the Universe will start collapsing and will reach the Big Crunch singularity in the age of 345 Gyrs. Therefore, the model with parameters  $\mathbf{q}_2$  is limited in time as opposed to the model with  $\mathbf{q}_1$ , though both match equally well the observational dataset corresponding to the past and present of the Universe (see Figs. 2.27–2.32). The differences between obtained best-fit parameters of these models are caused by differences of SNe Ia distance moduli obtained by SALT2 and MLCS2k2 methods of light-curve fitting.

Let us analyze now the possibility of distinguishing between the quintessential scalar field models with decreasing and increasing EoS parameters as well as with classical and tachyonic Lagrangian. Note, that the difference in the Lagrangian manifests only in the development of cosmological perturbations due to the different effective sound speed of scalar fields, so we consider two sets of parameters  $\mathbf{q}_1$  and  $\mathbf{q}_2$  for both Lagrangian.

The differences of dynamics of expansion of the Universe in the cosmological models with best-fit parameters  $\mathbf{q}_1$  and  $\mathbf{q}_2$  are shown in the left panel of

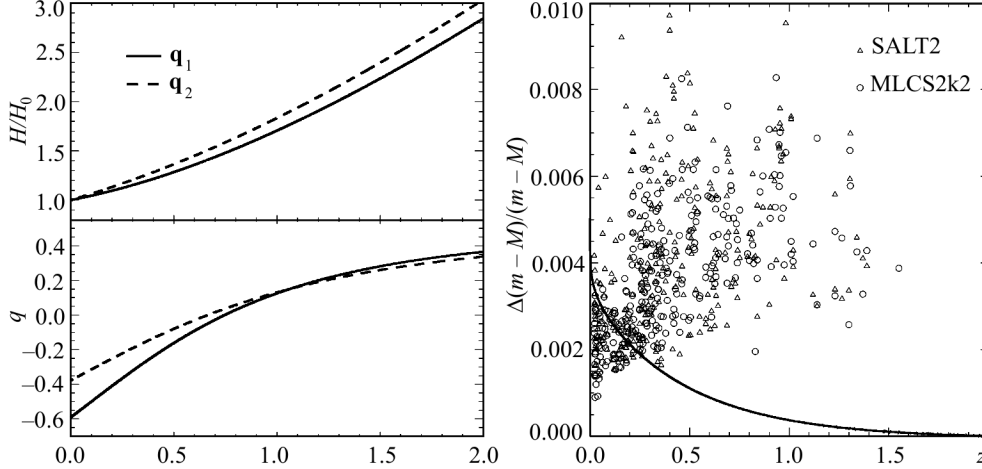


**Fig. 2.16.** Dynamics of expansion of the Universe in the redshift range  $0 \leq z \leq 2$  for cosmological models with best-fit parameters  $\mathbf{q}_1$  and  $\mathbf{q}_2$  (left panel) and relative differences of distance moduli  $[(m - M)_{q_2} - (m - M)_{q_1}]/(m - M)_{q_1}$  (solid line in the right panel). The symbols show the uncertainties of distance moduli determination of SN SDSS SALT2 and SN SDSS MLCS2k2 data

Fig. 2.16. The rate of expansion in the model  $\mathbf{q}_1$  increases slower than in the model  $\mathbf{q}_2$ , since  $q_0$  in it is essentially lower. Both characteristics,  $H(z)/H_0$  and  $q(a)$ , could be deduced from SNe Ia luminosity distances, if their number would be sufficient. In their absence the dependence of SNe Ia luminosity distance on redshift is used. In the right panel the relative differences of distance moduli  $[(m - M)_{q_2} - (m - M)_{q_1}]/(m - M)_{q_1}$  as well as the statistical and systematical uncertainties of distance moduli determinations of SDSS SNe Ia are presented. One can see that observational uncertainties are comparable with the model differences only at low redshifts  $z < 0.3$ .

Other tests are based on the evolution of cosmological perturbations in the multicomponent Universe. The scalar field dark energy affects the evolution of matter density perturbations via growth factor (dynamics of expansion) and gravitational influence of its own scalar perturbations [131, 255]. The evolution of density perturbations of main components in the cosmological models with parameters  $\mathbf{q}_1$ ,  $\mathbf{q}_2$ ,  $\mathbf{t}_1$  and  $\mathbf{t}_2$  is shown in Fig. 2.17. They have been computed using synchronous gauge, the initial conditions are adiabatic for matter components and subdominant asymptotic ones for the scalar field (eqs. (2.26)). The general property is inherent for all models: for positive matter density perturbation the QSF density perturbation is positive from initial moment to horizon crossing one, after that it changes the sign and decays. At the current epoch the density perturbations of QSF are by  $\sim 2$ – $3$  orders lower than matter ones and have opposite sign, so, their imprint in the large scale structure of the Universe is expected to be small. In the left panel of

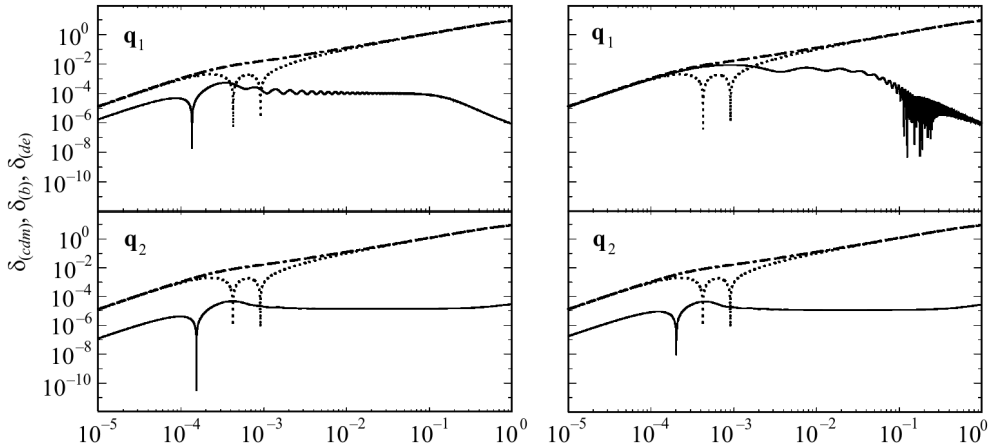


**Fig. 2.17.** Evolution of Fourier amplitude ( $k = 0.05 \text{ Mpc}^{-1}$ ) of density perturbations for cold dark matter (dashed line), baryonic matter (dotted) and QSF (solid). In the left column the scalar field is classical, in the right one tachyonic. The cosmological parameters for the computations were taken from Table 2.1

Fig. 2.18 the relative differences of matter power spectra in the models with  $\mathbf{q}_1$  and  $\mathbf{q}_2$  best-fit parameters for classical (solid line) and tachyonic (dashed line) Lagrangians are shown:  $|P(k; \mathbf{q}_2) - P(k; \mathbf{q}_1)|/P(k; \mathbf{q}_1)$ . The maximal differences  $\sim 8\%$  are for large scale perturbations where observational errors are essentially larger. At the scales  $k \sim 0.1 \text{ Mpc}^{-1}$ , where errors of determinations of matter power spectrum are minimal  $\sim 6\text{--}7\%$ , the relative differences between power spectra for  $\mathbf{q}_1$  and  $\mathbf{q}_2$  best-fit parameters are  $\sim 4\text{--}6\%$  and we hope that the current observational program will improve accuracy and possibility to distinguish this models.

In the right panel of Fig. 2.18 the relative differences of matter power spectra in the models with classical and tachyonic Lagrangians  $|P_{TSF}(k; \mathbf{q}_i) - P_{CSF}(k; \mathbf{q}_i)|/P_{CSF}(k; \mathbf{q}_i)$  are shown for  $\mathbf{q}_1$  (solid line) and  $\mathbf{q}_2$  (dashed line). Here differences are caused solely by influence of scalar field density perturbations on matter density ones. The maximal differences here are  $\sim 1\text{--}2\%$  for the model with  $\mathbf{q}_1$  and  $< 1\%$  for the model with  $\mathbf{q}_2$ . So, distinguishing of classical scalar field from tachyonic one by the observational data on matter density power spectra in the nearest future looks problematic.

In the procedure of determination of cosmological parameters the data on the BAO relative distance measure  $R \equiv r_s(z_{drag})/D_V(z)$  [143] (see subsection 1.4) have been used instead of data on  $P(k)$  because their accuracy is 2–3 times better. In the left panel of Fig. 2.19 the relative differences of the BAO distance measure  $|R(\mathbf{q}_1) - R(\mathbf{q}_2)|/R(\mathbf{q}_1)$  in the cosmological models with best fitting parameters  $\mathbf{q}_1$  and  $\mathbf{q}_2$  are shown for classical and tachyonic scalar fields. One can see that increasing of accuracy of measurement of this parameter will

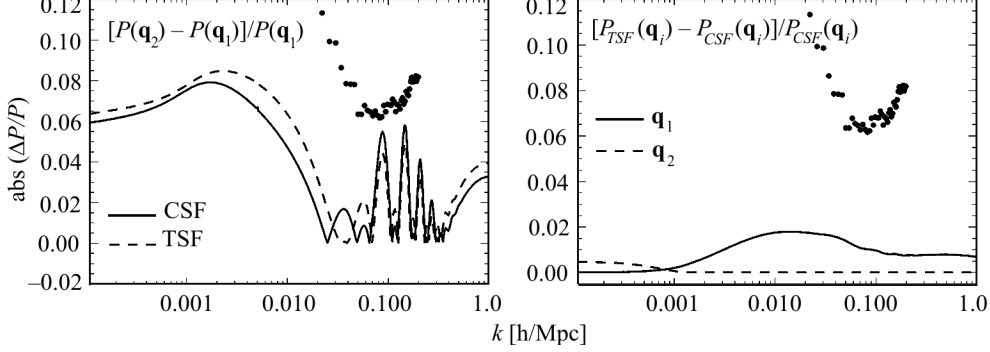


**Fig. 2.18.** Left panel: the relative difference of matter density power spectra  $|\Delta P(k)|/P(k)$  in the models with best fitting parameters  $\mathbf{q}_1$  and  $\mathbf{q}_2$  for classical scalar field (solid line) and tachyonic one (dashed line). Right panel: the relative difference of matter density power spectra  $|\Delta P/P|$  in the models with classical and tachyonic scalar fields for two sets of the best fitting parameters  $\mathbf{q}_1$  (solid line) and  $\mathbf{q}_2$  (dashed line). Dots show observational uncertainties ( $1\sigma$ ) of SDSS LRG DR7 data [163]

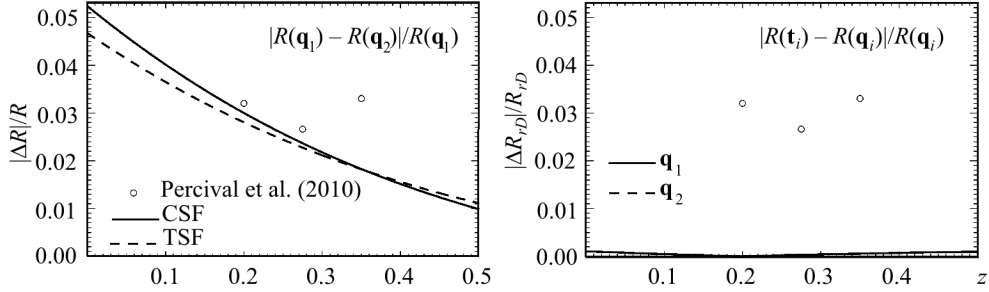


**Fig. 2.19.** Left panel: the relative differences of the BAO distance measure  $R \equiv r_s(z_{drag})/D_V(z)$  in the cosmological models with best fitting parameters  $\mathbf{q}_1$  and  $\mathbf{q}_2$  ( $|R(\mathbf{q}_1) - R(\mathbf{q}_2)|/R(\mathbf{q}_1)$ ) for classical scalar field (solid line) and tachyonic one (dashed line). Right panel: the relative differences of the BAO distance measure  $|R(\mathbf{t}_i) - R(\mathbf{q}_i)|/R(\mathbf{q}_i)$  ( $i = 1, 2$ ) in the models with best fitting parameters  $\mathbf{t}_i$  and  $\mathbf{q}_i$  ( $i = 1, 2$ ). Dots show the observational  $1\sigma$  uncertainties of  $R$  extracted from SDSS DR7 galaxy redshift survey [143] (symbols)

give possibility to distinguish between QSF + CDM models with increasing and decreasing EoS parameter. But these data cannot be used for distinguishing between classical and tachyonic scalar fields since they do not contain the information about evolution of matter density perturbations and their power spectrum. In the right panel of Fig. 2.19 the relative differences of the BAO distance measure  $|R(\mathbf{t}_i) - R(\mathbf{q}_i)|/R(\mathbf{q}_i)$  ( $i = 1, 2$ ) it is shown, they are essentially smaller than  $|P_{TSF}(k; \mathbf{q}_1) - P_{CSF}(k; \mathbf{q}_1)|/P_{CSF}(k; \mathbf{q}_1)$ , because are caused only by small differences of cosmological parameters  $\mathbf{t}_1$  and  $\mathbf{q}_1$ . Therefore, the high precision power spectrum of matter density perturbations is more informative about the nature of dark energy than BAO relative distance measure.

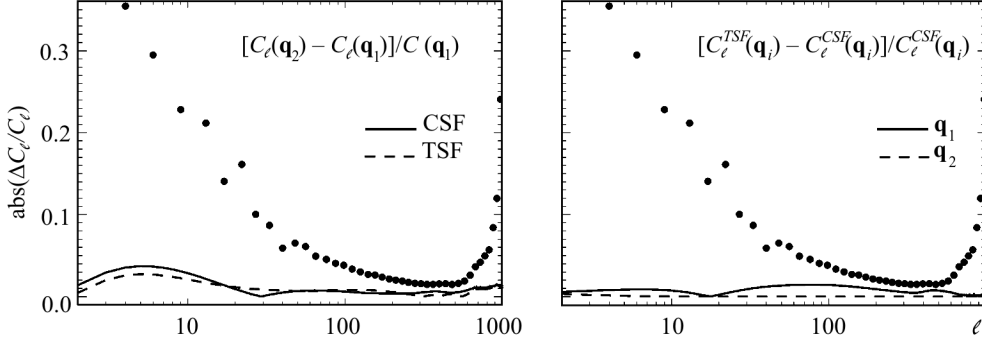


**Fig. 2.20.** Left panel: the relative difference of CMB temperature fluctuations power spectra  $|\Delta C_\ell|/C_\ell$  in the models with best fitting parameters  $\mathbf{q}_1$  and  $\mathbf{q}_2$  for classical (solid line) and tachyonic (dashed line) scalar fields (Table 2.1). Right panel: the relative difference of CMB temperature fluctuations power spectra  $|\Delta C_\ell|/C_\ell$  in the models with classical and tachyonic scalar fields for two sets of the best fitting parameters  $\mathbf{q}_1$  (solid line) and  $\mathbf{q}_2$  (dashed line). Dots show observational uncertainties ( $1\sigma$ ) of WMAP7 data

The dynamical properties of scalar field dark energy and its perturbations leave slight fingerprints in the map of temperature fluctuations and polarization of CMB radiation that have been already discussed above (see also [131]). Here we show the relative differences of CMB power spectra  $|C_\ell(\mathbf{q}_1) - C_\ell(\mathbf{q}_2)|/C_\ell(\mathbf{q}_1)$  for decreasing ( $\mathbf{q}_1$ ) and increasing ( $\mathbf{q}_2$ ) EoS parameters (left panel of Fig. 2.20) as well as  $|C_\ell^{CSF}(\mathbf{q}_i) - C_\ell^{TSF}(\mathbf{q}_i)|/C_\ell^{CSF}(\mathbf{q}_i)$  (right panel) for parameter sets  $\mathbf{q}_1$  and  $\mathbf{q}_2$ . In the left panel the differences at low spherical harmonics ( $\ell < 10$ ) for both scalar fields are caused mainly by different contribution of the late Sachs–Wolfe effect ( $\sim 2\text{--}4\%$ ), at higher ones mainly by different cold dark matter content ( $< 2\%$ ) and, partially, by different optical depth ( $\sim 0.2\%$ ) and geometrical effect<sup>7</sup> ( $\sim 0.3\%$ ). In the right panel the lines show the differences caused solely by influence of scalar field density perturbations on formation of CMB anisotropy. They do not exceed ( $\sim 1\text{--}2\%$ ) for model with decreasing EoS, in which the differences between amplitudes of CSF and TSF density perturbations are most substantial, and are  $\ll 1\%$  for model with increasing EoS parameters  $\mathbf{q}_2$ . The relative errors of binned CMB power spectrum  $|\Delta C_\ell|/C_\ell$ , obtained in WMAP seven-year experiment, are somewhat larger even in the range of acoustic peaks, where accuracy is highest. So, the SN SDSS SALT2 data prefer the model with decreasing EoS parameter, while SN SDSS MLCS2k2 data prefer the model with increasing EoS parameter, but the difference of maxima of likelihood functions for both models is statistically insignificant. It means, that current observational data do not distinct these models as well as the models with classical and tachyonic Lagrangian.

<sup>7</sup> The particle horizon for model with  $\mathbf{q}_1$  is 14430 Mpc, for model with  $\mathbf{q}_2$  is 14470 Mpc.



## 2.7. Phantom scalar fields with barotropic EoS

It was mentioned above that current observations allow the possibility of the equation of state  $w_{de} < -1$ , which is generally referred to as phantom dark energy (PDE) [51, 279]. On the other hand PDE emerges effectively from the gravity sector of brane-world models [308, 309] (see also section 4.6 of this book), from superstring theory [310, 311], from Brans–Dicke scalar-tensor gravity [312, 313] and quantum effects that lead to violations of the weak energy condition on cosmological scales [314, 315]. Some of these models have phantom properties only at the current stage of evolution of the Universe but did not have them at early time or they lose this feature in the future. Let us analyze the possibility of modeling of such dark energy by a single minimally coupled scalar field.

Primarily note, that scalar fields with classical or tachyonic Lagrangians cannot be PDE since the field variables for them become imaginary (see eqs. (2.59)–(2.65)). So, another form of Lagrangians must be considered. The simplest one is modified canonical Lagrangian with altered sign before the kinetic term:

$$L_{de} = -X - U(\phi). \quad (2.66)$$

In this case the energy density and pressure are following linear combinations of  $X$  and  $U$ :

$$\rho_{de} = -X + U(\phi), \quad p_{de} = -X - U(\phi). \quad (2.67)$$

The EoS parameter

$$w_{de} = \frac{-X - U}{-X + U} \quad (2.68)$$

for positive values of  $X$  and  $U$  is  $\leq -1$ . For explanation of accelerated expansion of the Universe at the current epoch ( $q_0 < 0$ ) the phantom scalar field must satisfy two conditions:

$$\text{a) } 0 < X^{(0)} < U^{(0)}, \quad \text{b) } U^{(0)} + 2X^{(0)} > \rho_m^{(0)}/2. \quad (2.69)$$

Assuming barotropic equation of state the field variable, potential and kinetic term can be presented in terms of density and EoS parameter as follows:

$$\begin{aligned} \phi(a) - \phi_0 &= \pm \sqrt{-(1 + w_0)\rho_{de}^{(0)}} \int_1^a \frac{da'}{a'^{\left(\frac{5}{2} + \frac{3}{2}c_a^2\right)} H(a')}, \\ U(a) &= \frac{(1 - c_a^2)(1 + w_0)a^{-3(1+c_a^2)} + 2(c_a^2 - w_0)}{2(1 + c_a^2)} \rho_{de}^{(0)}, \\ X(a) &= -\frac{1 + w_0}{2} a^{-3(1+c_a^2)} \rho_{de}^{(0)}. \end{aligned} \quad (2.70)$$

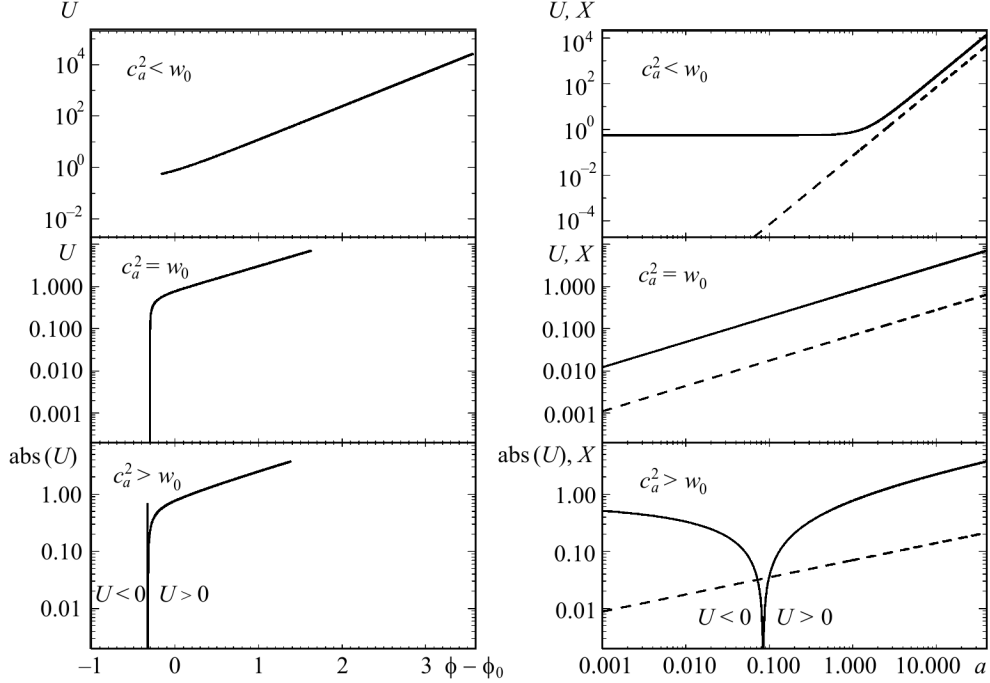


**Fig. 2.21.** Potentials  $U(\phi - \phi_0)$  (left) and dependences of potentials and kinetic terms on scale factor  $a$  (right) for phantom scalar field with Lagrangian (2.66) and barotropic EoS. In the top panels  $c_a^2 = -2.0$ , in the middle ones  $c_a^2 = -1.2$  and in the bottom ones  $c_a^2 = -1.1$ , in all panels  $w_0 = -1.2$ . Potential and kinetic term are in the units of current critical energy density,  $3c^2 H_0^2 / 8\pi G$ , the field variable in units of  $\sqrt{3c^2 / 8\pi G}$ . The current epoch in the left panels corresponds to  $\phi - \phi_0 = 0$  and field evolves from left to right

One can see that phantom barotropic scalar field ( $w_0 < -1$ ,  $c_a^2 < -1$ ) has real values of field variable and potential if current density of dark energy is positive. Its kinetic term  $X(a)$  is positive at any  $a$ , the potential  $U(a)$  is always positive only in the case  $c_a^2 \leq w_0$ . If  $w_0 < c_a^2 < -1$ , then  $U(a)$  starts from negative energy density  $(c_a^2 - w_0)\rho_{de}^{(0)} / (1 + c_a^2)$  at  $a = 0$ , changes the sign from “-” to “+” at  $a_{\rho=0} = [2(w_0 - c_a^2) / (1 - c_a^2)(1 + w_0)]^{-\frac{1}{3(1+c_a^2)}}$ , which is always  $\leq 1$  for phantom case. In any case  $U(a)$  increases with  $a$ , that distinguishes phantom scalar field from the quintessential one. The potentials  $U(\phi - \phi_0)$ , evolution of potentials and kinetic terms for models with  $c_a^2 < w_0 < -1$ ,  $c_a^2 = w_0 < -1$  and  $w_0 < c_a^2 < -1$  are shown in Fig. 2.21. One can see that accelerated expansion of the Universe is caused by rolling up of field to maximum of its potential, inversely as in the case of quintessential scalar field. We must note, that energy density and pressure are smooth monotonous functions of  $a$  for all relations between  $c_a^2$  and  $w_0$ , both  $< -1$ , while  $w_{de}$  has the second kind discontinuity, caused the passing of scalar field energy density over zero (see Fig. 2.7).

The effective sound speed (2.10) for phantom scalar field (2.66) is equal to the speed of light ( $c_s^2 = 1$ ) like in the case of classical one.

One can construct the Lagrangian like DBI one (2.61) for phantom range of EoS with positive defined kinetic term. Indeed, “relativistic” generalization of (2.66) is following:

$$L_{de} = -\tilde{U}(\xi)\sqrt{1+2\tilde{X}}. \quad (2.71)$$

The energy density, pressure and EoS parameter for this field are as follows:

$$\rho_{tach} = \frac{\tilde{U}(\xi)}{\sqrt{1+2\tilde{X}}}, \quad p_{tach} = -\tilde{U}(\xi)\sqrt{1+2\tilde{X}}, \quad (2.72)$$

$$w_{de} = -2\tilde{X} - 1. \quad (2.73)$$

One can see, that in the case of phantom field (2.71) the EoS parameter is always  $\leq -1$  for positive values of  $\tilde{X}$  independently on the value and sign of  $\tilde{U}$ . For explanation of accelerated expansion of the Universe at the current epoch ( $q_0 < 0$ ) such field must satisfy two conditions:

$$\text{a) } \tilde{X}^{(0)}, \tilde{U}^{(0)} > 0, \quad \text{b) } \tilde{U}^{(0)} \frac{1+3\tilde{X}^{(0)}}{\sqrt{1+2\tilde{X}^{(0)}}} > \rho_m^{(0)}/2, \quad (2.74)$$

where index (0) marks the current values of corresponding variables.

In the case of phantom field (2.71) its field variable, potential and kinetic term can be presented in terms of dark energy density (2.51) and EoS parameter (2.49) as follows:

$$\begin{aligned} \xi(a) - \xi_0 &= \pm \int_1^a \frac{da' \sqrt{-(1+w_{de}(a'))}}{a' H(a')}, \\ \tilde{U}(a) &= \rho_{de}(a) \sqrt{-w_{de}(a)}, \\ \tilde{X}(a) &= -\frac{1+w_{de}(a)}{2}. \end{aligned} \quad (2.75)$$

The potentials  $U(\xi - \xi_0)$ , evolution of potentials and kinetic terms for models with decreasing, constant and increasing EoS parameters are shown in Fig. 2.22. As it is in previous case, the accelerated expansion of the Universe is caused by rolling up of field to maximum of its potential. We must note, that energy density and pressure are smooth monotonous functions of  $a$  for all relations between  $c_a^2$  and  $w_0$ , both  $< -1$ , while  $w_{de}$  has discontinuity of second kind, caused by passing of scalar field energy density over zero (see Fig. 2.7) in the case  $w_0 < c_a^2$ . Moreover, as it follows from (2.75) and Fig. 2.7,

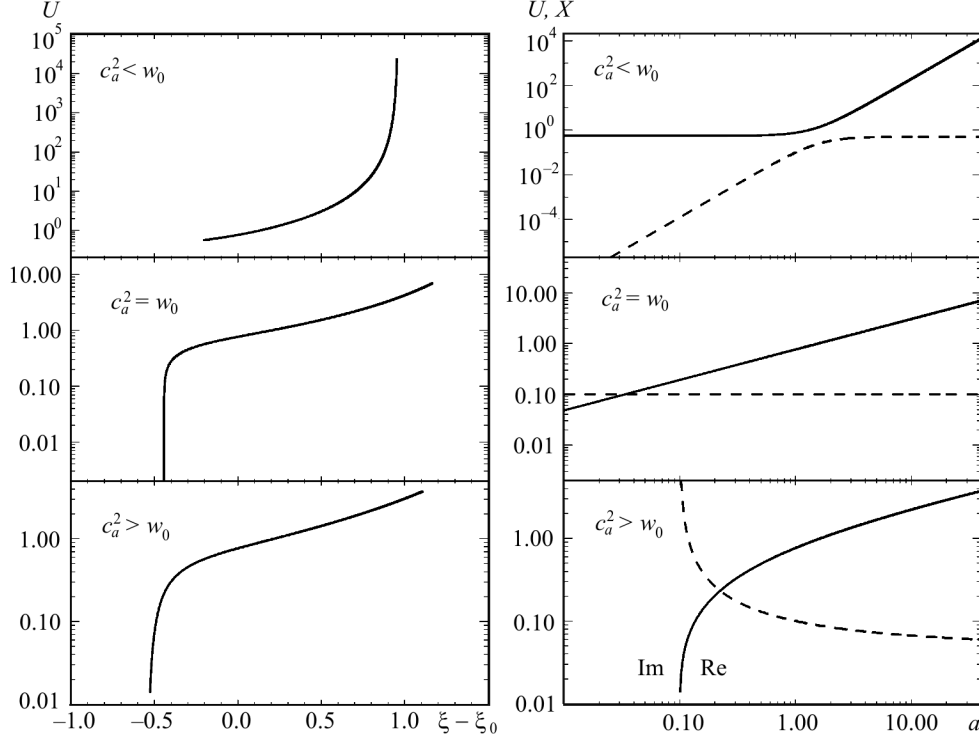
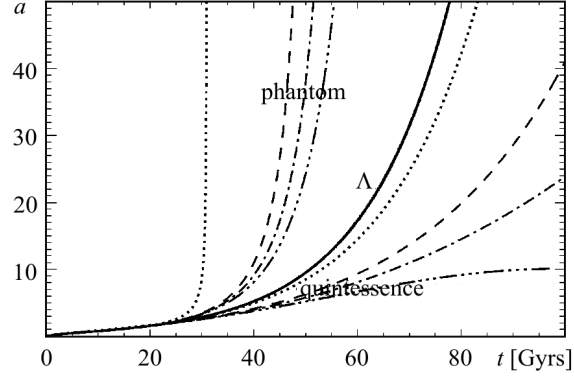


**Fig. 2.22.** Potentials  $U(\xi - \xi_0)$  (left) and dependences of potentials and kinetic terms on scale factor  $a$  (right) for phantom scalar field with Lagrangian (2.71) and barotropic EoS. In the top panels  $c_a^2 = -2.0$ , in the middle ones  $c_a^2 = -1.2$  and in the bottom ones  $c_a^2 = -1.1$ , in all panels  $w_0 = -1.2$ . Potential and kinetic term are in the units of current critical energy density,  $3c^2 H_0^2 / 8\pi G$ , the field variable is in units of  $\sqrt{3c^2 / 8\pi G}$ . The current epoch in the left panels corresponds to  $\phi - \phi_0 = 0$  and field evolves from left to right

the field variable  $\xi(a)$  and potential  $\tilde{U}(a)$  are imaginary at  $a < a_{\rho=0}$ , while measurable values,  $\rho_{de}(a)$  and  $p_{de}(a)$ , are real. Other intriguing property of such field is effective sound speed: according to (2.10) it is equal to  $-w_{de}$  and for phantom range is superluminal. Therefore, the phantom scalar field (2.71) can be theoretically interesting model of dark energy but unlikely for realization in our Universe. So, below we will analyse only phantom scalar field (2.66).

Other distinction of PSF from QSF consists in their asymptotic behavior: PSF mimics cosmological constant at the Beginning for any  $c_a^2 < -1$  ( $w_{de}$  goes to  $-1$  when  $a$  goes to 0), while QSF mimics it at  $a$ -infinity. So, such PSF always starts as cosmological constant with  $\rho_{de}(a = 0) = \rho_{de}^{(0)}(c_a^2 - w_0)/(1 + c_a^2)$ , which is positive for  $c_a^2 < w_0$  and negative when  $w_0 < c_a^2 < -1$ . This property distinguishes PSF from “standard” PDE [51, 279], the density of which starts from zero at  $a = 0$ . But one can see, that PDE is the special case of our barotropic PSF, when  $c_a^2 = w_0$ . In far future, when  $a \gg 1$ , its energy density

**Fig. 2.23.** Dependences of scale factors on time,  $a(t)$ , for cosmological models with quintessence/phantom scalar fields with  $w_0 = -1 \pm 0.2$  and  $c_a^2 = -1 \pm 1$  (dotted line),  $-1 \pm \pm 0.3$  (dashed line),  $-1 \pm 0.2$  (dash-dotted line),  $-1 \pm 0.1$  (dash-three-dotted line). The upper sign is for QSF, lower one is for PSF. For the  $\Lambda$ CDM model  $a(t)$  is shown by thick solid line. In all models  $\Omega_m = 0.3$ ,  $\Omega_{de} = 0.7$ ,  $H_0 = 70$  km/s · Mpc



will increase as  $\rho_{de}(a) \propto (1 + w_0)/(1 + c_a^2)\rho_{de}^{(0)}a^{-3(1+c_a^2)}$  while  $w_{de}$  will go to  $c_a^2$  (see eqs. (2.49) and (2.51)). So, its repulsion properties will increase and in finite time reach and outmatch firstly forces of gravitationally bound objects, then electrically ones, then strong force ones. All elements of structure of our Universe — galaxies, stars, planets, atoms and protons, will be ripped in finite time. This moment is dubbed the Big Rip<sup>8</sup> [279] and the moment when it happens can be estimated from the time dependence of scale factor,

$$t = \int_0^a \frac{da'}{a'H(a')}, \quad (2.76)$$

which can be calculated numerically using (1.15) for any cosmological models and parameters of scalar field with barotropic EoS. In Fig. 2.23 we present the time dependences of scale factors,  $a(t)$ , for cosmological models with PSF with the same parameters as in Fig. 2.7. For comparison we show also  $a(t)$  for  $\Lambda$ CDM and QSF+CDM models with symmetrical values of  $w_0$  and  $c_a^2$  relative to the phantom divide line. The phantom range of  $a - t$  space is above  $a(t)$ -line for  $\Lambda$ CDM with the same cosmological parameters, the quintessence range is below one.

At  $a \gg 1$ , when radiation and matter terms in (1.15) can be neglected, we obtain the approximate analytic formula for  $a(t)$ :

$$a(t) \approx \left[ \frac{3}{2} H_0 (1 + c_a^2) \sqrt{\frac{(1 + w_0)\Omega_{de}}{1 + c_a^2}} (t - t_0) + 1 \right]^{\frac{2}{3(1+c_a^2)}}. \quad (2.77)$$

It shows, that  $a$ -infinity is reached in finite time

$$t_{BR} - t_0 \approx \frac{2}{3} \frac{1}{H_0} \frac{1}{|1 + c_a^2|} \sqrt{\frac{1 + c_a^2}{(1 + w_0)\Omega_{de}}}, \quad (2.78)$$

<sup>8</sup> The first name of this singularity was “Big Smash”, proposed in the paper [316].

which is noted as time of Big Rip. Such fast expansion leads also to freezing of the particle horizon  $r_p$  at some  $r_p^{max}$  and contraction of the event horizon  $r_e$  to point when  $t \rightarrow t_{BR}$ . Really, in the co-moving coordinates they are as follows:

$$r_p(t) = c \int_0^a \frac{da'}{a'^2 H(a')}, \quad r_e(t) = c \int_0^\infty \frac{da'}{a'^2 H(a')} - r_p(a),$$

so, starting from  $a_f \gg 1$ , when matter component in (1.15) can be omitted, the rest of  $r_p$ -integral from  $a_f$  to  $a \gg a_f$  has analytic representation

$$I(a_f, a) = \frac{2c}{(1 + 3c_a^2)H_0} \sqrt{\frac{1 + c_a^2}{(1 + w_0)\Omega_{de}}} a_f^{\frac{(1+3c_a^2)}{2}}$$

and goes to 0 when  $a_f \rightarrow \infty$ .

Therefore, the positive energy density of PSF becomes infinite at finite time (2.78), overcoming all other forms of matter. The phantom scalar field dark energy rips at first the clusters of galaxies, later Milky Way and other galaxies, then Solar System, a bit later Earth, Sun and stars and ultimately “the molecules, atoms, nuclei, and nucleons of which we are composed, before the death of the Universe in a Big Rip” (see Table 1 in [279]). Will this be the end of Everything? Maybe this will be the beginning of new worlds — if PSF reaches the Planck density, the quantum fluctuations or interaction of field with the particles (the phenomenon of confinement) will lead to inflation in some regions of Planck scales. In the paper [312] it has been demonstrated that in the case of phantom Big Rip the consideration of quantum gravity effects might drastically change the future of our Universe, removing the singularity in a quite natural way.

Another feature of phantom dark energy, discussed in the literature, is its influence on quantum stability of vacuum. It was shown [317, 318] that minimally coupled scalar fields with a linear negative kinetic term may cause a UV quantum instability of the vacuum manifesting itself in the production of pairs of ghosts, photons or gravitons as a consequence of the violation of the null energy condition. It can be prevented by introducing the squared kinetic term in the Lagrangian as in the ghost condensate model [319, 320] or by second derivatives of the scalar field as in the kinetic braiding scalar-tensor model [321]. For late type phantom scalar fields the produced ghosts typically carry low energy, so, their decay rates are strongly time-dilated. On the other hand, the time scale of this instability for phantom dark energy can be much larger than the cosmological one, making this effect unsuitable for constraining the parameters of the model at the present level of observations. This is why in this chapter we concentrate our attention on the classical properties of scalar

field models of dark energy and on possibilities to determine their parameters by comparison of predictions with available observational data.

### 2.7.1. Gravitation instability of PSF and large scale structure formation

Before determination of PSF parameters let us discuss shortly the gravitational instability of such scalar field and its impact on the matter clustering. The complete system of evolution equations for cosmological perturbations of cold dark matter, baryons, massless and massive neutrinos and radiation based on General Relativity, differential conservation law and Boltzmann equations is presented in [116, 128, 130]. To understand the gravitational instability of PSF and its impact on the large scale structure formation in the matter and dark energy dominated epochs it is enough to analyze the subset of differential equations (2.14)–(2.17) with initial conditions (2.18)–(2.19) or (2.21)–(2.25) with initial conditions (2.26). At  $\eta_{init}$  for positive matter density perturbation<sup>9</sup> ( $\delta_m > 0$ ) the gravitational potential  $h_{init}$  in synchronous gauge (or  $\Psi_{init}$  in conformal Newtonian gauge) is negative and the dark energy density perturbation has opposite sign ( $\delta_{de} < 0$ ) for any  $w_0$ ,  $c_a^2 < -1$  and  $c_s^2 > 0$  (see equations (2.26)). The absolute values of their amplitudes in synchronous gauge increase  $\propto a$  at superhorizon stage of evolution, but amplitudes of density perturbations of phantom scalar field change the sign and decay after entering into horizon at  $\eta \approx k^{-1}$ . It is shown in Fig. 2.24, where the evolution of Fourier mode  $k = 0.05 \text{ Mpc}^{-1}$  of density perturbations for dark matter, baryons and phantom scalar field is presented for two cases:  $c_a^2 < w_0$  and  $c_a^2 = w_0$ .

One can see, that in the case of  $c_a^2 = w_0$  the absolute value of initial amplitude of  $|\delta_{de}|$  is higher than in the case of  $c_a^2 < w_0$ , but at the epoch of structure formation and at current epoch they are essentially lower than  $\delta_m$ . It means that perturbations of minimally coupled scalar fields with initial conditions (2.26) practically do not impact structure formation in matter components.

Nevertheless the parameters of barotropic scalar field can be constrained by data on the large scale structure of the Universe, since the rate of increasing of amplitude of matter density perturbations is enough sensitive to them. It is illustrated in Fig. 2.25, where the matter density evolution,  $\delta_m(a)$ , is shown for models with PSF dark energy. In order to eliminate the  $k$ -dependence caused by the baryonic component at small scales and emphasize the influence of dark energy we have normalized the amplitude of matter density perturbations to 0.1 at  $a = 0.1$  (free normalization). Then  $\rho_m/\rho_{de} \sim 1000$ ,  $q \approx 0.5$  and amplitudes of all Fourier modes evolve practically equally. For comparison the same

<sup>9</sup>In the early Universe for superhorizon scale it includes also relativistic components, which are density dominating.

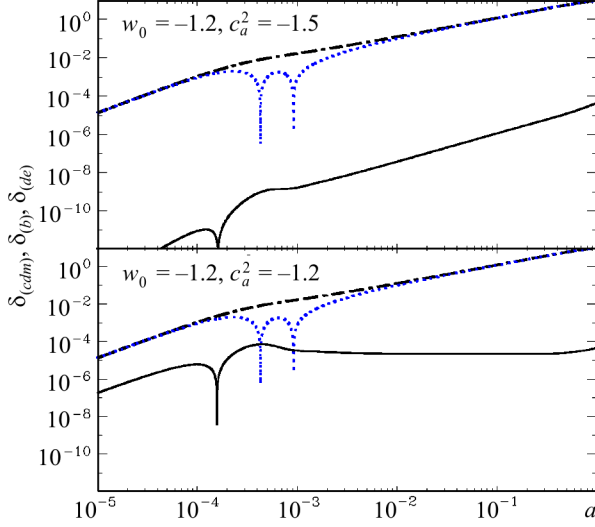
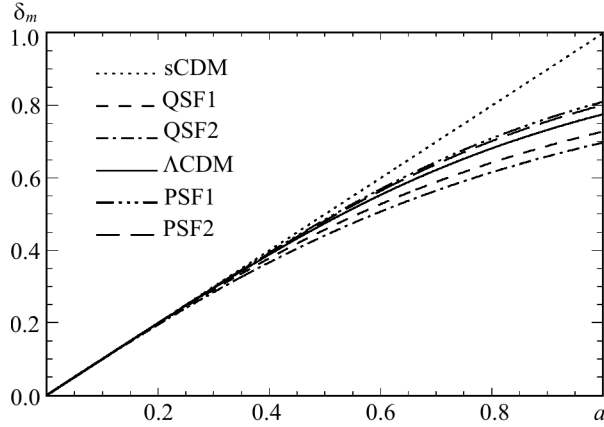


**Fig. 2.24.** Evolution of Fourier amplitude ( $k = 0.05 \text{ Mpc}^{-1}$ ) of density perturbations of cold dark matter (dashed line), baryonic matter (dotted line) and PSF (solid line) with  $c_a^2 < w_0$  (top panel) and  $c_a^2 = w_0$  (bottom panel)

**Fig. 2.25.** Evolution of matter density perturbations from Dark Ages to current epoch in sCDM,  $\Lambda$ CDM, QSF+CDM (1:  $w_0 = -0.8$ ,  $c_a^2 = -0.8$ ; 2:  $w_0 = -0.8$ ,  $c_a^2 = -0.5$ ) and PSF+CDM (1:  $w_0 = -1.2$ ,  $c_a^2 = -1.2$ ; 2:  $w_0 = -1.2$ ,  $c_a^2 = -1.5$ ) models. Amplitudes are normalized to 0.1 at  $z = 10$  ( $a = 0.1$ ). In the models with dark energy  $\Omega_m = 0.3$ ,  $\Omega_{de} = 0.7$



variables for QSF + CDM,  $\Lambda$ CDM and the standard CDM (sCDM) models are also presented. So, for the amplitude of large scale structure inhomogeneities the cosmological model with PSF is distinctive from one with QSF by  $\sim 10\%$  and from  $\Lambda$ CDM one by few percents at  $0 \leq z \leq 1$ .

Let us analyze the evolution of linear density perturbations in the future. The first question for elucidation is gravitational instability of PSF at strongly dark energy dominated epoch. We have integrated the system of differential equations (2.21)–(2.25) with initial conditions (2.26) up to  $a = 200$ , when expansion is already superfast (see Fig. 2.23) and  $\rho_{de}/\rho_m \sim 10^8\text{--}10^{10}$ . The results for PSF density perturbations are shown in Fig. 2.26 (left column) for different  $k$ -modes (0.0005, 0.001, 0.0015, 0.002, 0.0025, 0.005, 0.01, 0.05, 0.1  $\text{Mpc}^{-1}$ ) and two expansion rates, which correspond to models with  $w_0 = -1.2$ ,  $c_a^2 = -1.5$  (top panel) and  $c_a^2 = -1.2$  (bottom panel). One can see, that



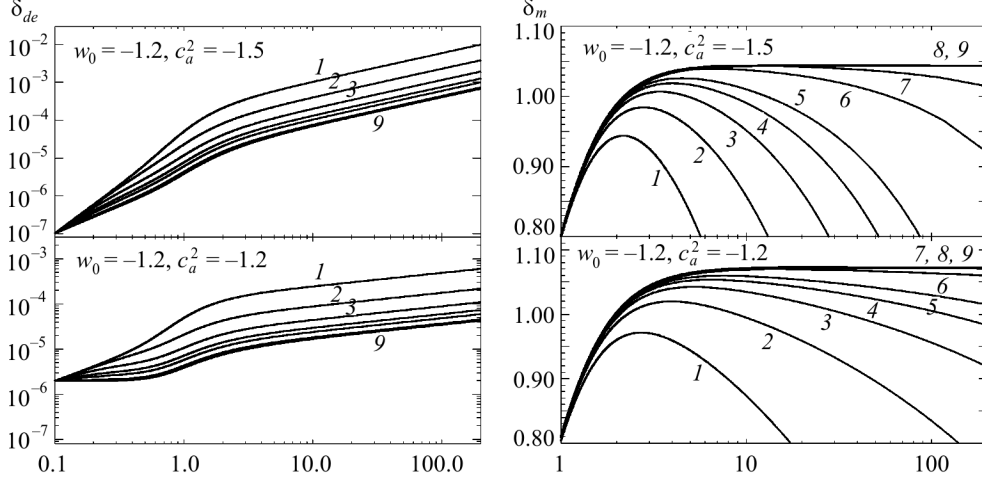


**Fig. 2.26.** Evolution of different Fourier amplitudes of PSF (left column) and matter (right column) density perturbations from  $a = 0.1$  to  $a = 200$  for models with  $w_0 = -1.2$ ,  $c_a^2 = -1.5$  (top panels) and  $w_0 = -1.2$ ,  $c_a^2 = -1.2$  (bottom panels). The rest parameters are the same as in Figs.2.24 and 2.25. The different lines correspond to wave numbers  $k$  (in  $\text{Mpc}^{-1}$ ) as follows: 1 – 0.0005, 2 – 0.001, 3 – 0.0015, 4 – 0.002, 5 – 0.0025, 6 – 0.005, 7 – 0.01, 8 – 0.05, 9 – 0.1  $\text{Mpc}^{-1}$ . The amplitudes of all  $k$ -modes of  $\delta_{de}$  are normalized to  $0.1\delta_{de}(k = 0.05; a = 0.1)/\delta_m(k = 0.05; a = 0.1)$ , the amplitudes of all  $k$ -modes of  $\delta_m$  are normalized to 0.1 at  $a = 0.1$

their amplitudes increase slowly and the rate depends on background expansion rate as well as on wave number. In order to visualize this  $k$ -dependence we remove the dependence on  $k$  caused by initial power spectrum and transition processes in the early epochs by renormalization of amplitudes at  $a = 0.1$  to  $\delta_{de}(k) = 0.1\delta_{de}(k = 0.05; a = 0.1)/\delta_m(k = 0.05; a = 0.1)$ . So, all  $k$ -modes of PSF density perturbations in Fig. 2.26 have the same amplitudes at  $a = 0.1$ , but the ratio of matter to PSF ones is the same as for  $k = 0.05 \text{ Mpc}^{-1}$  mode at that moment, as computed by CAMB and shown in Fig. 2.24. One can see, that rates of increasing of amplitudes are higher for lower  $k$  in the range  $a = 0.1$ –10 and are practically the same for all  $k$ -modes at  $a > 10$ :  $\delta_{de} \propto a^{-3(1+c_a^2)/2}$ . For the PSF with  $w_0 = -1.2$  and  $c_a^2 = -1.5$  the amplitude of  $k = 0.1 \text{ Mpc}^{-1}$  mode increases from  $a = 0.1$  to  $a = 10$  by 693 times, while the amplitude of  $k = 0.0005 \text{ Mpc}^{-1}$  mode increases by 10307 times. For the PSF with  $w_0 = c_a^2 = -1.2$  these numbers are 9 and 125 correspondingly. Since the evolution of amplitude of gravitational potential  $h$  is driven by term  $\rho_m\delta_m + \rho_{de}(1 + 3w_{de})\delta_{de}$  (Eq. 2.25), shortly after  $a = 1$  the perturbations of PSF will become crucial firstly on the largest scales and later on less and less. They affect the evolution of matter density perturbations, that is shown in the right panels of Fig. 2.26 in the log-norm scales. At scales with  $k \geq 0.05 \text{ Mpc}^{-1}$  (superimposed lines 8, 9 in both panels) the amplitudes of matter density

perturbations in the models with PSF will increase from  $a = 1$  to  $a = 10$  only by  $\sim 1.3$  times and will freeze at this value. At these scales in this range of  $a$  the influence of PSF density perturbations on the evolution of matter density ones is inappreciable. In the  $\Lambda$ CDM and QSF + CDM models all  $k$ -modes will evolve similarly as it is shown by line 9. In the PSF + CDM models at scales with  $k < 0.05 \text{ Mpc}^{-1}$  the effect of PSF density perturbations on the evolution of matter density ones becomes important: increasing of amplitude of PSF density perturbations causes the decaying of matter density ones. The greater is scale of perturbation, the earlier its amplitude starts to decay<sup>10</sup>.

Note, that this decaying of matter density perturbations is caused solely by influence of phantom scalar field perturbations, not superfast expansion of background (at  $a \sim 2$  the rates of expansion in PSF models are close to ones in  $\Lambda$ CDM and QSF, as it can be seen from Figs. 2.7 and 2.23). Excluding the effect of perturbations, the amplitudes of all  $k$ -modes freeze as it is shown by line 9. This is not the beginning of the Big Rip mentioned above, but its analog for linear perturbations.

### 2.7.2. Best-fit parameters of PSF

Let us estimate the parameters of PSF using the same data, method and codes which have been applied for QSF (see subsection 2.6.4). To find the best-fit values of parameters of cosmological model with PSF and their confidence limits we perform the MCMC analysis for two combined datasets: WMAP7 + HST + BBN + BAO + SN SDSS SALT2 and WMAP7 + HST + BBN + BAO + SN SDSS MLCS2k2. The difference in the search procedure consists only in the flat priors for  $w_0$  and  $c_a^2$  and starting values for them. In the case of PSF the priors are as follows:  $-2 \leq w_0 \leq -1$  and  $-2 \leq c_a^2 \leq -1$ . Since in the PSF models with  $w_0 < c_a^2 < -1$  the EoS parameter has second kind discontinuity at  $a < 1$ , we exclude them from likelihood analysis by the additional condition  $c_a^2 \leq w_0$ .

The results of estimation of the PSF parameters jointly with the minimal set of cosmological parameters for two sets of observational data (WMAP7 + HST + BBN + BAO + SN SDSS SALT2 and WMAP7 + HST + BBN + BAO + SN SDSS MLCS2k2) are presented in Table 2.2. We denote the sets of best-fit parameters by  $\mathbf{p}_1$  and  $\mathbf{p}_2$ . Here  $\mathbf{p}_i = (\Omega_{de}, w_0, c_a^2, \Omega_b, \Omega_{cdm}, H_0, n_s, A_s, \tau_{rei})$ . Both SN SDSS distance moduli datasets prefer values of  $w_0$  slightly lower than  $-1$ . In the past, when  $a \rightarrow 0$ ,  $w_{de} \rightarrow -1$ . Hence, the PSFs with parameters  $\mathbf{p}_1$  and  $\mathbf{p}_2$  mimic the  $\Lambda$ -term from the Big Bang up to the current epoch, but, due to instability of the value  $w_{de} = -1$ , even such a small difference changes drastically the future fate of the Universe: in  $\Lambda$ CDM model

<sup>10</sup>In order to visualize this effect in Fig. 2.26 we have normalized all  $k$ -modes of  $\delta_m$  to 0.1 at  $a = 0.1$ .

**Table 2.2. The best-fit values for cosmological parameters of PSF + CDM model and their  $1\sigma$  limits from the extremal values of the N-dimensional distribution determined by the MCMC technique from the combined datasets WMAP7 + HST + BBN + BAO + SN SDSS SALT2 ( $\mathbf{p}_1$ ) and WMAP7 + HST + BBN + BAO + SN SDSS MLCS2k2 ( $\mathbf{p}_2$ ). All units and notation are the same as in Table 2.1**

Parameters	$\mathbf{p}_1$	$\mathbf{p}_2$	Parameters	$\mathbf{p}_1$	$\mathbf{p}_2$
$\Omega_{de}$	$0.72^{+0.04}_{-0.04}$	$0.69^{+0.05}_{-0.04}$	$H_0$	$70.4^{+4.0}_{-3.2}$	$67.8^{+4.2}_{-2.9}$
$w_0$	$-1.043^{+0.043}_{-0.24}$	$-1.002^{+0.002}_{-0.14}$	$n_s$	$0.96^{+0.04}_{-0.03}$	$0.96^{+0.03}_{-0.04}$
$c_a^2$	$-1.12^{+0.12}_{-0.50}$	$-1.19^{+0.19}_{-0.42}$	$\log(10^{10} A_s)$	$3.09^{+0.09}_{-0.09}$	$3.11^{+0.08}_{-0.11}$
$10\omega_b$	$0.223^{+0.016}_{-0.013}$	$0.223^{+0.014}_{-0.013}$	$\tau_{rei}$	$0.085^{+0.041}_{-0.031}$	$0.086^{+0.036}_{-0.038}$
$\omega_{cdm}$	$0.115^{+0.011}_{-0.010}$	$0.119^{+0.009}_{-0.010}$	$-\log L$	3864.86	3859.30

the Universe as well as existing structures (in principle) are time-unlimited, while in the PSF + CDM model it reaches the Big Rip singularity in finite time, preceded by the destruction of the structure from clusters of galaxies to elementary particles. More precisely, in the PSF + CDM with parameters  $\mathbf{p}_1$  this happens in  $\approx 152$  Gyrs, with  $\mathbf{p}_2$  in  $\approx 594$  Gyrs. Long before  $t_{BR}$  the particle horizon<sup>11</sup> becomes  $r_p^{max} \approx 18710$  Mpc in model  $\mathbf{p}_1$  and  $\approx 19200$  in model  $\mathbf{p}_2$ , just  $\approx 1.3$  times larger than the current particle horizon.

## 2.8. Distinguishing of scalar field models of dark energy

The key parameters of barotropic scalar field are its current density in units of critical one  $\Omega_{de}$ , EoS parameter  $w_0$ , adiabatic sound speed  $c_a^2$  and effective sound speed  $c_s^2$ . Their reliable determination will unveil the inherent properties of dark energy: whether it is the cosmological constant ( $w_0 = c_a^2 = -1$ ) or dynamical dark energy in the form of QSF or PSF. The best-fit values and confidential ranges of cosmological parameters for flat QSF + CDM and PSF + CDM models determined by MCMC method on the base of WMAP7 + HST + BBN + BAO + SN SDSS SALT2 and WMAP7 + HST + BBN + BAO + SN SDSS MLCS2k2 datasets are presented in Tables 2.1 and 2.2 correspondingly. Similar computations have been carried out for  $\Lambda$ CDM model and the best-fit values and confidential ranges of cosmological parameters  $\mathbf{l}_1$  and  $\mathbf{l}_2$  are presented in Table 2.3.

If we compare the maxima of likelihood functions  $\chi^2 = -\log(L_{max})$ , presented in the last rows of Tables 2.1–2.3, we see that the current observational dataset including SN SDSS SALT2 prefers phantom scalar field model

<sup>11</sup> At the current epoch  $r_p^{(0)} = 14260$  Mpc in the model with  $\mathbf{p}_1$  and 14170 Mpc in the model with  $\mathbf{p}_2$ .

of dark energy, since  $\chi_{PSF}^2 < \chi_{\Lambda CDM}^2 < \chi_{QSF}^2$ . The opposite trend is for the dataset including SN SDSS MLCS2k2,  $\chi_{QSF}^2 < \chi_{\Lambda CDM}^2 < \chi_{PSF}^2$ , so, it prefers quintessential scalar field model of dark energy. The differences between all  $\chi^2$  in the tables are not statistically significant, but a clear trend supports that. In the paper [77] the differences between 2 methods of light-curve fitting, SALT2 and MLCS2k2, are thoroughly analyzed but convincing arguments for one or the other are not given. So, we can conclude only that WMAP7 + HST + BBN + BAO + SN SDSS SALT2 dataset prefers slightly the phantom scalar field model of dark energy, while WMAP7 + HST + BBN + BAO + SN SDSS MLCS2k2 dataset prefers slightly the quintessence one, but none of considered QSF + CDM,  $\Lambda$ CDM and PSF + CDM models with best-fit parameters has statically significant advantages by current datasets, used for their determination. All these models match well the observational data on SNe Ia distance moduli (Fig. 2.27), BAO relative distance measure (Fig. 2.29), power spectrum of matter density perturbations (Fig. 2.30), CMB temperature fluctuations (Fig. 2.31) and temperature-polarization (Fig. 2.32) power spectra. Let us analyze the possibility to distinguish QSF + CDM and PSF + CDM by each type of observational data.

The lines corresponding to different DE models, QSF, PSF and  $\Lambda$ , in the left panel of Fig. 2.27) look as perfectly superimposed, that means the complete model degeneracy. The maximal values of relative differences of SNe Ia distance moduli  $\Delta(m - M)/(m - M) \sim 0.4\%$  at low redshifts are for QSF models with  $\mathbf{q}_1$  and  $\mathbf{q}_2$  shown in Fig. 2.16. The similar relative differences between these dependences for QSF + CDM and PSF + CDM models with best-fit parameters determined with the same fitters ( $|\mu(\mathbf{q}_i) - \mu(\mathbf{p}_i)|/\mu(\mathbf{q}_i)$ ) are  $\leq 0.1\%$  (right panel of Fig. 2.27), that makes these data still quite useless to set the type of scalar field as dark energy.

Fortunately, other characteristics of dynamics of expansion of the Universe, based on the measurements of the first and second time derivatives of

**Table 2.3. The best-fit values for cosmological parameters of  $\Lambda$ CDM model and their  $1\sigma$  limits from the extremal values of the N-dimensional distribution determined by the MCMC technique from the combined datasets WMAP7 + HST + BBN + BAO + SN SDSS SALT2 ( $l_1$ ) and WMAP7 + HST + BBN + BAO + SN SDSS MLCS2k2 ( $l_2$ ). All units and notation are the same as in Tables 2.1 and 2.2.**

Parameters	$l_1$	$l_2$	Parameters	$l_1$	$l_2$
$\Omega_\Lambda$	$0.73^{+0.03}_{-0.04}$	$0.70^{+0.04}_{-0.04}$	$n_s$	$0.97^{+0.03}_{-0.03}$	$0.96^{+0.03}_{-0.03}$
$10\omega_b$	$0.226^{+0.012}_{-0.013}$	$0.224^{+0.013}_{-0.013}$	$\log(10^{10} A_s)$	$3.08^{+0.09}_{-0.09}$	$3.10^{+0.08}_{-0.08}$
$\omega_{cdm}$	$0.112^{+0.009}_{-0.008}$	$0.118^{+0.008}_{-0.009}$	$\tau_{rei}$	$0.087^{+0.041}_{-0.031}$	$0.082^{+0.038}_{-0.030}$
$H_0$	$70.4^{+2.9}_{-3.4}$	$68.2^{+3.3}_{-3.1}$	$-\log L$	3864.96	3859.15

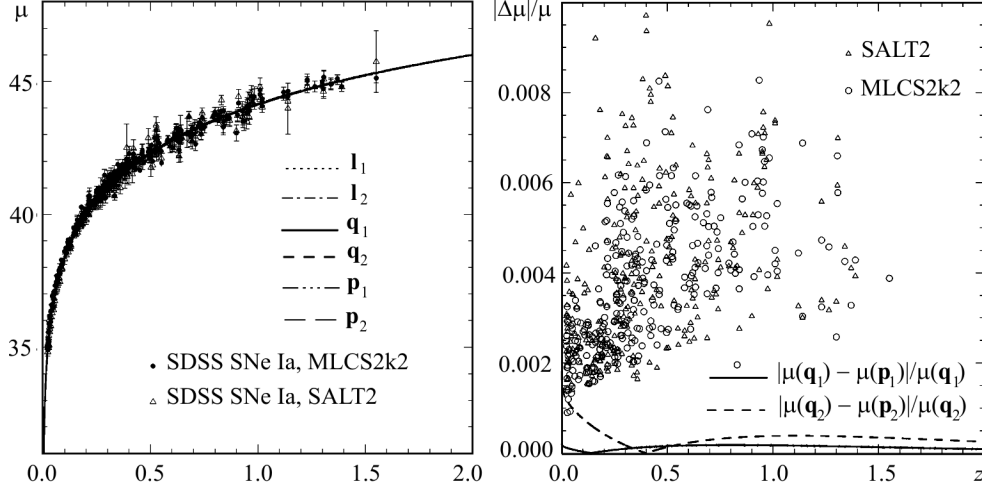


**Fig. 2.27.** Left panel: the dependences of distance modulus  $\mu \equiv m - M$  on redshift  $z$  for SNe Ia in the models with best-fit parameters  $\mathbf{l}_1$ ,  $\mathbf{l}_2$ ,  $\mathbf{q}_1$ ,  $\mathbf{q}_2$ ,  $\mathbf{p}_1$  and  $\mathbf{p}_2$  (superimposed lines) and observational data SDSS SNe Ia (signs). Right panel: the relative differences of distance moduli between QSF + CDM and PSF + CDM models with best-fit parameters determined for the same datasets (lines) and observational uncertainties for SDSS SNe Ia (signs)

Hubble parameter<sup>12</sup>  $H(\eta)$ , are essentially more sensitive to the value and time dependence of EoS parameter. The dependences of dimensionless parameters describing the dynamics of expansion of the Universe on redshift, such as the rate of expansion  $H/H_0$ , the deceleration parameter  $q = -\dot{H}/(aH^2) - 1$  and the statefinder parameters [322]  $r = \ddot{H}/(a^2H^3) + 2\dot{H}/(aH^2) + 1$  and  $s \equiv (r - 1)/3(q - 1/2)$ , are shown in Fig. 2.28 for the models with best-fit parameters  $\mathbf{l}_1$ ,  $\mathbf{l}_2$ ,  $\mathbf{q}_1$ ,  $\mathbf{q}_2$ ,  $\mathbf{p}_1$  and  $\mathbf{p}_2$ . Here the  $r$ -parameter is *jerk* (1.25), the  $s$ -parameter is linear combination of  $q$  and  $r$ , not snap one, discussed in the section 1.3. For matter plus dark energy dominated epoch they can be presented in our parametrization (2.49) as follows:

$$r = 1 + 4.5(1 + w_{de})c_a^2\Omega_{de}(a), \quad s = (1 + w_{de})c_a^2/w_{de},$$

where  $\Omega_{de}(a) \equiv 8\pi G\rho_{de}(a)/3H^2$ . One can see that the differences between  $s(\mathbf{q}_i)$  and  $s(\mathbf{p}_i)$  at high  $z$  as well as between  $r(\mathbf{q}_i)$  and  $r(\mathbf{p}_i)$  at low  $z$  are essentially larger than for parameters  $H$  and  $q$ . Maybe the future high-precision measurements of dynamics of expansion of the Universe will give possibility to distinguish the QSF and PSF models of DE.

The BAO relative distance measure  $R_{rD}(z) \equiv r_s(z_{drag})/D_V(z)$  (see subsection 1.4) extracted from SDSS DR7 galaxy redshift survey [143] is matched well by QSF+CDM, PSF+CDM and  $\Lambda$ CDM models with best-fit parameters

<sup>12</sup>  $\mu(z)$  dependence is integral of  $1/H$  over redshift (Eq. 1.23).

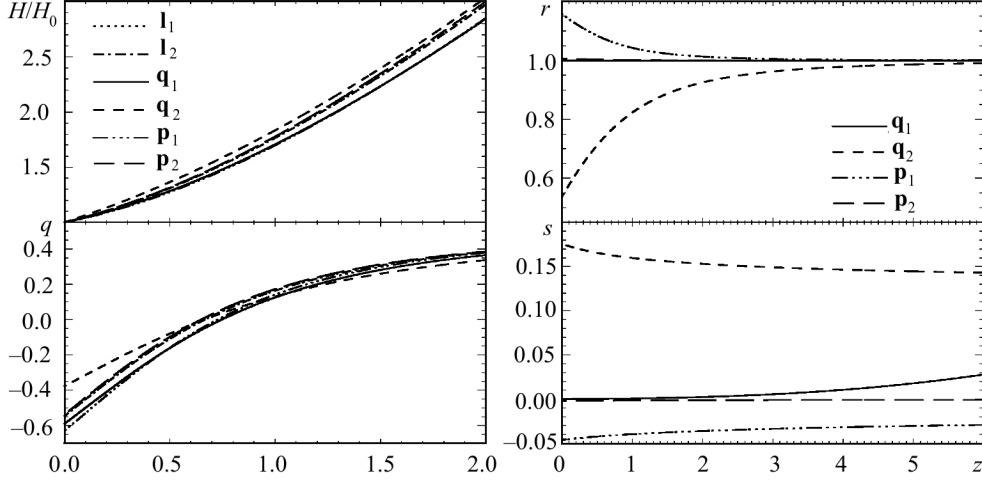


**Fig. 2.28.** The dependences of dimensionless parameters describing the dynamics of expansion of the Universe on redshift in the models with best-fit parameters  $\mathbf{l}_1$ ,  $\mathbf{l}_2$ ,  $\mathbf{q}_1$ ,  $\mathbf{q}_2$ ,  $\mathbf{p}_1$  and  $\mathbf{p}_2$ : the rate of expansion  $H/H_0$  (left panel, top), the deceleration parameter  $q = -\dot{H}/(aH^2) - 1$  (left panel, bottom) and the statefinder parameters  $r = \ddot{H}/(a^2H^3) + 2\dot{H}/(aH^2) + 1$  and  $s \equiv (r - 1)/3(q - 1/2)$  (right panel). For the  $\Lambda$ CDM model the last two parameters equal 1 and 0 correspondingly

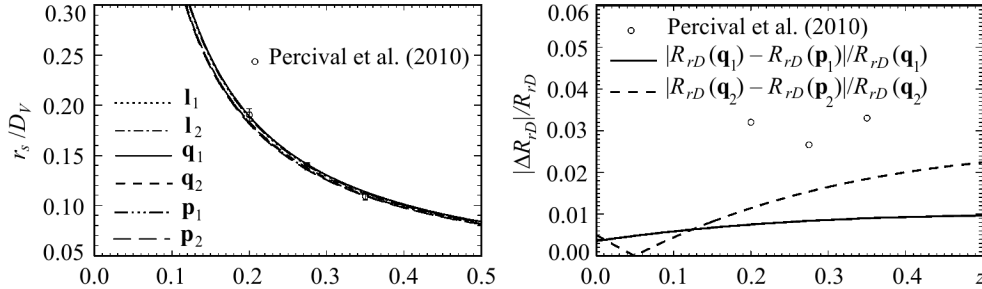


**Fig. 2.29.** Left panel: the BAO relative distance measure  $R_{rD} \equiv r_s(z_{drag})/D_V(z)$  in the cosmological models with best-fit parameters  $\mathbf{l}_1$ ,  $\mathbf{l}_2$ ,  $\mathbf{q}_1$ ,  $\mathbf{q}_2$ ,  $\mathbf{p}_1$  and  $\mathbf{p}_2$  (lines) and observational data extracted from SDSS DR7 galaxy redshift survey [143] (symbols). Right panel: the relative difference of the BAO distance measure  $|\Delta R_{rD}|/R_{rD}$  in the models with best fitting parameters  $\mathbf{q}_i$  and  $\mathbf{p}_i$ . Dots show observational  $1\sigma$  relative errors of data in the left panel

$\mathbf{q}_1$ ,  $\mathbf{q}_2$ ,  $\mathbf{p}_1$ ,  $\mathbf{p}_2$ ,  $\mathbf{l}_1$  and  $\mathbf{l}_2$  correspondingly. (Fig. 2.29, left panel). The relative differences of  $R_{rD}(z)$  for models with QSF and PSF are  $\leq 2\%$  at  $z \leq 0.4$ , while observational errors are  $\sim 3\%$  at  $0.2 \leq z \leq 0.35$  (right panel of Fig. 2.29). It means that future extensive measurements of galaxy space inhomogeneities in principle can distinguish these scalar fields of dark energy. The power spectrum of matter density perturbations extracted from luminous red galaxies of SDSS DR7 catalogue by Reid et al. (2010) [163] has not been used for determination

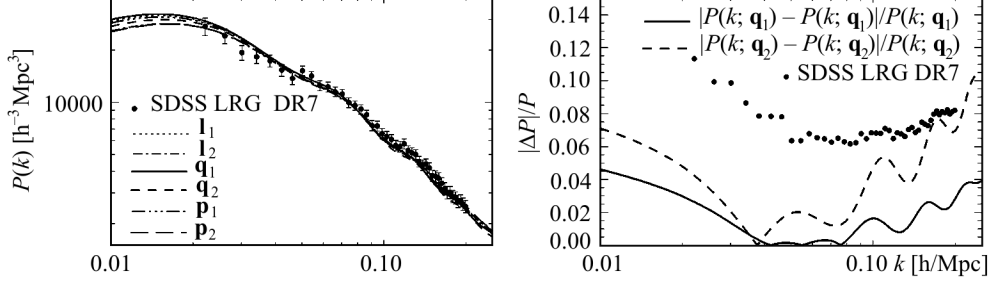


**Fig. 2.30.** Left panel: the power spectrum of matter density perturbations in the cosmological models with best-fit parameters  $l_1$ ,  $l_2$ ,  $q_1$ ,  $q_2$ ,  $p_1$  and  $p_2$ . Dots show observational SDSS LRG DR7 power spectrum [163]. Right panel: the relative difference of matter density power spectra  $|\Delta P(k)|/P(k)$  in the models with best fitting parameters  $q_i$  and  $p_i$ . Dots show observational uncertainties ( $1\sigma$ ) of SDSS LRG DR7 data [163]

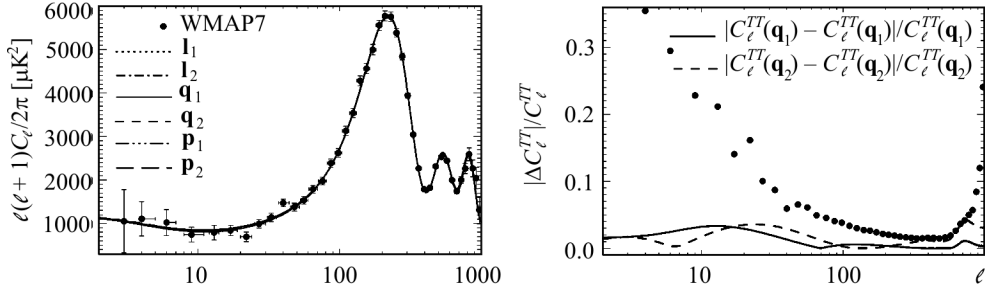


**Fig. 2.31.** Left panel: the power spectra of CMB temperature fluctuations  $\ell(\ell+1)C_\ell^{TT}/2\pi$  in the cosmological models with best-fit parameters  $l_1$ ,  $l_2$ ,  $q_1$ ,  $q_2$ ,  $p_1$  and  $p_2$  (superimposed lines) and observational one from WMAP7 [93] (dots). Right panel: the relative differences of CMB temperature fluctuations power spectra  $|\Delta C_\ell^{TT}|/C_\ell^{TT}$  in the models with best fitting parameters  $q_i$  and  $p_i$  (Tables 2.1 and 2.2). Dots show observational uncertainties ( $1\sigma$ ) of WMAP7  $\ell(\ell+1)C_\ell^{TT}/2\pi$

of best-fit parameters of QSF + CDM, PSF + CDM and  $\Lambda$ CDM models, however the computed for them power spectra match it perfectly too. The experimental errors of its determination are still too large (8–12%) to distinguish between different scalar field models of dark energy. In addition, at the small scales ( $k \geq 0.1 \text{ hMpc}^{-1}$ ) there are uncertainties in the computation of the power spectrum associated with the non-linear evolution of perturbations and unknown type of dark matter, cold or warm, that is being actively discussed in the literature.

Above we have discussed the importance of data on CMB anisotropy for determination of cosmological parameters and, particularly, the dark energy ones. The key cosmological data now are WMAP all sky maps, which contain information about position and amplitude of acoustic peaks at decoupling epoch as well as the amplitudes of large scale matter density perturbations

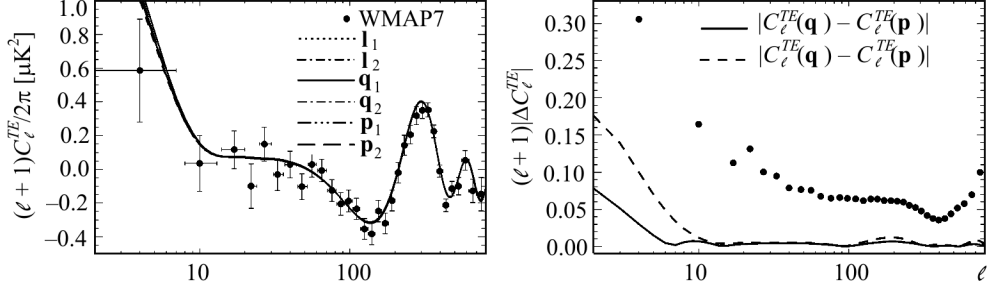


**Fig. 2.32.** Left panel: the temperature-polarization power spectra of CMB  $(\ell + 1)C_\ell^{TE}/2\pi$  in the cosmological models with best-fit parameters  $\mathbf{l}_1$ ,  $\mathbf{l}_2$ ,  $\mathbf{q}_1$ ,  $\mathbf{q}_2$ ,  $\mathbf{p}_1$  and  $\mathbf{p}_2$  (superimposed lines) and observational one from WMAP7 [93] (dots). Right panel: the relative differences of CMB temperature-polarization power spectra  $|\Delta C_\ell^{TE}|/C_\ell^{TE}$  in the models with best fitting parameters  $\mathbf{q}_i$  and  $\mathbf{p}_i$  (Tables 2.1 and 2.2). Dots show observational uncertainties ( $1\sigma$ ) of WMAP7  $(\ell + 1)C_\ell^{TE}/2\pi$

at the late epoch causing the integrated Sachs–Wolfe effect. In Fig. 2.31 (left panel) the binned power spectrum of temperature fluctuations extracted from the 7-year WMAP all sky measurements [93–95] is shown. Its accuracy is maximal (minimal errors  $\sim 2\text{--}4\%$ ) in the range of acoustic peaks ( $\ell \sim 200\text{--}600$ ), this allows the accurate determination of main cosmological parameters. The maximal accuracy of determination of parameters of dark energy is achieved when these data are used together with SNe Ia and BAO relative distance measure or matter density power spectrum. The computed power spectra  $\ell(\ell + 1)C_\ell^{TT}/2\pi$  for cosmological models  $\Lambda$ CDM, QSF + CDM and PSF + CDM with best-fit parameters  $\mathbf{l}_1$ ,  $\mathbf{l}_2$ ,  $\mathbf{q}_1$ ,  $\mathbf{q}_2$ ,  $\mathbf{p}_1$  and  $\mathbf{p}_2$  match well the observational one. The relative differences between power spectra in QSF+CDM and PSF+CDM models, shown in the right panel of Fig. 2.31, do not exceed the relative observational uncertainties of  $\ell(\ell + 1)C_\ell^{TT}/2\pi$ . Additional constraints on the cosmological parameters are obtained when CMB polarization data are included. For the illustration of agreement between theory and observations in the left panel of Fig. 2.32 the power spectra of CMB temperature-polarization  $(\ell + 1)C_\ell^{TE}/2\pi$  in the cosmological models with best-fit parameters  $\mathbf{l}_1$ ,  $\mathbf{l}_2$ ,  $\mathbf{q}_1$ ,  $\mathbf{q}_2$ ,  $\mathbf{p}_1$  and  $\mathbf{p}_2$  as well as WMAP7 [93] one are presented. All lines are superimposed at  $\ell > 10$  with sub-percent accuracy, while minimal errors of observational power spectrum at high spherical harmonics are  $\sim 4\text{--}6\%$  (right panel of Fig. 2.32).

In the paper [323] we have used the newer data on SNe Ia distance moduli from SNLS3 compilation (hereafter SNLS3) [84] and Union2.1 compilation (hereafter Union2.1) [324] together with data on BAO from the WiggleZ Dark Energy Survey (hereafter WiggleZ) [325]. The results for the combined datasets WMAP7 + HST + BBN + BAO + WiggleZ + SNLS3 and WMAP7 + HST + + BBN + BAO + WiggleZ + Union2.1 are presented in Tables 2.4 and 2.5 correspondingly.



Both these combined datasets prefer phantom fields,  $\chi_{PSF}^2 < \chi_{\Lambda CDM}^2 < \chi_{QSF}^2$ , and for both the differences of maximum of likelihoods between PSF + CDM,  $\Lambda$ CDM and QSF + CDM are still statistically insignificant too.

The results of determination of cosmological parameters, especially  $H_0$ ,  $\Omega_{de}$ ,  $w_{de}$  and  $c_a^2$ , presented in Tables 2.1–2.3, also indicate certain inconsistency or tension between fitters SALT2 and MLCS2k2 applied to the same SNe Ia. It was clearly highlighted and analyzed in the papers [77, 326], but up to now we have no decisive arguments for favor of one of them.

Therefore, any of the used observational data at the current level of accuracy cannot prefer QSF + CDM, PSF + CDM or  $\Lambda$ CDM at statistically significant level. In the framework of each of them the model with best-fit parameters exists, it matches well each type of data and all together with close goodness. The increasing of accuracy of observational CMB power spectra jointly with high precision matter density one and SNe Ia luminosity distance measurements will give possibility to establish the dynamical properties of dark

**Table 2.4. The best-fit values and  $1\sigma$  confidence ranges of the N-dimensional distribution for the dark energy parameters in QSF + CDM,  $\Lambda$ CDM and PSF + CDM models determined by the Markov chain Monte Carlo technique using the dataset WMAP7 + HST + BBN + BAO + WiggleZ + SNLS3. The current Hubble parameter  $H_0$  is in units  $\text{km s}^{-1} \text{Mpc}^{-1}$ . (From [323])**

Parameters	QSF + CDM	$\Lambda$ CDM	PSF + CDM
$\Omega_{de}$	$0.72^{+0.04}_{-0.04}$	$0.73^{+0.04}_{-0.04}$	$0.73^{+0.04}_{-0.04}$
$w_0$	$-0.994^{+0.14}_{-0.006}$	-1	$-1.10^{+0.10}_{-0.27}$
$c_a^2$	$-0.72^{+0.72}_{-0.28}$	-1	$-1.29^{+0.29}_{-0.33}$
$H_0$	$70.1^{+3.6}_{-4.6}$	$70.3^{+3.5}_{-3.4}$	$71.5^{+5.1}_{-4.1}$
$-\log L$	3947.00	3946.75	3945.98

**Table 2.5. The best-fit values and  $1\sigma$  confidence ranges of the N-dimensional distribution for the dark energy parameters in QSF + CDM,  $\Lambda$ CDM and PSF + CDM determined by the Markov chain Monte Carlo technique using the observational dataset WMAP7 + HST + BBN + BAO + WiggleZ + Union2.1. The current Hubble parameter  $H_0$  is in units  $\text{km s}^{-1} \text{Mpc}^{-1}$ . (From [323])**

Parameters	QSF + CDM	$\Lambda$ CDM	PSF + CDM
$\Omega_{de}$	$0.72^{+0.03}_{-0.04}$	$0.72^{+0.04}_{-0.04}$	$0.73^{+0.03}_{-0.04}$
$w_0$	$-0.995^{+0.17}_{-0.005}$	-1	$-1.13^{+0.13}_{-0.23}$
$c_a^2$	$-0.55^{+0.55}_{-0.45}$	-1	$-1.54^{+0.54}_{-0.09}$
$H_0$	$69.7^{+3.1}_{-4.5}$	$69.8^{+3.2}_{-3.2}$	$71.4^{+4.7}_{-4.4}$
$-\log L$	3800.89	3800.76	3800.48

energy and, maybe, its nature. Indeed, in the papers [327, 328] it was shown that accuracy of the power spectra that are expected in the experiment Planck will significantly narrow the allowable range of values of parameters for the scalar field models of dark energy.

## 2.9. Summary

In the chapter the different methods of modeling of dark energy by single scalar field are analyzed. The main attention was paid to the scalar field with barotropic equation of state and classical or tachyonic (DBI) Lagrangians. Such field has only three free parameters,  $\Omega_{de}$ ,  $w_0$  and  $c_a^2$ , which define completely its dynamical behavior from the Big Bang to the current epoch and in the future as well as the dynamics of expansion of the Universe. The different combinations of values of  $w_0$  and  $c_a^2$  from the range  $[-2, 0]$  correspond to different types of dark energy, quintessence and phantom, to different character of evolution of EoS parameter, decreasing, increasing or constant, and, accordingly, different repulsion properties, raising, receding or stable. The well studied  $\Lambda$ CDM and  $w$ CDM models of dark energy are partial cases of this barotropic scalar field model when  $w_0 = -1$  and  $w_0 = c_a^2$  correspondingly. If  $c_a^2 = 0$  and  $-1 < w_0 < -1/3$  then the scalar field with tachyon Lagrangian at the Beginning mimics dust-like matter, but later becomes quintessential dark energy with decreasing EoS parameter, which becomes  $w_0$  at current epoch and goes asymptotically to  $-1$ , mimicking  $\Lambda$ -term in far future. When Lagrangian of scalar field is classical then dark energy is never dust-like with the same time evolution of  $w_{de}$  since its effective sound speed is always  $c_s^2 = 1$ . If  $-1 < w_0 < c_a^2 < 0$  then we have quintessential scalar field model of dark energy with decreasing EoS parameter and raising repulsion:  $w_{de}$  monotonically decreases from  $c_a^2$  at the Big Bang to  $w_0$  now and will continue decreasing to  $-1$  up to time infinite. For the other order of inequality,  $-1 < c_a^2 < w_0 < 0$ , we have opposite evolution of  $w_{de}$ : it monotonically increases from  $c_a^2$  in the Big Bang to  $w_0$  now and will continue increase in the future, will become zero, then positive and will go to discontinuity of second kind since the energy density of scalar field,  $\rho_{de}$ , during decreasing will pass zero. In this model, in contrast to previous ones, the accelerated expansion will not last forever — it will be changed by the decelerated one, will reach the turnaround point, then will start to collapse and finally it will end in the Big Cranch singularity. The accelerated expansion in all these cases is caused by slow roll of scalar field to minimum of its potential. The energy density of quintessence scalar field decreases at the stage of expansion of the Universe much more slowly than for any other component, that explains its crucial role in the later epochs.

If  $w_0$  and  $c_a^2 < -1$ , then the scalar field with barotropic EoS has phantom properties — its density monotonically increases, that causes the superexponen-

tial expansion of the Universe and reaching of the Big Rip singularity in finite time. The field variable  $\phi$  and potential  $U$  are always real when the Lagrangian, classical or tachyonic, has the opposite sign before kinetic term. Moreover, the potential and kinetic term are always positive also if  $c_a^2 < w_0 < -1$ . The superfast expansion in this model is caused by roll up of the phantom scalar field to maximum of its potential which is  $+\infty$ , but is reached in finite time. The repulsion properties of PSF increase and in finite time they reach and outmatch firstly the gravitational force, then electromagnetic forces and finally strong interactions. All bound structures in the Universe — galaxies, stars, planets, atoms and protons — will be ripped in finite time. A distinctive feature of this class of phantom dark energy is that in a general case it mimics the positive or negative cosmological constant ( $w_{de}(a) \rightarrow -1$ ) in the early epoch ( $a \rightarrow 0$ ), that is defined by inequality  $c_a^2 < w_0$  or  $w_0 < c_a^2$  correspondingly. The inherent “phantom” property, when field starts from zero value of energy density, occurs only in the particular case  $w_0 = c_a^2$ . In the opposite asymptotic range,  $a \rightarrow +\infty$ , the equation of state parameter  $w_{de}(a)$  asymptotically goes to  $c_a^2$ , that defines the physical meaning of the term “adiabatic sound speed” in the case of phantom scalar field with barotropic EoS.

Here it has been shown also that dynamics of expansion of the Universe depends on values of parameters  $\Omega_{de}$ ,  $w_0$  and  $c_a^2$  of scalar field with barotropic EoS and this fact allows to estimate them using the cosmological test based on relations “luminosity distance — redshift” and “angular diameter distance — redshift” for different classes of astrophysical objects. The “strength” of scalar field repulsion and its time dependence, defined by these parameters, affect also the formation of large scale structure of the Universe via growth factor of linear matter density perturbations.

The important feature of the scalar fields is their gravitational instability, which was carefully analyzed in the chapter. It was shown that in the case of adiabatic initial conditions for matter density perturbations and subdominant asymptotic ones for dark energy the amplitudes of scalar field density perturbations in the past and current epochs are essentially lower than matter density ones. However, they leave their subtle “fingerprints” via gravitational interaction between dark energy and dark matter scalar density perturbations. It can be used as additional source of information about the nature of dark energy since it is sensitive to another important parameter of scalar field model of DE — the effective sound speed  $c_s^2$ . It was shown that the effect is more noticeable for smaller values of  $c_s^2$ . In the case of phantom scalar field the distinctive property is that the perturbation of energy density and gravitational potential have the same sign. It causes the decay of large scale linear density perturbations of matter long before the Big Rip singularity.

So, the determination of values of  $\Omega_{de}$ ,  $w_0$  and  $c_a^2$  for barotropic scalar field with given Lagrangian by comparison of theoretical predictions with observati-

onal data gives possibility to define the type and main dynamical properties of dark energy. The best-fit parameters of quintessence and phantom scalar fields with barotropic EoS have been determined jointly with all relevant cosmological parameters by MCMC method using the datasets WMAP7 + HST + + BBN + BAO + SN SDSS SALT2 and WMAP7 + HST + BBN + BAO + + SN SDSS MLCS2k2. It was shown that the dataset including SNe Ia distance moduli obtained with SALT2 fitter prefers slightly the phantom model of dark energy ( $\Omega_{de} = 0.72 \pm 0.04$ ,  $w_0 = -1.043_{-0.24}^{+0.043}$ ,  $c_a^2 = -1.12_{-0.50}^{+0.12}$ ), while the dataset with the same SNe Ia but obtained with MLCS2k2 prefers slightly the quintessence model ( $\Omega_{de} = 0.70 \pm 0.05$ ,  $w_0 = -0.83_{-0.17}^{+0.22}$ ,  $c_a^2 = -0.88_{-0.12}^{+0.88}$ ). However, the difference of the maximum likelihoods between them is statistically insignificant. The same conclusions apply to the datasets WMAP7 + + HST + BBN + BAO + WiggleZ + SNLS3 and WMAP7 + HST + BBN + + BAO + WiggleZ + Union2.1. The possibility of distinguishing between quintessence and phantom scalar fields by current and expected datasets is analyzed and it is concluded that more accurate future observations will enable us to do that.

# 3

## CHAPTER

---

# KALUZA—KLEIN MODELS

---

### 3.1. Introduction

As we have already pointed out in the previous chapters, the large-scale dynamics of the observable part of our present time Universe is well described by the  $\Lambda$ CDM model with the four-dimensional Friedmann—Robertson—Walker (FRW) metric. However, it is possible that space-time at short (Fermi or Planck) distances might have a dimensionality of more than four and possess a rather complex topology [329]. This idea takes its origin from the pioneering papers by Kaluza and Klein (KK) [330,331]. They were first who indicated how to unify gravity with electromagnetism. Moreover, Klein introduced the idea of compactification of the extra (fifth) dimension which provides the natural explanation of the extra dimension unobservability (see [332–334] for review of the KK models).

String theory [335,336] and its recent generalizations — p-brane, M- and F-theory [337,338] — widely use this concept and give it a new foundation. The most consistent formulations of these theories are possible in space-times with critical dimensions  $D_c > 4$ , for example, in string theory there are  $D_c = 26$  or 10 for the bosonic and supersymmetric version, respectively. In KK models, it is supposed that a  $D$ -dimensional manifold  $M$  undergoes a “spontaneous compactification” [339–342]:  $M \rightarrow M^4 \times B^{D-4}$ , where  $M^4$  is the four-dimensional external space-time and  $B^{D-4}$  is a compact internal space. So it is natural to consider cosmological consequences of such compactifications. With this in mind, we shall investigate multidimensional cosmological models (MCM) with the topology

$$M = M_0 \times M_1 \times \dots \times M_n, \quad (3.1)$$

where  $M_0$  denotes the  $(D_0 = d_0 + 1)$ -dimensional (usually  $d_0 = 3$ ) external space-time and  $M_i$  ( $i = 1, \dots, n$ ) are  $d_i$ -dimensional internal spaces. To make the extra dimensions unobservable at the present time these internal spaces  $M_i$  have to be compact and reduced to scales near the Fermi length  $L_F \sim 10^{-17}$  cm.

This scale is dictated by the level of energies achieved up to now in the accelerators and which were less than 1 TeV. In KK models, each type of particles of the Standard Model has infinite number of partners (the Kaluza–Klein tower of massive states commonly referred to KK particles (see e.g. [343])) with masses inversely proportional to the size of the internal space. KK particles were not detected in all previous experiments. This result can be interpreted in such a way that energies up to 1 TeV were not enough to excite them. In other words, the size of the internal spaces should be of the order or less than  $(1 \text{ TeV})^{-1} \sim 10^{-17}$  cm. On the other hand, it was not also registered any reaction where usual particles disappear in the extra dimensions. For considered models, it occurs if wavelength of these particles are bigger than the size of the extra dimensions. In the case of TeV energy particles, their wavelength is of order of  $L_F$ . We again arrive at the indicated above restriction on the size of the internal space. To discover the extra dimensions, it is necessary to increase energies of accelerators.

Large Hadronic Collider in CERN should reach 14 TeV. Therefore, if the internal spaces have the Fermi length size, we shall detect them in this experiment. Thus, in subsequent sections, we assume that scale factors  $a_i$  of the internal spaces should be of order or less of  $L_F$ .

There is no problem in constructing compact spaces with a positive curvature [344,345]. (For example, every Einstein manifold with constant positive curvature is necessarily compact [346].) However, Ricci-flat spaces and negative curvature spaces also can be compact. This can be achieved by appropriate periodicity conditions for the coordinates [347–351] or, equivalently, through the action of discrete groups  $\Gamma$  of isometries related to face pairings and to the manifold’s topology. For example, three-dimensional spaces of constant negative curvature are isometric to the open, simply connected, infinite hyperbolic (Lobachevsky) space  $H^3$  [344,345]. However, there exist also an infinite number of compact, multiply connected, hyperbolic coset manifolds  $H^3/\Gamma$ , which can be used for the construction of FRW metrics with negative curvature [347, 349]. These manifolds are built from a fundamental polyhedron (FP) in  $H^3$  with faces pairwise identified. The FP determines a tessellation of  $H^3$  into cells that are replicas of the FP, through the action of the discrete group  $\Gamma$  of isometries [349]. The simplest example of Ricci-flat compact spaces is given by  $D$ -dimensional tori  $T^D = \mathbb{R}^D/\Gamma$ . Thus internal spaces may have non-trivial global topology, being compact (i.e. closed and bounded) for any sign of spatial curvature.

In the cosmological context, internal spaces can be called compactified, when they are obtained by a compactification in the usual mathematical understanding (e.g. by replacements of the type  $\mathbb{R}^D \rightarrow S^D$ ,  $\mathbb{R}^D \rightarrow \mathbb{R}^D/\Gamma$  or  $H^D \rightarrow H^D/\Gamma$ ) with additional contraction of the sizes to Fermi scale. There are a number of interesting cosmological and astrophysical exact solutions (see, e.g., Refs. [352–367]). For the most of exact cosmological solutions, the internal spaces have dynamical behavior (see section 3.6 below). However, the physical constants that appear in the effective four-dimensional theory after dimensional reduction of an originally higher-dimensional model are the result of integration over the extra dimensions. If the volumes of the internal spaces would change, so would the observed constants (see Eq. (3.119) below). Because of limitation on the variability of these constants (see the relevant discussion in the subsequent sections), the internal spaces should be static or at least slowly variable since the time of primordial nucleosynthesis and, as we mentioned above, their sizes are of the order of the Fermi length. Obviously, such compactifications have to be stable against small fluctuations of the sizes (the scale factors  $a_i$ ) of the internal spaces. This means that the effective potential of the model obtained under dimensional reduction to a four-dimensional effective theory should have minima at  $a_i \sim L_F$  ( $i = 1, \dots, n$ ). These minima play the role of the cosmological constant (dark energy!) in our effective four-dimensional Universe.

Additionally, small excitations of a system near a minimum can be observed as massive scalar fields in the external space-time. These scalar fields very weakly interact with the Standard Model (SM) particles. Therefore, they belong to a class of the dark matter particles.

In the next section, we consider in detail the procedure of the dimensional reduction of KK models. Before that, it is worthy to note that the idea of the multidimensionality of our Universe has received a great deal of renewed attention over the last few years within the “brane-world” description of the Universe. In this approach the  $SU(3) \times SU(2) \times U(1)$  Standard Model fields, related to usual four-dimensional physics, are localized on a three-dimensional space-like hypersurface (brane) whereas the gravitational field propagates in the whole (bulk) space-time. This approach is different from KK one and will be the subject of the third part of our book.

## 3.2. Dimensional reduction, stable compactification, gravitational excitons, effective cosmological constant

### 3.2.1. General setup

In this section we present a sketchy outline of the basics of dimensional reduction and gravitational excitons. A more detailed description can be found, e.g., in the papers [368–370].

Let us consider a multidimensional space-time manifold  $M$  with warped product topology (3.1) and metric

$$g = g_{MN}(X)dX^M \otimes dX^N = g^{(0)} + \sum_{i=1}^n e^{2\beta^i(x)} g^{(i)}, \quad (3.2)$$

where  $x$  are some coordinates of the ( $D_0 = 4$ )-dimensional manifold  $M_0$  and

$$g^{(0)} = g_{\mu\nu}^{(0)}(x)dx^\mu \otimes dx^\nu. \quad (3.3)$$

Let further the internal factor manifolds  $M_i$  be  $d_i$ -dimensional warped Einstein spaces with warp factors  $e^{\beta^i(x)}$  and metrics  $g^{(i)} = g_{m_i n_i}^{(i)}(y_i) dy_i^{m_i} \otimes dy_i^{n_i}$ , i.e.,

$$R_{m_i n_i} [g^{(i)}] = \lambda^i g_{m_i n_i}^{(i)}, \quad m_i, n_i = 1, \dots, d_i \quad (3.4)$$

and

$$R [g^{(i)}] = \lambda^i d_i \equiv R_i. \quad (3.5)$$

In the case of constant curvature spaces parameter  $\lambda^i$  are normalized as  $\lambda^i = k_i(d_i - 1)$  with  $k_i = 0, \pm 1$ . Let  $b_i \equiv e^{\beta^i}$  and  $b_{(0)i} \equiv e^{\beta_0^i}$  denote the scales factors of the internal spaces  $M_i$  at arbitrary and at present time. (Obviously, to get scale factors in dimensional units, we must multiply them by the Planck length  $L_{\text{Pl}} \sim 10^{-33}$  cm, e.g.  $b_{(0)i} = L_{\text{Pl}} e^{\beta_0^i}$ .) Then the total volume of the internal spaces at the present time is given by

$$V_{D'} \equiv V_I \times v_0 \equiv \prod_{i=1}^n \int_{M_i} d^{d_i} y \sqrt{|g^{(i)}|} \times \left( \prod_{i=1}^n e^{d_i \beta_0^i} \right) = V_I \times \prod_{i=1}^n b_{(0)i}^{d_i}, \quad (3.6)$$

where  $D' = \sum_{i=1}^n d_i$  is the total number of the extra dimensions. The factor  $V_I$  is dimensionless and defined by geometry and topology of the internal spaces. We also denote the deviations of the internal scale factors from their present day values:

$$\tilde{\beta}^i = \beta^i - \beta_0^i. \quad (3.7)$$

For the demonstration of the dimensional reduction we consider a multi-dimensional action with a bare  $D$ -dimensional cosmological constant  $\Lambda$  and a minimal scalar field  $\Phi$ :

$$\begin{aligned} S &= \frac{1}{2\kappa_D^2} \int_M d^D x \sqrt{|g|} \{R[g] - 2\Lambda\} + S_m + S_{YGH}, \\ S_m &= -\frac{1}{2} \int_M d^D x \sqrt{|g|} [g^{MN} \partial_M \Phi \partial_N \Phi + 2U(\Phi)], \end{aligned} \quad (3.8)$$



where  $\kappa_D^2$  is a  $D$ -dimensional gravitational constant<sup>1</sup> and  $S_{YGH}$  is the standard York–Gibbons–Hawking boundary term [371, 372]. The field  $\Phi$  itself can be considered in its zero-mode approximation. This means that  $\Phi$  and its potential  $U(\Phi)$  depend only on the coordinates of the external space, and the dimensional reduction of the model can be performed by a simple integration over the coordinates of the internal spaces. Moreover, we usually assume that  $\Phi$  depends only on time to be in concordance with the homogeneity and isotropy of the Universe.

Scalar curvature of the metric (3.2) reads

$$R[g] = R[g^{(0)}] + \sum_{i=1}^n e^{-2\beta^i} R[g^{(i)}] - \sum_{i,j=1}^n (d_i \delta_{ij} + d_i d_j) g^{(0)\mu\nu} \frac{\partial \beta^i}{\partial x^\mu} \frac{\partial \beta^j}{\partial x^\nu} - 2 \sum_{i=1}^n d_i \Delta[g^{(0)}] \beta^i. \quad (3.9)$$

where  $\Delta[\bar{g}^{(0)}]$  is the Laplace–Beltrami operator on  $M_0$ :

$$\Delta[g^{(0)}] = \frac{1}{\sqrt{|g^{(0)}|}} \frac{\partial}{\partial x^\mu} \left( \sqrt{|g^{(0)}|} g^{(0)\mu\nu} \frac{\partial}{\partial x^\nu} \right), \quad (3.10)$$

Taking into account the relation

$$\begin{aligned} & \frac{1}{\kappa_D^2} \int_M d^D x \sqrt{|g|} \sum_{i=1}^n d_i \Delta[g^{(0)}] \beta^i = \\ &= \frac{\mu}{\kappa_D^2} \sum_{i=1}^n d_i \int_{M_0} d^{D_0} x \sqrt{|g^{(0)}|} \prod_{l=1}^n e^{d_l \beta^l} \frac{1}{\sqrt{|g^{(0)}|}} \frac{\partial}{\partial x^\lambda} \left( \sqrt{|g^{(0)}|} g^{(0)\lambda\nu} \frac{\partial}{\partial x^\nu} \beta^i \right) = \\ &= \frac{1}{\kappa_0^2} \sum_{i=1}^n d_i \int_{M_0} d^{D_0} x \left[ \frac{\partial}{\partial x^\lambda} \left( \sqrt{|g^{(0)}|} g^{(0)\lambda\nu} \prod_{l=1}^n e^{d_l \beta^l} \frac{\partial}{\partial x^\nu} \beta^i \right) - \right. \\ & \quad \left. - \sqrt{|g^{(0)}|} g^{(0)\lambda\nu} \frac{\partial \beta^i}{\partial x^\nu} \prod_{l=1}^n e^{d_l \beta^l} \sum_{j=1}^n d_j \frac{\partial \beta^j}{\partial x^\lambda} \right] = \\ &= S_{YGH} - \frac{1}{\kappa_0^2} \int_{M_0} d^{D_0} x \sqrt{|g^{(0)}|} \prod_{l=1}^n e^{d_l \beta^l} \sum_{i,j=1}^n d_i d_j g^{(0)\lambda\nu} \frac{\partial \beta^i}{\partial x^\lambda} \frac{\partial \beta^j}{\partial x^\nu}, \quad (3.11) \end{aligned}$$

<sup>1</sup>  $\kappa_D^2$  is connected with the multidimensional fundamental mass scale  $M_{\text{Pl}(D)}$  and the surface area  $S_{D-1} = 2\pi^{(D-1)/2}/\Gamma[(D-1)/2]$  of a unit sphere in  $D-1$  dimensions by the relation

$$\kappa_D^2 = 2S_{D-1}/M_{\text{Pl}(D)}^{D'+2}.$$

the action (3.8) can be easily reduced to the following expression

$$\begin{aligned}
 S = \frac{1}{2\kappa_0^2} \int_{M_0} d^{D_0}x \sqrt{|g^{(0)}|} \prod_{i=1}^n e^{d_i \tilde{\beta}^i} & \left\{ R[g^{(0)}] - G_{ij} g^{(0)\mu\nu} \partial_\mu \tilde{\beta}^i \partial_\nu \tilde{\beta}^j + \right. \\
 & \left. + \sum_{i=1}^n \tilde{R}_i e^{-2\tilde{\beta}^i} - 2\Lambda - g^{(0)\mu\nu} \kappa_D^2 \partial_\mu \Phi \partial_\nu \Phi - 2\kappa_D^2 U(\Phi) \right\}, \quad (3.12)
 \end{aligned}$$

where the notations  $\tilde{R}_i := R_i e^{-2\tilde{\beta}_0^i}$ ,  $G_{ij} = \delta_{ij} d_i - d_i d_j$  are used. Here,  $D_0$ -dimensional gravitational constant  $\kappa_0^2 \equiv 8\pi G_N = 8\pi/M_{\text{Pl}(4)}^2$  ( $G_N$  is the Newton gravitational constant and  $M_{\text{Pl}(4)}$  is the four-dimensional Planck mass) is given as

$$\kappa_0^2 = \kappa_D^2 / V_{D'} \quad (3.13)$$

Action (3.12) of the four-dimensional effective model is written in Brans–Dicke frame, i.e., it has the form of a generalized Brans–Dicke theory. As next step, we remove the explicit dilatonic coupling term in (3.12) by conformal transformation

$$g_{\mu\nu}^{(0)} = \Omega^2 \tilde{g}_{\mu\nu}^{(0)} := \left( \prod_{i=1}^n e^{d_i \tilde{\beta}^i} \right)^{-2/(D_0-2)} \tilde{g}_{\mu\nu}^{(0)} \quad (3.14)$$

and obtain the effective action in the Einstein frame

$$\begin{aligned}
 S = \frac{1}{2\kappa_0^2} \int_{M_0} d^{D_0}x \sqrt{|\tilde{g}^{(0)}|} & \left\{ \tilde{R}[\tilde{g}^{(0)}] - \bar{G}_{ij} \tilde{g}^{(0)\mu\nu} \partial_\mu \tilde{\beta}^i \partial_\nu \tilde{\beta}^j - \right. \\
 & \left. - \tilde{g}^{(0)\mu\nu} \kappa_D^2 \partial_\mu \Phi \partial_\nu \Phi - 2U_{\text{eff}} \right\}. \quad (3.15)
 \end{aligned}$$

The tensor components of the midisuperspace metric (target space metric on  $\mathbb{R}_T^n$ )  $\bar{G}_{ij}$  ( $i, j = 1, \dots, n$ ), its inverse metric  $\bar{G}^{ij}$  and the effective potential are given as

$$\bar{G}_{ij} = d_i \delta_{ij} + \frac{1}{D_0 - 2} d_i d_j, \quad \bar{G}^{ij} = \frac{\delta^{ij}}{d_i} + \frac{1}{2 - D} \quad (3.16)$$

and

$$U_{\text{eff}}[\tilde{\beta}, \Phi] = \left( \prod_{i=1}^n e^{d_i \tilde{\beta}^i} \right)^{-\frac{2}{(D_0-2)}} \left[ -\frac{1}{2} \sum_{i=1}^n \tilde{R}_i e^{-2\tilde{\beta}^i} + \Lambda + \kappa_D^2 U(\Phi) \right]. \quad (3.17)$$

It is obvious that the internal spaces can stabilize if the effective potential (3.17) has at least one minimum with respect to the scale factors  $\tilde{\beta}^i$ . Because

the conformal transformation (3.14) was performed only with respect to the external metric  $g^{(0)}$ , the stability of the internal space configurations does not depend on the concrete choice of the frame (Einstein or Brans–Dicke). In general, the effective potential  $U_{\text{eff}}$  can have more than one minimum so that transitions between these minima should be possible. In the following we consider models with the internal space scale factors localized at their present day values:  $\tilde{\beta}^i = 0$ ,  $\partial U_{\text{eff}}/\partial \tilde{\beta}^i \Big|_{\tilde{\beta}^i=0} = 0$ .

With the help of a regular coordinate transformation  $\psi = Q\beta$ ,  $\beta = Q^{-1}\psi$  midsuperspace metric (target space metric)  $\bar{G}$  can be transformed to a pure Euclidean form:  $\kappa_0^{-2}\bar{G}_{ij}d\beta^i \otimes d\beta^j = \sigma_{ij}d\psi^i \otimes d\psi^j = \sum_{i=1}^n d\psi^i \otimes d\psi^i$ ,  $\sigma = \text{diag}(+1, +1, \dots, +1)$ . An appropriate transformation to normal modes  $\psi^j = Q_i^j \beta^i$  can be found e.g. in [369]. In the special case of only one internal space ( $n = 1$ ), this procedure reduces to a simple rescaling<sup>2</sup>

$$\tilde{\beta}^1 = -\kappa_0 \sqrt{\frac{D_0 - 2}{d_1(D - 2)}} \psi^1, \quad (3.18)$$

It is usually assumed that metric  $\tilde{g}^{(0)}$  in action (3.15) is the Friedmann–Robertson–Walker one. Then, the dynamics of scale factor and scalar fields for arbitrary form of potential  $U_{\text{eff}}$  can be described with the help of numerical calculation of the system of the first order ordinary differential equations (ODEs) (A.13)–(A.16).

Below, we show that the stabilization of the internal spaces in model with the minimal coupled scalar field takes place if scalar field is in its minimum position  $\Phi_0$  too. For small fluctuations of the normal modes and scalar field in the vicinity of the minimum of the effective potential, action (3.15) reads

$$\begin{aligned} S = & \frac{1}{2\kappa_0^2} \int_{M_0} d^{D_0}x \sqrt{|\tilde{g}^{(0)}|} \left\{ \tilde{R}[\tilde{g}^{(0)}] - 2\Lambda_{\text{eff}} \right\} - \\ & - \frac{1}{2} \int_{M_0} d^{D_0}x \sqrt{|\tilde{g}^{(0)}|} \left\{ \sum_{i=1}^n \left( \tilde{g}^{(0)\mu\nu} \psi_{,\mu}^i \psi_{,\nu}^i + m_i^2 \psi^i \psi^i \right) + \tilde{g}^{(0)\mu\nu} \phi_{,\mu} \phi_{,\nu} + m_\phi^2 \phi \phi \right\}, \end{aligned} \quad (3.19)$$

where  $\Lambda_{\text{eff}} \equiv U_{\text{eff}}(\tilde{\beta}^i = 0, \Phi = \Phi_0)$  plays the role of a  $D_0$ -dimensional effective cosmological constant,  $m_i^2$  and  $m_\phi^2$  are mass squared of the normal modes and scalar field, respectively, and for convenience we use the normalizations for

<sup>2</sup> The relation between  $\tilde{\beta}^1$  and  $\psi^1$  is determined up to sign. For definiteness, we chose the minus sign.

scalar field fluctuations:  $\sqrt{V_{D'}}(\Phi - \Phi_0) \equiv \phi$ . In the case of one internal space

$$m_1^2 = \frac{D_0 - 2}{d_1(D - 2)} \frac{\partial^2 U_{\text{eff}}}{\partial(\tilde{\beta}^1)^2} \Big|_{\tilde{\beta}^1=0, \Phi=\Phi_0}. \quad (3.20)$$

Summarizing this section, we conclude that conformal zero-mode excitations of the internal factor spaces  $M_i$  have the form of massive scalar fields developing on the background of the external space-time  $M_0$ . In analogy with excitons in solid state physics (excitations of the electronic subsystem of a crystal), we called these conformal excitations of the internal spaces *gravitational excitons* [369]. Later, since Refs. [373, 374] these geometrical moduli excitations are also known as radions. Within the framework of multi-dimensional cosmological models such excitations were investigated in [375–378]. Obviously, positive  $\Lambda_{\text{eff}}$  plays the role of the **dark energy** in our Universe and weakly interacting gravexcitons form the **dark matter** (see the following sections).

Now we consider some specific examples of stable compactification.

### 3.2.2. Stable compactification with minimal scalar fields

This model is described by effective action (3.15). It is clear now that stabilization of the internal spaces can be achieved if the effective potential  $U_{\text{eff}}$  (3.17) has a minimum with respect to fields  $\tilde{\beta}^i$  (or fields  $\psi^i$ ). Let us find conditions which ensure a minimum at  $\tilde{\beta}^i = 0$ .

The extremum condition yields:

$$\frac{\partial U_{\text{eff}}}{\partial \tilde{\beta}^k} \Big|_{\tilde{\beta}^i=0} = 0 \implies \tilde{R}_k = -\frac{d_k}{D_0 - 2} \left( \sum_{i=1}^n \tilde{R}_i - 2(\Lambda + \kappa_D^2 U(\Phi)) \right). \quad (3.21)$$

The left-hand side of this equation is a constant but the right-hand side is a dynamical function. Thus, stabilization of the internal spaces in such type of models is possible only when the effective potential has also a minimum with respect to the scalar field  $\Phi$  (in Ref. [379] it was proved that for this model the only possible solutions with static internal spaces correspond to the case when the minimal coupled scalar field is in its extremum position too). Let  $\Phi_0$  be the minimum position for field  $\Phi$ . From the structure of the effective potential (3.17) it is clear that minimum positions of the potentials  $U_{\text{eff}}[\tilde{\beta}, \Phi]$  and  $U(\Phi)$  with respect to field  $\Phi$  coincide with each other:

$$\frac{\partial U_{\text{eff}}}{\partial \Phi} \Big|_{\Phi_0} = 0 \iff \frac{\partial U(\Phi)}{\partial \Phi} \Big|_{\Phi_0} = 0. \quad (3.22)$$

Hence, we should look for parameters which ensure a minimum of  $U_{\text{eff}}$  at the point  $\tilde{\beta}^i = 0, \Phi = \Phi_0$ . Eqs. 3.21 show that there exists a fine tuning condition for the scalar curvatures of the internal spaces:

$$\frac{\tilde{R}_k}{d_k} = \frac{\tilde{R}_i}{d_i}, \quad (i, k = 1, \dots, n). \quad (3.23)$$

Introducing the auxiliary quantity

$$\tilde{\Lambda} \equiv \Lambda + \kappa_D^2 U(\Phi)|_{\Phi_0}, \quad (3.24)$$

we get the useful relations

$$\Lambda_{\text{eff}} := U_{\text{eff}} \Big|_{\tilde{\beta}^i=0, \Phi=\Phi_0} = \frac{D_0 - 2}{D - 2} \tilde{\Lambda} = \frac{D_0 - 2}{2} \frac{\tilde{R}_k}{d_k}, \quad (3.25)$$

which show that  $\text{sign } \Lambda_{\text{eff}} = \text{sign } \tilde{\Lambda} = \text{sign } R_k$ . As we already mentioned above,  $\Lambda_{\text{eff}}$  plays the role of an effective cosmological constant in the external space-time. For the masses of the normal mode excitations of the internal spaces (gravitational excitons) and of the scalar field near the extremum position we obtain respectively [369]:

$$m_1^2 = \dots = m_n^2 = -\frac{4\Lambda_{\text{eff}}}{D_0 - 2} = -2\frac{\tilde{R}_k}{d_k} > 0, \quad (3.26)$$

$$m_\Phi^2 := \frac{d^2 U(\Phi)}{d\Phi^2} \Big|_{\Phi_0}.$$

These equations show that for our specific model a global minimum can only exist in the case of compact internal spaces with negative curvature  $R_k < 0$  ( $k = 1, \dots, n$ ). The effective cosmological constant is negative also:  $\Lambda_{\text{eff}} < 0$ . Obviously, in this model it is impossible to trap the internal spaces at a minimum of  $U_{\text{eff}}$  if they are tori ( $\tilde{R}_i = 0$ ) because for Ricci-flat internal spaces the effective potential has no minimum at all. Equations (3.25) and (3.26) show also that a stabilization by trapping takes place only for  $\tilde{\Lambda} < 0$ . This means that the minimum of the scalar field potential should be negative  $U(\Phi_0) < 0$  for non-negative bare cosmological constant  $\Lambda \geq 0$  or it should satisfy inequality  $\kappa_D^2 U(\Phi_0) < |\Lambda|$  for  $\Lambda < 0$ . In paper [376], it is shown a possibility of the early inflation in this model. However, because of the negative sign of  $\Lambda_{\text{eff}}$ , the configurations with stabilized extra dimensions do not provide a late-time acceleration of our Universe in the model with minimal scalar field. This configurations are asymptotically anti-De Sitter. Therefore, there is no dark energy in this model. To get dark energy, it is necessary to include additional matter. It may shift a minimum of the effective potential from negative to positive values. Different forms of matter can be described with the help of a perfect fluid.

### 3.2.3. Perfect fluid: no-go theorem

In conventional cosmology matter fields are taken into account in a phenomenological way as a perfect fluid with equal pressure in all three spatial directions. It provides homogeneous (if energy density and pressure depends only on time) and isotropic picture of the Universe. In multidimensional case we generalize this approach to a  $m$ -component perfect fluid with energy-momentum tensor [355, 356, 360, 362]

$$T_N^M = \sum_{c=1}^m T^{(c)M}_N, \quad (3.27)$$

$$T^{(c)M}_N = \text{diag} \left( -\rho^{(c)}(\tau), \underbrace{P_0^{(c)}(\tau), \dots, P_0^{(c)}(\tau)}_{d_0 \text{ times}}, \dots, \underbrace{P_n^{(c)}(\tau), \dots, P_n^{(c)}(\tau)}_{d_n \text{ times}} \right). \quad (3.28)$$

The conservation equations we impose on each component separately

$$T^{(c)M}_{N;M} = 0. \quad (3.29)$$

To investigate dynamical behavior of our Universe and internal spaces for a model with such perfect fluid, the metric (3.2) should be also written in homogeneous form:

$$\begin{aligned} g &= g^{(0)}(x) + \sum_{i=1}^n e^{2\beta^i(\tau)} g^{(i)}(y) \equiv \\ &\equiv -e^{2\gamma(\tau)} d\tau \otimes d\tau + e^{2\beta^0(\tau)} q^{(0)}(\vec{x}) + \sum_{i=1}^n e^{2\beta^i(\tau)} g^{(i)}(y), \end{aligned} \quad (3.30)$$

where  $q^{(0)}$  is a metric of the constant curvature space:  $R[q^{(0)}] = kd_0(d_0 - 1)$  with  $k = 0, \pm 1$ . The choice of the function  $\gamma(\tau)$  defines different gauges, e.g. the synchronous time gauge  $\gamma = 0$  or the conformal time gauge  $\gamma(\tau) = \beta^0(\tau)$ , etc. In what follows, we use the notations  $a \equiv e^{\beta^0}$  and  $b_i \equiv e^{\beta^i}$  ( $i = 1, \dots, n$ ) to describe scale factors of the external and internal spaces, respectively.

Denoting by an overdot differentiation with respect to time  $\tau$ , the conservation equations (3.29) for the tensors (3.28) read

$$\dot{\rho}^{(c)} + \sum_{i=0}^n d_i \dot{\beta}^i \left( \rho^{(c)} + P_i^{(c)} \right) = 0. \quad (3.31)$$

If the pressures and energy density are related via equations of state

$$P_i^{(c)} = \left( \alpha_i^{(c)} - 1 \right) \rho^{(c)}, \quad i = 0, \dots, n, \quad c = 1, \dots, m, \quad (3.32)$$

then Eq. (3.31) has the simple integral

$$\rho^{(c)}(\tau) = A^{(c)} a^{-d_0 \alpha_0^{(c)}} \times \prod_{i=1}^n b_i^{-d_i \alpha_i^{(c)}}, \quad (3.33)$$

where  $A^{(c)}$  is the constant of integration.

To investigate the problem of the stable compactification, it is helpful to use the equivalence between the Einstein equations and the Euler–Lagrange equations for Lagrangian obtained by dimension reduction of the action (3.8) with

$$S_m = - \int_M d^D x \sqrt{|g|} \rho, \quad (3.34)$$

where  $\rho$  is given by Eq. (3.33) (see [355, 356, 360, 362] for details). This equivalence takes place for homogeneous model (3.30). However, we can generalize it to the inhomogeneous case allowing inhomogeneous fluctuations  $\tilde{\beta}^i(x)$  ( $i = 1, \dots, n$ ) over stably compactified background  $\beta_0^i = \text{const}$  (see Eq. (3.7)). It can be easily seen that the dimensional reduction of action (3.8) with the matter term (3.34) results in effective theory (3.15) (where we should drop the scalar field) with the effective potential

$$U_{\text{eff}} = \left( \prod_{i=1}^n e^{d_i \tilde{\beta}^i} \right)^{-2/(D_0-2)} \left[ -\frac{1}{2} \sum_{i=1}^n \tilde{R}_i e^{-2\tilde{\beta}^i} + \Lambda_D + \kappa_D^2 \sum_{c=1}^m \rho^{(c)} \right], \quad (3.35)$$

where  $\rho^{(c)}$  is defined by Eq. (3.33). If we suppose that the external space-time metric in the Einstein frame has also FRW form:

$$\tilde{g}^{(0)} = \Omega^{-2} g^{(0)} = \tilde{g}_{\mu\nu}^{(0)} dx^\mu \otimes dx^\nu := -e^{2\tilde{\gamma}} d\tilde{\tau} \otimes d\tilde{\tau} + e^{2\tilde{\beta}^0(x)} q^{(0)}, \quad (3.36)$$

which results in the following connection between the external scale factors in the Brans–Dicke frame  $a \equiv e^{\beta^0}$  and in the Einstein frame  $\tilde{a} \equiv e^{\tilde{\beta}^0}$ :

$$a = \left( \prod_{i=1}^n e^{d_i \tilde{\beta}^i} \right)^{-1/(D_0-2)} \tilde{a}, \quad (3.37)$$

then, expression (3.33) for  $\rho^{(c)}$  can be rewritten in the form:

$$\kappa_D^2 \rho^{(c)} = \kappa_0^2 \rho_{(d_0)}^{(c)} \prod_{i=1}^n e^{-\xi_i^{(c)} \tilde{\beta}^i}, \quad (3.38)$$

where

$$\rho_{(d_0)}^{(c)} = \tilde{A}^{(c)} \tilde{a}^{-d_0 \alpha_0^{(c)}}, \quad \tilde{A}^{(c)} = A^{(c)} V_I \prod_{i=1}^n b_{(0)i}^{d_i(1-\alpha_i^{(c)})} \quad (3.39)$$

and

$$\xi_i^{(c)} = d_i \left( \alpha_i^{(c)} - \frac{\alpha_0^{(c)} d_0}{d_0 - 1} \right). \quad (3.40)$$

It can be easily verified that  $\tilde{A}^{(c)}$  has dimension  $\text{cm}^{d_0 \alpha_0^{(c)} - D_0}$ .

Thus, the problem of stabilization of the extra dimensions is reduced now to search of minima of the effective potential  $U_{\text{eff}}$  with respect to the fluctuations  $\tilde{\beta}^i$ :

$$\left. \frac{\partial U_{\text{eff}}}{\partial \tilde{\beta}^k} \right|_{\tilde{\beta}=0} = 0,$$

implying

$$\tilde{R}_k = -\frac{d_k}{D_0 - 2} \left[ \sum_{i=1}^n \tilde{R}_i - 2\Lambda_D \right] + \kappa_0^2 \sum_{c=1}^m \rho_{(d_0)}^{(c)} \left( \xi_k^{(c)} + \frac{2d_k}{D_0 - 2} \right), \quad k = 1, \dots, n. \quad (3.41)$$

The left-hand side of this equation is a constant but the right-hand side is a dynamical function because of dynamical behavior of the effective  $d_0$ -dimensional energy density  $\rho_{(d_0)}^{(c)}$ . Thus, we arrived at the following *no-go theorem* [380]:

*Multidimensional cosmological Kaluza–Klein models with the perfect fluid as a matter source do not admit stable compactification of the internal spaces with exception of two special cases:*

$$\text{I. } \alpha_0^{(c)} = 0, \quad \forall \alpha_i^{(c)}, \quad i = 1, \dots, n, \quad c = 1, \dots, m. \quad (3.42)$$

$$\text{II. } \xi_i^{(c)} = -\frac{2d_i}{d_0 - 1} \implies \begin{cases} \alpha_0^{(c)} = \frac{2}{d_0} + \frac{d_0 - 1}{d_0} \alpha^{(c)}, \\ \alpha_i^{(c)} = \alpha^{(c)}, \quad i = 1, \dots, n, \quad c = 1, \dots, m. \end{cases} \quad (3.43)$$

First case corresponds to vacuum in the external space  $\rho_{(d_0)}^{(c)} = \tilde{A}^{(c)} = \text{const}$  and arbitrary equations of state in the internal spaces. Some bulk matter can mimic such behavior, e.g. vacuum fluctuations of quantum fields (Casimir effect) [369, 381], monopole form fields [369, 378] and gas of branes [382].

In the second case, the energy density in the external space is not a constant but a dynamical function with the following behavior:

$$\rho_{(d_0)}^{(c)}(\tilde{a}) = \tilde{A}^{(c)} \frac{1}{\tilde{a}^{2+(d_0-1)\alpha^{(c)}}} \implies \rho_{(3)}^{(c)} = \tilde{A}^{(c)} \frac{1}{\tilde{a}^{2(1+\alpha^{(c)})}}. \quad (3.44)$$

The corresponding equation of state is:

$$P_{(d_0)}^{(c)} = (1/3)(2\alpha^{(c)} - 1)\rho_{(d_0)}^{(c)} \implies P_{(3)}^{(c)} = (\alpha_0^{(c)} - 1)\rho_{(3)}^{(c)}, \quad (3.45)$$

It can be easily seen from Eq. (3.38) that in the case of stabilized internal spaces (i.e.  $\tilde{\beta}^i = 0$ )  $\rho_{(d_0)}^{(c)} = \rho^{(c)} V_{D'}$  where the internal space volume  $V_{D'}$  is defined in Eq. (3.6). Similar relation takes place for  $P_{(d_0)}^{(c)}$  and  $P_0^{(c)}$ :  $P_{(d_0)}^{(c)} =$



$= P_0^{(c)} V_{D'}$ . Therefore, second case corresponds to ordinary matter in our three-dimensional space. For example, for  $d_0 = 3$ , besides the exotic case of gas of cosmic strings with  $\alpha^{(c)} = 0$ , the choice  $\alpha^{(c)} = 1/2$  provides dust in our space:  $\alpha_0^{(c)} = 1 \rightarrow P_{(3)}^{(c)} = 0$  and equation of state  $\alpha_i^{(c)} = 1/2 \rightarrow P_i^{(c)} = -(1/2)\rho^{(c)}$  in the internal spaces. It is worth noting that these equations are exactly the black string/branes equations of state (see section 3.7).

It is clear that the cases I and II are the necessary but not sufficient conditions for stabilization. As we shall show below, stability is ensured by the matter from the first case with a proper choice of the parameters of models. The matter related to the second case provides the standard evolution of the Universe and does not spoil the stabilization.

The no-go theorem (the case II) clearly shows that the condition of the internal space stabilization requires the violation of symmetry (in terms of equations of state) between our three dimensions and the extra dimensions. The need for such a violation is especially seen in the example of radiation. It is well known that radiation satisfies the equation of state  $P = (1/3)\rho$ . If we assume equality of all dimensions and allow light to move around all multidimensional space, then equation of state will be  $P = (1/D)\rho$ , which apparently contradicts the observations for  $D > 3$ . Therefore, radiation should not move in the extra dimensions. Exactly this situation we have in case II. If we take  $\alpha^{(c)} = 1$ , then we obtain the usual equation of state for radiation in our Universe  $\alpha_0^{(c)} = 4/3 \rightarrow P_{(3)}^{(c)} = (1/3)\rho_{(3)}^{(c)}$  and dust in the internal space:  $\alpha_i^{(c)} = 1 \rightarrow P_i^{(c)} = 0$ . The latter means that the light does not move in the extra dimensions. Such situation is realized if light is localized on a brane [383].

### 3.2.4. Conventional cosmology from multidimensional models

Now, we want to present toy models with stabilized internal spaces and the standard Friedmann-like behavior of the external space (our Universe). These models give a possibility to demonstrate the typical problems of KK multidimensional cosmological models.

**Dark energy from extra dimensions: fine tuning problem.** Let us consider a model where multicomponent perfect fluid is the combination of the cases I and II. To be more precise, additionally to the the perfect fluid of the type II, we endow our model with the monopole form fields [369, 378]:

$$S_m = -\frac{1}{2} \int_M d^D x \sqrt{|g|} \sum_{i=1}^n \frac{1}{d_i!} \left(F^{(i)}\right)^2 = - \int_M d^D x \sqrt{|g|} \sum_{i=1}^n \frac{f_i^2}{b_i^{2d_i}}, \quad (3.46)$$

where  $f_i \equiv \text{const}$  are arbitrary constants of integration (free parameters of the model) and for real form fields  $f_i^2 > 0$  (see, e.g., Eqs. (3.199)–(3.202)).

Comparison of this expression with Eqs. (3.34) and (3.33) shows that such monopole form fields are equivalent to  $n$ -component perfect fluid with  $\alpha_0^{(c)} = 0$ ,  $\alpha_i^{(c)} = 2\delta_i^c$ ,  $c, i = 1, \dots, n$ , i.e. belong to the case I.

Without loss of generality, we can perform our analysis in the case of one internal space  $n = 1$ . Then, the effective potential (3.35) for such combined model undergoes the following separation:

$$U_{\text{eff}} = \underbrace{\left( e^{d_1 \tilde{\beta}^1} \right)^{-2/(D_0-2)} \left[ -\frac{1}{2} \tilde{R}_1 e^{-2\tilde{\beta}^1} + \Lambda_D + \tilde{f}_1^2 e^{-2d_1 \tilde{\beta}^1} \right]}_{U_{\text{int}}(\tilde{\beta}^1)} + \underbrace{\kappa_0^2 \sum_{c=1}^m \rho_{(d_0)}^{(c)}(\tilde{a})}_{U_{\text{ext}}(\tilde{a})}, \quad (3.47)$$

where  $\rho_{(d_0)}^{(c)}(\tilde{a})$  is defined by Eq. (3.44) and  $\tilde{f}_1^2 \equiv \kappa_D^2 f_1^2 / b_{(0)1}^{2d_1}$ . These two terms  $U_{\text{int}}(\tilde{\beta}^1)$  and  $U_{\text{ext}}(\tilde{a})$  depend only on scale factors of the internal and external spaces, respectively. Therefore, the first term is responsible for the internal space stabilization due to its minimum and the second term provides the Friedmann-like behavior of the external space.

First, we investigate the problem of stable compactification of the internal space. It is clear that such stabilization for our model takes place if potential  $U_{\text{int}}$  has a minimum with respect to the fluctuation field  $\tilde{\beta}^1$ :

$$\left. \frac{\partial U_{\text{int}}}{\partial \tilde{\beta}^1} \right|_{\tilde{\beta}^1=0} = 0 \implies \frac{D-2}{2d_1} \tilde{R}_1 = \Lambda_D + d_0 \tilde{f}_1^2. \quad (3.48)$$

The value of this potential at the minimum plays the role of the effective four-dimensional cosmological constant:

$$\Lambda_{\text{eff}} := U_{\text{int}}|_{\tilde{\beta}^1=0} = -\frac{1}{2} \tilde{R}_1 + \Lambda_D + \tilde{f}_1^2. \quad (3.49)$$

With the help of the extremum condition (3.48),  $\Lambda_{\text{eff}}$  can be written in the form

$$\Lambda_{\text{eff}} = \frac{D_0-2}{2d_1} \tilde{R}_1 - (D_0-2) \tilde{f}_1^2 = \quad (3.50)$$

$$= \frac{D_0-2}{D-2} \Lambda_D - \left( \frac{d_0 d_1}{D-2} - 1 \right) \tilde{f}_1^2 = \quad (3.51)$$

$$= \frac{d_0-1}{d_0} \Lambda_D - \frac{1}{2} \left( 1 - \frac{D-2}{d_0 d_1} \right) \tilde{R}_1. \quad (3.52)$$

Second derivative of  $U_{int}$  in the extremum position reads

$$\left. \frac{\partial^2 U_{int}}{\partial \tilde{\beta}^2} \right|_{\tilde{\beta}^2=0} = -2 \left( \frac{D-2}{D_0-2} \right)^2 \tilde{R}_1 + \left( \frac{2d_1}{D_0-2} \right)^2 \Lambda_D + \left( \frac{2d_0 d_1}{D_0-2} \right)^2 \tilde{f}_1^2 = \quad (3.53)$$

$$= \frac{4}{D_0-2} \left[ -\frac{1}{2}(D-2)\tilde{R}_1 + 4d_0 d_1^2 \tilde{f}_1^2 \right] = \quad (3.54)$$

$$= \frac{4d_1}{(D_0-2)^2} \left[ -(D_0-2)\Lambda_D + (D-2)d_0 \left( \frac{d_0 d_1}{D-2} - 1 \right) \tilde{f}_1^2 \right] = \quad (3.55)$$

$$= \frac{4}{(D_0-2)^2} \left[ -d_1^2(d_0-1)\Lambda_D + \frac{1}{2}(D-2)^2 \left( \frac{d_0 d_1}{D-2} - 1 \right) \tilde{R}_1 \right]. \quad (3.56)$$

For stable compactification, this extremum should be a minimum. Then, small fluctuations above it describe minimal scalar field (gravitational excitons [369]) propagated in the external space with the mass squared

$$m_1^2 \equiv \frac{D_0-2}{d_1(D-2)} \left. \frac{\partial^2 U_{int}}{\partial \tilde{\beta}^2} \right|_{\tilde{\beta}^2=0} > 0. \quad (3.57)$$

Additionally, the effective four-dimensional cosmological constant should be positive  $\Lambda_{\text{eff}} > 0$ . This is the necessary condition for the late time acceleration of the Universe in considered model. Both of these conditions (the positiveness of  $\Lambda_{\text{eff}}$  and  $m_1^2$ ) lead to the following inequalities

$$d_1 \tilde{f}_1^2 < \frac{1}{2} \tilde{R}_1 < \frac{4d_0 d_1}{D-2} \times d_1 \tilde{f}_1^2, \quad (3.58)$$

$$\frac{D-2}{D_0-2} \left( \frac{d_0 d_1}{D-2} - 1 \right) \tilde{f}_1^2 < \Lambda_D < d_0 \times \frac{D-2}{D_0-2} \left( \frac{d_0 d_1}{D-2} - 1 \right) \tilde{f}_1^2, \quad (3.59)$$

$$\frac{1}{2} \frac{D-2}{d_1(d_0-1)} \left( \frac{d_0 d_1}{D-2} - 1 \right) \tilde{R}_1 < \Lambda_D < \frac{D-2}{d_1} \times \frac{1}{2} \frac{D-2}{d_1(d_0-1)} \left( \frac{d_0 d_1}{D-2} - 1 \right) \tilde{R}_1. \quad (3.60)$$

The inequality on the left-hand side follow from the condition  $\Lambda_{\text{eff}} > 0$  applied to Eqs. (3.50)–(3.52), whereas the inequalities on the right-hand side follow from the minimum condition  $m_1^2 > 0$  applied to Eqs. (3.54)–(3.56). Thus, for the most reasonable case  $\tilde{f}_1^2 > 0$  of the real form field we get  $\tilde{R}_1, \Lambda_D > 0$ . It can be easily seen that the case  $\tilde{f}_1^2 = 0$  results in negative effective cosmological constant [384]. To shift it to non-negative values we introduced the real form fields.

According to the present day observations, our Universe undergoes the late time accelerating expansion due to dark energy. The origin of the dark energy is the great challenge of the modern theoretical physics and cosmology.

The cosmological constant is one of the most probable candidate for it. The observations give  $\Lambda_{DE} \sim 10^{-123} \Lambda_{\text{Pl}(4)} \sim 10^{-57} \text{ cm}^{-2}$ . Let us estimate now a possibility for our effective cosmological constant to admit this quantity:  $\Lambda_{\text{eff}} \sim \Lambda_{DE} \sim 10^{-57} \text{ cm}^{-2}$ .

As we noted in section (3.1), in KK models the size of the extra dimensions at present time should be of the order or less than  $b_{(0)1} \sim 10^{-17} \text{ cm} \sim 1 \text{ TeV}^{-1}$ . In the case of the upper limit  $b_{(0)1} \sim 10^{-17} \text{ cm}$ , we get  $\tilde{R}_1 \sim b_{(0)1}^{-2} \sim 10^{34} \text{ cm}^{-2}$ . On the other hand, inequalities (3.58)–(3.60) show that  $\tilde{R}_1$ ,  $\Lambda_D$  and  $\tilde{f}_1^2$  are of the same order of magnitude, i.e.  $\tilde{R}_1 \sim \Lambda_D \sim \tilde{f}_1^2 \sim 10^{34} \text{ cm}^{-2}$ , and have the same sign. Thus, these parameters should be extremely fine tuned (in Eq. (3.49)) to compensate each other in such a way that to leave only  $10^{-57} \text{ cm}^{-2}$ . One of possibilities to avoid this problem consists in inclusion of different form fields/fluxes which may result in a big number of minima (landscape) [385] with sufficient large probability to find oneself in a dark energy minimum.

It is clear that extreme fine tuning has arisen because of two extremely different scales present in the model, namely  $\Lambda_{\text{eff}} \sim 10^{-57} \text{ cm}^{-2}$  and  $\tilde{R}_1 \sim 10^{34} \text{ cm}^{-2}$ . We can avoid this problem by removing one of the scales (or both of them). Let us consider these possibilities.

(i)  $\tilde{R}_1 = \Lambda_{\text{eff}} = 0$  This case does not work because Eqs. (3.48) and (3.49) contradict each other for  $d_0 > 1$ .

(ii)  $\tilde{R}_1 \neq 0$ ,  $\Lambda_{\text{eff}} = 0$  Here,  $\tilde{R}_1 = 2d_1 \tilde{f}_1^2$  and  $\Lambda_D = (d_1 - 1) \tilde{f}_1^2$ . Hence,  $\tilde{R}_1 \sim \Lambda_D \sim \tilde{f}_1^2$ . Additionally, condition  $m_1^2 > 0$  requires that these parameters are positive. Therefore, if  $b_{(0)1} \sim 10^{-17} \text{ cm} \sim 1 \text{ TeV}^{-1}$ , then we obtain the physically reasonable result that all parameters in this model are of the TeV scale, e.g.  $m_1 \sim 1 \text{ TeV}$ . Unfortunately, the condition  $\Lambda_{\text{eff}} = 0$  makes it impossible to solve the problem of dark energy.

(iii)  $\tilde{R}_1 = 0$ ,  $\Lambda_{\text{eff}} > 0$  Here,  $\Lambda_D = -2d_0 \tilde{f}_1^2$  and  $\Lambda_{\text{eff}} = -(d_0 - 1) \tilde{f}_1^2 = [(d_0 - 1)/d_0] \Lambda_D$  which result in conditions  $\Lambda_D > 0$ ,  $\tilde{f}_1^2 < 0$  for  $\Lambda_{\text{eff}} > 0$ . However, the condition  $m_1^2 > 0$  requires the opposite inequalities:  $\Lambda_D < 0$ ,  $\tilde{f}_1^2 > 0$ . Therefore, we arrive at a contradiction. Nevertheless, models with Ricci-flat ( $\tilde{R}_1 = 0$ ) internal spaces are not excluded. For example, this space can be an orbifold with branes in fixed points [386]. This model is investigated in the next section.

Now, we turn to the dynamical behavior of the external factor space. We consider zero order approximation, when all excitations are frozen out (or heavy enough to decay long before the present time<sup>3</sup>). Because our Universe (external

<sup>3</sup> Gravexcitons with masses  $m_1 \sim 1 \text{ TeV}$  decay (e.g. due to reaction  $\psi \rightarrow 2\gamma$ ) before primordial nucleosynthesis and they do not contradict the observational data [387, 388] (see section 3.4.3). Therefore, in this case the effective potential contributes in the form of the effective cosmological constant (3.49).

space) is homogeneous and isotropic, functions  $\hat{\gamma}$  and  $\hat{\beta}^0$  depends only on time:  $\hat{\gamma} = \hat{\gamma}(\hat{\tau})$  and  $\hat{\beta}^0 = \hat{\beta}^0(\hat{\tau})$ . Then, the action functional (3.15) (without scalar field and for the effective potential (3.47)) after dimensional reduction reads:

$$\begin{aligned} S &= \frac{1}{2\kappa_0^2} \int_{M_0} d^{D_0} x \sqrt{|\tilde{g}^{(0)}|} \left\{ \tilde{R}[\tilde{g}^{(0)}] - 2U_{\text{eff}} \right\} = \\ &= \frac{V_0}{2\kappa_0^2} \int d\hat{\tau} \left\{ e^{\hat{\gamma}+d_0\hat{\beta}^0} e^{-2\hat{\beta}^0} R[q^{(0)}] + d_0(1-d_0)e^{-\hat{\gamma}+d_0\hat{\beta}^0} \left( \frac{d\hat{\beta}^0}{d\hat{\tau}} \right)^2 - \right. \\ &\quad \left. - 2e^{\hat{\gamma}+d_0\hat{\beta}^0} \left( \Lambda_{\text{eff}} + \kappa_0^2 \sum_{c=1}^m \rho_{(d_0)}^{(c)} \right) \right\} + \frac{V_0}{2\kappa_0^2} d_0 \int d\hat{\tau} \frac{d}{d\hat{\tau}} \left( e^{-\hat{\gamma}+d_0\hat{\beta}^0} \frac{d\hat{\beta}^0}{d\hat{\tau}} \right), \quad (3.61) \end{aligned}$$

where  $V_0 := \int_{M_0} d^{d_0} x \sqrt{|q^{(0)}|}$  is the volume of the external space,  $\rho_{(d_0)}^{(c)}$  is defined by Eq. (3.44) and usually  $R[q^{(0)}] = kd_0(d_0 - 1)$ ,  $k = \pm 1, 0$ . The constraint equation  $\partial L / \partial \hat{\gamma} = 0$  in the synchronous time gauge  $\hat{\gamma} = 0$  yields

$$\left( \frac{1}{\tilde{a}} \frac{d\tilde{a}}{d\tilde{t}} \right)^2 = -\frac{k}{\tilde{a}^2} + \frac{2}{d_0(d_0 - 1)} \left( \Lambda_{\text{eff}} + \kappa_0^2 \sum_{c=1}^m \rho_{(d_0)}^{(c)}(\tilde{a}) \right), \quad (3.62)$$

which results in

$$\begin{aligned} \tilde{t} + \text{const} &= \int \frac{d\tilde{a}}{\left[ -k + \frac{2\Lambda_{\text{eff}}}{d_0(d_0 - 1)} \tilde{a}^2 + \frac{2\kappa_0^2}{d_0(d_0 - 1)} \sum_{c=1}^m \frac{\tilde{A}^{(c)}}{\tilde{a}^{(d_0-1)\alpha^{(c)}}} \right]^{1/2}}, \\ &= \int \frac{d\tilde{a}}{\left[ -k + \frac{\Lambda_{\text{eff}}}{3} \tilde{a}^2 + \frac{\kappa_0^2}{3} \sum_{c=1}^m \frac{\tilde{A}^{(c)}}{\tilde{a}^{2\alpha^{(c)}}} \right]^{1/2}}, \quad (3.63) \end{aligned}$$

where in the last line we put  $d_0 = 3$ .

Thus in zero order approximation we arrived at a Friedmann model in the presence of positive cosmological constant  $\Lambda_{\text{eff}} > 0$  and a multicomponent perfect fluid. It is assumed that  $\Lambda_{\text{eff}}$  defines dark energy observed now. The perfect fluid has the form of a dust for  $\alpha^{(c)} = 1/2$  and radiation for  $\alpha^{(c)} = 1$ .

There is also a possibility for a primordial inflation. For this purpose we can consider one component perfect fluid with  $\alpha^{(1)} < 0$ , e.g.  $\alpha^{(1)} = -1/2 \Rightarrow \alpha_0^{(1)} = 1/3$  which describes a frustrated network of domain walls in the external space. It is well known that such perfect fluid results in acceleration of the Universe. The flat Universe ( $k = 0$ ) in the case  $\alpha_0^{(1)} = 1/3$  undergoes the power law inflation at early times:  $\tilde{a} \sim \tilde{t}^2$ . If domain walls decay into ordinary matter, then the described above Friedmann-like scenario follows the inflation.

**Dark energy in the universal extra dimension models.** In this section, to avoid the fine tuning problem, we consider Ricci-flat internal spaces. In this case scalar curvatures of the internal spaces are absent and there is no need for extreme fine tuning of the parameters to get the observable dark energy.

Among such models, Universal extra dimension models (UED) are of special interest [386]. Here, the internal spaces are orbifolds<sup>4</sup> with branes in fixed points. The compactification of the extra dimensions on orbifolds has a number of very interesting and useful properties, e.g. breaking (super)symmetry and obtaining chiral fermions in four dimensions (see, e.g., paper by H.-C. Cheng at al in [386]). The latter property gives a possibility to avoid famous no-go theorem of KK models (see e.g. [389]).

In UED models, the Standard Model fields are not localized on the brane but can move in the bulk. Branes in fixed points contribute in action functional (3.8) in the form:

$$\sum_{\substack{\text{fixed} \\ \text{points}}} \int d^4x \sqrt{g^{(0)}(x)} L_b \Big|_{\substack{\text{fixed} \\ \text{point}}}, \quad (3.64)$$

where  $g^{(0)}(x)$  is induced metric (which for our geometry (3.2) coincides with the metric of the external space-time in the Brans–Dicke frame) and  $L_b$  is the matter Lagrangian on the brane. In what follows, we consider the case where branes are characterized by their tensions  $L_{b(k)} = -\tau_{(k)}$ ,  $k = 1, 2, \dots, m$  and  $m$  is the number of branes.

After conformal transformation (3.14), the action (3.64) reads

$$\frac{1}{2\kappa_0^2} \int d^4x \sqrt{\tilde{g}^{(0)}(x)} \left( \prod_{i=1}^n e^{d_i \tilde{\beta}^i} \right)^{-2/(D_0-2)} \left[ -2\kappa_0^2 \sum_{k=1}^m \tau_{(k)} \prod_{i=1}^n e^{-d_i \tilde{\beta}^i} \right]. \quad (3.65)$$

The comparison of this expression with Eqs. (3.33) and (3.35) shows that branes contribute in the effective potential in the form of one component perfect fluid ( $c = 1$ ) with equations of state:  $\alpha_0^{(1)} = 0$ ,  $\alpha_i^{(1)} = 1$ ,  $i = 1, \dots, n$ , i.e., from the case I of the no-go theorem. It means that they contribute only to the  $U_{\text{int}}$ :

$$U_{\text{int}} = \left( e^{d_1 \tilde{\beta}^1} \right)^{-2/(D_0-2)} \left[ \Lambda_D + \tilde{f}_1^2 e^{-2d_1 \tilde{\beta}^1} - \lambda e^{-d_1 \tilde{\beta}^1} \right], \quad (3.66)$$

where we consider the case of one internal space  $i = 1$  and introduce notation  $\lambda \equiv -\kappa_0^2 \sum_{k=1}^m \tau_{(k)}$ .

Obviously, the internal space is stabilized if potential (3.66) has a minimum with respect to  $\tilde{\beta}^1$ . The extremum condition reads:

$$\left. \frac{\partial U_{\text{int}}}{\partial \tilde{\beta}^1} \right|_{\tilde{\beta}^1=0} = 0 \implies \frac{d_1 D_0}{D_0 - 2} \lambda = \frac{2d_1}{D_0 - 2} \Lambda_D + \frac{2d_1(D_0 - 1)}{D_0 - 2} \tilde{f}_1^2. \quad (3.67)$$

<sup>4</sup>For example,  $S^1/Z_2$  and  $T^2/Z_2$  which represent circle and square folded onto themselves due to  $Z_2$  symmetry.

The value of this potential at the minimum plays the role of effective four-dimensional cosmological constant:

$$\Lambda_{\text{eff}} := U_{\text{int}}|_{\tilde{\beta}^1=0} = \Lambda_D + \tilde{f}_1^2 - \lambda > 0, \quad (3.68)$$

which we assume to be positive. For the mass of gravexcitons we obtain:

$$\begin{aligned} m_1^2 &\sim \left. \frac{\partial^2 U_{\text{int}}}{\partial \tilde{\beta}^{1^2}} \right|_{\tilde{\beta}^1=0} = \left( \frac{2d_1}{D_0 - 2} \right)^2 \Lambda_D + \\ &+ \left( \frac{2d_1(D_0 - 1)}{D_0 - 2} \right)^2 \tilde{f}_1^2 - \left( \frac{d_1 D_0}{D_0 - 2} \right)^2 \lambda > 0. \end{aligned} \quad (3.69)$$

It can be easily seen from condition (3.67) and inequality (3.68) that all three parameters are positive:  $\tilde{f}_1^2, \Lambda_D, \lambda > 0$ . Thus, from  $\lambda > 0$  follows that summarized tensions of branes should be negative. Taking into account inequality (3.69), it can be easily verified that all these parameters have the same order of magnitude:

$$\tilde{f}_1^2 \sim \Lambda_D \sim \lambda \sim \Lambda_{\text{eff}} \sim m_1^2. \quad (3.70)$$

Therefore, there is no need for fine tuning of parameters to obtain the observable value of dark energy. To get it, it is sufficient to suppose that all these parameters, including  $\Lambda_{\text{eff}}$ , are of the order of  $\Lambda_{\text{DE}} \sim 10^{-123} \Lambda_{\text{Pl}(4)} \sim \sim 10^{-57} \text{ cm}^{-2}$ . However, it is natural to assume that parameters of the model have the same order of magnitude. On the other hand, our model does not answer why this value is equal to  $10^{-123} L_{\text{Pl}}$ . According to the anthropic principle, it takes place because human life is possible only at this value of dark energy.

If we assume that our parameters are defined by  $\Lambda_{\text{DE}} \sim 10^{-123} \Lambda_{\text{Pl}(4)}$ , then we get for the gravexciton masses  $m_1 \sim 10^{-33} \text{ eV} \sim 10^{-61} M_{\text{Pl}(4)}$ . These ultra-light particles have a period of oscillations  $t \sim 1/m_1 \sim 10^{18} \text{ sec}$  (see section 3.4.2) which is of the order of the Universe age. So, up to now these cosmological gravexcitons did not start to oscillate but slowly move to the position of minimum of the effective potential. In this case it is hardly possible to speak about stabilization of the internal space (the effective potential  $U_{\text{int}}$  is too flat) and we arrive at the problem of the fundamental constant variations (see section 3.4.4).

Of course, this problem is absent for gravexcitons with sufficiently large masses. For example, we can put  $m_1 \sim 1 \text{ TeV}$ . Then, as it follows from (3.69),  $\Lambda_D, \tilde{f}_1^2, \lambda \sim m_1^2 \sim 1 \text{ TeV}^2$  and to get observable dark energy  $\Lambda_{\text{eff}} \sim \Lambda_{\text{DE}} \sim \sim 10^{-123} M_{\text{Pl}(4)}^2 \sim 10^{-91} \text{ TeV}^2$  the parameters  $\Lambda_D, \tilde{f}_1^2, \lambda$  should be extremely fine tuned each other.

Similarly to the previous section, we can avoid this problem, if we give up the dark energy in this model:  $\Lambda_{\text{eff}} = 0$ . In this case we get  $\Lambda_D = \tilde{f}_1^2 = \lambda/2$  and  $m_1^2 = 2d_1^2\Lambda_D$ . Thus, if we naturally assume that  $\Lambda_D \sim 1 \text{ TeV}$ , then all parameters of the model (including  $m_1$ ) are of the TeV scale, which is physically reasonable.

Thus, the two previous sections demonstrate the typical problems of the KK models, when we want to both stabilize the internal spaces and to solve the problem of dark energy. Either we are faced with an extremely fine tuning of parameters or the effective potential is very flat, which leads to the problem of variation of fundamental constants.

### 3.3. Abelian gauge fields in KK models, dimensional reduction

In the section 3.2.1 we have shown that conformal zero-mode excitations of the internal factor spaces  $M_i$  have the form of massive scalar fields (gravexcitons/radions) developing on the background of the external space-time  $M_0$  i.e. in our Universe. It is of interest to consider the interaction of these scalar particles with fields from the Standard Model. In this section, we study the interaction of gravitational excitons with Abelian gauge fields, and in particular with the standard electromagnetic field of  $U(1)_{EM}$  symmetry. Strictly speaking, the photon will not exist as a separate gauge boson at temperatures higher than the electroweak scale  $M_{EW} \sim 246 \text{ GeV}$  where the full electroweak  $SU(2) \times U(1)$  model should be considered. Nevertheless, our results should reproduce the correct coupling term between the gravexciton sector and the EM gauge field sector of the theory. In the next section we will use this coupling term for estimating the strength of cosmological and astrophysical effects related to the corresponding interaction channel.

In order to derive the concrete form of the coupling term in the dimensionally reduced, four-dimensional effective theory, we start from the simplified toy model ansatz

$$S_{EM} = -\frac{1}{2} \int_M d^D X \sqrt{|g|} F_{MN} F^{MN}, \quad (3.71)$$

where the gauge field is assumed Abelian also in the higher-dimensional setup. Additionally, we work in the zero mode approximation for these fields, i.e. we keep only the zero modes of the harmonic expansion in mass eigenstates of the higher-dimensional fields<sup>5</sup>, [391, 392]. In this case, the Abelian vector potential depends only on the external coordinates,  $A_M = A_M(x)$ , ( $M = 1, \dots, D$ ), and the corresponding non-zero components of the field strength

<sup>5</sup>The excitation of Kaluza–Klein modes of Abelian gauge fields was considered, e.g., in Ref. [390].



tensor are  $F_{\mu\nu} = \partial_\mu A_\nu - \partial_\nu A_\mu$ , ( $\mu, \nu = 1, \dots, D_0$ ) and  $F_{\mu m_i} = \partial_\mu A_{m_i} - \partial_{m_i} A_\mu = \partial_\mu A_{m_i}$ , ( $m_i = 1, \dots, d_i$ ;  $i = 1, \dots, n$ ).

Dimensional reduction of the gauge field action (3.71) yields

$$S_{EM} = -\frac{1}{2} \int_{M_0} d^{D_0} x \sqrt{|g^{(0)}|} \prod_{i=1}^n e^{d_i \tilde{\beta}^i} \times \left\{ F_{\mu\nu} F^{\mu\nu} + 2g^{(0)\mu\nu} \sum_{i=1}^n e^{-2\tilde{\beta}^i(x)} \bar{g}^{(i)m_i n_i} \partial_\mu A_{m_i} \partial_\nu A_{n_i} \right\}, \quad (3.72)$$

where we introduced the metric integral

$$\bar{g}^{(i)m_i n_i} := \frac{1}{V_{d_i}} \int_{M_i} d^{d_i} y \sqrt{|g^{(i)}|} g^{(i)m_i n_i}(y^i) \quad (3.73)$$

and included the factor  $\sqrt{V_{D'}}$  into  $A_M$  for convenience:  $\sqrt{V_{D'}} A_M \rightarrow A_M$ . Due to this redefinition, the field strength tensor  $F_{\mu\nu}$  acquires the usual dimensionality  $\text{cm}^{-D_0/2}$  (in geometrical units  $\hbar = c = 1$ ). In Eq. (3.72) we assumed  $F^{\mu\nu} = g^{(0)\mu\kappa} g^{(0)\nu\delta} F_{\kappa\delta}$ .

It is easily seen that the  $A_{m_i}$  components play the role of scalar fields in the  $D_0$ -dimensional space-time. In what follows, we will not investigate the dynamics of these fields. Instead, we will concentrate on the interaction between gravexcitons and the 2-form field strength  $F = dA$ ,  $A = A_\mu dx^\mu$  which is described by the first term of the action functional (3.72). The corresponding truncated action (without  $A_{m_i}$  terms) will be denoted by  $\bar{S}_{EM}$ .

The exact field strength 2-form  $F = dA$  with components  $F_{\mu\nu}$  is invariant under gauge transformations  $A \mapsto A^f = A + df$ ,  $F^f = dA + d^2 f = dA = F$ , with  $f(x)$  any smooth and single-valued function. Accordingly,  $\bar{S}_{EM}$  is gauge invariant too (see Eq. (3.72)).

The action functional (3.72) is written in a Brans–Dicke frame. For passing by the conformal transformation (3.14) to the Einstein frame we choose an ansatz

$$A = \Omega^k \tilde{A} \quad (3.74)$$

for the vector potential and introduce the auxiliary field strength  $\bar{F}$  by the relation

$$\begin{aligned} F &= dA = d(\Omega^k \tilde{A}) = \Omega^k \bar{F}, \\ \bar{F} &= d(\ln \Omega^k) \wedge \tilde{A} + d\tilde{A}. \end{aligned} \quad (3.75)$$

The conformally transformed effective action reads then

$$\bar{S}_{EM} = -\frac{1}{2} \int_{M_0} d^{D_0} x \sqrt{|\tilde{g}^{(0)}|} \left\{ \Omega^{2(k-1)} \bar{F}_{\mu\nu} \bar{F}^{\mu\nu} \right\}, \quad (3.76)$$

where the external space indices are raised and lowered by the metric  $\tilde{g}^{(0)}$ . With  $\tilde{F} = d\tilde{A}$ , we have in Eq. (3.76) explicitly

$$\begin{aligned} \bar{F}_{\mu\nu}\bar{F}^{\mu\nu} &= \tilde{F}_{\mu\nu}\tilde{F}^{\mu\nu} - 2\tilde{F}^{\mu\nu} \left[ \tilde{A}_\mu\partial_\nu(\ln\Omega^k) - \tilde{A}_\nu\partial_\mu(\ln\Omega^k) \right] + \\ &+ 2 \left[ \tilde{g}^{(0)\mu\kappa}\partial_\mu(\ln\Omega^k)\partial_\kappa(\ln\Omega^k)\tilde{A}^\nu\tilde{A}_\nu - \left( \tilde{A}^\mu\partial_\mu(\ln\Omega^k) \right)^2 \right]. \end{aligned} \quad (3.77)$$

In order to fix the conformal weight  $k$  of the vector potential in Eq. (3.74), we require the effective external field strength tensor  $\bar{F}_{\mu\nu}$  in Eq. (3.76) to be gauge-invariant, i.e. to be invariant under  $\tilde{A} \mapsto \tilde{A}^f = \tilde{A} + df$ . From Eq. (3.75) we have for this transformation

$$\bar{F} \mapsto \bar{F}^f = d\tilde{A} + d^2f + d(\ln\Omega^k) \wedge (\tilde{A} + df) = \bar{F} + d(\ln\Omega^k) \wedge df, \quad (3.78)$$

so that for non-trivial  $\Omega \neq 1$  the gauge invariance  $\bar{F} = \bar{F}^f$  is only achieved for zero conformal weight  $k = 0$ . The same result follows also directly from the gauge invariance of the field strength tensor  $F$  in Eq. (3.72) and the ansatz (3.74): One checks immediately that  $\bar{F}$  is invariant under a transformation  $\tilde{A} \mapsto \tilde{A} = \tilde{A} + \Omega^{-k}df$ , which only for  $k = 0$  is a gauge transformation.

This means that in order to preserve the gauge invariance of the action functional, when passing from the Brans–Dicke frame to the Einstein frame, we have to keep the vector potential unchanged, i.e. we have to fix the conformal weight at  $k = 0$ . As a result, we arrive at the action functional

$$\bar{S}_{EM} = -\frac{1}{2} \int_{M_0} d^{D_0}x \sqrt{|\tilde{g}^{(0)}|} \left\{ e^{\frac{2}{D_0-2} \sum_{i=1}^n d_i \tilde{\beta}^i(x)} F_{\mu\nu} F^{\mu\nu} \right\} \quad (3.79)$$

with dilatonic coupling of the Abelian gauge fields to the gravitational excitons [387].

For completeness, we note that for  $k = 1$ , according to Eqs. (3.76) and (3.77), we obtain a theory with a pure free action term  $\tilde{F}_{\mu\nu}\tilde{F}^{\mu\nu}$  without any prefactor ( $\Omega^{2(k-1)} = 1$ ) but with explicitly destroyed gauge invariance. The corresponding effective action reads

$$\begin{aligned} \bar{S}_{EM} &= -\frac{1}{2} \int_{M_0} d^{D_0}x \sqrt{|\tilde{g}^{(0)}|} \left\{ \tilde{F}_{\mu\nu}\tilde{F}^{\mu\nu} - 4\tilde{F}^{\mu\nu} \tilde{A}_{[\mu}\partial_{\nu]}(\ln\Omega) + \right. \\ &\left. + 2 \left[ \tilde{g}^{(0)\mu\kappa}\partial_\mu(\ln\Omega)\partial_\kappa(\ln\Omega)\tilde{A}^\nu\tilde{A}_\nu - \left( \tilde{A}^\mu\partial_\mu \ln\Omega \right)^2 \right] \right\}. \end{aligned} \quad (3.80)$$

Obviously, the localization of the internal space scale factors at their present values implies  $\tilde{\beta}^i = 0$  which yields  $\Omega \equiv 1$ . Then, both approaches (3.79) and (3.80) coincide with each other. However, the presence of small scale factor fluctuations above this background will restore the dilatonic coupling of Eq. (3.79) (see also the next section).

### 3.4. Gravitational excitons and their cosmological and astrophysical implications. Dark matter from extra dimensions

In this section, we discuss some cosmological and astrophysical implications related to the possible existence of gravitational excitons. We suppose that the scale factor background of the internal spaces is localized in one of the minima of the effective potential and that gravexcitons are present as small fluctuations above this static background. Our analysis is based on the dilatonic coupling (3.79) which describes the interaction between gravexcitons and zero mode photons<sup>6</sup>. Hereafter, we treat these KK zero mode photons as our usual SM matter photons. In particular, the vector potential  $A_\mu(x)$  of the previous section corresponds to our 4D photons.

In the following we consider the simplest example — the interaction between gravitational excitons and photons in a system with only one internal space ( $n = 1$ ) with its scale factor  $\beta^1$  localized in one of the minima of the effective potential (e.g. potential (3.35)). Then, for small scale factor fluctuations  $\tilde{\beta}^1 \ll 1$  action (3.19) (without minimal scalar field) together with (3.79) reads

$$\begin{aligned}
S = & \frac{1}{2\kappa_0^2} \int_{M_0} d^{D_0}x \sqrt{|\tilde{g}^{(0)}|} \left\{ \tilde{R}[\tilde{g}^{(0)}] - 2\Lambda_{\text{eff}} \right\} + \\
& + \frac{1}{2} \int_{M_0} d^{D_0}x \sqrt{|\tilde{g}^{(0)}|} \left\{ -\tilde{g}^{(0)\mu\nu} \psi_{,\mu} \psi_{,\nu} - m_\psi^2 \psi \psi \right\} - \\
& - \frac{1}{2} \int_{M_0} d^{D_0}x \sqrt{|\tilde{g}^{(0)}|} \left\{ F_{\mu\nu} F^{\mu\nu} - 2\sqrt{\frac{d_1}{(D_0-2)(D-2)}} \kappa_0 \psi F_{\mu\nu} F^{\mu\nu} \right\} + \dots \quad (3.81)
\end{aligned}$$

We have used the notation of the action (3.19),  $m_\psi := m_1$  and relation (3.18) between  $\tilde{\beta}^1$  and the rescaled fluctuational component  $\psi \equiv \psi^1$ . As mentioned in section 3.2.1,  $\kappa_0^2 = 8\pi/M_{\text{Pl}(4)}^2$  is the  $D_0$ -dimensional (usually  $D_0 = 4$ ) gravitational constant. The last term in Eq. (3.81) describes the interaction between gravitational excitons and photons. In the lowest-order tree-level approximation, this term corresponds to the vertex  $1/M_{\text{Pl}(4)}$  of Fig. 3.1 [387] and describes the decay of a gravitational exciton into two photons. The probability of this decay is easily estimated as<sup>7</sup>

$$\Gamma \sim \left( \frac{1}{M_{\text{Pl}(4)}} \right)^2 m_\psi^3 = \left( \frac{m_\psi}{M_{\text{Pl}(4)}} \right)^3 \frac{1}{t_{\text{Pl}}} \ll m_\psi, \quad (3.82)$$

<sup>6</sup> Brane-world models with on-brane dilatonic coupling terms have been considered, e.g., in Refs. [393, 394]. In a rough approximation, the results of the present section will also hold for these models.

<sup>7</sup> Exact calculations give  $\Gamma = [2d_1/(d_1 + 2)](m_\psi^3/M_{\text{Pl}(4)}^2)$ .

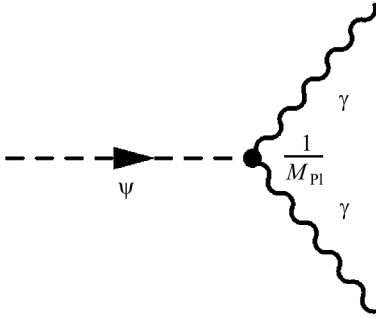


**Fig. 3.1.** Planck-scale suppressed gravexciton decay:  $\psi \rightarrow 2\gamma$

which results in a life-time  $\tau$  of the gravitational excitons with respect to this decay channel of

$$\tau = \frac{1}{\Gamma} \sim \left( \frac{M_{\text{Pl}(4)}}{m_\psi} \right)^3 t_{\text{Pl}}. \quad (3.83)$$

For example, for light excitons with masses  $m_\psi \leq 10^{-21} M_{\text{Pl}} \sim 10^{-2} \text{ GeV} \sim 20m_e$  (where  $m_e$  is the electron mass) we get that their life-time  $\tau$  is greater than the age of the Universe  $\tau \geq 10^{19} \text{ sec} > t_{\text{univ}} \sim 10^{18} \text{ sec}$  (see also section 3.4.2).

Similar to Polonyi particles in spontaneously broken supergravity [395, 396], scalarons in the  $(R + R^2)$  fourth order theory of gravity [397] or moduli fields in the hidden sector of SUSY [398–401], gravitational excitons are WIMPs (Weakly-Interacting Massive Particles [402]) because their coupling to the observable matter is suppressed by powers of the Planck scale. Thus, the gravexcitons/radions can contribute to **dark matter**<sup>8</sup> (DM). As we have shown above, light gravexcitons with masses  $m_\psi \leq 10^{-21} M_{\text{Pl}(4)} \sim 10^{-2} \text{ GeV}$  have life-time  $\tau$  greater than the age of the Universe. However, there are strong cosmological restrictions on masses of gravexcitons. To show it, we investigate now the role of gravexcitons in different cosmological scenarios [388].

### 3.4.1. Effective equation of motion for gravexcitons

The effective equation of motion for massive gravexcitons in FRW metric (3.36) is

$$\ddot{\psi} + (3H + \Gamma)\dot{\psi} + m_\psi^2\psi = 0, \quad (3.84)$$

where  $H = \dot{\tilde{a}}/\tilde{a}$  is the Hubble constant,  $\tilde{a}$  is the scale factor of the external space in the Einstein frame, and dots denote the derivatives with respect to the synchronous time  $\tilde{t}$  in the Einstein frame. In sections 3.4.1–3.4.5, for simplicity of notations we shall write  $a$  and  $t$  without symbol tilde above them. In Eq. (3.84) (by analogy with Ref. [403]) we took into account the effective decay of gravexcitons into ordinary matter, e.g. into 4D photons (3.82). In Refs. [387, 404] it was shown that the gravexciton production due to interactions with matter fields is negligible for the models under consideration.

<sup>8</sup> The type of the DM depends on the masses of the particles which constitute it. It is hot for  $m_{\text{DM}} \leq 50\text{--}100 \text{ eV}$ , warm for  $100 \text{ eV} \leq m_{\text{DM}} \leq 10 \text{ KeV}$  and cold for  $m_{\text{DM}} \geq 10\text{--}50 \text{ KeV} \sim 10^{-5} \text{ GeV}$ .

A corresponding source term on the right-hand side of Eq. (3.84) can, hence, be omitted.

The investigation of Eq. (3.84) is most conveniently started by a substitution

$$\psi := B(t)u(t) := M_{\text{Pl}(4)} e^{-\frac{1}{2} \int (3H+\Gamma) dt} u(t), \quad (3.85)$$

which, for constant  $\Gamma$ , leads to the following differential equation for the auxiliary function  $u(t)$ :

$$\ddot{u} + \left[ m_\psi^2 - \frac{1}{4}(3H + \Gamma)^2 - \frac{3}{2}\dot{H} \right] u = 0. \quad (3.86)$$

This equation shows that at times when the Hubble parameter  $H = s/t \sim 1/t$  is less than the mass

$$H < m_\psi \implies t > t_{in} \sim H_{in}^{-1} \sim \frac{1}{m_\psi}, \quad (3.87)$$

the scalar field oscillates

$$\psi \approx CB(t) \cos(m_\psi t + \delta). \quad (3.88)$$

The time  $t_{in}$  roughly indicates the beginning of the oscillations. Substituting the Hubble parameter  $H = s/t$  into the definition of  $B(t)$  we obtain

$$B(t) = M_{\text{Pl}(4)} e^{-\frac{1}{2}\Gamma t} \frac{1}{(M_{\text{Pl}(4)} t)^{3s/2}}, \quad (3.89)$$

where  $s = 1/2, 2/3$  for radiation dominated (RD) and matter dominated (MD) stages, respectively. The parameter  $C$  in Eq. (3.88) can be obtained from the amplitude of the initial oscillation  $\psi_{in}$ :

$$\psi_{in} \sim CB(t_{in}) \implies C_r \sim \frac{\psi_{in}}{M_{\text{Pl}(4)}} \left( \frac{M_{\text{Pl}(4)}}{m_\psi} \right)^{3/4}, \quad C_m \sim \frac{\psi_{in}}{m_\psi}. \quad (3.90)$$

$C_r$  and  $C_m$  correspond to particles which start to oscillate during the RD and MD stages. Additionally, we took into account that  $\Gamma t_{in} \sim \Gamma/m_\psi \ll 1$ .

Further useful differential relations are those for  $B(t)$  in (3.85), (3.89) and for the energy density  $\rho_\psi$  and the number density  $n_\psi$  of the gravexcitons. It can be easily seen from the definition of  $B(t)$  that this function satisfies the differential equation

$$\frac{d}{dt} (a^3 B^2) = -\Gamma a^3 B^2, \quad (3.91)$$

with  $a(t) \sim t^s$  as scale factor of the Friedmann Universe. The energy density of the gravexciton field and the corresponding number density, which can be approximated as

$$\rho_\psi = \frac{1}{2} \dot{\psi}^2 + \frac{1}{2} m_\psi^2 \psi^2 \approx \frac{1}{2} C^2 B^2 m_\psi^2, \quad n_\psi \approx \frac{1}{2} C^2 B^2 m_\psi, \quad (3.92)$$

satisfy the DEs

$$\frac{d}{dt}(a^3 \rho_\psi) = -\Gamma a^3 \rho_\psi \text{ and } \frac{d}{dt}(a^3 n_\psi) = -\Gamma a^3 n_\psi \quad (3.93)$$

with solutions 
$$\rho_\psi \sim e^{-\Gamma t} a^{-3} \text{ and } n_\psi \sim e^{-\Gamma t} a^{-3}. \quad (3.94)$$

This means that during the stage  $m_\psi > H \gg \Gamma$  the gravexcitons perform damped oscillations and their energy density behaves like a red-shifted dust-like perfect fluid ( $\rho_\psi \sim a^{-3}$ ) with slow decay  $e^{-\Gamma t} \sim 1$ :

$$\rho_\psi \approx \psi_{in}^2 m_\psi^2 \left( \frac{T}{T_{in}} \right)^3. \quad (3.95)$$

$T_{in}$  denotes the temperature of the Universe when the gravexcitons started to oscillate. According to the Friedmann equation (the 00-component of the Einstein equation), the Hubble parameter and the energy density (which defines the dynamics of the Universe) are connected (for flat spatial sections) by the relation

$$H(t) M_{\text{Pl}(4)} = \sqrt{\frac{8\pi}{3} \rho(t)} \sim \sqrt{\rho(t)}. \quad (3.96)$$

During the RD stage it holds  $\rho(t) \sim T^4$  and, hence,  $H^2 \sim T^4 / M_{\text{Pl}(4)}^2$ . For gravexcitons which start their oscillations during this stage, the temperature  $T_{in}$  is now easily estimated as

$$H_{in} \sim m_\psi \sim \frac{T_{in}^2}{M_{\text{Pl}(4)}} \implies T_{in} \sim \sqrt{m_\psi M_{\text{Pl}(4)}}. \quad (3.97)$$

If there is no broad parametric resonance (“preheating”) [403], then the decay plays the essential role when  $H \lesssim \Gamma$  and the evolution of the energy density of the gravexcitons is dominated by an exponential decrease. The most effective decay takes place at times

$$t_D \sim H_D^{-1} \sim \Gamma^{-1} \sim \left( \frac{M_{\text{Pl}(4)}}{m_\psi} \right)^2 m_\psi^{-1}. \quad (3.98)$$

### 3.4.2. Light and ultra-light gravexcitons: $m_\psi \leq 10^{-2}$ GeV

If the decay time  $t_D$  of the gravexcitons exceeds the age of the Universe  $t_{univ} \sim 10^{18}$  sec then the decay can be neglected. Eq. (3.98) shows that this is the case for particles with masses  $m_\psi \leq 10^{21} M_{\text{Pl}(4)} \sim 10^{-2}$  GeV  $\sim \sim 20m_e$  (where  $m_e$  is the electron mass).

Subsequently, we split our analysis, considering separately particles which start to oscillate before matter/radiation equality  $t_{eq} \sim H_{eq}^{-1}$  (i.e. during the RD stage) and after  $t_{eq}$  (i.e. during the MD stage). According to present WMAP data for the  $\Lambda$ CDM model, the following holds:

$$H_{eq} \equiv m_{eq} \sim 10^{-56} M_{\text{Pl}(4)} \sim 10^{-28} \text{ eV}. \quad (3.99)$$

An obvious requirement is that gravexciton should not over-close the observable Universe. This means that for particles with masses  $m_\psi > m_{eq}$  the energy density at the time  $t_{eq}$  should not exceed the critical density<sup>9</sup>:

$$\sqrt{\rho_\psi} \Big|_{t_{eq} \sim H_{eq}^{-1}} \lesssim H_{eq} M_{\text{Pl}(4)} \implies m_\psi \lesssim m_{eq} \left( \frac{M_{\text{Pl}(4)}}{\psi_{in}} \right)^4. \quad (3.100)$$

Here we used the estimate  $\rho_\psi \sim (\psi_{in}/t)^2 (m_\psi t)^{1/2}$  which follows from Eqs. (3.89), (3.90) and (3.92). For particles with masses  $m_\psi \gtrsim m_{eq}$ , relation (3.100) implies the additional consistency condition  $\psi_{in} \lesssim M_{\text{Pl}(4)}$ , or more exactly

$$\psi_{in} \lesssim \left( \frac{m_{eq}}{m_\psi} \right)^{1/4} M_{\text{Pl}(4)} \lesssim M_{\text{Pl}(4)}. \quad (3.101)$$

Let us now consider particles with masses  $m_\psi \lesssim m_{eq}$  which start to oscillate during the MD stage. From Eqs. (3.89), (3.90) and (3.92) one finds for these particles  $\rho_\psi \sim (\psi_{in}/t)^2$  so that the inequality

$$\sqrt{\rho_\psi} \Big|_{t_{in} \sim H_{in}^{-1}} \lesssim H_{in} M_{\text{Pl}(4)} \implies \psi_{in} \lesssim M_{\text{Pl}(4)} \quad (3.102)$$

ensures under-criticality of the energy density with respect to over-closure of the Universe.

It is worth noting that the combination  $-(9/4)H^2 - (3/2)\dot{H}$  in (3.86) vanishes for the MD stage because of  $H = 2/(3t)$ . Hence, for times  $t \geq t_{eq} \sim 1/m_{eq}$  the solutions of equation (3.86) have an oscillating behavior (provided that  $m_\psi > \Gamma$ ) with a period of oscillations  $t_{osc} \sim 1/m_\psi$ . For light particles with masses  $m_\psi \leq m_{eq}$  this implies that the initial oscillations start at  $t_{in} \sim 1/m_\psi$ .

Particles with masses  $m_\psi \sim 10^{-33} \text{ eV} \sim 10^{-61} M_{\text{Pl}(4)}$  are of special interest because via  $\Lambda_{\text{eff}} \sim m_\psi^2$  (see section 3.2.4) they are related to the recently observed value of the effective cosmological constant (dark energy)  $\Lambda_{\text{eff}} \sim 10^{-123} \Lambda_{\text{Pl}(4)} \sim 10^{-57} \text{ cm}^{-2}$ . These ultra-light particles begin to oscillate at characteristic times  $t \sim 10^{18} \text{ sec}$  which is of order of the Universe age. Thus, these particles did not oscillate coherently up to the present time and a splitting of the scale factor of the internal space into a background component and gravexcitons makes no sense. A more adequate interpretation of the scale factor dynamics would be in terms of a slowly varying background in the sense of a quintessence scenario [236, 405]. However, such light gravexcitons will lead to a temporal variability of the fine structure constant above the experimentally established value [387] (see section 3.4.4).

<sup>9</sup> It is clear that the ratio between the energy densities of gravexciton and matter becomes fixed after  $t_{eq}$ . If  $\rho_\psi$  is less than the critical density at this moment then it will remain under-critical forever.

Finally, it should be noted that light gravexcitons can lead to the appearance of a fifth force with characteristic length scale  $\lambda \sim 1/m_\psi$ . Recent gravitational (Cavendish-type) experiments (see e.g. [406]) exclude fifth force particles with masses  $m_\psi \lesssim 1/(10^{-2} \text{ cm}) \sim 10^{-3} \text{ eV}$ . This sets an additional restriction on the allowed mass region of gravexcitons. Thus, physically sensible models should allow for parameter configurations which exclude such ultra-light gravexcitons.

### 3.4.3. Heavy gravexcitons: $m_\psi \geq 10^{-2} \text{ GeV}$

This section is devoted to the investigation of gravexcitons/radions with masses  $m_\psi \geq 10^{-2} \text{ GeV}$  for which the decay plays an important role. Because of  $m_\psi \gg m_{eq}$ , the corresponding modes begin to oscillate during the RD stage. We consider two scenarios separately. The first one contains an evolutionary stage with transient gravexciton dominance ( $\psi$ -dominance), whereas in the second one gravexcitons remain always sub-dominant.

**The transiently  $\psi$ -dominated Universe.** In this subsection we consider a scenario where the Universe is already at the RD stage when the gravexcitons begin their oscillations. The initial heating could be induced, e.g., by the decay of some additional very massive (inflaton) scalar field. We assume that the Hubble parameter at this stage is defined by the energy density of the radiation. The gravexcitons start their oscillations when the radiation cools down to the temperature  $T_{in} \sim \sqrt{m_\psi M_{\text{Pl}(4)}}$  (see Eq. (3.97)). From the dust-like red-shifting of the energy density  $\rho_\psi$  (see Eq. (3.95)) follows that the ratio  $\rho_\psi/\rho_{rad}$  increases like  $1/T$  when  $T$  decreases. At some critical temperature  $T_{crit}$  this ratio reaches  $\sim 1$  and the Universe becomes  $\psi$ -dominated:

$$m_\psi^2 \psi_{in}^2 \left( \frac{T}{T_{in}} \right)^3 \sim T^4 \implies T_{crit} \sim T_{in} \left( \frac{\psi_{in}}{M_{\text{Pl}(4)}} \right)^2. \quad (3.103)$$

After that the Hubble parameter is defined by the energy density of the gravexcitons:  $H^2 M_{\text{Pl}(4)}^2 \sim \rho_\psi$  (with  $\rho_\psi$  from Eq. 3.95). This stage is transient and ends when the gravexcitons decay at the temperature  $T_D$ :

$$\begin{aligned} H_D^2 M_{\text{Pl}(4)}^2 &\sim \Gamma^2 M_{\text{Pl}(4)}^2 \sim m_\psi^2 \psi_{in}^2 \left( \frac{T_D}{T_{in}} \right)^3 \implies \\ \implies T_D &\sim T_{in} \left( \frac{M_{\text{Pl}(4)}}{\psi_{in}} \right)^{2/3} \left( \frac{m_\psi}{M_{\text{Pl}(4)}} \right)^{4/3}. \end{aligned} \quad (3.104)$$

We assume that, due to the decay, all the energy of the gravexcitons is converted into radiation and that a reheating occurs. The corresponding reheating temperature can be estimated as:

$$H_D^2 M_{\text{Pl}(4)}^2 \sim \Gamma^2 M_{\text{Pl}(4)}^2 \sim T_{RH}^4 \implies T_{RH} \sim \sqrt{\frac{m_\psi^3}{M_{\text{Pl}(4)}}}. \quad (3.105)$$



Because the Universe before the gravexciton decay was gravexciton-dominated, it is clear that the reheating temperature  $T_{RH}$  should be higher than the decay temperature  $T_D$ . This provides a lower bound for  $\psi_{in}$ :

$$T_{RH} \geq T_D \implies \psi_{in} \geq \sqrt{m_\psi M_{\text{Pl}(4)}} \sim T_{in}. \quad (3.106)$$

Substitution of this estimate into Eq. (3.103) shows that the minimal critical temperature (at which the Universe becomes  $\psi$ -dominated) is equal to the reheating temperature:  $T_{crit(min)} \sim T_{RH}$ .

If we additionally assume the natural initial condition  $\psi_{in} \sim M_{\text{Pl}(4)}$ , then it holds  $T_{crit} \sim T_{in}$  and the Universe will be  $\psi$ -dominated from the very beginning of the gravexciton oscillations. The upper bound on  $\psi_{in}$  is set by the exclusion of quantum gravity effects:  $m_\psi^2 \psi_{in}^2 \leq M_{\text{Pl}(4)} q_u$ . Hence, in the considered scenario it should hold

$$T_{in} \leq \psi_{in} \leq M_{\text{Pl}(4)} \left( \frac{M_{\text{Pl}(4)}}{m_\psi} \right). \quad (3.107)$$

A successful nucleosynthesis requires a temperature  $T \gtrsim 1$  MeV during the RD stage. If we assume that this lower bound is fulfilled for the reheating temperature (3.105), then we find the lower bound on the gravexciton mass

$$m_\psi \gtrsim 10^4 \text{ GeV}. \quad (3.108)$$

It is also possible to consider a scenario where the  $\psi$ -field acts as inflaton itself. In such a scenario, the Universe is  $\psi$ -dominated from the very beginning and for the amplitude of the initial oscillations one obtains:

$$HM_{\text{Pl}(4)} \sim \sqrt{\rho_\psi} \implies H_{in} M_{\text{Pl}(4)} \sim m_\psi M_{\text{Pl}(4)} \sim \psi_{in} m_\psi \implies \psi_{in} \sim M_{\text{Pl}(4)}. \quad (3.109)$$

The reheating temperature is then again given by the estimate (3.105) and the gravexciton masses should also fulfill the requirement (3.108).

**Sub-dominant gravexcitons.** In this subsection we consider a scenario where the  $\psi$ -field undergoes a decay, but the gravexcitons never dominate the dynamics of the Universe. The Hubble parameter of the Universe is then defined by the energy density of other (matter) fields which behave as radiation for  $t \leq t_{eq}$  and as dust for  $t \geq t_{eq}$ . The energy density  $\rho_\psi$  is always much less than the total energy density of the other fields.

i. *Decay during the RD stage*

Here, we analyze the behavior of  $\psi$ -particles that decay during the RD stage, when  $H^2 \sim T^4/M_{\text{Pl}(4)}^2$ . Again we will clarify for which masses  $m_\psi$  and initial oscillation amplitudes  $\psi_{in}$  such a scenario can hold. A decay during RD

implies that the decay temperature  $T_D$ , estimated as

$$\Gamma \sim H_D \sim \frac{T_D^2}{M_{\text{Pl}(4)}} \implies T_D \sim \sqrt{\frac{m_\psi^3}{M_{\text{Pl}(4)}}}, \quad (3.110)$$

should be higher than the temperature

$$T_{eq} \sim \sqrt{H_{eq} M_{\text{Pl}(4)}} \sim 1 \text{ eV} \quad (3.111)$$

of the matter/radiation equality. This yields the following restriction on the gravexciton masses:

$$T_D \gtrsim T_{eq} \implies m_\psi \gtrsim M_{\text{Pl}(4)} \left( \frac{T_{eq}}{M_{\text{Pl}(4)}} \right)^{2/3} \equiv m_d \sim 1 \text{ GeV}. \quad (3.112)$$

The mass parameter  $m_d$  corresponds to particles which decay at the moment  $t_{eq}$ :  $\Gamma \sim H_{eq}$ . The bound on the initial oscillation amplitude  $\psi_{in}$  can be found from the energy sub-dominance condition for the gravexcitons at the moment of their decay  $t_D$

$$\rho_\psi|_{t_D} \approx \psi_{in}^2 m_\psi^2 \left( \frac{T_D}{T_{in}} \right)^3 < T_D^4. \quad (3.113)$$

It reads

$$\psi_{in} < \sqrt{m_\psi M_{\text{Pl}(4)}} \sim T_{in}, \quad (3.114)$$

where  $T_{in}$  is defined by Eq. (3.97). It can be easily seen that condition (3.114) is supplementary to the condition (3.106). During the decay, the energy of the gravexcitons is converted into radiation:  $\rho_\psi \rightarrow \rho_{r,2}$  with temperature  $T_r^4 \sim \sim \rho_\psi|_{t_D}$ . For a scenario with  $\rho_\psi|_{t_D} \ll T_D^4$ , and hence  $T_r \ll T_D$ , the energy density  $\rho_{r,2}$  contributes only negligibly to the total energy density and the gravexciton decay does not spoil the standard picture of a hot Universe with successful big bang nucleosynthesis (BBN).

ii. *Gravexciton decay during the MD stage*

At the MD stage (for  $t > t_{eq}$ ) the Hubble parameter reads (see e.g. [402], page 504)

$$t \sim H^{-1} \sim \frac{M_{\text{Pl}(4)}}{T^{3/2} T_{eq}^{1/2}} \implies H M_{\text{Pl}(4)} \sim T^{3/2} T_{eq}^{1/2}, \quad (3.115)$$

and the decay temperature  $T_D$  of the gravexcitons can be estimated as

$$\begin{aligned} \Gamma \sim H_D \sim \frac{T_D^{3/2} T_{eq}^{1/2}}{M_{\text{Pl}(4)}} &\implies \\ \implies T_D^3 \sim \frac{(\Gamma M_{\text{Pl}(4)})^2}{T_{eq}} \sim T_{eq}^3 \left( \frac{m_\psi}{M_{\text{Pl}(4)}} \right)^4 \left( \frac{m_\psi}{m_{eq}} \right)^2. &\quad (3.116) \end{aligned}$$

For a decay during MD this decay temperature should be less than  $T_{eq}$ , and as implication a restriction on the mass of the  $\psi$ -field can be obtained

$$T_D < T_{eq} \implies m_\psi < M_{\text{Pl}(4)} \left( \frac{T_{eq}}{M_{\text{Pl}(4)}} \right)^{2/3} = m_d, \quad (3.117)$$

which is supplementary to the inequality (3.112). The restriction on the initial amplitude  $\psi_{in}$  can be found from the condition of matter dominance and the fact that heavy gravexcitons begin to oscillate at the RD stage when  $T_{in} \sim \sqrt{m_\psi M_{\text{Pl}(4)}}$

$$\begin{aligned} \psi_{in}^2 m_\psi^2 \left( \frac{T_D}{T_{in}} \right)^3 &\sim T_r^4 < H_D^2 M_{\text{Pl}(4)}^2 \sim \frac{T_D^3 T_{eq}}{M_{\text{Pl}(4)}^2} M_{\text{Pl}(4)}^2 \implies \\ \implies \psi_{in} < M_{\text{Pl}(4)} \left( \frac{T_{eq}}{T_{in}} \right)^{1/2} &\sim M_{\text{Pl}(4)} \left( \frac{H_{eq}}{m_\psi} \right)^{1/4} \ll M_{\text{Pl}(4)}. \end{aligned} \quad (3.118)$$

Condition (3.118) guarantees that there is no additional reheating and the BBN is not spoiled.

In this section, we discussed different cosmological scenarios affected by the dynamics of gravitational excitons/radions. These massive moduli fields describe the conformal excitations of the internal spaces in higher dimensional models and are WIMPs in the external space-time. We demonstrated that observable cosmological data set strong constraints on the gravexciton masses and the amplitudes of their initial oscillations.

#### 3.4.4. Variation of the fine-structure constant

As we have seen in section (3.4.2), light gravexcitons with masses  $m_\psi \leq 10^{-2}$  GeV have a decay time greater than the age of the Universe. Moreover, ultra-light particles with masses  $m_\psi \leq 10^{-33}$  eV have not yet started to oscillate. It means that, in the case of such ultra-light particles, the internal spaces are not stabilized up to present time in the minimum of the effective potential. However, there is very strong restrictions on dynamical behavior of the internal spaces following from experiments on the time variation of the fine-structure constant  $\alpha = e^2/\hbar c$ . In KK models the effective fine-structure constant is inversely proportional to the volume of the internal spaces:  $\alpha \sim V_{D'}^{-1}(t)$ , where  $V_{D'}(t) = \exp(\sum_{i=1}^n d_i \tilde{\beta}^i) V_{D'}$  is the internal space volume at the moment  $t$  and  $V_{D'}$  is defined in Eq. (3.6). The origin of such dependence can be easily seen from action (3.79) where the Lagrangian density can be rewritten in the form<sup>10</sup>  $\mathcal{L} = -(1/2)\sqrt{|\tilde{g}^{(0)}|}(V_{D'}(t)/V_{D'})(1/e^2)F^2$  and we chose  $D_0 = 4$ .

<sup>10</sup> It is well known that the theory of electromagnetic field can be described with the help of the Lagrangian density of the form  $\mathcal{L} = -(1/2)\sqrt{|g|}(1/e^2)F^2$  where  $e$  is the electron charge.

Therefore, we can introduce an effective electron charge  $e_{\text{eff}}^2(t) = e^2 V_{D'}/V_{D'}(t)$ , which defines the written above dependence of the fine-structure constant on the internal space volume. Thus, for the variation of  $\alpha$  with time we obtain the following equation <sup>11</sup>:

$$\left| \frac{\dot{\alpha}}{\alpha} \right| = \left| \frac{\dot{V}_{D'}(t)}{V_{D'}(t)} \right|. \quad (3.119)$$

In the case of one internal space  $n = 1$  this formula yields

$$\left| \frac{\dot{\alpha}}{\alpha} \right| = d_1 |\dot{\beta}^1| = \frac{\sqrt{8\pi}}{M_{\text{Pl}(4)}} \sqrt{\frac{2d_1}{D-2}} |\dot{\psi}^1| = \frac{\sqrt{8\pi}}{M_{\text{Pl}(4)}} \sqrt{\frac{2d_1}{D-2}} \left| \frac{\Delta\psi^1}{\Delta t} \right|, \quad (3.120)$$

where we used the relation (3.18).

The experimental bounds on the time variation of  $\alpha$  have been considerably refined during recent years (see, e.g., [407–411] and references therein). Different experiments give different bounds on  $|\dot{\alpha}/\alpha|$  (see Table II in [411]), from  $\lesssim 10^{-12} \text{ yr}^{-1}$  (following from the data analysis of the observed cosmic microwave background [407]) to  $\lesssim 10^{-17} \text{ yr}^{-1}$  (following from the Oklo experiment [412]). Estimates on primordial nucleosynthesis require  $|\Delta\alpha/\alpha| \lesssim 10^{-4}$  at a redshift of order  $z = 10^9\text{--}10^{10}$  [413], i.e.  $|\dot{\alpha}/\alpha| \lesssim 10^{-14} \text{ yr}^{-1}$ . The WMAP data analysis [414] gives upper bounds on the variation of  $\alpha$  during the time from re-ionization/recombination ( $z \sim 1100$ ) until today:  $|\Delta\alpha/\alpha| \lesssim 2 \times 10^{-2}\text{--}6 \times 10^{-2}$ , i.e.  $|\dot{\alpha}/\alpha| \lesssim 2 \times 10^{-12}\text{--}6 \times 10^{-12} \text{ yr}^{-1}$ . In all these estimates  $\dot{\alpha} = \Delta\alpha/\Delta t$  is the average rate of change of  $\alpha$  during the time interval  $\Delta t$  (corresponding to a redshift  $z$ ). For our estimates, we use the bound  $|\dot{\alpha}/\alpha| \lesssim 10^{-15} \text{ yr}^{-1}$  [409], which follows from observations of the spectra of quasars at a Hubble time scale  $\Delta t \sim H^{-1} \sim 10^{10}$  years.

Coming back to Eq. (3.120) for the fine-structure constant variation, we obtain in our model

$$\left| \frac{\dot{\alpha}}{\alpha} \right| \sim \sqrt{8\pi} \sqrt{\frac{2d_1}{D-2}} 10^{-10} \text{ yr}^{-1}, \quad (3.121)$$

where for the Hubble time scale  $\Delta t \sim H^{-1} \sim 10^{10}$  we used  $|\Delta\psi^1| \sim \psi_{in} \sim \sim M_{\text{Pl}(4)} \text{ yr}$  which is usual assumption for light gravexcitons (see section 3.4.2). It is obvious that this value is many orders of magnitude larger than the experimental bounds  $10^{-15} \text{ yr}^{-1}$ . This contradiction means that light gravexcitons with masses  $m_\psi \lesssim 10^{-2} \text{ GeV}$  and initial amplitude  $\psi_{in} \sim M_{\text{Pl}(4)}$  should have decayed at sufficiently early times of the evolution of the Universe in order not to contradict the experimental bounds on the variation of the fine

<sup>11</sup> We remind that dots denote the derivatives with respect to the synchronous time in the Einstein frame. We omit here the symbol “tilde” for  $t$ .

structure constant. From this point of view, the presence of such light gravexcitons is unacceptable for the time after the end of primordial nucleosynthesis. This restriction can be circumvented in the case  $\psi_{in} \ll M_{\text{Pl}(4)}$  (see the next section 3.4.5).

The above estimate shows that too much variation of the fine-structure constant is a typical problem of models with dynamical behavior of the internal spaces if they are not stabilized at sufficiently early times (see, e.g., section 3.6).

### 3.4.5. Lorentz invariance violation

Obviously, the term, describing interaction between gravexcitons and photons in action (3.81), modifies the Maxwell equations, and, consequently, results in a modified dispersion relation for photon [415]. In this section we demonstrate that this modification has a rather specific form. For simplicity we assume that  $\tilde{g}^0$  in action (3.81) is the flat FRW metric and for the scale factors  $\tilde{a}$  and synchronous time  $\tilde{t}$ , we omit the tilde symbol. It is worth noting that action (3.81) (the third line) is conformally invariant in the case when  $D_0 = 4$ ,  $D_0$ -dimensional field strength tensor,  $F_{\mu\nu}$ , is gauge invariant and the electromagnetic field is antisymmetric as usual,  $F_{\mu\nu} = \partial_\mu A_\nu - \partial_\nu A_\mu$ . Varying (3.81) with respect to the electromagnetic vector potential,

$$\partial_\nu [\sqrt{-g}(1 - \mathcal{G}\kappa_0\psi) F^{\mu\nu}] = 0, \quad (3.122)$$

where  $\mathcal{G} := 2\sqrt{d_1/[(D_0 - 2)(D - 2)]}$ . The second term in the round brackets  $\mathcal{G}\kappa_0\psi F^{\mu\nu}$  reflects the interaction between photons and the scalar field  $\psi$ , and as we show below, it is responsible for Lorentz invariance violation (LV). In particular, coupling between photons and the scalar field  $\psi$  makes the speed of photons different from the standard speed of light. Eq. (3.122) together with Bianchi identity,  $F_{(\mu\nu,\lambda)} = 0$ , (which is preserved in the considered model due to gauge-invariance of the tensor  $F_{\mu\nu}$  [387]) defines a complete set of the generalized Maxwell equations. As we noted, the electromagnetic part of action (3.81) is conformally invariant in the  $4D$  dimensional space-time. So, it is convenient to present the flat FRW metric  $\tilde{g}^0$  in the conformally flat form:  $\tilde{g}_{\mu\nu}^0 = a^2\eta_{\mu\nu}$ , where  $\eta_{\mu\nu}$  is the Minkowski metric.

Using the standard definition of the electromagnetic field tensor  $F_{\mu\nu}$ :

$$F_{\mu\nu} = \begin{pmatrix} 0 & -E_1 & -E_2 & -E_3 \\ E_1 & 0 & B_3 & -B_2 \\ E_2 & -B_3 & 0 & B_1 \\ E_3 & B_2 & -B_1 & 0 \end{pmatrix}, \quad F^{\mu\nu} = \begin{pmatrix} 0 & E_1 & E_2 & E_3 \\ -E_1 & 0 & B_3 & -B_2 \\ -E_2 & -B_3 & 0 & B_1 \\ -E_3 & B_2 & -B_1 & 0 \end{pmatrix}, \quad (3.123)$$

we obtain the complete set of the Maxwell equations in vacuum <sup>12</sup>,

$$\nabla \cdot \mathbf{B} = 0, \quad (3.124)$$

$$\nabla \cdot \mathbf{E} = \frac{\mathcal{G}\kappa_0}{1 - \mathcal{G}\kappa_0\psi} (\nabla\psi \cdot \mathbf{E}), \quad (3.125)$$

$$\nabla \times \mathbf{B} = \frac{\partial \mathbf{E}}{\partial \eta} - \frac{\mathcal{G}\kappa_0 \dot{\psi}}{1 - \mathcal{G}\kappa_0\psi} \mathbf{E} + \frac{\mathcal{G}\kappa_0}{1 - \mathcal{G}\kappa_0\psi} [\nabla\psi \times \mathbf{B}], \quad (3.126)$$

$$\nabla \times \mathbf{E} = -\frac{\partial \mathbf{B}}{\partial \eta}, \quad (3.127)$$

where all operations are performed in the Minkowski space-time,  $\eta$  denotes conformal time related to physical time  $t$  as  $dt = a(\eta)d\eta$ , and an overdot represents a derivative with respect to conformal time  $\eta$ .

Eqs. (3.124) and (3.127) correspond to Bianchi identity, and since it is preserved, Eqs. (3.124) and (3.127) keep their usual forms. Eqs. (3.125) and (3.126) are modified due to interactions between photons and gravexcitons ( $\propto \kappa_0\psi$ ). These modifications have simple physical meaning: the interaction between photons and the scalar field  $\psi$  acts in Eq. (3.125) as an effective electric charge  $e_{\text{eff}}$ . This effective charge is proportional to the scalar product of the  $\psi$  field gradient and the  $\mathbf{E}$  field, and it vanishes for an homogeneous  $\psi$  field. The modification of Eq. (3.126) corresponds to an effective current  $\mathbf{J}_{\text{eff}}$ , which depends on both electric and magnetic fields. This effective current is determined by variations of the  $\psi$  field over the time ( $\dot{\psi}$ ) and space ( $\nabla\psi$ ). For the case of a homogeneous  $\psi$  field the effective current is still present and LV takes place. The modified Maxwell equations are conformally invariant. To account for the expansion of the Universe we rescale the field components as  $\mathbf{B}, \mathbf{E} \rightarrow \mathbf{B}a^2, \mathbf{E}a^2$  [416]. Thus, the components of the physical electric and magnetic field are diluted as  $1/a^2$ .

To obtain a dispersion relation for photons, we use the Fourier transform between position and wave number spaces as,

$$\begin{aligned} \mathbf{F}(\mathbf{k}, \omega) &= \int \int d\eta d^3x e^{-i(\omega\eta - \mathbf{k}\cdot\mathbf{x})} \mathbf{F}(\mathbf{x}, \eta), \\ \mathbf{F}(\mathbf{x}, \eta) &= \frac{1}{(2\pi)^4} \int \int d\omega d^3k e^{i(\omega\eta - \mathbf{k}\cdot\mathbf{x})} \mathbf{F}(\mathbf{k}, \omega). \end{aligned} \quad (3.128)$$

Here,  $\mathbf{F}$  is a vector function describing either the electric or the magnetic field,  $\omega$  is the angular frequency of the electromagnetic wave measured today,

---

<sup>12</sup> The electric ( $\mathbf{E}$ ) and magnetic ( $\mathbf{B}$ ) fields are related to the vector potentials (scalar  $\phi$  and vector  $\mathbf{A}$ ) as

$$\mathbf{B} = \nabla \times \mathbf{A}, \quad \mathbf{E} = -\nabla\phi - \frac{\partial \mathbf{A}}{\partial \eta},$$

where the operator  $\nabla$  denotes the spatial derivatives in 3-dimensional flat space.

and  $\mathbf{k}$  is the wave vector. We assume that the field  $\psi$  is an oscillatory field with the frequency  $\omega_\psi$  and the momentum  $\mathbf{q}$ , so  $\psi(\mathbf{x}, \eta) = C \exp[i(\omega_\psi \eta - \mathbf{q} \cdot \mathbf{x})]$ ,  $C = \text{const.}$  Eq. (3.124) implies  $\mathbf{B} \perp \mathbf{k}$ . Without loosing of generality, and for simplicity of description we assume that the wave vector  $\mathbf{k}$  is oriented along the  $\mathbf{z}$  axis. Using Eq. (3.127) we get  $\mathbf{E} \perp \mathbf{B}$ . Therefore, Eqs. (3.125) and (3.127) in the component form read

$$(1 - \mathcal{G}\kappa_0\psi)kE_z = \mathcal{G}\kappa_0\psi(q_x E_x + q_y E_y + q_z E_z) \quad (3.129)$$

and

$$kE_y = \omega B_x, \quad (3.130)$$

$$kE_x = -\omega B_y. \quad (3.131)$$

Eq. (3.126) in components can be rewritten as

$$(1 - \mathcal{G}\kappa_0\psi)kB_y = -(1 - \mathcal{G}\kappa_0\psi)\omega E_x + \mathcal{G}\kappa_0\psi(\omega_\psi E_x + q_z B_y), \quad (3.132)$$

$$(1 - \mathcal{G}\kappa_0\psi)kB_x = (1 - \mathcal{G}\kappa_0\psi)\omega E_y - \mathcal{G}\kappa_0\psi(\omega_\psi E_y - q_z B_x), \quad (3.133)$$

$$0 = (1 - \mathcal{G}\kappa_0\psi)\omega E_z - \mathcal{G}\kappa_0\psi(\omega_\psi E_z + q_y B_x - q_x B_y). \quad (3.134)$$

A linearly polarized wave can be expressed as a superposition of left (L,  $-$ ) and right (R,  $+$ ) circularly polarized (LCP and RCP) waves. Using the polarization basis of Sec. 1.1.3 of Ref. [417], we derive  $E^\pm = (E_x \pm iE_y)/\sqrt{2}$ . From Eqs. (3.130)–(3.133), for LCP and RCP waves we get

$$(1 - n_+^2)E^+ = 0, \quad (1 - n_-^2)E^- = 0, \quad (3.135)$$

where  $n_+$  and  $n_-$  are refractive indices for RCP and LCP electromagnetic waves

$$n_+^2 = \frac{k^2 [1 - \mathcal{G}\kappa_0\psi(1 + q_z/k)]}{\omega^2 [1 - \mathcal{G}\kappa_0\psi(1 + \omega_\psi/\omega)]} = n_-^2. \quad (3.136)$$

In the case when Lorentz invariance is preserved, the electromagnetic waves propagating in vacuum have  $n_+ = n_- = n = k/\omega \equiv 1$ . For the electromagnetic waves propagating in the magnetized plasma,  $k/\omega \neq 1$ , and the difference between the LCP and RCP refractive indices describes the Faraday rotation effect,  $\alpha \propto \omega(n_+ - n_-)$  [418]. In the considered model, since  $n_+ = n_-$  the rotation effect is absent, but the speed of electromagnetic waves propagation in vacuum differs from the speed of light  $c$  (see also Ref. [419] for LV induced by electromagnetic field coupling to other generic field). This difference implies the propagation time delay effect

$$\Delta t = \Delta l \left( 1 - \frac{\partial k}{\partial \omega} \right), \quad (3.137)$$

where  $\Delta l$  is a propagation distance,  $\Delta t$  is the difference between the photon travel time and that for a “photon” which travels at the speed of light  $c$ . Here,  $t$  is physical synchronous time. This formula does not take into account the evolution of the Universe. However, it is easy to show that the effect of the Universe expansion is negligibly small. To get  $\partial k/\partial\omega$ , we should note that we have defined the system of 6 equations (3.129)–(3.134) with respect to 6 components of the vectors  $\mathbf{E}$  and  $\mathbf{B}$ . This system has non-trivial solutions only if its determinant is zero. From this condition we get the dispersion relation:

$$\omega^2 \left(1 - \mathcal{G}\kappa_0\psi \left(1 + \frac{\omega\psi}{\omega}\right)\right) = k^2 \left(1 - \mathcal{G}\kappa_0\psi \left(1 + \frac{q_z}{k}\right)\right). \quad (3.138)$$

Solving the dispersion relation as a square equation with respect to  $k$ , we can obtain

$$\frac{\partial k}{\partial\omega} \simeq \pm \left\{1 + \frac{1}{2} \left[\frac{\omega_\psi^2 - q_z^2}{4\omega^2}\right] (\mathcal{G}\kappa_0\psi)^2\right\}, \quad (3.139)$$

where  $\pm$  signs correspond to photons forward and backward directions respectively.

The modified inverse group velocity (3.138) shows that the LV effect can be measured if we know the gravexciton frequency  $\omega_\psi$ ,  $z$ -component of the momentum  $q_z$  and its amplitude  $\psi$ . For our estimates, we assume that  $\psi$  is the oscillatory field, satisfying (in local Lorentz frame) the dispersion relation,  $\omega_\psi^2 = m_\psi^2 + \mathbf{q}^2$ , where  $m_\psi$  is the mass of gravexcitons<sup>13</sup>. Unfortunately, we do not have any information concerning parameters of gravexcitons (some estimates are given in sections 3.4.2 and 3.4.3). Thus, we intend to use possible LV effects (supposing it is caused by interaction between photons and gravexcitons) to set limits on gravexciton parameters. For example, from Eqs. (3.137) and (3.139) we can easily get the following estimate for the upper limit of the amplitude of gravexciton oscillations:

$$|\psi| \approx \frac{1}{\sqrt{\pi\mathcal{G}}} \sqrt{\left|\frac{\Delta t}{\Delta l}\right|} \frac{\omega}{m_\psi} M_{\text{Pl}(4)}, \quad (3.140)$$

where for  $\omega$  and  $m_\psi$  we can use their physical values. In the case of gamma-ray burst (GRB) with  $\omega \sim 10^{21} \div 10^{22}$  Hz  $\sim 10^{-4} \div 10^{-3}$  GeV and  $\Delta l \sim 3 \div 5 \times 10^9$  y  $\sim 10^{17}$  sec, the typical upper limit for the time delay is  $\Delta t \sim \sim 10^{-4}$  sec [420].

For these values the upper limit on gravexciton amplitude of oscillations is

$$|\kappa_0\psi| \approx \frac{10^{-13} \text{ GeV}}{m_\psi}. \quad (3.141)$$

<sup>13</sup> To get physical values of the corresponding parameters we should rescale them by the scale factor  $a$ .



This estimate shows that our approximation  $\kappa_0\psi < 1$  works for gravexciton masses  $m_\psi > 10^{-13}$  GeV. Future measurements of the time-delay effect for GRBs at frequencies  $\omega \sim 1\text{--}10$  GeV would increase significantly the limit up to  $m_\psi > 10^{-9}$  GeV. On the other hand, as we wrote in section 3.4.2, the Cavendish-type experiments exclude fifth force particles with masses  $m_\psi \lesssim \lesssim 1/(10^{-2} \text{ cm}) \sim 10^{-12}$  GeV, which is rather close to our lower bound for  $\psi$  field masses. Respectively, we slightly shift the considered mass lower limit to be  $m_\psi \geq 10^{-12}$  GeV. These masses are considerably higher than the mass corresponding to the equality between the energy densities of the matter and radiation (matter/radiation equality),  $m_{eq} \sim H_{eq} \sim 10^{-37}$  GeV, where  $H_{eq}$  is the Hubble “constant” at matter/radiation equality. It means that such  $\psi$ -particles start to oscillate during the radiation dominated epoch (see section 3.4.2). Another bound on the  $\psi$ -particles masses comes from the condition of their stability. With respect to decay  $\psi \rightarrow \gamma\gamma$  the life-time of  $\psi$ -particles is  $\tau \sim (M_{\text{Pl}(4)}/m_\psi)^3 t_{\text{Pl}}$  (see Eq. (3.83)), and the stability conditions requires that the decay time should be greater than the age of the Universe. According to this we consider light gravexcitons with masses  $m_\psi \leq 10^{-21} M_{\text{Pl}(4)} \sim 10^{-2}$  GeV  $\sim \sim 20m_e$  (where  $m_e$  is the electron mass).

An additional restriction arises from the condition that such cosmological gravexcitons should not overclose the observable Universe. This results in conditions (3.100) and (3.101) for  $m_\psi$  and  $\psi_{in}$ , respectively. Thus, for the range of masses<sup>14</sup>  $10^{-12}$  GeV  $\leq m_\psi \leq 10^{-2}$  GeV, we obtain respectively  $\psi_{in} \lesssim \lesssim 10^{-6} M_{\text{Pl}(4)}$  and  $\psi_{in} \lesssim 10^{-9} M_{\text{Pl}(4)}$ . Now, we want to estimate the amplitude of oscillations of the considered gravexciton at the present time. To perform it, we should mention that prefactors  $C_r$  and  $B(t)$  in Eq. (3.88) are given by (Eqs. 3.90) and (3.89), respectively. We are interested in the gravexciton oscillations at the present time  $t = t_{univ}$ . In this case  $s = 2/3$  and for  $B(t_{univ})$  we obtain:  $B(t_{univ}) \sim t_{univ}^{-1} \approx 10^{-61} M_{\text{Pl}(4)}$ , where we took into account that for considered masses  $\Gamma t_{univ} \lesssim 1$ . Thus, the amplitude of the light gravexciton oscillations at the present time reads:

$$|\kappa_0\psi| \sim 10^{-60} \frac{\psi_{in}}{M_{\text{Pl}(4)}} \left( \frac{M_{\text{Pl}(4)}}{m_\psi} \right)^{3/4}. \quad (3.142)$$

Together with the nonovercloseness condition, we obtain from this expression that  $|\kappa_0\psi| \sim 10^{-43}$  for  $m_\psi \sim 10^{-12}$  GeV and  $\psi_{in} \sim 10^{-6} M_{\text{Pl}(4)}$  and  $|\kappa_0\psi| \sim \sim 10^{-53}$  for  $m_\psi \sim 10^{-2}$  GeV and  $\psi_{in} \sim 10^{-9} M_{\text{Pl}(4)}$ . Obviously, it is much less than the upper limit (3.141). Note, as we mentioned above, gravexcitons with masses  $m_\psi \gtrsim 10^{-2}$  GeV can start to decay at the present epoch. However, taking into account the estimate  $|\kappa_0\psi| \sim 10^{-53}$ , we can easily get that their energy density  $\rho_\psi \sim (|\kappa_0\psi|^2/8\pi) M_{\text{Pl}(4)}^2 m_\psi^2 \sim 10^{-55}$  g/cm<sup>3</sup> is much less than

<sup>14</sup> Gravexcitons with such masses are either warm or cold **dark matter** (see footnote 8).

the present energy density of the radiation  $\rho_\gamma \sim 10^{-34} \text{ g/cm}^3$ . Thus,  $\rho_\psi$  contributes negligibly in  $\rho_\gamma$ . Otherwise, the gravexcitons with masses  $m_\psi \gtrsim 10^{-2} \text{ GeV}$  should be observed at the present time, which, obviously, is not the case.

Additionally, it follows from section 3.4.4 that to avoid the problem of the fine structure constant variation, the amplitude of the initial oscillations should satisfy the condition:  $\psi_{in} \lesssim 10^{-5} M_{\text{Pl}(4)}$  which, obviously, completely agrees with our upper bound  $\psi_{in} \lesssim 10^{-6} \text{ GeV}$ .

In summary, we shown that LV effects can give additional restrictions on parameters of gravexcitons. First, gravexcitons should not be lighter than  $10^{-13} \text{ GeV}$ . It is very close to the limit following from the fifth-force experiment. Moreover, experiments for GRB at frequencies  $\omega > 1 \text{ GeV}$  can result in significant shift of this lower limit making it much stronger than the fifth-force estimates. Together with the nonovercloseness condition, this estimate leads to the upper limit on the amplitude of the gravexciton initial oscillations. It should not exceed  $\psi_{in} \lesssim 10^{-6} \text{ GeV}$ . Thus, the bound on the initial amplitude obtained from the fine structure constant variation is one magnitude weaker than the bound found from LV even for the limiting case of the gravexciton masses. This limit becomes stronger for heavier gravexcitons. Our estimates for the present-day amplitude of the gravexciton oscillations, following from the above obtained limitations, show that we cannot use the LV effect for the direct detections of the gravexcitons. Nevertheless, the obtained bounds can be useful for astrophysical and cosmological applications. For example, let us suppose that gravexcitons with masses  $m_\psi > 10^{-2} \text{ GeV}$  are produced during late stages of the Universe expansion in some regions and GRB photons travel to us through these regions. Then, Eq. (3.142) is not valid for such gravexcitons having astrophysical origin and the only upper limit on the amplitude of their oscillations (in these regions) follows from Eq. (3.141). In the case of TeV masses we get  $|\kappa_0 \psi| \sim 10^{-16}$ . If GRB photons have frequencies up to 1 TeV,  $\omega \sim 1 \text{ TeV}$ , then this estimate is increased by six orders of magnitude.

### 3.5. Dark energy in curvature-non-linear $f(R)$ multidimensional cosmological models

Starting from the pioneering paper [397], the non-linear (with respect to the scalar curvature  $R$ ) theories of gravity  $f(R)$  have attracted the great deal of interest because these models can provide a natural mechanism of the early inflation. Non-linear models may arise either due to quantum fluctuations of matter fields including gravity [421], or as a result of compactification of extra spatial dimensions [422]. Compared, e.g., to others higher-order gravity theories,  $f(R)$  theories are free of ghosts and of Ostrogradski instabilities [423]. Recently, it was realized that these models can also explain the late-time acceleration of the Universe. This fact resulted in a new wave of papers devoted to this topic (see e.g., recent reviews [424, 425]).

The most simple, and, consequently, the most studied models are polynomials of  $R$ :  $f(R) = \sum_{n=0}^k C_n R^n$  ( $k > 1$ ), e.g., quadratic  $R + R^2$  and quartic  $R + R^4$  ones. Active investigation of these models, which started in 80-th years of the last century [426, 427], continues up to now. Obviously, the correction terms (to the action of Hilbert–Einstein type) with  $n > 1$  give the main contribution in the case of large  $R$ , e.g., in the early stages of the Universe’s evolution. As it was shown first in [397] for the quadratic model, such modification of gravity results in early inflation. On the other hand, function  $f(R)$  may also contain negative degrees of  $R$ . For example, the simplest model is  $R + R^{-n}$ ,  $n \geq 1$ . In this case the correction term plays the main role for small  $R$ , e.g., at the late stage of the Universe’s evolution (see, e.g., numerous references in [428, 429]). Such modification of gravity may result in the late-time acceleration of our Universe [430]. Non-linear models with polynomial as well as  $R^{-n}$ -type correction terms have also been generalized to the multidimensional case (see, e.g., [377, 378, 428, 429, 431–435]). Special emphasis was laid on finding parameter regions (regions in moduli space) which ensure the existence of at least one minimum of the effective potential for the volume moduli of the internal spaces and which in this way allow for their stabilization. Additionally, positive minimum of the effective potential plays the role of the positive cosmological constant which gives the possibility to resolve the dark energy problem. It is well known that non-linear models are equivalent to linear-curvature models with additional minimal scalar field  $\phi$  (dubbed scalaron in [397]). This scalar field corresponds to additional degree of freedom of non-linear models. This equivalence is very useful tool for the investigation of the problems of the internal space stabilization and the external space acceleration. Let us show it in more detail.

### 3.5.1. Internal space stabilization for pure geometrical $f(R)$ models

We consider a  $D = (4 + D')$  – dimensional non-linear pure gravitational theory with action

$$S = \frac{1}{2\kappa_D^2} \int_M d^D x \sqrt{|\bar{g}|} f(\bar{R}), \quad (3.143)$$

where  $f(\bar{R})$  is an arbitrary smooth function with mass dimension  $\mathcal{O}(m^2)$  ( $m$  has the unit of mass) of a scalar curvature  $\bar{R} = R[\bar{g}]$  constructed from the  $D$ -dimensional metric  $\bar{g}_{ab}$  ( $a, b = 1, \dots, D$ ).

The equation of motion for this theory reads

$$f' \bar{R}_{ab} - \frac{1}{2} f \bar{g}_{ab} - \bar{\nabla}_a \bar{\nabla}_b f' + \bar{g}_{ab} \bar{\square} f' = 0, \quad (3.144)$$

where  $f' = df/d\bar{R}$ ,  $\bar{R}_{ab} = R_{ab}[\bar{g}]$ .  $\bar{\nabla}_a$  is the covariant derivative with respect to the metric  $\bar{g}_{ab}$ ; and the corresponding Laplacian is denoted by

$$\bar{\square} = \square[\bar{g}] = \bar{g}^{ab}\bar{\nabla}_a\bar{\nabla}_b = \frac{1}{\sqrt{|\bar{g}|}}\partial_a\left(\sqrt{|\bar{g}|}\bar{g}^{ab}\partial_b\right). \quad (3.145)$$

Eq. (3.144) can be rewritten in the form

$$f'\bar{G}_{ab} + \frac{1}{2}\bar{g}_{ab}(\bar{R}f' - f) - \bar{\nabla}_a\bar{\nabla}_bf' + \bar{g}_{ab}\bar{\square}f' = 0, \quad (3.146)$$

where  $\bar{G}_{ab} = \bar{R}_{ab} - \frac{1}{2}\bar{R}\bar{g}_{ab}$ . The trace of Eq. (3.144) is

$$(D-1)\bar{\square}f' = \frac{D}{2}f - f'\bar{R} \quad (3.147)$$

and can be considered as a connection between  $\bar{R}$  and  $f$ .

It is well known, that for<sup>15</sup>  $f'(\bar{R}) > 0$  the conformal transformation

$$g_{ab} = \Omega^2\bar{g}_{ab}, \quad (3.148)$$

with

$$\Omega = [f'(\bar{R})]^{1/(D-2)}, \quad (3.149)$$

reduces the non-linear theory (3.143) to a linear one with an additional scalar field. The equivalence of the theories can be easily proven with the help of the following auxiliary formulas:

$$\square = \Omega^{-2}\left[\bar{\square} + (D-2)\bar{g}^{ab}\Omega^{-1}\Omega_{,a}\partial_b\right] \iff \bar{\square} = \Omega^2\square - (D-2)g^{ab}\Omega\Omega_{,a}\partial_b, \quad (3.150)$$

$$R_{ab} = \bar{R}_{ab} + \frac{D-1}{D-2}(f')^{-2}\bar{\nabla}_af'\bar{\nabla}_bf' - (f')^{-1}\bar{\nabla}_a\bar{\nabla}_bf' - \frac{1}{D-2}\bar{g}_{ab}(f')^{-1}\bar{\square}f' \quad (3.151)$$

and

$$R = (f')^{2/(2-D)}\left\{\bar{R} + \frac{D-1}{D-2}(f')^{-2}\bar{g}^{ab}\partial_af'\partial_bf' - 2\frac{D-1}{D-2}(f')^{-1}\bar{\square}f'\right\}. \quad (3.152)$$

Thus, Eqs. (3.146) and (3.147) can be rewritten as

$$G_{ab} = \phi_{,a}\phi_{,b} - \frac{1}{2}g_{ab}g^{mn}\phi_{,m}\phi_{,n} - \frac{1}{2}g_{ab}e^{\frac{-D}{\sqrt{(D-2)(D-1)}}\phi}(\bar{R}f' - f) \quad (3.153)$$

<sup>15</sup> We consider the positive branch  $f'(\bar{R}) > 0$ . Although the negative  $f' < 0$  branch can be considered as well (see e.g. Refs. [378, 427, 428]). However, negative values of  $f'(\bar{R})$  result in negative effective gravitational “constant”  $G_{\text{eff}} = \kappa_D^2/f'$ . Thus  $f'$  should be positive for the graviton to carry positive kinetic energy (see, e.g., [425]).

and

$$\square\phi = \frac{1}{\sqrt{(D-2)(D-1)}} e^{\frac{-D}{\sqrt{(D-2)(D-1)}}\phi} \left( \frac{D}{2}f - f'\bar{R} \right), \quad (3.154)$$

where

$$f' = \frac{df}{d\bar{R}} := e^{A\phi} > 0, \quad A := \sqrt{\frac{D-2}{D-1}}. \quad (3.155)$$

Eq. (3.155) can be used to express  $\bar{R}$  as a function of the dimensionless field (scalon)  $\phi$ :  $\bar{R} = \bar{R}(\phi)$ .

It is easily seen that Eqs. (3.153) and (3.154) are the equations of motion for the action

$$S = \frac{1}{2\kappa_D^2} \int_M d^D x \sqrt{|g|} \left( R[g] - g^{ab} \phi_{,a} \phi_{,b} - 2U(\phi) \right), \quad (3.156)$$

where

$$U(\phi) = \frac{1}{2} e^{-B\phi} \left[ \bar{R}(\phi) e^{A\phi} - f(\bar{R}(\phi)) \right], \quad B := \frac{D}{\sqrt{(D-2)(D-1)}} \quad (3.157)$$

and they can be written as follows:

$$G_{ab} = T_{ab}[\phi, g], \quad (3.158)$$

$$\square\phi = \frac{\partial U(\phi)}{\partial \phi}. \quad (3.159)$$

Here,  $T_{ab}[\phi, g]$  is the standard expression of the energy–momentum tensor for the minimally coupled scalar field with potential (3.157). Eq. (3.159) can be considered as a constraint equation following from the reduction of the non-linear theory (3.143) to the linear one (3.156).

Let us consider what will happen if, in some way, the scalar field  $\phi$  tends asymptotically to a constant:  $\phi \rightarrow \phi_0$ . From Eq. (3.155) we see that in this limit the non-linearity disappears and (3.143) becomes a linear theory  $f(\bar{R}) \sim c_1 \bar{R} + c_2$  with  $c_1 = f' = \exp(A\phi_0)$  and a cosmological constant  $-c_2/(2c_1)$ . In the case of homogeneous and isotropic space-time manifolds, linear purely geometrical theories with constant  $\Lambda$ -term necessarily imply an (A)dS geometry. Thus, in the limit  $\phi \rightarrow \phi_0$  the D-dimensional theory (3.143) can asymptotically lead to an (A)dS with scalar curvature:

$$\bar{R} \rightarrow -\frac{D}{D-2} \frac{c_2}{c_1}. \quad (3.160)$$

Clearly, the linear theory (3.156) would reproduce this asymptotic (A)dS-limit for  $\phi \rightarrow \phi_0$ :

$$R \rightarrow 2 \frac{D}{D-2} U(\phi_0) = -\frac{D}{D-2} c_2 c_1^{-\frac{D}{D-2}}. \quad (3.161)$$

Hence, in this limit  $\bar{R}/R \rightarrow c_1^{\frac{D}{D-2}}$  in accordance with Eq. (3.152) and  $f' = c_1$ .

Next, we assume that the  $D$ -dimensional bulk space-time  $M$  undergoes a spontaneous compactification to a warped product manifold

$$M = M_0 \times M_1 \times \dots \times M_n \quad (3.162)$$

with metric

$$\bar{g} = \bar{g}_{ab}(X)dX^a \otimes dX^b = \bar{g}^{(0)} + \sum_{i=1}^n e^{2\bar{\beta}^i(x)} g^{(i)}. \quad (3.163)$$

The coordinates on the  $(D_0 = d_0 + 1)$ -dimensional manifold  $M_0$  (usually interpreted as our observable  $(D_0 = 4)$ -dimensional Universe) are denoted by  $x$  and the corresponding metric by

$$\bar{g}^{(0)} = \bar{g}_{\mu\nu}^{(0)}(x) dx^\mu \otimes dx^\nu. \quad (3.164)$$

The internal factor manifolds  $M_i$  are taken in the form of  $d_i$ -dimensional Einstein spaces (3.4) and (3.5). The specific metric ansatz (3.163) leads to a scalar curvature  $\bar{R}$  which depends only on the coordinates  $x$  of the external space:  $\bar{R}[\bar{g}] = \bar{R}(x)$ . Correspondingly, also the non-linearity field  $\phi$  depends on  $x$  only:  $\phi = \phi(x)$ .

Passing from the  $\bar{R}$ -non-linear theory (3.143) to the equivalent  $R$ -linear theory (3.156) the metric (3.163) undergoes the conformal transformation  $\bar{g} \mapsto g$  [see relation (3.148)]

$$g = \Omega^2 \bar{g} = \left( e^{A\phi} \right)^{2/(D-2)} \bar{g} := g^{(0)} + \sum_{i=1}^n e^{2\beta^i(x)} g^{(i)} \quad (3.165)$$

with

$$g_{\mu\nu}^{(0)} := \left( e^{A\phi} \right)^{2/(D-2)} \bar{g}_{\mu\nu}^{(0)}, \quad \beta^i := \bar{\beta}^i + \frac{A}{D-2} \phi. \quad (3.166)$$

Therefore, the problem of the internal spaces stabilization can be solved in full analogy with sections 3.2.1 and 3.2.2 where in formulas of the latter section we should put  $\Lambda = 0$  (for simplicity of notations, in the present section 3.5 we use  $\phi$  instead of  $\Phi$  of section 3.2.2.). In section 3.2.2, we have shown that in the case  $\Lambda = 0$ , the stabilization<sup>16</sup> of the extra dimensions automatically results in

<sup>16</sup> It is worth noting that despite the existence of a negative minimum of the effective potential, the internal spaces are not fully stabilized in the case of flat external space. This follows easily from the equations of Appendix A. Indeed, for the Hubble parameter  $H > 0$  (expanding external space), the friction term in (A.9) results in decrease of the amplitude of  $\varphi^i$  and its velocity  $\dot{\varphi}^i$  with time (see also section 3.4.1). This decrease continues until  $H$  in (A.4) becomes equal to 0. Then, the scale factor of the Universe reaches its maximum and  $H$  changes the sign (respectively, the friction term in (A.9) changes its sign). After that, scalar fields  $\varphi^i$  start to oscillate around the minimum position with increasing amplitude. Therefore, at the present stage of expanding Universe, the internal spaces are not fully stabilized at the minimum position but oscillate with decreasing amplitude. The frequency of oscillations is equal to the gravexciton masses (see Eq. (3.88)) and the period of oscillations  $T_{osc}$  is quite short for sufficiently large masses. For example,  $T_{osc} \sim 10^{-12}$  sec for  $m_\psi \sim 10^{-2}$  GeV. Obviously, for time intervals  $t \gg T_{osc}$ , with a high degree of accuracy, the internal space scale factors are equal to their values at the equilibrium positions.

condition  $\phi \rightarrow \phi_0$  with  $U(\phi_0) < 0$ . Thus, the D-dimensional space-time (bulk) becomes asymptotically AdS<sub>D</sub> (see Eq. (3.161)) and there is no dark energy in these pure geometrical theories. The main difference from section 3.2.2 is that in non-linear  $f(R)$  models the potential of the scalar field is not arbitrary, but completely determined by the form of the scalar curvature non-linearity. Let us consider a few examples.

*i.  $1/R$  non-linearity:*

$$f(\bar{R}) = \bar{R} - \mu/\bar{R}, \quad \mu > 0. \quad (3.167)$$

In front of the  $\bar{R}^{-1}$ -term, the minus sign is chosen, because otherwise the potential  $U(\phi)$  will have no extremum. With the help of definition (3.155), we express the scalar curvature  $\bar{R}$  in terms of scalaron  $\phi$  and obtain two real-valued solution branches

$$\bar{R}_{\pm} = \pm\sqrt{\mu} \left( e^{A\phi} - 1 \right)^{-1/2} \implies \phi > 0 \quad (3.168)$$

of the quadratic equation  $f'(\bar{R}) = e^{A\phi}$ .

The corresponding potentials (3.157)

$$U_{\pm}(\phi) = \pm\sqrt{\mu} e^{-B\phi} \sqrt{e^{A\phi} - 1} \quad (3.169)$$

have extrema for curvatures

$$\bar{R}_{0,\pm} = \pm\sqrt{\mu} \sqrt{\frac{D+2}{D-2}} \implies e^{A\phi_0} = \frac{2B}{2B-A} = \frac{2D}{D+2} > 1 \text{ for } D \geq 3 \quad (3.170)$$

and take for these curvatures the values

$$U_{\pm}(\phi_0) = \pm\sqrt{\mu} \sqrt{\frac{D-2}{D+2}} e^{-B\phi_0} = \pm\sqrt{\mu} \sqrt{\frac{D-2}{D+2}} \left( \frac{2D}{D+2} \right)^{-D/(D-2)}. \quad (3.171)$$

The stability defining second derivatives at the extrema (3.170),

$$\begin{aligned} \partial_{\phi}^2 U_{\pm} \Big|_{\phi_0} &= \mp\sqrt{\mu} \frac{D}{D-1} \sqrt{\frac{D+2}{D-2}} e^{B\phi_0} = \\ &= \mp\sqrt{\mu} \frac{D}{D-1} \sqrt{\frac{D+2}{D-2}} \left( \frac{2D}{D+2} \right)^{-D/(D-2)}, \end{aligned} \quad (3.172)$$

shows that only the negative curvature branch  $\bar{R}_-$  yields a minimum with stable internal space components. The positive branch has a maximum with  $U_+(\phi_0) > 0$ . According to (3.25) (where  $\Lambda = 0$ ) it can provide an effective **dark energy** contribution with  $\Lambda_{\text{eff}} > 0$ , but due to its tachyonic behavior with  $\partial_{\phi}^2 U(\phi_0) < 0$  it cannot give stably frozen internal dimensions [428].

*ii. curvature-squared non-linearity:*

$$f(\bar{R}) = \bar{R} + \alpha \bar{R}^2 - 2\Lambda_D, \quad (3.173)$$

For this theory we obtain

$$1 + 2\alpha \bar{R} = e^{A\phi} \iff \bar{R} = \frac{1}{2\alpha} (e^{A\phi} - 1), \quad -\infty < \phi < \infty, \quad (3.174)$$

and

$$U(\phi) = \frac{1}{2} e^{-B\phi} \left[ \frac{1}{4\alpha} (e^{A\phi} - 1)^2 + 2\Lambda_D \right]. \quad (3.175)$$

The parameter region which ensures the stabilization of the internal space is described in [377]. In this region, the effective potential has a negative global minimum. Thus, the D-dimensional space-time becomes asymptotically AdS.

*iii. curvature-quartic non-linearity:*

$$f(\bar{R}) = \bar{R} + \gamma \bar{R}^4 - 2\Lambda_D. \quad (3.176)$$

For this model,  $\bar{R}$  and scalaron  $\phi$  are related as

$$\bar{R} = (4\gamma)^{-1/3} (e^{A\phi} - 1)^{1/3}, \quad -\infty < \phi < \infty, \quad (3.177)$$

and potential  $U(\phi)$  reads

$$U(\phi) = \frac{1}{2} e^{-B\phi} \left[ \frac{3}{4} (4\gamma)^{-1/3} (e^{A\phi} - 1)^{4/3} + 2\Lambda_D \right]. \quad (3.178)$$

The internal space stability region in parameter space is described in [428]. It is shown that this stability region depends on the total dimension  $D = \dim(M)$  of the higher dimensional space-time  $M$ . For  $D > 8$  the stability region consists of a single (absolutely stable) sector which is shielded from a conformal singularity (and an antigravity sector beyond it) by a potential barrier of infinite height and width. This sector is smoothly connected with the stability region of a curvature-linear model. For  $D < 8$  an additional (meta-stable) sector exists which is separated from the conformal singularity by a potential barrier of finite height and width so that systems in this sector are prone to collapse into the conformal singularity. This second sector is not smoothly connected with the first (absolutely stable) one. As we mentioned above, the external space-time in this model is necessary AdS and the corresponding negative effective cosmological constant,  $\Lambda_{\text{eff}} < 0$ , forbids a late-time acceleration.

*iv. curvature-squared and curvature-quartic non-linearities:*

$$f(\bar{R}) = \bar{R} + \alpha \bar{R}^2 + \gamma \bar{R}^4 - 2\Lambda_D. \quad (3.179)$$



The relation between the scalar curvature  $\bar{R}$  and the scalaron field  $\phi$  is

$$f' = e^{A\phi} = 1 + 2\alpha\bar{R} + 4\gamma\bar{R}^3. \quad (3.180)$$

This equation has three solutions  $\bar{R}_{1,2,3}(\phi)$ , where one or three of them are real-valued. Therefore, in general, the potential

$$U(\phi) = (1/2)e^{-B\phi} (\alpha\bar{R}^2 + 3\gamma\bar{R}^4 + 2\Lambda_D) \quad (3.181)$$

is multivalued and consists of a number of branches. The case of one real-valued solution for ( $D = 8$ )-dimensional space-time was investigated in [432] where the parameter region for the freezing stabilization of the internal spaces was described. The external space-time is asymptotically AdS.

Very interesting case of multivalued solutions for ( $D = 4$ )-dimensional space-time was considered in [435]. Here, the branches of the potential  $U(\phi)$  are fitted with each other in the branching and monotonic points. It was shown that the monotonic points are penetrable for the scalaron, while in the vicinity of the branching points, the scalaron has the bouncing behavior and cannot cross these points. Moreover, there are branching points where the scalaron bounces an infinite number of times with decreasing amplitude, and the Universe asymptotically approaches the de Sitter stage. Such accelerating behavior was called bouncing inflation. For this accelerating expansion, there is no need for original potential  $U(\phi)$  to have a minimum or to check the slow-roll conditions. A necessary condition for such inflation is the existence of the branching points. This is a new type of inflation. Such bouncing inflation takes place both in the Einstein and Brans–Dicke frames. This type of inflation was found for the model with the curvature-squared and curvature-quartic correction terms which play an important role during the early stages of the Universe evolution. However, the branching points take also place in models with  $\bar{R}^{-1}$ -type correction terms [436]. These terms play an important role at late times of the evolution of the Universe. Therefore, bouncing inflation may be responsible for the late-time accelerating expansion of the Universe (**dark energy**).

### 3.5.2. Dark energy in $f(R)$ models with form fields

As we saw above, in the pure geometrical non-linear models, the internal space freezing stabilization is achieved due to negative minimum of the effective potential. Thus, these models are asymptotically AdS without accelerating behavior of our Universe (see, however, comments with respect to the bouncing inflation). However, the inclusion of matter can uplift potential to the positive values. In this section, we shall demonstrate such uplifting for non-linear models with form fields.

To start with, let us present general theory of such models [378]. We consider a  $D = (4 + D')$ -dimensional non-linear gravitational theory with action

$$S = \frac{1}{2\kappa_D^2} \int_M d^D x \sqrt{|\bar{g}|} f(\bar{R}) - \frac{1}{2} \int_M d^D x \sqrt{|\bar{g}|} \sum_{i=1}^n \frac{1}{d_i!} \left(F^{(i)}\right)^2, \quad (3.182)$$

where  $f(\bar{R})$  is an arbitrary smooth function with mass dimension  $\mathcal{O}(m^2)$  ( $m$  has the unit of mass) of the scalar curvature  $\bar{R} = R[\bar{g}]$  constructed from the  $D$ -dimensional metric  $\bar{g}_{ab}$  ( $a, b = 1, \dots, D$ ). In action (3.182),  $F^{(i)} = F_{m_i n_i \dots q_i}^{(i)}$ ,  $i = 1, \dots, n$  is an antisymmetric tensor field of rank  $d_i$  (a  $d_i$ -form field strength) with indices from an index set  $s_{(i)} = \{m_i : \max(m_i) - \min(m_i) = d_i\}$ , where  $m_i, n_i, \dots, q_i \in s_{(i)}$ . For simplicity, we suppose that the index sets  $s_{(i)}$ ,  $s_{(j)}$  of tensors  $F^{(i)}$ ,  $F^{(j)}$  with  $i \neq j$  contain no common elements as well as no indices corresponding to the coordinates of the  $D_0$ -dimensional external space-time (usually  $D_0 = 4$ ). Additionally, we assume that for the sum of the ranks holds  $\sum_{i=1}^n d_i = D - D_0 := D'$ . Obviously, this model can be generalized to tensor configurations  $F^{(i)}$ ,  $F^{(j)}$  with intersecting (overlapping) index sets. In this case explicit field configuration can be obtained, e.g., when the indices satisfy special overlapping rules [364]. Such a generalization is beyond the scope of our consideration. Furthermore, we assume in our subsequent considerations that the index sets  $m_i, n_i, \dots, q_i \neq 0$  do not contain the coordinates of the external space-time  $M_0$  and, hence, the field strengths  $F^{(i)}$  can be associated with a magnetic (solitonic)  $p$ -brane system located in the extra dimensions as discussed, e.g., in Refs. [364, 437, 438].

The equation of motion for the gravitational sector of (3.182) reads

$$f' \bar{R}_{ab} - \frac{1}{2} f \bar{g}_{ab} - \bar{\nabla}_a \bar{\nabla}_b f' + \bar{g}_{ab} \bar{\square} f' = \kappa_D^2 T_{ab}[F, \bar{g}], \quad (3.183)$$

where  $a, b = 1, \dots, D$ ,  $f' = df/d\bar{R}$ ,  $\bar{R}_{ab} = R_{ab}[\bar{g}]$ ,  $\bar{R} = R[\bar{g}]$ .  $\bar{\nabla}_a$  and  $\bar{\square}$  denote the covariant derivative and the Laplacian with respect to the metric  $\bar{g}_{ab}$  (see equation (3.145)). Eq. (3.183) can be rewritten in the form

$$f' \bar{G}_{ab} + \frac{1}{2} \bar{g}_{ab} (\bar{R} f' - f) - \bar{\nabla}_a \bar{\nabla}_b f' + \bar{g}_{ab} \bar{\square} f' = \kappa_D^2 T_{ab}[F, \bar{g}], \quad (3.184)$$

where  $\bar{G}_{ab} = \bar{R}_{ab} - \frac{1}{2} \bar{R} \bar{g}_{ab}$ , with its trace

$$(D-1) \bar{\square} f' = \frac{D}{2} f - f' \bar{R} + \kappa_D^2 T[F, \bar{g}]. \quad (3.185)$$

The energy momentum tensor (EMT)  $T_{ab}[F, \bar{g}]$  is defined in the standard way as

$$T_{ab}[F, \bar{g}] \equiv \frac{1}{\sqrt{|\bar{g}|}} \frac{\delta \left( \sqrt{|\bar{g}|} \sum_{i=1}^n \frac{1}{d_i!} (F^{(i)})^2 \right)}{\delta \bar{g}^{ab}} = \sum_{i=1}^n T_{ab}[F^{(i)}, \bar{g}], \quad (3.186)$$

where

$$T_{ab} [F^{(i)}, \bar{g}] = \frac{1}{d_i!} \left( -\frac{1}{2} \bar{g}_{ab} F_{m_i n_i \dots q_i}^{(i)} F^{(i) m_i n_i \dots q_i} + d_i F_{a n_i \dots q_i}^{(i)} F_b^{(i) n_i \dots q_i} \right). \quad (3.187)$$

For the trace of this tensor we obtain

$$T [F, \bar{g}] = \sum_{i=1}^n T [F^{(i)}, \bar{g}] \quad (3.188)$$

with

$$T [F^{(i)}, \bar{g}] = \frac{2d_i - D}{2(d_i!)} F_{m_i n_i \dots q_i}^{(i)} F^{(i) m_i n_i \dots q_i}. \quad (3.189)$$

The field strengths  $F^{(i)}$  satisfy the equations of motion

$$F^{(i) m_i n_i \dots q_i}{}_{; q_i} = 0 \iff \frac{1}{\sqrt{|\bar{g}|}} \left( \sqrt{|\bar{g}|} F^{(i) m_i n_i \dots q_i} \right)_{; q_i} = 0, \quad i = 1, \dots, n. \quad (3.190)$$

and the Bianchi identities

$$F_{[m_i n_i \dots q_i, a]}^{(i)} = 0, \quad i = 1, \dots, n. \quad (3.191)$$

Similar to the previous section, we perform the conformal transformation (3.148) and reduce the non-linear gravitational theory to a linear one with additional scalar field  $\phi$  (scalon). This transformation is well defined for  $f'(\bar{R}) > 0$  (see footnote 15). The equivalence of the theories can be easily proven with the help of the auxiliary formulas (3.150)–(3.152).

Defining the scalar  $\phi$  by the relation (3.155), and making use of (3.150)–(3.152), equations (3.184) and (3.185) can be rewritten as

$$G_{ab} = \kappa_D^2 T_{ab} [F, \phi, g] + T_{ab} [\phi, g] \quad (3.192)$$

and

$$\begin{aligned} \square \phi &= \frac{1}{\sqrt{(D-1)(D-2)}} e^{\frac{-D}{\sqrt{(D-1)(D-2)}} \phi} \left( \frac{D}{2} f - f' \bar{R} \right) + \\ &+ \frac{1}{\sqrt{(D-1)(D-2)}} \kappa_D^2 T [F, \phi, g]. \end{aligned} \quad (3.193)$$

The EMTs read

$$T_{ab} [\phi, g] = \phi_{,a} \phi_{,b} - \frac{1}{2} g_{ab} g^{mn} \phi_{,m} \phi_{,n} - \frac{1}{2} g_{ab} e^{\frac{-D}{\sqrt{(D-1)(D-2)}} \phi} (\bar{R} f' - f), \quad (3.194)$$

$$T_{ab} [F, \phi, g] = \sum_{i=1}^n e^{\frac{2d_i - D}{\sqrt{(D-1)(D-2)}} \phi} T_{ab} [F^{(i)}, g] \quad (3.195)$$

and

$$T[F, \phi, g] = \sum_{i=1}^n e^{\frac{2d_i-D}{\sqrt{(D-1)(D-2)}}\phi} T[F^{(i)}, g], \quad (3.196)$$

where  $T_{ab}[F^{(i)}, g]$ ,  $T[F^{(i)}, g]$  are given by replacing  $\bar{g} \rightarrow g$  in equations (3.187), (3.189). The indices of the field strengths  $F^{(i)}$  are now raised and lowered with the metric  $g$ .

The equations of motion (3.190) for  $F^{(i)}$  transform to

$$\frac{1}{\sqrt{|g|}} \left( \sqrt{|g|} e^{\frac{2d_i-D}{\sqrt{(D-1)(D-2)}}\phi} F^{(i) m_i n_i \dots q_i} \right)_{, q_i} = 0, \quad i = 1, \dots, s, n, \quad (3.197)$$

whereas the Bianchi identities (3.191) do not change.

It can be easily checked that Eqs. (3.192), (3.193) and (3.197) are the equations of motion for the action

$$S = \frac{1}{2\kappa_D^2} \int_M d^D x \sqrt{|g|} \left\{ R[g] - g^{ab} \phi_{,a} \phi_{,b} - 2U(\phi) - \kappa_D^2 \sum_{i=1}^n \frac{1}{d_i!} e^{\frac{2d_i-D}{\sqrt{(D-1)(D-2)}}\phi} F_{m_i n_i \dots q_i}^{(i)} F^{(i) m_i n_i \dots q_i} \right\}, \quad (3.198)$$

where potential  $U(\phi)$  is defined by formula (3.157). The scalaron  $\phi$  is the result and the carrier of the curvature non-linearity of the original theory (3.182). Correspondingly, Eq. (3.193) has a two-fold interpretation. It is the equation of motion for the field  $\phi$  and at the same time it can be considered as constraint equation following from the reduction of the non-linear theory (3.182) to the linear one (3.198). Furthermore, we note that in the linear theory (3.198) the form fields are non-minimally coupled with the scalaron  $\phi$ . (A minimal coupling occurs only for a model with  $n = 1$ ,  $d_1 = D_0$ , where according to (3.189) the trace of the form field EMT vanishes.) A comparison of the action functional with (3.195) shows that the last term in (3.198) coincides with the expression for the energy density  $-T_0^0[F, \phi, g]$  of the solitonic form field (due to  $F_{0n_i \dot{q}_i}^{(i)} \equiv 0$  by the definition of  $F^{(i)}$ ).

Now, we assume that the multidimensional space-time manifold undergoes a spontaneous compactification (3.162) in accordance with the block-orthogonal structure of the field strength  $F$ , and that the form fields  $F^{(i)}$ , each nested in its own  $d_i$ -dimensional factor space  $M_i$ , respect a generalized Freund–Rubin ansatz [439] (see also [364, 438, 440, 441]). The factor spaces  $M_i$  are then Einstein spaces with metrics  $\hat{g}^{(i)} \equiv e^{2\beta^i(x)} g^{(i)}$  which depend only through the warp factors  $a_i(x) := e^{2\beta^i(x)}$  on the coordinates  $x$  of the external space-time  $M_0$  (see Eqs. (3.163)–(3.166)). This allows us to perform a dimensional reduction

of our model and the internal space stabilization along the lines of section 3.2. Additionally, it is not difficult to show that in the case of the freezing stabilization<sup>17</sup> ( $\beta^i = 0, \phi = \phi_0$ ), the asymptotic multidimensional space-time is built up from Einstein-space blocks, but is itself a non-Einsteinian space due to an additional terms which depend on form fields [378].

Similar to the previous section, it can be easily seen that for considered product manifold ansatz, the scalar curvature  $\bar{R}$  depends only on the coordinate  $x$  of the  $D_0$ -dimensional external space-time  $M_0$ :  $\bar{R}[\bar{g}] = \bar{R}(x)$ . This implies that the scalaron field  $\phi$  is also a function only of  $x$ :  $\phi = \phi(x)$ .

We choose the form-field components in the generalized Freund–Rubin ansatz as

$$\begin{aligned} F_{m_i n_i \dots q_i}^{(i)} &= \sqrt{2} \sqrt{|\hat{g}^{(i)}|} \varepsilon_{m_i n_i \dots q_i} f^{(i)}(x), \\ F^{(i) m_i n_i \dots q_i} &= \left( \sqrt{2} / \sqrt{|\hat{g}^{(i)}|} \right) \varepsilon^{m_i n_i \dots q_i} f^{(i)}(x). \end{aligned} \quad (3.199)$$

For the Levi–Civita symbol  $\varepsilon_{m_i n_i \dots q_i}$  we use conventions where for Riemann spaces holds  $\varepsilon_{m_i n_i \dots q_i} = \varepsilon^{m_i n_i \dots q_i}$  and  $\varepsilon_{m_i n_i \dots q_i} \varepsilon^{m_i n_i \dots q_i} = d_i!$ . It can be easily seen that the ansatz (3.199) satisfies Eq. (3.197) (because  $\phi$  and  $f$  depend only on  $x$  and the  $\sqrt{|g^{(i)}|}$  factors cancel). The Bianchi identities (3.191) reduce to the equations

$$\frac{\partial \left( a_i^{d_i}(x) f^{(i)}(x) \right)}{\partial x^\mu} = 0 \quad (3.200)$$

with solutions

$$f^{(i)}(x) = \frac{f_i}{a_i^{d_i}} \quad (3.201)$$

and  $f_i \equiv \text{const}$ . With (3.201) the energy density of the solitonic form field, and correspondingly the last term in action (3.198), reads

$$\begin{aligned} -T_0^0[F, \phi, g] &= \frac{1}{2} \sum_{i=1}^n \frac{1}{d_i!} e^{\frac{2d_i - D}{\sqrt{(D-1)(D-2)}} \phi} F_{m_i n_i \dots q_i}^{(i)} F^{(i) m_i n_i \dots q_i} = \\ &= \sum_{i=1}^n e^{\frac{2d_i - D}{\sqrt{(D-1)(D-2)}} \phi} \frac{f_i^2}{2d_i a_i^{2d_i}} := \rho(\beta, \phi), \end{aligned} \quad (3.202)$$

where for real form fields  $f_i^2 \geq 0$ . Again we see that for models with  $n = 1$  and  $d_1 = D_0$  this energy density decouples from the scalaron field  $\phi$ :  $\rho(\beta^1, \phi) \rightarrow \rho(\beta^1)$ .

<sup>17</sup> Without loss of generality, we can choose the stability position  $\beta_0^i = 0$ . Then, the internal space fluctuations  $\tilde{\beta}^i$  in section 3.2 coincide with  $\beta^i$ .

Let us consider now a model with only one  $d_1$ -dimensional internal space. After dimensional reduction and subsequent conformal transformation to the Einstein frame (along the lines of section 3.2), the action functional (3.198) reads

$$\begin{aligned}
 S = \frac{1}{2\kappa_0^2} \int_{M_0} d^{D_0}x \sqrt{|\tilde{g}^{(0)}|} & \left\{ R[\tilde{g}^{(0)}] - \tilde{g}^{(0)\mu\nu} \partial_\mu \varphi \partial_\nu \varphi - \right. \\
 & \left. - \tilde{g}^{(0)\mu\nu} \partial_\mu \phi \partial_\nu \phi - 2U_{\text{eff}}(\varphi, \phi) \right\}, \tag{3.203}
 \end{aligned}$$

where field  $\varphi$  is defined by equation (3.18):

$$\varphi = -\sqrt{\frac{d_1(D-2)}{D_0-2}} \beta^1. \tag{3.204}$$

A stable compactification of the internal space  $M_1$  is ensured when its scale factor  $\varphi$  is frozen at one of the minima of the effective potential

$$\begin{aligned}
 U_{\text{eff}}(\varphi, \phi) = e^{2\varphi \sqrt{\frac{d_1}{(D-2)(D_0-2)}}} & \times \\
 \times \left[ -\frac{1}{2} R_1 e^{2\varphi \sqrt{\frac{D_0-2}{d_1(D-2)}}} + U(\phi) + \kappa_D^2 \rho(\varphi, \phi) \right], \tag{3.205}
 \end{aligned}$$

where  $R[g^{(1)}] \equiv R_1$  is the scalar curvature of the factor-space  $M_1$  (see Eq. (3.5)) and the energy density (3.202) of the solitonic form field reads

$$\kappa_D^2 \rho(\varphi, \phi) = \kappa_D^2 f_1^2 e^{\frac{2d_1-D}{\sqrt{(D-1)(D-2)}} \phi} e^{2\varphi \sqrt{\frac{d_1(D_0-2)}{D-2}}}. \tag{3.206}$$

The value of the effective potential at the minimum plays the role of the effective  $D_0$ -dimensional cosmological constant:  $U_{\text{eff}}|_{\text{min}} \equiv \Lambda_{\text{eff}}$ . It can be **dark energy** in the case of positive  $\Lambda_{\text{eff}} > 0$ .

The potential  $U(\phi)$  of the scalaron field is given by Eq. (3.157) and its exact expression depends on the form of non-linearity  $f(R)$ . The  $1/R$  and  $R^2$  non-linearities were considered in detail in papers [378] and [429]. It was shown that for all these models, there exist parameter configurations that can provide positive values of the effective four-dimensional cosmological constant. Thus, an accelerated expansion of the Universe (dark energy) is possible in accordance with observational data. However, the observational value of dark energy is achieved with the help of fine tuning of parameters, similar to how it happens for the linear model in section 3.2.4.

To conclude this section, we would like to note that there is also a possibility to consider non-linear models with form fields where the action functional reads [434]:

$$S = \frac{1}{2\kappa_D^2} \int_M d^D x \sqrt{|\bar{g}|} f(\bar{R}) - \frac{1}{2} \int d^D x \sqrt{|g|} \frac{1}{d_1!} \left(F^{(1)}\right)^2 - \sum_{k=1}^m \int_{M_0} d^4 x \sqrt{|g^{(0)}(x)|} \tau_{(k)}. \quad (3.207)$$

The main difference between this expression and the action functional (3.182) is that the form field  $F^{(1)}$  is originally coupled with metric  $g$  but not with  $\bar{g}$ . Additionally, we suppose that the internal space  $M_1$  is a flat orbifold with  $m$  branes in fixed points and branes are uniquely characterized by their tensions  $\tau_k$  (see section 3.2.4). Then, the effective potential for this model reads

$$U_{\text{eff}}(\varphi, \phi) e^{2\varphi \sqrt{\frac{d_1}{(D-2)(D_0-2)}}} \times \left[ U(\phi) + \kappa_D^2 f_1^2 e^{2\varphi \sqrt{\frac{d_1(D_0-2)}{D-2}}} - \lambda e^{\varphi \sqrt{\frac{d_1(D_0-2)}{D-2}}} \right], \quad (3.208)$$

Therefore, in this approach the energy density of the solitonic form field decouples from the scalaron field  $\phi$  for any number of dimensions  $d_1$ :  $\rho(\varphi, \phi) \rightarrow \rho(\varphi)$ , and this greatly simplifies the calculations. This model was investigated in [434] for  $R^2$  and  $R^4$  non-linearities. To avoid the fine-tuning problem, the main attention was paid to the case of zero effective cosmological constant  $\Lambda_{\text{eff}} = 0$ . Conditions, that ensure stable compactification of the internal space in zero minimum of the effective potentials, were defined. Such effective potentials have interesting and rather complicated form with a number of local minima, maxima and saddle points. It was shown (with the help of numerical calculation of equations in Appendix A) that the  $R^2$ - and  $R^4$  models can produce up to 10 and 22 e-foldings, respectively. These values are not sufficient to solve the homogeneity and isotropy problem but big enough to explain the recent CMB data. Additionally, the  $R^4$  model, with saddle points of the effective potential, can provide conditions for eternal topological inflation. The main drawback of the obtained inflationary models consists in a spectral index  $n_s$  that is less than the presently observed  $n_s \approx 1$ . For the  $R^4$  model, e.g.,  $n_s \approx 0.61$ .

### 3.6. *Sp*-branes. Dynamical dark energy from extra dimensions

As we have repeatedly noted above, recent astronomical observations abundantly evidence that our Universe underwent stages of accelerating expansion during its evolution. There are at least two of such stages: early inflation and late-time acceleration. The latter began approximately at the redshift  $z \sim 0.35$  (see, e.g., [442]) and continues until now. Thus, the

construction and investigation of models with stages of acceleration is one of the main challenge of the modern cosmology. In previous sections (3.2)–(3.5), we demonstrated theories where dark energy appears in multidimensional models due to minima of the effective potentials. Such dark energy is time independent. There are also models with dynamical dark energy. Among such models, the models originating from fundamental theories (e.g. string/M-theory) are of the most of interest. For example, it was shown that some of space-like brane (S-brane) solutions have a stage of the accelerating expansion. In  $D$ -dimensional manifold,  $Sp$ -branes are time dependent solutions with  $(p + 1)$ -dimensional Euclidean world volume and, apart from time, they have  $(D - p - 2)$ -dimensional hyperbolic, flat or spherical spaces as transverse/additional dimensions [443]:

$$ds_D^2 = -e^{2\gamma(\tau)} d\tau^2 + a_0^2(\tau) (dx_1^2 + \dots + dx_{p+1}^2) + a_1^2(\tau) d\Sigma_{(D-p-2),\sigma}^2, \quad (3.209)$$

where  $\gamma(\tau)$  fixes the gauge of time,  $a_0(\tau)$  and  $a_1(\tau)$  are time dependent scale factors, and  $\sigma = -1, 0, +1$  for hyperbolic, flat or spherical spaces respectively. Obviously,  $p = 2$  if brane describes our 3-dimensional space. These branes are known as SM2-branes if original theory is 11-dimensional M-theory and SD2-branes in the case of 10-dimensional Dirichlet strings. For this choice of  $p$ , the evolution of our Universe is described by the scale factor  $a_0$ . In general, the scale factor  $a_1$  can also determine the behavior of our 3-dimensional Universe. Hence,  $D - p - 2 = 3$  and we arrive to SM6-brane in the case of the M-theory and SD5-brane for the Dirichlet string. Usually,  $Sp$ -brane models include form fields (fluxes) and massless scalar fields (dilaton) as a matter sources. If SD $p$ -branes are obtained by dimensional reduction of 11-dimensional M-theory, then the dilaton is associated with the scale factor of a compactified 11-th dimension.

Starting from [443], the S-brane solutions were also found, e.g., in Refs. [444–447]. It was quite natural to test these models for the accelerating expansion of our Universe. Really, it was shown in [448] that the SM2-brane as well as the SD2-brane have stages of the accelerating behavior. This result generalizes conclusions of [449] for models with hyperbolic compact internal spaces. Here, the cosmic acceleration (in Einstein frame) is possible due to a negative curvature of the internal space that gives a positive contribution to an effective potential. This acceleration is not eternal but has a short period and the mechanism of such short acceleration was explained in [450]. It was indicated in [448] that the solution of [449] is the vacuum case (the zero flux limit) of the S-branes. It was natural to suppose that if the acceleration takes place in the vacuum case, it may also happen in the presence of fluxes. Indeed, it was confirmed for the case of the compact hyperbolic internal space. Even more, it was found that periods of the acceleration occur in the cases of flat and spherical internal spaces due to the positive contributions of fluxes into the effective potential. Similar effect of uplifting of the effective potential due to the form field was already considered in section 3.5.2 for non-linear models.



Along with Ref. [448] mentioned above, the accelerating S-brane cosmologies (in the Einstein frame) were obtained and investigated, e.g., in Refs. [451–455]. Accelerating solutions closely related to them were also found in Refs. [456, 457]. It should be noted that some of these solutions are not new ones but either rediscovered or written in different parametrization (see corresponding comments in Refs. [445, 457]). For example, the first vacuum solution for a product manifold (consisting of  $(n - 1)$  Ricci-flat spaces and one Einstein space with non-zero constant curvature) was found in [359]. This solution was generalized to the case of a massless scalar field in Refs. [353, 354]. Obviously, solutions in Refs. [353, 354, 359] are the zero flux limit of the *Sp*-branes and the result of [449] is a particular case of [354]. Some of solutions in [454, 456] coincides with corresponding solutions in Refs. [353, 354, 359, 458]. An elegant minisuperspace approach for the investigation of the product space manifolds consisting of Einstein spaces was proposed in [368]. Here, it was shown that the equations of motion have the most simple form in a harmonic time gauge<sup>18</sup> because the minisuperspace metric is flat in this gauge. Even if the authors of the above-mentioned papers were not aware of it, they intuitively used this gauge to get exact solutions. New solutions also can be generated (from the known solutions) with the help of a topological splitting when the Einstein space with non-zero curvature is split into a number of Einstein spaces of the same sign of the curvature (see Refs. [459, 460]). This kind of solutions was found, e.g., in Refs. [454, 456].

Now, to show the main characteristic properties of *Sp*-brane solutions, we consider some particular solutions from [353] and [354]. To start with, we derive the connection between different quantities in the Einstein and Brans–Dicke frames. The dimensionally reduced actions in these frames have, e.g., forms of equations (3.12) and (3.15). The conformal transformation between the external space-time metrics in the Einstein and Brans–Dicke frames is given by Eq. (3.14). For simplicity, we consider the case of one internal space, i.e.  $n = 1$  in (3.14). Additionally, for the model with dynamical internal spaces, there is no sense to split the internal space scale factors into background and fluctuations. Therefore,  $\tilde{\beta}^i \equiv \beta^i$  in (3.14) and  $\Omega^2 = \left(e^{d_1\beta^1}\right)^{-2/(d_0-1)} = \left(a_1^{d_1}\right)^{-2/(d_0-1)}$ . Thus, the metric (3.209) in different gauges reads (see also Eqs. (3.36) and (3.37))

$$\begin{aligned} g &= -e^{2\gamma_0} d\tau \otimes d\tau + a_0^2 q^{(0)} + a_1^2 g^{(1)} = -dt \otimes dt + a_0^2 q^{(0)} + a_1^2 g^{(1)} = \\ &= \Omega^2 \left(-d\tilde{t} \otimes d\tilde{t} + \tilde{a}_0^2 q^{(0)}\right) + a_1^2 g^{(1)}, \end{aligned} \quad (3.210)$$

where the first equality is the metric in the harmonic time gauge ( $\gamma = \gamma_0 = d_0\beta^0 + d_1\beta^1$ ) in the Brans–Dicke frame, the second equality is the metric in

<sup>18</sup> For Eq. (3.209), it reads  $\gamma = (p + 1) \ln a_0 + (D - p - 2) \ln a_1$ . In the harmonic time gauge, time satisfies equation  $\Delta[g]\tau = 0$  [368].

the synchronous time gauge in the Brans–Dicke frame, and the third equality is the metric in the synchronous time gauge in the Einstein frame. Equations (3.210) show that the external scale factors in the Einstein and Brans–Dicke frames are related as in Eq. (3.37):

$$\tilde{a}_0 = \Omega^{-1} a_0 \quad (3.211)$$

and there exists the following correspondence between different times<sup>19</sup>:

$$dt = e^{\gamma_0(\tau)} d\tau \implies t = \int e^{\gamma_0(\tau)} d\tau + \text{const}, \quad (3.212)$$

$$d\tilde{t} = \Omega^{-1} e^{\gamma_0(\tau)} d\tau \implies \tilde{t} = \int \Omega^{-1} e^{\gamma_0(\tau)} d\tau + \text{const}. \quad (3.213)$$

For two component cosmological model with  $R[q^{(0)}] = 0$ ,  $R[g^{(1)}] \equiv R_1 \neq 0$  and minimally coupled free scalar field, the explicit expressions for the scale factors (in the Brans–Dicke frame) and scalar field as functions of harmonic time read [353, 354]:

$$a_0(\tau) = \exp(\beta^0(\tau)) = A_0 \exp\left(\frac{\xi_1}{d_0} \tau\right), \quad (3.214)$$

$$a_1(\tau) = \exp(\beta^1(\tau)) = a_{(c)1} \exp\left(-\frac{\xi_1}{d_1 - 1} \tau\right) \times \frac{1}{g_{\pm}(\tau)}, \quad (3.215)$$

$$\varphi(\tau) = p^2 \tau + q, \quad (3.216)$$

where

$$g_+ = \cosh^{1/(d_1-1)}(\xi_2 \tau), \quad (-\infty < \tau < +\infty), \quad (3.217)$$

for  $R_1 > 0$  and

$$g_- = \sinh^{1/(d_1-1)}(\xi_2 |\tau|), \quad (|\tau| > 0), \quad (3.218)$$

for  $R_1 < 0$ . Here,  $a_{(c)1} = A_1 (2\varepsilon/|R_1|)^{1/2(d_1-1)}$ ,  $\xi_1 = [d_0(d_1 - 1)/(D - 2)]^{1/2} p^1$ ,  $\xi_2 = [(d_1 - 1)/d_1]^{1/2} (2\varepsilon)^{1/2}$  and  $2\varepsilon = (p^1)^2 + (p^2)^2$ . Parameters  $A_0, A_1, p^1, p^2$  and  $q$  are the constants of integration and  $A_0, A_1$  satisfy the following constraint:  $A_0^{d_0} A_1^{d_1} = A_0$ . It was shown in [461] that  $p^1$  and  $p^2$  are the momenta in the minisuperspace ( $p^1$  is related to the momenta of the scale factors and  $p^2$  is responsible for the momentum of the scalar field) and  $\varepsilon$  plays the role of energy. Obviously, these solutions are the zero flux limit of the  $S_p$ -branes.

This model was investigated in detail in [462]. Here, both the Ricci-flat space and non-zero curvature space may play the role of our Universe (with corresponding changes in Eqs. (3.210)–(3.213)). The analysis was performed in the Brans–Dicke and Einstein frames. It was shown that in the context of the considered models, the Brans–Dicke gravity provides more possibilities for accelerating cosmologies than the Einsteinian one. Such different behavior

<sup>19</sup>To have the same directions of the arrows of time, we choose the plus sign for the square root.

of the external space scale factors in both of these frames is not surprising because these scale factors are described by different variables connected with each other via the conformal transformation in Eqs. (3.210)–(3.213). Moreover, the synchronous times in both of these frames are also different. As a consequence of these discrepancies, the scale factors of the external space in both frames behave differently. In the Brans–Dicke frame, stages of the accelerating expansion exist for all types of the external space (flat, spherical and hyperbolic). However, in the Einstein frame, the model with flat external space and hyperbolic compactification of the internal space is the only one with the stage of the accelerating expansion. The presence of a minimally coupled free scalar field does not help the acceleration because this field does not contribute to the potential. Nevertheless, it make sense to include such field in the model because it results in more reach and interesting dynamical behavior. For example, it was shown that scalar field can prevent the acceleration in the Einstein frame.

As it was shown in section 3.4.4, the dynamical behavior of the internal spaces results in the variation of the fine-structure constant (see Eq. (3.119)). Thus, any multidimensional cosmological models with time dependent internal spaces should be tested from this point of view. It was demonstrated that the examined model runs into significant problems related to the too large variations of the fine-structure constant. The case of the hyperbolic external space in the Brans–Dicke frame is the only possibility to avoid this problem.

### 3.6.1. Dark energy in pure geometrical *Sp*-brane model with hyperbolic internal space

The considered above *Sp*-brane model was carefully investigated in [462] for an arbitrary range of parameters. Is it possible to fix these parameters with the help of the modern observational data? This interesting problem was investigated in paper [463] where the metric (3.210) is defined on the manifold with product topology

$$M = \mathbb{R} \times \mathbb{R}^{d_0} \times \mathbb{H}^{d_1}/\Gamma, \quad (3.219)$$

where  $\mathbb{R}^{d_0}$  is  $d_0$ -dimensional Ricci-flat external (our) space with metric  $q^{(0)}$ :  $R[q^{(0)}] = 0$  and scale factor  $a_0$ , and  $\mathbb{H}^{d_1}/\Gamma$  is  $d_1$ -dimensional hyperbolic (compact) internal space with metric  $g^{(1)}$ :  $R[g^{(1)}] = -d_1(d_1 - 1)$  and scale factor  $a_1$ . Both  $a_0$  and  $a_1$  depend only on time. As we already mentioned, the first equality in (3.210) is the metric in the Brans–Dicke frame in the harmonic time gauge where  $e^{\gamma_0} = a_0^{d_0} a_1^{d_1}$ . The third equality in (3.210) is the metric in the Einstein frame in the synchronous time gauge. According to formulas (3.37) and (3.211), the scale factors  $a_0$  of the external space in the Brans–Dicke frame is connected with the scale factor  $\tilde{a}_0$  in the Einstein frame as follows:  $\tilde{a}_0 = \Omega^{-1} a_0$ , where

conformal factor  $\Omega = a_1^{-d_1/(d_0-1)}$ . Harmonic time  $\tau$  is related to synchronous time  $\tilde{t}$  as  $d\tilde{t} = f(\tau)d\tau$ , where  $f(\tau) = \Omega^{-1}a_0^{d_0}a_1^{d_1} = \tilde{a}_0^{d_0}$ . Hereafter we consider 3-dimensional external space:  $d_0 = 3$ . Taking into account these relations, the solutions (3.214) and (3.215) (in the case of the absence of scalar field:  $p^2 \equiv 0$ ) in the Einstein frame can be rewritten as follows:

$$\tilde{a}_0(\tau) = A_1^{\frac{d_1+2}{6}} \left( \sqrt{\frac{2\varepsilon}{|R_1|}} \right)^{\frac{d_1}{2(d_1-1)}} \frac{\exp\left(-\sqrt{\frac{d_1+2}{12(d_1-1)}} 2\varepsilon \tau\right)}{\sinh^{d_1/[2(d_1-1)]}\left(-\sqrt{\frac{d_1-1}{d_1}} 2\varepsilon \tau\right)}, \quad (3.220)$$

and

$$a_1(\tau) = A_1 \left( \sqrt{\frac{2\varepsilon}{|R_1|}} \right)^{\frac{1}{d_1-1}} \frac{\exp\left(-\sqrt{\frac{3}{(d_1-1)(d_1+2)}} 2\varepsilon \tau\right)}{\sinh^{1/(d_1-1)}\left(-\sqrt{\frac{d_1-1}{d_1}} 2\varepsilon \tau\right)}, \quad (3.221)$$

where  $A_1$  and  $\varepsilon$  are the constants of integration. The function  $f(\tau)$  can be easily obtained from Eq. (3.220) via expression  $f(\tau) = \tilde{a}_0^3(\tau)$ .

Solutions (3.220) and (3.221) for the metric (3.210) is a particular case of the  $Sp$ -branes with  $(p+1 = d_0)$ -dimensional Ricci-flat external space. In the case  $d_0 = 3$  we obtain  $p = 2$ . Therefore, if underlying model is  $(D = 11)$ -dimensional M-theory, we arrive at M2-branes where the number of internal dimensions is equal to 7. As we already mentioned above, such models with hyperbolic internal space undergo the stage of accelerating expansions [462]. However, the parameters of the model in (3.220) and (3.221) are still not connected with observational data. So, now we want to use the modern cosmological data (the present day value for the Hubble parameter and the redshift when our external space transits from deceleration to acceleration) to fix all arbitrary parameters of the considered model and obtain corresponding dynamical behavior for the scale factors, the Hubble parameter, the deceleration parameter and the fine-structure ‘‘constant’’.

Besides the external  $\tilde{a}_0$  and internal  $a_1$  scale factors described by Eqs. (3.220) and (3.221), we also consider the Hubble parameter for each of the factor spaces

$$\begin{aligned} H_0 &= \frac{1}{\tilde{a}_0} \frac{d\tilde{a}_0}{d\tilde{t}} = \frac{1}{\tilde{a}_0 f(\tau)} \frac{d\tilde{a}_0}{d\tau} = \\ &= -\frac{\sqrt{2\varepsilon}}{f(\tau)} \left( \sqrt{\frac{d_1+2}{12(d_1-1)}} + \sqrt{\frac{d_1}{4(d_1-1)}} \coth\left(\sqrt{\frac{d_1-1}{d_1}} 2\varepsilon \tau\right) \right), \end{aligned} \quad (3.222)$$

$$\begin{aligned}
 H_1 &= \frac{1}{a_1} \frac{da_1}{d\tilde{t}} = \frac{1}{a_1 f(\tau)} \frac{da_1}{d\tau} = \\
 &= -\frac{\sqrt{2\varepsilon}}{f(\tau)} \sqrt{\frac{3}{(d_1-1)(d_1+2)}} \left( 1 + \sqrt{\frac{d_1+2}{3d_1}} \coth \left( \sqrt{\frac{d_1-1}{d_1}} 2\varepsilon \tau \right) \right), \quad (3.223)
 \end{aligned}$$

the external space deceleration parameter<sup>20</sup>

$$\begin{aligned}
 q_0 &= -\frac{d^2 \tilde{a}_0}{d\tilde{t}^2} \frac{1}{H_0^2 \tilde{a}_0} = -\frac{1}{f(\tau)} \frac{d}{d\tau} \left( \frac{1}{f(\tau)} \frac{d\tilde{a}_0}{d\tau} \right) \frac{1}{H_0^2 \tilde{a}_0} = \\
 &= -2 \sinh^{-2} \left( \sqrt{\frac{d_1-1}{d_1}} 2\varepsilon \tau \right) \times \\
 &\times \left[ \sqrt{\frac{d_1+2}{3(d_1-1)}} + \sqrt{\frac{d_1}{d_1-1}} \coth \left( \sqrt{\frac{d_1-1}{d_1}} 2\varepsilon \tau \right) \right]^{-2} + 2 \quad (3.224)
 \end{aligned}$$

and the variation of the fine-structure constant (as a function of redshift  $z$ )

$$\Delta\alpha = \frac{\alpha(z) - \alpha(0)}{\alpha(0)} = \frac{a_1^{d_1}(0)}{a_1^{d_1}(z)} - 1, \quad (3.225)$$

where we took into account that for  $d_0 = 3$  the fine-structure constant  $\alpha \sim a_1^{-d_1}$  (see section 3.4.4). We also assume that the solution (3.220), (3.221) describes the M2-brane, that is  $d_1 = 7$ .

According to the recent observational data (see, e.g., [442, 464]), the present acceleration stage began at redshift  $z \approx 0.35$  and the Hubble parameter now is  $H_0(\tilde{t}_p) \equiv H_p \approx 72 \text{ km/sec/Mpc} = 2.33 \times 10^{-18} \text{ sec}^{-1}$ . Hereafter, the letter  $p$  denotes the present day values. Additionally, at the present time the value of the external space scale factor can be estimated as  $\tilde{a}_0(\tilde{t}_p) \approx cH_p^{-1} \approx 1.29 \times 10^{28} \text{ cm}$ . We shall use these observational conditions to fix the free parameters of the model  $A_1$  and  $\varepsilon$  (the constants of integration) and to define the present time<sup>21</sup>  $\tilde{t}_p$ . Observational data also show that for different redshifts the fine structure constant variation does not exceed  $10^{-5}$ :  $|\Delta\alpha| < 10^{-5}$  [411].

Below, all quantities are measured in the Hubble units. For example, the scale factors are measured in  $cH_p^{-1}$  and synchronous time  $t$  is measured in  $H_p^{-1}$ . Therefore,  $\tilde{a}_0(\tilde{t}_p) = 1$  and  $H_p = 1$ .

<sup>20</sup> Note that overdots in definition of Hubble and deceleration parameters after Eqs. (1.15) and (1.16) denote the derivatives with respect to the conformal time  $\eta$ .

<sup>21</sup> It is obvious that our model cannot pretend to describe the full history of the Universe. We try to apply this model to explain the late time acceleration of the Universe which starts at the redshift  $z \approx 0.35$ . Before this time, the Universe evolution is described by the standard Big Bang cosmology. Therefore, in our model  $\tilde{t} = 0$  corresponds to  $z = 0.35$  (i.e.  $q_0(z = 0.35) = 0$ ) and  $\tilde{t}_p$  is the time from this moment to the present day.

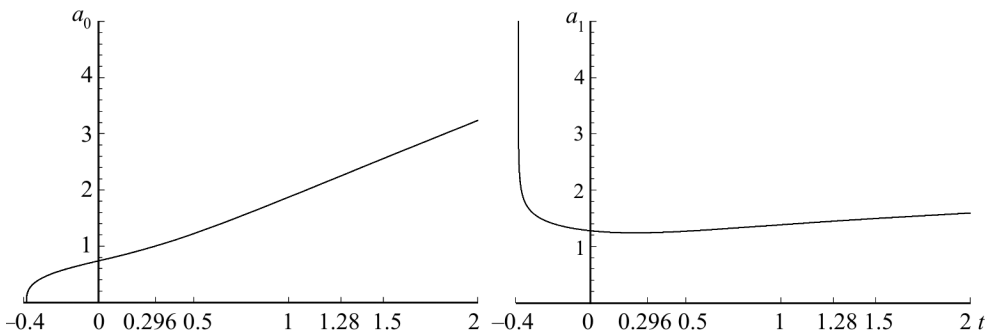


**Fig. 3.2.** The scale factors (in the Einstein frame) of the external space (left panel) and internal space (right panel) versus synchronous time  $\tilde{t}$

To fix all free parameters of the model, we use the following logic chain. First, from the equation  $q_0(\tau) = 0$  we obtain the harmonic time  $\tau_{in}$  of the beginning of the stage of acceleration. We find that this equation has two roots which describe the beginning and end of the acceleration. Second, we define the constant of integration  $A_1$  from the equation  $z = 0.35 = 1/\tilde{a}_0(\tau_{in}) - 1$  where we use the condition that acceleration starts at  $z = 0.35$  and that  $\tilde{a}_0(\tau_p) = 1$ . Third, we find the present harmonic time  $\tau_p$  from the condition  $\tilde{a}_0(\tau_p) = 1$ . It is worth noting that  $\tau_{in}, \tau_p$  and  $A_1$  are the functions of  $\varepsilon$ . To fix this parameter, we can use the condition  $H_0(\tau_p) = 1$ . Finally, to find the value of the present synchronous time, we use the equation  $\tilde{t}_p = \int_{\tau_{in}}^{\tau_p} f(\tau) d\tau$  where  $f(\tau) = \tilde{a}_0^3(\tau)$ . In the case  $d_1 = 7$ , direct calculations give for the constants of integration  $A_1 = 1.23468$  and  $\varepsilon = 1.53097$ . It results in  $\tilde{t}_p = 0.296 \sim 4\text{Gyr}$ ,  $q_0(\tilde{t}_p) = -0.960572$  and for the internal space  $a_1(\tilde{t}_p) = 1.24319$ ,  $H_1(t_p) = 0.0500333$ .

Dynamical behavior of the considered model is depicted in Figs. 3.2–3.4 [463]. Fig. 3.2 shows the dynamics of the external space scale factor  $\tilde{a}_0(\tilde{t})$  (left panel) and the internal space scale factor  $a_1(\tilde{t})$  (right panel). Here,  $\tilde{t} = 0.296$  is the present time, and  $\tilde{t} = 0$  and  $\tilde{t} = 1.28$  correspond to the beginning and the end of the stage of acceleration, respectively. It follows that the internal space is the same order of magnitude as the external one at the present time. However, for the standard Kaluza–Klein models there is the experimental restriction on sizes of the extra dimensions:  $l_{extra} \leq 10^{-17}\text{ cm}$ . That is  $\tilde{a}_0/a_1 \geq 10^{45}$ . Obviously, our model does not satisfy this condition. One of the possible way to avoid this problem consists in proposal that the Standard Model matter is localized on a brane. In this case the extra dimensions can be much bigger than  $10^{-17}\text{ cm}$  (even an infinite). However, such model requires the generalization of our metric (3.210) to the non-factorisable case and this investigation is out of the scope of this section.

We plot in Fig. 3.3 the evolution of the Hubble parameters  $H_0(\tilde{t})$  (left panel) and  $H_1(\tilde{t})$  (right panel). We can see that their values are comparable

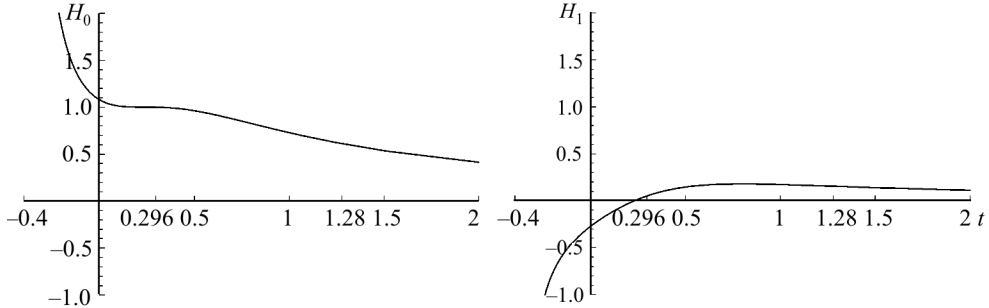


**Fig. 3.3.** The Hubble parameters of the external space (left panel) and internal space (right panel) versus synchronous time  $\tilde{t}$

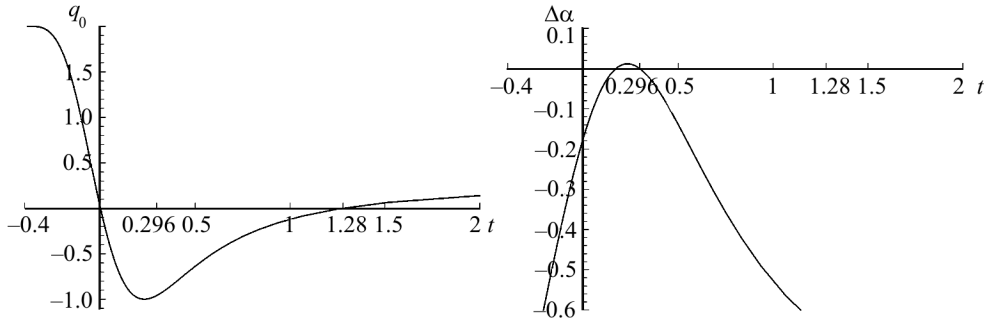


**Fig. 3.4.** The deceleration parameter of the external space (left panel) and variation of the fine structure constant (right panel) versus synchronous time  $\tilde{t}$

with each other. Thus, the internal space is rather dynamical and this fact is the main reason of too large variations of the fine structure constant (see Fig. 3.4).

We present in Fig. 3.4 the evolution of the deceleration parameter  $q_0(\tilde{t})$  (left panel) and the variation of the fine structure constant  $\Delta\alpha(\tilde{t})$  (right panel). Left picture clearly shows that the acceleration stage has the final period for the considered model. It starts at  $\tilde{t} = 0$  and finishes at  $\tilde{t} = 1.28$ . The right picture demonstrates that  $\Delta\alpha$  does not satisfy the observable restrictions  $|\Delta\alpha| < 10^{-5}$ . There is the only very narrow region in the vicinity of  $z = 0.13$  (or equivalently  $\tilde{t} = 0.17$  in synchronous time) where  $\Delta\alpha$  changes its sign. However, it is the exceptional region but restriction  $|\Delta\alpha| < 10^{-5}$  works for very large diapason of redshifts  $z$  [411].

Therefore, despite the satisfactory description of the accelerated expansion of our Universe at the late stages of its evolution, this model has two significant drawbacks. On the one hand, the internal space is too big with respect to the standard Kaluza–Klein restrictions  $a_{\text{internal}} \leq 10^{-17}\text{cm}$  and, on the other hand, this space is not sufficiently constant to satisfy the observable

limits on the fine-structure constant variations. These are typical problems for the Kaluza–Klein multidimensional cosmological models with dynamical internal spaces.

### 3.7. Problematic aspects of Kaluza–Klein models

In this section we want to point out some problems of Kaluza–Klein models. We first consider a model with a matter source in the form of a point-like mass. This approximation seems physically reasonable at sufficiently large distances from the compact material sources. Moreover, this approach works very well in General Relativity for calculation in a weak-field limit of the formulas for the well known gravitational experiments: perihelion shift, deflection of light and time delay of radar echoes [465]. Thus, we expect that such approach will be also applicable to Kaluza–Klein models. However, it is not the case.

To prove it, we can use asymptotic expression for the metric coefficients<sup>22</sup> in  $(\mathcal{D} = 1 + D)$ -dimensional space-time with toroidal extra dimensions. For a point-like mass  $m$  at rest the line element is [466]:

$$\begin{aligned}
 ds^2 \approx & \left(1 - \frac{r_g}{r_3} + \frac{r_g^2}{2r_3^2}\right) c^2 dt^2 - \left(1 + \frac{1}{D-2} \frac{r_g}{r_3}\right) (dr_3^2 + r_3^2 d\Omega_2^2) - \\
 & - \left(1 + \frac{1}{D-2} \frac{r_g}{r_3}\right) \sum_{i=1}^N ds_i^2, \tag{3.226}
 \end{aligned}$$

where  $r_3$  is the length of a radius vector in three-dimensional space,  $r_g = 2G_N m/c^2$  is three-dimensional Schwarzschild radius,  $G_N$  is the Newtonian gravitational constant,  $ds_i^2 = \sum_{j=1}^{d_i} d\xi_{(i)j}^2$  is a metric of  $d_i$ -dimensional torus, and we used three-dimensional isotropic (with respect to our three-dimensional space) coordinates. We suppose that the  $(D = 3 + D')$ -dimensional space has the factorisable geometry of a product manifold  $M_D = \mathbb{R}^3 \times T_1^{d_1} \times \dots \times T_N^{d_N}$ .  $\mathbb{R}^3$  describes the three-dimensional asymptotically flat external (our) space and the internal space consists of  $N$   $d_i$ -dimensional tori with the total number of the extra dimensions  $D' = \sum_{i=1}^N d_i$ .

We would like to mention that metrics (3.226) is written for the distances from gravitating mass  $m$  which much larger than periods of tori. In this case we can restrict ourselves to the zero Kaluza–Klein mode (see [472, 473]). For example, this approximation is very well satisfied for the planets of the solar

<sup>22</sup> In this section 3.7, we use the sign convention of the book [465]. We also indicate explicitly the speed of light  $c$ , because in weak-field approximation we expand quantities in powers of  $1/c$ . It is also convenient to use the letter  $D$  to indicate the total number of spatial dimensions and the dimension of space-time is denoted by the letter  $\mathcal{D}$ , i.e.  $\mathcal{D} = 1 + D$ .



system because the inverse-square law experiments show that the extra dimensions in Kaluza–Klein models should not exceed submillimeter scales [406]. Then, the gravitational potential reads  $\varphi(\mathbf{r}) \approx -G_N m/r_3 = -r_g c^2/(2r_3)$ . Moreover, in the case of gravitating mass uniformly smeared over the extra dimensions, the Newton’s law preserves its shape for arbitrary distances and this approximate formula for  $\varphi(\mathbf{r})$  becomes the exact equality [472, 473].

Now, we can use the metric (3.226) to calculate the perihelion shift and deflection of light, and to compare the results with the observations. Such calculations were performed in [466] where it was shown that considered model significantly contradicts the experimental data. However, there is more short way to show it with the help of parameterized post-Newtonian (PPN) parameters. According to PPN formalism (see, e.g., Refs. [467, 468]), the static spherically symmetric metrics in isotropic coordinates is parameterized as follows:

$$ds^2 = \left(1 - \frac{r_g}{r_3} + \beta \frac{r_g^2}{2r_3^2}\right) c^2 dt^2 - \left(1 + \gamma \frac{r_g}{r_3}\right) (dr_3^2 + r_3^2 d\Omega_2^2). \quad (3.227)$$

In General Relativity we have  $\beta = \gamma = 1$ . To get  $\beta$  and  $\gamma$  in the case of a point-like mass, it is sufficient to compare the metric coefficients in (3.227) with the corresponding asymptotic expression (3.226) what immediately gives the PPN parameters for the point-like mass

$$\beta = 1, \quad \gamma = \frac{1}{1 + D'}. \quad (3.228)$$

The latter expression shows that parameter  $\gamma$  coincides with the corresponding value of General Relativity if the number of extra dimensions  $D' = 0$ . Only in this case  $\gamma = 1$ . According to the experimental data,  $\gamma$  should be very close to 1. The tightest constraint on  $\gamma$  comes from the Shapiro time-delay experiment using the Cassini spacecraft:  $\gamma - 1 = (2.1 \pm 2.3) \times 10^{-5}$  [469–471]. On the other hand, for the point-like mass we get  $\gamma - 1 = -D'/(1 + D') \sim \mathcal{O}(1)$  what is very far from the experimental data.

After this negative (and, to some extent unexpected) result with respect to point-like masses, it is of interest to find metrics which are in good agreement with observations. From this point the soliton solutions play important role. These solutions belong to a class of metrics of the form

$$ds^2 = A(r_3) c^2 dt^2 + B(r_3) (dr_3^2 + r_3^2 d\Omega_2^2) + \sum_{i=1}^N C_i(r_3) ds_i^2. \quad (3.229)$$

They are vacuum solutions of Einstein equations with the proper boundary conditions. The dependence of the metric coefficients in (3.229) only on  $r_3$  means that the matter source for such metrics is uniformly smeared over the

extra dimensions [472, 473]. It is clear that in this case the non-relativistic gravitational potential depends only on  $r_3$  and exactly coincides with the Newtonian one. However, as we shall see below, in general case this coincidence is not sufficient to be agreement with observations.

In 5-dimensional space-time, soliton solutions were found in papers [474–476]. Then, they have been generalized to an arbitrary number of dimensions in [358, 477–479]. To our knowledge, the most general form of these solutions was given in [478] and in isotropic coordinates it reads

$$ds^2 = \left(\frac{ar_3 - 1}{ar_3 + 1}\right)^{2\alpha} c^2 dt^2 - \left(1 - \frac{1}{a^2 r_3^2}\right)^2 \left(\frac{ar_3 + 1}{ar_3 - 1}\right)^{2\alpha(1-\tau)} (dr_3^2 + r_3^2 d\Omega_2^2) - \sum_{i=1}^N \left(\frac{ar_3 + 1}{ar_3 - 1}\right)^{2\alpha\gamma_i} ds_i^2, \quad (3.230)$$

where parameters  $\alpha$  and  $\gamma_i$  satisfy the condition

$$\alpha^2[(\tau - 1)^2 + \sigma + 1] = 2, \quad \tau \equiv \sum_{i=1}^N d_i \gamma_i, \quad \sigma \equiv \sum_{i=1}^N d_i \gamma_i^2. \quad (3.231)$$

In the weak-field limit  $1/(ar_3) \ll 1$ , the metric coefficients are

$$A(r_3) \approx 1 - \frac{4\alpha}{ar_3} + \frac{16\alpha^2}{a^2} \frac{1}{2r_3^2}, \quad (3.232)$$

$$B(r_3) \approx -1 - \frac{4\alpha(1-\tau)}{ar_3}, \quad (3.233)$$

$$C_i(r_3) \approx -1 - \frac{4\alpha\gamma_i}{ar_3}. \quad (3.234)$$

The comparison of these asymptotes with the metric coefficients in Eq. (3.226) gives a possibility to single out the soliton solution which corresponds to the point-like mass. To get such correspondence, first, the following relation must hold:

$$\frac{4\alpha}{a} = r_g. \quad (3.235)$$

It follows that  $\text{sign } a = \text{sign } \alpha$ . Because the solution (3.230) is invariant under the simultaneous change  $a \rightarrow -a, \alpha \rightarrow -\alpha$ , we can choose  $a, \alpha > 0$ . Second, the parameters  $\gamma_i$  should take the same value for all internal spaces:

$$\gamma_1 = \gamma_2 = \dots = \gamma_N = \frac{1}{1 + D'}, \quad (3.236)$$

and, third, the parameters  $\alpha$  and  $a$  are

$$\alpha = \sqrt{\frac{2(1 + D')}{2 + D'}}, \quad a = \frac{4}{r_g} \sqrt{\frac{2(1 + D')}{2 + D'}}, \quad (3.237)$$

where we also took into account the constraint (3.231) and the relation (3.235).

Therefore, Eqs. (3.235)–(3.237) completely define the point-mass soliton, i.e. the solution where delta-shaped  $T_{00}$  is the only non-zero component of the energy-momentum tensor. To demonstrate it, we derive in the next subsection equations of state for general soliton solution (3.230). In 5-dimensional space-time, the experimental bounds as well as equations of state for soliton solutions were investigated in [480]. In the present section we consider the general case (3.230) of arbitrary number of dimensions and perform our investigations following Ref. [481].

### 3.7.1. Equations of state in general case

As we noted above, the dependence of the metric coefficients in (3.230) only on  $r_3$  means that the matter source for such metrics is uniformly “smeared” over the extra dimensions. It is clear that in this case the non-relativistic gravitational potential depends only on  $r_3$  and exactly coincides with the Newtonian one [472, 473]. Because the function  $A(r_3)$  is the metric coefficient  $g_{00}$  (which in the weak-field limit defines the non-relativistic potential) this demand leads to the condition of the form of (3.235):  $4\alpha/a = r_g = 2G_N m/c^2$ . Then, the expansions (3.232)–(3.234) become

$$A(r_3) \approx 1 - \frac{r_g}{r_3} + \frac{1}{2} \frac{r_g^2}{r_3^2}, \quad (3.238)$$

$$B(r_3) \approx -1 - (1 - \tau) \frac{r_g}{r_3}, \quad (3.239)$$

$$C_i(r_3) \approx -1 - \gamma_i \frac{r_g}{r_3}. \quad (3.240)$$

From these expressions, we can easily get the perturbations  $h_{00} = -r_g/r_3$ ,  $h_{\alpha\alpha} = -(1 - \tau)r_g/r_3$  and  $h_{\mu_i\mu_i} = -\gamma_i r_g/r_3$  of the order of  $1/c^2$  over the flat space-time, that gives us the possibility to find components of Ricci tensor up to the same order:

$$R_{00} \approx \frac{1}{2} \Delta h_{00} = \frac{1}{2} \kappa_0^2 m \delta(\mathbf{r}_3) c^2 = \frac{1}{2} \kappa_0^2 \rho_{(3)} c^2, \quad (3.241)$$

$$R_{\alpha\alpha} \approx \frac{1}{2} \Delta h_{\alpha\alpha} = \frac{1}{2} (1 - \tau) \kappa_0^2 \rho_{(3)} c^2, \quad \alpha = 1, 2, 3, \quad (3.242)$$

$$R_{\mu_i\mu_i} \approx \frac{1}{2} \Delta h_{\mu_i\mu_i} = \frac{1}{2} \gamma_i \kappa_0^2 \rho_{(3)} c^2, \quad (3.243)$$

$$\mu_i = 1 + \sum_{j=0}^{i-1} d_j, \quad \dots, \quad d_i + \sum_{j=0}^{i-1} d_j; \quad i = 1, \dots, N,$$

where  $d_0 = 3$ ,  $\kappa_0^2 \equiv 8\pi G_N/c^4$  and  $\Delta = \delta^{ik} \partial^2 / \partial x^i \partial x^k$  is the  $D$ -dimensional Laplace operator (see [466] for details). We also introduced the non-relativistic

three-dimensional mass density  $\rho_{(3)} = m\delta(\mathbf{r}_3)$ , which is connected with  $D$ -dimensional mass density  $\rho = \rho_{(3)}/V_{D'}$ . Here,  $V_{D'}$  is the total volume of the internal spaces. For example, if  $i$ -th torus has periods  $a_{(i)j}$ , then  $V_{D'} = \prod_{i=1}^N \prod_{j=1}^{d_i} a_{(i)j}$ .

Now, we want to define the components of the energy-momentum tensor with the help of Einstein equation in  $(1 + D)$ -dimensional space-time:

$$R_{ik} = \frac{2S_D\tilde{G}_D}{c^4} \left( T_{ik} - \frac{1}{D-1}g_{ik}T \right), \quad (3.244)$$

where  $S_D = 2\pi^{D/2}/\Gamma(D/2)$  is the total solid angle (surface area of the  $(D-1)$ -dimensional sphere of unit radius) and  $\tilde{G}_D$  is the gravitational constant in the  $(\mathcal{D} = 1 + D)$ -dimensional space-time. Introducing the quantity  $\kappa_D^2 \equiv 2S_D\tilde{G}_D/c^4$  (see also footnote 1 where we should replace  $D$  by  $\mathcal{D} = 1 + D$ ) and keeping in mind that we consider compact astrophysical object at rest in our three-dimensional space (it results in  $T_{11} = T_{22} = T_{33} = 0$ ), we arrive at the following Einstein equations:

$$\frac{1}{2}\kappa_0^2\rho_{(3)}c^2 \approx \kappa_D^2 \left( T_{00} - \frac{1}{D-1}Tg_{00} \right), \quad (3.245)$$

$$\frac{1}{2}(1-\tau)\kappa_0^2\rho_{(3)}c^2 \approx \kappa_D^2 \left( -\frac{1}{D-1}Tg_{\alpha\alpha} \right), \quad (3.246)$$

$$\frac{1}{2}\gamma_i\kappa_0^2\rho_{(3)}c^2 \approx \kappa_D^2 \left( T_{\mu_i\mu_i} - \frac{1}{D-1}Tg_{\mu_i\mu_i} \right). \quad (3.247)$$

Therefore, the required components of the energy-momentum are

$$T_{00} \approx \frac{\kappa_0^2V_{D'}}{\kappa_D^2} \left( 1 - \frac{\tau}{2} \right) \rho c^2, \quad T_{\alpha\alpha} = 0, \quad (3.248)$$

$$T_{\mu_i\mu_i} \approx \frac{\kappa_0^2V_{D'}(\gamma_i - 1 + \tau)}{2\kappa_D^2} \rho c^2. \quad (3.249)$$

The equation for the 00-component shows that the parameter  $\tau$  cannot be equal to 2 because for  $\tau = 2$  we get  $T_{00} = 0$ , what corresponds to uninteresting case of absence of matter. Moreover,  $T_0^0 = \varepsilon$  is the energy density of matter (remind that in this section we use the sign convention of the book [465]). Therefore, up to the terms  $1/c^2$ , we have  $T_{00} \approx \varepsilon \approx \rho c^2$ . It requires the following relation between Newtonian and multidimensional gravitational constants:

$$\kappa_0^2 = \frac{2}{2-\tau}\kappa_D^2/V_{D'} \implies 4\pi G_N = \frac{2}{2-\tau}S_D\tilde{G}_D/V_{D'}. \quad (3.250)$$

In the particular case of a point-like mass source with  $\tau = D'/(1 + D')$ , this relation was given in [473, 480]. From Eqs. (3.248) and (3.249) we also obtain the relation

$$T_{\mu_i\mu_i} \approx \frac{\gamma_i - 1 + \tau}{2 - \tau} T_{00}. \quad (3.251)$$

Taking into account that up to the terms  $1/c^2$ , components  $T_{\mu_i\mu_i}$  define pressure in  $i$ -th internal space:  $T_{\mu_i\mu_i} \approx P_i$ , we get from Eq. (3.251) the following equations of state in these spaces:

$$P_i = \frac{\gamma_i - 1 + \tau}{2 - \tau} \varepsilon, \quad i = 1, \dots, N. \quad (3.252)$$

Since  $T_{11} = T_{22} = T_{33} = 0$ , in our three-dimensional space we have dust-like equation of state:  $P_0 = 0$ . In the case of a point-like mass, the parameters  $\gamma_i$  satisfy the condition (3.236). It can be easily seen that for these values of  $\gamma_i$ , all  $T_{\mu_i\mu_i}$  are equal to zero. Therefore, in this case,  $T_{00}$  is the only non-zero component and in the external/our space, as well as in all internal spaces, we have the same dust-like equations of state:  $P_i = 0$ ,  $i = 0, \dots, N$ .

### 3.7.2. Latent solitons

Asymptotic expressions (3.238) and (3.239) also enable to get the PPN parameters in general case. Comparing these equations with the corresponding metric coefficients in (3.227), we immediately find for solitons:

$$\beta_s = 1, \quad \gamma_s = 1 - \tau. \quad (3.253)$$

With the help of these PPN parameters, we can easily get formulas for the famous gravitational experiments [467, 470]:

#### (i) *Perihelion shift*

$$\begin{aligned} \delta\psi &= \frac{6\pi m G_N}{\lambda(1-e^2)c^2} \frac{1}{3} (2 + 2\gamma_s - \beta_s) = \\ &= \frac{6\pi m G_N}{\lambda(1-e^2)c^2} \frac{3-2\tau}{3} = \frac{\pi r_g}{\lambda(1-e^2)} (3-2\tau), \end{aligned} \quad (3.254)$$

where  $\lambda$  is the semi-major axis of the ellipse and  $e$  is its eccentricity.

#### (ii) *Deflection of light*

$$\delta\psi = (1 + \gamma_s) \frac{r_g}{\rho} = (2 - \tau) \frac{r_g}{\rho}, \quad (3.255)$$

where  $\rho$  is the distance of closest approach (impact parameter) of the ray's path to the gravitating mass  $m$ .

(iii) *Time delay of radar echoes (Shapiro time-delay effect)*

$$\begin{aligned}\delta t &= (1 + \gamma_s) \frac{r_g}{c} \ln \left( \frac{4r_{\text{Earth}} r_{\text{planet}}}{R_{\text{Sun}}^2} \right) = \\ &= (2 - \tau) \frac{r_g}{c} \ln \left( \frac{4r_{\text{Earth}} r_{\text{planet}}}{R_{\text{Sun}}^2} \right).\end{aligned}\quad (3.256)$$

Comparison of the formulas (3.254)–(3.256) with the experimental data gives the possibility to restrict parameters of the soliton solutions. In fact, as in the case of the point-like mass, we can also get it directly from experimental restriction on PPN parameter  $\gamma$ :  $\gamma - 1 = (2.1 \pm 2.3) \times 10^{-5}$ . Thus, from (3.253) we find that solitonic parameter  $\tau$  should satisfy the condition

$$\tau = -(2.1 \pm 2.3) \times 10^{-5}.\quad (3.257)$$

In the case of the point-like massive soliton described by Eqs. (3.235)–(3.237), we have  $\tau = D'/(1 + D') \sim \mathcal{O}(1)$ , what obviously contradicts to Eq. (3.257).

Equation (3.253) shows that there is very interesting class of solitons which are defined by the condition

$$\tau = \sum_{i=1}^N d_i \gamma_i = 0.\quad (3.258)$$

With the help of the gravitational experiments mentioned above, it is impossible to differ these Kaluza–Klein solitons from general relativity because they have  $\gamma_s = 1$  as in general relativity<sup>23</sup>. For this reason we called these solutions *latent solitons* [481]. For these latent solitons, equations of state (3.252) in the internal spaces are

$$P_i = \frac{\gamma_i - 1}{2} \varepsilon, \quad i = 1, \dots, N.\quad (3.259)$$

Black strings ( $N = 1$ ,  $d_1 = 1$ ) and black branes ( $N > 1$ ) are characterized by the condition that all  $\gamma_i = 0$ ,  $i \geq 1$ . Obviously, they belong to the class of latent solitons and they have the equations of state

$$P_i = -\frac{1}{2} \varepsilon, \quad i = 1, \dots, N.\quad (3.260)$$

<sup>23</sup> It can be easily seen from equations (3.238)–(3.240) that the parameter  $\tau$  defines also the difference between perturbations  $h_{00}$  and  $h_{\alpha\alpha}$ :  $h_{00} - h_{\alpha\alpha} = -\tau r_g / r_3$ . Precisely because of this difference gravitational experiments in KK models and in General Relativity lead to different results. When  $\tau \rightarrow 0$ , this difference disappears. The additional limit  $\gamma_i \rightarrow 0 \implies h_{\mu_i \mu_i} \rightarrow 0$  provides stabilization of the internal spaces [380, 480].

It is known (see section (3.2.3) and Refs. [380, 480]) that in the case of three-dimensional external/our space such equations of state are the only ones which do not spoil the condition of the internal space stabilization for the compact astrophysical objects with the dust-like equation of state  $P_0 = 0$  in the external space. Therefore, it is tempting to treat non-zero parameters  $\gamma_i$  as a measure of the latent soliton destabilization<sup>24</sup>. However, a careful analysis (see [483]) shows that the variation of the total volume of the internal space is equal to zero. Consequently, in the case of latent solitons variation of fundamental constants are also absent.

We would like to stress the following: It is well known that black strings (branes) have the topology

$$(4\text{-dimensional Schwarzschild space-time}) \times (\text{flat internal spaces}).$$

In this case, it does not seem surprising that gravitational experiments lead to the same results as for general relativity. However, the latent solitons, in general case, do not have either Schwarzschildian metrics for 4-dimensional part of space-time nor flat metrics for the extra dimensions. Nevertheless, within the considered accuracy, it is also impossible to distinguish them from General Relativity. This is really surprising.

To conclude this section, we would like to mention that the relation between Newtonian and multidimensional gravitational constants for latent solitons is reduced to the equation (3.13):

$$4\pi G_N = S_D \tilde{G}_D / V_{D'}. \quad (3.261)$$

### 3.7.3. Experimental restrictions on the equations of state of a multidimensional perfect fluid

Now, we want to show in general case that for static spherically symmetric perfect fluid with dust-like equation of state in our space, the condition  $h_{00} = h_{\alpha\alpha}$  (which ensures the agreement with the gravitational experiments at the same level of accuracy as General Relativity) results in the latent soliton condition (3.258) and equations of state (3.259), and additional condition  $R_{\mu_i\mu_i} = 0 \implies h_{\mu_i\mu_i} = 0$  reduces (3.259) to (3.260) (which is necessary for the internal space stability) and singles out  $d_0 = 3$  for the number of the external dimensions.

<sup>24</sup> If we rewrite equations of state in the form of Eq. (3.32)  $P_i = (\alpha_i - 1)\varepsilon$ ,  $i = 0, \dots, N$ , then for the latent solitons we have  $\alpha_0 = 1$ ,  $\alpha_i = (1 + \gamma_i)/2$ ,  $i = 1, \dots, N$ . For these values of  $\alpha_0, \alpha_i$ , we get on the right-hand side of the equation (3.41) (for  $d_0 = 3$ ) the terms  $(\gamma_i d_i / 2) \kappa_N \rho_{(3)}$ . These terms are dynamical functions because of dynamical behavior of the energy density  $\rho_{(3)}$ . This results in violation of the necessary condition for the internal space stabilization.

Let us consider a static spherically symmetric perfect fluid with energy-momentum tensor (see footnote 22 about the sign convention in this section):

$$T^i_k = \text{diag} \left( \varepsilon, \underbrace{-P_0, \dots, -P_0}_{d_0 \text{ times}}, \dots, \underbrace{-P_N, \dots, -P_N}_{d_N \text{ times}} \right). \quad (3.262)$$

We recall that we are using the notations:  $i, k = 0, 1, \dots, D$ ;  $a, b = 1, \dots, D$ ;  $\alpha, \beta = 1, \dots, d_0$  and  $\mu_i = 1 + \sum_{j=0}^{i-1} d_j, \dots, d_i + \sum_{j=0}^{i-1} d_j$ ,  $i = 1, \dots, N$ . For static spherically symmetric configurations we have  $g_{0a} = 0$  and  $g_{ab} = 0$ ,  $a \neq b$ . Since we want to apply this model to ordinary astrophysical objects where the condition  $T^0_0 \gg |T^\alpha_\alpha|$  usually holds, we assume the dust-like equation of state in  $d_0$ -dimensional external space:  $P_0 = 0$ , but the equations of state are arbitrary ones in  $i$ -th internal space:  $P_i = \omega_i \varepsilon$ . Obviously,  $\varepsilon$  is equal to zero outside the compact astrophysical objects.

Moreover, we consider the weak-field approximation where the metric coefficients can be expressed in the form

$$g_{00} \approx 1 + h_{00}, \quad g_{aa} \approx -1 + h_{aa}, \quad h_{00}, h_{aa} \sim O(1/c^2). \quad (3.263)$$

As an additional requirement, we impose that the considered configuration does not contradict the observations. It will be so if the following conditions hold:  $h_{00} = h_{\alpha\alpha}$  and  $h_{\mu_i\mu_i} = 0$  (see Ref. [480]). In what follows, we define which equations of state are obtained as a result of these restrictions. Taking into account that  $T = \sum_{i=0}^D T^i_i = \varepsilon(1 - \sum_{i=1}^N \omega_i d_i)$ ,  $T_{\alpha\alpha} = 0$ ,  $\varepsilon \sim O(c^2)$  and, up to terms  $c^2$ , that  $T_{00} \approx T^0_0$ ,  $T_{\mu_i\mu_i} \approx -T^{\mu_i}_{\mu_i}$ , we get from the Einstein equation (3.244) the non-zero components of Ricci tensor (up to  $1/c^2$ ):

$$R_{00} \approx \frac{\varepsilon \kappa_{\mathcal{D}}}{D-1} \left[ d_0 - 2 + \sum_{i=1}^N d_i (1 + \omega_i) \right], \quad (3.264)$$

$$R_{\alpha\alpha} \approx \frac{\varepsilon \kappa_{\mathcal{D}}}{D-1} \left[ 1 - \sum_{i=1}^N d_i \omega_i \right], \quad (3.265)$$

$$R_{\mu_i\mu_i} \approx \frac{\varepsilon \kappa_{\mathcal{D}}}{D-1} \times \left[ \omega_i \left( \sum_{j=0}^N 'd_j - 1 \right) + 1 - \sum_{j=1}^N 'd_j \omega_j \right], \quad (3.266)$$

where  $\kappa_{\mathcal{D}} \sim O(1/c^4)$  is defined in section 3.7.1 and the prime in the summation of Eq. (3.266) means that we must not take into account the  $i$ -th term. Eqs. (3.264) and (3.265) shows that  $R_{00}$  and  $R_{\alpha\alpha}$  components are related as follows:

$$R_{\alpha\alpha} = \frac{1 - \sum_{i=1}^N d_i \omega_i}{d_0 - 2 + \sum_{i=1}^N d_i (1 + \omega_i)} R_{00}. \quad (3.267)$$



On the other hand, in weak-field limit the components of Ricci tensor read

$$R_{00} \approx \frac{1}{2} \Delta h_{00}, \quad R_{aa} \approx \frac{1}{2} \Delta h_{aa}, \quad a = 1, \dots, D, \quad (3.268)$$

where as usual we can put  $h_{00} \equiv 2\varphi/c^2$  and  $\Delta$  is  $D$ -dimensional Laplace operator defined in Eqs. (3.241)–(3.243). Therefore, from equations (3.267) and (3.268) we obtain

$$h_{\alpha\alpha} = \frac{1 - \sum_{i=1}^N d_i \omega_i}{d_0 - 2 + \sum_{i=1}^N d_i (1 + \omega_i)} h_{00}, \quad \alpha = 1, \dots, d_0. \quad (3.269)$$

As we have mentioned above, to be in agreement with experiment at the same level of accuracy as General Relativity we should demand  $h_{\alpha\alpha} = h_{00}$ , what leads to the restriction on the parameters  $\omega_i$  of the equations of state:

$$3 - d_0 - \sum_{i=1}^N d_i = 2 \sum_{i=1}^N d_i \omega_i. \quad (3.270)$$

In the case of three-dimensional external space ( $d_0 = 3$ ), this constraint is reduced to

$$\sum_{i=1}^N d_i \left( \omega_i + \frac{1}{2} \right) = 0. \quad (3.271)$$

If we parameterize

$$\omega_i = \frac{\gamma_i - 1}{2}, \quad i = 1, \dots, N, \quad (3.272)$$

then we arrive at the latent soliton condition (3.258). Therefore, the demand that multidimensional perfect fluid (with dust-like equation of state in the external space  $P_0 = 0$ ) provides the same results for gravitational experiments as General Relativity, leads to the latent soliton equations of state (3.259) in the internal spaces. However, it is known (see section 3.2.3) that the internal spaces can be stabilized if multidimensional perfect fluid (with  $P_0 = 0$ ) has the same equations of state  $\omega_i = -1/2$  in all internal spaces and the external space is three-dimensional  $d_0 = 3$ . In other words, it takes place if all  $\gamma_i = 0$  in (3.272). Let us show that the additional requirement  $R_{\mu_i \mu_i} = 0$  ensures the fulfillment of these conditions. Indeed, from Eq. (3.266) we get

$$R_{\mu_i \mu_i} = 0 \implies \omega_i = -\frac{1}{2}, \quad i = 1, \dots, N, \quad (3.273)$$

where we used the constraint (3.270)<sup>25</sup>. Now, substitution  $\omega_i = -1/2$  in (3.270) singles out  $d_0 = 3$ . Therefore, the demand of the internal space stabilizati-

<sup>25</sup> It can be also easily seen that  $R_{\mu_i \mu_i} = 0 \implies \Delta h_{\mu_i \mu_i} = 0$ , what, together with the boundary conditions (finiteness of  $h_{\mu_i \mu_i}$  at  $r_3 = 0$  and  $h_{\mu_i \mu_i} \rightarrow 0$  for  $r_3 \rightarrow +\infty$ ), gives  $h_{\mu_i \mu_i} = 0$ .

on leads, for multidimensional perfect fluid (with  $P_0 = 0$ ), to the black string/brane equations of state (3.260) in the internal spaces and, additionally, it selects uniquely the number of the external spaces to be  $d_0 = 3$ .

To conclude the consideration of this perfect fluid, we want to get the metric coefficients up to  $\mathcal{O}(1/c^2)$  (see Eq. (3.263)). To do so, it is sufficient to define the function  $\varphi$ . It can be easily seen from (3.264) and (3.268) that this function satisfies the equation

$$\Delta\varphi = \frac{c^2}{2}\Delta h_{00} \approx c^2 R_{00} \approx S_D \tilde{G}_D \rho, \quad (3.274)$$

where we use the constraint (3.270) for arbitrary  $d_0$  and relation  $\varepsilon \approx \rho c^2$ . Therefore, to get the metric coefficients we need to solve this equation with proper boundary conditions. We want to reduce this equation to ordinary Poisson equation in three-dimensional external space  $d_0 = 3$ . To do so, we consider the case in which matter is uniformly smeared over the extra dimensions, then  $\rho = \rho_{(3)}/V_{D'}$  (see section 3.7.1).

In this case the non-relativistic potential  $\varphi$  depends only on our external coordinates and  $\Delta$  is reduced to three-dimensional Laplace operator  $\Delta_3$ . Therefore, Eq. (3.274) is reduced to

$$\Delta_3\varphi \approx (S_D \tilde{G}_D / V_{D'})\rho_{(3)} = 4\pi G_N \rho_{(3)}, \quad (3.275)$$

where we use the relation (3.261) between Newtonian and multidimensional gravitational constants. This is usual Poisson equation. It is worth noting that  $\rho_{(3)} = 0$  outside the compact astrophysical object and it is necessary to solve (3.275) inside and outside of the object, followed by matching these solutions at the boundary.

We can summarize the main conclusion of this section as follows. For compact astrophysical objects with dust-like equation of state in the external space ( $P_0 = 0$ ), the demand of the agreement with the gravitational experiments requires the condition (3.257), namely:  $\tau = -(2.1 \pm 2.3) \times 10^{-5}$ . However, to be at the same level of accuracy as General Relativity, we must have  $\tau = 0$ . In other words, we should consider the latent solitons with equations of state (3.259) in the internal spaces (in the case  $d_0 = 3$ ). Moreover, the condition of stability of the internal spaces singles out black strings/branes from the latent solitons and leads uniquely to  $P_i = -(1/2)\varepsilon$  as the black string/brane equations of state in the internal spaces, and to the number of the external dimensions  $d_0 = 3$ . The main problem with the black strings/branes is to find a physically reasonable mechanism which can explain how the ordinary particles forming the astrophysical objects can acquire rather specific equations of state ( $P_i = -\varepsilon/2$ ) in the internal spaces.

As we have seen above, to be in agreement with the observations, it is necessary to break the symmetry (in terms of equations of state) between the

external/our and internal spaces. In our opinion, braneworld models are the most promising alternative to the KK models because they naturally break the symmetry between our three-dimensional Universe and the extra dimensions, and the following chapter is devoted to the problems of dark energy and dark matter in the braneworld models.

### 3.8. Summary

In this chapter, we have considered a possibility for our space-time to have extra spatial dimensions, and what observational consequences follow from this. In particular, can we explain dark matter and dark energy due to the existence of the extra dimensions? We supposed that fields from the Standard Model of particle physics are not localized on a three-dimensional hypersurface but can propagate throughout the multidimensional space-time. Such models are called Kaluza–Klein ones. The case of localization will be considered in the following chapter 4.

We first investigated an important problem of stable compactification of the internal space. The point is that in Kaluza–Klein models, to make the extra dimensions unobservable at the present time, the internal spaces have to be compact and reduced to very small scales (of the order of or less than the Fermi length). Therefore, we proposed general mechanism of dimension reduction of multidimensional models. We have shown that after such reduction the considered models take the form of an effective four-dimensional Brans–Dicke or Einstein (after conformal transformation) theories with scalar fields. These scalar fields are defined by scale factors of the internal spaces. The form of a potential energy of these fields depends on topology of the internal spaces and matter content of considered models. Moreover, to avoid a problem of too large variations of the fine structure constant, the compactification have to be stable against fluctuations of these fields (i.e. small fluctuations of the scale factors of the internal spaces). This means that the effective potential of the model obtained under dimensional reduction to a four-dimensional effective theory should have minima with respect to these fluctuations. These minima play the role of the cosmological constant in our observable Universe and can be dark energy in the case of positive values. We have also shown that small excitations of a system near a minimum of the effective potential can be observed as massive scalar fields in the external (our) space-time. These scalar fields very weakly interact with the Standard Model particles. Therefore, they belong to a class of the dark matter particles. We called these particles gravitational excitons. They may play an important role during the Universe evolution. Therefore, we have investigated the dynamical behavior of gravexcitons depending on the value of their mass. We have also considered effects of Lorentz invariance violation due to interaction between gravexcitons and four-dimensional photons. It was

shown that experimental limitations on such violation can restrict parameters (e.g. masses of gravexcitons) of the models.

In conventional cosmology matter fields are taken into account in a phenomenological way as a perfect fluid. Therefore, we have proven an important theorem (the no-go theorem) which defines the classes of the perfect fluid allowing the stable compactification of the internal spaces.

Non-linear gravitational  $f(R)$  models have attracted the great deal of interest from the eighties of last century because these models can provide a natural mechanism of the early inflation. Recently, it was realized that these models can also explain the late-time acceleration of the Universe (dark energy). This fact resulted in a new wave of papers devoted to this topic. Therefore, we have generalized these theories to the case of multidimensional space-time. We have shown that these models are reach enough to explain both early inflation and accelerated expansion of the Universe at a late stage of its evolution. However, there are still problems with fine-tuning of parameters of the models as well as with sufficient number of e-foldings.

We have also considered multidimensional cosmological models which can mimic dynamical dark energy. They are the so-called  $Sp$ -branes. In this case, there are no minima of the effective potential for gravexcitons and acceleration has different origin. For example, the negative curvature of the internal space can lead to such acceleration. However, we have shown that, despite the satisfactory description of the accelerated expansion of our Universe at the late stages of its evolution, this model has two significant drawbacks. On the one hand, the internal space is too big with respect to the standard Kaluza–Klein restrictions and, on the other hand, this space is not sufficiently invariable to satisfy the observable limits on the fine-structure constant variations. These are typical problems for the Kaluza–Klein multidimensional cosmological models with dynamical internal spaces.

It is well known that General Relativity in four-dimensional space-time is in good agreement with gravitational experiments such as perihelion shift, deflection of light, time delay of radar echoes and PPN parameters. Therefore, it is important to verify Kaluza–Klein models as to their conformity with these experiments. We first have considered models with toroidal compactification of the extra dimensions. A matter source was taken in the form of a point-like mass with a dust-like  $p = 0$  equation of state in all (external and internal) spatial dimensions. This approach works very well in General Relativity for calculation in a weak field limit of the formulas for the gravitational experiments. However, in the case of considered Kaluza–Klein models, we found that PPN parameters demonstrate good agreement with the experimental data only in the case of ordinary three-dimensional space. Therefore, the point-like gravitational source with dust-like equations of state strongly contradicts the observations. It is important to note that the result does not depend on the

---

point-like approximation. Instead of the delta-shaped form, we can consider a compact object in the form of a perfect fluid with the dust-like equation of state in all spatial dimensions, and we obtain the same negative result. It turned out that to satisfy the experimental data, the matter source should have negative equations of state (tension) in the internal spaces. For example, latent solitons (which are exact solutions (3.230) with condition (3.258)) have such tension and they satisfy the gravitational tests at the same level of accuracy as General Relativity. The uniform black strings and black branes are particular examples of the latent solitons. It is of interest to understand why some models meet the classical gravitational tests, while others do not. In our recent paper [483], we have shown that the variation of the total volume of the internal spaces generates the fifth force in the case of toroidal models with the dust-like equations of state in all spatial dimensions. This is the main reason of the problem. However, in the case of the latent solitons, tension of the gravitating source fixes the internal space volume, eliminating the fifth force contribution and resulting in agreement with the observations. Therefore, tension plays a crucial role here. In the case of spherical compactification of the internal space, the fifth force is replaced by the Yukawa interaction for models with the stabilized internal space [484–486]. For large Yukawa masses (gravexciton masses), the effect of this interaction is negligibly small, and considered models satisfy the gravitational tests at the same level of accuracy as General Relativity. It happens for an arbitrary equation of state (including the dust-like  $p = 0$ ) in the internal space. However, we have shown [486, 487] for this model that gravitating masses acquire effective relativistic pressure in the external space. Such pressure contradicts the observations of compact astrophysical objects (e.g., the Sun). The tension (with the parameter of equation of state  $\omega = -1/2$ ) in the internal space is the only possibility to preserve the dust-like equation of state in the external space. Therefore, in spite of agreement with the gravitational experiments for an arbitrary value of  $\omega$ , tension ( $\omega = -1/2$ ) also plays a crucial role for the models with spherical compactification. The problematic aspect of all these models with tension consists in physically reasonable explanation of the origin of tension for ordinary astrophysical objects.

# 4

## CHAPTER

---

# BRANEWORLD MODELS

---

### 4.1. Introduction

Cosmological brane-world models constitute the branch of physics with non-compact (“large”) extra-dimensions in which our world is a four-dimensional hypersurface (the brane) embedded in a higher-dimensional manifold. This represents an alternative to the Kaluza–Klein compactification of extra dimensions that was described in Sec. 3.1 of chapter 3.

One of the first models with localization of matter on the brane was constructed in [488] (see also [489] and reviews in [383, 490]). In this model, the brane represented a domain wall (kink) in a five-dimensional space-time, constructed of a real scalar field  $\varphi$  with spontaneous breaking of the discrete  $Z_2$  symmetry with respect to the transformation  $\varphi \rightarrow -\varphi$ . A Dirac fermion field coupled to this scalar has a zero Kaluza–Klein mode (i.e., with zero four-dimensional invariant mass) which is localized in the neighborhood of the brane and has left chirality. Such massless fermions can imitate matter localized on the brane. At high interaction energies, such zero modes can create excitations from the continuum of the Kaluza–Klein spectrum, which then would correspond to the process of particles leaving the brane and going into higher dimension [492–493]. It is also possible (but more difficult) to confine vector gauge fields on the brane in the field-theoretical setup [494].

More recent motivation for alternative compactification of extra dimensions is the discovery of  $p$ -branes — extended dynamical submanifolds in the multidimensional space — in string theory [337, 338]. Some types of  $p$ -branes can confine matter fields; for instance, gauge fields can live on the so-called Dirichlet-branes, or D-branes (see a review in [495]).  $Dp$ -branes are  $(p + 1)$ -dimensional time-like hypersurfaces

at which the ends of open strings can be localized (see Fig. 4.1). Since the ends of open strings carry gauge fields, these fields on a fundamental level are  $(p + 1)$ -dimensional objects residing entirely on the brane and having no Kaluza–Klein counterparts. On the other hand, closed strings, describing excitations of spin two (i.e., gravitons), can freely propagate in the multidimensional volume. This explains the basic structural features of the new picture of extra dimensions, in which matter fields and gravity play different role.

The idea of a “braneworld” arises naturally in the context of the fundamental M-theory (see [496] as a review). Although the phenomenological models usually under consideration in cosmology are quite simplistic, one can hope that the analogs of at least some of their properties can be found in a realistic fundamental theory. This relates, in particular, to the properties of gravity and dark energy in the braneworld model, which is the subject of the present chapter.

In the end of 1990ies, the braneworld theory gave a fresh view of the problem of the Planck hierarchy, which served as one of the motivations for its subsequent development. In the model proposed by Arkani-Hamed, Dimopoulos and Dvali (the ADD model) [497] (see also [498]), a multidimensional gravitational action of Hilbert–Einstein type

$$S = M^{D-2} \int \mathcal{R} \sqrt{-g} d^D x, \quad (4.1)$$

was under consideration, where  $M$  is the Planck mass in a  $D$ -dimensional space-time, and  $\mathcal{R}$  is the curvature scalar of the corresponding metric  $g_{ab}$ .

In the presence of a three-brane, under compactification of the extra  $d = D - 4$  dimensions and under the assumption of independence of the graviton wave function on the extra coordinates, action (4.1) reduces to a four-dimensional effective action on the brane of the form

$$S_{\text{brane}} = M_{\text{P}} \int R \sqrt{-h} d^4 x, \quad (4.2)$$

where  $R$  is the curvature scalar of the induced metric  $h_{ab}$  on the brane, and the Planck mass  $M_{\text{P}}$  is expressed through the fundamental mass  $M$  and characteristic compactification radius of extra dimensions  $L$  as follows:

$$M_{\text{P}} = M (ML)^{d/2}. \quad (4.3)$$

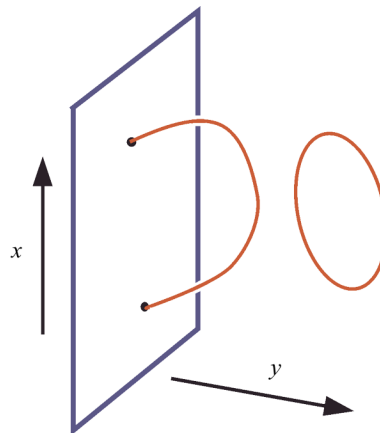


**Fig. 4.1.** An open string whose ends are attached to a D-brane, and a closed string that can propagate freely in a higher-dimensional space

By setting  $M \sim 1$  TeV, one can estimate the value of  $L$ :

$$L \sim M^{-1} \left( \frac{M_{\text{P}}}{M} \right)^{2/d} \sim 10^{32/d-17} \text{ cm.} \quad (4.4)$$

Of interest is the case  $d = 2$ , for which we have  $L \sim 1$  mm. The analysis of the processes of graviton production during supernovae explosions leads to a somewhat stronger constraint on the quantity  $M$ , namely [383, 499],  $M > 30$  TeV, which gives  $L \sim 1\text{--}10$   $\mu\text{m}$  for  $d = 2$ . Thus, compactification of extra dimensions on very large (from particle-physics viewpoint) spatial scale, in principle, could solve the problem of the Planck hierarchy, at the same time leading to modifications of the law of gravity at small distances. This observation stimulated search of the deviation of the gravitational law from Newtonian at submillimeter distances.

The ADD model did not address the problem of hierarchy connected with a large spatial compactification scale  $L$ . Moreover, this model neglected the curvature of the multidimensional space, in particular, caused by possible gravitational effect of the brane in this space. Both shortcomings were removed in the model due to Randall and Sundrum (the RS model) [500, 501]. Inspired by the eleven-dimensional Hořava–Witten model [502, 503] on the orbifold  $R^{10} \times S^1/Z_2$ , this version of the theory had only one large extra spatial dimension. The arising effective five-dimensional space-time was curved, and the four-dimensional character of the laws of gravity on the brane was achieved by localization of the massless gravitational mode in the neighborhood of the brane. The flat character of the brane (i.e., the absence of a large effective cosmological constant on the brane) was achieved by fine tuning the brane tension  $\sigma$  and the gravitational and cosmological constants in the five-dimensional space-time.

The next important step in the construction of braneworld models was made in [504, 505] (and, independently, in [506]), where it was pointed out that the quantum character of the fields localized on the brane, in general, leads to the appearance of the term with the curvature scalar of the induced metric on the brane. (This mechanism of generating an effective action for gravity was, in fact, first considered by Sakharov [507].) It is this version of the theory that will be the focus of our discussion in this chapter.

## 4.2. General setup and notation

Throughout this chapter, our main object of investigation will be a time-like hypersurface (called brane) in a five-dimensional manifold  $\mathcal{B}$  (the bulk). In this case it is convenient to use the conventions of [508]. Specifically, the vectors and tensors tangent to the brane are regarded as vectors also tangent to the five-dimensional manifold, and thus all tensors carry the five-dimensional abstract indices  $a, b, c, \dots$  By a tensor field tangent to the



brane, we mean any tensor field  $T^{a\dots b\dots}$  defined at the position of the brane and such that

$$n_a T^{a\dots b\dots} = n^b T^{a\dots b\dots} = \dots = 0 \quad (4.5)$$

for any vector field  $n^a$  normal to the brane.

The metric in the bulk is denoted by  $g_{ab}$ , while the induced metric on the brane is  $h_{ab} = g_{ab} - n_a n_b$ , where  $n^a$  is the *unit* vector field normal to the brane, which we always set to be the inner normal, pointed *from* the brane in the direction of the bulk space. Everywhere we employ the space-time signature  $(-, +, +, +, +)$ .

The induced metric on the brane defines the unique covariant derivative on the brane compatible with this metric, which we denote by  $D_a$ , to distinguish it from the covariant derivative in the five-dimensional bulk space  $\nabla_a$ . The curvature tensor for  $g_{ab}$  in the bulk is denoted by  $\mathcal{R}^a{}_{bcd}$ . The curvature tensor of  $h_{ab}$  on the brane is denoted as  $R^a{}_{bcd}$ ; regarded as a tensor in  $\mathcal{B}$ , it is tangent to the brane by construction. The tensor of extrinsic curvature of the brane in  $\mathcal{B}$  is defined as

$$K_{ab} = h^c{}_a \nabla_c n_b \equiv -\frac{1}{2} \mathcal{L}_n h_{ab}, \quad (4.6)$$

where  $\mathcal{L}_n$  denotes the lie derivative along the vector field  $n^a$  (arbitrarily but smoothly extended from the brane to the bulk space). It is also tangent to the brane by definition, as can easily be verified.

We consider a braneworld model described by the following simple yet generic action, which includes gravitational and cosmological constants in the bulk ( $\mathcal{B}$ ) and on the brane:

$$\begin{aligned} S = & \sum_{i=1}^N M_i^3 \left[ \int_{\mathcal{B}_i} (\mathcal{R}_i - 2\Lambda_i) - 2 \int_{\text{brane}} K_i \right] + \\ & + \int_{\text{brane}} (m^2 R - 2\sigma) + \int_{\text{brane}} L(h_{ab}, \phi). \end{aligned} \quad (4.7)$$

Here,  $\mathcal{R}_i$  is the scalar curvature of the five-dimensional metric  $g^i_{ab}$  on  $\mathcal{B}_i$ ,  $i = 1, \dots, N$ , the  $N$  bulk spaces for which the brane is a boundary (see the left panel in Fig. 4.2), and  $R$  is the scalar curvature of the induced metric  $h_{ab}$  on the brane. The quantity  $K_i = K^i{}_{ab} h^{ab}$  is the trace of the symmetric tensor of extrinsic curvature  $K^i{}_{ab}$  of the brane in the space  $\mathcal{B}_i$ . The symbol  $L(h_{ab}, \phi)$  denotes the Lagrangian density of the four-dimensional matter fields  $\phi$  the dynamics of which is restricted to the brane so that they interact only with the induced metric  $h_{ab}$ . All integrations over  $\mathcal{B}_i$  and over the brane are taken with the corresponding natural volume elements. The symbols  $M_i$ ,  $i = 1, \dots, N$ , and  $m$  denote the Planck masses of the corresponding spaces,  $\Lambda_i$ ,  $i = 1, \dots, N$ , are the five-dimensional cosmological constants on each side of the brane, and  $\sigma$  is the brane tension.

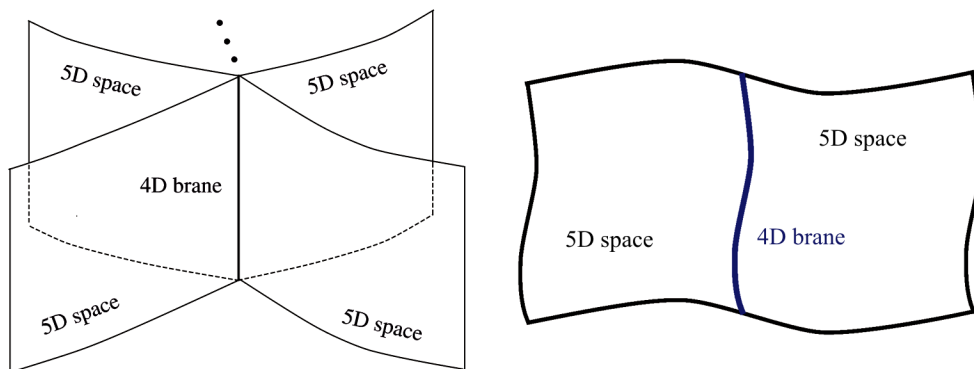


**Fig. 4.2.** On the left: A brane as a boundary of several volume spaces. The field theory of this configuration is studied in [509]. On the right: A special, physical, case of two volume spaces

Action (4.7) can be regarded as the simplest local action for gravity in the braneworld setup under consideration. Indeed, it is the lowest-order non-trivial action in the number of derivatives acting on the metric. The braneworld model described by (4.7) can be classified according to the number of the bulk spaces  $N$  for which the brane is a boundary, and according to the values taken by the fundamental constants  $M_i$ ,  $\Lambda_i$ ,  $m$ , and  $\sigma$ . We do it as follows:

- The case  $N = 1$  is the simplest one and most frequently discussed in the literature. It describes a brane which is a boundary of a five-dimensional bulk space. Alternatively, it can be obtained from the physically more natural case  $N = 2$  (see the right panel in Fig. 4.2) by making identification between the two sides of the brane, or by imposing the so-called mirror symmetry of reflection of the bulk space with respect to the brane. The cases with  $N \geq 2$  need not have this mirror symmetry.

In most of this chapter, we consider the simple case  $N = 1$  (or brane with mirror symmetry). The case of  $N = 2$  (without the mirror symmetry) will be considered in Sec. 4.11.

- A special case where  $m = 0$  will be referred to as the Randall–Sundrum (RS) type of model since it is this form of action that was employed in the original papers [500, 501].

- A more general case where  $m \neq 0$  will be referred to as models with induced gravity on the brane, and a special case of such models with vanishing cosmological constants on the brane and in the bulk, i.e.,  $\sigma = 0$  and  $\Lambda_i = 0$ , will be referred to as the Dvali–Gabadadze–Porrati (DGP) type of model owing to its first appearance in [504].

Variation of action (4.7) with respect to the metric  $g_{ab}$  gives rise to the Einstein equations in each of the  $i$  bulk spaces:

$$\mathcal{G}_{ab} + \Lambda_i g_{ab} = 0 \quad (4.8)$$

and the junction conditions on the brane

$$m^2 G_{ab} + \sigma h_{ab} = \sum_i M_i^3 (K_{ab}^i - h_{ab} K_i) + T_{ab}, \quad (4.9)$$

where  $G_{ab}$  and  $\mathcal{G}_{ab}$  are the Einstein tensors on the brane and in the bulk, respectively, and  $T_{ab}$  is the stress-energy tensor on the brane — the variation of the matter action with respect to  $h_{ab}$ :

$$T_{ab} = \frac{1}{\sqrt{h}} \frac{\delta}{\delta h^{ab}} \int_{\text{brane}} L(h_{ab}, \phi). \quad (4.10)$$

The York–Gibbons–Hawking [371, 372] boundary terms  $-2 \int_{\text{brane}} K_i$  are required for consistency of this variational problem. Treatment of the variational problem in (4.7) with the presence of boundary can be found in Appendix B.1.

### 4.3. Cosmological solutions

A brane with FRW metric

$$ds^2 = -dt^2 + a^2(t) \gamma_{ij}(x) dx^i dx^j, \quad (4.11)$$

where  $\gamma_{ij}(x)$  is the Euclidean metric of the homogeneous and isotropic three-space, is embedded into the Schwarzschild–(anti)-de Sitter solution of the bulk equations (4.8):

$$ds_{\text{bulk}}^2 = -f(r) d\tau^2 + \frac{dr^2}{f(r)} + r^2 \gamma_{ij}(x) dx^i dx^j, \quad (4.12)$$

where <sup>1</sup>

$$f(r) = \kappa - \frac{C}{r^2} - \frac{\Lambda_b}{6} r^2, \quad (4.13)$$

$\kappa = 0, \pm 1$  in this chapter denotes the spatial curvature of the metric  $\gamma_{ij}$ , and  $C$  is an arbitrary constant of integration describing the presence of a black hole in the bulk. The embedding is described by the trajectory

$$r = a(\tau), \quad (4.14)$$

which is the scale factor of the FRW metric (4.11). The cosmological time  $t$  on the brane in (4.11) is then related to the time  $\tau$  in the bulk by

$$\frac{dt}{d\tau} = \sqrt{f(a(\tau)) - \frac{a'(\tau)}{f(a(\tau))}}. \quad (4.15)$$

<sup>1</sup> The variables  $(\tau, r)$  denote the coordinates of the bulk space in this section. Where only one bulk space is under consideration, we omit the index  $i$  and denote the bulk cosmological constant by  $\Lambda_b$ .

The coordinate  $r$  is related to the Gaussian normal coordinate  $y$  in the bulk by

$$y = \int^r \frac{dx}{\sqrt{f(x)}}. \quad (4.16)$$

The extrinsic curvature of the hypersurface (4.14) with unit normal  $n^a$  pointing in the direction of increasing  $r$  is calculated straightforwardly, so that, in the  $t, x^i$  coordinates on the brane, we have

$$K^\alpha{}_\beta - h^\alpha{}_\beta K = \left\{ -\frac{3\sqrt{f(a) - \dot{a}^2}}{a}, -\delta^i{}_j \frac{1}{a^2 \dot{a}} \frac{d}{dt} \left( a^2 \sqrt{f(a) + \dot{a}^2} \right) \right\}, \quad (4.17)$$

where the dot denotes the derivative with respect to  $t$ .

After embedding the brane in the bulk via (4.14), we can make it a boundary by leaving only one of the two sides of the bulk solution,  $r > a(\tau)$  or  $r < a(\tau)$ . This gives rise to one of two possible branches in each of the bulk spaces  $\mathcal{B}_i$ ,  $i = 1, \dots, N$ . Using this fact and substituting (4.17) into the brane equation (4.9), we obtain the following equation for the cosmological evolution of the scale factor  $a(t)$ :

$$H^2 + \frac{\kappa}{a^2} = \frac{\rho + \sigma}{3m^2} + \frac{1}{m^2} \sum_{i=1}^N \zeta_i M_i^3 \sqrt{H^2 + \frac{\kappa}{a^2} - \frac{\Lambda_i}{6} - \frac{C_i}{a^4}}, \quad (4.18)$$

where  $\rho$  is the total energy density of matter on the brane, and  $\zeta_i = \pm 1$  correspond to the two possible ways of bounding each of the bulk spaces  $\mathcal{B}_i$ ,  $i = 1, \dots, N$ , by the brane [505, 506, 510]. The branch with the bulk space  $r > a(\tau)$  corresponds to  $\zeta = 1$ . All the richness of the braneworld homogeneous and isotropic cosmology is encoded in equation (4.18).

The simplest case in braneworld cosmology is, of course,  $N = 1$  in (4.7), where the brane is a boundary of a single bulk space. It is equivalent to the case of arbitrary  $N$  with identical bulk spaces (as was noted in Sec. 4.2, in the case  $N = 2$ , this is called mirror symmetry of reflection of the bulk space with respect to the brane).

For  $N = 1$ , omitting the index  $i$ , we have the cosmological equation on the brane

$$H^2 + \frac{\kappa}{a^2} = \frac{\rho + \sigma}{3m^2} \pm \frac{M^3}{m^2} \sqrt{H^2 + \frac{\kappa}{a^2} - \frac{\Lambda_b}{6} - \frac{C}{a^4}}, \quad (4.19)$$

where the  $\pm$  sign corresponds to the two branches arising from two possible ways of bounding the bulk space by the brane, as described in the previous section.

The cosmological solution based on the Randall–Sundrum model [500, 501], which has  $m = 0$ , is obtained as the lower branch of (4.19) in this limit [511–514]:

$$H^2 + \frac{\kappa}{a^2} = \left( \frac{\rho + \sigma}{3M^3} \right)^2 + \frac{\Lambda_b}{6} + \frac{C}{a^4}. \quad (4.20)$$

Since the last term enters the modified Friedmann equation and has dependence on the scale factor exactly like radiation, it was called “dark radiation” in the literature. The name extends to the term  $C/a^4$  under the square root of (4.19).

The cosmological solution based on the DGP model [504] is obtained by setting  $\sigma = 0$ ,  $C = 0$  and  $\Lambda_b = 0$  in (4.19) [515, 516]:

$$H^2 + \frac{\kappa}{a^2} = \frac{\rho}{3m^2} \pm \frac{M^3}{m^2} \sqrt{H^2 + \frac{\kappa}{a^2}}. \quad (4.21)$$

A remarkable property of this model is that it can describe an accelerating Universe even in the absence of cosmological constants either on the brane or in the bulk. Indeed, the branch with the upper sign in (4.21) in the asymptotic future tends to the de Sitter regime with the Hubble constant

$$H_{\text{DGP}} = \frac{M^3}{m^2}. \quad (4.22)$$

This is the reason why it received the name “self-accelerating branch” in the literature. This simple alternative model of the cosmic acceleration at present appears to be ruled out both observationally and theoretically, since it has a ghost perturbation in its spectrum [517–521]. The branch with the lower sign in (4.21) can self-accelerate only in the presence of cosmological constants; it is called “normal branch” in the literature. The “normal branch” is free from ghosts and is in agreement with all current observations.

The case of  $N = 1$  can be treated in an alternative way. By contracting the Gauss identity

$$R_{abc}{}^d = h_a{}^f h_b{}^g h_c{}^k h^d{}_j \mathcal{R}_{fgk}{}^j + K_{ac} K_b{}^d - K_{bc} K_a{}^d \quad (4.23)$$

on the brane and using Eq. (4.8), one obtains the constraint equation

$$R - 2\Lambda_b + K_{ab} K^{ab} - K^2 = 0, \quad (4.24)$$

which, together with (4.9) taken in the case  $N = 1$ , implies the following closed scalar equation on the brane:

$$\begin{aligned} M^6 (R - 2\Lambda_b) + (m^2 G_{ab} + \sigma h_{ab} - T_{ab}) \left( m^2 G^{ab} + \sigma h^{ab} - T^{ab} \right) - \\ - \frac{1}{3} (m^2 R - 4\sigma + T)^2 = 0, \end{aligned} \quad (4.25)$$

where  $T = h^{ab} T_{ab}$ .

One method for obtaining solutions of the theory consists in first solving the scalar equation (4.25) on the brane together with the stress-energy conservation equation, and then integrating the Einstein equations in the bulk with the given data on the brane [522–524]. The gravitational equations in the bulk can be integrated by using, for example, Gaussian normal coordinates. Specifically, in the Gaussian normal coordinates  $(x, y)$ , where  $x = \{x^\alpha\}$  are the coordinates on the brane and  $y$  is the fifth coordinate in the bulk, the metric in the bulk is written as

$$ds_5^2 = dy^2 + h_{\alpha\beta}(x, y)dx^\alpha dx^\beta. \quad (4.26)$$

Introducing also the tensor of extrinsic curvature  $K_{ab}$  of every hypersurface  $y = \text{const}$  in the bulk, one can obtain the following system of differential equations for the components  $h_{\alpha\beta}$  and  $K^\alpha{}_\beta$ :

$$\begin{aligned} \frac{\partial K^\alpha{}_\beta}{\partial y} &= R^\alpha{}_\beta - K K^\alpha{}_\beta - \frac{1}{6}\delta^\alpha{}_\beta (R + 2\Lambda_b + K^\mu{}_\nu K^\nu{}_\mu - K^2) = \\ &= R^\alpha{}_\beta - K K^\alpha{}_\beta - \frac{2}{3}\delta^\alpha{}_\beta \Lambda_b, \end{aligned} \quad (4.27)$$

$$\frac{\partial h_{\alpha\beta}}{\partial y} = 2h_{\alpha\gamma} K^\gamma{}_\beta, \quad (4.28)$$

where  $R^\alpha{}_\beta$  are the components of the Ricci tensor of the metric  $h_{\alpha\beta}$  induced on the hypersurface  $y = \text{const}$ ,  $R = R^\alpha{}_\alpha$  is its scalar curvature, and  $K = K^\alpha{}_\alpha$  is the trace of the tensor of extrinsic curvature. The second equality in (4.27) is true by virtue of the constraint equation (4.24). Equations (4.27) and (4.28) together with the constraint equation (4.24) represent the 4 + 1 splitting of the Einstein equations in the Gaussian normal coordinates. The initial conditions for these equations are defined on the brane through Eq. (4.9). We emphasize that, to obtain a complete braneworld theory in the general case (including a stability analysis), one must also specify additional conditions in the bulk such as the presence of other branes or certain regularity conditions. In this section, we deal only with the homogeneous and isotropic cosmology on the brane, so this issue does not arise. In this sense, we are studying here the cosmological features common to the whole class of braneworld models described by action (4.7) with arbitrary boundary conditions in the bulk.

#### 4.4. Vacuum and static branes

In this section, we discuss the situation pertaining to a vacuum brane, i.e., when the matter stress-energy tensor  $T_{ab} = 0$ . It is interesting that the brane approaches this condition during the course of cosmological evolution provided it expands forever and its matter density asymptotically

declines to zero. In the simplifying case of  $N = 1$  (brane as a boundary of a single bulk space), Eq. (4.25) takes the form

$$\left(M^6 + \frac{2}{3}\sigma m^2\right) R + m^4 \left(R_{ab}R^{ab} - \frac{1}{3}R^2\right) - 4M^6\Lambda_{\text{RS}} = 0, \quad (4.29)$$

where

$$\Lambda_{\text{RS}} = \frac{\Lambda_{\text{b}}}{2} + \frac{\sigma^2}{3M^6} \quad (4.30)$$

is the expression arising in the Randall–Sundrum model [500, 501].

It is important to note that the second term in Eq. (4.29) has *precisely* the form of one of the terms in the expression for the conformal anomaly, which describes the vacuum polarization at the one-loop level in curved space-time (see, e.g., [421])<sup>2</sup>. It therefore immediately follows that all *symmetric spaces* are solutions of Eq. (4.29) with appropriate  $\Lambda_{\text{RS}}$ , just as they are solutions of the Einstein equations with one-loop quantum-gravitational corrections [525]. Symmetric spaces satisfy the condition  $D_a R_{bcde} = 0$ , which implies that geometrical invariants such as  $R_{abcd}R^{abcd}$ ,  $R_{ab}R^{ab}$ , and  $R$  are constants so that Eq. (4.29) becomes an algebraic equation. Prominent members of this family include:

- the homogeneous and isotropic de Sitter space-time

$$ds^2 = -dt^2 + \frac{1}{H^2} \cosh^2 Ht [d\chi^2 + \sin^2 \chi (d\theta^2 + \sin^2 \theta d\phi^2)], \quad (4.31)$$

where  $-\infty < t < \infty$ ,  $0 \leq \chi, \theta \leq \pi$ ,  $0 \leq \phi \leq 2\pi$ . The four-dimensional metric (4.31) has the property  $R^a_b = 3H^2 h^a_b$ . It formed the basis for Starobinsky's first inflationary model sustained by the quantum conformal anomaly [397];

- the homogeneous and anisotropic Nariai metric [526–528]

$$ds^2 = k^2 (-dt^2 + \cosh^2 t dr^2 + d\theta^2 + \sin^2 \theta d\phi^2), \quad (4.32)$$

where  $k = \text{constant}$ ,  $-\infty < t < \infty$ ,  $0 \leq \theta \leq \pi$ ,  $0 \leq \phi \leq 2\pi$  and for which  $R^a_b = h^a_b/k^2$ . In fact, it is easy to show that any metric for which  $R$  and  $R_{ab}R^{ab}$  are constants will automatically be a solution to Eq. (4.29) with an appropriate choice of  $\Lambda_{\text{RS}}$ .

Both de Sitter space and the Nariai metric belong to the class of space-times which satisfy the vacuum Einstein equations with a cosmological constant

$$R_{ab} = \Lambda_{\text{eff}} h_{ab}. \quad (4.33)$$

---

<sup>2</sup> It is interesting that, while the conformal anomaly term  $R_{ab}R^{ab} - \frac{1}{3}R^2$  cannot be obtained by the variation of a local four-dimensional Lagrangian, the very same term is obtained via the variation of a local Lagrangian in the five-dimensional braneworld theory under investigation.

Such space-times also satisfy Eq. (4.29) if

$$\Lambda_{\text{eff}} = \frac{1}{m^2} \left[ \left( \frac{3M^6}{2m^2} + \sigma \right) \pm \sqrt{\left( \frac{3M^6}{2m^2} + \sigma \right)^2 - 3M^6 \Lambda_{\text{RS}}} \right]. \quad (4.34)$$

Equation (4.34) expresses the resulting cosmological constant on the brane in terms of the coupling constants of the theory. For the Randall–Sundrum model ( $m = 0$ ), one obtains  $\Lambda_{\text{eff}} = \Lambda_{\text{RS}}$ . The two signs in (4.34) again correspond to the two different ways in which the lower-dimensional brane can form the boundary of the higher-dimensional bulk.

The condition  $\Lambda_{\text{RS}} = 0$  is the well-known fine-tuning condition of Randall and Sundrum [500, 501] and leads to the vanishing of the cosmological constant on an empty brane if we set  $m = 0$  in (4.7). Note that, under the Randall–Sundrum condition, expression (4.34) with the sign opposite to the sign of the quantity  $3M^6/2m^2 + \sigma$  also gives a zero value for the resulting cosmological constant on the brane, but the other sign usually leads to  $\Lambda_{\text{eff}} \neq 0$ .

We would like to draw the reader’s attention to the fact that Eq. (4.34) is meaningful only when the expression under the square root is non-negative. When it is negative, solutions describing the corresponding empty Universe simply do not exist. This leads to the following important conclusion: a Universe which contains matter and satisfies

$$\frac{3M^6 \Lambda_{\text{RS}}}{(3M^6/2m^2 + \sigma)^2} > 1, \quad (4.35)$$

*cannot expand forever.*

For the special case  $3M^6/2m^2 + \sigma = 0$ , the expression for  $\Lambda_{\text{eff}}$  on the brane is given by

$$\Lambda_{\text{eff}} = \pm \frac{M^3}{m^2} \sqrt{-3\Lambda_{\text{RS}}}. \quad (4.36)$$

In this case, both  $\sigma$  and  $\Lambda_{\text{RS}}$  must be negative in order that the corresponding empty Universe exist, but the resulting cosmological constant on the brane can be of any sign.

Another interesting example is that of a static empty Universe. The radius (scale factor)  $a$  of such a Universe is easily determined from (4.29) to be

$$a^2 = \frac{\kappa}{\Lambda_{\text{RS}}} \left( \frac{3}{2} + \frac{\sigma m^2}{M^6} \right), \quad (4.37)$$

where  $\kappa = \pm 1$  is the sign of the spatial curvature. One can see that the radius of the Universe can be arbitrarily large. In the general case, the development of this solution to the five-dimensional bulk leads to a Schwarzschild–anti-de Sitter metric. It was shown in [506] that, for  $\kappa = 1$ , this metric is purely



anti-de Sitter (with zero Schwarzschild mass) if the constants of the theory satisfy the condition

$$\frac{\sigma}{m^2} - \frac{\Lambda_b}{2} + \frac{3M^6}{4m^4} = 0, \quad (4.38)$$

which implies negative brane tension  $\sigma$ . It should be pointed out that the static and empty braneworld solution described by (4.37) does not possess a general-relativistic analog, since, in General Relativity, a static cosmological model (the ‘static Einstein Universe’) *cannot* be empty (see, for instance, [236]). Furthermore, from (4.37) we find that the static empty Universe can be spatially open ( $\kappa = -1$ ) – for example, in the case  $\Lambda_{\text{RS}} < 0$  and  $\sigma > -3M^6/2m^2$ , – again a situation without an analog in General Relativity.

For static homogeneous and isotropic braneworlds filled with matter, Eq. (4.25) gives the following relation:

$$a^2 [\rho_{\text{tot}}(\rho_{\text{tot}} + 3p_{\text{tot}}) - 3\Lambda_b M^6] = 3\kappa [m^2(\rho_{\text{tot}} + 3p_{\text{tot}}) - 3M^6], \quad (4.39)$$

where the total energy density  $\rho_{\text{tot}}$  and pressure  $p_{\text{tot}}$  include the contribution from the brane tension, i.e.,

$$\rho_{\text{tot}} = \rho + \sigma, \quad p_{\text{tot}} = p - \sigma, \quad (4.40)$$

and  $\kappa = 0, \pm 1$  corresponds to the sign of the spatial curvature. This relation reduces to (4.37) for  $\rho = p = 0$ .

Having obtained all these solutions on the brane, one can find the corresponding solutions in the bulk by integrating Eqs. (4.27) and (4.28) with the initial conditions on the brane given by Eq. (4.9). In doing this, one can consider various additional conditions in the bulk, for example, the existence of other branes, or one can impose certain regularity conditions. It is worth noting that one and the same cosmological solution on the given brane can correspond to different global solutions in the bulk, for example, other branes may be present or absent, be static or evolving, close or far away from our brane, etc. In the most general case (for instance in the absence of special symmetries on the brane) integration on the brane needs to be performed in conjunction with dynamical integration in the bulk. All such situations must be separately studied and issues such as their stability to linearized perturbations must be examined on a case-by-case basis.

Consider any solution to (4.33) on the brane with effective cosmological constant  $\Lambda_{\text{eff}}$  given by (4.34). It is obvious that the solution of system (4.27), (4.28), describing the metric in the Gaussian normal coordinates  $y \geq 0$  with the brane situated at  $y = 0$ , can be sought for in the form

$$h_{\alpha\beta}(x, y) = f(y)h_{\alpha\beta}(x, 0), \quad K^\alpha{}_\beta = \frac{1}{4}K(y)\delta^\alpha{}_\beta, \quad (4.41)$$

with  $f(0) = 1$ . For this metric, we have

$$R^\alpha{}_\beta(x, y) = \frac{\Lambda_{\text{eff}}}{f(y)} \delta^\alpha{}_\beta, \quad G^\alpha{}_\beta(x, y) = -\frac{\Lambda_{\text{eff}}}{f(y)} \delta^\alpha{}_\beta. \quad (4.42)$$

The brane junction condition (4.9) for the case  $N = 1$  under consideration then gives the initial condition for  $K(y)$ :

$$K(0) = \frac{4}{3M^3} (m^2 \Lambda_{\text{eff}} - \sigma). \quad (4.43)$$

Equations (4.27), (4.28) then lead to a system of differential equations for  $K(y)$  and  $f(y)$ :

$$K' = \frac{4\Lambda_{\text{eff}}}{f} - K^2 - \frac{8}{3}\Lambda_{\text{b}}, \quad (4.44)$$

$$f' = \frac{1}{2}Kf. \quad (4.45)$$

In the simplifying case of a Ricci-flat brane with  $\Lambda_{\text{eff}} = \Lambda_{\text{RS}} = 0$ , we have  $K^2(0) = -8\Lambda_{\text{b}}/3$ , and the solution is

$$K(y) \equiv K(0) = -\frac{4\sigma}{3M^3}, \quad (4.46)$$

$$f(y) = \exp\left(-\frac{2\sigma}{3M^3}y\right) = \exp\left(\pm\sqrt{-\frac{2}{3}\Lambda_{\text{b}}}y\right), \quad (4.47)$$

where the sign in the last exponent depends on the sign of the brane tension. For the flat metric  $h_{\alpha\beta} = \eta_{\alpha\beta}$  on the brane, this gives the famous Randall–Sundrum solution [500, 501].

### 4.5. Properties of braneworld gravity

In this section, we discuss some generic properties of braneworld gravity. We will restrict ourselves to the simplest case  $N = 1$  in (4.7).

Action (4.7) in the case  $N = 1$  has two important scales, namely, the length scale

$$\ell = \frac{2m^2}{M^3}, \quad (4.48)$$

which describes the interplay between the bulk and brane gravity, and the energy scale

$$k_\sigma = \frac{\sigma}{3M^3}, \quad (4.49)$$

which determines the role of the brane tension in the dynamics of the brane. In a model characterized by the Randall–Sundrum constraint [500, 501]

$$\Lambda_{\text{RS}} \equiv \frac{\Lambda_{\text{b}}}{2} + \frac{\sigma^2}{3M^6} = 0, \quad (4.50)$$

the absolute value of  $k_\sigma$  is equal to the inverse curvature  $\ell_{\Lambda_b} = \sqrt{-6/\Lambda_b}$  of the bulk space. Note that  $k_\sigma$  is negative in the case  $\sigma < 0$ . The quantity  $M$  has to be taken positive since, in the opposite case, the massive Kaluza–Klein gravitons become ghosts [529, 530].

Following the procedure first employed in [522] for the Randall–Sundrum (RS) model [500, 501] and subsequently applied in [531] to the more general model under consideration, we make one contraction of indices in the Gauss identity

$$R_{abc}{}^d = h_a{}^f h_b{}^g h_c{}^k h^d{}_j \mathcal{R}_{fgk}{}^j + K_{ac} K_b{}^d - K_{bc} K_a{}^d \quad (4.51)$$

on the brane and, using Eq. (4.8), obtain the equation

$$G_{ab} + \Lambda_{\text{eff}} h_{ab} = 8\pi G_{\text{eff}} T_{ab} + \frac{1}{\beta + 1} \left( \frac{1}{M^6} Q_{ab} - C_{ab} \right), \quad (4.52)$$

where

$$\beta = \frac{2\sigma m^2}{3M^6} = k_\sigma \ell \quad (4.53)$$

is a dimensionless parameter,

$$\Lambda_{\text{eff}} = \frac{\Lambda_{\text{RS}}}{\beta + 1} \quad (4.54)$$

is the effective cosmological constant,

$$8\pi G_{\text{eff}} = \frac{\beta}{\beta + 1} \frac{1}{m^2} \quad (4.55)$$

is the effective gravitational constant,

$$Q_{ab} = \frac{1}{3} E E_{ab} - E_{ac} E^c{}_b + \frac{1}{2} \left( E_{cd} E^{cd} - \frac{1}{3} E^2 \right) h_{ab} \quad (4.56)$$

is a quadratic expression with respect to the “bare” Einstein equation  $E_{ab} \equiv m^2 G_{ab} - T_{ab}$  on the brane, and  $E = h^{ab} E_{ab}$ . The symmetric traceless tensor  $C_{ab} \equiv n^c n^d C_{acbd}$  in (4.52) is a projection of the bulk Weyl tensor  $C_{abcd}$ . It is related to the tensor  $Q_{ab}$  through the covariant conservation equation on the brane

$$D_a (Q^a{}_b - M^6 C^a{}_b) = 0. \quad (4.57)$$

It is important to note that all couplings in Eq. (4.52), including the effective cosmological and gravitational constants, are inversely proportional to  $\beta + 1$ , which indicates that the theory becomes singular for the special case  $\beta = -1$  (see [530, 532]). We are not going to study this degenerate case here.

In the absence of the curvature term on the brane ( $m = 0$ ), we obtain Eq. (4.52) in which  $8\pi G_{\text{eff}} = 2\sigma/3M^6$  is the gravitational constant in the RS model [500, 501], and  $\beta = 0$ ; in this form, Eq. (4.52) was first derived in [522]. The conditions  $\sigma = 0$  and  $\Lambda_b = 0$  are characteristic of the DGP model [504], which also has  $\beta = 0$ . In this model, the effective gravitational constant (4.55)

turns to zero, i.e., the term linear in the stress–energy tensor on the brane vanishes in Eq. (4.52).

Equation (4.52) is not closed on the brane in the sense that it contains the symmetric traceless tensor  $C_{ab}$  whose dynamics on the brane is not determined by the dynamics of matter alone. Some additional information from the bulk is needed to solve the braneworld equations completely, e.g., some boundary conditions in the bulk are to be specified. However, for the homogeneous and isotropic cosmology, this ambiguity manifests itself only in the appearance of the dark-radiation term  $C/a^4$  in (4.19), characterized by one constant.

Consider now some properties of braneworld gravity. The expression for  $Q_{ab}$  in Eq. (4.56) is quadratic in the curvature as well as in the stress–energy tensor. On the other hand, the tensor  $C_{ab}$  is related to  $Q_{ab}$  through the conservation equation (4.57). One might, therefore, expect that the term in the parentheses on the right-hand side of Eq. (4.52), namely  $Q_{ab}/M^6 - C_{ab}$ , will be insignificant on sufficiently large length scales, and that the braneworld theory on those scales should reduce to Einstein gravity with the effective constants given by (4.54) and (4.55). This expectation is borne out by a detailed analysis [530] carried out for a positive-tension brane ( $\sigma > 0$ ) in the specific case when the braneworld satisfies the RS constraint (4.50). In this case, the gravitational potential of a unit mass on large scales (on the positive-tension brane) has the Newtonian form with a small RS correction [530]:

$$V(r) = -\frac{G_{\text{eff}}}{r} \left[ 1 + \frac{2}{3(\beta + 1)(k_\sigma r)^2} \right], \quad k_\sigma r \gg 1, \quad (4.58)$$

where  $G_{\text{eff}}$  is given by (4.55).

On smaller spatial scales,  $k_\sigma r \ll 1, \beta$ , the potential in linear theory again has the Newtonian form with a small logarithmic correction:

$$V(r) = -\frac{\tilde{G}_{\text{eff}}}{r} - \left( \frac{15}{8} + \frac{2}{\beta} \right) \frac{k_\sigma}{3\pi^2 m^2} \log \left[ \left( \frac{15}{8} + \frac{2}{\beta} \right) k_\sigma r \right], \quad k_\sigma r \ll 1, \beta, \quad (4.59)$$

but with a different expression for the effective gravitational constant [530]

$$\tilde{G}_{\text{eff}} = \left[ 1 + \frac{1}{3(1 + \beta)} \right] \frac{1}{8\pi m^2} = \left( 1 + \frac{4}{3\beta} \right) G_{\text{eff}}. \quad (4.60)$$

For  $k_\sigma \rightarrow 0$  (hence, also  $\beta \rightarrow 0$ ), this reproduces the result obtained for the DGP model in [533–535] on scales  $r \ll \ell$ .

It is worth noting that gravity on these smaller scales  $k_\sigma r \ll 1, \beta$ , in principle, involves the massless scalar radion, i.e., it is of scalar–tensor type. As a consequence, for the spherically symmetric solution, it violates the property  $h_{00}(r) = -h_{rr}^{-1}(r)$ , or, in the linear approximation,  $\gamma_{00}(r) = \gamma_{rr}(r)$ , where

$\gamma_{\alpha\beta}(r)$  are the components of metric perturbation in the spherically symmetric coordinate system. Specifically, in the model with the RS constraint  $\Lambda_{\text{RS}} = 0$ , one can obtain the relation:

$$\frac{\Delta\gamma}{\gamma_{00}} \equiv \frac{\gamma_{00} - \gamma_{rr}}{\gamma_{00}} = \frac{1}{1 + 3\beta/4}. \quad (4.61)$$

Since there are stringent experimental upper bounds [467, 469] on the left-hand side of (4.61) in the neighborhood of the solar system (it should not exceed  $10^{-5}$  by order of magnitude), if solution (4.59) were applicable in this domain, it would imply that only very large values of  $\beta$  are permissible in the braneworld theory under consideration [namely, the braneworld model (4.7) with  $N = 1$  and with the RS constraint (4.50)].

We should stress, however, that the applicability region of the linear approximation (4.59) is bounded from below by a length scale which depends upon the mass of the central source, as has been demonstrated for the DGP model in [533–535]. Specifically, the dynamics of the radion develops strong non-linear corrections on sufficiently small scales, leading to the breakdown of linearized theory. (This also creates the so-called strong-coupling problem in the DGP model [536, 537].) In this case, in order to study gravity at small distances from the source, one should turn to the fully non-linear theory.

To determine the distances at which the linearized theory breaks down and to establish the correct behavior of the potential on such scales, we turn to the effective equation (4.52). Taking the trace of Eq. (4.52), we get the following closed scalar equation on the brane:

$$-R + 4\Lambda_{\text{eff}} - 8\pi G_{\text{eff}}T = \frac{Q}{(\beta + 1)M^6}, \quad (4.62)$$

where the left-hand side contains terms which are linear in the curvature and in the stress–energy tensor while the right-hand side contains the quadratic term  $Q = h^{ab}Q_{ab}$ .

Suppose that we are interested in the behavior of gravity in the neighborhood of a spherically symmetric source with density  $\rho_s$ , total mass  $\mathcal{M}_s$ , and radius  $r_s$ . First of all, we assume that one can neglect the tensor  $C_{ab}$  and the effective cosmological constant in the neighborhood of the source. As regards the effective cosmological constant, this assumption is natural since the observed cosmological constant is small. Concerning the tensor  $C_{ab}$ , its smallness in the neighborhood of the source represents some additional condition on the spherically symmetric solution. A condition of this sort is likely to arise in any consistent and viable braneworld theory as, without it, one has a large number of spherically symmetric solutions on the brane, many of them non-physical (see [538] for a comprehensive treatment in the framework of the RS model).

Within the source itself, we have two qualitatively different options: an approximate solution can be sought either neglecting the quadratic part or linear part of Eqs. (4.52) and (4.62). We should choose the option that gives smaller error of approximation in Eq. (4.62). In the first case, neglecting the quadratic part and the effective cosmological constant, we have

$$G_{ab} - 8\pi G_{\text{eff}} T_{ab} \approx 0 \Rightarrow \frac{Q}{(\beta + 1)M^6} \sim \frac{\rho_s^2}{(\beta + 1)^3 M^6}. \quad (4.63)$$

In the second case, we neglect the linear part, so that

$$Q_{ab} \approx 0 \Rightarrow E_{ab} \approx 0 \Rightarrow R + 8\pi G_{\text{eff}} T \sim \frac{\rho_s}{(\beta + 1)m^2}. \quad (4.64)$$

The final expression on the right-hand side of (4.64) is smaller than the corresponding expression in (4.63) if

$$\rho_s > (\beta + 1)^2 \frac{M^6}{m^2} \Rightarrow r_s^3 < r_*^3 \sim \frac{\mathcal{M}_s \ell^2}{(\beta + 1)^2 m^2}, \quad (4.65)$$

where we have used the relation  $\mathcal{M}_s \sim \rho_s r_s^3$ . Thus, we can expect that, in the neighborhood of the source, on distances smaller than  $r_*$  given by (4.65), the solution is determined mainly by the quadratic part  $Q_{ab}$  in Eq. (4.52), which means that it respects the “bare” Einstein equation  $m^2 G_{ab} = T_{ab}$  to a high precision. This effect is sometimes described as the “gravity filter” of the DGP model [504], which screens the scalar graviton in the neighborhood of the source making the gravity effectively Einsteinian. Some aspects of this interesting phenomenon are discussed in [539, 540].

Expression (4.65) generalizes the length scale [533–535] of the DGP model, below which non-linear effects become important, to the case of non-zero brane tension (non-zero  $\beta$ ) and bulk cosmological constant satisfying the RS constraint (4.50). The observable gravitational constant on scales much smaller than  $r_*$  is then given by

$$8\pi G_{\text{obs}} = \frac{1}{m^2}. \quad (4.66)$$

For the Sun, the scale  $r_*$  is estimated as

$$r_*^\odot \sim \frac{10^{16} \text{ km}}{(\beta + 1)^{2/3} \Omega_\ell^{1/3}}, \quad (4.67)$$

where  $\Omega_\ell = 1/\ell^2 H_0^2$ . For interesting values of  $\beta \sim 1$  and  $\Omega_\ell \sim 1$ , this distance will be very large. The corresponding radius for the Earth is smaller only by two orders of magnitude.

This, however, is not the full story. As argued in [541, 542], the gravitational potential of a spherically symmetric body on scales  $r_* \lesssim r \ll \ell$  is corrected by the cosmological expansion. Moreover, the critical scale  $r_*$  becomes dependent

on the value of the Hubble parameter, and can be different from (4.65) for values of  $\ell$  of the order of the Hubble length. One also should note that gravity on scales  $r \ll r_*$ , although close to Einstein gravity, is not exactly Einsteinian, and these deviations can be used to test braneworld theory on solar-system scales [533–535, 541–543]. Specifically, in the case of the DGP model ( $m = 0$ ,  $\sigma = 0$  and  $\Lambda_b = 0$ ), the authors of [541, 542] obtain a small correction to the locally static metric:

$$ds^2 = -[1 + 2n(r)] dt^2 + [1 + 2a(r)] dr^2 + r^2 [1 + 2b(r)] d\Omega^2. \quad (4.68)$$

Here,

$$a(r) = \frac{r_g}{2r} [1 - \delta(r)] + \frac{1}{2} H^2 r^2, \quad (4.69)$$

and  $n(r)$  satisfies the differential equation

$$rn'(r) = \frac{r_g}{2r} [1 + \delta(r)] - H^2 r^2, \quad (4.70)$$

where

$$\delta(r) = \frac{3r^3}{\ell^2 r_g} (1 \pm \ell H) \left[ \sqrt{1 + \frac{2\ell^2 r_g}{9r^3 (1 \pm \ell H)^2}} - 1 \right], \quad (4.71)$$

and  $r_g = \mathcal{M}/4\pi m^2$  is the gravitational radius of a central body. For

$$r \ll r_* = \left( \frac{r_g}{H^2} \right)^{1/3}, \quad (4.72)$$

one obtains

$$n(r) = -\frac{r_g}{2r} \pm \sqrt{\frac{2r_g r}{\ell^2}}, \quad a(r) = \frac{r_g}{2r} \mp \sqrt{\frac{r_g r}{4\ell^2}}. \quad (4.73)$$

The last terms in these expressions, in particular, lead to orbit precession with constant rate

$$\frac{d}{dt} \Delta\phi_{\text{DGP}} = \mp \frac{3}{4\ell} = \mp 5 \frac{\mu\text{as}}{\text{year}} \quad (4.74)$$

for the value of  $\ell \simeq 10$  Gpc, which is a best-fit value for the DGP cosmological model by supernovae Ia.

Although the preceding reasoning is applicable to both the positive-tension and the negative-tension brane, the current understanding of the braneworld gravitational physics supports only the positive-tension case. From Eq. (4.52), one might expect that a negative-tension brane will show reasonable physical behavior in the case  $|\beta| > 1$  (note that  $\beta < 0$  for a negative-tension brane), in which the gravitational constant (4.55) is positive. However, direct calculation (along the lines of [530]) in the two-brane model with the RS constraint (4.50) shows that, in this case, the gravitational interaction between material bodies on large scales is dominated by the ghost-like radion, with the effective gravitational coupling

$$G_{\text{radion}} = -\frac{1}{3} G_{\text{eff}}, \quad k_\sigma r \gg 1, \quad (4.75)$$

where  $G_{\text{eff}}$  is given by the same expression (4.55). The radion-dominated gravity on these scales is formally attractive in the case  $G_{\text{eff}} < 0$ , and is repulsive for  $G_{\text{eff}} > 0$ . However, on smaller spatial scales  $k_{\sigma} r_* \lesssim k_{\sigma} r \ll 1, |\beta|$ , Newton's law similar to (4.59) is reproduced with the gravitational constant given by (4.60), which is positive if  $|\beta| > 4/3$ . The gravity on these scales is of scalar-tensor character. On still smaller distances from the central source,  $r < r_*$ , the theory may approach Einstein gravity with the effective gravitational constant (4.66).

#### 4.6. Phantom property of braneworld dark energy

We proceed in this section to a more detailed investigation of the specific features of braneworld cosmology. The first such interesting feature is the phantom-like behavior of the dark energy in a braneworld, which is a generic property of one of the branches in (4.19). This equation can be solved with respect to the Hubble parameter:

$$H^2 + \frac{\kappa}{a^2} = \frac{\rho + \sigma}{3m^2} + \frac{2}{\ell^2} \left[ 1 \pm \sqrt{1 + \ell^2 \left( \frac{\rho + \sigma}{3m^2} - \frac{\Lambda_b}{6} - \frac{C}{a^4} \right)} \right], \quad (4.76)$$

where  $\ell$  is given by (4.48).

It is convenient to introduce the dimensionless cosmological parameters

$$\begin{aligned} \Omega_m &= \frac{\rho_0}{3m^2 H_0^2}, & \Omega_{\kappa} &= -\frac{\kappa}{a_0^2 H_0^2}, & \Omega_{\sigma} &= \frac{\sigma}{3m^2 H_0^2}, \\ \Omega_{\ell} &= \frac{1}{\ell^2 H_0^2}, & \Omega_{\Lambda_b} &= -\frac{\Lambda_b}{6H_0^2}, & \Omega_C &= -\frac{C}{a_0^4 H_0^2}, \end{aligned} \quad (4.77)$$

where the subscript “0” refers to the current values of cosmological quantities. The cosmological equation (4.76) with the energy density  $\rho$  dominated by dust-like matter can now be written in the form:

$$\begin{aligned} \frac{H^2(z)}{H_0^2} &= \Omega_m(1+z)^3 + \Omega_{\kappa}(1+z)^2 + \Omega_{\sigma} + \\ &+ 2\Omega_{\ell} \pm 2\sqrt{\Omega_{\ell}} \sqrt{\Omega_m(1+z)^3 + \Omega_{\sigma} + \Omega_{\ell} + \Omega_{\Lambda_b} + \Omega_C(1+z)^4}. \end{aligned} \quad (4.78)$$

The model satisfies the constraint equation

$$\Omega_m + \Omega_{\kappa} + \Omega_{\sigma} \pm 2\sqrt{\Omega_{\ell}} \sqrt{1 - \Omega_{\kappa} + \Omega_{\Lambda_b} + \Omega_C} = 1 \quad (4.79)$$

reducing the number of independent  $\Omega$  parameters. The sign choices in Eqs. (4.78) and (4.79) always correspond to each other if  $1 - \Omega_{\kappa} + \Omega_{\Lambda_b} + \Omega_C > > \Omega_{\ell}$ . This condition is necessary for the model to have physical meaning and we assume it to be valid in what follows. The signs in (4.79) correspond to the two possible ways of bounding the Schwarzschild–(anti)-de Sitter bulk space by the brane [505, 506, 510], as discussed in Sec. 4.3.



In what follows, we consider a spatially flat Universe ( $\kappa = 0$ ) without dark radiation ( $C = 0$ ). In the physical case  $1 + \Omega_{\Lambda_b} > \Omega_\ell$ , substituting  $\Omega_\sigma$  from (4.79) into (4.78), we get

$$\begin{aligned} \frac{H^2(z)}{H_0^2} &= \Omega_m(1+z)^3 + 1 - \Omega_m + 2\Omega_\ell \mp 2\sqrt{\Omega_\ell} \sqrt{1 + \Omega_{\Lambda_b}} \pm \\ &\pm 2\sqrt{\Omega_\ell} \sqrt{\Omega_m(1+z)^3 - \Omega_m + \left(\sqrt{1 + \Omega_{\Lambda_b}} \mp \sqrt{\Omega_\ell}\right)^2}. \end{aligned} \quad (4.80)$$

The cosmological models with the lower and upper sign were called BRANE1 and BRANE2 models in [308], respectively. In the physical region of parameters, they are equivalent to the previously introduced “normal” and “self-accelerating” branches, respectively. As we noted already in Sec. 4.3, the latter name is obtained due to the property of the branch with the upper sign that, even in the absence of cosmological constants on the brane ( $\sigma = 0$ ) and in the bulk space ( $\Lambda_b = 0$ ), one passes to the de Sitter space in the future with the asymptotic Hubble parameter that follows from (4.78):

$$H_{\text{DGP}}^2 = 4H_0^2\Omega_\ell. \quad (4.81)$$

Typical values of the  $\Omega$  parameters (4.77) that we consider in this section are of order  $\Omega \sim 1$ . For such values, the fundamental constants of the theory have the following orders of magnitude:

$$m^2 \simeq M_{\text{P}}^2 \sim 10^{19} \text{ GeV}, \quad M \sim 100 \text{ MeV}, \quad \Lambda_b \sim \frac{\sigma}{m^2} \sim H_0^2 \sim 10^{-56} \text{ cm}^{-2}. \quad (4.82)$$

The smallness of the bare cosmological constants in the bulk and on the brane represents a fine-tuning similar to what is the case for the cosmological constant in the standard  $\Lambda$ CDM (or  $\Lambda$ CDM) model. However, even with such small values of the bare cosmological constants in action (4.7), the braneworld model of dark energy exhibits qualitatively new properties when compared to the case where these constants are set to zero.

Observations of high-redshift type Ia supernovae indicate that these objects are fainter than they would be in a standard cold dark matter cosmology (SCDM) with  $\Omega_m = 1$  [3]. This observation is taken as support for a Universe which is accelerating, fueled by a form of energy with negative pressure (dark energy). In standard FRW cosmology the acceleration of the Universe is described by the equation

$$\frac{\ddot{a}}{a} = -\frac{4\pi G}{3} \sum_i (\rho_i + 3p_i), \quad (4.83)$$

where the summation is over all matter fields contributing to the dynamics of the Universe. It is easy to show that a necessary (but not sufficient) condition

for acceleration ( $\ddot{a} > 0$ ) is that the strong energy condition is violated for *at least one* of the matter fields in (4.83), so that  $\rho + 3p < 0$ . In the case of the popular LCDM model, this requirement is clearly satisfied since  $p_m = 0$  in pressureless (cold) matter, while  $p_\Lambda = -\rho_\Lambda \equiv -\Lambda/8\pi G$  in the cosmological constant.

The situation with respect to braneworld models is different since the braneworld evolution is distinct from FRW evolution at late times. However it is easy to show that braneworld models can accelerate. We demonstrate this by noting that a completely general expression for the deceleration parameter  $q = -\ddot{a}/aH^2$  is provided by

$$q(z) = \frac{H'(z)}{H(z)}(1+z) - 1, \quad (4.84)$$

where the derivative is with respect to  $z$ . In our case,  $H(z)$  is given by (4.78) or (4.80), and the current value of the deceleration parameter is easily calculated to be

$$q_0 = \frac{3}{2}\Omega_m \left( 1 - \frac{\sqrt{\Omega_\ell}}{\sqrt{\Omega_\ell} \mp \sqrt{1 + \Omega_{\Lambda_b}}} \right) - 1, \quad (4.85)$$

where the lower and upper signs correspond to BRANE1 and BRANE2 models, respectively. The present Universe will accelerate for brane parameter values which satisfy  $q_0 < 0$ .

Observationally, a pivotal role in the case for an accelerating Universe is played by the *luminosity distance*  $d_L(z)$ , since the flux of light received from a distant source varies inversely to the square of the luminosity distance,  $F \propto d_L^{-2}$ . This effect is quantitatively described by the magnitude–luminosity relation:  $m_B = M_0 + 25 + 5 \log_{10} d_L$ , where  $m_B$  is the corrected apparent peak  $B$  magnitude and  $M_0$  is the absolute peak luminosity of the supernova. A supernova will therefore appear fainter in a Universe which possesses a larger value of the luminosity distance to a given redshift.

In a FRW Universe, the luminosity distance (1.23) is determined by the Hubble parameter and three-dimensional spatial curvature as [236]

$$d_L(z) = \frac{1+z}{H_0 \sqrt{|\Omega_{\text{total}} - 1|}} S(\eta_0 - \eta), \quad (4.86)$$

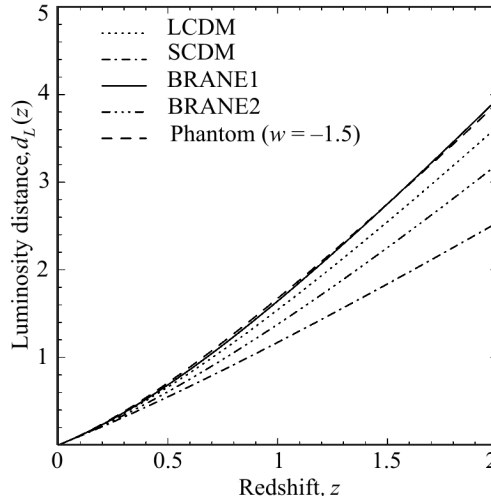
where

$$\eta_0 - \eta = H_0 \sqrt{|\Omega_{\text{total}} - 1|} \int_0^z \frac{dz'}{H(z')}, \quad (4.87)$$

and  $S(x)$  is defined as follows:  $S(x) = \sin x$  if  $\kappa = 1$  ( $\Omega_{\text{total}} > 1$ ),  $S(x) = \sinh x$  if  $\kappa = -1$  ( $\Omega_{\text{total}} < 1$ ), and  $S(x) = x$  if  $\kappa = 0$  ( $\Omega_{\text{total}} = 1$ ). For a spatially flat Universe under consideration in this section, Eq. (1.23) or (4.86) simplifies to

$$d_L(z) = (1+z) \int_0^z \frac{dz'}{H(z')}. \quad (4.88)$$

**Fig. 4.3.** The luminosity distance is shown as a function of redshift for the two braneworld models BRANE1 & BRANE2, LCDM, SCDM, and ‘phantom energy’. All models, with the exception of SCDM, have  $\Omega_m = 0.3$ . SCDM has  $\Omega_m = 1$ . The BRANE1 & BRANE2 models have  $\Omega_\ell = 0.3$  and vanishing cosmological constant in the bulk. LCDM and the phantom model have the same dark energy density  $\Omega_\Lambda = \Omega_X = 0.7$ . The equation of state for dark energy is  $w_\Lambda = -1$  for LCDM and  $w = p_X/\rho_X = -1.5$  for phantom. The luminosity distance is greatest for BRANE1 & phantom, and least for SCDM. BRANE1 & BRANE2 lie on either side of LCDM



In Fig. 4.3 we show the luminosity distances for the BRANE1 & BRANE2 models. Also shown for comparison is the value of  $d_L(z)$  in a spatially-flat two-component FRW Universe with the Hubble parameter

$$H(z) = H_0 \left[ \Omega_m (1+z)^3 + \Omega_X (1+z)^{3(1+w)} \right]^{1/2}, \quad (4.89)$$

where  $\Omega_X$  describes dark energy with equation of state  $w = p_X/\rho_X$ . Three cosmological models will be of interest to us in connection with (4.89):

- (i) **SCDM:** The standard cold dark matter Universe with  $\Omega_m = 1$  and  $\Omega_X = 0$ .
- (ii) **LCDM:** Cold dark matter + a cosmological constant with  $w = -1$ .
- (iii) **Phantom models:** Cold dark matter + ‘phantom energy’ satisfying  $w < -1$  [51].

We find from Fig. 3 that the luminosity distance in both braneworld models exceeds that in SCDM. In fact, BRANE1 models have the unusual feature that their luminosity distance can even exceed that in LCDM (for a fixed value of  $\Omega_m$ ). In fact it can easily be shown that

$$d_L^{\text{dS}}(z) \geq d_L^{\text{BRANE1}}(z) \geq d_L^{\text{LCDM}}(z), \quad (4.90)$$

where  $d_L^{\text{dS}}(z)$  refers to the luminosity distance in the spatially flat coordinatization of de Sitter space (equivalently, the steady state Universe). The second inequality presumes a fixed value of  $\Omega_m$ . BRANE2 models show complementary behavior

$$d_L^{\text{LCDM}}(z) \geq d_L^{\text{BRANE2}}(z) \geq d_L^{\text{SCDM}}(z), \quad (4.91)$$

where the first inequality is valid for a fixed value of  $\Omega_m$ . In the case  $\Omega_\ell = 0$ , the equations of the braneworld theory formally reduce to those of General Relativity, and we have  $d_L^{\text{BRANE1}}(z) = d_L^{\text{BRANE2}}(z) = d_L^{\text{LCDM}}(z)$ .

One might add that the behavior of BRANE1 is mimicked by FRW models with  $w \leq -1$ , whereas BRANE2 resembles dark energy with  $-1 \leq w \leq 0$  [236]. In fact, from Fig. 4.3 we see that the luminosity distance in the BRANE1 model is quite close to what one gets from ‘phantom energy’ described by (4.89) with  $w = -1.5$ . (The parameters for this BRANE1 model are  $\Omega_m = \Omega_\ell = 0.3$ ,  $\Omega_{\Lambda_b} = 0$ , and  $\Omega_\sigma = 1 - \Omega_m + 2\sqrt{\Omega_\ell} \approx 1.8$ .) It should be pointed out that phantom energy models were introduced by Caldwell [51], who made the observation that dark energy with  $w < -1$  appeared to give a better fit to the current supernova observations than LCDM (which has  $w = -1$ ). However, the models with phantom energy have several bizarre properties, some of which are summarized below (see also [51, 544]):

(i) A negative equation of state suggests that the effective velocity of sound in the medium  $v = \sqrt{|dp/d\rho|}$  can become larger than the velocity of light.

(ii) The expansion factor of a Universe dominated by phantom energy grows as

$$a(t) \simeq a(t_{\text{eq}}) \left[ (1+w) \frac{t}{t_{\text{eq}}} - w \right]^{2/3(1+w)}, \quad w < -1, \quad (4.92)$$

where  $t_{\text{eq}}$  marks the epoch when the densities in matter and phantom energy are equal:  $\rho_m(t_{\text{eq}}) \simeq \rho_X(t_{\text{eq}})$ . It immediately follows that the scale factor diverges in a *finite* amount of cosmic time

$$a(t) \rightarrow \infty \quad \text{as} \quad t \rightarrow t_* = \left( \frac{w}{1+w} \right) t_{\text{eq}}. \quad (4.93)$$

Substitution of  $z \rightarrow -1$  and  $w < -1$  in (4.89) shows that the Hubble parameter also diverges as  $t \rightarrow t_*$ , implying that an infinitely rapid expansion rate for the Universe has been reached in the *finite* future.

As the Universe expands, the density of phantom energy ( $w < -1$ ) *grows* instead of decreasing ( $w > -1$ ) or remaining constant ( $w = -1$ ),

$$\rho(t) \propto \left[ (1+w) \frac{t}{t_{\text{eq}}} - w \right]^{-2}, \quad (4.94)$$

reaching a singular value in a finite interval of time  $\rho(t) \rightarrow \infty$ ,  $t \rightarrow t_*$ . This behavior should be contrasted with the density of ordinary matter which drops to zero:  $\rho_m \rightarrow 0$  as  $t \rightarrow t_*$ . A Universe dominated by phantom energy is thus doomed to *expand towards a physical singularity* which is reached in a finite amount of proper time. (An exact expression for the time of occurrence of the

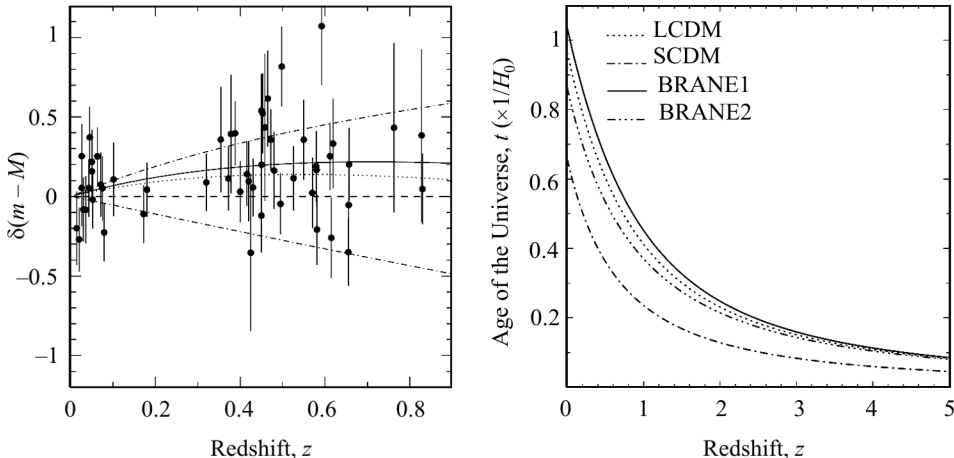


**Fig. 4.4.** The distance modulus ( $m - M$ ) of Type Ia supernovae (the primary fit of the Supernova cosmology project) is shown relative to an empty  $\Omega_m \rightarrow 0$  Milne Universe (dashed line). The solid line refers to the distance modulus in BRANE1 with  $\Omega_\ell = \Omega_m = 0.3$ , and vanishing cosmological constant in the bulk. The dotted line (below the solid) is LCDM with  $(\Omega_\Lambda, \Omega_m) = (0.7, 0.3)$ . The uppermost and lowermost (dot-dashed) lines correspond to de Sitter space  $(\Omega_\Lambda, \Omega_m) = (1, 0)$  and SCDM  $(\Omega_\Lambda, \Omega_m) = (0, 1)$ , respectively. Figure taken from [308]

**Fig. 4.5.** The age of the Universe (in units of the inverse Hubble parameter) is plotted as a function of the cosmological redshift for the models discussed in Fig. 4.3. (The phantom model is not shown.) BRANE1 models have the oldest age while SCDM is youngest. Figure taken from [308]

phantom singularity can be found in [545], which also contains an interesting discussion of related issues.)

At this stage one must emphasize that, although the BRANE1 model has several features in common with phantom energy (which is the reason why it also provides a good fit to supernova data; see Fig. 4.4 as an illustration), it is not necessarily afflicted with phantom's pathologies. Indeed, in a broad range of parameters, both BRANE1 and BRANE2 are physically well motivated and remain *well behaved during all times*. The model safely passes both the geometrical tests using supernovae type Ia and baryon acoustic oscillations [546,547] and the tests connected with the integrated Sachs–Wolfe effect [548]. The development of braneworld cosmology, therefore, added an important new dimension to the debate about the acceleration of the Universe by showing that cosmological models with  $d_L(z) > d_L^{\text{LCDM}}(z)$  are possible to construct within the framework of the braneworld scenario and should be taken seriously.

The angular diameter distance  $d_A$  is related to the luminosity distance  $d_L$  through the equation (see Sec. 1.4)

$$d_A(z) = \frac{d_L(z)}{(1+z)^2}. \quad (4.95)$$

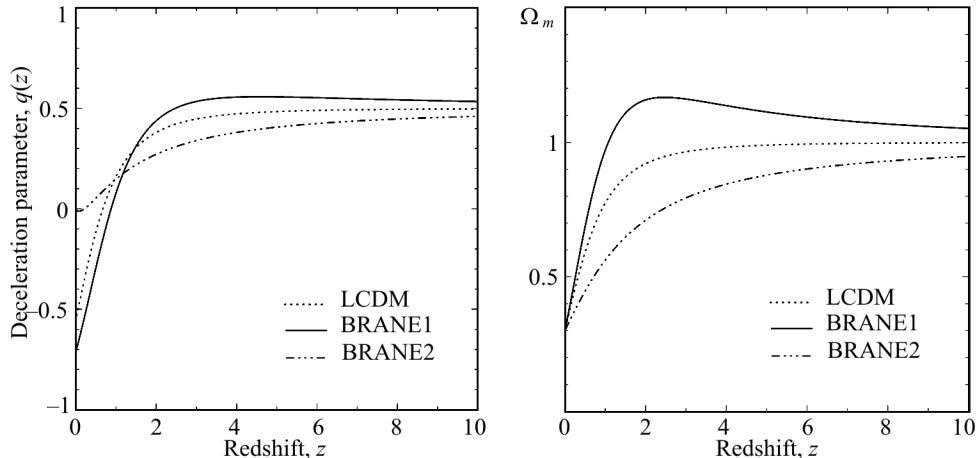


**Fig. 4.6.** The deceleration parameter  $q(z)$  is shown for BRANE1, BRANE2 and LCDM. The model parameters are as in Fig. 4.3. For reference it should be noted that  $q = 0.5$  for SCDM while de Sitter space has  $q = -1$ . Figure taken from [308]

**Fig. 4.7.** The dimensionless matter density  $\Omega_m(z)$  is shown for the two braneworld models and LCDM. ( $\Omega_m = 1$  in SCDM.) Parameter values are the same as in previous figures. BRANE1 has the interesting feature that  $\Omega_m(z)$  *exceeds unity* for  $z \gtrsim 1$ . Figure taken from [308]

Therefore, much of the above analysis carries over when one discusses properties of the angular diameter distance within the framework of braneworld models. Some cosmological features of braneworld models are shown in Figs. 4.5–4.7. In Fig. 4.5, the age of the Universe at a given cosmological redshift

$$t(z) = \int_z^\infty \frac{dz'}{(1+z')H(z')} \quad (4.96)$$

is shown for the two braneworld models and for LCDM & SCDM. We find that the age of the Universe in BRANE1 (BRANE2) is larger (smaller) than in LCDM for identical values of the cosmological density parameter  $\Omega_m$ . This is a direct consequence of the fact that the Hubble parameter in BRANE1 (BRANE2) is smaller (larger) than in LCDM. Both braneworld models are significantly older than SCDM.

Considerable insight into the dynamics of the Universe is provided by the cosmological deceleration parameter (4.84). The results obtained in [308], shown in Fig. 4.6, indicate that at late times the BRANE1 (BRANE2) Universe accelerates at a faster (slower) rate than LCDM (with identical  $\Omega_m$ ). Curiously, the BRANE1 Universe shows an earlier transition from deceleration to acceleration than any of the other models. (For the given choice of parameters this transition takes place at  $z \simeq 1$  for BRANE1 and at  $z \simeq 0.7$  for LCDM. The

BRANE2 model begins accelerating near the present epoch at  $z \simeq 0$ .) A related point of interest is that at  $z \gtrsim 2$  the deceleration parameter in BRANE1 marginally exceeds that in SCDM indicating that the BRANE1 model is decelerating at a faster rate than SCDM ( $q = 0.5$ ). In conventional models of dark matter this behavior can occur only if the equation of state of the dark component is stiffer than dust, implying  $w > 0$  in (4.89), or if the Universe is spatially closed. On the other hand, the current *acceleration* rate of BRANE1 in our example ( $q_0 \simeq -0.7$ ) significantly exceeds that of LCDM ( $q_0 \simeq -0.55$ ) with an identical value of  $\Omega_m = 0.3$  in both models. Within the framework of four-dimensional Einstein gravity, this situation can only arise if the equation of state of dark energy is strongly negative:  $w < -1$  in (4.89).

The unusual high- $z$  behavior of the deceleration parameter in BRANE1 can be better understood if we consider the cosmological density parameter

$$\Omega_m(z) = \left[ \frac{H_0}{H(z)} \right]^2 \Omega_m(0)(1+z)^3. \quad (4.97)$$

Here  $H(z)$  again should be given by (4.80) for braneworld models. From Fig. 4.7 we notice that, for  $z \gtrsim 1$ , the value of  $\Omega_m(z)$  in BRANE1 *exceeds* its value in SCDM ( $\Omega_m = 1$ ). This is precisely the redshift range during which  $q(z)_{\text{BRANE1}} > q(z)_{\text{SCDM}}$ . Thus, the rapid deceleration of BRANE1 at high redshifts can be partly attributed to the larger value of the matter density  $\Omega_m(z)$  at those redshifts, relative to SCDM.

Having established partial similarity of BRANE1 with phantom models at low redshifts, we can investigate the analogy further and calculate the effective equation of state of dark energy

$$w(z) = \frac{2q(z) - 1}{3[1 - \Omega_m(z)]}, \quad (4.98)$$

where  $\Omega_m(z)$  is given by (4.97). One notes that  $w(z)$  has a pole-like singularity at  $z \simeq 1$  for BRANE1, which arises because  $\Omega_m(z)$  crosses the value of unity at  $z \simeq 1$  (see Fig. 4.7). This demonstrates that the notion of ‘effective equation of state’ is of limited utility for this model. Equations (4.80), (4.84), and (4.98) also illustrate the important fact that dark energy in braneworld models, though similar to phantom energy in some respects, differ from it in others. For instance, in both braneworld models,  $w(z) \rightarrow -0.5$  at  $z \gg 1$  and  $w(z) \rightarrow -1$  as  $z \rightarrow -1$ , whereas phantom energy has  $w(z) < -1$  at *all* times.

A useful quantity is the *current value* of the effective equation of state of dark energy in braneworld theories:

$$w_0 = \frac{2q_0 - 1}{3(1 - \Omega_m)} = -1 - \left( \frac{\Omega_m}{1 - \Omega_m} \right) \frac{\sqrt{\Omega_\ell}}{\sqrt{\Omega_\ell} \mp \sqrt{1 + \Omega_{\Lambda_b}}}, \quad (4.99)$$

where the lower and upper signs, as usual, correspond to BRANE1 and BRANE2 models, respectively. We easily see that  $w_0 < -1$  for BRANE1, whereas  $w_0 > -1$  for BRANE2.

The reason for the effect of phantom-like behavior of the BRANE1 model can be seen directly from equation (4.78) or (4.80), which can be written in the form

$$\frac{H^2(z)}{H_0^2} = \Omega_m(1+z)^3 + \Omega_{\Lambda_{\text{eff}}}(z), \quad (4.100)$$

where

$$\begin{aligned} \Omega_{\Lambda_{\text{eff}}}(z) &= \Omega_\sigma + 2\Omega_\ell \pm 2\sqrt{\Omega_\ell} \sqrt{\Omega_m(1+z)^3 + \Omega_\sigma + \Omega_\ell + \Omega_{\Lambda_b}} = \\ &= 1 - \Omega_m + 2\Omega_\ell \mp 2\sqrt{\Omega_\ell} \sqrt{1 + \Omega_{\Lambda_b}} \pm \\ &\pm 2\sqrt{\Omega_\ell} \sqrt{\Omega_m(1+z)^3 - \Omega_m + \left(\sqrt{1 + \Omega_{\Lambda_b}} \mp \sqrt{\Omega_\ell}\right)^2} \end{aligned} \quad (4.101)$$

is the omega parameter for the effective time-dependent cosmological constant. One can see that, for the branch with the lower sign (BRANE1),  $\Omega_{\Lambda_{\text{eff}}}(z)$  increases with time, while, for the branch with the upper sign (BRANE2), it decreases. This explains the properties (4.90) and (4.91).

### 4.7. Disappearing dark energy

The braneworld models admit an intriguing possibility that the current acceleration of the Universe may not be a lasting feature. It may be recalled that most models of dark energy, including the cosmological constant, have the property that, once the Universe begins to accelerate, it accelerates forever. Although this is not a problem from the viewpoint of cosmology; nevertheless, as shown in a number of papers, an eternally accelerating Universe is endowed with a cosmological event horizon which prevents the construction of a conventional S-matrix describing particle interactions within the framework of string or M-theory [549–551]. In this section we show that, provided the Randall–Sundrum constraint relation (4.50) is satisfied, the acceleration of the Universe can be a transient phenomenon in braneworld models. An anisotropic solution of Bianchi V class with the same feature was described in [552].

From Eq. (4.80) we obtain the following asymptotic expressions for the Hubble parameter  $H_\infty$  as  $z \rightarrow -1$ , assuming that the Universe expands forever:

$$\left(\frac{H_\infty}{H_0}\right)^2 = \Omega_\sigma + 2\Omega_\ell \pm 2\sqrt{\Omega_\ell} \sqrt{\Omega_\sigma + \Omega_\ell + \Omega_{\Lambda_b}}, \quad (4.102)$$

where the lower and upper signs correspond to BRANE1 and BRANE2 models, respectively. In applying the Randall–Sundrum constraint (4.50), we first



consider the case where  $\Omega_\sigma > 0$ . Then

$$\Omega_\sigma = 2\sqrt{\Omega_\ell \Omega_{\Lambda_b}} \quad (4.103)$$

and

$$\left(\frac{H_\infty}{H_0}\right)^2 = 2\sqrt{\Omega_\ell} \left[ \sqrt{\Omega_\ell} + \sqrt{\Omega_{\Lambda_b}} \pm \left( \sqrt{\Omega_\ell} + \sqrt{\Omega_{\Lambda_b}} \right) \right]. \quad (4.104)$$

One can see that this expression vanishes for the lower sign. Thus, for positive  $\Omega_\sigma$ , it is the BRANE1 model that leads to vanishing effective cosmological constant in the future. However, in this case, the constraint equation (4.79) becomes

$$\Omega_m - 2\sqrt{\Omega_\ell} \left( \sqrt{1 + \Omega_{\Lambda_b}} - \sqrt{\Omega_{\Lambda_b}} \right) = 1 \quad (4.105)$$

and implies  $\Omega_m > 1$ , which is hardly compatible with the observations.

In the case of  $\Omega_\sigma < 0$ , we have

$$\Omega_\sigma = -2\sqrt{\Omega_\ell \Omega_{\Lambda_b}} \quad (4.106)$$

and

$$\left(\frac{H_\infty}{H_0}\right)^2 = 2\sqrt{\Omega_\ell} \left( \sqrt{\Omega_\ell} - \sqrt{\Omega_{\Lambda_b}} \pm \left| \sqrt{\Omega_\ell} - \sqrt{\Omega_{\Lambda_b}} \right| \right). \quad (4.107)$$

If  $\Omega_\ell > \Omega_{\Lambda_b}$ , then this expression vanishes for the lower sign, which brings us back to the non-physical BRANE1 models with  $\Omega_m > 1$ . In the case  $\Omega_\ell \leq \Omega_{\Lambda_b}$ , expression (4.107) vanishes for the upper sign, which corresponds to BRANE2 models. The constraint equation (4.79) now reads

$$\Omega_m + 2\sqrt{\Omega_\ell} \left( \sqrt{1 + \Omega_{\Lambda_b}} - \sqrt{\Omega_{\Lambda_b}} \right) = 1 \quad (4.108)$$

and implies  $\Omega_m < 1$ .

Therefore, BRANE2 with  $\Omega_\sigma < 0$  and  $\Omega_\ell \leq \Omega_{\Lambda_b}$ , provides us with an interesting example of a physically meaningful cosmological model in which the current acceleration of the Universe is a *transient phenomenon*. An example of this behavior as probed by the deceleration parameter is shown in Fig. 4.8, which demonstrates that the current period of cosmic acceleration takes place between two matter-dominated epochs. We emphasize that these models require negative brane tension  $\sigma$ . Since an observer in this model resides on a negative-tension brane, one must ponder over the issue of whether such a braneworld will be perturbatively stable and hence physically viable. We consider this to be an open question for future investigations. Remarks made at the end of Sec. 4.4 are relevant, however, since one and the same cosmological solution on the ‘visible’ (negative tension) brane can correspond to many different global conditions in the bulk, for instance, other (‘hidden’)

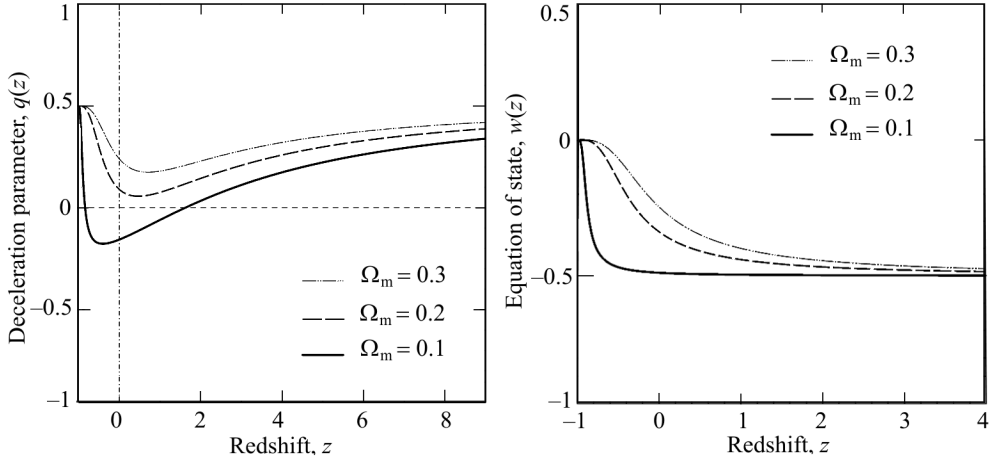


**Fig. 4.8.** The deceleration parameter is plotted as a function of redshift for the BRANE2 model with the Randall–Sundrum constraint (4.50),  $\Omega_{\Lambda_b} = 2$ , and  $(\Omega_m, \Omega_\ell) = (0.3, 1.2)$ ,  $(0.2, 1.6)$ ,  $(0.1, 1.98)$  (top to bottom). The vertical (dot-dashed) line at  $z = 0$  marks the present epoch, while the horizontal (dashed) line at  $q = 0$  corresponds to a Milne Universe [ $a(t) \propto t$ ] which neither accelerates nor decelerates. Note that the Universe *ceases to accelerate* and becomes matter dominated in the future. Figure taken from [308]

**Fig. 4.9.** The effective equation of state for dark energy in the BRANE2 model is shown as a function of redshift. Model parameters are as in the previous figure. Note that the past and future asymptotes of  $w(z)$  are quite different:  $w(z) \rightarrow -1/2$  for  $z \gg 0$ , while  $w(z) \rightarrow 0$  for  $z \rightarrow -1$ . Braneworld dark energy therefore effectively disappears in the future, giving rise to a matter-dominated Universe. Figure taken from [308]

branes may be present or absent, static or evolving, close to or far away from our brane, etc.

Useful insight into the BRANE2 model is also provided by the effective equation of state of dark energy (4.98). Our results [308], shown in Fig. 4.9, indicate that the past and future behavior of dark energy in the braneworld Universe can be very different. The past behavior  $w(z) \rightarrow -0.5$  for  $z \gg 1$  arises because, in a spatially flat braneworld, the second most important contribution to braneworld expansion at high redshifts is caused by the  $(1+z)^{3/2}$  term in (4.80); see also [515, 516]. The future behavior  $w(z) \rightarrow 0$  as  $z \rightarrow -1$ , on the other hand, reflects the decreasing importance of dark energy as the Universe expands. The acceleration of the Universe is therefore a transient phenomenon which ends once the Universe settles back into the matter-dominated regime.

Finally, we should mention that a transiently accelerating regime also arises in a class of BRANE2 models which do not satisfy the Randall–Sundrum constraint (4.50). In these models the current epoch of acceleration is succeeded by an epoch during which the deceleration parameter grows without bound. This unusual ‘future singularity’ is reached in a *finite* interval of expansion time and is characterized by the fact that both the matter density and the

Hubble parameter remain finite, while  $\ddot{a} \rightarrow \infty$  (a feature that distinguishes it from the phantom singularities discussed in Sec. 4.6). A detailed discussion of the ‘new’ singularities which occur in braneworld models will be made in Sec. 4.10.

### 4.8. Cosmic mimicry

It was noted [531] that the cosmological evolution in braneworld theory, from the viewpoint of the Friedmannian Universe, proceeds with a time-dependent gravitational constant. Indeed, the cosmological equation on the brane (4.76) can be written in the form of one of the Friedmann equations

$$H^2 + \frac{\kappa}{a^2} = \frac{8\pi G_{\text{eff}}(\rho)}{3}\rho, \quad (4.109)$$

where  $G_{\text{eff}}(\rho)$  is the effective time-dependent gravitational constant that can be read-off from (4.76).

In this section, we describe another interesting feature of braneworld cosmology, which we call “cosmic mimicry” [553]. It turns out that, for a broad range of parameter values, the braneworld model behaves *exactly as a LCDM* ( $\Lambda + \text{Cold Dark Matter}$ ) *Universe* with different values of the effective cosmological density parameter  $\Omega_m$  at different epochs. Moreover, the cosmological density parameter inferred from the observations of the large-scale structure and CMB and that determined from neoclassical cosmological tests such as observations of supernovae (SN) can potentially have different values.

An important feature of this model is that, although it is very similar to LCDM at the present epoch, its departure from “concordance cosmology” can be significant at intermediate redshifts, leading to new possibilities for the Universe at the end of the “dark ages” which may be worth exploring.

We relate the “mimicry” properties of the braneworld cosmology with the properties of gravity in braneworld theories. In particular, we show that the change in the cosmological density parameter  $\Omega_m$  as the Universe evolves can be related to the spatial scale dependence of the effective gravitational constant in braneworld theory [533–535]. This can have important consequences for cosmological models based on the braneworld theory and calls for more extensive analysis of their cosmological history.

The basic equation describing the cosmological evolution is (4.80). For sufficiently high redshifts, the first term on the right-hand side of this equation dominates, and the model reproduces the matter-dominated Friedmann Universe with the density parameter  $\Omega_m$ . Now we note that, for the values of  $z$  and parameters  $\Omega_{\Lambda_b}$  and  $\Omega_\ell$  which satisfy

$$\Omega_m(1+z)^3 \ll \left( \sqrt{1 + \Omega_{\Lambda_b}} \mp \sqrt{\Omega_\ell} \right)^2, \quad (4.110)$$

Eq. (4.80) can be well approximated as

$$\frac{H^2(z)}{H_0^2} \simeq \Omega_m(1+z)^3 + 1 - \Omega_m - \frac{\sqrt{\Omega_\ell}}{\sqrt{\Omega_\ell} \mp \sqrt{1 + \Omega_{\Lambda_b}}} [\Omega_m(1+z)^3 - \Omega_m]. \quad (4.111)$$

We introduce the positive parameter  $\alpha$  by the equation

$$\alpha = \frac{\sqrt{1 + \Omega_{\Lambda_b}}}{\sqrt{\Omega_\ell}}. \quad (4.112)$$

Then, defining a new density parameter by the relation

$$\Omega_m^{\text{LCDM}} = \frac{\alpha}{\alpha \mp 1} \Omega_m, \quad (4.113)$$

we get

$$\frac{H^2(z)}{H_0^2} \simeq \Omega_m^{\text{LCDM}}(1+z)^3 + 1 - \Omega_m^{\text{LCDM}}, \quad (4.114)$$

which is precisely the Hubble parameter describing a LCDM Universe. [Note that the braneworld parameters  $\Omega_\ell$  and  $\Omega_{\Lambda_b}$  have been effectively absorbed into a “renormalization” of the matter density  $\Omega_m \rightarrow \Omega_m^{\text{LCDM}}$ , defined by (4.113).]

Thus, our braneworld displays the following remarkable behavior which we refer to as “*cosmic mimicry*”:

- A BRANE1 model, which at high redshifts expands with density parameter  $\Omega_m$ , at lower redshifts *masquerades as a LCDM Universe* with a *smaller value* of the density parameter. In other words, at low redshifts, the BRANE1 Universe expands as the LCDM model (4.114) with  $\Omega_m^{\text{LCDM}} < \Omega_m$  [where  $\Omega_m^{\text{LCDM}}$  is determined by (4.113) with the lower (“+”) sign].

- A BRANE2 model at low redshifts also masquerades as LCDM but with a *larger value* of the density parameter. In this case,  $\Omega_m^{\text{LCDM}} > \Omega_m$  with  $\Omega_m^{\text{LCDM}}$  being determined by (4.113) with the upper (“−”) sign<sup>3</sup>.

The range of redshifts over which this cosmic mimicry occurs is given by  $0 \leq z \ll z_m$ , with  $z_m$  determined by (4.110). Specifically,

$$z_m = \frac{(\sqrt{1 + \Omega_{\Lambda_b}} \mp \sqrt{\Omega_\ell})^{2/3}}{\Omega_m^{1/3}} - 1, \quad (4.115)$$

which can also be written as

$$(1 + z_m)^3 = \frac{\Omega_m(1 + \Omega_{\Lambda_b})}{(\Omega_m^{\text{LCDM}})^2} \quad (4.116)$$

for both braneworld models.

---

<sup>3</sup>For  $\alpha < 1$ , the BRANE2 model behaves like that with *negative* matter density and demonstrates unwanted bouncing at low redshifts.

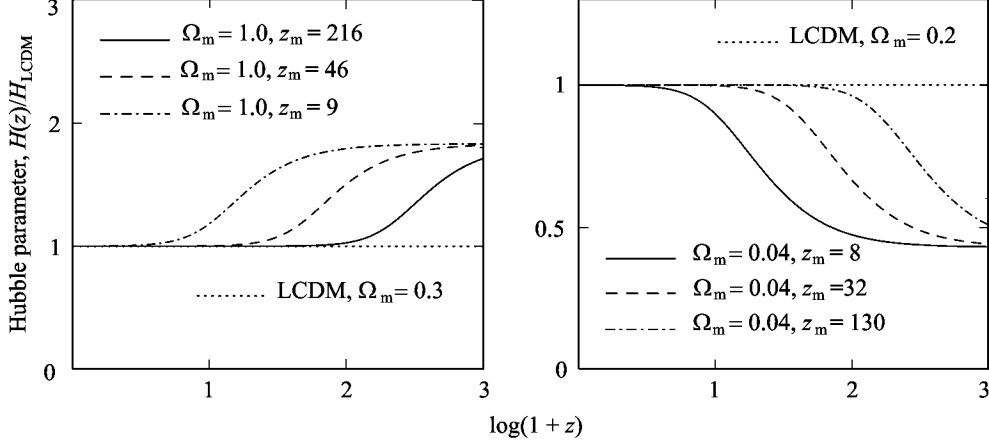


**Fig. 4.10.** An illustration of cosmic mimicry for the BRANE1 (left) and BRANE2 (right) models. The Hubble parameter in three high-density BRANE1 models with  $\Omega_m = 1$  and low-density BRANE2 models with  $\Omega_m = 0.04$  is shown. Also shown is the Hubble parameter in the LCDM model (dotted line) which closely mimics this braneworld but has a lower mass density  $\Omega_m^{\text{LCDM}} = 0.3$  ( $\Omega_\Lambda = 0.7$ ) for BRANE1 and a higher mass density  $\Omega_m^{\text{LCDM}} = 0.2$  ( $\Omega_\Lambda = 0.8$ ) for BRANE2. The brane matter density ( $\Omega_m$ ) and the matter density in LCDM are related through  $\Omega_m = \Omega_m^{\text{LCDM}} \left[ 1 \pm \sqrt{\Omega_\ell / (1 + \Omega_{\Lambda_b})} \right]$ , so that  $\Omega_m \gtrsim \Omega_m^{\text{LCDM}}$  for BRANE1 (lower sign) and  $\Omega_m \lesssim \Omega_m^{\text{LCDM}}$  for BRANE2 (upper sign). The braneworld model masquerades as LCDM for  $z \ll z_m$ , where  $z_m = 9, 46, 216$  for BRANE1 and  $z_m = 8, 32, 130$  for BRANE2 (left to right) for three different choices of parameters. Figure taken from [553]

Examples of cosmic mimicry are shown in Fig. 4.10 for the BRANE1 model (left) and BRANE2 model (right). One striking consequence of the BRANE2 model in Fig. 4.10 is that a low-density ( $\Omega_m = 0.04$ ) Universe consisting *entirely* of baryons mimics a higher-density LCDM model ( $\Omega_m^{\text{LCDM}} = 0.3$ ) and can therefore be in excellent agreement with the SN data.

In view of relation (4.116), it is interesting to note that we can use the equations derived in this section to relate the three free parameters in the braneworld model:  $\{\Omega_\ell, \Omega_{\Lambda_b}, \Omega_m\}$  to  $\{\Omega_m, z_m, \Omega_m^{\text{LCDM}}\}$ . These relations (which turn out to be the same for BRANE1 and BRANE2 models) are:

$$\frac{1 + \Omega_{\Lambda_b}}{\Omega_m^{\text{LCDM}}} = \frac{\Omega_m^{\text{LCDM}}}{\Omega_m} (1 + z_m)^3, \quad (4.117)$$

$$\frac{\Omega_\ell}{\Omega_m^{\text{LCDM}}} = \left[ \sqrt{\frac{\Omega_m^{\text{LCDM}}}{\Omega_m}} - \sqrt{\frac{\Omega_m}{\Omega_m^{\text{LCDM}}}} \right]^2 (1 + z_m)^3. \quad (4.118)$$

Furthermore, if we assume that the value of  $\Omega_m^{\text{LCDM}}$  is known (say, from the analysis of SN data), then the two braneworld parameters  $\Omega_\ell$  and  $\Omega_{\Lambda_b}$  can be related to the two parameters  $\Omega_m$  and  $z_m$  using (4.117), so it might

be more convenient to analyze the model in terms of  $\Omega_m$  and  $z_m$  (instead of  $\Omega_\ell$  and  $\Omega_{\Lambda_b}$ ).

We also note that, under condition (4.110), the brane tension  $\sigma$ , determined by (4.79), is positive for BRANE1 model, and negative for BRANE2 model.

Since the Hubble parameter in braneworld models departs from that in LCDM at *intermediate* redshifts ( $z > z_m$ ), this could leave behind an important cosmological signature especially since several key cosmological observables depend upon the Hubble parameter either differentially or integrally. Examples include:

- the luminosity distance  $d_L(z)$ , given by (4.88),
- the angular diameter distance (4.95),
- the product  $d_A(z)H(z)$ , which plays a key role in the Alcock–Paczynski anisotropy test [554, 555],
- the product  $d_A^2(z)H^{-1}(z)$ , which is used in the volume-redshift test [556],
- the deceleration parameter (4.84),
- the effective equation of state of dark energy (4.98),
- the age of the Universe (4.96),
- the “statefinder pair” [322, 557]:

$$r = \frac{\ddot{a}}{aH^3} \equiv 1 + \left[ \frac{H''}{H} + \left( \frac{H'}{H} \right)^2 \right] (1+z)^2 - 2 \frac{H'}{H} (1+z), \quad (4.119)$$

$$s = \frac{r-1}{3(q-1/2)},$$

- the electron-scattering optical depth to a redshift  $z_{\text{reion}}$  [558, 559]

$$\tau(z_{\text{reion}}) = c \int_0^{z_{\text{reion}}} \frac{n_e(z) \sigma_T dz}{(1+z)H(z)}, \quad (4.120)$$

where  $n_e$  is the electron density and  $\sigma_T$  is the Thomson cross-section describing scattering between electrons and CMB photons.

A degree of caution should be exercised when comparing the late-time LCDM behavior (4.114) of the model under consideration with different sets of observations, since the parameter  $\Omega_m^{\text{LCDM}}$ , residing in (4.114), which is effectively used in determinations of the luminosity distance (4.88) and angular diameter distance (4.95), may very well be different from the value of  $\Omega_m$  inferred from observations of gravitational clustering. These issues should be kept in mind when performing a maximum-likelihood analysis using data belonging to different observational streams.

Cosmological tests based on the luminosity distance and angular diameter distance typically probe lower redshifts  $z \lesssim 2$ . Therefore, if the mimicry redshift

is  $z_m \geq 2$ , the braneworld model will, for all practical purposes, be indistinguishable from the LCDM cosmology on the basis of these tests alone. However, tests which probe higher redshifts should be able to distinguish between these models. For instance, since  $H(z) < H_{\text{LCDM}}(z)$  in BRANE2 at redshifts larger than the mimicry redshift, it follows that the age of the Universe will be greater in this model than in the LCDM cosmology. This is illustrated in Fig. 4.11 for three distinct values of the cosmological density parameter:  $\Omega_m = 0.2, 0.1, 0.04$ , all of which are lower than  $\Omega_m^{\text{LCDM}} = 0.3$ . Since the late-time evolution of the Universe is

$$t(z) \simeq \frac{2}{3H_0\sqrt{\Omega_m}}(1+z)^{-3/2}, \quad (4.121)$$

one finds, for  $z \gg 1$ ,

$$\frac{t_{\text{brane}}}{t_{\text{LCDM}}}(z) \simeq \sqrt{\frac{\Omega_m^{\text{LCDM}}}{\Omega_m}}. \quad (4.122)$$

Since  $\Omega_m < \Omega_m^{\text{LCDM}}$  in the BRANE2 model, we find that the age of a BRANE2 Universe is greater than that of a LCDM Universe. (The reverse is true for the BRANE1 model, for which  $\Omega_m > \Omega_m^{\text{LCDM}}$ .)

The altered rate of expansion in the braneworld model at late times ( $z > z_m$ ) also affects other cosmological quantities including the redshift of reionization which, for the BRANE2 model, becomes smaller than that in the LCDM cosmology. This is because the lower value of  $H(z)$  in the BRANE2 model (relative to the LCDM model), when substituted to (4.120), gives a correspondingly lower value for  $z_{\text{reion}}$  for an identical value of the optical depth  $\tau$  in both models. (In fact, it is easy to see that, for the BRANE2 model, the value of  $z_{\text{reion}}$  decreases with decreasing  $z_m$  and  $\Omega_m$ .)

Both an increased age of the Universe and a lower redshift of reionization are attractive properties of the braneworld model which, as we have seen, mimics the LCDM cosmology at lower redshifts  $z < z_m$ <sup>4</sup>. It is important to note that the presence of high-redshift quasi-stellar objects (QSO's) and galaxies at redshifts  $z \gtrsim 6$  indicates that the process of structure formation was already in full swing at that early epoch when the LCDM Universe was less than a billion years old. Most models of QSO's rely on a central supermassive black hole ( $M_{\text{BH}} \gtrsim 10^9 M_\odot$ ) to power the quasar luminosity via accretion. Since structure forms hierarchically in the cold dark matter scenario, the presence of such supermassive black holes at high redshift suggest that they formed through an assembly mechanism involving either accretion or mergers or both. It is not clear whether either of these processes is efficient enough to assemble a large number of high-redshift QSO's in a LCDM cosmology [561, 562]. We

<sup>4</sup> Note that the decreased redshift of reionization and the increased age of the Universe are properties that the BRANE2 model shares with the loitering Universe [560] discussed in Sec. 4.9.

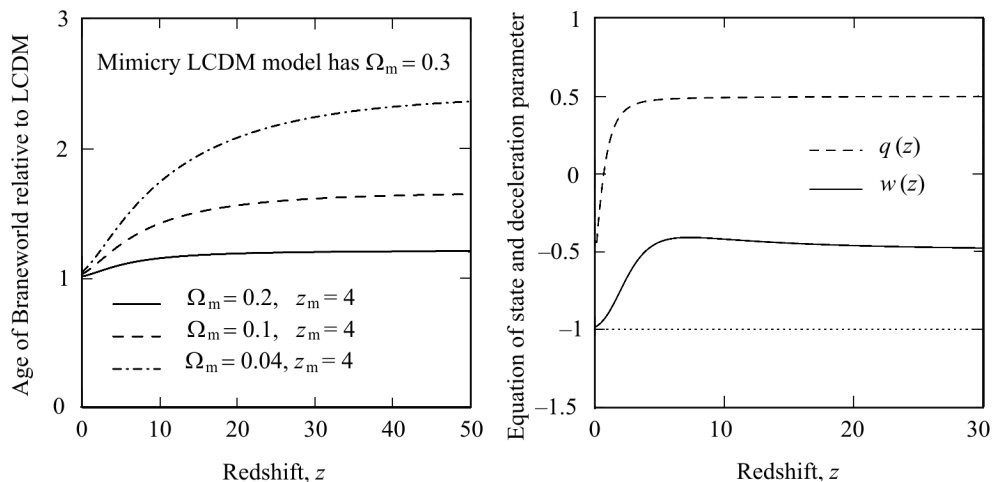


**Fig. 4.11.** The age of the Universe in the BRANE2 model is shown with respect to the LCDM value. The mimicry redshift (4.116) is  $z_m = 4$  so that  $H_{\text{brane}}(z) \simeq H_{\text{LCDM}}(z)$  at  $z \ll 4$ . The braneworld models have  $\Omega_m = 0.2, 0.1, 0.04$  (bottom to top) whereas  $\Omega_m^{\text{LCDM}} = 0.3$ . Note that the braneworld models are older than LCDM. Figure taken from [553]

**Fig. 4.12.** The effective equation of state (solid line) and the deceleration parameter (dashed line) of the BRANE2 model are shown. (The dotted line shows  $w = -1$  which describes the LCDM model.) The mimicry redshift (4.116) is  $z_m = 4$  so that  $H_{\text{brane}}(z) \simeq H_{\text{LCDM}}(z)$  at  $z \lesssim 4$ . The braneworld has  $\Omega_m = 0.2$  whereas  $\Omega_m^{\text{LCDM}} = 0.3$ . Figure taken from [553]

would like to note in this section that braneworld cosmology may successfully alleviate some of the tension currently existing between theory and observations at moderate redshifts, while allowing the Universe to be “LCDM-like” at the present epoch.

The effective equation of state and the deceleration parameter of the BRANE2 model are shown in Fig. 4.12. The braneworld has  $\Omega_m = 0.2$  and, at  $z \lesssim 4$ , masquerades as a higher-density LCDM model with  $\Omega_m^{\text{LCDM}} = 0.3$ . Note that the *effective* equation of state (4.98) is a *model-dependent* quantity, involving the model-dependent cosmological parameter  $\Omega_m$  in its definition. In our case, we use the braneworld theory as our model with  $\Omega_m$  defined in (4.77), and the effective equation of state (4.98) is then *redshift-dependent* even during the mimicry period when  $H_{\text{brane}}(\Omega_m, z) \simeq H_{\text{LCDM}}(\Omega_m^{\text{LCDM}}, z)$ . A theorist who is unaware of the possibility of cosmic mimicry, when reconstructing the cosmic equation of state from (4.98) with  $\Omega_m^{\text{LCDM}} = 0.3$  in the place of  $\Omega_m$ , will arrive at a different conclusion that  $w = -1$ . This example demonstrates some of the pitfalls associated with the cosmological reconstruction of the equation of state, which depends on the underlying theoretical model and for which an accurate knowledge of  $\Omega_m$  is essential; see [322, 557, 563–566] for a discussion of related issues.



The “cosmic mimicry” exhibited by braneworld cosmology can be related to the gravitational properties of braneworld theory described in Sec. 4.5. In this context, it is remarkable that the parameter  $\beta$  introduced in (4.53) is very close (in absolute terms) to the parameter  $\alpha$  introduced in (4.112) in our discussion of mimicry models. Specifically,

$$\beta = \frac{1 - \Omega_m}{2\Omega_\ell} \mp \alpha, \quad (4.123)$$

so that

$$|\beta| \approx \alpha \quad (4.124)$$

when  $|1 - \Omega_m| \ll \Omega_\ell$ . This last inequality follows naturally from condition (4.110) for values of  $\alpha$  of order unity, which are of interest to us. As a consequence, the term which appears in the “renormalization” of the cosmological mass density  $\Omega_m$  in (4.113) is almost identical to the term which redefines the gravitational constant in (4.55). This coincidence can be explained by inspecting the brane equation (4.52). First, we recall that cosmological solutions without dark radiation are embeddable in the anti-de Sitter bulk space-time (see Sec. 4.2), so that  $C_{ab} = 0$  for these solutions. For high cosmological matter densities, the quadratic expression (4.56) dominates in Eq. (4.52), and the Universe is described by the “bare” Einstein equation  $m^2 G_{ab} - T_{ab} = 0$ , with the effective gravitational coupling being equal to  $1/m^2$ . As the matter density decreases, the role of this quadratic term becomes less and less important, and the effective gravitational coupling eventually is determined by the linear part of Eq. (4.52), i.e., by the gravitational constant (4.55).

Thus, comparing (4.55) and (4.113), one has the following natural relation, valid to a high precision in view of (4.124):

$$\Omega_m^{\text{LCDM}} = \frac{8\pi G_{\text{eff}} \rho_0}{3H_0^2}. \quad (4.125)$$

Since, in our case, interesting values of the parameters  $\Omega_\ell$  and  $\Omega_{\Lambda_b}$  are considerably greater than unity, the RS constraint (4.50), which can also be written in the form

$$\Omega_\sigma \pm 2\sqrt{\Omega_\ell \Omega_{\Lambda_b}} = 0, \quad (4.126)$$

is satisfied to a good precision in view of Eq. (4.79). Note that  $\Omega_m^{\text{LCDM}} \approx 1$  in the case of the RS constraint. A slight violation of the RS constraint causes the appearance of a small effective cosmological constant (4.54) on the brane, which can be thought to be inessential for the discussion of the Newtonian part of the gravitational physics performed in Sec. 4.5.

The cosmological model under consideration appears to safely pass the existing constraints on the variation of the gravitational constant from primordial abundances of light elements synthesized in the big-bang nucleosynthesis

(BBN) and from CMB anisotropy [567]. The value of the gravitational constant at the BBN epoch in our model coincides with the value measured on small scales (4.66), and the effective gravitational constant (4.60) or (4.55) that might affect the large-scale dynamics of the Universe responsible for the CMB fluctuations is within the uncertainties estimated in [567].

Cosmic mimicry in braneworld models is most efficient in the case of parameter  $\alpha \sim 1$ , which, according to (4.112), implies that the two spatial scales, namely, the brane length scale given by (4.48) and the curvature scale of the bulk are of the same order:  $\ell \sim \ell_{\text{warp}} = \sqrt{-6/\Lambda_b}$ . This coincidence of the orders of magnitude of completely independent scales can be regarded as some tuning of parameters, although it is obviously a mild one.

## 4.9. Loitering

### 4.9.1. Loitering Universe

In the models of dark energy, the deceleration parameter at some point changes sign while the Hubble parameter is usually assumed to be a monotonically decreasing function of the cosmic time<sup>5</sup>. In the present section, we show that this need not necessarily be the case in braneworld models, and that compelling dark-energy models can be constructed in which  $H(z)$  dips in value at high redshifts. In these models,  $dH(z)/dz \simeq 0$  at  $z_{\text{loit}} \gg 1$ , which is called the “loitering redshift”. (A Universe which loiters has also been called a “hesitating” Universe, since, if  $H(z_{\text{loit}}) \simeq 0$ , the Universe hesitates at the redshift  $z_{\text{loit}}$  for a lengthy period of time — before either collapsing or re-expanding.) Loitering increases the age of the Universe at high  $z$  and also provides a boost to the growth of density inhomogeneities, thereby endowing a dark-energy model with compelling new properties.

Before discussing loitering in braneworld models [560], we briefly review the status of loitering in standard General Relativity in this subsection. Within a FRW setting, loitering can only arise in a Universe which is spatially closed and which is filled with matter and a cosmological constant (or some other form of dark energy — see [569]). The evolution of such a Universe is described by the equation

$$H^2 = \frac{8\pi G}{3} \frac{\rho_0 a_0^3}{a^3} + \frac{\Lambda}{3} - \frac{\kappa}{a^2}, \quad \kappa = 1, \quad (4.127)$$

where  $\rho_0$  is the present matter density. Loitering in (4.127) arises if the curvature term ( $1/a^2$ ) is large enough to substantially offset the dark-matter + + dark-energy terms but not so large that the Universe collapses. The redshift at which the Universe loitered can be determined by rewriting (4.127) in the

<sup>5</sup> Phantom models may provide an exception to this rule; see [568] and references therein.

form

$$h^2(z) \equiv \frac{H^2(z)}{H_0^2} = \Omega_m(1+z)^3 + \Omega_\Lambda + \Omega_\kappa(1+z)^2, \quad (4.128)$$

where  $\Omega_\kappa = -\kappa/a_0^2 H_0^2$ ,  $\Omega_m = 8\pi G\rho_0/3H_0^2$ ,  $\Omega_\Lambda = \Lambda/3H_0^2$ , the subscript “0” refers to present epoch, and the constraint equation requires  $\Omega_\kappa = 1 - \Omega_m - \Omega_\Lambda$ .

The loitering condition  $dh/dz = 0$  gives

$$1 + z_{\text{loit}} = \frac{2|\Omega_\kappa|}{3\Omega_m}, \quad (4.129)$$

and it is easy to show that  $z_{\text{loit}} \leq 2$  for  $\Omega_m \geq 0.1$  [569]. (Note that a large value of  $|\Omega_\kappa|$  can cause the Universe to recollapse.) The value of the Hubble parameter at loitering can be determined by substituting  $z_{\text{loit}}$  into (4.128). Note that, since  $\ddot{a}/a = \dot{H} + H^2$ , it follows that  $(\ddot{a}/a)|_{z=z_{\text{loit}}} = H^2(z_{\text{loit}})$  at loitering. (The special case  $\dot{a} = 0$ ,  $\ddot{a} = 0$  corresponds to the static Einstein Universe [236]. For a detailed discussion of loitering in FRW models with dark energy see [569]. Loitering in more general contexts has been discussed in [570, 571].)

Interest in loitering FRW models has waxed and waned ever since the original discovery of a loitering cosmology by Lemaitre over seventy years ago [48]. Among the reasons why the interest in loitering appears to have declined in more recent times are the following: (i) even though loitering models can accommodate an accelerating Universe, the loitering redshift is usually small:  $z_{\text{loit}} \leq 2$  in LCDM; (ii) loitering models require a large spatial curvature, which is at variance with inflationary predictions and CMB observations both of which support a flat Universe. As we shall show, in marked contrast with the above scenario, loitering in braneworld models can take place in a spatially flat Universe and at high redshifts ( $z \gtrsim 6$ ). At late times, the loitering braneworld model has properties similar to those of LCDM.

#### 4.9.2. Loitering in braneworld models

Loitering can be realized in a braneworld model described by action (4.7) with  $N = 1$  and cosmological equation (4.80), which, for a spatially flat Universe ( $\kappa = 0$ ) can be written in the form

$$H^2(a) = \frac{A}{a^3} + B + \frac{2}{\ell^2} \left[ 1 \pm \sqrt{1 + \ell^2 \left( \frac{A}{a^3} + B - \frac{\Lambda_b}{6} - \frac{C}{a^4} \right)} \right], \quad (4.130)$$

where

$$A = \frac{\rho_0 a_0^3}{3m^2}, \quad B = \frac{\sigma}{3m^2}, \quad \ell = \frac{2m^2}{M^3}. \quad (4.131)$$

Of crucial importance to the present analysis is the dark-radiation term  $C/a^4$  in (4.130) whose presence is a generic feature in braneworld models

and which describes the projection of the bulk degrees of freedom onto the brane. [As was noted in the remark following Eq. (4.13), it corresponds to the presence of the bulk black hole.] An interesting situation arises when  $C < 0$  and  $\ell^2|C|/a^4 \gg 1$ . In this case, if  $\ell^2|C|/a^4$  is larger than the remaining terms under the square root in (4.130), then that equation reduces to<sup>6</sup>

$$H^2(a) \approx \frac{A}{a^3} + B \pm \frac{2\sqrt{-C}}{\ell a^2}. \quad (4.132)$$

Equation (4.132) bears a close formal resemblance to (4.127), which gave rise to loitering solutions in standard FRW geometry for  $\kappa = 1$ . Indeed, the role of the spatial curvature in (4.132) is played by the dark-radiation term; consequently, a spatially open Universe is mimicked by the BRANE2 model [the upper sign in (4.130)] while a closed Universe is mimicked by BRANE1 [the lower sign in (4.130)]. In analogy with standard cosmology, one might expect the braneworld model (4.130) to show loitering behavior in the BRANE1 case. This is indeed the case, and strongly loitering solutions to (4.130) and (4.132) can be found by requiring  $H'(a) = 0$ .

Although this is the general procedure which we follow, for practical purposes it is more suitable to rewrite (4.130) in the form (4.78). When the dark-radiation term is strongly dominating, Eq. (4.130) or, for that matter (4.78) with  $\kappa = 0$ , then reduces to

$$\frac{H^2(z)}{H_0^2} \simeq \Omega_m(1+z)^3 + \Omega_\sigma - 2\sqrt{\Omega_\ell\Omega_C}(1+z)^2, \quad (4.133)$$

which is the braneworld analog of (4.128). The loitering redshift in this case can be defined by the condition  $H'(z_{\text{loit}}) = 0$ ; as a result, one gets

$$1 + z_{\text{loit}} \simeq \frac{4}{3} \frac{\sqrt{\Omega_C\Omega_\ell}}{\Omega_m}. \quad (4.134)$$

From this expression we find that the Universe will loiter at a large redshift  $z_{\text{loit}} \gg 1$  provided  $\Omega_C\Omega_\ell \gg \Omega_m^2$ . Since  $\Omega_m^2 \ll 1$ , this is not difficult to achieve in practice. Successful loitering of this type requires the following two conditions to be satisfied:

$$\begin{aligned} \Omega_C(1 + z_{\text{loit}})^4 &\gg \Omega_m(1 + z_{\text{loit}})^3 + \Omega_\sigma + \Omega_\ell + \Omega_{\Lambda_b}, \\ \Omega_\sigma &\sim \sqrt{\Omega_\ell\Omega_C}(1 + z_{\text{loit}})^2. \end{aligned} \quad (4.135)$$

---

<sup>6</sup> The negative value of the dark-radiation term implies the presence of black hole with negative mass – hence, naked singularity – in the complete extension of the bulk geometry. In principle, this singularity could be “closed from our view” by another (invisible) brane.

The first inequality ensures that the dark-radiation term dominates over the remaining terms under the square root of (4.80) during loitering, while the second makes sure that this term is never so large as to cause the Universe to recollapse.

Substituting the value for  $1 + z_{\text{loit}}$  from (4.134) into (4.135), we obtain

$$\Omega_\sigma \sim \frac{(\Omega_C \Omega_\ell)^{3/2}}{\Omega_m^2} \gg \Omega_\ell, \quad (4.136)$$

which is a necessary condition for loitering in our braneworld model.

Finally, the Hubble parameter at loitering is given by the approximate expression

$$\frac{H^2(z_{\text{loit}})}{H_0^2} \simeq \Omega_\sigma - \frac{32}{27} \frac{(\Omega_C \Omega_\ell)^{3/2}}{\Omega_m^2}. \quad (4.137)$$

Note that conventional loitering is usually associated with a vanishingly small value for the Hubble parameter at the loitering redshift [569]. The Hubble parameter at loitering can be set as close to zero as possible; however, we do not require it to be *very* close to zero. A small “dip” in the value of  $H(z)$ , which is sufficient for our purposes, arises for a far larger class of parameter values than the more demanding condition  $H(z_{\text{loit}}) \simeq 0$ .

Moreover, in a wide range of parameters, the Universe evolution may not exhibit a minimum of the Hubble parameter  $H(z)$ . In this case, the definition of the loitering redshift by the condition  $H'(z_{\text{loit}}) = 0$  is not appropriate and can be generalized in several different ways, one of which is described in Sec. 4.9.3.

An example of a loitering model is shown in Fig. 4.13, where the Hubble parameter of a Universe which loitered at  $z \simeq 18$  is plotted against the redshift, keeping  $\Omega_m$ ,  $\Omega_\ell$ , and  $\Omega_C$  fixed and varying the value of  $\Omega_{\Lambda_b}$ . The right-hand panel of Fig. 4.13 illustrates the fact that the loitering Universe can show a variety of interesting behavior: (i) top curve,  $H(z)$  is monotonically increasing and  $H'(z) \simeq \text{constant}$  in the loitering interval; (ii) middle curve,  $H(z)$  appears to have an inflexion point ( $H' \simeq 0$ ,  $H'' \simeq 0$ ) during loitering; (iii) lower curve,  $H(z)$  has both a maximum and a minimum, the latter occurring in the loitering regime.

At this point, we would like to stress an important difference existing between the Randall–Sundrum braneworld (4.20) and our Universe (4.130) due to which the latter can accommodate a large value of dark radiation without violating nucleosynthesis constraints whereas the former cannot. In the Randall–Sundrum braneworld (4.20), the dark-radiation term ( $C/a^4$ ) affects cosmological expansion in *exactly the same way* as the usual radiation density  $\rho_r$ , so that this model comes into serious conflict with the predictions of the big-bang nucleosynthesis if  $|C|$  is very large [572]. In the loitering braneworld, on the other hand, the dark-radiation term resides under the square root in

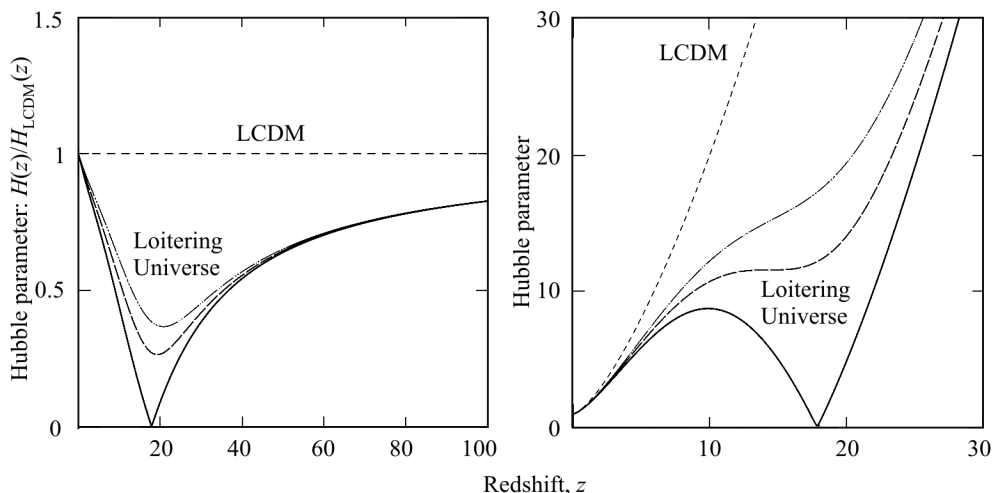


**Fig. 4.13.** The Hubble parameter for a Universe that loiters at  $z_{\text{loit}} \simeq 18$ . Parameter values are  $\Omega_m = 0.3$ ,  $\Omega_C = 8.0$ ,  $\Omega_\ell = 3.0$ , and  $\Omega_{\Lambda_b}/10^5 = 6, 4.5, 3.4$  (solid lines, from top to bottom). The left panel shows the Hubble parameter with respect to the LCDM value while, in the right panel, the LCDM (dashed) and loitering (solid) Hubble parameters are shown separately. Figure taken from [560]

(4.130); due to this circumstance its effect on the cosmological expansion is less severe and, more importantly, *transient*. Indeed, even if the dark-radiation term is very large ( $|C|/a^4 > \rho_m, \rho_r$ ), its influence on expansion can only be  $\propto 1/a^2$ , which does not pose a serious threat to the standard predictions of the big-bang nucleosynthesis.

A loitering Universe could have several important cosmological consequences:

(i) The age of the Universe during loitering *increases*, as shown in Fig. 4.14. The reason for this can be seen immediately from expression (4.96). Clearly, a lower value of  $H(z)$  close to loitering will boost the age of the Universe at that epoch. In Fig. 4.14, the age of the Universe is plotted with reference to a LCDM Universe, which has been chosen as our fiducial model. It is interesting to note that, while the *age at loitering* can be significantly larger in the loitering model than in LCDM [ $t_{\text{loit}}(z_{\text{loit}}) \sim \text{few} \times t_{\text{LCDM}}(z_{\text{loit}})$ ], the present age of the Universe in both models is comparable [ $t_{\text{loit}}(0) \lesssim 1.2 \times t_{\text{LCDM}}(0)$ ]<sup>7</sup>. An important consequence of having a larger age of the Universe at  $z \sim 20$  (or so) is that astrophysical processes at these redshifts have more time in which to develop. This is especially important for gravitational instability which forms gravitationally bound systems from the extremely tiny fluctuations existing at

<sup>7</sup> The age of a LCDM Universe at  $z \gg 1$  is  $t(z) \simeq (2/3H_0\sqrt{\Omega_m})(1+z)^{-3/2} = 5.38 \times 10^8(1+z/10)^{-3/2}$  years for  $\Omega_m = 0.3$  and  $h = 0.7$ .

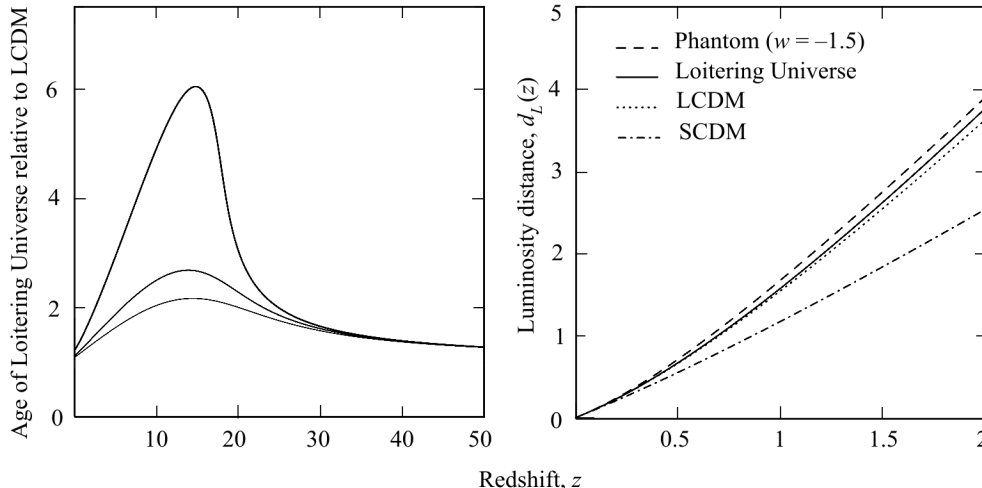


**Fig. 4.14.** In the left panel, the age of three loitering models is shown relative to the age in LCDM (model parameters are the same as in Fig. 4.13). Note that the age of the Universe near loitering ( $z_{\text{loit}} \sim 18$ ) is significantly greater than that in LCDM although, at the present epoch, the difference in ages between the two models is relatively small. In the right panel, the luminosity distance in a Universe that loiters at  $z_{\text{loit}} \simeq 18$  is shown in comparison with other models. Note that the luminosity distance in the loitering model is only slightly larger than that in LCDM and smaller than that in a phantom model with  $w = -1.5$ . Figure taken from [560]

the epoch of last scattering. Thus, an early loitering epoch may be conducive to the formation of Population III stars and low-mass black holes at  $z \sim 17$  and also of  $\sim 10^9 M_\odot$  black holes at lower redshifts ( $z \sim 6$ ).

(ii) In Fig. 4.14, the luminosity distance (4.88) for the loitering model is shown, again with LCDM as the base model. One finds from Fig. 4.14 that the luminosity distance in the loitering model, although somewhat larger than in LCDM, is smaller than in a phantom model with  $w = -1.5$ . Since both phantom and LCDM models provide excellent fits to type Ia supernova data [3, 279, 564, 565], we expect our family of “high redshift loitering models” to also be in good agreement with observations. (A detailed comparison of loitering models with observations lies outside of the scope of the present book.)

The reason why both the luminosity distance and the current age of the Universe have values which are close to those in the LCDM model is clear from Fig. 4.13, where we see that the difference between the Hubble parameters for the loitering models and LCDM model is small at low redshifts. Since both  $d_L(z)$  and  $t(z)$  probe  $H^{-1}(z)$ , and since the value of the Hubble parameter at low  $z$  is much smaller than its value at high  $z$  (unless parameter values are chosen to give  $H(z_{\text{loit}}) \simeq 0$  with a high precision), it follows that  $|d_L^{\text{loit}}(z) - d_L^{\text{LCDM}}(z)| \ll d_L^{\text{LCDM}}(z)$  and  $|t^{\text{loit}}(z) - t^{\text{LCDM}}(z)| \ll t^{\text{LCDM}}(z)$  for  $z \ll 1$ .

(iii) The growth of density perturbations depends sensitively upon the behavior of the Hubble parameter, as can be seen from the following equation describing the growth of linearized density perturbations  $\delta = (\rho - \bar{\rho})/\bar{\rho}$  in a FRW Universe (ignoring the effects of pressure):

$$\ddot{\delta} + 2H\dot{\delta} - 4\pi G\bar{\rho}\delta = 0. \quad (4.138)$$

In Eq. (4.138), the second term  $2H\dot{\delta}$  damps the growth of perturbations; consequently, a lower value of  $H(z)$  during loitering will boost the growth rate in density perturbations, as originally demonstrated in [569].

Here we should note that Eq. (4.138) for perturbations is perfectly valid only in General Relativity and, in principle, may be corrected or modified in the braneworld theory under consideration. Thus, for the DGP braneworld model [504] (which corresponds to setting  $\sigma = 0$ ,  $\Lambda_b = 0$  and  $C = 0$  in Eq. (4.130)), the linearized equation

$$\ddot{\delta} + 2H\dot{\delta} - 4\pi G\bar{\rho}\left(1 + \frac{1}{3\beta_{\text{DGP}}}\right)\delta = 0 \quad (4.139)$$

was derived in [541, 542], where

$$\beta_{\text{DGP}} = -\frac{1 + \Omega_m^2(t)}{1 - \Omega_m^2(t)}, \quad \Omega_m(t) \equiv \frac{8\pi G\bar{\rho}(t)}{3H^2(t)}. \quad (4.140)$$

It is important to note the similarities as well as differences between (4.138) and (4.139). Thus, cosmological expansion works in the same way for both models and introduces the damping term  $2H\dot{\delta}$  in (4.138) as well as in (4.139). However, in contrast to (4.138), the braneworld perturbation Eq. (4.139) has a time-dependent (decreasing) effective gravitational constant

$$G_{\text{eff}} = G\left(1 + \frac{1}{3\beta_{\text{DGP}}}\right), \quad (4.141)$$

which is expected to affect the growth rate of linearized density perturbations in this model. For the generic braneworld models which we study in this book [which has non-zero brane and bulk cosmological constants and especially non-zero dark radiation:  $C \neq 0$  in Eq. (4.130)], the corresponding equation for cosmological perturbations remains to be derived. We expect the form of this equation to be dependent on the additional boundary conditions in the bulk or on the brane. However, we anticipate that such an equation will contain the damping term  $2H\dot{\delta}$  which serves to enhance the growth of perturbations in the case of loitering. At the same time, braneworld-specific effects may act in the opposite direction leading to the suppression of the growth of perturbations



relative to the FRW model, as is the case, for instance, with the last term in (4.139) for the DGP model [541, 542].

(iv) The deceleration parameter  $q$  and the effective equation of state  $w$  in our loitering model are given by the expressions (4.84) and (4.98), respectively, in which  $H(z)$  is to be determined from (4.80) and (4.79). The current values of these quantities are

$$q_0 = \frac{3}{2}\Omega_m \left[ 1 - \frac{\sqrt{\Omega_\ell}}{\sqrt{\Omega_\ell} + \sqrt{1 + \Omega_{\Lambda_b} + \Omega_C}} \left( 1 + \frac{4}{3} \frac{\Omega_C}{\Omega_m} \right) \right] - 1, \quad (4.142)$$

$$w_0 = -1 - \frac{\Omega_m}{(1 - \Omega_m)} \cdot \frac{\sqrt{\Omega_\ell}}{\sqrt{\Omega_\ell} + \sqrt{1 + \Omega_{\Lambda_b} + \Omega_C}} \left( 1 + \frac{4}{3} \frac{\Omega_C}{\Omega_m} \right). \quad (4.143)$$

From Eq. (4.143) we find that  $w_0 < -1$  if  $\Omega_C \geq 0$ ; in other words, our loitering Universe has a phantom-like effective equation of state. (In particular, for the loitering models shown in Fig. 4.13, we have  $w_0 = -1.035, -1.04, -1.047$  (top to bottom), all of which are in excellent agreement with observations [573].) However, in contrast to phantom models, the Hubble parameter in a loitering Universe (4.80) does not encounter a future singularity since  $\Omega_C, \Omega_\sigma > 0$  is always satisfied in models which loitered in the past. (Future singularities can arise in braneworld models if  $\Omega_C, \Omega_\sigma < 0$  — see [574] for a comprehensive discussion of this issue and [575, 576] for related ideas.)

An interesting consequence of the loitering braneworld is that the time-dependent density parameter  $\Omega_m(z) = 8\pi G\rho_m(z)/3H^2(z)$  *exceeds* unity at some time in the past. This follows immediately from the fact that, since the value of  $H(z)$  in the loitering braneworld model is *smaller* than its counterpart in LCDM, the value of  $\Omega_m(z)$  is larger than its counterpart in LCDM. One important consequence of this behavior is that, as expected from (4.143), the effective equation of state blows up precisely when  $\Omega_m(z) = 1$ . In Fig. 4.15, we show that, in contrast to the singular behavior of the equation of state, the deceleration parameter remains finite and well behaved even as  $w \rightarrow \infty$ . Note that the finite behavior of  $q(z)$  reflects the fact that the equation of state for the braneworld is an *effective* quantity and not a real physical property of the theory — see [322, 557] for a related discussion of this issue and [577] for an example of a different dark-energy model displaying similar behavior. (The deceleration parameter experiences near-singular behavior at the higher, loitering redshift, as  $H \rightarrow 0$  so that  $q \rightarrow \infty$ .)

(v) Finally, we draw attention to the fact that a loitering epoch at  $z_{\text{loit}}$  can significantly alter the reionization properties of the Universe at lower redshifts. The electron scattering optical depth to a redshift  $z_{\text{reion}}$  is given by Eq. (4.120). Clearly, were  $H(z)$  to drop below its value in LCDM it would imply a lower value for  $z_{\text{reion}}$ . Since this is precisely what happens in a loitering cosmology,

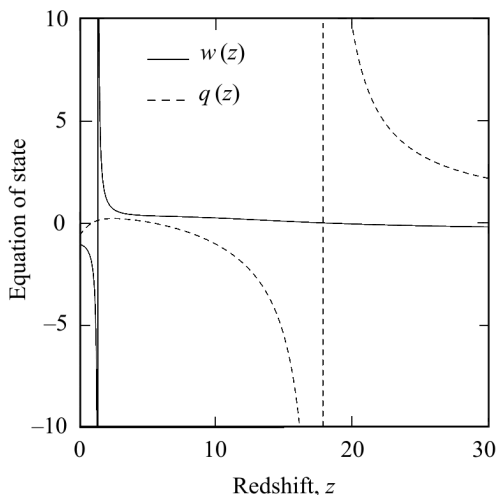


**Fig. 4.15.** The effective equation of state of dark energy (solid) and the deceleration parameter (dashed) are shown for a Universe which loitered at  $z \simeq 18$ . Note that the effective equation of state of dark energy becomes infinite at low redshifts when  $\Omega_m(z) = 1$ . However, this behavior is not reflected in the deceleration parameter, which becomes large only near the loitering redshift. Figure taken from [560]

one expects  $z_{\text{reion}}|_{\text{loitering}} < z_{\text{reion}}|_{\text{LCDM}}$  if  $z_{\text{loit}} \lesssim 20$ . As an example, consider the loitering models shown for illustrative purposes in Fig. 4.13. Not surprisingly, the redshift of reionization drops to  $z_{\text{reion}} \leq 12$  (from the value  $z_{\text{reion}} \simeq 17$ ) for the loitering models shown in Fig. 4.13. By decreasing the redshift of reionization as well as increasing the age of the Universe, the loitering braneworld may help in alleviating the possible tension between the high-redshift Universe and dark-energy cosmology.

### 4.9.3. The parameter space in loitering models

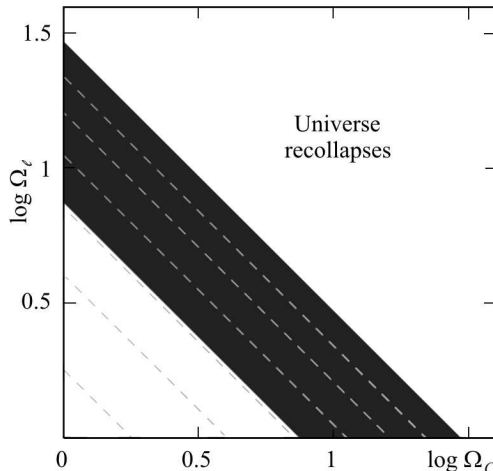
As pointed out earlier, while not all loitering models pass through a minimum of the Hubble parameter, a minimum value of the ratio  $H(z)/H_{\text{LCDM}}(z)$  is generic and is exhibited by all models. It is therefore useful to supplement the definition of loitering given in (4.134) by defining the loitering redshift  $z_{\text{loit}}$  as the epoch associated with the minimum of  $H(z)/H_{\text{LCDM}}(z)$  (both models are assumed to have the same value of  $\Omega_m$ ). In order to quantify the degree of loitering, it is useful to introduce the function

$$f(z) \equiv 1 - \frac{H^2(z)}{H_{\text{LCDM}}^2(z)}, \quad (4.144)$$

where  $0 \leq f < 1$ . Small values  $0 \leq f \leq 1/2$  imply *weak loitering*, whereas larger values  $1/2 < f < 1$  correspond to *strong loitering*. It is straightforward to derive expressions for the loitering redshift  $z_{\text{loit}}$  and the degree of loitering  $f(z_{\text{loit}})$ :

$$(1 + z_{\text{loit}})^4 \approx \frac{3(\sqrt{1 + \Omega_{\Lambda_b} + \Omega_C} + \sqrt{\Omega_\ell})^2}{\Omega_C}, \quad (4.145)$$

**Fig. 4.16.** The parameter space  $\{\Omega_\ell, \Omega_C\}$  is shown for models which exhibit (i) weak loitering:  $f(z_{\text{loit}}) \leq 1/2$  in (4.144) (lower left corner); (ii) strong loitering:  $1/2 < f(z_{\text{loit}}) < 1$  in (4.144) (shaded region). The prohibited region corresponding to braneworld models which recollapse *before* reaching the present epoch is shown on the far right. The dashed lines show contours of  $\{\Omega_\ell, \Omega_C\}$  with current values of the effective equation of state:  $w_0 = -1.01, -1.015, -1.02, -1.025, -1.03, -1.035$  (from left to right). All models loiter at  $z_{\text{loit}} = 20$  and have  $\Omega_m = 0.3$ . Figure taken from [560]



$$f(z_{\text{loit}}) \approx \frac{2\sqrt{\Omega_\ell} (\sqrt{1 + \Omega_{\Lambda_b} + \Omega_C} + \sqrt{\Omega_\ell})}{\Omega_m (1 + z_{\text{loit}})^3}, \quad (4.146)$$

which are valid under the single assumption  $\Omega_m (1 + z_{\text{loit}})^3 \ll \Omega_C (1 + z_{\text{loit}})^4$ , or

$$\Omega_m \ll \Omega_C^{3/4} \left( \sqrt{1 + \Omega_{\Lambda_b} + \Omega_C} + \sqrt{\Omega_\ell} \right)^{1/2}. \quad (4.147)$$

From (4.145) and (4.146) one has the useful approximate conditions

$$2\sqrt{\Omega_\ell} \left( \sqrt{1 + \Omega_{\Lambda_b} + \Omega_C} + \sqrt{\Omega_\ell} \right) \approx \Omega_m f(z_{\text{loit}}) (1 + z_{\text{loit}})^3, \quad (4.148)$$

$$\Omega_C \Omega_\ell \approx \frac{3}{4} \left[ \Omega_m f(z_{\text{loit}}) (1 + z_{\text{loit}}) \right]^2. \quad (4.149)$$

In practice, it is often convenient to take the values of  $\Omega_m$ ,  $(1 + z_{\text{loit}})$ , and  $f(z_{\text{loit}})$  as control parameters and to determine the approximate ranges of  $\Omega_\ell$ ,  $\Omega_C$ , and  $\Omega_{\Lambda_b}$  from equations (4.145)–(4.149). In Fig. 4.16, we show, as an example, the range of allowed values for the parameter pair  $\{\Omega_\ell, \Omega_C\}$  for a model which loiters at  $z_{\text{loit}} = 20$  and has  $\Omega_m = 0.3$ .

It is necessary to draw the reader's attention to the fact that not every set of parameter values gives rise to a “realistic” cosmology. For some of them, the Universe recollapses before reaching the present epoch. (The loitering braneworld shares this property with a closed FRW Universe, and the reader is referred to [578] for an extensive discussion of this issue.) It is obvious that the model approaches a recollapsing Universe as the loitering parameter  $f(z_{\text{loit}}) \rightarrow 1$ . Thus, setting  $f(z_{\text{loit}}) = 1$  in estimate (4.149), we obtain the approximate boundary of the region of recollapsing universes in the parameter space  $\{\Omega_\ell, \Omega_C\}$ :

$$\Omega_C \Omega_\ell \gtrsim \frac{3}{4} \Omega_m^2 (1 + z_{\text{loit}})^2, \quad (4.150)$$

which corresponds to the “prohibited” region in Fig. 4.16 for the particular choice of  $z_{\text{loit}} = 20$  and  $\Omega_m = 0.3$ .

#### 4.9.4. Inflation in braneworld models with loitering

The loitering braneworld models considered in the previous section place certain constraint on the duration of the inflationary stage, as we are going to show. First, we note that, during the inflationary stage, the Hubble parameter as a function of the scale factor can be approximated with a great precision as follows [cf. with (4.132)]:

$$H^2(a) = \frac{\rho_i(a)}{3m^2} - 2\frac{\sqrt{-C}}{\ell a^2}, \quad (4.151)$$

where  $\rho_i(a)$  is the energy density during inflation, which typically changes very slowly with the scale factor  $a$ . Since, on the contrary, the last term in (4.151) changes rapidly during inflation, one can easily see that inflation *should have a beginning* in this model at the scale factor roughly given by the estimate

$$a_i^2 \simeq \frac{6m^2\sqrt{-C}}{\ell\rho_i}, \text{ or } \left(\frac{a_i}{a_0}\right)^2 \simeq \frac{2\rho_0}{\rho_i}\sqrt{\Omega_\ell\Omega_C}. \quad (4.152)$$

Using (4.149), one can write the following estimate for the redshift  $z_i$  at the beginning of inflation:

$$(1 + z_i)^2 \simeq \frac{\rho_i}{\rho_0} \left[ \sqrt{3}\Omega_m f(z_{\text{loit}}) (1 + z_{\text{loit}}) \right]^{-1}, \quad (4.153)$$

where the loitering redshift  $z_{\text{loit}}$  and the quantity  $f(z_{\text{loit}})$ , which quantifies the degree of loitering and takes values in the range between zero and unity, are defined in Sec. 4.9.3.

To estimate the *total number* of the inflationary  $e$ -foldings, we consider a simple model of inflation based on the inflaton  $\phi$  with potential  $V(\phi) = \frac{1}{2}m_\phi^2\phi^2$ . In this case, as can be shown, inflation proceeds at the values of the scalar field  $\phi_i \simeq M_P \equiv \sqrt{8\pi}m$  and ends approximately at  $\phi_f \simeq M_P^2/\sqrt{12\pi}$ . This leads to the following relation between the typical energy density during inflation and at its end:

$$\frac{\rho_i}{\rho_f} \simeq 12\pi. \quad (4.154)$$

Then using (4.153) and the estimate for the redshift at the end of inflation

$$1 + z_f = \frac{a_0}{a_f} \simeq \frac{T_{\text{rh}}}{T_0} \simeq \left(\frac{\rho_f}{\Omega_r\rho_0}\right)^{1/4} \quad (4.155)$$

which assumes that preheating takes place instantaneously with effective temperature  $T_{\text{rh}}$ , we can estimate the redshift ratio

$$\begin{aligned} \frac{z_i}{z_f} &\simeq \left[ \frac{4\rho_i^2}{27\rho_0\rho_f} \frac{\Omega_r}{\Omega_m^2 f^2(z_{\text{loit}})(1+z_{\text{loit}})^2} \right]^{1/4} \simeq \\ &\simeq \left[ \frac{16\pi\rho_i}{9\rho_0} \frac{\Omega_r}{\Omega_m^2 f^2(z_{\text{loit}})(1+z_{\text{loit}})^2} \right]^{1/4}. \end{aligned} \quad (4.156)$$

Here,  $\Omega_r \simeq 10^{-5}$  is the current value of the radiation density parameter.

For our typical loitering redshift  $z_{\text{loit}} \approx 18$ , for the degree of loitering  $f(z_{\text{loit}}) \sim 1$ , and for the estimate of the inflationary energy density in agreement with the CMB fluctuations spectrum as [579]  $\rho_i/\rho_0 \sim 10^{112}$ , this will restrict the total number of inflationary  $e$ -foldings  $N$  by

$$e^N \equiv \frac{z_i}{z_f} \lesssim 10^{26} \simeq e^{60}. \quad (4.157)$$

It is interesting that the *total* number of inflationary  $e$ -foldings in the loitering braneworld is close to the expected number of  $e$ -foldings associated with horizon crossing in inflationary models [579]. The exact upper bound on the number of inflationary  $e$ -foldings depends on a concrete model of braneworld inflation in the presence of loitering, and we propose to study this issue in greater detail in a future work.

Returning to (4.151), we would like to draw the reader's attention to the fact that, depending upon the form of the inflaton potential, the evolution of the Hubble parameter at very early times could have proceeded in two fundamentally different and complementary ways:

(i) If the shape of the inflaton potential  $V(\phi)$  is sufficiently flat, then, for a field rolling slowly,  $\rho_i = \rho_\phi$  behaves like a slowly varying  $\Lambda$  term. As a result, the  $1/a^2$  term is expected to dominate at early times giving rise to a cosmological "bounce" ( $H \simeq 0$ ) when the two terms in (4.151) become comparable.

(ii) Alternatively, it might well be that the potential  $V(\phi)$  is not uniformly flat, but changes its form and becomes steep for large values of  $\phi$  (within the context of chaotic inflation). In this case, the bounce will be avoided if, for small values of  $a$ ,  $\rho_i(a)$  increases faster than the  $1/a^2$  term in (4.151). Such a rapid change in  $\rho_i(a)$  at early times will be accompanied by the fast rolling of the inflaton field until the latter evolves to values where the potential is sufficiently flat for inflation to commence.

Interestingly, both (i) and (ii) lead to departures from scale invariance of the primordial fluctuation spectrum on very large scales, and have been discussed in [580] and [581], respectively, as providing a means of suppressing power on very large angular scales in the CMB fluctuation spectrum. In analogy with the discussion in these papers, we expect that the present loitering

scenario too may give rise to a smaller amplitude for scalar perturbations on the largest scales, thereby providing better agreement with the CMB anisotropy results obtained by COBE [14, 582] and WMAP [94].

## 4.10. Quiescent singularities

### 4.10.1. Homogeneous case

In this section, we describe another interesting property of the braneworld theory, namely, that it admits cosmological singularities of very unusual form and nature [574]. Let us first consider the case with  $N = 1$  in action (4.7). The corresponding cosmological equation of the theory is (4.76), where the integration constant  $C$  corresponds to the presence of a black hole in the five-dimensional bulk solution, and the term  $C/a^4$  (occasionally referred to as ‘dark radiation’) arises due to the projection of the bulk gravitational degrees of freedom onto the brane.

The new singularities that we are going to discuss in this section are connected with the fact that the expression under the square root of (4.76) *turns to zero* at some point during evolution, so that solutions of the cosmological equations *cannot be continued* beyond this point. There are essentially two types of ‘quiescent’ singularities displaying this behavior:

A **type 1** singularity (S1) is essentially induced by the presence of the ‘dark radiation’ term under the square root of (4.76) and arises in either of the following two cases:

- $C > 0$  and the density of matter increases *slower* than  $a^{-4}$  as  $a \rightarrow 0$ . Such singularities occur if the Universe is filled with matter having equation of state  $p/\rho < 1/3$ , an example is provided by pressureless matter (dust) for which  $\rho \propto a^{-3}$ . A special case is an empty Universe ( $\rho = 0$ ).

- The energy density of the Universe is radiation-dominated so that  $\rho = \rho_0/a^4$  and  $C > \rho_0$ .

The singularities discussed above can take place either in the past of an expanding Universe or in the future of a collapsing one.

A **type 2** singularity (S2) arises if

$$\ell^2 \left( \frac{\sigma}{3m^2} - \frac{\Lambda_b}{6} \right) < -1. \quad (4.158)$$

In this case, it is important to note that the combination  $\rho/3m^2 - C/a^4$  decreases monotonically as the Universe expands. The expression under the square root of (4.76) can therefore become zero at suitably late times, in which case the cosmological solution cannot be extended beyond this time. Singularity S2 is even more interesting than S1 since: (i) it can occur during the late time expansion of the Universe; (ii) it can occur *even if* dark radiation is entirely absent ( $C = 0$ ).

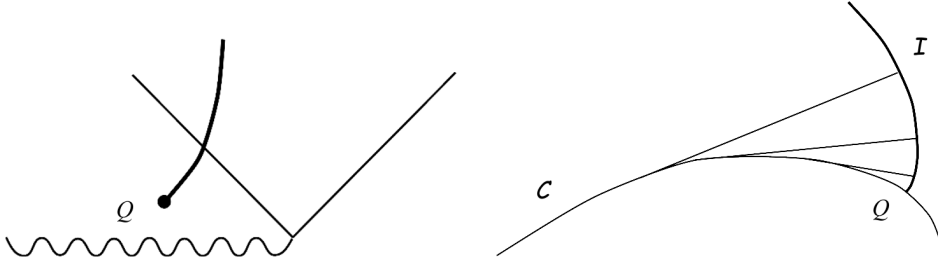


**Fig. 4.17.** Conformal diagram showing the trajectory of a spatially spherical braneworld embedded in the five-dimensional Schwarzschild space-time. The trajectory is not smoothly extendable beyond the point  $Q$

**Fig. 4.18.** The involute  $\mathcal{I}$  of a planar curve  $\mathcal{C}$  is not smoothly extendable beyond the starting point  $Q$

For both S1 and S2, the scale factor  $a(t)$  and its first time derivative remain finite, while all the higher time derivatives of  $a(t)$  tend to infinity as the singularity is approached. As an example consider a type 2 singularity with  $C = 0$ , for which

$$\frac{d^n a}{dt^n} = \mathcal{O}([\rho(t) - \alpha]^{3/2-n}), \quad n \geq 2, \quad (4.159)$$

as  $\rho(t) \rightarrow \alpha = \Lambda_b m^2/2 - \sigma - 3m^2/\ell^2$ . We therefore find that the scalar curvature  $R \rightarrow \infty$  near the singularity, while the energy density and pressure remain finite. Although this situation is quite unusual from the viewpoint of the intrinsic dynamics on the brane, it becomes comprehensible when one considers the embedding of the brane in the bulk. As we already know, the cosmological braneworld under consideration can be isometrically embedded in the five-dimensional solution of the vacuum Einstein equations described by metric (4.12), (4.13). The embedding of the brane is defined by the function (4.14), and one can then proceed to define evolution in terms of the proper cosmological time  $t$  of the induced metric on the brane, given by (4.15). The cosmological singularity under consideration is connected with the fact that the brane embedding is not extendable beyond some moment of time  $T$  because the function  $a(T)$  that defines the embedding cannot be smoothly continued beyond this point (see Fig. 4.17).

This specific feature of the brane embedding can be compared to the behavior of the involute of a planar curve. The involute  $\mathcal{I}$  of a convex planar curve  $\mathcal{C}$  is a line which intersects the tangent lines of  $\mathcal{C}$  orthogonally [583].  $\mathcal{I}$  can be visualized as the trajectory described by the end of a strained thread winding up from  $\mathcal{C}$  (see Fig. 4.18). The involute of a typical curve is sharp at the starting point  $Q$  so that it is not smoothly extendable beyond the point  $Q$ .

This analogy can be traced further. Note that the evolution of the brane in theory (4.7) is described by equation (4.9) which, for the case  $N = 1$ , reads

$$m^2 G_{ab} + \sigma h_{ab} = M^3 (K_{ab} - h_{ab}K) + T_{ab}. \quad (4.160)$$

One can see that it is the influence of the extrinsic curvature on the right-hand side that leads to the singularities under investigation, so that the singularity of the Einstein tensor  $G_{ab}$  is accompanied by the singularity of the extrinsic curvature  $K_{ab}$ , while the induced metric  $h_{ab}$  and the stress-energy tensor  $T_{ab}$  on the brane remain finite. Quite similarly, the involute of a curve is defined through the extrinsic curvature of its embedding in the plane, as is clear from Fig. 4.18, and its singularity at the point  $Q$  is connected with the fact that the extrinsic curvature diverges at this point. Specifically, the parametric equation for the involute  $\mathbf{x}_*(s)$ ,  $s \geq 0$ , in Cartesian coordinates on the plane can be written as [583]

$$\mathbf{x}_*(s) = \mathbf{x}(q - s) + s \cdot \mathbf{x}'(q - s), \quad (4.161)$$

where  $\mathbf{x}(s)$  is the curve  $\mathcal{C}$  parametrized by the natural parameter  $s$ , and  $\mathbf{x}(q) = \mathbf{x}_*(0)$  is the coordinate of the starting point  $Q$  of the involute. The extrinsic curvature of the involute is

$$k(s) = \frac{1}{s}, \quad (4.162)$$

which diverges at the starting point  $Q$  corresponding to  $s = 0$ .

One should also highlight an important difference between the 1D and 4D embeddings: the involute being one-dimensional, a singularity in its extrinsic curvature does not lead to a singularity in its intrinsic geometry. As we have seen, this is not the case with the brane for which the extrinsic and intrinsic curvatures are related through (4.9), so that a singularity in  $K_{ab}$  is reflected in a singularity in  $G_{ab}$ .

Interestingly, an S2 singularity can arise in the distant future of a Universe resembling our own. To illustrate this we can consider Eq. (4.78) with  $\Omega_C = 0$ . For simplicity, we shall only discuss the solution corresponding to the upper sign in (4.80) (called BRANE2 in Sec. 4.6 and in [308]). Our model satisfies the constraint equation (4.79) with  $\Omega_C = 0$ . Inequality (4.158) now becomes

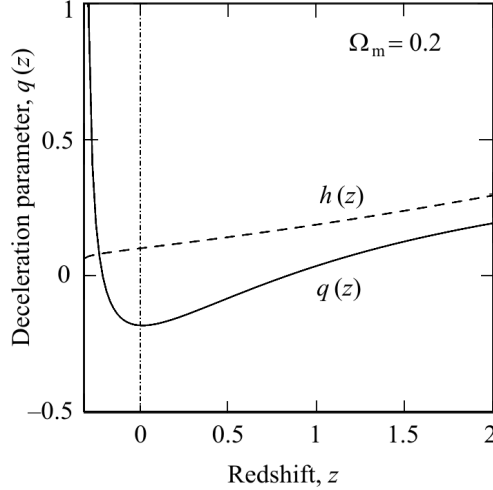
$$\Omega_\sigma + \Omega_\ell + \Omega_{\Lambda_b} < 0, \quad (4.163)$$

and the limiting redshift,  $z_s = a_0/a(z_s) - 1$ , at which the braneworld becomes singular is given by

$$z_s = \left( -\frac{\Omega_\sigma + \Omega_\ell + \Omega_{\Lambda_b}}{\Omega_m} \right)^{1/3} - 1. \quad (4.164)$$



**Fig. 4.19.** The deceleration parameter (solid line) is shown for a braneworld model with  $\Omega_m = 0.2$ ,  $\Omega_\ell = 0.4$ ,  $\Omega_{\Lambda_b} = \Omega_\kappa = 0$ , and  $\Omega_\sigma$  determined from (4.79). We find that  $q(z) \rightarrow 0.5$  for  $z \gg 1$  while  $q(z) \rightarrow \infty$  as  $z \rightarrow -0.312779\dots$  Currently  $q_0 < 0$ , which indicates that the Universe is accelerating. Also shown is the dimensionless Hubble parameter  $h(z) = 0.1 \times H(z)/H_0$  (dashed line) for this model. The vertical line at  $z = 0$  shows the present epoch. Figure taken from [574]



The time of occurrence of the singularity (measured from the present moment) can easily be determined from

$$\Delta t_s = t(z = z_s) - t(z = 0) = \int_{z_s}^0 \frac{dz}{(1+z)H(z)}, \quad (4.165)$$

where  $H(z)$  is given by (4.80) (see also [545]). In Fig. 4.19 we show a specific braneworld model having  $\Omega_m = 0.2$ ,  $\Omega_\ell = 0.4$ ,  $\Omega_{\Lambda_b} = \Omega_\kappa = 0$ . In keeping with observations of high-redshift supernovae, our model Universe is currently accelerating [3], but will become singular at  $z_s \simeq -0.3 \Rightarrow a(z_s) \simeq 1.4 \times a_0$ , i.e. after  $\Delta t_s \simeq 4.5 h^{-1}$  Gyr ( $h = H_0/100$  km/sec/Mpc). Figure 4.19 demonstrates that the deceleration parameter (4.84) becomes singular as  $z_s$  is approached:  $\lim_{z \rightarrow z_s} q(z) \rightarrow \infty$ , while the Hubble parameter remains finite:

$$\frac{H^2(z_s)}{H_0^2} = \Omega_\ell - \Omega_{\Lambda_b}. \quad (4.166)$$

It should be noted that, for a subset of parameter values, inequality (4.163) can be satisfied simultaneously with  $\Omega_{\Lambda_b} > \Omega_\ell$ . In these models, the Universe will recollapse (under the influence of the negative brane tension) before the S2 singularity is reached. (The marginal case  $\Omega_{\Lambda_b} = \Omega_\ell$  corresponds to the Hubble parameter vanishing *at* the singularity.)

### 4.10.2. Inhomogeneous case

The preceding discussion focused on a homogeneous and isotropic Universe whose expansion was governed by the brane equations of motion. Since the real Universe is quite inhomogeneous on spatial scales  $\lesssim 100$  Mpc, it is worthwhile to ask whether any of our previous results may be generalized to this case.

Although we are not yet able to provide a self-consistent treatment of the brane equations for this important case, still, some aspects of the problem can be discussed at the phenomenological level. Consider, for instance, the expansion law (4.76) with  $C = 0$ . A necessary condition for the existence of a quiescent singularity is that the matter density  $\rho$  drops to a value which is small enough for the square root on the right-hand side of (4.76) to vanish. When this happens, the Universe encounters the quiescent singularity at which  $\rho$  and  $H$  remain finite, but  $\ddot{a}$  and higher derivatives of the scale factor diverge. Note, however, that, according to (4.76), the Universe encounters the quiescent singularity *homogeneously*, i.e., every part of the (spatially infinite) Universe encounters the singularity at *one and the same* instant of time. This follows from the fact that the density in (4.76) depends only upon the cosmic time and nothing else. In practice, however, the Universe is anything but homogeneous: its density varies from place to place. For instance, it is well known that the density of matter in galaxies is  $\gtrsim 10^6$  times the average value while, in voids, it drops to only a small fraction of the average value. This immediately suggests that the brane should encounter the quiescent singularity in a very inhomogeneous fashion. Underdense regions (voids) will be the first to encounter the singularity. Even in this case, since the density in individual voids is inhomogeneously distributed, more underdense regions lying closer to the void center will be the first to experience the singularity. It therefore follows that the quiescent singularity will first form near the centers of very underdense regions. As the void expands, its density at larger radii will drop below  $\rho_s$ , where

$$\sqrt{1 + \ell^2 \left( \frac{\rho_s + \sigma}{3m^2} - \frac{\Lambda_b}{6} \right)} = 0; \quad (4.167)$$

consequently, the singularity will propagate outward from the void center in the form of a quasi-spherical singular front. (For simplicity, we have assumed that all voids have a spherical density profile; this assumption may need to be modified for more realistic cases; see [584–588] and references therein.)

The above approach provides us with a very different perspective of the quiescent singularity than that adopted in the previous subsection (and in [574]). For one thing, the singularity may be present in certain regions of the Universe *right now*, so it concerns us directly (as astrophysicists) and not as some abstract point to which we may (or may not) evolve in the distant future. The second issue is related to the first, since the singularity could already exist

within several voids (there are as many as a million voids in the visible Universe in at least some of which the condition  $\rho \simeq \rho_s$  could be satisfied), a practical observational strategy needs to be adopted to search for singularities in voids. (Similar strategies combined with strenuous observational efforts have led to the discovery of dozens of black holes in the centers of galaxies [589].)

A number of important issues therefore need to be addressed:

1. Since  $R_{iklm}R^{iklm} \rightarrow \infty$  within a finite region at the very center of a void, it follows that, unless this region is contained within an event horizon, we will find ourselves staring at a naked singularity. (As shown in [590], quantum effects do soften the singularity so that  $R_{iklm}R^{iklm}$  may remain finite if these effects are included.)

2. The moment we drop the homogeneity assumption, the issue of particle production immediately crops up, and we must take it into account if our treatment is to be at all complete [591, 592]. (In a related context, the quantum creation of gravitons takes place even in a homogeneous and isotropic Universe, since these fields couple minimally, and not conformally, to gravity [593, 594].)

Let us discuss the possible effect of particle production in more detail. First, we consider the model of homogeneous Universe taking it as an approximation to the situation inside an underdensity region (void). Gravitational quantum particle production occurs as the singularity is approached. Since the local value of the Hubble parameter remains finite at the singularity, production of the conformally coupled particles (like photons) is expected to be negligible. However, particles that are non-conformally coupled to gravity (which could be, for example, Higgs bosons in the Standard Model) will be copiously produced as the acceleration of the Universe  $\ddot{a}$  rapidly increases. The rate of particle production depends not only on their coupling to gravity but also on their coupling between themselves. Gravitationally created primary particles will decay into conformally coupled secondaries (electrons, photons, neutrino, etc.), which will influence the rate of production of the primaries by causing decoherence in their quantum state. The whole process is thus not easy to calculate in detail. However, from very general arguments it can be seen that creation of matter due to quantum particle production is important for the dynamics of the Universe during its later stages<sup>8</sup>.

For the sake of physical simplicity, we restrict ourselves to the case of vanishing bulk cosmological constant  $\Lambda_b$  and write Eq. (4.76) in the form

$$H = \frac{1}{\ell} + \sqrt{\frac{\Delta\rho}{3m^2}}, \quad (4.168)$$

<sup>8</sup> Effects of particle production are negligible in the neighborhood of the usual cosmological singularity of the Friedmann Universe because the energy density of ordinary matter and radiation strongly diverges and thus dominates at this singularity [421, 591, 592]. In our case, the energy density of ordinary matter remains finite during the classical approach to the quiescent singularity, hence, particle production effects are of crucial significance.

where

$$\Delta\rho = \rho - \rho_s, \quad \rho_s = -\sigma - \frac{3m^2}{\ell^2}, \quad (4.169)$$

and where we have chosen the physically interesting “+” sign in Eq. (4.76). Thus, we have two free parameters in our theory, namely,  $\ell$  and  $\rho_s$ . The value of  $m$  is assumed to be of the order of the Planck mass. In this case the early-time behavior of the Universe follows the standard Friedmann model, as can be seen from (4.76) or (4.168).

Let the average particle energy density production rate be  $\dot{\rho}_{\text{prod}}$ . Then, differentiating Eq. (4.168), we obtain

$$\dot{H} = \frac{\dot{\rho}_{\text{prod}} - \gamma H \rho}{2(3m^2 \Delta\rho)^{1/2}}, \quad (4.170)$$

where  $\gamma > 0$  corresponds to the effective equation of state of matter in the Universe: if  $p = w\rho$ , then  $\gamma = 3(1 + w)$ . The second term in the numerator of (4.170) follows from the conservation law and describes the effect of the Universe expansion on the matter density. (Note that  $\rho$  includes contributions from quantum and classical matter.)

In order to qualitatively assess the effects of particle production, let us examine two fundamentally distinct possibilities.

1. Suppose that, in the course of evolution,  $\Delta\rho \rightarrow 0$  is reached in a finite interval of time. Since the Hubble parameter is a unique function of the energy density, given by (4.168), and since the singularity value  $\rho_s$  of the energy density is approached from above, it follows that  $\dot{H} \leq 0$  in the neighborhood of the singular point. In the purely classical case we find, after setting  $\dot{\rho}_{\text{prod}}$  to zero in (4.170), that  $\dot{H} \rightarrow -\infty$  as the quiescent singularity is approached. It is well known, however, that particle production effects are sensitive to the change in the rate of expansion [421], and it is expected that  $\dot{\rho}_{\text{prod}}$  will go to infinity as  $\dot{H} \rightarrow -\infty$ . Since  $\dot{\rho}_{\text{prod}} \gg \gamma H \rho$ , this will result in  $\dot{H}$  becoming positive, which contradicts the assumption that  $\dot{H} \leq 0$ .

Therefore, under the assumption that the critical density  $\rho_s$  is reached in a finite time, the only possibility for  $\dot{H}$  is to *remain bounded*. In other words, the rate of particle production should exactly balance the decrease in the matter density due to expansion, turning the numerator in (4.170) to zero:

$$\dot{\rho}_{\text{prod}} - \gamma H \rho \rightarrow 0 \Rightarrow \dot{\rho}_{\text{prod}} \rightarrow \frac{\gamma \rho_s}{\ell} \text{ as } \rho \rightarrow \rho_s. \quad (4.171)$$

In this case, the Universe reaches its singular state with the energy density due to particle production exactly balancing the density decrease caused by expansion, as given by (4.171).

2. It is not clear whether the above regime will be realized or whether, if realized, it will be stable, since it requires the exact balancing of rates (4.171)

at the singularity. A second distinct possibility is that, due to the presence of particle production, the value of  $\Delta\rho = \rho - \rho_s$  always remains bounded from below by a non-zero density. In this scenario,  $\dot{H}$  initially decreases ( $|\dot{H}|$  increases) under the influence of the increasing factor  $1/\sqrt{\Delta\rho}$  in (4.170). However, a large value of  $|\dot{H}|$  induces active particle production from the vacuum which leads to an increase in the value of  $\dot{\rho}_{\text{prod}}$  in (4.170). As the value of  $\Delta\rho$  reaches its (non-zero) minimum, we have  $\dot{H} = 0$  at this point, according to (4.168), after which the rate  $\dot{H}$  becomes positive due to self-sustained particle production that continues because of the large value of the second time derivative  $\ddot{H}$ . After a period of extensive particle production, the Universe reaches another turning point  $\dot{H} = 0$  after which it continues to expand according to (4.168) with decreasing energy density. Thus, we arrive at a model of cyclic evolution with periods of extensive particle production alternating with periods of classical expansion during which quantum particle production is negligible. This scenario bears a formal resemblance to quasi-steady-state cosmology proposed in a very different context by Hoyle, Burbidge, and Narlikar [595–597]. The particle production rate in our case is estimated by the quantity  $\dot{\rho}_{\text{prod}}$  given in (4.171), which is approximately the value it takes at the turning points where  $\dot{H} = 0$ . The Hubble parameter in this scenario periodically varies being of the order of  $H \sim \ell^{-1}$ , and the energy density is of the order  $\rho_s$ , so that particle production rate is

$$\dot{\rho}_{\text{prod}} \sim \frac{\gamma\rho_s}{\ell}. \quad (4.172)$$

Our discussion thus far was limited to quantum processes within a single underdense region (void) which was assumed for simplicity to be perfectly homogeneous. Let us now (qualitatively) discuss whether this scenario can be generalized to the real (inhomogeneous) Universe. Clearly, the particle production rate  $\dot{\rho}_{\text{prod}}$  in this case should be regarded as being averaged over the entire Universe, to which several significantly underdense voids are contributing. Equation (4.170) should therefore be treated as an ensemble average, where the *mean* particle production rate depends upon the distribution as well as dynamics of *local* underdensity regions. As a result, equation (4.170) is not expected to explicitly depend upon the behavior of the Hubble parameter and, in principle, particle production can proceed even in a De Sitter-like Universe, in which the Hubble parameter  $H$  remains constant in time. The rate of particle production in this case is given by equality (4.170) with zero left-hand side:

$$\dot{\rho}_{\text{prod}} = \gamma H \rho. \quad (4.173)$$

The value of the Hubble parameter in such a steady-state Universe can be related to the  $\Omega$ -parameter in matter

$$\Omega_{\text{m}} = \frac{\rho}{\rho_s} = \frac{\rho}{3m^2 H^2}, \quad (4.174)$$

where we have used the basic Eq. (4.168). For the average energy density, we obviously have  $\rho - \rho_s \approx \rho$ . Hence,

$$H = \frac{1}{\ell} + \sqrt{\frac{\Delta\rho}{3m^2}} \approx \frac{1}{\ell} + \sqrt{\frac{\rho}{3m^2}} = \frac{1}{\ell} + H\sqrt{\Omega_m}, \quad (4.175)$$

or, finally<sup>9</sup>,

$$H \approx \frac{1}{\ell(1 - \sqrt{\Omega_m})}. \quad (4.176)$$

In principle, one might use these preliminary results to construct a braneworld version of steady-state cosmology, in which matter is being created at a steady rate in voids rather than in overdense regions (as hypothesized in the original version [595, 596]). This would then add one more model to the steadily growing list of dark-energy cosmologies [236, 568]. These conclusions must, however, be substantiated by a more detailed treatment which takes into account the joint effect of vacuum polarization and particle production near the quiescent singularity.

#### 4.11. Asymmetric branes

In this section, we consider the properties of a more generic braneworld model with  $N = 2$ , i.e., the physical case where the brane is a boundary of two bulk spaces (has two sides). Two possibilities of principle exist in this case: either the bulk space is constrained to be symmetric with respect to the  $Z_2$  group of reflections relative to the brane, or such a symmetry is not imposed. The case where the bulk is symmetric is equivalent to the geometrical setting with  $N = 1$ , which we were considering up to now. An embedded brane without the  $Z_2$  symmetry is, however, a more general case with rich possibilities for cosmology [505, 598–614]).

We consider a braneworld model described by action (4.7) with  $N = 2$ . We shall focus on the asymmetric case with  $\Lambda_1 \neq \Lambda_2$  and  $M_1 \neq M_2$ , which appears to be preferable from a string-theory perspective. For instance, the dilaton stabilized in different vacuum states on adjacent sides of the brane would lead to an effective five-dimensional theory with  $M_1 \neq M_2$ . The string landscape is likely to favor  $\Lambda_1 \neq \Lambda_2$ , which also occurs in domain wall scenarios.

In the absence of  $Z_2$  symmetry, cosmological evolution of the brane is described by the general equation (4.18), in which we set  $N = 2$ . In that equation,  $\rho$  is the total energy density of matter on the brane, and  $\zeta_i = \pm 1$ ,  $i = 1, 2$ , correspond to the two possible ways of bounding each of the bulk spaces  $\mathcal{B}_i$ ,  $i = 1, 2$ , by the brane. We classify the resulting four branches according

<sup>9</sup>For comparison, the late-time value of the Hubble parameter in LCDM is [236]  $H = H_0\sqrt{1 - \Omega_m}$ .

to the signs of  $\zeta_1$  and  $\zeta_2$  as  $(++)$ ,  $(+-)$ ,  $(-+)$ , or  $(--)$ <sup>10</sup>. In the limit of  $Z_2$  symmetry, the branches  $(--)$  and  $(++)$  become the normal branch (BRANE1) and self-accelerating branch (BRANE2), respectively (see Sec. 4.6). The other two so-called *mixed* branches are characterized by  $\zeta_1\zeta_2 = -1$ .

In this section, we study the implications of (4.18) for a spatially flat Universe ( $\kappa = 0$ ) without dark radiation ( $C_i = 0$ ,  $i = 1, 2$ ). Equation (4.18) then simplifies to

$$H^2 = \frac{\rho + \sigma}{3m^2} + \frac{1}{m^2} \sum_{i=1,2} \zeta_i M_i^3 \sqrt{H^2 - \frac{\Lambda_i}{6}} = \frac{\rho + \sigma}{3m^2} + \sum_{i=1,2} \frac{\zeta_i}{\ell_i} \sqrt{H^2 + \lambda_i^{-2}}, \quad (4.177)$$

where we have introduced the fundamental lengths

$$\ell_i = \frac{m^2}{M_i^3}, \quad \lambda_i = \sqrt{-\frac{6}{\Lambda_i}}, \quad i = 1, 2, \quad (4.178)$$

assuming negative values of the bulk cosmological constants.

Note that (4.177) can be rewritten in terms of an *effective* cosmological constant,  $\Lambda_{\text{eff}}$ , as

$$H^2 = \frac{\rho}{3m^2} + \frac{\Lambda_{\text{eff}}}{3}, \quad (4.179)$$

where

$$\frac{\Lambda_{\text{eff}}}{3} = \frac{\sigma}{3m^2} + \sum_{i=1,2} \frac{\zeta_i}{\ell_i} \sqrt{H^2 + \lambda_i^{-2}}, \quad (4.180)$$

which is useful for the study of the cosmological properties of this braneworld. A pictorial representation of the branches described by (4.177) is given in Appendix 5.5.

We consider the late-time evolution of the Universe, in which the energy density  $\rho$  is dominated by matter with the equation of state  $p = 0$ . Then, introducing the cosmological parameters as in (4.77),

$$\Omega_m = \frac{\rho_0}{3m^2 H_0^2}, \quad \Omega_\sigma = \frac{\sigma}{3m^2 H_0^2}, \quad \Omega_{\ell_i} = \ell_i^{-2} H_0^{-2}, \quad \Omega_{\lambda_i} = \lambda_i^{-2} H_0^{-2}, \quad (4.181)$$

where  $\rho_0$  and  $H_0$  are the current values of the matter density and Hubble parameter, respectively, we rewrite (4.177) in terms of the cosmological redshift  $z$ :

$$h^2(z) \equiv \frac{H^2(z)}{H_0^2} = \Omega_m (1+z)^3 + \Omega_\sigma + \sum_{i=1,2} \zeta_i \sqrt{\Omega_{\ell_i}} \sqrt{h^2(z) + \Omega_{\lambda_i}}. \quad (4.182)$$

<sup>10</sup> Note that, in the case of  $Z_2$  symmetry, there are only two ways of bounding the bulk by the brane, and these were called BRANE1 and BRANE2 in [308] and in Sec. 4.6. Of these, BRANE2 contains the self-accelerating DGP brane as a subclass, while BRANE1 can lead to phantom acceleration.

This equation implicitly determines the function  $h(z)$ , and explicitly the inverse function  $z(h)$ . Note that the dimensionless cosmological parameters are related through the constraint equation

$$\Omega_m + \Omega_\sigma + \sum_{i=1,2} \zeta_i \sqrt{\Omega_{\ell_i}} \sqrt{1 + \Omega_{\lambda_i}} = 1. \quad (4.183)$$

We now proceed to describe the specific features of braneworld cosmology without  $Z_2$  symmetry, some of which reproduce those discussed in the preceding sections for the  $Z_2$ -symmetric case.

#### 4.11.1. Induced cosmological constant on the brane

One way of accounting for cosmic acceleration within the framework of braneworld theory with mirror symmetry was suggested in [515, 516] and described by Eq. (4.21). An extension of this model to the case when mirror symmetry is absent is obtained by setting to zero the cosmological constants on the brane and in the bulk, so that  $\sigma = 0$ ,  $\Lambda_i = 0$ ,  $i = 1, 2$ . The expansion law (4.177) then simplifies to

$$H^2 - H \sum_{i=1,2} \frac{\zeta_i}{\ell_i} = \frac{\rho}{3m^2}, \quad (4.184)$$

which evolves to a De Sitter limit at late times

$$\lim_{z \rightarrow -1} H(z) = H_{\text{DS}} = \sum_{i=1,2} \frac{\zeta_i}{\ell_i}, \quad (4.185)$$

provided  $\sum_{i=1,2} \zeta_i/\ell_i$  is positive, which is true for branches  $(++)$  and  $(+-)$ , provided  $M_1 > M_2$  in the latter case. If  $m$  is of the order of the Planck mass  $M_{\text{P}} \simeq 10^{19}$  GeV, then the values of  $M_i \sim 100$  MeV can explain the observed cosmic acceleration. [The self-accelerating solution (4.21) corresponds to the  $(++)$  branch with  $\ell_1 = \ell_2$ .]

The absence of mirror symmetry provides a new avenue for this mechanism. Specifically, the observed cosmic acceleration can be produced on one of the mixed branches with *arbitrarily high* values of the bulk Planck masses  $M_1$  and  $M_2$ , provided these values are sufficiently close to each other. If  $0 < \Delta M \equiv M_1 - M_2 \ll M_1$ , then we have

$$H_{\text{DS}} = \frac{M_1^3 - M_2^3}{m^2} \approx \frac{3M_1^2}{m^2} \Delta M \quad (4.186)$$

on the  $(+-)$  branch, and, by adjusting the value of  $\Delta M$ , one can always achieve an observationally suitable value of  $H_{\text{DS}}$ . For example, if  $M_1, M_2 \sim m$ , then one needs  $\Delta M \sim H_0$ .

The previous model gave one example of late-time acceleration in the absence of the (brane) cosmological constant. We now derive another model



with the same property but with a more flexible assumption  $\Lambda_i \neq 0$ . Setting  $\sigma = 0$  and  $\Lambda_i \neq 0$  in (4.177) leads to

$$H^2 - \sum_{i=1,2} \frac{\zeta_i}{\ell_i} \sqrt{H^2 - \frac{\Lambda_i}{6}} = \frac{\rho}{3m^2}, \quad (4.187)$$

which evolves to a different De Sitter limit, expressed by the equation

$$\lim_{z \rightarrow -1} H^2(z) = H_{\text{DS}}^2 = \sum_{i=1,2} \frac{\zeta_i}{\ell_i} \sqrt{H_{\text{DS}}^2 + \lambda_i^{-2}}, \quad (4.188)$$

where the length scales  $\ell_i$  and  $\lambda_i$  are defined in (4.178).

It is interesting that a tiny asymmetry between the two bulk spaces can lead to a small cosmological constant being induced on the brane [614]. Provided the bulk parameters  $M_1$  and  $M_2$  as well as  $\Lambda_1$  and  $\Lambda_2$  are close to each other, a neat cancellation on the right-hand side of (4.188), which occurs for  $\zeta_1 \zeta_2 = -1$ , leads to a small value of  $H_{\text{DS}}$ . Remarkably, this can happen even for very large values of the bulk constants. In particular, assuming that  $\lambda_i \ll H_{\text{DS}}^{-1}$ , we have

$$H_{\text{DS}}^2 \approx \left| \frac{1}{\ell_1 \lambda_1} - \frac{1}{\ell_2 \lambda_2} \right| \quad (4.189)$$

for one of the mixed branches. Thus, for bulk parameters of the order of a TeV,  $M_i \sim 1 \text{ TeV}$ ,  $\lambda_i \sim 1 \text{ TeV}^{-1}$ , we recover the current value of the Hubble parameter ( $H_{\text{DS}} \sim H_0$ ) provided

$$|\ell_1 \lambda_1 - \ell_2 \lambda_2|^{1/2} \sim 10^{-13} \text{ TeV}^{-1} \sim 10^{-30} \text{ cm}. \quad (4.190)$$

Equations such as (4.186) or (4.189), (4.190) certainly represent fine tuning, with a tiny difference between bulk parameters only slightly breaking the smoothness of the metric across the brane<sup>11</sup>. In the limit of exact equality of the bulk constants on the two sides of the brane, the branches with  $\zeta_1 \zeta_2 = -1$  describe a smooth bulk space, and the brane approaches the limit of a stealth brane [611], evolving according to the usual Einstein equations without affecting the bulk space.

#### 4.11.2. Cosmic mimicry

For large values of the bulk parameters, we encounter the phenomenon of *cosmic mimicry* which, in the context of  $Z_2$  symmetry, was described in Sec. 4.8 and in [553]. Note that, during the radiation and matter-dominated epochs, the expansion of the Universe follows the general-relativistic prescription

$$H^2 \approx \frac{\rho + \sigma}{3m^2}, \quad (4.191)$$

<sup>11</sup> Perhaps, the small asymmetry in the fundamental constants characterizing the bulk can be explained by the presence of the brane itself. For instance, the presence of the brane could lead to a small difference in the quantum contribution to the effective action of the bulk on its two sides, inducing slightly different bulk constants.

where  $\sigma/m^2$  plays the role of the cosmological constant on the brane. However, at very late times, cosmic expansion gets modified due to extra-dimensional effects. Indeed, if  $\lambda_i \ll H_0^{-1}$ , then the square root in the last term of (4.177) can be expanded in the small parameter  $\lambda_i^2 H^2$  at late times, and the braneworld expands according to LCDM, namely

$$H^2 = \frac{8\pi G\rho}{3} + \frac{\Lambda}{3} \quad (4.192)$$

with

$$8\pi G = m^{-2} \left( 1 - \sum_{i=1,2} \frac{\zeta_i \lambda_i}{2\ell_i} \right)^{-1}, \quad (4.193)$$

$$\Lambda = \left( \frac{\sigma}{m^2} + \sum_{i=1,2} \frac{3\zeta_i}{\ell_i \lambda_i} \right) \left( 1 - \sum_{i=1,2} \frac{\zeta_i \lambda_i}{2\ell_i} \right)^{-1}. \quad (4.194)$$

Note that both  $G$  and  $\Lambda$  are *independent of time*. Equations (4.192)–(4.194) have important ramifications. They inform us that the ‘bare’ value of the cosmological constant on the brane,  $\sigma$ , is ‘screened’ at late times by extra-dimensional effects resulting in its effective value  $\Lambda$ . Thus, the early-time and late-time values of the cosmological constant are likely to be different, and this makes our model open to verification.

Also note that one can have  $\Lambda \neq 0$  even if  $\sigma = 0$ . Then, a small  $\Lambda$ -term can be induced during late-time evolution on the brane *solely by extra-dimensional effects*, as pointed out in the previous section. The mechanism by which the induced  $\Lambda$ -term becomes relatively small consists in a compensation of two potentially large terms with opposite signs in equation (4.194). Specifically, for small values of  $\lambda_i$  (which correspond to large values of  $\Lambda_i$ ) such that  $\lambda_i/\ell_i \ll 1$ , in the case  $\sigma = 0$ , we have, approximately,

$$\Lambda \approx \sum_{i=1,2} \frac{3\zeta_i}{\ell_i \lambda_i}, \quad (4.195)$$

which is another form of the result (4.189) for one of the mixed branches. What is remarkable here is that a *positive* cosmological constant on the brane can be sourced by bulk cosmological constants which are *negative*.

From (4.192), (4.193) we also find that the effective gravitational constants during the early and late epochs are related by a multiplicative factor

$$1 - \sum_{i=1,2} \frac{\zeta_i \lambda_i}{2\ell_i}, \quad (4.196)$$

which can be larger as well as smaller than unity, depending on the braneworld branch. This factor will be closer to unity for the mixed branches ( $\zeta_1 \zeta_2 =$

$= -1$ ) than it is for the usual branches ( $\zeta_1 \zeta_2 = 1$ ) which survive in the case of  $Z_2$  symmetry.

Focusing on the important case where  $\sigma = 0$  and the effective four-dimensional cosmological constant is induced entirely by five-dimensional effects, we find that, at redshifts significantly below the *mimicry redshift*

$$z_m \simeq \left( \frac{\Omega_{\lambda_i}}{\Omega_m} \right)^{1/3} - 1, \quad \Omega_{\lambda_1} \simeq \Omega_{\lambda_2}, \quad (4.197)$$

the brane expansion mimics LCDM

$$h^2(z) = \tilde{\Omega}_m (1+z)^3 + \Omega_\Lambda, \quad z \ll z_m, \quad (4.198)$$

with ‘screened’ values of the cosmological parameters:

$$\tilde{\Omega}_m = \Omega_m \left( 1 - \sum_{i=1,2} \frac{\zeta_i}{2} \sqrt{\frac{\Omega_{\ell_i}}{\Omega_{\lambda_i}}} \right)^{-1}, \quad (4.199)$$

$$\Omega_\Lambda = \sum_{i=1,2} \zeta_i \sqrt{\Omega_{\ell_i}} \sqrt{\Omega_{\lambda_i}} \left( 1 - \sum_{i=1,2} \frac{\zeta_i}{2} \sqrt{\frac{\Omega_{\ell_i}}{\Omega_{\lambda_i}}} \right)^{-1}. \quad (4.200)$$

On the other hand, from (4.192) it follows that, at high redshifts, the Universe expands as SCDM

$$h^2(z) = \Omega_m (1+z)^3, \quad z \gg z_m. \quad (4.201)$$

An important distinguishing feature of this model is that the (screened) matter density,  $\tilde{\Omega}_m$ , inferred via geometrical tests based on standard candles and rulers, may not match its (bare) dynamical value  $\Omega_m$ . This allows cosmic mimicry to be distinguished from other cosmological scenarios by means of the *Om diagnostic* suggested in [615]. The fact that brane expansion also follows different laws at low and high redshift provides another important observational test of this model.

### 4.11.3. Phantom branes

In the presence of  $Z_2$  symmetry, the BRANE1 branch of the generic model (4.18) exhibits phantom-like behavior [308] (see Sec. 4.6) which is in excellent agreement with observations [546–548] (see also [309]). Let us see whether this behavior persists when mirror symmetry is absent. Note first that the condition for phantom acceleration,  $w(z) < -1$ , where  $w(z)$  is given by (4.98), has two equivalent formulations:

$$\Omega_m(z) > \frac{2}{3} \frac{d \log H(z)}{d \log(1+z)} \quad \text{and} \quad \dot{\Lambda}_{\text{eff}} > 0, \quad (4.202)$$

where  $\Lambda_{\text{eff}}$  is the effective cosmological constant in (4.180), and differentiation is carried out with respect to the physical time variable. In the case of the  $(--)$  brane ( $\zeta_1 = \zeta_2 = -1$ ), one has

$$\Lambda_{\text{eff}} = \frac{\sigma}{3m^2} - \sum_{i=1,2} \frac{\sqrt{H^2 + \lambda_i^{-2}}}{\ell_i}, \quad (4.203)$$

and we find immediately that  $\Lambda_{\text{eff}}$  *increases with time* when the expansion rate,  $H$ , decreases. It is also quite clear that one (and only one) of the mixed branches will necessarily have a negative value of the sum term in (4.180), again exhibiting phantom behavior.

It is straightforward to verify that  $\dot{\Lambda}_{\text{eff}} > 0$  and  $\dot{H} < 0$  on the two branches exhibiting phantom behavior. Differentiating (4.177) and (4.180), we find

$$\dot{H} = -\frac{\rho}{m^2} \left[ 2 - \sum_{i=1,2} \frac{\zeta_i}{\ell_i \sqrt{H^2 + \lambda_i^{-2}}} \right]^{-1} < 0, \quad (4.204)$$

$$\dot{\Lambda}_{\text{eff}} = 3H\dot{H} \sum_{i=1,2} \frac{\zeta_i}{\ell_i \sqrt{H^2 + \lambda_i^{-2}}} > 0 \quad (4.205)$$

for

$$\sum_{i=1,2} \frac{\zeta_i}{\ell_i \sqrt{H^2 + \lambda_i^{-2}}} < 0.$$

Note that phantom models [51] with constant equation of state,  $w < -1$ , are marked by  $\dot{\Lambda}_{\text{eff}} > 0$  and *super-acceleration*:  $\dot{H} > 0$  at late times<sup>12</sup>. This is related to the fact that the dark-energy (phantom) density in such models *increases*, as the Universe expands, according to

$$\rho_{\text{phantom}} \propto a^{3|1+w|}, \quad w < -1, \quad (4.207)$$

which causes the Hubble parameter to grow at late times, eventually leading to a Big-Rip singularity at which  $H$  diverges. By contrast, although the behavior of our braneworld is phantom-like ( $w_{\text{eff}} < -1$ ), the Universe never super-accelerates since  $\dot{H} < 0$  always holds. Furthermore, since  $H$  decreases during expansion, a Big-Rip-type future singularity which plagues phantom cosmology is absent in the braneworld. From the definition of  $q$  and property  $\dot{H} < 0$ , we find  $q > -1$ . In fact, the deceleration parameter in our model always remains larger than the de Sitter value of  $q = -1$ , approaching it only in the limit of  $t \rightarrow \infty$ .

<sup>12</sup> It is easy to show that, in phantom models, the turning point  $\dot{H} = 0$  occurs at

$$1 + z_* \equiv \frac{a_0}{a(t_*)} = \left( \frac{1 - \Omega_m}{\Omega_m} |1 + w| \right)^{1/3|w|}, \quad w < -1. \quad (4.206)$$

#### 4.11.4. Disappearing dark energy

An important property of this class of braneworld models is that the current acceleration of the Universe need not be eternal. In other words, for a specific relationship between the fundamental parameters in (4.177), the acceleration of the Universe is a *transient* phenomenon, and the Universe reverts back to matter-dominated expansion in the future. Within the context of mirror symmetry, this scenario was called *disappearing dark energy* and discussed in [308] and in Sec. 4.7. In the absence of mirror symmetry, it was studied in [612] under the name *stealth-acceleration* (which should not be confused with the ‘stealth brane’ of [611]).

Transient acceleration implies the property  $H \rightarrow 0$  in the asymptotic future, which requires the following condition to be satisfied:

$$\frac{\sigma}{3m^2} + \sum_{i=1,2} \frac{\zeta_i}{\ell_i \lambda_i} = 0 \Rightarrow \Omega_\sigma + \sum_{i=1,2} \zeta_i \sqrt{\Omega_{\ell_i} \Omega_{\lambda_i}} = 0. \quad (4.208)$$

On the  $(--)$  and  $(++)$  branches, this condition is realized with the following respective values of the brane tension:

$$\frac{\sigma}{3m^2} = \pm \left( \frac{1}{\ell_1 \lambda_1} + \frac{1}{\ell_2 \lambda_2} \right) \Rightarrow \Omega_\sigma = \pm \left( \sqrt{\Omega_{\ell_1} \Omega_{\lambda_1}} + \sqrt{\Omega_{\ell_2} \Omega_{\lambda_2}} \right). \quad (4.209)$$

On the new mixed branches  $(+-)$  and  $(-+)$ , the required brane tension is smaller by absolute value:

$$\frac{\sigma}{3m^2} = \pm \left| \frac{1}{\ell_1 \lambda_1} - \frac{1}{\ell_2 \lambda_2} \right| \Rightarrow \Omega_\sigma = \pm \left| \sqrt{\Omega_{\ell_1} \Omega_{\lambda_1}} - \sqrt{\Omega_{\ell_2} \Omega_{\lambda_2}} \right|. \quad (4.210)$$

Under constraint (4.208), the cosmological evolution equation (4.182) becomes

$$h^2(z) = \Omega_m(1+z)^3 + \sum_{i=1,2} \zeta_i \sqrt{\Omega_{\ell_i}} \left( \sqrt{h^2(z) + \Omega_{\lambda_i}} - \sqrt{\Omega_{\lambda_i}} \right). \quad (4.211)$$

Condition (4.208) is necessary but not sufficient to speak about transient acceleration on a particular branch. A distinguishing property of a transiently accelerating brane is that  $q(z) \rightarrow 0.5$  in the remote past ( $10^5 \gg z \gg 1$ ) as well as in the remote future ( $z \rightarrow -1$ ), reflecting the fact that the Universe is matter dominated in the past and in the future, while, during the current phase, the deceleration parameter is negative,  $q_0 < 0$ . This last condition is realized only if the cosmological expansion law  $H^2(\rho)$  is convex upwards to a sufficiently high degree. Specifically, in view of (4.84), the condition  $q_0 < 0$  can be presented in the form

$$\frac{dH^2(\rho_0)}{d\rho} < \frac{2H_0^2}{3\rho_0}. \quad (4.212)$$

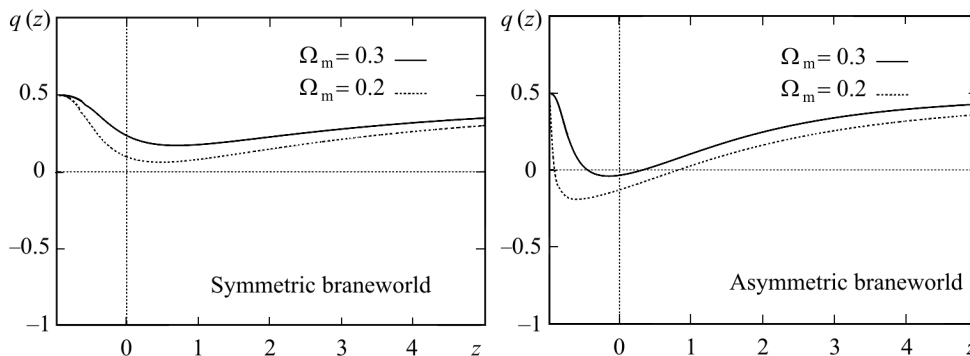


**Fig. 4.20.** The deceleration parameter versus redshift is plotted for the  $(++)$  branch in the case of  $Z_2$  symmetry. The model has the parameters  $\Omega_{\lambda_1} = \Omega_{\lambda_2} = 2$ . We present plots for two different values of the matter density parameter:  $\Omega_m = 0.3$  and  $\Omega_m = 0.2$ . The sets of other parameters are calculated to be  $\Omega_{\ell_1} = \Omega_{\ell_2} = 1.21$ ,  $\Omega_\sigma = -3.11$  and  $\Omega_{\ell_1} = \Omega_{\ell_2} = 1.58$ ,  $\Omega_\sigma = -3.56$ , respectively. In this case, an accelerated regime is not realized, although deceleration is significantly slowed down at the present cosmological epoch. Figure taken from [614]

**Fig. 4.21.** The deceleration parameter versus redshift is plotted for the  $(+-)$  branch in the case of absence of  $Z_2$  symmetry. The model has the parameters  $\Omega_{\lambda_1} = 2$  and  $\Omega_{\lambda_2} = 2.1$ . We present plots for two different sets of values of the remaining two independent parameters:  $(\Omega_m, \Omega_{\ell_1}) = (0.3, 10000)$ , which results in  $(\Omega_{\ell_2}, \Omega_\sigma) = (9954.68, 3.16)$ , and  $(\Omega_m, \Omega_{\ell_1}) = (0.2, 5000)$ , which results in  $(\Omega_{\ell_2}, \Omega_\sigma) = (4840.15, 0.82)$ . Both plots show acceleration at the present cosmological epoch, which generically becomes more prominent for lower values of  $\Omega_m$ . Figure taken from [614]

Looking at figures B.1 and B.2 in Appendix B.2, one can see that this property can be realized only on two of the four branches: on the  $(++)$  branch and on one of the mixed branches.

The expression for the current value of the deceleration parameter can be calculated by using the formula

$$q_0 = \frac{3\Omega_m}{2 - \sum_i \zeta_i \sqrt{\frac{\Omega_{\ell_i}}{1 + \Omega_{\lambda_i}}}} - 1. \quad (4.213)$$

One should note that only four out of five  $\Omega$  parameters are independent in this expression because of the normalization condition  $h^2(0) = 1$  applied to the evolution equation (4.211). In the  $Z_2$ -symmetric case, there remain only two independent  $\Omega$  parameters. It is clear then that transient acceleration can be realized more easily in the  $Z_2$ -asymmetric case. This is illustrated in Figs. 4.20 and 4.21, which show the corresponding behavior of the deceleration parameter  $q(z)$ .

In a transiently accelerating Universe, cosmic acceleration is sandwiched between two matter-dominated regimes. A transiently accelerating braneworld

clearly does not possess the Big Rip of phantom cosmology, nor even the event horizon of de Sitter space. An in-depth study of this class of models [612] has revealed the existence of regions in parameter space which are stable (ghost-free).

We have demonstrated that it is possible to construct braneworld models with transient acceleration. What is less clear is whether such transiently accelerating branches will pass key cosmological tests based on observations of high-redshift type Ia supernovae, baryon acoustic oscillations, etc. This important issue is open for further study.

#### 4.11.5. Quiescent singularities

As discussed in Sec. 4.10, a new feature of brane cosmology is a possible presence of *quiescent* singularities at which the density, pressure and expansion rate remain finite, while the deceleration parameter and the Kretschman invariant,  $R_{iklm}R^{iklm}$ , diverge [574, 590]. The Universe encounters such a singularity in the future if a point is reached during expansion where the derivative of  $H^2$  with respect to  $\rho$  goes to infinity or, equivalently, where the derivative of  $\rho$  with respect to  $H^2$  vanishes. Using (4.177), we can express this condition as the existence of a positive root  $H_s^2$  of the equation

$$\sum_{i=1,2} \frac{\zeta_i}{\ell_i \sqrt{H_s^2 + \lambda_i^{-2}}} = 2, \quad (4.214)$$

and a quiescent singularity is approached as  $H \rightarrow H_s$ . At this moment, expansion formally ceases, and one cannot extend the classical evolution of the brane beyond this point. Such a singular point obviously exists on the  $(++)$  branch if and only if

$$\frac{\lambda_1}{\ell_1} + \frac{\lambda_2}{\ell_2} > 2 \Rightarrow \sqrt{\frac{\Omega_{\ell_1}}{\Omega_{\lambda_1}}} + \sqrt{\frac{\Omega_{\ell_2}}{\Omega_{\lambda_2}}} > 2, \quad (4.215)$$

and it is reachable on this branch if the brane tension  $\sigma$  is sufficiently negative:

$$\frac{\sigma}{3m^2} < H_s^2 - \sum_{i=1,2} \frac{1}{\ell_i} \sqrt{H_s^2 + \lambda_i^{-2}} < 0, \quad (4.216)$$

or, equivalently,

$$\Omega_\sigma < \frac{H_s^2}{H_0^2} - \sum_{i=1,2} \sqrt{\Omega_{\ell_i}} \sqrt{\frac{H_s^2}{H_0^2} + \Omega_{\lambda_i}} < 0. \quad (4.217)$$

Condition (4.214) may or may not be realized on the mixed branches. For example, in the simplifying case  $\ell_1 = \ell_2 = \ell$ , condition (4.214) is realized on the mixed branch  $(+-)$  provided  $\lambda_1 > \lambda_2$ . One can show that the values of the parameters  $\ell_i$ ,  $\lambda_i$ ,  $i = 1, 2$ , in principle can be chosen so that equation (4.214)

has positive roots for three branches  $(++)$ ,  $(+-)$  and  $(-+)$ . To achieve this, one only needs to satisfy the conditions  $\ell_1 > \ell_2$  and  $\lambda_1 \ell_2 > \lambda_2 \ell_1$  and choose sufficiently small values of  $\ell_1, \ell_2$ .

For a graphical presentation of the reasons for the existence of quiescent singularities, the reader can look into Appendix B2. As in the case of mirror symmetry, quantum effects may play an important role in the vicinity of a quiescent singularity [590]; see also [616–618].

We also note that, in the case of mirror symmetry, realization of quiescent singularity requires either negative brane tension or positive bulk cosmological constant (both conditions are suspicious from the viewpoint of possible instabilities). However the quiescent singularity can easily be realized without these assumptions in the asymmetric case on a mixed branch.

The presence of a quiescent singularity in the future of the cosmological evolution does not threaten the past cosmological scenario. Therefore, this issue, just like the issue of Big Rip of phantom cosmology, is mainly of academic interest. Here, we only wish to point out that the possibility of quiescent singularity can be realized rather easily in braneworld theory in certain domain of its parameters without any additional ingredients (such as phantom fields, which lead to Big Rip singularities).

#### 4.11.6. Stability issues

The stability issues of the class of braneworld models without  $Z_2$  mirror symmetry were studied in [612, 613]. It is notable that ghost-free settings of the model with transient acceleration (and phantom acceleration) appear to exist [612]. On the other hand, the analysis in paper [613] reveals the presence of ghosts on a background with a De Sitter vacuum brane on the three branches  $(++)$ ,  $(+-)$ ,  $(-+)$  (i.e., which have at least one ‘+’, so that the bulk at least on one side of the brane has ‘infinite volume’ in terminology of [613]). Whether this situation is critical for the cosmology under investigation remains to be seen. In this connection, it should be noted that the  $(++)$  branch, surviving in the  $Z_2$  symmetric case, contains a ghost and is, therefore, linearly unstable [517–521]. On the other hand, the  $(--)$  branch, responsible for ‘phantom acceleration’ ( $w_0 < -1$ ), is ghost-free in the  $Z_2$  symmetric case and, apparently, also in the general case without  $Z_2$  symmetry.

#### 4.12. Gravitational instability on the brane

In this section, we proceed to the study of cosmological perturbations in a braneworld theory. This subject is not so well developed as the homogeneous cosmology because of evident difficulties connected with the necessity of solving the perturbations equations in the five-dimensional



space and imposing certain boundary conditions. We will concentrate here on the most general features of scalar perturbations, which are of most relevance to the structure formation.

#### 4.12.1. Scalar cosmological perturbations on the brane

The unperturbed metric on the brane is described by the Robertson–Walker line element and brane expansion is described by Eq. (4.76). The two signs in (4.76) describe two different branches corresponding to the two different ways in which a brane can be embedded in the Schwarzschild–anti-de Sitter bulk. In Sec. 4.6, we classified models with lower (upper) sign as BRANE1 (BRANE2). Models with the upper sign can also be called *self-accelerating* because they lead to late-time cosmic acceleration even in the case of zero brane tension and bulk cosmological constant [515, 516]. Throughout this section, we consider the spatially flat case ( $\kappa = 0$ ) for simplicity.

Scalar metric perturbations of this cosmological solution are most conveniently described by the relativistic potentials  $\Phi$  and  $\Psi$  in the so-called longitudinal gauge:

$$ds^2 = -(1 + 2\Phi)dt^2 + a^2(1 - 2\Psi)\gamma_{ij}dx^i dx^j, \quad (4.218)$$

where  $\gamma_{ij}(x)$  is the spatial part of the metric, which is used to raise and lower the spatial indices. The components of the linearly perturbed stress-energy tensor of matter in the coordinate basis are defined by

$$T^\alpha{}_\beta = \begin{pmatrix} -(\rho + \delta\rho), & -\nabla_i v \\ \frac{\nabla^i v}{a^2}, & (p + \delta p)\delta^i{}_j + \frac{\zeta^i{}_j}{a^2} \end{pmatrix}, \quad (4.219)$$

where  $\delta\rho$ ,  $\delta p$ ,  $v$ , and  $\zeta_{ij} = \left(\nabla_i \nabla_j - \frac{1}{3}\gamma_{ij}\nabla^2\right)\zeta$  are small quantities. The symbol  $\nabla_i$  in this section denotes the spatial covariant derivative compatible with the spatial metric  $\gamma_{ij}$  present in (4.218),  $\nabla^2 \equiv \nabla^i \nabla_i$  is the scalar Laplacian, and the spatial indices are raised and lowered using  $\gamma_{ij}$ . Similarly, we introduce the scalar perturbations  $\delta\rho_C$ ,  $v_C$ , and  $\delta\pi_C$  of the tensor  $C_{ab}$  in the coordinate basis:

$$m^2 C^\alpha{}_\beta = \begin{pmatrix} \frac{3m^2 C}{a^4} - \delta\rho_C, & -\nabla_i v_C \\ \frac{\nabla^i v_C}{a^2}, & \left(\frac{\delta\rho_C}{3} - \frac{m^2 C}{a^4}\right)\delta^i{}_j + \frac{\delta\pi^i{}_j}{a^2} \end{pmatrix}, \quad (4.220)$$

where  $\delta\pi_{ij} = \nabla_i \nabla_j \delta\pi_C - \frac{1}{3}\delta_{ij}\nabla^2 \delta\pi_C$ . We call  $v$  and  $v_C$  the momentum potentials for matter and dark radiation, respectively.

Equation (4.52) together with the stress-energy conservation equation for matter and conservation equation (4.57) for dark radiation result in the following complete system of equations describing the evolution of scalar perturbations on the brane:

$$\begin{aligned} \ddot{\Psi} + 3(1 + \gamma)H\dot{\Psi} + H\dot{\Phi} + \left[2\dot{H} + 3H^2(1 + \gamma)\right] \Phi - \frac{\gamma}{a^2} \nabla^2 \Psi - \frac{\kappa(1 + 3\gamma)}{a^2} \Psi + \\ + \frac{1}{3a^2} \nabla^2(\Phi - \Psi) = \left[ c_s^2 - \gamma + \frac{2}{\lambda} \left( c_s^2 - \frac{1}{3} \right) \right] \frac{\delta\rho}{2m^2} + \left( 1 + \frac{2}{\lambda} \right) \frac{\tau\delta S}{2m^2}, \end{aligned} \quad (4.221)$$

$$\delta\dot{\rho} + 3H(\delta\rho + \delta p) = \frac{1}{a^2} \nabla^2 v + 3(\rho + p)\dot{\Psi}, \quad (4.222)$$

$$\dot{v} + 3Hv = \delta p + (\rho + p)\Phi + \frac{2}{3a^2} (\nabla^2 + 3\kappa) \zeta, \quad (4.223)$$

$$\delta\dot{\rho}_C + 4H\delta\rho_C = \frac{1}{a^2} \nabla^2 v_C - \frac{12m^2 C}{a^4} \dot{\Psi}, \quad (4.224)$$

$$\begin{aligned} \dot{v}_C + 3Hv_C = \frac{1}{3} \delta\rho_C - \frac{4m^2 C}{a^4} \Phi + \frac{1}{6} \lambda(1 - 3\gamma) \Delta_m - \frac{2 + \lambda}{3a^2} (\nabla^2 + 3\kappa) \zeta - \\ - \frac{m^2 \lambda}{3a^2} (\nabla^2 + 3\kappa) [\Phi - 3\gamma\Psi], \end{aligned} \quad (4.225)$$

$$\frac{1}{a^2} (\nabla^2 + 3\kappa) \nabla^2 \Psi = \left( 1 + \frac{2}{\lambda} \right) \frac{\Delta_m}{2m^2} + \frac{\Delta_C}{m^2 \lambda}, \quad (4.226)$$

$$m^2 \lambda (\dot{\Psi} + H\Phi) = \left( 1 + \frac{\lambda}{2} \right) v + v_C, \quad (4.227)$$

$$\delta\pi_C = -\frac{m^2}{4} \lambda(3\gamma + 1) \left( \Phi - \Psi + \frac{\zeta}{m^2} \right) - \zeta. \quad (4.228)$$

Here, we use the following notation:  $S$  is the entropy density of the matter content of the Universe,  $\tau = (\partial p / \partial S)_\rho$ ,  $c_s^2 = (\partial p / \partial \rho)_S$  is the adiabatic sound velocity, the time-dependent dimensionless functions  $\lambda$  and  $\gamma$  are given by

$$\lambda \equiv \ell^2 \left( H^2 - \frac{\rho + \sigma}{3m^2} \right) - 2 = \pm 2 \sqrt{1 + \ell^2 \left( \frac{\rho + \sigma}{3m^2} - \frac{\Lambda_b}{6} - \frac{C}{a^4} \right)}, \quad (4.229)$$

$$\gamma \equiv \frac{1}{3} \left( 1 + \frac{\dot{\lambda}}{H\lambda} \right) = \frac{1}{3} \left[ 1 - \frac{\frac{\rho + p}{m^2} - \frac{4C}{a^4}}{2 \left( \frac{\rho + \sigma}{3m^2} + \frac{1}{\ell^2} - \frac{\Lambda_b}{6} - \frac{C}{a^4} \right)} \right], \quad (4.230)$$

and the perturbations  $\Delta_m$  and  $\Delta_C$  are defined as

$$\Delta_m = \delta\rho + 3Hv, \quad \Delta_C = \delta\rho_C + 3Hv_C. \quad (4.231)$$

The overdot, as usual, denotes the partial derivative with respect to the time  $t$ .

The system of equations (4.221)–(4.228) generalizes the result obtained in [510] (for the DGP brane) to the case of a generic braneworld scenario described by (4.7), which allows non-zero values for the brane tension and bulk cosmological constant. It describes two dynamically coupled fluids: matter and dark radiation. It is important to emphasize that the evolution equations (4.224), (4.225) for the dark-radiation component are *not quite* the same as those for ordinary radiation. Of special importance are the source terms on the right-hand side of (4.225) which lead to non-conservation of the dark-radiation density. Thus, the behavior of this component is rather non-trivial, as will be demonstrated in next sections.

It is also interesting to note that the perturbations in dark radiation formally decouple from those in ordinary matter in the important limiting case  $M \rightarrow 0$  (equivalently,  $\ell \rightarrow \infty$ ), for which the system (4.221)–(4.228) reproduces the corresponding equations of General Relativity (after setting  $\gamma = c_s^2$ ).

From equations (4.222)–(4.227), one can derive the following useful system for perturbations in *pressureless* matter and dark radiation in the important case  $C = 0$ :

$$\ddot{\Delta} + 2H\dot{\Delta} = \left(1 + \frac{6\gamma}{\lambda}\right) \frac{\rho\Delta}{2m^2} + (1 + 3\gamma) \frac{\delta\rho_C}{m^2\lambda}, \quad (4.232)$$

$$\dot{v}_C + 4Hv_C = \gamma\Delta_C + \left(\gamma - \frac{1}{3}\right) \Delta_m + \frac{4}{3(1 + 3\gamma)a^2} (\nabla^2 + 3\kappa) \delta\pi_C, \quad (4.233)$$

$$\delta\dot{\rho}_C + 4H\delta\rho_C = \frac{1}{a^2} \nabla^2 v_C, \quad (4.234)$$

where

$$\Delta \equiv \frac{\Delta_m}{\rho} \quad (4.235)$$

is the conventional dimensionless variable describing matter perturbations.

#### 4.12.2. Simplified boundary conditions for scalar perturbations

The system of equations (4.221)–(4.228), or (4.232)–(4.234), describing scalar cosmological perturbations, is not closed on the brane since the quantity  $\delta\pi_C$  in (4.228) or (4.233) (hence, the difference  $\Phi - \Psi$ ) is undetermined and, in principle, can be set arbitrarily from the brane viewpoint. For this reason, one should also consider equations for perturbations in the bulk and impose certain boundary conditions. This will be under consideration further in Sec. 4.13.

From a broad perspective of solving equations in the brane-bulk system, boundary conditions can be regarded as any conditions which restrict the space of solutions. In view of the difficult problems of solving the perturbation equations in the bulk, what some researches usually do in practice is to specify such

conditions directly on the brane by making various reasonable assumptions (see, e.g., [619, 620] for the issue of cosmological perturbations; and [562] for the case of spherically symmetric solutions on the brane). The behavior of the metric in the bulk is of no further concern in this approach, since this metric is, for all practical purposes, unobservable directly. The described approach to the problem of boundary conditions effectively “freezes” certain degrees of freedom in the bulk; but its merit is that it apparently leads to a well-defined closed, local, causal, and, in principle, verifiable theory of gravity in four dimensions. On the other hand, it corresponds to a certain class of approximations to the perturbation equations on the brane [621–623].

As first noted in [522], the intrinsic non-locality and non-closure of the braneworld equations is connected with the dynamical properties of the bulk Weyl tensor projected on to the brane. It, therefore, seems logical to impose certain restrictions on this tensor in order to obtain a closed system of equations on the brane. A general family of boundary conditions on the brane is obtained by relating the quantities  $\pi_{\mathcal{C}}$  and  $\rho_{\mathcal{C}}$ . As a simplest class of such relation which does not involve dimensional parameters, one can set

$$\frac{1}{a^2} \nabla^2 \delta\pi_{\mathcal{C}} = A \delta\rho_{\mathcal{C}}. \quad (4.236)$$

In most of this section,  $A$  shall be assumed to be a (dimensionless) constant. We also consider the simplifying case where the spatial curvature is equal to zero ( $\kappa = 0$ ) and the matter anisotropic stresses are absent ( $\zeta = 0$ ). Then, by virtue of (4.228), this relates the difference  $\Phi - \Psi$  between the gravitational potentials to the perturbation of the dark-radiation density  $\delta\rho_{\mathcal{C}}$ :

$$\frac{1}{a^2} \nabla^2 (\Phi - \Psi) = -\frac{4A}{m^2 \lambda (1 + 3\gamma)} \delta\rho_{\mathcal{C}}. \quad (4.237)$$

For the boundary condition (4.236), one can derive a second-order differential equation for  $\delta\rho_{\mathcal{C}}$  by substituting for  $v_{\mathcal{C}}$  from (4.234) into (4.233):

$$\begin{aligned} \delta\dot{\rho}_{\mathcal{C}} + (10 - \gamma)H\delta\rho_{\mathcal{C}} + 4 \left[ \dot{H} + 3(2 - \gamma)H^2 \right] \delta\rho_{\mathcal{C}} = \\ = \frac{1}{a^2} \nabla^2 \left[ \gamma\delta\rho_{\mathcal{C}} + \frac{4A}{3(1 + 3\gamma)} \delta\rho_{\mathcal{C}} + \left( \gamma - \frac{1}{3} \right) \Delta_{\text{m}} \right]. \end{aligned} \quad (4.238)$$

Equations (4.232) and (4.238) then form a closed system of two coupled second-order differential equations for  $\Delta$  and  $\delta\rho_{\mathcal{C}}$ . From the form of the right-hand side of (4.238) one expects this system to have regions of stability as well as instability. Specifically, a necessary condition for stability on small spatial scales is that the sign of the coefficient of  $\nabla^2 \delta\rho_{\mathcal{C}}$  on the right-hand side of

(4.238) be positive. This leads to the condition<sup>13</sup>

$$A \geq -\frac{3}{4}\gamma(1 + 3\gamma). \quad (4.239)$$

From (4.230), we find that  $\gamma \approx -1/6$  in a matter-dominated Universe, and condition (4.239) simplifies to

$$A \geq \frac{1}{16}. \quad (4.240)$$

We consider two important subclasses of (4.236) which we call the minimal boundary condition and the Koyama–Maartens boundary condition, respectively.

**Minimal boundary condition.** Our simplest condition corresponds to setting  $A = 0$ . In this case, from (4.228) we obtain the relation  $\Phi = \Psi$ , the same as in General Relativity. Under this condition, equations (4.221)–(4.223) constitute a complete system of equations for scalar cosmological perturbations on the brane in which initial conditions for the relativistic potential  $\Phi$ ,  $\dot{\Phi}$  and matter perturbations  $\delta\rho$ ,  $\delta p$ ,  $v$  can be specified quite independently. Once a solution of this system is given, one can calculate all components of dark-radiation perturbations using (4.226) and (4.227). Thus, with this boundary condition, equations (4.224)–(4.227) can be regarded as auxiliary and can be used to facilitate and elucidate the dynamics described by the main system (4.221)–(4.223). We should stress that only the quantities pertaining to the induced metric on the brane ( $\Phi$ ,  $\Psi$ ) and those pertaining to matter ( $\delta\rho$ ,  $\delta p$ ,  $v$ ) can be regarded as directly observable, while those describing dark radiation ( $\delta\rho_C$ ,  $v_C$ ) are not directly observable.

**Koyama–Maartens boundary condition.** In an important paper [621], Koyama and Maartens arrived at condition (4.236) with  $A = -1/2$ :

$$\frac{1}{a^2}\nabla^2\delta\pi_C = -\frac{1}{2}\delta\rho_C. \quad (4.241)$$

This boundary condition was derived in [621, 622] as an approximate relation in the DGP model valid only on small (subhorizon) spatial scales under the assumption of quasi-static behavior. It was later re-derived in [623] under a similar approximation. We call it, therefore, the Koyama–Maartens boundary condition, although one should be aware of the different status of this relation in the present section, where it is regarded as an exact additional relation, and in [621–623], where it is derived as an approximation.

<sup>13</sup> In the absence of matter on the brane,  $\Delta_m = 0$ , equation (4.238) becomes a closed wave-like equation for the scalar mode of gravity, and condition (4.239) becomes the boundary of its stability domain. The existence of such a scalar gravitational mode is due to the presence of an extra dimension.

In discussing the small-scale approximation in quasi-static regime, it was argued in [621,622] that equation (4.234) permits one to neglect the perturbation  $v_C$  in (4.233), which, together with (4.236), will then transform (4.232) into a closed equation for matter perturbations<sup>14</sup>:

$$\ddot{\Delta} + 2H\dot{\Delta} = \Theta_{\text{KM}} \frac{\rho\Delta}{2m^2}, \quad \Theta_{\text{KM}} = 1 + \frac{12A\gamma + 3\gamma + 1}{\lambda [2A + \frac{3}{2}\gamma(1 + 3\gamma)]}. \quad (4.242)$$

Some cosmological consequences of this approach are discussed in [624]. As in General Relativity, this equation does not contain spatial derivatives; hence, the evolution of  $\Delta$  is independent of the spatial scale. We would obtain equation of the type (4.242) for perturbations had we followed the route of [621–623] in finding approximate solutions of perturbation equations in the bulk and using the quasi-static approximation. However, in the approach adopted in this section, as will be shown in the following two sections, numerical integration of the exact linearized system (4.232)–(4.234) does not support approximation (4.242). No matter what initial conditions for dark radiation are set initially, one observes a strong dependence of the evolution of matter perturbations on the wave number. In particular, it is incorrect to neglect the quantity  $v_C$  on small spatial scales, since it is precisely this quantity which is responsible for the dramatic growth of perturbations both in  $\Delta_m$  and in  $\delta\rho_C$  on such scales.

From equations (4.239) and (4.240), we can see that the minimal and Koyama–Maartens boundary conditions generally lead to unstable evolution. This will be confirmed by numerical simulations in the next section.

**Scale-free boundary conditions.** Evolution of perturbations in the stability region (4.239) & (4.240) shows little dependence on spatial scale. It is interesting that there also exists an important class of boundary conditions leading to *exact* scale-independence. We call these, for simplicity, *scale-free boundary conditions*. To remove the dependence on wave number altogether and thereby obtain a theory in which perturbations in matter qualitatively evolve as in standard (post-recombination) cosmology, it suffices to set the right-hand side of (4.233) identically zero:

$$\frac{1}{a^2} \nabla^2 \delta\pi_C = \frac{1 + 3\gamma}{4} [(1 - 3\gamma)\Delta_m - 3\gamma\Delta_C], \quad (4.243)$$

which, in view of equation (4.226), can also be expressed in a form containing only the geometrical quantities  $\delta\pi_C$ ,  $\Delta_C$ , and  $\Psi$ . In this case, the perturbations  $\delta v_C$  and  $\delta\rho_C$  in dark radiation decay very rapidly, according to equations (4.233)

<sup>14</sup>Equation (4.242) was derived in [621,622] only for the DGP model and for the case  $A = -1/2$ ; however, the argument can be extended to a general braneworld model and a general value of  $A$  in (4.236).

and (4.234), and (4.232) reduces to the simple equation

$$\ddot{\Delta} + 2H\dot{\Delta} = \Theta \frac{\rho\Delta}{2m^2}, \quad \Theta = \left(1 + \frac{6\gamma}{\lambda}\right), \quad (4.244)$$

valid on all spatial scales. Equations (4.226) and (4.228) then lead to simple relations between the gravitational potentials  $\Phi$  and  $\Psi$  and matter perturbations:

$$\frac{1}{a^2}\nabla^2\Phi = \Theta \frac{\Delta_m}{2m^2}, \quad \frac{1}{a^2}\nabla^2\Psi = \left(1 + \frac{2}{\lambda}\right) \frac{\Delta_m}{2m^2}. \quad (4.245)$$

The difference  $\Phi - \Psi$  can be conveniently determined from

$$\frac{1}{a^2}\nabla^2(\Phi - \Psi) = \frac{3\gamma - 1}{m^2\lambda}\Delta_m. \quad (4.246)$$

As can easily be seen from (4.228) or (4.246), the general-relativistic relation  $\Phi = \Psi$  is not usually valid in braneworld models. An important exception to this rule is provided by the mimicry models discussed in Sec. 4.12.4.

One can propose other conditions of type (4.243) that lead to scale-independent behavior. For instance, one can equate to zero the right-hand side of (4.238). It remains unclear how these conditions involving perturbations may be generalized to the fully non-linear case. Nevertheless, in view of the interesting properties of scale-independence and the fact that perturbations in the stability region (4.239) and (4.240) behave in this manner, the consequences of (4.244) need to be further explored, and we shall return to this important issue later on in this section.

Having described the system of linearized equations governing the evolution of scalar perturbations in pressureless matter and dark radiation, we now proceed to apply them to two important braneworld models: the popular DGP model [504, 515, 516] and the ‘mimicry’ model suggested in [553] and described in Sec. 4.8. It should be noted that these two models are complementary in the sense that the mimicry model arises for *large values* of the bulk cosmological constant  $\Lambda_b$  and brane tension  $\sigma$ , whereas the DGP cosmology corresponds to the opposite situation  $\Lambda_b = 0$  and  $\sigma = 0$ .

### 4.12.3. Scalar perturbations in the DGP model

Amongst alternatives to LCDM, the Dvali–Gabadadze–Porrati (DGP) model [504] stands out because of its stark simplicity. Like the cosmological constant which features in LCDM, the DGP model too has an extra parameter  $\ell = 2m^2/M^3$ , the length scale beyond which gravity effectively becomes five-dimensional. However, unlike the cosmological constant whose value must be extremely small in order to satisfy observations, the

value  $\ell \sim cH_0^{-1}$ , required to explain cosmic acceleration, can be obtained by a ‘reasonable’ value of the five-dimensional Planck mass  $M \sim 10$  MeV. As pointed out earlier, DGP cosmology belongs to the class of induced gravity models which we examine and is obtained from (4.7) after setting to zero the brane tension and the cosmological constant in the bulk (i.e.,  $\sigma = 0$  and  $\Lambda_b = 0$ ). Under the additional assumption of spatial flatness ( $\kappa = 0$ ), the modified Friedmann equation (4.21) for the upper sign becomes [515, 516]

$$H^2 - \frac{2H}{\ell} = \frac{\rho}{3m^2}. \quad (4.247)$$

In a spatially flat Universe, given the current value of the matter density and Hubble constant,  $\ell$  ceases to be a free parameter and becomes related to the matter density by the following relation

$$\Omega_\ell \equiv \frac{1}{\ell^2 H_0^2} = \left( \frac{1 - \Omega_m}{2} \right)^2, \quad (4.248)$$

which may be contrasted with  $\Omega_{\Lambda_b} = 1 - \Omega_m$  in LCDM.

Linear perturbation equations for this model were discussed in [510, 541, 542, 621, 622, 626, 627]. An approximate boundary condition for scalar perturbations was obtained by Koyama and Maartens [621, 622] on subhorizon scales; it is described by (4.241). For convenience, we present system (4.232)–(4.234) for this case:

$$\ddot{\Delta} + 2H\dot{\Delta} = \left(1 + \frac{6\gamma}{\lambda}\right) \frac{\rho\Delta}{2m^2} + (1 + 3\gamma) \frac{\delta\rho_C}{m^2\lambda}, \quad (4.249)$$

$$\dot{v}_C + 4Hv_C = \gamma\Delta_C + \left(\gamma - \frac{1}{3}\right) \Delta_m - \frac{2}{3(1 + 3\gamma)}\delta\rho_C, \quad (4.250)$$

$$\delta\dot{\rho}_C + 4H\delta\rho_C = \frac{1}{a^2}\nabla^2 v_C. \quad (4.251)$$

In the DGP model, the general expressions (4.229) and (4.230) for  $\lambda$  and  $\gamma$  in the case of pressureless matter reduce to

$$\lambda = 2(\ell H - 1), \quad \gamma = \frac{1}{2(\ell H - 1)^2} - \frac{1}{6}. \quad (4.252)$$

The results of a typical integration of the exact system of equations (4.249)–(4.251) for different values of the wave number  $k$  are shown in Fig. 4.22. We observe a dramatic escalation in the growth of perturbations at moderate redshifts and a strong  $k$ -dependence for perturbations in matter as well as in dark-radiation (the y-axis is plotted in logarithmic units). These results do not support the approximation made in [621, 622], which assumes



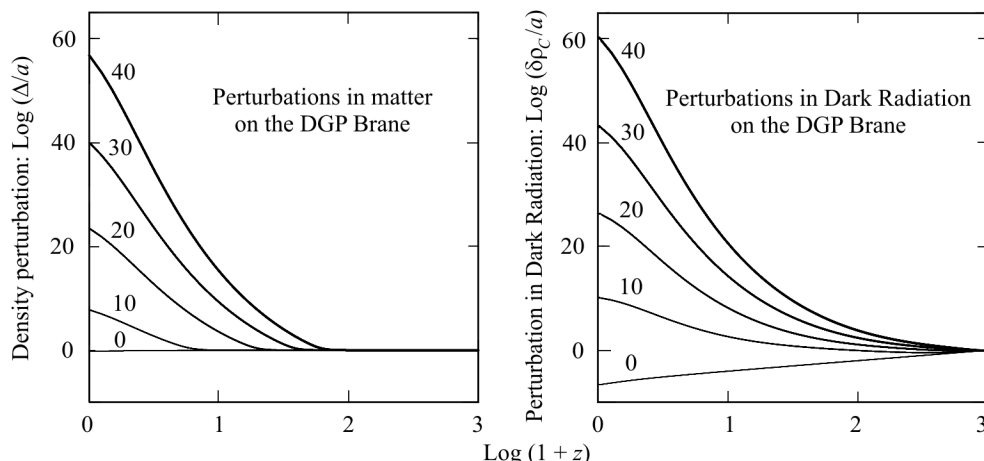


**Fig. 4.22.** The DGP brane with the Koyama–Maartens boundary condition  $A = -1/2$ . Growth of perturbations in matter (left) and dark radiation (right) on the DGP brane are shown for different values of the comoving wave number  $k/a_0 H_0$  (indicated by numbers above the corresponding curves). The current matter density is chosen to be  $\Omega_m = 0.22$ , and the initial value of  $v_C$  is set to zero. (Our results remain qualitatively the same for other values of the density parameter.) Note the dramatic  $k$ -dependence in the growth of perturbations both in matter and in dark radiation. For comparison,  $\Delta/a = 1$  at these redshifts in the standard CDM model with  $\Omega_m = 1$ . Figure taken from [625]

the left-hand side of equation (4.250) to be much smaller than individual terms on its right-hand side for sufficiently large values of  $k$ , and which leads, subsequently, to the scale-independent equation (4.242).

We would like to stress that our conclusions themselves are not based on the small-scale or quasi-static approximation. Indeed, we integrate the *exact* system of equations (4.232)–(4.234) on the brane, and the only ansatz that we set in this system is the boundary condition (4.241).

The strong  $k$ -dependence of the evolution of perturbations can be explained by the presence of the term  $\nabla^2 v_C$  on the right-hand side of (4.251), which leads to the generation of large perturbations of dark radiation  $\delta\rho_C$ . The quantity  $v_C$  is being generated by the right-hand side of equation (4.250). The instability in the growth of perturbations for the Koyama–Maartens boundary condition is in agreement with the fact that the value of  $A = -1/2$  lies well beyond the stability domain (4.240).

As demonstrated earlier, depending upon the value of  $A$ , perturbations on the brane can be either unstable or quasi-stable. By unstable is meant  $\Delta/a \gg 1$  while quasi-stability implies  $\Delta/a \sim O(1)$ . The quasi-stable region (4.239) is illustrated in Fig. 4.23, in which we show the results of a numerical integration of equations (4.232)–(4.234) for  $A = 1/2$ . It is instructive to compare this figure with the left panel of Fig. 4.22. One clearly sees the much weaker growth of perturbations as well as their scale-independence in this case. We

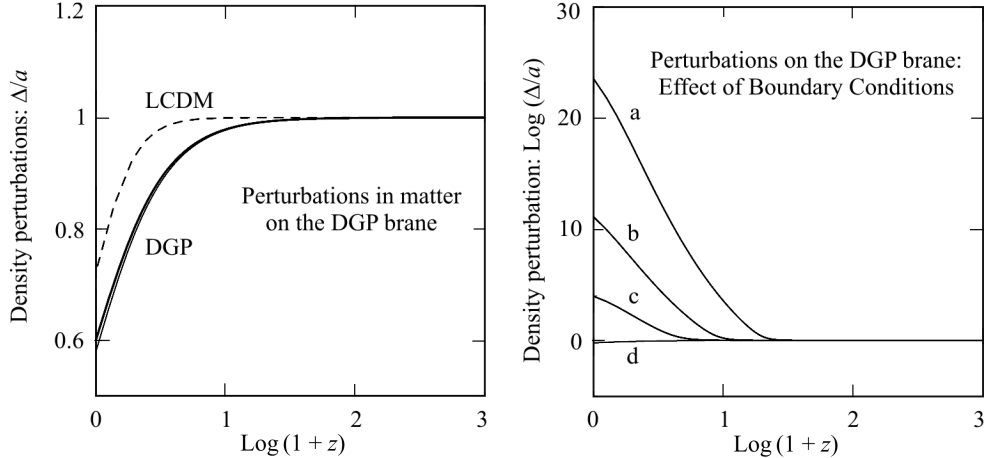


**Fig. 4.23.** The DGP brane with the boundary condition  $A = 1/2$ . The parameters of the model are the same as in figure 4.22 but the y-axis is no longer plotted in logarithmic units. The two solid curves show the evolution of scalar perturbations corresponding to the comoving wave numbers  $k/a_0 H_0 = 0$  (thin curve) and 40 (thick curve). Note that these two curves are almost indistinguishable which illustrates that the growth of perturbations is virtually scale-independent in this case. The dashed line shows the behavior of scalar perturbations in the LCDM model. (In all cases  $\Omega_m = 0.22$  is assumed.) Figure taken from [625]

**Fig. 4.24.** Growth of scalar perturbations in matter on the DGP brane is shown for different boundary conditions in the brane-bulk system. (The comoving wave number  $k/a_0 H_0 = 20$  in all cases.) Boundary conditions are specified by (4.236) and differ in the expression for  $A$ ; namely: (a) the Koyama–Maartens condition  $A = -1/2$ , (b)  $A = -(1 + 3\gamma)/4$ , (c) the minimal condition  $A = 0$ , and (d)  $A = 1/2$ . Condition (b) with time-dependent value of  $A$  was chosen because it simplifies equation (4.225), and condition (d) because it lies well inside the stability domain (4.239). For comparison, note that  $\Delta/a = 1$  for all values of  $k$  in the standard CDM model with  $\Omega_m = 1$ . Figure taken from [625]

therefore conclude that boundary conditions can strongly influence the evolution of perturbations on the brane. Our results are summarized in Fig. 4.24, which shows the evolution  $\Delta/a$  obtained by integrating the system (4.232)–(4.234) for different boundary conditions. (Results for the wave number  $k/a_0 H_0 = 20$  are shown.) We see that the growth of perturbations becomes weaker as the value of  $A$  approaches the stability domain (4.239), and quasi-stability is observed for  $A = 1/2$ .

The behavior of scalar perturbations on the DGP brane in the case of scale-free boundary conditions (4.243) is very similar to that shown in Fig. 4.23. As in [541, 542, 621, 622], we also find that perturbation growth on the DGP brane is slower than that in LCDM.

#### 4.12.4. Scalar perturbations in the mimicry model

*Scale-dependent boundary conditions.* As expected, perturbations in the mimicry model crucially depend upon the type of boundary condition which has been imposed. Generally speaking, brane perturbations grow moderately for BC's which lie in the stability domain (4.239) or (4.240) and more rapidly in the instability region. This remains true for mimicry models. In this section, we explore the behavior of perturbations in this model for the boundary condition  $A = 0$ , which belongs to the instability class. In the next section, we shall explore BC's which give rise to more moderate and scale-independent behavior.

The growth of perturbations if  $A = 0$  is substituted in (4.236) is illustrated in Fig. 4.25. The  $k$ -dependence, clearly seen in this figure, can be understood by inspecting the system of equations (4.232)–(4.234). Even if we start with zero initial conditions for the dark-radiation components  $\delta\rho_C$  and  $v_C$ , the non-trivial right-hand side of Eq. (4.233) leads to the generation of  $v_C$ ; then, via the  $k$ -dependent right-hand side of (4.234), the density  $\delta\rho_C$  is generated, which later influences the growth of perturbations of matter in (4.232). The instability in the growth of perturbations is explained by the fact that the value of  $A = 0$  lies outside the stability domain (4.239) or (4.240). However, the growth of perturbations is not as dramatic in this case as in the DGP model with the Koyama–Maartens BC's, mainly because the value  $A = 0$  lies much closer to the boundary (4.240) than the Koyama–Maartens value  $A = -1/2$ .

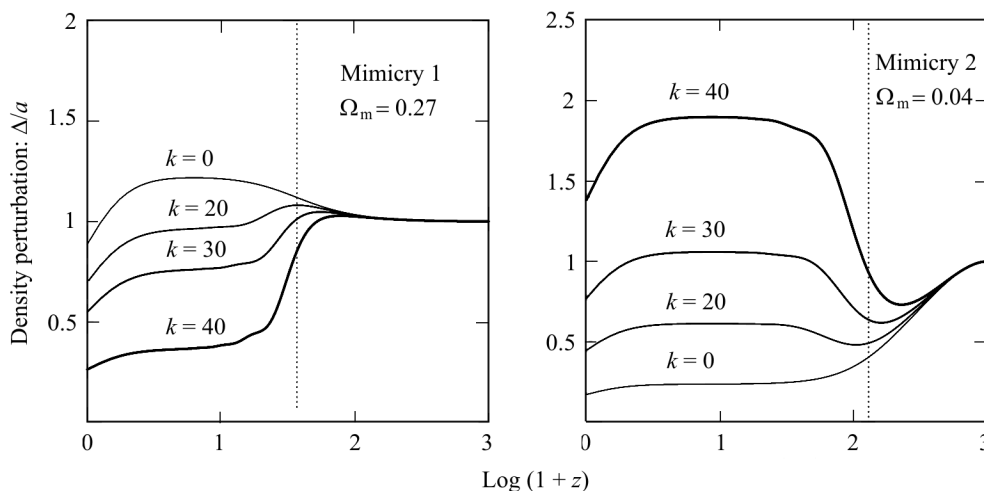


**Fig. 4.25.** Growth of matter perturbations in the Mimicry 1 and Mimicry 2 models are shown for different values of the comoving wave number  $k/a_0H_0$  (indicated by numbers above the corresponding curves) and for the minimal boundary condition  $A = 0$  in (4.236). Both models have the same effective parameter  $\Omega_m^{\text{LCDM}} = 0.22$ , hence, quite different matter content, indicated by the parameter  $\Omega_m$ . The value of  $v_C$  is set to zero initially. The position of the mimicity redshift  $z_m$  is indicated by the vertical dotted lines. Figure taken from [625]

Qualitatively, the evolution of matter perturbations in mimicry models can be understood as follows: during the early stages of matter-domination the last term on the right-hand side of equation (4.232) is not very important, which transforms (4.232) into a closed equation for the matter perturbation. Indeed, in the pre-mimicry regime, for  $z \gg z_m$ , we have  $|\lambda| \gg 1$  for the quantity in the denominator of the last term on the right-hand side of (4.232), which makes this term relatively small for moderate values of  $\delta\rho_C$ . Thus, perturbations in matter evolve according to (4.244) on all spatial scales, for redshifts greater than the mimicry redshift  $z_m$ . For  $z \leq z_m$ , the quantity  $|\lambda|$  is of order unity. By this time, the perturbations  $\delta\rho_C$  have grown large, and their amplitude strongly depends on the wave number. Through the last term in equation (4.232), they begin to influence the growth of matter perturbations for  $z \sim z_m$ , resulting in the  $k$ -dependent growth of the latter. The reason for the opposite  $k$ -dependence of matter perturbations in Mimicry 1 and Mimicry 2 shown in Fig. 4.25 is connected with the difference in the sign of  $\lambda$  — defined in (4.230) — for the two models. Thus, the last term in (4.232) comes with opposite signs in Mimicry 1 and Mimicry 2, and therefore works in opposite directions in these two models.

Well inside the mimicry regime, for  $z \ll z_m$ , we have  $\gamma \approx 1/3$ , so that the second term on the right-hand side of (4.233) can be ignored if matter perturbations are not too large. Then equations (4.233), (4.234), and (4.236) lead to a closed system of equations for the evolution of dark-radiation perturbations. Substituting  $\gamma = 1/3$  into this system, we obtain:

$$v_C = a^{-7/2}\xi, \quad \delta\rho_C = \frac{3}{(1+2A)a^3} \frac{\partial}{\partial t} (a^3 v_C), \quad (4.253)$$

where we assumed  $A \not\approx -1/2$  to be constant. The function  $\xi$  obeys an oscillator-type equation

$$\ddot{\xi} - \left( \frac{1}{2}\dot{H} + \frac{1}{4}H^2 + \frac{1+2A}{3a^2}\nabla^2 \right) \xi = 0. \quad (4.254)$$

This means that both  $\delta\rho_C$  and  $v_C$  rapidly decay during the mimicry regime (oscillating approximately in opposite phase) and the last term on the right-hand side of (4.232) again becomes unimportant. In particular, this will describe the behavior of the mimicry model with the minimal boundary condition  $A = 0$ . The transient oscillatory character of  $\delta\rho_C$  induces transient oscillations with small amplitude in  $\Delta$  through the last term in (4.234). These small oscillations can be noticed in Fig. 4.25 for  $\log(1+z) \gtrsim 1$ , particularly for values 40 and 30 of the comoving wave number<sup>15</sup>.

<sup>15</sup> For the Koyama–Maartens boundary condition  $A = -1/2$ , the approximation described above is not valid during the mimicry stage. Instead, during mimicry, the value of  $v_C$  decays without oscillating approximately as  $v_C \propto 1/a^3$ , as can be seen from equations (4.233), (4.236), and the value of  $\delta\rho_C$  also decays, which follows from (4.234).

Two important features of mimicry models deserve to be highlighted:

1. As demonstrated in Fig. 4.25, there is a strong suppression of long-wavelength modes in Mimicry 2.
2. From this figure, we also find that the growth of short-wavelength modes in Mimicry 2 can be substantial, even in a low-density Universe.

Both properties could lead to interesting cosmological consequences. For instance, the relative suppression of low- $k$  modes may lead to a corresponding suppression of low-multipole fluctuations in the CMB, while the increased amplitude of high- $k$  modes could lead to an earlier epoch of structure formation. (Since the mimicry models behave as  $\Lambda$ CDM at low redshifts, they satisfy the supernova constraints quite well.) A detailed investigation of both effects, however, requires that we know the form of the transfer function of fluctuations in matter (and dark radiation) at the end of the radiative epoch. This open issue lies outside the scope of the present book<sup>16</sup>.

For the minimal boundary condition ( $A = 0$ ), assumed in this section, equations (4.226) and (4.237) imply  $\Phi = \Psi$  and

$$\frac{1}{a^2} \nabla^2 \Phi = \left(1 + \frac{2}{\lambda}\right) \frac{\Delta_m}{2m^2} + \frac{\Delta_c}{m^2 \lambda}, \quad (4.255)$$

which is a generalization of the Poisson equation for the mimicry brane.

Mimicry models with the Koyama–Maartens boundary condition exhibit much stronger instability in the growth of  $\delta\rho_c$  for high values of  $k$ , enhancing the growth of matter perturbations (not shown). This can be explained by the fact that  $A = 0$  is much closer to the boundary of the stability domain (4.240) than the Koyama–Maartens value  $A = -1/2$ . For the latter, the density perturbation  $\Delta$  in the Mimicry 1 model grows to be large and negative, while the perturbation  $\delta\rho_c$  becomes large and positive; for instance, both  $\Delta$  and the dimensionless quantity  $\delta\rho_c/m^2 H^2$  grow by a factor of  $10^{11}$  for  $k/a_0 H_0 = 40$ . This provides another example of the very strong dependence of perturbation evolution on boundary conditions.

In our calculations, we have not found any significant dependence of the eventual growth of perturbations on initial conditions for dark radiation specified in a reasonable range (at  $z = 10^3$ ).

**Scale-free boundary conditions.** As mentioned earlier, BC's lying in the stability region (4.239) lead to an almost scale-free growth of density perturbations. A similar result is obtained if we assume the scale-free boundary condition (4.243) of Sec. 4.12.2. In this case, the momentum potential  $v_c$  decays as  $v_c \propto a^{-4}$ , and its spatial gradients in (4.234) can therefore be neglected. The

<sup>16</sup> For simplicity, the amplitudes of all  $k$ -modes were assumed to be equal at high redshifts in figures 4.22, 4.24 and 4.25. A more realistic portrayal of  $\Delta(k)$  should take into consideration the initial spectrum and the properties of the transfer function for matter and dark radiation.

same is true, of course, if one considers super-horizon modes with  $k \ll aH$ . In both cases, we have approximately  $\delta\rho_{\mathcal{C}} \propto 1/a^4$ , suggesting that the dynamical role of perturbations in dark radiation is unimportant. This results in a radical simplification: as in the DGP model, for BC's lying in the stability region, the growth of perturbations in matter can be effectively described by a single second-order differential equation (4.244), namely,

$$\ddot{\Delta} + 2H\dot{\Delta} = \Theta \frac{\rho\Delta}{2m^2}, \quad \Theta = \left(1 + \frac{6\gamma}{\lambda}\right), \quad (4.256)$$

where  $\lambda$  and  $\gamma$  are defined in (4.229) and (4.230), respectively. We shall call  $\Theta(z)$  in (4.256) the ‘*gravity term*’ since it incorporates the effects of modified gravity on the growth of perturbations. The value of this term on the brane can depart from the canonical  $\Theta = 1$  in General Relativity.

Figure 4.26 shows the behavior of  $\Theta(z)$  for a typical mimicry model. At redshifts significantly larger than the mimicry redshift,  $z \gg z_m$ , we have  $\Theta(z) \simeq 1$ , whereas at low redshifts,  $z \ll z_m$ , the value of  $\Theta(z)$  changes to

$$\Theta(z) \simeq \frac{\Omega_m^{\text{LCDM}}}{\Omega_m} = \frac{\rho^{\text{LCDM}}}{\rho} \quad \text{for } z \ll z_m, \quad (4.257)$$

where  $\rho^{\text{LCDM}}$  is defined in (4.113). The solid line in the same figure shows the ratio of the Hubble parameter on the brane to that in LCDM. The consequences of this behavior for the growth equation (4.244) are very interesting. Substituting (4.257) into (4.244) and noting that  $H(z) \simeq H^{\text{LCDM}}$  during mimicry, we recover the standard equation describing perturbation growth in the LCDM model

$$\ddot{\Delta} + 2H^{\text{LCDM}}\dot{\Delta} = \frac{\rho^{\text{LCDM}}\Delta}{2m^2}. \quad (4.258)$$

Thus, ordinary matter in mimicry models gravitates in agreement with the effective value of the gravitational constant which appears in the cosmological relation (4.125).

We therefore conclude that, deep in the mimicry regime ( $z \ll z_m$ ), perturbations grow *at the same rate* on the brane and in LCDM. This is borne out by Fig. 4.27, which shows the results of a numerical integration of (4.244) for Mimicry 1 [integrating the exact system (4.232)–(4.234) gives indistinguishable results]. Notice that the *total* amplitude of fluctuations during mimicry in this model is *greater on the brane* than in LCDM. Indeed, for mimicry models, we have

$$\frac{\Delta_{\text{brane}}}{\Delta_{\text{LCDM}}} \simeq \frac{\Omega_m}{\Omega_m^{\text{LCDM}}} \quad \text{for } z \ll z_m, \quad (4.259)$$

and this ratio is greater than unity for Mimicry 1.

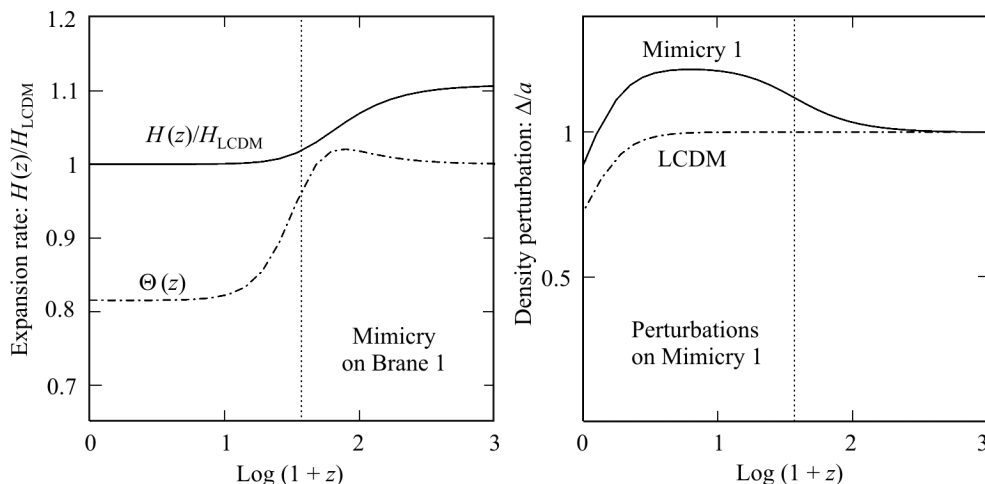


**Fig. 4.26.** The Hubble parameter in the braneworld ‘Mimicry 1’ is shown relative to LCDM (solid). The LCDM model has  $\Omega_m^{\text{LCDM}} = 0.22$  while  $\Omega_m = 0.27$  on the brane. Also shown is the ‘gravity term’  $\Theta(z)$  defined in (4.244) whose value diminishes from unity at high redshifts to the asymptotic form (4.257) at low redshifts. The dotted vertical line shows the mimicry redshift  $z_m \approx 37$ . Figure taken from [625]

**Fig. 4.27.** Density perturbations on the Mimicry 1 brane (dot-dash) and in LCDM (solid). The evolution of perturbations in Mimicry 1 in this case is effectively described by (4.244). In both cases, the perturbation amplitude is scaled by the expansion factor  $a(t)$ . (It may be noted that  $\Delta/a = 1$  in standard CDM with  $\Omega_m = 1$ .) The dotted vertical line shows the mimicry redshift  $z_m \approx 37$ . The braneworld has  $\Omega_m = 0.27$  while  $\Omega_m^{\text{LCDM}} = 0.22$ . This leads to a moderate enhancement in the amplitude of brane perturbations over LCDM. Figure taken from [625]

Since the contribution from perturbations in dark radiation can be neglected, the growth of matter perturbations in Mimicry 2 is again described by (4.244) and by (4.259). However, since  $\Omega_m < \Omega_m^{\text{LCDM}}$  in this case, the final amplitude of perturbations will be *smaller* in Mimicry 2 than the corresponding quantity in LCDM, which is the opposite of what we have for Mimicry 1.

It is interesting that during mimicry, when  $\gamma \approx 1/3$ , the relation between the gravitational potentials  $\Phi$  and  $\Psi$  reduces to the general-relativistic form  $\Phi = \Psi$ , as can be seen from (4.246), where  $\Phi$  satisfies the generalized Poisson equation (4.245), namely,

$$\frac{1}{a^2} \nabla^2 \Phi = \Theta \frac{\Delta_m}{2m^2}. \quad (4.260)$$

An interesting feature of Mimicry 1 is that, at early times, the expansion rate in this model *exceeds* that in LCDM, i.e.,  $H(z)|_{\text{Mimicry1}} > H(z)|_{\text{LCDM}}$  for  $z > z_m$  (see Figs. 4.10 and 4.26). [The opposite is the case for Mimicry 2: the expansion rate in this model is *lower* than that in LCDM at early times, i.e.,

$H(z)|_{\text{Mimicry 2}} < H(z)|_{\text{LCDM}}$  for  $z > z_m$ .] As we can see, this has important consequences for the growth of structure in this model. The increase in the growth of perturbations in Mimicry 1 relative to LCDM occurs during the period before and slightly after the mimicry redshift has been reached, when the relative expansion rate  $H(z)/H^{\text{LCDM}}$  is declining while the ‘gravity term’  $\Theta(z)$  has still not reached its asymptotic form (4.257). A lower value of  $H(z)$  in (4.244) diminishes the damping of perturbations due to cosmological expansion while a slower drop in  $\Theta(z)$  signifies a much more gradual decrease in the force of gravity. Consequently, there is a net increase in the growth of perturbations on the Mimicry 1 brane relative to LCDM<sup>17</sup>. For the models in Fig. 4.27, which have  $\Omega_m^{\text{LCDM}} = 0.22$  and  $\Omega_m = 0.27$ , the increase is about 20%. The increased amplitude of perturbations in Mimicry 1 stands in contrast to the DGP model as well as Quintessence model, in both of which linearized perturbations grow at a *slower* rate than in the LCDM cosmology [541, 542, 621, 622, 628, 629].

It is important to note that observations of galaxy clustering by the 2dFGRS survey provide the following estimate [630, 631] for perturbation growth at a redshift  $z = 0.15$ :

$$\frac{d \log \delta}{d \log a} \equiv - (1 + z) \frac{d \log \delta}{dz} \Big|_{z=0.15} = 0.51 \pm 0.11, \quad (4.261)$$

where  $\delta \equiv \delta\rho/\rho$ . Since the growth of perturbations during the mimicry regime stays proportional to that in the LCDM model ( $\delta_{\text{mimic}} \propto \delta_{\text{LCDM}}$ ,  $z \ll z_m$ ), it follows that if perturbations in the LCDM model satisfy (4.261) (which they do), then so will those in the mimicry scenario. Nevertheless, as we have seen, the *net increase* in the amplitude of perturbations on the brane is *larger than* that in the LCDM model. This clearly has important cosmological consequences since it can enhance structure formation at high redshifts as well as lead to higher values of  $\sigma_8$ . Thus, while preserving the many virtues of the LCDM model, the mimicry models add important new features which could be tested by current and future observations.

## 4.13. Perturbations of the bulk

### 4.13.1. General system of equations

In this section, we consider the full physical problem with perturbations described dynamically also in the bulk [632]. The background bulk metric can be written in the form (4.12), where  $\gamma_{ij}$  is the metric of a maximally symmetric space with coordinates  $x^i$ , and the function  $f(r)$  in our

<sup>17</sup> Figure 4.26 clearly shows that  $H(z)$  reaches its asymptotic form much sooner than  $\Theta(z)$ . Notice that, at redshifts slightly larger than  $z_m$ , the value of  $\Theta(z)$  exceeds unity. The dependence of perturbation growth on the mimicry redshift  $z_m$  is very weak, and (4.259) is a robust result which holds to an accuracy of better than 2% for a wide range of parameter values.



case of  $C = 0$  is given by

$$f(r) = \kappa - \frac{\Lambda_b}{6} r^2. \quad (4.262)$$

The brane is moving along the trajectory (4.14), and the relevant part of the bulk is given by  $r \leq a(\tau)$ . In what follows, we will be interested in the case of a closed Universe  $\kappa = 1$  and  $\Lambda_b \leq 0$ . This makes the brane a spherical boundary of a ball, and the boundary conditions in the bulk are then specified simply as the requirement of regularity in this ball (this can be called “no-boundary conditions”).

It is convenient to present the first part of metric (4.12) in the form  $\gamma_{ab} dx^a dx^b$ , where  $x^a$ ,  $a = 1, 2$  are arbitrary coordinates in place of  $(\tau, r)$ . Thus, for the background metric, we have

$$ds_{\text{bulk}}^2 = \gamma_{ab} dx^a dx^b + r^2 \gamma_{ij} dx^i dx^j, \quad (4.263)$$

where  $r = r(x^a)$ . Some auxiliary expressions for the curvature of this metric are presented in Appendix B.3.

The scalar (with respect to the isometries of  $\gamma_{ij}$ ) perturbations of this metric can be described as in [626]<sup>18</sup>:

$$\begin{aligned} \delta g_{AB} dx^A dx^B = & \sum_k \left( h_{ab} Y dx^a dx^b + 2h_a V_i dx^a dx^i + \right. \\ & \left. + [h_L T_{(L)ij} + h_Y T_{(Y)ij}] dx^i dx^j \right), \end{aligned} \quad (4.264)$$

where  $Y$ ,  $V_i \equiv \nabla_i Y$ ,  $T_{(L)ij} \equiv 2\nabla_i \nabla_j Y - \frac{2}{3} \gamma_{ij} \nabla^2 Y$ , and  $T_{(Y)ij} \equiv \gamma_{ij} Y$  are the harmonics defined in [626], depending on the coordinates  $x^i$  and all expressible through the scalar harmonic  $Y$ , and  $h_{ab}$ ,  $h_a$ ,  $h_L$ , and  $h_Y$  are the perturbation coefficients depending on  $x^a$ . Here, as before,  $\nabla_i$  is the covariant derivative with respect to the metric  $\gamma_{ij}$ . The number  $k$  characterizes the Laplacian eigenvalue of the scalar harmonics  $Y$  as defined in [626].

Infinitesimal coordinate transformations of scalar type are defined by the vector field  $\xi^A$  which has the form

$$\xi_A dx^A = \sum_k (\xi_a Y dx^a + \xi V_i dx^i). \quad (4.265)$$

Under diffeomorphisms, perturbations transform as follows:

$$h_{ab} \rightarrow h_{ab} - \nabla_a \xi_b - \nabla_b \xi_a, \quad (4.266)$$

$$h_a \rightarrow h_a - \xi_a - r^2 \nabla_a (r^{-2} \xi), \quad (4.267)$$

$$h_L \rightarrow h_L - \xi, \quad (4.268)$$

$$h_Y \rightarrow h_Y - \xi^a \nabla_a r^2 + \frac{2}{3} k^2 \xi. \quad (4.269)$$

<sup>18</sup> In this subsection, we denote the five-dimensional space-time indices by capital Latin letters.

Here,  $\nabla_a$  is the covariant derivative in the two-dimensional space spanned by  $(\tau, r)$ , compatible with the metric  $\gamma_{ab}$ . From these quantities, one can construct gauge-invariant variables

$$F_{ab} = h_{ab} - \nabla_a X_b - \nabla_b X_a, \quad (4.270)$$

$$F = h_Y - X^a \nabla_a r^2 + \frac{2}{3} k^2 h_L, \quad (4.271)$$

where

$$X_a = h_a - r^2 \nabla_a (r^{-2} h_L) \quad (4.272)$$

is a gauge-dependent combination that transforms as  $X_a \rightarrow X_a - \xi_a$ .

Note that perturbations of the tensors which are equal to zero for the background solution are gauge-invariant: if  $T_{\dots}$  is any such tensor, then, under the infinitesimal coordinate transformations  $x^A \rightarrow x^A - \xi^A$ , its components transform as

$$\delta T_{\dots} = \mathcal{L}_\xi T_{\dots} = 0, \quad (4.273)$$

i.e., are invariant. In particular, perturbations of the Weyl tensor  $C^A{}_{BCD}$  (and all its contractions and derivatives) as well as perturbations of the Einstein–De Sitter tensor

$$E_{AB} = G_{AB} + \Lambda_b g_{AB} \quad (4.274)$$

are gauge-invariant because these tensors are identically equal to zero for the background solution (4.12).

Using the gauge transformations (4.267), (4.268), one can fix the gauge in such a way as to turn the coefficients  $h_L$  and  $h_a$  to zero (at least, this is possible to do locally). In this gauge, the coefficients  $h_{ab}$  and  $h_Y$  coincide with the gauge invariants  $F_{ab}$  and  $F$ , respectively, and the metric perturbation then simplifies to

$$\delta g_{AB} dx^A dx^B = \sum_k Y \left( F_{ab} dx^a dx^b + F \gamma_{ij} dx^i dx^j \right). \quad (4.275)$$

Expression in this gauge can be used whenever one is to calculate gauge-invariant perturbations, such as perturbations of the Weyl tensor  $C^A{}_{BCD}$ , which is zero for the background solution.

Another set of simplifications can be obtained by taking into account the equations of motions in the bulk (4.8), which can be presented as

$$\mathcal{R} = \frac{10}{3} \Lambda_b, \quad \mathcal{R}_{AB} = \frac{2}{3} \Lambda_b g_{AB}. \quad (4.276)$$

Using these relations, one can express the Weyl tensor in the bulk as follows:

$$\begin{aligned} \mathcal{C}_{ABCD} &\equiv \mathcal{R}_{ABCD} - \frac{2}{3} (g_{A[C} \mathcal{R}_{D]B} - g_{B[C} \mathcal{R}_{D]A}) + \frac{1}{6} \mathcal{R} g_{A[C} g_{D]B} = \\ &= \mathcal{R}_{ABCD} - \frac{1}{3} \Lambda_b g_{A[C} g_{D]B}. \end{aligned} \quad (4.277)$$

However, when calculating the curvature tensor  $\mathcal{R}_{ABCD}$  to get the perturbed equations of motion in the bulk, one needs to deal with the complete metric perturbation (4.275).

Using (4.277) and equations (B.20), (B.21) and (B.22) from Appendix B.4, one easily computes the components of the perturbed bulk Weyl tensor  $\mathcal{C}_{ABCD}$  in the gauge  $h_L = 0$ ,  $h_a = 0$ . After that, the coefficients  $h_{ab}$  and  $h_Y$  can be replaced with gauge invariants  $F_{ab}$  and  $F$ , respectively. Thus, using (4.12) and (4.262), one can express the perturbed bulk Weyl tensor as

$$\delta\mathcal{C}_{abcd} = \sum_k \left[ \frac{\Lambda_b}{6} (\gamma_{d[a} F_{b]c} - \gamma_{c[a} F_{b]d}) + \nabla_d \nabla_{[a} F_{b]c} - \nabla_c \nabla_{[a} F_{b]d} \right] Y, \quad (4.278)$$

$$\delta\mathcal{C}_{iabc} = \sum_k \left( \nabla_{[c} F_{b]a} - \frac{1}{r} F_{a[b} \nabla_{c]} r \right) \nabla_i Y, \quad (4.279)$$

$$\delta\mathcal{C}_{abij} = 0, \quad (4.280)$$

$$\begin{aligned} \delta\mathcal{C}_{aibj} = & -\frac{1}{2} \sum_k F_{ab} (\nabla_i \nabla_j Y) + \\ & + \frac{1}{2} \gamma_{ij} \sum_k \left[ r (\nabla_e r) (\nabla_a F^e_b + \nabla_b F^e_a - \nabla^e F_{ab}) - \right. \\ & \left. - \frac{\Lambda_b r^2}{3} F_{ab} - \frac{\Lambda_b}{6} \gamma_{ab} F - r \nabla_a \nabla_b \left( \frac{F}{r} \right) \right] Y, \end{aligned} \quad (4.281)$$

$$\delta\mathcal{C}_{aijk} = \sum_k \left[ r^2 \nabla_a \left( \frac{F}{r^2} \right) - r (\nabla^b r) F_{ab} \right] \gamma_{i[j} \nabla_{k]} Y, \quad (4.282)$$

$$\begin{aligned} \delta\mathcal{C}_{ijkl} = & \sum_k F (\gamma_{i[l} \nabla_{k]} \nabla_j Y - \gamma_{j[l} \nabla_{k]} \nabla_i Y) + \\ & + 2 \gamma_{i[k} \gamma_{l]j} \sum_k \left[ r^2 (\nabla_a r) (\nabla_b r) F^{ab} + \left( \kappa - \frac{\Lambda_b r^2}{3} \right) F - r (\nabla_a r) (\nabla^a F) \right] Y. \end{aligned} \quad (4.283)$$

Expressed in this way, the perturbed bulk Weyl tensor is not obviously traceless. In fact, as follows from (4.277),  $\delta\mathcal{C} = \delta\mathcal{R}$ , and  $\delta\mathcal{C} = 0$  only if the perturbed equations of motion in the bulk are taken in to account.

It was shown by Mukohyama (see [626]) that the gauge invariants  $F_{ab}$  and  $F$ , satisfying the perturbed bulk equations of motion, can be expressed through a scalar master variable  $\Omega$  as

$$r F_{ab} = \nabla_a \nabla_b \Omega - \frac{2}{3} \nabla^2 \Omega \gamma_{ab} - \frac{\Lambda_b}{18} \Omega \gamma_{ab}, \quad (4.284)$$

$$F = \frac{r}{3} \left( \nabla^2 \Omega + \frac{\Lambda_b}{3} \Omega \right), \quad (4.285)$$

where  $\Omega$  is a solution of the master equation

$$\nabla^2 \Omega - \frac{3}{r} \nabla_a r \nabla^a \Omega - \left( \frac{k^2 - 3\kappa}{r^2} + \frac{\Lambda_b}{6} \right) \Omega + \frac{U}{r^2} = 0 \quad (4.286)$$

with some function  $U$ , which, in general case, is a solution of

$$\nabla_a \nabla_b U + \frac{\Lambda_b}{6} \gamma_{ab} U = 0. \quad (4.287)$$

One can verify that the trace  $\delta\mathcal{C}$  of the perturbed bulk Weyl tensor  $\delta\mathcal{C}_{ABCD}$ , defined by (4.278)–(4.283), can be expressed through the Mukohyama master variable  $\Omega$  as

$$\delta\mathcal{C} = -\frac{1}{3r^3} \sum_k \left[ \nabla^2 (r^2 \Sigma) + \frac{\Lambda_b r^2}{3} \Sigma \right] Y, \quad (4.288)$$

where

$$\Sigma \equiv \nabla^2 \Omega - \frac{3}{r} \nabla_a r \nabla^a \Omega - \left( \frac{k^2 - 3\kappa}{r^2} + \frac{\Lambda_b}{6} \right) \Omega. \quad (4.289)$$

Obviously, the Mukohyama master equation (4.286) implies the condition  $\delta\mathcal{C} = 0$ .

#### 4.13.2. Perturbations on the flat background bulk geometry

The general problem of solving the Mukohyama master equation and subsequent projection of the bulk Weyl tensor to the brane is greatly simplified if the background bulk geometry is simply a Minkowski space-time:  $\gamma_{ab} = \eta_{ab}$  and  $\Lambda_b = 0$ . In this case, the Mukohyama master equation (4.286) takes the form:

$$-\partial_\tau^2 \Omega + \partial_r^2 \Omega - \frac{3}{r} \partial_r \Omega - \frac{(n^2 + 2n - 3)}{r^2} \Omega = 0, \quad (4.290)$$

where we have used the fact that, for a compact three-dimensional manifold, the Laplacian eigenvalues  $k$  of the scalar harmonics  $Y$  are discrete:  $k_n^2 = n(n + 2)$ ,  $n = 0, 1, 2, \dots$ . We also have restricted ourselves to the case  $n \geq 2$ , for which the function  $U$  from (4.286) can be set to zero [626].

Equation (4.290) is a partial differential equation of hyperbolic type. Its simple form allows one to separate variables<sup>19</sup>:  $\Omega(\tau, r) = \xi(\tau) \chi(r)$  with the

---

<sup>19</sup> Such a simplification of the problem becomes possible due to the choice of the coordinate system in the form (4.12). In the Gaussian normal coordinates, separation of variables can be performed for the special case of a de Sitter brane (with constant Hubble parameter  $H$ ), which is of great interest because the bulk solution for the master variable in this case can be obtained analytically [633, 634].

functions  $\xi(\tau)$  and  $\chi(r)$  satisfying the ordinary differential equations

$$\frac{d^2\xi(\tau)}{d\tau^2} + B\xi(\tau) = 0, \quad (4.291)$$

$$\frac{d^2\chi(r)}{dr^2} - \frac{3}{r} \frac{d\chi(r)}{dr} + \left[ B - \frac{(n^2 + 2n - 3)}{r^2} \right] \chi(r) = 0, \quad (4.292)$$

where  $B$  is some constant, which can be chosen arbitrary until some boundary or regulatory conditions are specified.

Using expressions (4.291), (4.292) and definitions (4.284) and (4.285), one can easily compute the components of the perturbed bulk Weyl tensor (4.278)–(4.283). Once this operation is done, the projection  $\delta C_{\mu\nu} = \delta C_{\mu A\nu B} n^A n^B$  of the bulk Weyl tensor to the brane is trivial<sup>20</sup>. Setting the brane trajectory to be  $r = a(\tau)$ , we get the components of  $\delta C_{\mu\nu}$  [see definition (4.220)] to be

$$\frac{1}{m^2} \delta \rho_{\mathcal{C}} = - \frac{n(n+2)(n^2 + 2n - 3)}{3a^5} \Omega_{\text{b}}, \quad (4.293)$$

$$\frac{1}{m^2} v_{\mathcal{C}}(t) = \frac{(n^2 + 2n - 3)}{3a^3} \left[ aH (\partial_r \Omega)_{\text{b}} + \sqrt{1 + a^2 H^2} (\partial_\tau \Omega)_{\text{b}} - H \Omega_{\text{b}} \right], \quad (4.294)$$

$$\begin{aligned} \frac{1}{m^2} \delta \pi_{\mathcal{C}} = & - \frac{1}{2a} \left[ (1 + 2a^2 H^2) (\partial_\tau^2 \Omega)_{\text{b}} + 2aH \sqrt{1 + a^2 H^2} (\partial_{\tau r}^2 \Omega)_{\text{b}} + \right. \\ & \left. + \frac{(1 + 3a^2 H^2)}{a} (\partial_r \Omega)_{\text{b}} + \frac{(n^2 + 2n - 3)(1 + 3a^2 H^2)}{3a^2} \Omega_{\text{b}} \right]. \end{aligned} \quad (4.295)$$

Here,  $a = a(t)$  is a scale factor of the background Friedmann–Robertson–Walker metric on the brane,  $H = \dot{a}/a$  is the Hubble parameter on the brane, and the function  $\tau = \tau(t)$  is defined by the differential equation  $d\tau/dt = \sqrt{1 + a^2 H^2}$ . The subscript  $(\dots)_{\text{b}}$  means that the corresponding function should be evaluated at the brane. For example,  $\Omega_{\text{b}}(t) \equiv \Omega(\tau(t), a(t))$ .

Using the differentiation rule

$$\dot{\Omega}_{\text{b}} = \sqrt{1 + a^2 H^2} (\partial_\tau \Omega)_{\text{b}} + aH (\partial_r \Omega)_{\text{b}}, \quad (4.296)$$

one can write (4.294) and (4.295), respectively, in the following form:

$$v_{\mathcal{C}} = \frac{(n^2 + 2n - 3)m^2}{3a^3} \left[ \dot{\Omega}_{\text{b}} - H \Omega_{\text{b}} \right], \quad (4.297)$$

<sup>20</sup> The perturbation  $\delta n^A$  of the unit vector  $n^A$  normal to the brane does not contribute to  $\delta C_{\mu\nu}$  because the Weyl tensor  $\mathcal{C}_{MANB} = 0$  for the background solution.

$$\begin{aligned} \delta\pi_{\mathcal{C}} = & -\frac{m^2}{2a} \left[ \ddot{\Omega}_{\text{b}} - \frac{a^2 H(\dot{H} + H^2)}{(1 + a^2 H^2)} \dot{\Omega}_{\text{b}} + \right. \\ & \left. + \frac{(1 - a^2 \dot{H})}{a(1 + a^2 H^2)} (\partial_r \Omega)_{\text{b}} + \frac{(n^2 + 2n - 3)}{3a^2} \Omega_{\text{b}} \right]. \end{aligned} \quad (4.298)$$

We observe that the function  $v_{\mathcal{C}}(t)$  can be related to the function  $\delta\rho_{\mathcal{C}}(t)$ , defined in (4.293), as

$$v_{\mathcal{C}} = -\frac{a^2}{n(n+2)} (\delta\dot{\rho}_{\mathcal{C}} + 4H\delta\rho_{\mathcal{C}}), \quad (4.299)$$

which is in accordance with equation (4.224), which we obtained as one of the conservation equations on the brane. The relation between functions  $\delta\pi_{\mathcal{C}}(t)$  and  $\delta\rho_{\mathcal{C}}(t)$  is not so trivial due to the presence of the third term in the square bracket on the right hand side of (4.298). To investigate the relation between  $\delta\pi_{\mathcal{C}}(t)$  and  $\delta\rho_{\mathcal{C}}(t)$ , one should find the general solution of the master equation (4.290) and specify  $\Omega_{\text{b}}(t)$ .

This can easily be done. As we can see from (4.291), the master variable  $\Omega$  demonstrates an oscillatory or exponential behavior depending on the sign of the arbitrary constant  $B$ . In what follows, we consider the constant  $B$  to be positive to avoid problems with stability of our solution. Setting  $B \equiv \omega^2$ , we get the solution of (4.292) for a given  $\omega$  in the form

$$\chi(r) = r^2 [A_{\omega} J_{n+1}(\omega r) + B_{\omega} Y_{n+1}(\omega r)], \quad (4.300)$$

where  $A_{\omega}$  and  $B_{\omega}$  are some constants that can be chosen arbitrary until the boundary conditions are specified, and  $J_{n+1}(\omega r)$  and  $Y_{n+1}(\omega r)$  are the Bessel and Neumann functions, respectively.

The asymptotic behavior of the function  $\chi(r)$  in the neighborhood of the point  $r = 0$  is determined in the leading order by the asymptotic of the Neumann functions:

$$\chi(r) \rightarrow -\frac{2^{n+1} n! B_{\omega}}{\pi \omega^{n+1}} \frac{1}{r^{n-1}}, \quad r \rightarrow 0. \quad (4.301)$$

Our boundary condition at  $r = 0$  is the absence of any singularities; hence,  $\chi(r)$  is regular at  $r = 0$ , which implies the condition  $B_{\omega} = 0$  for all modes with  $n \geq 2$ .

Finally, the *general solution* of the master equation (4.290) can be written in the form of an integral over all possible values of the parameter  $\omega$ :

$$\Omega(\tau, r) = \int_{-\infty}^{\infty} d\omega \Omega(\omega) r^2 J_{n+1}(\omega r) e^{i\omega\tau}, \quad (4.302)$$

where  $\Omega(\omega)$  is some complex function which we expect to be specified from the boundary equations on the brane. We would like to note that the same result may be obtained by applying the method of Fourier transform to equation (4.290).

Substituting (4.302) in to (4.293), (4.295), we obtain

$$\frac{1}{m^2}\delta\rho_{\mathcal{C}} = -\frac{n(n+2)(n^2+2n-3)}{3a^3} \int_{-\infty}^{\infty} d\omega \Omega(\omega) J_{n+1}(\omega a) e^{i\omega\tau(t)}, \quad (4.303)$$

$$\begin{aligned} \frac{1}{m^2}\delta\pi_{\mathcal{C}} = & - \int_{-\infty}^{\infty} d\omega \Omega(\omega) e^{i\omega\tau(t)} \times \\ & \times \left[ \omega a J_n(\omega a) \left( \frac{1+3a^2H^2}{2a} + i\omega a H \sqrt{1+a^2H^2} \right) + \right. \\ & + J_{n+1}(\omega a) \left( \frac{n(n-1)(1+3a^2H^2)}{6a} - \frac{\omega^2 a(1+2a^2H^2)}{2} - \right. \\ & \left. \left. - i(n-1)\omega a H \sqrt{1+a^2H^2} \right) \right]. \end{aligned} \quad (4.304)$$

### 4.13.3. Quasi-static approximation

The quasi-static approximation was proposed by Koyama and Maartens in [621,622] as a simplification of the general equations describing the structure formation problem in the braneworld model. The main assumption of this approximation is that the terms with time derivatives can be neglected relative to those with spatial gradients. Specifically, this assumption implies  $H\dot{\Omega}_{\text{b}}, \ddot{\Omega}_{\text{b}} \ll (n^2/a^2)\Omega_{\text{b}}$ , where the values of  $n$  should be taken sufficiently large ( $n \gg 1$ ). In this case, our general expressions (4.293) and (4.298) turn into the approximate ones:

$$\frac{1}{m^2}\delta\rho_{\mathcal{C}}^{(qs)} \approx -\frac{n^4}{3a^5}\Omega_{\text{b}}, \quad (4.305)$$

$$\frac{1}{m^2}\delta\pi_{\mathcal{C}}^{(qs)} \approx -\frac{1}{6a} \left[ \frac{n^2}{a^2}\Omega_{\text{b}} + \frac{3(1-a^2\dot{H})}{a(1+a^2H^2)} (\partial_r\Omega)_{\text{b}} \right]. \quad (4.306)$$

This reproduces the result presented in [621,622] in the limit  $H^2, \dot{H} \gg 1/a^2$  corresponding to the spatially flat brane geometry. The regularity conditions imposed in [621,622] for the master variable in the bulk enabled the authors of that work to neglect the term with  $(\partial_r\Omega)_{\text{b}}$  on the right hand side of (4.306)

in the quasi-static approximation, arriving at a relation between the functions  $\delta\rho_{\mathcal{C}}(t)$  and  $\delta\pi_{\mathcal{C}}(t)$  in the form

$$\delta\rho_{\mathcal{C}}^{(qs)} \approx \frac{2n^2}{a^2} \delta\pi_{\mathcal{C}}^{(qs)}, \quad (4.307)$$

which is just the mode transform of (4.241). Whether this approximation can work for the general solution (4.302) is a matter of debates and future investigation.

#### 4.14. Summary

In this chapter, we have considered cosmological implications of a popular braneworld model with a single extra dimension, described by action (4.7), which contains both bulk and brane curvature terms and cosmological constants.

We first considered an important case where the brane forms the boundary of the five-dimensional bulk space. This is equivalent to endowing the bulk with the  $Z_2$  reflection isometry with respect to the brane. The presence of the curvature term in the action leads to two families of braneworld models, which we called BRANE1 & BRANE2. They differ in the manner in which the brane forms the boundary of the five-dimensional bulk. Alternatively, the two different families of braneworld models can be regarded as corresponding to the two possible signs of the five-dimensional Planck mass  $M$ .

Braneworld models of dark energy have an interesting and unusual property that their luminosity distance  $d_L$  can *exceed* that in the LCDM model with the same matter content. This is unusual since, within the general-relativistic framework, the luminosity distance has this property *only if* the equation of state of dark energy is strongly negative ( $w < -1$ ). Phantom dark energy, which realizes this feature [51], is beset with a host of undesirable properties which makes this model of dark energy unattractive. We have shown that braneworld models have all the advantages and none of the disadvantages of phantom models and therefore endow dark energy with exciting new possibilities. A recent analysis of braneworld models in [546–548] has demonstrated that BRANE1 models (which generically have  $w \leq -1$ ) are consistent with observations of supernovae combined with baryon acoustic oscillations and integrated Sachs–Wolfe effect.

Another feature of the braneworld scenario discussed in this chapter is that it allows for a Universe which is *transiently accelerating*. Recent investigations indicate that an eternally accelerating Universe, which possesses a cosmological event horizon, prevents the construction of a conventional  $S$ -matrix describing particle interactions within the framework of string or  $M$ -theory [549–551]. We have demonstrated that braneworld models can enter into a regime of



accelerated expansion at late times *even if* the brane tension and the bulk cosmological constant are tuned to satisfy the Randall–Sundrum constraint (4.50) on the brane. In this case, braneworld dark energy and the acceleration of the Universe are *transient* phenomena. In this class of models, the Universe, after the current period of acceleration, re-enters the matter-dominated regime. We have shown that viable models realizing this behavior are those of BRANE2 type.

We have shown that braneworld cosmology, in a certain broad region of the values of fundamental constants, exhibits a property which we called *cosmic mimicry*. During early cosmological epochs, the braneworld behaves like a matter-dominated Friedmann Universe with the value of the cosmological parameter  $\Omega_m$  that would be inferred from observations of the local matter density. At late times, however, the Universe evolves almost exactly like in the LCDM scenario but with a *renormalized* value of the cosmological density parameter  $\Omega_m^{\text{LCDM}}$ . Specifically, a positive-tension BRANE1 model, which at high redshifts expands with density parameter  $\Omega_m$ , at lower redshifts mimics the LCDM cosmology with a *smaller value* of the density parameter  $\Omega_m^{\text{LCDM}} < \Omega_m$ . A negative-tension BRANE2 model at low redshifts also mimics LCDM but with a *larger value* of the density parameter  $\Omega_m^{\text{LCDM}} > \Omega_m$ .

The cosmic-mimicry scenario has interesting cosmological properties. For instance, in the case of BRANE1 (BRANE2), the Universe expands faster (slower) than in the LCDM scenario at redshifts greater than the mimicry redshift  $z_m$ , whereas, for  $z < z_m$ ,  $H_{\text{brane}}(z) \equiv H_{\text{LCDM}}(z)$  in both models. The smaller value of the Hubble parameter at intermediate redshifts ( $z > \text{few}$ ) in the case of BRANE2 leads to an older Universe and also to a redshift of reionization which can be significantly lower than that inferred for the LCDM model from the WMAP data [94].

The effect of cosmic mimicry and the existence of two asymptotic density parameters  $\Omega_m$  and  $\Omega_m^{\text{LCDM}}$  is a consequence of the time-dependence of the *effective* gravitational coupling in braneworld theory [531], which can be related to the well known property of the scale-dependence of the effective gravitational coupling in braneworld models [533–535]. On large spatial scales,  $kr \gg 1$ , the braneworld model with positive brane tension (BRANE1) exhibits gravity with the renormalized effective gravitational constant (4.55), and we have shown that this renormalization corresponds to a renormalization of the cosmological density parameter (4.125).

Only two effective gravitational constants appear in the cosmology under consideration, given by (4.55) and (4.66), respectively, for low and high energy densities. However, in the local gravitational physics, there also appears the spatial distance  $r_*$  defined in (4.65) and depending upon the mass of the central source, so that gravity in the range of distances

$$r_* \lesssim r \lesssim \ell \tag{4.308}$$

from the source has a different value of the gravitational constant, given by (4.60), and, moreover, has a scalar–tensor character manifest, e.g., in (4.61). This may be important for the estimates of masses from the dynamics of clusters of galaxies and from gravitational lensing on these scales in the braneworld theory [533–535, 541, 542].

On small distances from the central source,  $r \ll r_*$ , both positive-tension and negative-tension branes apparently behave similarly reproducing the Einstein gravity to a high precision with the gravitational constant  $1/m^2$ , which is the bare gravitational coupling in the braneworld action (4.7). However, this expectation is to be verified by refined calculations in braneworld models with arbitrary sign of brane tension and without the RS constraint (4.50). In this respect, we should note that solution with a spherically symmetric source (the analog of the Schwarzschild and interior solution in General Relativity) largely remains to be an open problem in braneworld theory (for recent progress in the DGP model, see [635]).

We have demonstrated that the braneworld models of dark energy allow one to construct a *loitering* Universe. An important aspect of braneworld loitering is that, in contrast to the conventional loitering scenarios that demand a closed Universe, loitering on the brane can easily occur in a spatially flat cosmological model. A key role in making the brane loiter is the presence of (negative) dark radiation — a generic five-dimensional effect associated with the projection of the bulk gravitational degrees of freedom onto the brane. The Universe can loiter at large redshifts ( $z \gtrsim 6$ ) while accelerating at the present epoch. During loitering, the value of the Hubble parameter decreases steadily before increasing again. As a result, the age of the loitering braneworld is larger than that of a LCDM Universe at a given redshift. This feature may help spur the formation of  $\sim 10^9 M_\odot$  black holes at redshifts  $\gtrsim 6$  whose presence (within high redshift QSO’s) could be problematic for standard LCDM cosmology [561, 562]. Loitering is also expected to increase the growth rate of density inhomogeneities and could, in principle, be used to reconcile structure formation models which predict a lower amplitude of initial ‘seed’ fluctuations with the observed anisotropies in the cosmic microwave background (see [559]).

Braneworld models give rise to cosmological singularities which are not commonly encountered in General Relativity. This is largely due to the possibility of different kinds of embedding of the brane in the higher dimensional (bulk) space-time. Singular embedding implies that the expansion (in time) of the brane cannot be continued indefinitely. The singularities which we have examined in this chapter have the property that, while the density, pressure, and Hubble parameter on the brane remain finite, higher derivatives of the Hubble parameter blow up as the singularity is approached. For this reason, we called them “quiescent singularities.” Despite its deceptively mild nature, the

quiescent singularity is a real curvature singularity at which the Kretschmann invariant diverges ( $R_{abcd}R^{abcd} \rightarrow \infty$ ). The importance of quantum effects in regions of large space-time curvature has been demonstrated in a number of papers [421], and it should therefore come as no surprise that these effects can significantly alter the classical behavior near the quiescent singularity, as demonstrated by us in this chapter.

Unlike the classical Big-Bang singularity, the quiescent singularity in braneworld models is reached in regions of *low density* and is therefore encountered during the course of the Universe expansion rather than its collapse. Densities lower than the mean value are known to occupy a large filling fraction within the cosmic web [587, 588]. Therefore, if the braneworld model is a reasonable representation of reality, one might expect that it is likely to encounter the quiescent singularity (or its quantum-corrected counterpart, the “soft singularity”) within large underdense regions, or voids. The rapidly varying space-time geometry near the quiescent singularity can, in addition to vacuum polarization, also give rise to quantum creation of fields which do not couple conformally to gravity. This allows one to suggest a cosmological scenario which, at later times, is reminiscent of quasi-steady-state cosmology, with the Hubble parameter showing oscillations about a constant value.

In this chapter, we have also considered the braneworld model without the mirror ( $Z_2$ ) symmetry of the bulk space with respect to the brane. We find that, depending upon the choice of the brane embedding, cosmological expansion on the brane can proceed along four independent branches, two of which survive in the case of  $Z_2$  symmetry. An important property of this class of models is that the four-dimensional gravitational and cosmological constants are effective quantities derivable from five-dimensional physics. In this case, brane expansion mimics  $\Lambda$ CDM at low redshifts, but the ‘screened’ matter density parameter  $\tilde{\Omega}_m$  does not equal to its bare (dynamical) value  $\Omega_m$ . This opens a new avenue for testing such models against observations (see [553, 615]). Another important property of these models would be the growth of density perturbations which is likely to differ from  $\Lambda$ CDM. Braneworld models can be phantom-like and also exhibit transient acceleration. Thus, brane phenomenology, with its basis in geometry, provides an interesting alternative to ‘physical’ dark energy scenarios such as quintessence.

Braneworld theories with large extra dimensions have one common property: while the dynamics of the higher-dimensional bulk space needs to be taken into account in order to understand brane dynamics, all observables are restricted to the four-dimensional brane. In field-theoretic language, the situation can be described in terms of an *infinite (quasi)-continuum* of Kaluza–Klein gravitational modes existing on the brane from the brane viewpoint. This property makes braneworld theory complicated, solutions on the brane non-unique and evolution non-local.

Fortunately, in situations possessing a high degree of symmetry, the above properties of braneworld theory do not affect its cosmological solutions (at least, in the simplest case of one extra dimension). Thus, homogeneous and isotropic cosmology on the brane is almost uniquely specified since it involves only one additional integration constant which is associated with the mass of a black hole in the five-dimensional bulk space. However, in order to turn a braneworld model into a *complete* theory of gravity viable in all physical circumstances, it is necessary to address the issue of boundary conditions.

In this chapter, we adopted a different approach to the issue of boundary conditions in the brane-bulk system. From a broader perspective, boundary conditions can be regarded as any conditions restricting the space of solutions. Our approach is to specify such conditions directly on the brane which represents the observable world, in order to arrive at a local and closed system of equations on the brane. The behavior of the metric in the bulk is of no further concern in this approach, since this metric is for all practical purposes unobservable. Since the non-locality of the braneworld equations is known to be connected with the dynamical properties of the bulk Weyl tensor projected onto the brane [522], it is natural to consider the possibility of imposing certain restrictions on this tensor. We have assumed the one-parameter family of boundary conditions (4.236) for perturbations. This family generalizes the boundary condition derived by Koyama and Maartens [621] (with  $A = -1/2$ ) for the DGP model in the small-scale and quasi-static approximation.

An important conclusion is that the growth of perturbations in braneworld models strongly depends upon our choice of boundary conditions. This was illustrated in figure 24 for the DGP model. Specifying boundary conditions in the form (4.236) allows us to determine regions of stability and instability in terms of the single parameter  $A$ ; they are described by Eq. (4.239). In the DGP model, perturbations are explicitly demonstrated to be quasi-stable for  $A = 1/2$  (figure 4.23) and unstable for  $A = -1/2$  (figure 4.22). In the instability domain, gradients in the momentum potential  $v_C$  of dark radiation, lead to the creation of perturbations in this quantity via equation (4.233). This effect can significantly boost the growth of perturbations in matter. An important implication of this effect is that perturbations in the baryonic component might overcome the ‘growth problem,’ which plagues them in standard General Relativity, and grow to acceptable values without requiring the presence of (deep potential wells in) dark matter. The Mimicry 2 model looks promising from this perspective. Note that, in this model, the expansion of a low-density Universe is virtually indistinguishable from that of a (higher-density) LCDM model.

The values of  $A$  lying in the stability region (4.239) or a scale-free boundary condition such as (4.243) may also be important. In this case, perturbations in

the DGP model grow *slower* than in LCDM whereas perturbations in Mimicry 1 grow somewhat faster. This suggests that structure formation may occur slightly earlier in Mimicry 1 than it does in LCDM.

It is well known that the expansion history,  $H(z)$ , does not characterize a given world model uniquely, and it is conceivable that cosmological models having fundamentally different theoretical underpinnings (such as different forms of the matter Lagrangian or different field equations for gravity) could have identical expansion histories (some examples may be found in [236, 636]).

Whether boundary conditions such as described by Eq. (4.243) will remain in place for a more fundamental extra-dimensional theory is presently a moot point. Perhaps, by comparing the consequences of different boundary conditions with observations we will gain a better understanding of the type of braneworld theory most consistent with reality.

# 5

## CHAPTER

---

### ENERGY IN GENERAL RELATIVITY IN VIEW OF SPINOR AND TENSOR METHODS

---

#### 5.1. Introduction

It is known that positive energy theorem (PET) in General Relativity [637,638], possessing independent principal significance, also creates the basis for solving of other problems, for example, stability of Minkowski space. Among assumptions at proving the theorem there is hypothesis about satisfying of one of the energy conditions — dominant energy condition (DEC). But just in the beginning of the proving PET searches the change of view of the energy conditions has taken place. Tipler [639] had analyzed the consequences of possible violation of strong energy condition on existence of singularities in space-time. Further Visser [640,641], Visser and Barcelo [642] pointed out the existence of quantum and classical effects which cause the violation of all energy conditions. Possibility for proving the positive energy theorem at more weak energy condition in comparison with standard one has been discussed by Shiromizu and Sugai [643]. Consequently the discovery of accelerated expansion of Universe, development of the dark energy concept and radical change of the energy conditions paradigm require detailed analysis of influence of this change on all PET aspects, including different methods of its proving.

From the moment of the first proof of this theorem [637] there were presented many simplified and complement proofs [644–647] within the limits of the Witten’s spinor method, as well as alternative to Wittenian one [648–650]. Among these alternative tensor methods the most developed one is Nester’s method of special orthonormal frame (SOF), on the basis of which there is a set of gauge conditions for

the choice of this orthonormal frame on a three-dimensional Riemannian manifold [651]. These conditions are purely geometrical, because they are expressed in terms of teleparallel geometry.

Application of SOF is not limited by proof of PET and investigating of quasilocalization. In particular, by adopting four-dimensional special orthonormal frames, the tetrad equations for vacuum gravity are put into explicitly causal and symmetric hyperbolic form, independent of any time slicing or other gauge or coordinate specialization [652]. Buchman and Bardeen [653] within a first order symmetric hyperbolic tetrad formulation of the Einstein equations developed by Estabrook and Wahlquist obtained stable unconstrained evolution for certain initial conditions in SOF, but not with some Lorentz gauge.

Dimakis and Müller-Hoissen have shown [650, 654] that Nester's gauge conditions are related to the three-dimensional Dirac equation. Since the solutions of the latter as elliptic equations can have zeros, as Ashtekar and Horowitz [646] have noticed for the first time (see also [654], where the additional arguments for support of this statement are presented together with corresponding references to works, in which zeros of elliptic equations are investigated), the special orthonormal frame (triad) as well as Dimakis and Müller-Hoissen SOF (tetrad) are determined only almost everywhere on space-like hypersurface in asymptotically Minkowskian manifold. From uniqueness theorem for system of linear equations of first order with smooth coefficients follows that nodal sets of codimension 1 of Sen–Witten spinor field are absent, and Bär [674] proved that nodal set of generalized Dirac equation is a countably  $(n - 2)$ -rectifiable set and thus has Hausdorff dimension  $(n - 2)$  at most. But it is important to obtain conditions for absence of all nodal points, because possible existence of zeros of spinor field even on the set of zero measure is the barrier for the correspondence of spinor and tensor methods as well as for distinguishing of SOF as constituent of frames of reference, since the latter in some physically non-singular points does not exist.

The connections between triads and Sen–Witten (SWE) equation were also investigated by Frauendiener [655]. He obtained the necessary and sufficient conditions that have to be satisfied by the triad in order to correspond to the spinor that satisfies the Sen–Witten equation. These conditions, as it was marked by Frauendiener, are closely connected with Nester's conditions, because they also include some cyclic conditions. But in the process of obtaining of these conditions the possibility of the situation, when the spinor equals zero in one or even on a set of points of nonvanishing measure, is not taken into account, therefore Frauendiener's theorem is correct only under the suitable additional assumption. SOF reflects general features, domain of SOF application is not limited by PET and asymptotically Minkowskian manifold. In particular, SOF is used in problem of quasilocalization of gravitational energy. Not long ago Frauendiener, Szabados and Nester performed additional investi-

gation of zeros absence conditions for Sen–Witten (SWE) equation [656]. Developing our idea of elimination of zeros for Sen–Witten equation by choice of appropriate boundary conditions [657–659] firstly (2005 Annual Meeting of Chinese Physics Society, Taipei) denied by Nester, they determined conditions for zeros absence in class of spaces nearest to the flat one — Petrov class  $O$ , the unique non-trivial representative of which is conformally flat pseudoriemannian space.

Our first purpose is to show that non-trivial solutions of SWE on defined by some conditions hypersurface and, generally, in algebraically more general space-time, will not have any node point, and to prove on this basis the equivalence of SWE and Nester’s gauge and therefore the existence of correspondence of spinor and tensor methods in investigations of the positive definition of the gravitational energy and its quasilocalization. Further we will prove that in such spaces even at violation of WEC by dark energy, the full energy can be positive definite.

## 5.2. Connection between spinor and tensor methods in the positive energy problem

In subsection 5.2.2 we review the ascertained by Skorobohat’ko properties of nodal sets of selfadjoint second order elliptic equations and strong elliptic systems of equations of second order.

In subsection 5.2.3 on the basis of these results we show at what boundary values for the spinor field the solution for SWE has not any nodal points in the bounded domain on the space-like spatial-constant mean curvature hypersurface in Petrov type  $N$  space-time. Then using the methods, introduced by Reula [645] and Ashtekar and Horowitz [646], we prove that in Petrov type  $N$  space-time non-trivial solutions of SWE with asymptotically flat initial data set do not equal zero in any point of finite or infinite domain on spatial-constant mean curvature (SCMC) hypersurface in asymptotically flat Petrov type  $N$  space-time.

This allows us to prove in subsection 5.2.4 the equivalence of SWE and Nester’s gauge, and also to complement Nester’s investigations, showing that the local rotation to Nester’s SOF exists not only for geometries in a neighborhood of Euclidean space, but everywhere on maximal hypersurface with good topological properties<sup>1</sup>. The latter circumstance allows to take down fully the negation of Dimakis and Müller-Hoissen against the Nester’s method [654], which was taken down partly by Nester earlier [660].

We use the Witten’s method in the interpretation, given by Reula [645]. In the basis of this interpretation lies the reduction of  $SL(2, C)$  spinors of

<sup>1</sup> Maximal surface are space-like submanifold which locally maximize the induced area functional.



space-time to  $SU(2)$  spinors on space-like hypersurface; this reduction was introduced by Sommers [661] and Sen [662].

From the point of view of theory of differential equations with partial derivatives the necessity for investigation of submanifolds, on which the solutions of elliptic equations are equal to zero, first of all is connected with the fact that the necessary and sufficient conditions for absence of such closed submanifolds of codimension one are simultaneously the necessary and sufficient conditions for uniqueness of the Dirichlet problem for these equations in the bounded domain (the existence and stability of solutions at sufficiently smoothed coefficients leads to its uniqueness). On the other hand, the uniqueness theorems for Dirichlet problem define conditions for absence of submanifolds of codimension one, on which the solutions of elliptic equations are equal to zero.

### 5.2.1. Sen—Witten equation in Petrov type $N$ space-time

In next sections we prove, that non-trivial solutions of Sen—Witten equation with asymptotically flat data set in Petrov type  $N$  on SCMC hypersurface does do not equal zero in any point of this hypersurface. On this basis we ascertain the correspondence between Witten’s spinor method and Nester’s tensor method.

Let  $(M, g)$  be an asymptotically Minkowskian space-time of Petrov type  $N$  with space-like foliation  $\Sigma_t \times \{t\}$  and metric  $g$  of signature  $(+, -, -, -)$ . We assume initial data set  $(\Sigma_t, h_{\mu\nu}, \mathcal{K}_{\pi\rho})$  to be asymptotically flat in introduced by Reula [645] sense and  $h_{\mu\nu}, \mathcal{K}_{\pi\rho}$  to be of  $C^\infty$  class on  $C^\infty$  hypersurface  $\Sigma_t$ . Assumptions about asymptotical properties (topology) are result of PET conditions; these are important for existence of SOF, but, as it will be seen later, these are not necessary for obtaining conditions of the nodal sets absence.

The constraint equations of general relativity on the space-like hypersurface  $\Sigma_t$  are

$$-R - \mathcal{K}_{\mu\nu}\mathcal{K}^{\mu\nu} + \mathcal{K}^2 = 2\mu, \quad (5.1)$$

$$D_\mu(\mathcal{K}^{\mu\nu} - \mathcal{K}h^{\mu\nu}) = \mathcal{J}^\nu, \quad (5.2)$$

where  $R$  is scalar curvature of  $\Sigma_t$ ,  $h = g - n \otimes n$  is induced metric on  $\Sigma_t$ .  $D_\mu$  is induced by connection  $\nabla_\mu$  on  $M$  connection on  $\Sigma_t$ ,  $\mathcal{K}_{\mu\nu}$  is extrinsic curvature of  $\Sigma_t$ ,  $\mathcal{K} = \mathcal{K}^\nu_\nu$ .  $\mu$  and  $\mathcal{J}^\nu$  are the energy density and momentum density respectively of the matter in the frame of reference of an observer, whose one-form of 4-velocity is  $\xi = dt$ . In the case of barionic matter  $\mu$  and  $\mathcal{J}^\nu$  satisfies the dominant energy condition

$$\mu \geq |\mathcal{J}^\nu \mathcal{J}_\nu|^{1/2}. \quad (5.3)$$

As it was shown by Witten [638], if on  $\Sigma_t$  exists the solution  $\beta^C$  of Sen—Witten equation

$$\mathcal{D}^B_C \beta^C = 0 \quad (5.4)$$

with  $\beta^C$  going asymptotically to a constant spinor  $\beta_0^C$ , then the total mass is non-negative. The action of Sen operator  $\mathcal{D}_{AB}$  on spinor field is

$$\mathcal{D}_{AB}\lambda_C = D_{AB}\lambda_C + \frac{\sqrt{2}}{2}\mathcal{K}_{ABC}{}^D\lambda_D. \quad (5.5)$$

For solving the problem of zeros existence for  $\beta^C$  solutions of the equation (5.4), when  $\beta^C$  is going asymptotically to the constant spinor  $\lambda_0^C \neq 0$ , we briefly review the results of Skorobohat'ko.

### 5.2.2. Nodal surfaces of selfadjoint elliptic second order equations

The unique solvability of Dirichlet problem for elliptic equations was studied in the works [663–666]. The results of these works were generalized in [667, 668] where the similar results were obtained independently. In particular, from the Aronszajn [667] and Cordes [668] theorem we see that non-trivial solutions of the equation

$$a^{\mu\nu} \left( x, u, \frac{\partial u}{\partial x} \right) \frac{\partial^2 u}{\partial x^\mu \partial x^\nu} = f \left( x, u, \frac{\partial u}{\partial x} \right), \quad u(x), a^{\mu\nu}(x) \in C^2$$

in  $R^n$ , which is elliptic for all  $x^1, \dots, x^n$  and  $u$ , in any point  $\xi_0$  cannot have zero of infinite order. Therefore this allows to exclude the existence of the solutions with zeros of infinite order only.

In the works of Skorobohat'ko [672, 673] the known theorems about the distribution of zeros for linearly independent solutions of the ordinary differential second order equation  $y'' + c(x)y = 0$  are generalized for selfadjoint elliptic type equations

$$\frac{\partial}{\partial x^\mu} \left[ a^{\mu\nu}(x^\pi) \frac{\partial u}{\partial x^\nu} \right] + a(x^\pi)u = 0, \quad (5.6)$$

where  $a^{\mu\nu}(x^\pi) \in C^2(\Omega)$ ,  $a(x^\pi) \in C^1(\Omega)$ . The point  $x_0^\pi$ , in which the solution  $u$  equals zero, is said to be a nodal point of this solution. The important property of the equation (5.6) is given in the following theorem.

**Theorem Skorobohat'ko V.** *The nodal points of any solution  $u$  of the equation (5.6) aren't isolated in domain  $\Omega$ , but create the surfaces, which divide the domain  $\Omega$ .*

From the theorem we can see, that nodal surfaces are closed, or their ends lie on the boundary of domain  $\Omega$ . The theorem is simply generalized for the case of  $n$ -dimensional space, where it takes the following form: nodal sets of codimension  $(n - 1)$  are not isolated and create hypersurfaces, which divide the domain. The theorem is simply generalized for the case of  $n$ -dimensional space, where it takes the following form: nodal sets of codimension  $(n - 1)$  are not isolated and create hypersurfaces, which divide the domain.

### 5.2.3. The solutions of Sen—Witten equation have no zeros

**Theorem 1.** *Let  $\lambda^C$  satisfies Reula's condition and is a solution of the equation (5.4) with asymptotically flat initial data set in Petrov type N space-time, that satisfies the dominant energy condition (5.3). Then the solution  $\lambda^C$  everywhere on the SCMC hypersurface  $\Sigma_t$  has no zeros.*

*Proof.* From Lemma [646] we obtain, that all solutions  $\lambda^C$  of equation

$$\mathcal{D}_A{}^B \mathcal{D}_{BC} \lambda^C = 0 \quad (5.7)$$

with the form  $\lambda^C = \lambda_0^C + \beta^C$ , where spinor field  $\lambda_0^C$  is asymptotically constant and  $\beta^C$  is element of Hilbert space  $\mathcal{H}$ , satisfy also the first order equation (5.4). Here the space  $\mathcal{H}$  is the Cauchy completion of  $C_0^\infty$  spinor fields under the norm

$$\|\beta^E\|_{\mathcal{H}}^2 = \int_{\Sigma_t} (\mathcal{D}^A{}_B \beta^B)^+ (\mathcal{D}_{AC} \beta^C) dV.$$

The equations (5.7) are elliptic system of equations. Indeed,

$$\mathcal{D}_A{}^B \mathcal{D}_{BC} \lambda^C = -D_{AB} D^B{}_C \lambda^C - \frac{\sqrt{2}}{2} D_{AB} \lambda^B - \frac{\sqrt{2}}{4} \lambda^B D_{AB} \mathcal{K} - \frac{1}{8} \mathcal{K}^2 \lambda_A;$$

taking into account that

$$-D_{AB} D^B{}_C \lambda^C = -\frac{1}{2} D^{BF} D_{BF} \lambda_A - \frac{1}{8} R^{(3)} \lambda_A,$$

and using the equation (5.1), we obtain:

$$\begin{aligned} \mathcal{D}_A{}^B \mathcal{D}_{BC} \lambda^C &= \frac{1}{2} D^{BC} D_{BC} \lambda_A - \frac{\sqrt{2}}{2} \mathcal{K} D_{AB} \lambda^B - \frac{\sqrt{2}}{2} \lambda^B D_{AB} \mathcal{K} - \\ &\quad - \frac{1}{4} \mathcal{K}^2 \lambda_A + \frac{1}{8} \mathcal{K}_{\mu\nu} \mathcal{K}^{\mu\nu} \lambda_A + \frac{1}{4} \mu \lambda_A. \end{aligned} \quad (5.8)$$

Let introduce on an open neighborhood of  $\Sigma_t$  the Gauß normal coordinates  $(t, x^\alpha)$ . Then

$$\begin{aligned} \mathcal{D}_A{}^B \mathcal{D}_{BC} \lambda^C &= \frac{1}{2\sqrt{-h}} \frac{\partial}{\partial x^\alpha} \left( \sqrt{-h} h^{\alpha\beta} \frac{\partial}{\partial x^\beta} \lambda_A \right) - \\ &\quad - \frac{\sqrt{2}}{2} \lambda^B D_{AB} \mathcal{K} + \frac{1}{8} \mathcal{K}_{\alpha\beta} \mathcal{K}^{\alpha\beta} \lambda_A + \frac{1}{4} \mu \lambda_A = 0, \end{aligned} \quad (5.9)$$

and ellipticity (5.6), as well as (5.4), follows from the negative definition of  $\|h^{\alpha\beta}\|$  matrix.

On the hypersurface  $\Sigma_t$  of spacial constant mean curvature<sup>2</sup> the system of equations (5.11) comes to two independent selfadjoint equations for the spinor in abstract form

$$\frac{1}{\sqrt{-h}} \frac{\partial}{\partial x^\alpha} \left( \sqrt{-h} h^{\alpha\beta} \frac{\partial}{\partial x^\beta} \lambda_A \right) + \frac{1}{4} \mathcal{K}_{\alpha\beta} \mathcal{K}^{\alpha\beta} \lambda_A + \frac{1}{2} \mu \lambda_A = 0. \quad (5.10)$$

Taking into account that space-time belongs to Petrov type  $N$ , we can make a conclusion that system of two equations for real and imaginary parts for one of components  $\lambda^\alpha$  of spinor in a spin-frame consists of two independent equations. Then, applying Skorobohat'ko's theorem, for every equation we obtain, that nodal surfaces of every solution are not isolated in arbitrary bounded domain  $\Omega$  and divide this domain. According to the dominant energy condition (5.3)

$$\mathcal{K}_{\alpha\beta} \mathcal{K}^{\alpha\beta} + 2\mu \geq 0, \quad (5.11)$$

then for (5.10) the maximum principle is fulfilled, and the solution of the Dirichlet problem for every from each of above mentioned equation is unique; that is why the nodal surfaces set of equation (5.10) does not include the closed surface. For the case, when real or imaginary part of this component does not vanish in any point on boundary, equation (5.12) has no node points. Since in asymptotically flat space-time  $\lambda^C$  asymptotically tends to  $\lambda_0^C \neq 0$ , then for the solution on  $\Sigma_t$  the nodal surfaces, which tend to infinity, are also absent.

Therefore the solution  $\lambda^C$  of equation (5.4) does not have a zero on  $\Sigma_t$ . Note that maximality condition is not necessary condition of splitting of equations. For splitting of equations in space-time of Petrov type  $N$  it is sufficiently to require for hypersurface to be spatial constant mean curvature hypersurface, in other words, one of realizations of well-known class of hypersurfaces of prescribed mean curvature [674, 675].

From Lemma 1 and Lemma [662] we can deduce, that the solution of the equation (5.4), which vanishes at a point on  $\Sigma_t$ , vanishes everywhere on  $\Sigma_t$ . But during the process of Lemma's 1 proof the Conjecture, which is based on the observation of the properties of the solutions for the equation (5.4) in Minkowski space and at  $\mathcal{K}_{\alpha\beta} = 0$ , is used; these assumptions are too strong.

For the general case  $D_{AB}\mathcal{K} \neq 0$  let us restrict by the notice, that the solutions of Sen–Witten equation do not have zero also everywhere on hypersurfaces in some neighborhood of the SCMC hypersurface. The proof can be obtained on the basis of the Lopatynsky [676] theorem, according to which the solutions of the Dirichlet problem for elliptic system of second-order equations continuously depend on its right parts, coefficients,  $\Omega$ -domain and values of the functions on  $\partial\Omega$ . In subsection 5.3 we strengthen this result significantly.

---

<sup>2</sup> It is known, that particular case of SCMC hypersurfaces — hypersurfaces of constant mean curvature (CMC) — are favored in cosmologies.

#### 5.2.4. Sen—Witten equations and SOF

**Definition 1.** A set of  $N$  ( $0 < N \leq 10$ ) equations for the components of orthonormal vector basis  $e_m{}^\mu$  (tetrad, vierbein)

$$\Phi_N(e_m{}^{\mu'}, \partial_{\nu'} e_m{}^{\nu'}, \partial_{\nu'}^2 e_p{}^{\pi'}) = 0, \quad (5.12)$$

which are not covariant relatively to the local Lorentz transformations and (or) coordinate basis transformations, is said to be auxiliary conditions.

**Definition 2.** The auxiliary conditions (5.12) are said to be gauge fixing conditions in some domain  $\Omega$ , if in this domain the solution  $x^{\mu'}(x^\nu)$ ,  $L_n^{m'}(x)$  of the system of equations

$$\Phi_N \left( e_n{}^\nu \frac{\partial x^{\mu'}}{\partial x^\nu} L_n{}^{m'}, \dots, \dots \right) = 0 \quad (5.13)$$

with arbitrary coefficients  $e_n{}^\nu$  exists.

The sets of additional and gauge fixing conditions are not identical [676—678]. This is caused firstly by the fact, that the coefficients of the system (5.13) are considered in general as the functions of  $C^\infty$  class, but not  $C^a$ , and the solutions of non-analytical equations may not exist; secondly, even the conditions of integrability for equations (5.13) can be not satisfied.

Nester [651] introduced the additional conditions for the choice of special orthonormal frame on three-dimensional Riemannian manifold. Let  $\theta^a$  denotes the corresponding orthonormal coframe field. Nester's conditions, written in terms of the differential forms

$$\tilde{q} = i_a d\theta^a, \quad q = \theta_a \wedge d\theta^a, \quad (5.14)$$

are given by

$$d\tilde{q} = 0, \quad d * q = 0. \quad (5.15)$$

The system of equations (5.13), corresponding to these additional conditions, is a non-linear second-order elliptic system for the rotation  $R^{a'}{}_b$ . Nester proved the existence and uniqueness of the solution of the linearization of this system for geometries within a neighborhood of Euclidean space and therefore the additional conditions (5.15) are gauge-fixing only asymptotically.

Analogously to Nester under investigations and application of the conditions (5.15) we would restrict ourselves to consideration of the spaces with “good” topology, where the forms  $\tilde{q}$  and  $*q$  are exact (vanishing of the first de Rahm cohomology class of the three-manifolds is sufficient but not necessary). Taking into account, that initial data set  $(\Sigma_t, h_{\mu\nu}, \mathcal{K}_{\pi\rho})$  is asymptotically flat, the conditions (5.15) are replaced by their first integrals:

$$\tilde{q} = -4d \ln \rho, \quad *q = 0. \quad (5.16)$$

Function  $\rho$  everywhere on  $\Sigma_t$  is positive.

**Theorem 2** [657]<sup>3</sup>. Let an initial data set  $(h_{\mu\nu}, \mathcal{K}_{\pi\rho})$  on maximal hypersurface  $\Sigma_t$  in Petrov type N space-time be asymptotically flat and satisfies the dominant energy condition. Then everywhere on  $\Sigma_t$  the Sen–Witten’s equations (5.4) with Reula conditions and Nester’s condition (5.15) are equivalent.

*Proof.* Let assume firstly that on  $\Sigma_t$  the equation (5.4) for  $SU(2)$  spinor  $\lambda_C$  is given. Then a spatial one-form  $L$  with components  $L_\nu = -\lambda_A \lambda_B$  satisfies “squared” SWE

$$\langle \tilde{L}, D \otimes L \rangle - \mathcal{K}L + 3! i * (n \wedge D \wedge L) = 0, \quad (5.17)$$

where  $n$  is one-form of unit normal to  $\Sigma_t$ ,  $\langle \tilde{L}, D \otimes L \rangle$  is one-form with components  $\tilde{L}_\nu D_\mu L^\nu$ ,  $\tilde{L} = |L|^{-1} * (L \wedge \bar{L})$  is non-zero spatial one-form. Because  $\Sigma_t$  as three-dimensional orientable manifold is parallelisable, it admits a globally defined orthonormal 3-coframe  $\theta^a$  and together with time-like unit one-form  $n$  of the normal to  $\Sigma_t$  it forms 4-coframe  $\theta^m$ .

Let us introduce 4-coframe  $\theta^m$  with the help of the correlations

$$L = \frac{\lambda}{\sqrt{2}}(\theta^1 + i\theta^2), \quad \theta^3 = \tilde{L}, \quad \theta^0 \equiv n = Ndt, \quad (5.18)$$

where  $\lambda = \lambda^{+A} \lambda_A$ , and let introduce metric  $\eta_{mn} = (1, -1, -1, -1)$  in which this frame is orthonormal. Let us substitute the expression for  $L$  from (5.18) into (5.17) and take into account that in agreement with theorem 1 the spinor  $\lambda^A$  everywhere on  $\Sigma_t$  does not equal zero. This allows to write instead of (5.17)

$$-\langle \theta^1, D \otimes \theta^3 \rangle - \mathcal{K}\theta^1 + 3! i * [n \wedge (D + F) \wedge \theta^2] = 0, \quad (5.19)$$

$$\langle \theta^2, D \otimes \theta^3 \rangle + \mathcal{K}\theta^3 + 3! i * [n \wedge (D + F) \wedge \theta^1] = 0, \quad (5.20)$$

where we denoted  $F = D \ln \lambda$ . Contracting the left parts of (5.19) and (5.20) with vector field  $e_b$  and taking into account that  $\varepsilon_{(0)abc} = \varepsilon_{abc}$ , we obtain

$$-\omega^{13}{}_b - \mathcal{K}\eta_b^1 + \varepsilon_{bca}\omega^{a2c} + \varepsilon^{c2}{}_b F_c = 0, \quad (5.21)$$

$$\omega^{23}{}_b + \mathcal{K}\eta_b^2 + \varepsilon_{bca}\omega^{a1c} + \varepsilon^{c1}{}_b F_c = 0. \quad (5.22)$$

The connection one-forms coefficients  $\omega^k{}_{mn}$  in (5.21)–(5.22) are defined as usually:  $\omega^k{}_{mn} = \langle \theta^k, \nabla_{e_m} e_n \rangle$ . The system of equations (5.21) and (5.22) includes only four independent equations:

$$\begin{aligned} \varepsilon^{abc}\omega_{abc} &\equiv *q = 0, \quad \omega^a{}_{1a} \equiv -\tilde{q}_1 = F_1, \\ \omega^a{}_{2a} &= -\tilde{q}_2 = F_2, \quad \omega^a{}_{3a} = -\tilde{q}_3 = \mathcal{K} + F_3. \end{aligned} \quad (5.23)$$

<sup>3</sup> Despite reconfirm our priority in [659], the result of our Theorem 2 is given by authors in [656, p. 5] as their own. In paper “On the zero set of solutions of the Witten equation on asymptotically euclidean hypersurfaces” (GR20/Amaldi10 Abstract Book, Warsaw July 6, 2013) Frauendiener repeatedly tried to declare the result of Theorem 2 own, but the publication of the report on the conference itself in our presence gave.

Let us choose the hypersurface  $\Sigma_t$  maximal and adjust the parametrization in  $V_3$  and on  $\Sigma_t$  identifying  $\rho$  with  $\lambda(x^\mu)|_{\Sigma_t}$ . After this the direct conjecture of the theorem becomes evident.

The converse is obvious.

### 5.2.5. Conclusion

The possibility of the proof of the Theorem 1 is provided by our splitting off two independent equations from SWE four equations on SCMC hypersurface in Petrov type  $N$  space-time.

Evidently the Theorem 1, which plays auxiliary role in the proof of the Theorem 2, possesses independent importance for spinor fields in Riemannian space-time. In particular, it is connected with the fact, that SWE generalizes the equation for neutrino “zero mode” for the case of curved space. Jackiw and Rebbi [680] introduced this equation for investigations of vacuum state structure in quantum gravity.

The main result of presented section — Theorem 2 — solves (under the defined conditions) the problem of relation between spinor and tensor formalism, ascertaining that Witten’s spinor formalisms and Nester’s tensor formalisms are isomorphic; this isomorphism is a result of zeros absence for Witten’s spinor (Theorem 1) and of isomorphism between complexified vector space  $R^3$  and three-dimensional complex vector space of symmetric second-rank  $SU(2)$  spinors.

We can also say, that on SCMC hypersurface in Petrov type  $N$  space-time there exists globally defined (nowhere degenerate) special orthonormal frame — Witten’s orthonormal frame, — and this SOF on maximal hypersurface is also Nester’s SOF.

### 5.3. Nodal points of elliptic equations and system of equations

From the mathematical point of view the necessity for investigation of submanifolds, on which the solutions of elliptic equations are equal to zero, is connected with the fact that the necessary and sufficient conditions for absence of such closed submanifolds of codimension one are simultaneously the necessary and sufficient conditions for uniqueness of the Dirichlet problem for these equations in the domain. The existence and stability of solutions (at sufficiently high smoothness of known functions) follows from its uniqueness. Since the elliptic equations refer to the static solutions of the given hyperbolic field equations, the non-uniqueness of solution for the boundary value problem from the physical point of view defines the instability of “zero modes” of given field equations. Additionally there appears the necessity to study not only the closed submanifolds and not only of codimension one, but all other ones, on which zeros of solutions are located.

The purpose of this section is to develop a new approach for establishing the conditions of solvability and zeros absence for general from the physical point of view elliptic systems of equations. This will give the possibility to prove the existence of the wide class of hypersurfaces, in all points of which there exists the two-to-one correspondence between Sen–Witten spinor and a certain three-frame; we will name it Sen–Witten orthonormal frame (SWOF). In all points on such hypersurfaces there exist also the well defined lapses and shifts, associated by Ashtekar and Horowitz [646] with Sen–Witten spinor. On a subclass of this class, including also the maximal hypersurfaces, we establish the existence of two-to-one correspondence between Sen–Witten spinor and Nester three-frame.

We introduce first three definitions.

**Definition 1.** *The nodal point of the component of the solution is a point, in which the component is equal to zero.*

**Definition 2.** *The nodal point of the solution for the elliptical system of equations is a point, in which the solution is equal to zero.*

From the general theory of elliptic differential equations it is known that non-trivial solutions cannot vanish on an open subdomain, but they can turn to zero on subsets of lower dimensions  $k$ ,  $k = 0, 1, \dots, n-1$ , where  $n$  is dimension of the domain.

**Definition 3.** *The nodal submanifold of dimension  $s$ ,  $s = 1, 2, \dots, n-1$ , is a maximal connected subset<sup>4</sup> of dimension  $s$  consisting of nodal points of the solution.*

Discrete set of nodal points is 0-submanifold. We will show further, that for the system of differential equations, interesting for us, all nodal subsets are formed by intersection of nodal surfaces of the components of the solution.

The connection between the unique solvability for the boundary value problem in  $\mathbf{R}^n$  and absence of  $(n-1)$ -dimensional closed nodal submanifolds was established by Picone [670, 671]. The existence of such connection follows from the next consideration: if the boundary value problem in a certain domain  $\Omega$  is uniquely solvable, then the boundary value problem is also uniquely solvable for any subdomain  $\Omega_1 \subseteq \Omega$ . This excludes the possibility of existence of non-trivial solutions which turn to zero on the boundary of the arbitrary domain  $\Omega_1$ , i.e., excludes the possibility of existence of closed nodal submanifolds of codimension one, and vice versa.

The known investigation of elliptical equations of general form does not allow to obtain the conditions for all nodal points absence. For example, even in the case of the only single equation of general form it is proved the absence of zeros only of infinite order is proven. [667, 668]. Bär [674], continuing Aronszajn

<sup>4</sup>Maximal connected subset  $A$  is a non-empty connected subset such that the only connected subset containing  $A$  is  $A$ .



[667] investigations, proved that the nodal set of Dirac equation is a countable  $(n - 2)$  rectifiable set and thus has Hausdorff dimension  $(n - 2)$  at most, but question about possibility of all nodal points absence remains free-answer. That is why further we will examine only such general equations, which possess also the necessary physical properties, in particular, symmetry properties and reflects embedding of the hypersurface into space-time.

Let  $\Omega$  be a bounded closed spherical-type domain on space like hypersurface in Petrov type  $N$  space-time, otherwise, (i) its boundary  $\partial\Omega$  in every point has a tangent plane; (ii) for every point  $P$  on the boundary there exists a sphere, which belongs to  $\Omega$ , and the boundary of sphere includes the point  $P$ .

In the domain  $\Omega$  let us consider the system of elliptic second order equations

$$D^{AB}D_{AB}u_E + C_E{}^B u_B = 0, \quad (5.24)$$

which generalized equation (5.10). The unknown functions  $u_A$  of independent variables  $x^\alpha$  are the elements of complex vector space  $\mathbf{C}^2$ , in which the skew symmetric tensor  $\varepsilon^{AB}$  is defined, and the group  $SU(2)$  acts.  $C_A{}^B$  is Hermitian  $(1, 1)$  spinorial tensor.

The equation (5.24) and every its summand is invariant under the arbitrary transformations of coordinates in  $V^3$ , and covariant under the local  $SU(2)$ -transformations of unknown functions in a local space isomorphic to the complexified tangent space in every point to  $V^3$ .

Long ago Picone had ascertained that at arbitrary coefficients of elliptic equations the boundary value problem is uniquely solvable, and the closed node submanifolds of codimension one are absent, respectively, only in the domains with enough small intrinsic diameter.

The general conditions for the absence of closed nodal surfaces for strong elliptic system (5.24) are ascertained by Theorem [672].

**Theorem.** *If in domain  $\Omega$  there exist symmetrical quadratic functional second-order matrices  $B_1, B_2, B_3$  of  $C^1$  class, such that matrix*

$$\sqrt{-h}C - \sum_{\alpha=1}^3 \frac{\partial B_\alpha}{\partial x^\alpha} + B^T G^{-1} B$$

*is positive definite, where*

$$B = (B_1, B_2, B_3), \quad G = \sqrt{-h} \text{diag}(\|h_{\alpha\beta}\|, \|h_{\alpha\beta}\|, \|h_{\alpha\beta}\|),$$

*then the solutions of system of equations (5.24) with matrix  $C = \|C_A{}^B\|$  of  $C^1$  class do not have the closed node surfaces in domain  $\Omega$ .*

The effective geometrical conditions of B-matrix existence and corresponding unique solvability of Dirichlet problem in dependence on the domain intrinsic diameter were obtained [672] for the Euclidean space. Since the conditions of nodal manifolds absence for quantum fields equations are the

point of our interest, further we will concentrate our attention on the conditions of nodal points absence in the domains of arbitrary as well as infinite intrinsic diameter.

Evidently, if matrix  $C$  is positive definite, then the conditions of Theorem 1 are fulfilled for  $B \equiv 0$ , and closed nodal surfaces are absent in the domain with arbitrary intrinsic diameter. Simultaneously, the boundary value problem for the system of equations (5.24) is uniquely solvable.

Above cite Theorem does not indicate the conditions at which nodal points, lines and node surfaces for solutions of equations (5.24) are absent. We will obtain them in the next subsection.

### 5.3.1. Conditions for the absence of nodal points

In the case of a single selfadjoint elliptic equation in  $V^3$  the nodal submanifolds can be only the surfaces which divide the domain, but in the case of a system of equations the topology of nodal submanifolds becomes more various: they can be also the lines and the points. We can take this fact into account and ascertain the conditions for the nodal manifolds absence exploiting the double covariance of the system of equations (5.24) and using Zaremba—Giraud Lemma, generalized at first by Keldysh and Lavrentiev [682] and later by Oleynik [683].

Let us introduce the matrix

$$R := \|R_{A'}{}^B\| := \begin{pmatrix} \alpha & \beta \\ -\beta & \bar{\alpha} \end{pmatrix}, \quad \alpha\bar{\alpha} + \beta\bar{\beta} = 1,$$

which is of the group  $SU(2)$ , and let its elements additionally satisfy the condition

$$C_0^1\beta^2 + (C_0^0 - C_1^1)\alpha\beta - C_0^1\alpha^2 = 0.$$

Therefore,

$$C_{0'}{}^{1'} = R_{0'}{}^A C_A{}^B R_{B'}{}^0 = 0,$$

and in accordance with Hermiticity of matrix  $C$  also  $\bar{C}_{0'}{}^{1'} = C_{1'}{}^{0'}$ . Then  $C_0 := C_{0'}{}^{0'}$  and  $C_1 := C_{1'}{}^{1'}$  are eigenvalues of matrix  $C = \|C_A{}^B\|$ . This follows from a fact that for arbitrary matrix  $R \in SU(2)$  the identity

$$-\varepsilon R \varepsilon \equiv R^{T+}$$

is valid, where  $\varepsilon = \|\varepsilon^{AB}\|$ . Therefore

$$C' = -\varepsilon R \varepsilon C R^{T+} = R^{T+} C R^T = \text{diag}(C_0, C_1). \quad (5.25)$$

Let us denote

$$\Delta := C_1^1 - C_0^0 - \left[ (C_1^1 - C_0^0)^2 + 4|C_0^1|^2 \right]^{1/2},$$

and let us denote by  $S$  a set of points in domain  $\Omega$ , in all points of which  $C_0^1$  does not equal to zero, and let us denote by  $T$  a set of points, in which  $C_0^1$  is

equal to zero. Then the elements of the matrix  $R$ , which transforms the matrix  $C$  to diagonal form, satisfy on the set  $S$  the conditions

$$\alpha\bar{\alpha}(1 + \Delta^2/4|C_0^1|^2) = 1, \quad \beta = \alpha\Delta/2C_0^1$$

and on the set  $T$  the conditions

$$\alpha\bar{\alpha} = 1, \quad \beta = 0.$$

Functions  $u_{0'}$  and  $u_{1'}$  on the set  $S$  will be following:

$$u_{0'} = \bar{\alpha} \left( u_0 + \frac{\Delta}{2C_0^1} u_1 \right), \quad u_{1'} = \alpha \left( -\frac{\Delta}{2C_0^1} u_0 + u_1 \right), \quad (5.26)$$

and on set  $T$  they will be

$$u_{0'} = \bar{\alpha}u_0, \quad u_{1'} = \alpha u_1. \quad (5.27)$$

Respectively, eigenvalue  $C_0$  on  $S$  is:

$$C_0 = \frac{4C_0^0|C_0^1|^4 + (4\Delta|C_0^1|^2 + C_1^1\Delta^2)(4|C_0^1|^2 + \Delta^2)}{4|C_0^1|^2(4|C_0^1|^2 + \Delta^2)}$$

and coincides with  $C_0^0$  on the set  $T$ .

**Lemma.** *If real and imaginary parts of functions  $u_A$  and of elements of matrix  $C_A^B$  are functions of class  $C^2$  in domain  $\Omega$ , then the real and imaginary parts of functions  $u_{A'}$  defined by conditions (5.26)–(5.27) are also the functions of class  $C^2$  in this domain.*

*Proof.* Taking into account that it is always possible to choose  $\Im m \alpha \in C^2(\Omega)$ , from direct calculation we obtain that on the set  $S$  there exists first and second derivatives of real and imaginary parts of functions  $u_{A'}$  and  $\alpha$  with respect to arguments  $(\Delta^2/4|C_0^1|^2)$  and  $(\Delta/2|C_0^1|^2)$  and that

$$\lim_{P \ni S \rightarrow Q \in T} \Re e \alpha^{(m)}(P) = \Re e \alpha^{(m)}(Q), \quad \lim_{P \ni S \rightarrow Q \in T} \Im m \alpha^{(m)}(P) = \Im m \alpha^{(m)}(Q), \quad (5.28)$$

$$\lim_{P \ni S \rightarrow Q \in T} \Re e u_{A'}^{(m)}(P) = \Re e u_{A'}^{(m)}(Q), \quad \lim_{P \ni S \rightarrow Q \in T} \Im m u_{A'}^{(m)}(P) = \Im m u_{A'}^{(m)}(Q), \quad (5.29)$$

where symbol  $f^{(m)}$  denotes arbitrary partial derivatives of order  $m = 0, 1, 2$ .

The following theorem is valid.

**Theorem 3.** *Let:*

a) *real and imaginary parts of the elements of matrix  $C$  be of  $C^2$  class in the domain  $\Omega$  on space-like hypersurface in Petrov  $N$  space-time;*

b) *at least one eigenvalue of matrix  $C$ , for definiteness  $C_0$ , be non-negative everywhere in  $\Omega$ ;*

c) *real or imaginary part of the function*

$$v := \begin{cases} \left( u_0 + \frac{\Delta}{2C_0^1} u_1 \right) \Big|_{S \cap \partial\Omega}, \\ u_0 \Big|_{T \cap \partial\Omega} \end{cases}$$

*be equal to zero in any point.*

Then solution  $u_A$  of class  $C^2$  for the system of equations (5.24) does not have any nodal points in the domain  $\Omega$  of spherical type.

*Proof.* The system of equations (5.24) is covariant under the arbitrary transformations of coordinates and under the local transformations from the group  $SU(2)$  that allows to use them independently. Let us apply at the first step the  $SU(2)$  spinor transformation  $u_A \rightarrow R_{A'}{}^B u_B$ , which transforms the matrix  $C$  to the diagonal form, and under which the equation (5.24) is covariant.

The eigenvalues of matrix  $C$  are real, therefore, the resulting system of equations (5.24) splits into two independent subsystem for  $u_{A'}$ . Taking into account that space-time is of Petrov type  $N$ , we can make a conclusion that in a spin-frame subsystem with  $C_0$  splits into two independent equations for real and imaginary parts of  $u_{0'}$  component. Taking into account that  $u_{A'}$ ,  $C_0$  and  $C_1$  are scalars under transformations of coordinates, and  $C_0 \geq 0$ , we can apply the Zaremba—Giraud principle in the general form grounded by Oleynik [683] to every equation containing  $C_0$ . According to this principle, if in a certain point  $P_0$  on the sphere the non-constant function in the ball turns to zero, and everywhere in the ball  $\Re u_{0'} < 0$ , then  $\langle d \Re u_{0'}, l \rangle|_{P_0} < 0$ . Here  $l$  — arbitrary vector field, for which  $\langle n, l \rangle|_{P_0} > 0$ , and  $n$  is one-form of intrinsic normal to the sphere in the point  $P_0$ .

Let us show further that a set of the nodal points for function  $\Re u_{0'}$  does not contain the isolated points. Let us assume that such point exists, i.e.  $\Re u_{0'} = 0$ , and in a certain neighborhood of the point  $P_0$  the function has a constant sign. For definiteness let in this neighborhood be  $u_{0'} < 0$ . Let us consider a sphere, on which the point  $P$  lies and which is so small that completely belongs to the mentioned neighborhood of the point  $P$ . Then, using Zaremba—Giraud principle, we obtain  $\langle d \Re u_{0'}, n \rangle|_{P_0} > 0$ , and therefore in any neighborhood of the point  $P_0$ , located outside the ball, the function  $\Re u_{0'}$  changes its sign, and that is why its zeros are not isolated. Therefore, they form the surfaces which divide  $\Omega$ . Since  $C_0 \geq 0$ , then it follows from the maximum principle that the closed nodal surfaces for the components of solution  $\Re u_{0'}$  are absent. Analogous conclusion is true also for the component of solution  $\Im u_{0'}$ . This means that the only surfaces having common points with the boundary of domain  $\Omega$  can be the nodal surfaces of real or imaginary part of function  $u_{0'}$ . According to condition c), if, for definiteness,

$$\Re \left( u_0 + \frac{\Delta}{2C_0^1} u_1 \right) \Big|_{S \cap \partial \Omega} \neq 0, \quad \Re u_0 \Big|_{T \cap \partial \Omega} \neq 0,$$

then we can choose

$$\begin{aligned} \Re \bar{\alpha} \Big|_{S \cap \partial \Omega} &\neq \left\{ \left[ \Re \left( u_0 + \frac{\Delta}{2C_0^1} u_1 \right) \right]^{-1} \Im \bar{\alpha} \Im \left( u_0 + \frac{\Delta}{2C_0^1} u_1 \right) \right\} \Big|_{S \cap \partial \Omega}, \\ \Re \bar{\alpha} \Big|_{T \cap \partial \Omega} &\neq \left[ (\Re u_0)^{-1} \Im \bar{\alpha} \Im u_0 \right] \Big|_{T \cap \partial \Omega} \end{aligned}$$

and obtain

$$\begin{aligned} & \left[ \Re \bar{\alpha} \Re \left( u_0 + \frac{\Delta}{2\bar{C}_0^1} u_1 \right) - \Im \bar{\alpha} \Im \left( u_0 + \frac{\Delta}{2\bar{C}_0^1} u_1 \right) \right] \Big|_{S \cap \partial\Omega} \equiv \\ & \equiv \Re u_{0'} \Big|_{S \cap \partial\Omega} \neq 0, \\ & (\Re \bar{\alpha} \Re u_0 - \Im \bar{\alpha} \Im u_0) \Big|_{T \cap \partial\Omega} \equiv \Re u_{0'} \Big|_{T \cap \partial\Omega} \neq 0. \end{aligned}$$

Therefore nodal surfaces as well as lines and points of the real (or imaginary) part are absent, and that is why any nodal points of complete solution  $u_A$  are also absent. The statement of the theorem is proven.

*Note.* If the conditions a) and b) of the Theorem are fulfilled, and the matrix  $C$  is non-negative definite in domain  $\Omega$ , then both eigenvalues are non-negative, and, therefore, the boundary value problem for the system of equations (5.24) is uniquely solvable in arbitrary bounded domain, as it follows from the classical maximum principle. Otherwise the solution in finite domain exists only in the case when its intrinsic diameter does not overcome a certain value.

### 5.3.2. The conditions of nodal points absence for the solutions of Sen—Witten equation

After Witten's positive energy proof the attempts of development of tensor method for proof were performed along two lines. The attempts of the tensor interpretation for Sen—Witten spinor field belong to the first line. In particular, Ashtekar and Horowitz [646] used Sen—Witten spinor field for determination of a class of preferred lapses  $T := \lambda$  and shifts  $T^a := -\sqrt{2} i \lambda^{+(A} \lambda^{B)}$ . Dimakis and Müller-Hoissen [650, 654] have defined a preferred class of orthonormal frame fields in which spinor field take a certain standard form. Frauendiener [655] has noticed a correspondence between Sen—Witten spinor field and a triad. But, as it was shown by Dimakis and Müller-Hoissen, frame fields cannot exist in the nodal points of the spinor field.

Let us weaken the conditions of zeros absence for SWE (5.4) on  $\Sigma_t$  using the results of subsection 5.3.1. From equation (5.4), taking into account the equation of Hamiltonian constraint on  $\Sigma_t$ , in Gauss normal coordinates we obtained (see also [657]):

$$\begin{aligned} \mathcal{D}_A{}^B \mathcal{D}_{BC} \lambda^C &= \frac{1}{2\sqrt{-h}} \frac{\partial}{\partial x^\alpha} \left( \sqrt{-h} h^{\alpha\beta} \frac{\partial}{\partial x^\beta} \lambda_A \right) - \\ &- \frac{\sqrt{2}}{2} \lambda^B D_{AB} \mathcal{K} + \frac{1}{4} \mathcal{K}^2 \lambda_A + \frac{1}{8} \mathcal{K}_{\alpha\beta} \mathcal{K}^{\alpha\beta} \lambda_A + \frac{1}{4} \mu \lambda_A = 0. \end{aligned} \quad (5.30)$$

Therefore, the system of equations (5.30) is a system of the form (5.24); if it does not have the nodal points, the SWE also does not have them.

Spinorial tensor

$$C_A{}^B := \frac{\sqrt{2}}{4} D_A{}^B \mathcal{K} + \frac{1}{4} \varepsilon_A{}^B \left( 2\mathcal{K}^2 + \frac{1}{2} \mathcal{K}_{\pi\rho} \mathcal{K}^{\pi\rho} + \mu \right) \quad (5.31)$$

is Hermitian because

$$(\mathcal{D}_A{}^B \mathcal{K})^+ = (\varepsilon^{BC} \mathcal{D}_{AC} \mathcal{K})^+ = (\varepsilon^{BC})^+ (\mathcal{D}_{AC} \mathcal{K})^+ = -(\mathcal{D}_{AC} \mathcal{K}) \varepsilon^{CB} = (\mathcal{D}_A{}^B \mathcal{K}).$$

So, the SWE solutions of class  $C^2$  do not have the nodal points in a bounded closed domain  $\Omega$  of spherical type on  $\Sigma_t$  in Petrov type  $N$  space-time, if for spinorial tensor  $C_A{}^B$  in this domain and for the boundary values of the solution the conditions of Theorem 3 are fulfilled.

Let us consider further a sequence  $\Omega_n$  of increasing domains of spherical type covering  $\Sigma_t$ . If in every domain the conditions of Theorem 3 are fulfilled, then all solutions of class  $C^2$  do not have the nodal points in  $\Omega_n$ . According to Reula, on  $\Sigma_t$  there exists the SWE solution of  $\lambda^C = \lambda_\infty^C + \beta^C$  form, where  $\lambda_\infty^C$  is asymptotically covariant constant spinor field on  $\Sigma_t$ ,  $\beta^C$  is an element of Hilbert space  $\mathcal{H}$ , which is the Cauchy completion of  $C_0^\infty$  spinor fields under the norm

$$\|\beta^E\|_{\mathcal{H}}^2 = \int_{\Sigma_t} (\mathcal{D}^A{}_B \beta^B)^+ (\mathcal{D}_{AC} \beta^C) dV.$$

Solution  $\lambda^C$  belongs properly to  $C^\infty$  class. From the asymptotical flatness condition it follows that  $(\Delta^2/(4|C_0^1|^2))$ , as well as real and imaginary parts of functions  $(\Delta/2\bar{C}_0^1)$  and  $(\Delta/2C_0^1)$  vanish asymptotically. Therefore, condition c) of Theorem 2 asymptotically takes the form:  $\Re \lambda_\infty^0 \neq 0$  or  $\Im \lambda_\infty^0 \neq 0$ . In such a way we obtain the following theorem:

**Theorem 4.** *Let:*

- a) *initial data set be asymptotically flat;*
- b) *everywhere on space-like hypersurface  $\Sigma_t$  in Petrov type  $N$  space-time the matrix of spinorial tensor (5.31) have at least one non-negative eigenvalue, for definiteness  $C_0$ ;*

- c)  *$\Re \lambda_\infty^0$  or  $\Im \lambda_\infty^0$  equal zero asymptotically nowhere.*

*Then the asymptotically constant nontrivial solution  $\lambda^C$  to SWE does not have the nodal points on  $\Sigma_t$ .*

The conditions of Theorem 4 are fully admissible from the physical point of view.

### 5.3.3. Towards Sen—Witten equation, special orthonormal frame and preferred time variables

Usually the question about existence of system of coordinates or orthonormal basis, which satisfy certain gauge conditions, is reduced to the question about existence of solution for non-linear system of differential equations and often can be solved only at some additional limitations and assumptions [649].

The existence theorem for Sen–Witten (linear) equation and the Theorem 4 about their zeros (subsection 4) on surfaces, which can be not maximal, allow us to prove the existence of a certain class of orthonormal three-frames in all points of these hypersurfaces which satisfies gauge conditions.

$$\begin{aligned} \varepsilon^{abc}\omega_{abc} \equiv *q = 0, \quad \omega^a{}_{1a} \equiv -\tilde{q}_1 = F_1, \\ \omega^a{}_{2a} = -\tilde{q}_2 = F_2, \quad \omega^a{}_{3a} = -\tilde{q}_3 = \mathcal{K} + F_3, \end{aligned} \quad (5.32)$$

and generalizes Nester’s SOF. Such three-frame we will name as Sen–Witten orthonormal frame (SWOF)

**Theorem 5.** *Let the conditions of Theorem 4 be fulfilled. Then everywhere on  $\Sigma_t$  there exists a two-to-one correspondence between Sen–Witten spinor and Sen–Witten orthonormal frame.*

*Proof.* Really, let all conditions of Theorem 3 be fulfilled on  $\Sigma_t$ . Then SWE solution  $\lambda_A$  does not have the nodal points anywhere on  $\Sigma_t$ . This allows to prove on such  $\Sigma_t$  the Sommers [661] assumption that spatial null one-form  $L = -\lambda_A\lambda_B$  on  $\Sigma_t$  is non-zero, and allows to turn everywhere on  $\Sigma_t$  to the “squared” SWE represented in the form:

$$\langle \tilde{L}, D \otimes L \rangle - \mathcal{K}L + 3!i * (n \wedge D \wedge L) = 0, \quad (5.33)$$

where  $\langle \tilde{L}, D \otimes L \rangle$  is one-form with components  $\tilde{L}_\nu D_\mu L^\nu$ ,  $\tilde{L} = |L|^{-1} * (L \wedge \bar{L})$  is non-zero spatial one-form, and  $n$  is one form of unit normal to  $\Sigma_t$ .

The bilinear form

$$\frac{1}{\sqrt{2}}n^{AA}\lambda_A\bar{\lambda}_{\dot{A}} = \lambda_A\lambda^{A+} \equiv \lambda,$$

where  $n$  is one-form of a unit normal to  $\Sigma_t$ , is Hermitian positive definite one, and the solution  $\lambda_A$  does not have the nodal points on  $\Sigma_t$ . Consequently, we can further introduce real nowhere degenerate orthonormal 4-coframe  $\theta^m$  as

$$\theta^0 \equiv n = Ndt, \quad \theta^1 = \frac{\sqrt{2}}{2\lambda}(L + \bar{L}), \quad \theta^2 = \frac{\sqrt{2}}{2\lambda i}(L - \bar{L}), \quad \theta^3 = \tilde{L} \quad (5.34)$$

and represent immediately (5.33) in the form

$$-\langle \theta^1, D \otimes \theta^3 \rangle - \mathcal{K}\theta^1 + 3! * [n \wedge (D + F) \wedge \wedge \theta^2] = 0, \quad (5.35)$$

$$\langle \theta^2, D \otimes \theta^3 \rangle + \mathcal{K}\theta^3 + 3! * [n \wedge (D + F) \wedge \theta^1] = 0, \quad (5.36)$$

where  $F = D \ln \lambda$ . The system of equations (5.35)–(5.36) includes only four independent equations, and they are equations (5.32) for the connection one-forms coefficients. From this it follows that if on  $\Sigma_t$  the conditions of Theorem 3 and SWE are fulfilled, then on  $\Sigma_t$  there exists three-frame  $\theta^a$  defined by (5.34) in which conditions (5.32) are fulfilled.

Inversely, if on  $\Sigma_t$  in some three-frame  $\theta^a$  the conditions of Theorem 4 and conditions (5.32) are fulfilled, then it follows from condition of Theorem

3 that these one-forms have a form  $\theta^a = \theta_\infty^a + \phi^a$ , where  $\theta_\infty^a$  tend asymptotically to the covariant constant forms and  $\phi^a$  belongs to  $\mathcal{H}$ . We can turn from four-frame  $\theta^m \equiv \{n, \theta^a\}$  to one-forms  $\theta^0, L, \tilde{L}$ , assuming  $\lambda_A|_{\Sigma_t} \neq 0$ . After this we obtain equation (5.33) and further (5.4)<sup>5</sup> for spinor field  $\lambda^A$ , which, as we have demonstrated previously, indeed does not have the nodal points on selected hypersurface  $\Sigma_t$  and which together with asymptotical conditions defines up to sign the spinor field  $\lambda^A$ . Mentioned in conditions of the Theorem correspondence between Sen–Witten spinor field and Nester’s SOF is defined by relationship (5.34).

We have proven in Section 5.2.4 that if initial set  $(\Sigma_t, h_{\mu\nu}, \mathcal{K}_{\pi\rho})$  on maximal hypersurface  $\Sigma_t$  is asymptotically flat and satisfies the dominant energy condition, then everywhere on  $\Sigma_t$  from existence of Sen–Witten spinor field follows existence Nester’s three-frame and conversely. Theorem 4 allows to strengthen significantly this result taking away the assumption that  $\Sigma_t$  is maximal. Indeed, if all conditions of Theorem 3 are fulfilled on  $\Sigma_t$ , and additionally the one-form  $\mathcal{K}\tilde{L}$  is globally exact, we can perform in conditions the identification  $F \equiv d \ln \lambda + \mathcal{K}\theta^3$  and obtain the Nester’s gauge (5.14), or to perform the inverse transition — from Nester’s gauge to SWE. Therefore, if on  $\Sigma_t$  the conditions of Theorem 3 are fulfilled, then SWE and Nester’s gauge are equivalent if and only if the one-form  $\mathcal{K}\lambda^{+(A}\lambda^{B)}$  is exact. In this case the correspondence between Sen–Witten spinor and Nester’s SOF is also ascertained by relationship (5.34).

Ashtekar and Horowitz [646] have accented on the necessity of zeros investigations for SWE solutions introducing the vector interpretation of Sen–Witten’s spinor which defines a preferred lapse and shift. Evidently, the fulfilling of the Theorem 4 conditions ensures the existence of corresponding lapses and shifts well defined everywhere on  $\Sigma_t$ . And also the preferred class of orthonormal four-frame fields introduced by Dimakis and Müller-Hoissen exists in all points of  $\Sigma_t$  under fulfilling of the Theorem 3 conditions.

The presence of zeros in the solutions of elliptic equations is rather ordinary than exceptional case, therefore, it is necessary to prove the absence of zeros for concrete cases.

The represented investigation demonstrates the possibility for obtaining the condition of the nodal manifolds absence for enough general system of elliptic second order equations owing to its double covariance.

The application of this result to SWE allows to prove the equivalence of SWE and gauge conditions (5.15), and, respectively, the existence of an everywhere well defined two-to-one correspondence between Sen–Witten spinor field and the SWOF, which is the Nester SOF in the particular case, when one of the one-forms  $\mathcal{K}\theta^a$  is exact. Therefore, the indicated correspondence

---

<sup>5</sup> The equivalence of the SWE (5.4) and of the equation (5.30) is proven by Reula [645].



exists not only on the unique — maximal — hypersurface, but on the whole set of asymptotically flat hypersurfaces.

Ashtekar and Horowitz [646] have shown that the Reula results hold even if the energy condition is mildly violated. Also the conclusion about existence of special three- and four-frames, as well as preferred lapses and shifts, is stable under the violation of the energy condition, because, as it is seen from (5.31), there exist the hypersurfaces, on which this condition of nodal points absence is fulfilled at violation of the energy condition.

#### 5.4. Sen—Witten orthonormal three-frame and gravitational energy quasilocalization

The equivalence principle excludes a possibility for existence of the gravitational energy density, however, in the Penrose conception [684] there is possible its quasilocalization. This conception is realized in several proposals for the quasilocal energy-momentum [684–689].

According to the Nester and coauthors approach, for each gravitational energy-momentum pseudotensor there is Hamiltonian boundary term, and the energy-momentum in a domain, bounded by close 2-surface, depends on the field values and the frame of reference on the 2-surface. Various criteria are insufficient and, most probably [689], will be insufficient for selecting a unique Hamiltonian boundary term. Variety of these terms is characterized by different choices of dynamic variables (metric, orthonormal frame, spinors), boundary conditions and reference configurations. According to this there a problem of the different Hamiltonians comparing [686, 691] appears. Among criteria that must be satisfied by the quasilocal energy-momentum density, at least in asymptotically Minkowskian space [692], must be positivity. It can be ensured by finding the locally non-negative Hamiltonian density dependent on the Sen—Witten spinor according to Witten [638], or by applying the ADM Hamiltonian and the Nester special orthonormal frame [649].

In the asymptotically flat space the Hamiltonian is of the general form [694]

$$H(N) = \int_{\Sigma} (N\mathcal{H} + N^a\mathcal{H}_a)dV + \oint_{\partial\Sigma} B \quad (5.37)$$

and includes the Regge—Teitelboim boundary term [695] at spatial infinity.

Grounding and developing the Wittenian proof of the positive energy theorem, Nester [696] proposed an expression for the Hamiltonian density as the 4-covariant quadratic spinor 3-form:

$$\mathcal{H}(\psi) := 2[D(\bar{\psi} \wedge \gamma_5 \gamma) \wedge D\psi - D\bar{\psi} \wedge D(\gamma_5 \gamma \psi)], \quad (5.38)$$

where

$$D\psi = \psi + \frac{1}{2}\omega^{\mu\nu}\sigma_{\mu\nu}\psi, \quad \sigma_{\mu\nu} = \frac{1}{2}[\gamma_{\mu}, \gamma_{\nu}], \quad \gamma = \gamma_{\mu}\theta^{\mu}, \\ \gamma_{\mu}\gamma_{\nu} + \gamma_{\nu}\gamma_{\mu} = 2g_{\mu\nu}, \quad \gamma_5^2 = -E, \quad \gamma_5 = \gamma^0\gamma^1\gamma^2\gamma^3.$$

From expression (5.38) one can obtain the following expression for  $\mathcal{H}(\psi)$ :

$$\mathcal{H}(\psi) = 4D\bar{\psi} \wedge \gamma_5 \gamma \wedge D\psi = 4\nabla_\pi \bar{\psi} (\gamma^\mu \sigma^{\pi\rho} + \sigma^{\pi\rho} \gamma^\mu) \nabla_\rho \psi d\Sigma_\mu, \quad (5.39)$$

where  $d\Sigma_\mu = \frac{1}{3!} \sqrt{|g|} \varepsilon_{\mu\nu\pi\sigma} dx^\nu \wedge dx^\pi \wedge dx^\sigma$ .

In the Gaussian normal system of coordinates in the neighborhood of arbitrary space-like hypersurface  $\Sigma$ , the Hamiltonian density (5.39) can be written as a sum of positive and negative definite components [696]

$$\mathcal{H}(\psi) = -4g^{ab} D_a \psi^+ D_b \psi + D_a \bar{\psi} \left( \gamma^d \gamma^a \gamma^b + \gamma^a \gamma^b \gamma^d \right) D_b \psi d\Sigma_0 \quad (5.40)$$

and be locally non-negative if  $SL(4, \mathbb{C})$ -spinor  $\psi$  on the space-like hypersurface  $\Sigma$  satisfies the Sen–Witten equation

$$\gamma^a D_a \psi = 0. \quad (5.41)$$

Expression (5.40) cannot give the true positive energy density for the gravitational field because  $\psi$ , as solution of the SWE, is a non-local functional on the initial data  $(h, K, \Sigma)$  set; therefore, a concept of the locally non-negative density of the gravitation energy is treated as the locally non-negative functional on the set of initial data  $(h, K, \Sigma)$  and the boundary values of function  $\psi$ . The gravitational Hamiltonian density (5.40) has significant advantages in comparison with the other ones: except a fact that it is explicitly 4-covariant, the gravitational Hamiltonian, which includes it, allows to prove that the total 4-momentum and the Bondi 4-momentum are time-like. To its liabilities Nester and Tung have referred the physical mysteriousness of the Sen–Witten spinor field, and absence of the direct relation to the Hamiltonian density in the SOF method [649, 651, 693]. For establishing such relation, Nester and Tung [686] had developed a new method of proving the PET and the gravitational energy localization, which employs the 3-dimensional spinors and a new identity connecting the 3-dimensional scalar curvature to the spinor expression in the Hamiltonian. The Einstein 3-spinor Hamiltonian with a zero shift the authors obtained in the form<sup>6</sup>

$$H = \int_{\Sigma} \left[ \varphi^+ \varphi g^{-1/2} \left( \pi^{ab} \pi_{ab} - \frac{1}{2} \pi^2 \right) - 4 \left( g^{ab} \nabla_a \varphi^+ \nabla_b \varphi + \nabla_a \varphi^+ \sigma^a \sigma^b \nabla_b \varphi \right) \right] d^3x, \quad (5.42)$$

from which follows a conclusion that the density is non-negative definite, if on the maximal hypersurface the asymptotically constant spinor  $\varphi$  satisfies the Dirac equation in the 3-dimensional space

$$\sigma^a \nabla_a \varphi = 0. \quad (5.43)$$

<sup>6</sup>In this formula and in some next formulas we change the signs, comparing with the original papers, according to the chosen here convention that a signature is  $(+, -, -, -)$ .

The main result of the Nester, Tung [686] and the Nester, Tung, Zhytnikov [697] works is formulated in the form of a statement that between the localization method, based on the 4-covariant spinor Hamiltonian, and the SOF-based method there exists a close connection owing to the 3-spinor Hamiltonian (5.42).

Such statement is grounded on the two circumstances: 1) among terms of which the 4-covariant spinor density consists, the 3-spinorial density is present; 2) between the 3-spinor field variables there exists, as Nester and Tung declared, a close relation, since from the 3-dimensional Dirac equation (5.43) it follows that

$$\sigma^a \nabla_a \varphi = \sigma^a \varphi_{,a} - \frac{1}{2} \tilde{q}_b \sigma^b \varphi + \frac{1}{4} i * q \varphi = 0, \quad (5.44)$$

where forms  $q$  and  $\tilde{q}$  are defined in the following way:

$$q = \theta_{\hat{a}} \wedge d\theta^{\hat{a}}, \quad \tilde{q} = i_{\hat{a}} d\theta^{\hat{a}} \quad (5.45)$$

and fix SOF on the asymptotically flat surfaces by means of the Nester gauge

$$*q = 0, \quad \tilde{q} = \Phi, \quad (5.46)$$

where  $\Phi$  is arbitrary exact one-form. Nester, Tung and Zhytnikov results do not connect the Dirac equation itself and the Nester gauge by the equivalence relationship of a certain type, and do not establish the explicit and unique connection in all points of  $\Sigma$  (see, for example, [650, 654, 693]) between the variables of the 3-spinor field and the SOF variables. That is why search for the valuable grounding of a statement about existence of a close correlation between both approaches remains topical.

We propose further a new insight into the problems of this correlation that is fully correct for the case of maximal hypersurface and is grounded asymptotically in the case of quite arbitrary hypersurfaces. The reason is known: the linear equations for the spinor fields become non-linear after transition to the respective tensor functions.

#### 5.4.1. Direct link between the 4-covariant spinor 3-form and the Einstein Hamiltonian

Taking into account that the Hamiltonian density (5.38) and the SWE were obtained by the spinor parameterization for the Hamiltonian displacement, we write in terms of the Sommers–Sen spinors

$$N^\mu = \lambda^A \lambda^{\dot{A}} = \lambda^{(A} \lambda^{B)+} + N^\mu n_\mu n^{AB} = \lambda^{(A} \lambda^{B)+} + \frac{1}{\sqrt{2}} \lambda_D \lambda^{D+} \varepsilon^{AB}. \quad (5.47)$$

That is why  $N \equiv N^0 = \lambda_A \lambda^{A+} = \Phi$ . Note, that the Nester SOF approach does not limit a choice of the dependence  $\Phi = \Phi(N)$ , but the only case of  $\Phi \equiv N$  seems to be meaningful and admissible [693].

We will further give the 4-covariant Hamiltonian density in terms of the Sen–Witten spinor using the SWE in the form

$$\mathcal{D}^B{}_C \lambda^C = 0. \quad (5.48)$$

An action of operator  $\mathcal{D}_{AB}$  on the spinor fields is

$$\mathcal{D}_{AB} \lambda_C = D_{AB} \lambda_C + \frac{\sqrt{2}}{2} \mathcal{K}_{ABC}{}^D \lambda_D,$$

where  $D_{AB}$  – the spinorial form of the derivative operator  $D_\alpha$  compatible with metric  $h_{\mu\nu}$  on the  $C^\infty$  hypersurface  $\Sigma_t$ ,  $\mathcal{K}_{ABCD}$  – the spinorial tensor of the extrinsic curvature of hypersurface  $\Sigma$ .

The standard substitution transforms (5.39) to the form

$$\begin{aligned} \mathcal{H}(\varphi, \chi) = & \left[ -2\sqrt{2} \left( n_{A\dot{A}} D_\mu \varphi^A D^\mu \bar{\varphi}^{\dot{A}} + n_{A\dot{A}} D_\mu \chi^A D^\mu \bar{\chi}^{\dot{A}} \right) + \right. \\ & \left. + 2 \left( n^{B\dot{C}} D_{B\dot{A}} \bar{\varphi}^{\dot{A}} D^\mu \varphi^A + n^{B\dot{C}} D_{B\dot{A}} \bar{\chi}^{\dot{A}} D^\mu \chi^A \right) \right] d^3 \Sigma. \end{aligned} \quad (5.49)$$

Let us take into account that

$$\begin{aligned} h^{\mu\nu} n_{A\dot{A}} D_\mu \varphi^A D_\nu \bar{\varphi}^{\dot{A}} &= \varepsilon^{\dot{B}\dot{D}} \varepsilon^{BD} n_{A\dot{A}} (D_{B\dot{B}} \varphi^A) (D_{D\dot{D}} \bar{\varphi}^{\dot{A}}) = \\ &= 2n^{R\dot{B}} n_R{}^{\dot{D}} \varepsilon^{BD} (D_{B\dot{B}} \varphi^A) (D_{D\dot{D}} \bar{\varphi}^{\dot{A}}) = (\mathcal{D}_B{}^R \varphi^A) (\mathcal{D}_R{}^B \bar{\varphi}^{\dot{A}}) n_{A\dot{A}}, \end{aligned} \quad (5.50)$$

and

$$(\mathcal{D}_R{}^B \bar{\varphi}^{\dot{A}}) n_{A\dot{A}} = \frac{1}{\sqrt{2}} \left[ -\mathcal{D}^{BR} \varphi_A^+ - \sqrt{2} (\mathcal{D}^{BR} n_{A\dot{A}}) \bar{\varphi}^{\dot{A}} \right], \quad (5.51)$$

$$\mathcal{D}^{BR} n_{A\dot{A}} = \mathcal{K}^{BR}{}_{A\dot{A}} + \frac{\sqrt{2}}{2} F_{A\dot{A}} \varepsilon^{(BR)} = \mathcal{K}^{BR}{}_{A\dot{A}}. \quad (5.52)$$

Then

$$\begin{aligned} n_{A\dot{A}} h^{\mu\nu} (D_\mu \varphi^A D_\nu \bar{\varphi}^{\dot{A}} + D_\mu \chi^A D_\nu \bar{\chi}^{\dot{A}}) &= \\ &= (\mathcal{D}_{BR} \varphi_A) \left( \frac{\sqrt{2}}{2} \mathcal{D}^{BR} \varphi^{+A} + \mathcal{K}_S{}^{BRA} \varphi^{+S} \right) + \\ &+ (\mathcal{D}^{BR} \chi^A) \left( \frac{\sqrt{2}}{2} \mathcal{D}_{BR} \chi_A^+ + \mathcal{K}_S{}^{BRA} \chi^{+S} \right). \end{aligned} \quad (5.53)$$

For transformation of the other terms we will use the identity

$$\begin{aligned} D_{B\dot{A}} \bar{\varphi}^{\dot{A}} &= D_{B\dot{A}} (2n^{\dot{A}C} n_{C\dot{C}} \bar{\varphi}^{\dot{C}}) = -\frac{2}{\sqrt{2}} D_{B\dot{A}} (n^{\dot{A}C} \varphi_C^+) = \\ &= -\frac{2}{\sqrt{2}} \left( \mathcal{K}_{B\dot{A}}{}^{\dot{A}C} \varphi_C^+ + \frac{1}{\sqrt{2}} \mathcal{D}_B{}^C \varphi_C^+ \right) = -\frac{2}{\sqrt{2}} \left( \mathcal{K}_B{}^C \varphi_C^+ + \frac{1}{\sqrt{2}} \mathcal{D}_B{}^C \varphi_C^+ \right) \end{aligned} \quad (5.54)$$

and, therefore,

$$n^{B\dot{C}}D_{B\dot{A}}\bar{\varphi}^{\dot{A}}D_{A\dot{C}}\varphi^A = \frac{\sqrt{2}}{2}(\mathcal{D}_A{}^B\varphi^A)(\mathcal{D}_{BC}\varphi^{+C}) - \frac{1}{2}\mathcal{K}_{BC}\varphi^{+C}\mathcal{D}_A{}^B\varphi^A. \quad (5.55)$$

The final expression for  $\mathcal{H}(\varphi, \chi)$  we will give in the form

$$\begin{aligned} \mathcal{H}(\varphi, \chi) = & \sqrt{2}\left\{(\mathcal{D}_{BR}\varphi_A)\left(\sqrt{2}\mathcal{D}^{BR}\varphi^{+A} + \mathcal{K}_S^{BRA}\varphi^{+S}\right) + \right. \\ & + (\mathcal{D}_A{}^B\varphi^A)(-\mathcal{D}_{BC}\varphi^{+C} + \mathcal{K}_{BC}\varphi^{+C}) + (\mathcal{D}_{BR}\chi_A)\left(\sqrt{2}\mathcal{D}^{BR}\chi^{+A} + \mathcal{K}_S^{BRA}\chi^{+S}\right) + \\ & \left. + (\mathcal{D}_A{}^B\chi^A)(-\mathcal{D}_{BC}\chi^{+C} + \mathcal{K}_{BC}\chi^{+C})\right\}dV. \quad (5.56) \end{aligned}$$

The Hamiltonian 3-form  $\mathcal{H}(\varphi, \chi)$  (5.4.1) in comparison with the Hamiltonian 3-form, obtained by Ashtekar and Horowitz [646], contains the terms with the external curvature of hypersurface  $\Sigma$ .

The first and the second terms are positive definite, and the next ones turn to zero if on hypersurface  $\Sigma$  the spinor fields  $\varphi^A$  and  $\chi^A$  satisfy the SWE (5.48).

On the other hand, the ADM Hamiltonian density, parameterized with orthonormal 3-frames  $\theta^{\dot{a}}$ , is of the form [686]

$$\begin{aligned} \mathcal{H}(N) = & -2|h|^{1/2}\tilde{q}^a\partial_a N + N|h|^{1/2}\left(\mathcal{K}^{ab}\mathcal{K}_{ab} - \mathcal{K}^2\right) - \\ & - 2|h|^{1/2}\left(\mathcal{K}^a{}_b - \delta^a{}_b\mathcal{K}\right)D_a N^b + N|h|^{1/2}\left[q^{ab}q_{ab} + \frac{1}{2}\tilde{q}^a\tilde{q}_a - \frac{1}{6}(*q)^2\right], \quad (5.57) \end{aligned}$$

where the symmetric tensor  $q_{ab}$ , vector  $\tilde{q}_a$ , and scalar  $*q$  are defined by irreducible decomposition

$$C^a{}_{bc} = q^{ad}\varepsilon_{dcb} + \frac{1}{2}(\delta_c^a\tilde{q}_b - \delta_b^a\tilde{q}_c) + \frac{1}{3}*q\varepsilon^a{}_{cb}.$$

Varying the lapse in (5.57), we obtain the super-Hamiltonian constraint in the form

$$\begin{aligned} & 2\partial_k\left(|h|^{1/2}q_k\right) + \frac{1}{2}|h|^{1/2}q^k q_k + \\ & + \frac{|h|}{2}\left[\mathcal{K}^{mn}\mathcal{K}_{mn} - \mathcal{K}^2 + q^{mn}q_{mn} + \frac{1}{2}\tilde{q}^a\tilde{q}_a - \frac{1}{6}(*q)^2\right]. \quad (5.58) \end{aligned}$$

If the spinor fields  $\varphi^A$  and  $\chi^A$  satisfy the SWE and conditions of Theorem 3, then condition (5.15) is fulfilled, and vice versa. Then, on the one hand,  $\mathcal{H}(\varphi, \chi)$  will be positive, and, on the other hand, this will permit us to write  $\mathcal{H}(N)$  in the SWOF, under the necessary in this context limitation for  $\Phi$  and at  $N^a = 0$ , in the form

$$\begin{aligned} \mathcal{H}^{SWOF}(N) = & N|h|^{1/2}\left(-\frac{3}{2}h^{mn}\partial_m \ln N \partial_n \ln N - \mathcal{K}\partial_3 \ln N - \right. \\ & \left. - \frac{3}{2}\mathcal{K}^2 + \mathcal{K}^{mn}\mathcal{K}_{mn} + q^{mn}q_{mn}\right). \quad (5.59) \end{aligned}$$

Here the lapse is determined by the super-Hamiltonian constraint

$$\begin{aligned}
 & 2\partial_m \left( |h|^{1/2} h^{mn} \partial_n \ln N \right) + 2\partial_m \left( |h|^{1/2} \theta^{\hat{3}m} \mathcal{K} \right) + \\
 & + |h|^{1/2} \left( \frac{1}{2} h^{mn} \partial_m \ln N \partial_n \ln N + 2\mathcal{K} \theta^{\hat{3}m} \partial_m \ln N - \frac{3}{2} \mathcal{K}^2 + \mathcal{K}^{mn} \mathcal{K}_{mn} + q^{mn} q_{mn} \right) = \\
 & = 2\partial_m \left( |h|^{1/2} h^{mn} \partial_m \ln N \right) + |h|^{1/2} \left( \frac{1}{2} h^{mn} \partial_m \ln N \partial_n \ln N + \right. \\
 & \left. + 2\mathcal{K} \partial_{\hat{3}} \ln N - 2\partial_{\hat{3}} \mathcal{K} + \frac{1}{2} \mathcal{K}^2 + \mathcal{K}^{mn} \mathcal{K}_{mn} + q^{mn} q_{mn} \right) = 0. \quad (5.60)
 \end{aligned}$$

Let us consider first of all the especially simple case of a maximal spatial Cauchy hypersurface. Then the Hamiltonian density (5.59) takes the form

$$\mathcal{H}^{SWOF}(N) = N |h|^{1/2} \left( -\frac{3}{2} h^{mn} \partial_m \ln N \partial_n \ln N + \mathcal{K}^{mn} \mathcal{K}_{mn} + q^{mn} q_{mn} \right) \quad (5.61)$$

and will be everywhere positive definite if on  $\Sigma$  exists an appropriate solution of the super-Hamiltonian constraint

$$\begin{aligned}
 & 2\partial_m \left( |h|^{1/2} h^{mn} \partial_m \ln N \right) + \\
 & + |h|^{1/2} \left( \frac{1}{2} h^{mn} \partial_m \ln N \partial_n \ln N + \mathcal{K}^{mn} \mathcal{K}_{mn} + q^{mn} q_{mn} \right) = 0. \quad (5.62)
 \end{aligned}$$

Unique positive solution  $N$  of this equation exists because Nester's gauge (5.14) has the property of conformal invariance and thus fits into the Lichnerowicz—Choquet-Bruhat—York initial-value problem analysis [693]. Therefore, we conclude, that owing to the correspondence between the SWE and the Nester gauge on the maximal hypersurface there exists the direct relationship between the Hamiltonian based positivity localization in the 4-covariant spinor method and in the ADM method based on the SOF.

Now, let us consider the hypersurface  $\Sigma$  which is not maximal, and let it be asymptotically  $N = a + O(r^{-1})$ ,  $\partial_m N = O(r^{-2})$ . Then the super-Hamiltonian constraint (5.60) for enough large  $r$  can be written as

$$2\partial_m \left( |h|^{1/2} h^{mn} \partial_m N \right) + N |h|^{1/2} \left( -2\partial_{\hat{3}} \mathcal{K} + \frac{1}{2} \mathcal{K}^2 + \mathcal{K}^{mn} \mathcal{K}_{mn} + q^{mn} q_{mn} \right) = 0. \quad (5.63)$$

The Dirichlet problem for equation (5.63) has the unique solution, if

$$C(x) = |h|^{1/2} \left( -2\partial_{\hat{3}} \mathcal{K} + \frac{1}{2} \mathcal{K}^2 + \mathcal{K}^{mn} \mathcal{K}_{mn} + q^{mn} q_{mn} \right) \geq 0. \quad (5.64)$$

The same condition and the condition that  $N$  is positive on the boundary or asymptotically ensure the non-occurrence of the nodal points of equation

(5.63), since the nodal submanifolds of elliptic equation of second order are closed or have common points with boundary. That is why everywhere  $N > 0$ , and we can choose  $a = 1$ .

Further, a general theorem for the elliptic second-order system claims [676] that its solutions continuously depend on coefficients, domain and values of the functions on the boundary, therefore the Hamiltonian density  $\mathcal{H}^{SWOF}(N(\mathcal{K}), N)$  (5.59) continuously depends on  $\mathcal{K}$  and thus is non-negative on the hypersurfaces which satisfy the condition

$$-2\partial_{\hat{3}}\mathcal{K} + \frac{1}{2}\mathcal{K}^2 \geq 0 \quad (5.65)$$

and lie in some neighborhood of the maximal one. The presence of the terms  $-2\partial_{\hat{3}}\mathcal{K}$  and  $\frac{1}{2}\mathcal{K}^2$  in the right-hand side of relationship (5.64) is caused just by the fact that we used the SWOF; the application of Nester's gauge does not give a possibility to prove the existence of this class of hypersurfaces, on which the Hamiltonian density in the SOF is non-negative.

In order to establish a correspondence between condition b) of Theorem 4 and (5.65), we write the following space spinors definition

$$D_A{}^B\mathcal{K} = -\sqrt{2}n_{\hat{\alpha}}\sigma_{AA}^{\hat{\alpha}}\sigma^{\hat{\beta}B\hat{A}}\partial_{\hat{\beta}}\mathcal{K} = -\sqrt{2}\sigma_{AA}^{\hat{0}}\sigma^{\hat{\beta}B\hat{A}}\partial_{\hat{\beta}}\mathcal{K}, \quad (5.66)$$

and obtain that the diagonal elements of matrix

$$\frac{\sqrt{2}}{4}D_A{}^B\mathcal{K} + \frac{1}{2}\varepsilon_A{}^B\mathcal{K}^2$$

are

$$\frac{1}{4}\partial_{\hat{3}}\mathcal{K} + \frac{1}{2}\mathcal{K}^2 \quad \text{and} \quad -\frac{1}{4}\partial_{\hat{3}}\mathcal{K} + \frac{1}{2}\mathcal{K}^2.$$

Therefore, the second of them is non-negative on the hypersurfaces which satisfy condition (5.65). This means that under fulfilling condition (5.65) condition b) of Theorem 3 is also fulfilled.

So, if the SWE and conditions a) and c) of Theorem 3 are fulfilled, then on hypersurfaces, which satisfy condition (5.65) and lie in some neighborhood of the maximal one, the Hamiltonian density  $\mathcal{H}(\varphi, \chi)$  (5.4.1) and the ADM Hamiltonian density  $\mathcal{H}^{SWOF}(N)$  (5.59) are locally non-negative simultaneously.

Let us note that just an absence of the result on connection between the SWE equation and the Nester gauge (a theorem like Theorem 3 and Theorem 4) did not permit Nester and Tung to obtain a direct relationship between the 4-spinor 3-form of the Hamiltonian density under fulfilling the SWE and the Hamiltonian density in the SOF formalism, both on the enough general hypersurfaces and even on the maximal ones. The 3-spinor formalism, developed by these authors and Zhytnikov, provides the partial solving of this problem;

in particular, the energy is guaranteed to be locally non-negative only on the maximal hypersurfaces.

Generalization of the SOF by the SWOF allows us to remove two liabilities of the SOF method: necessity of the restriction to the maximal hypersurfaces, and impossibility of extension to the future null infinity and, hence, description of the Bondi 4-momentum. Therefore, for the quasilocal Hamiltonian density (5.38) investigation not the Dirac equation and the 3-spinors are suitable, but the SWE and the space spinors introduced by Sommers [661]. Although the 3-dimensional Dirac equation and the SWE are very similar, we see that fixing of the spinor field by the Dirac equation or by the SWE leads to different physical consequences. The mathematical consequences for application of these gauge conditions for the spinor field are also different; in particular, the conditions for existence of solutions differ in domains of finite measure [658].

The equivalence of the Sen–Witten spinor field and the SWOF, under the reasonable from the physical point of view fulfilling of conditions of Theorem 3, permits to establish that the method of the 4-covariant quadratic spinor Hamiltonian and the SOF method are very close. The spinor parameterization of the Hamiltonian displacement and correlations (5.34) are the key for the orthonormal frame interpretation of the Hamiltonian 4-covariant spinor form (5.38) and the spinor interpretation of the ADM Hamiltonian density even in the case when the spinor field or the orthonormal frame are not fixed.

Note at the end that conditions of (5.64) and (5.65) type are the only sufficient ones, and we expect to weaken them significantly or to exclude completely.

#### 5.4.2. In which cases the conditions of Theorem 4 are fulfilled?

Theorem 4 implies that the absence of nodal submanifolds can be ensured in accordance with condition 2) at least for some hypersurfaces  $\Sigma_t$  in Petrov type  $N$  space-time with tensor of extrinsic curvature  $\mathcal{K}_{\pi\rho}$  and for some physical fields with density of energy in comoving frame  $\mu$ . Further we will work out in detail these constituents of condition 2).

Apparently, nodal sets are absent on SCMC hypersurfaces in empty space and hence by continuity — in a neighborhood. However, significantly more strong result takes place.

**Theorem 6.** *Let:*

a) everywhere in the bounded domain on the space-like hypersurface on  $\Sigma_t$  in Petrov type  $N$  space-time the dominant energy conditions be fulfilled;

b) the functions  $\operatorname{Re} \lambda^0$  or  $\operatorname{Im} \lambda^0$ , which correspond to non-negative eigenvalue  $C_0$ , nowhere on domain boundary equal zero.

Then the non-trivial solution  $\lambda^C$  to SWE does not have the nodal points in domain  $\Omega$ .



This theorem is a corollary of the following lemma:

**Lemma.** *If in a point of the domain  $\Omega$  the dominant energy condition is fulfilled, then in this point the matrix of spinorial tensor*

$$C_A{}^B := \frac{\sqrt{2}}{2} D_A{}^B \mathcal{K} + \frac{1}{4} \varepsilon_A{}^B \left( 2\mathcal{K}^2 + \frac{1}{2} \mathcal{K}_{\pi\rho} \mathcal{K}^{\pi\rho} + \mu \right) \quad (5.67)$$

has at least one non-negative eigenvalue.

*Proof.* Applying strengthening of Descartes theorem we see that this is possible in two cases:

1.  $\frac{1}{2} \mathcal{K}^2 + \frac{1}{8} \mathcal{K}_{\pi\rho} \mathcal{K}^{\pi\rho} + \mu \geq 0.$
  2.  $\frac{1}{2} \mathcal{K}^2 + \frac{1}{8} \mathcal{K}_{\pi\rho} \mathcal{K}^{\pi\rho} + \mu < 0,$
- $$\frac{1}{2} \left( \mathcal{K}^2 + \frac{1}{8} \mathcal{K}_{\pi\rho} \mathcal{K}^{\pi\rho} + \mu \right)^2 - \frac{1}{4} [(\partial_1 \mathcal{K})^2 + (\partial_2 \mathcal{K})^2 + (\partial_3 \mathcal{K})^2] \geq 0.$$

Condition 1 is fulfilled, if the dominant energy condition is fulfilled.

Taking into account this lemma, let us substitute condition b) of Theorem 5 by the dominant energy condition, let us denote non-negative eigenvalue by  $C_0$  and refine condition c). Then we obtain Theorem 6.

Now we can strengthen significantly Theorem 6.

**Theorem 7.** *Let on  $\Sigma_t$  in Petrov type N space-time Einstein constraints and the dominant energy condition be fulfilled. Then everywhere on  $\Sigma_t$  there exists a two-to-one correspondence between Sen–Witten spinor and Sen–Witten orthonormal frame.*

Since for all physical fields, whose existence hitherto is confirmed experimentally, the dominant energy condition is fulfilled, then Theorem 7 permits to state that Sen–Witten spinor and Sen–Witten orthonormal frame are equivalent in majority of physical models. Nevertheless, in recent years the physical situations in which the dominant energy condition will be violated (primarily of dark energy, but also in wormhole space-time, in sudden future singularity or in gravastar) appear. That is why we note that Theorem 7 does not exhaust all cases, when Sen–Witten spinor and Sen–Witten orthonormal frame are equivalent. In particular, from condition 1) it follows, that even if the dominant energy condition is violated ( $\mu < 0$ ), Sen–Witten spinor and Sen–Witten orthonormal frame are equivalent on hypersurfaces, which satisfy condition

$$\frac{1}{2} \mathcal{K}^2 + \frac{1}{8} \mathcal{K}_{\pi\rho} \mathcal{K}^{\pi\rho} \geq -\mu$$

or simultaneously two conditions

$$\frac{1}{2} \mathcal{K}^2 + \frac{1}{8} \mathcal{K}_{\pi\rho} \mathcal{K}^{\pi\rho} \leq -\mu,$$

$$\frac{1}{2} \left( \mathcal{K}^2 + \frac{1}{8} \mathcal{K}_{\pi\rho} \mathcal{K}^{\pi\rho} + \mu \right)^2 - \frac{1}{4} [(\partial_1 \mathcal{K})^2 + (\partial_2 \mathcal{K})^2 + (\partial_3 \mathcal{K})^2] \geq 0.$$

The result of our investigations shows that mystery, above mentioned by Nester and Bartnik, is eliminated for all spaces with typical geometrical properties and fields with typical physical properties.

### 5.5. Summary

Spinor methods in general relativity became not only a tool for description of interaction between gravity field and particles with half-integer spin, but one of main methods for description of algebraic properties of curvature tensor and gravitational and electromagnetic radiation in the curved space-time. This confirmed their efficiency for proving the positive gravity energy theorem that became not only proof for correspondence of properties for gravity and other physical fields, but opened a way for establishing of conditions of stability or spontaneous compactification of Minkowski space in multidimensional theories of Kaluza—Klein type. Discovery of Witten spinor method for positive energy theorem (PET) proof increased significantly an interest to study all aspects of spinor fields behavior in Riemannian spaces.

Schoen and Yau proof of Einstein hypothesis about positive energy of asymptotically flat space solved one of longstanding problems in General Relativity, nevertheless its complexity stimulated an appearance of alternative methods of proving, and first of all the most prospective one from the physical point of view — Wittenian spinor method (with significant contribution of Reula, Ashtekar, Horowitz, Nester). Despite the fact that Wittenian proof after its refinement obtained a perfect mathematical form, the physical interpretation of proof is treated up to date ambiguously because of decisive part of auxiliary spinor field in proof. According to common view (Goldberg, Nester, Bartnik) this spinor field remains physically mysterious. Establishing of correspondence between Witten spinor method and tensor methods became a subject of many investigations. Taking into account that local orthorepers may not exist on subsets of asymptotically flat manifolds, Dimakis and Müller-Hoissen made final conclusion about impossibility of tensor method of proving PET.

In Chapter 5 we ground the Nester tensor method for proving PET, taking into account its criticism by Dimakis and Müller-Hoissen, and generalize it for systems with radiation. Such grounding establishes the connection between Witten spinor method and Nester tensor method.

The main ideas of realized approach are the following. Firstly, we take into account that existence of nodal points of Sen—Witten equation is not a barrier for existence of correspondence between the local orthoreper field and Witten spinor field, because for Sommers transformation we can use such SWE solutions that do not have the nodal points. Secondly, we show that the reason for existence of the nodal points comes from the properties of SWE and boundary values first of all, but not topological properties of space. On this basis we

develop the theory of nodal manifolds for physically meaningful elliptic systems of equations, the most wide class among which consists of double-covariant systems, and establish conditions for coefficients and boundary values, for which the nodal points are absent. Absence of nodal sets of dimension  $n - 1$  for generalized Dirac (and SWE) equation is the known fact, but for the case of nodal sets of lower dimensions the consideration of the system of first order equations gives the possibility to obtain the only conclusion that the nodal set of solutions of generalized Dirac equation on an  $n$ -dimensional manifold has the dimension at most  $n - 2$  and does not ascertain when the nodal sets of such or lower dimension are absent. That is why we consider the differential consequence of SWE in form of the second-order equation and formulate the conditions, under which zeros of solution are absent independently on dimension of nodal sets. It is clear that for nodal sets of dimension 2 these conditions are not necessary, but they are not too rigid from the physical point of view.

After ensuring the absence of zeros of SWE we obtain the possibility to use the Sommers transformation and prove the existence of correspondence between Witten spinor field and some orthonormal frame, which on maximal hypersurface coincides with Nester special orthonormal frame.

Nester method did not cover the systems with radiation. Generalization of tensor method on radiating systems, i.e. nonmaximal hypersurfaces, is presented in Chapter 5, where we prove the existence of tensor interpretation of Wittenian spinor field also on nonmaximal hypersurfaces.

Equivalence principle excludes the possibility of existence of the gravitational energy density, but one can describe the distribution of energy as integrals over finite regions, as it was proposed by Penrose and known as quasilocalization. As it was mentioned above, in theory of quasilocal values there appears a problem of comparison of different Hamiltonian three-forms, in particular, Hamiltonian density with spinor variables and Arnowitt–Deser–Misner density, parametrized by special Nester orthonormal frame. We establish existence and correspondence between these forms.

One of necessary conditions for possibility of existence of tensor interpretation of Wittenian spinor field and for existence of correspondence between Hamiltonian density with spinor variables and Arnowitt–Deser–Misner density in SOF is fulfilling of dominant energy condition. Existence of dark energy, which violates the dominant energy condition, puts the question about possible change of status for Wittenian spinor field in its presence. We show that at violation of DEC the correspondence between Witten spinor field and SOF continues to exist, i.e. Witten spinor field keeps its geometrical (gauge) nature.

---

■

---

## APPENDIXS

---

### APPENDIX A

#### FRIEDMANN EQUATIONS FOR THE MULTICOMPONENT SCALAR-FIELD MODEL

We consider  $n$  scalar fields minimally coupled to gravity in four dimensions. The effective action of this model reads as (see, e.g., (3.15))

$$S = \frac{1}{16\pi G_N} \int d^4x \sqrt{|\tilde{g}^{(0)}|} \left( R[\tilde{g}^{(0)}] - G_{ij} \tilde{g}^{(0)\mu\nu} \partial_\mu \varphi^i \partial_\nu \varphi^j - 2U(\varphi^1, \varphi^2, \dots) \right), \quad (\text{A.1})$$

where the kinetic term is usually taken in the canonical form  $G_{ij} = \text{diag}(1, 1, \dots)$  (flat  $\sigma$  model). We use the usual conventions  $c = \hbar = 1$ , i.e.  $L_{\text{Pl}} = t_{\text{Pl}} = 1/M_{\text{Pl}(4)}$  and  $8\pi G_N = 8\pi/M_{\text{Pl}(4)}^2$ . Here, scalar fields are dimensionless and potential  $U$  has dimension  $[U] = \text{length}^{-2}$ .

Because we want to investigate the dynamical behavior of our Universe in the presence of scalar fields, we suppose that scalar fields are homogeneous:  $\varphi^i = \varphi^i(t)$  and four-dimensional metric is spatially flat Friedmann–Robertson–Walker one:  $\tilde{g}^{(0)} = -dt \otimes dt + a^2(t) d\vec{x} \otimes d\vec{x}$ .

For the energy density and pressure we easily get (see also Eqs. (2.5) and (2.6)):

$$\begin{aligned} \rho &= \frac{1}{8\pi G_N} \left( \frac{1}{2} G_{ij} \dot{\varphi}^i \dot{\varphi}^j + U \right), \\ P &= \frac{1}{8\pi G_N} \left( \frac{1}{2} G_{ij} \dot{\varphi}^i \dot{\varphi}^j - U \right) \end{aligned} \quad \Longrightarrow \quad (\text{A.2})$$

$$\begin{aligned} \implies \frac{1}{2}G_{ij}\dot{\varphi}^i\dot{\varphi}^j &= 4\pi G_N(\rho + P), \\ U &= 4\pi G_N(\rho - P), \end{aligned} \quad (\text{A.3})$$

where overdots denote the derivatives with respect to the synchronous time  $t$ . In chapter 1, overdots denote the derivatives with respect to the conformal time  $\eta$ .

The Friedmann equations for considered model are

$$3\left(\frac{\dot{a}}{a}\right)^2 \equiv 3H^2 = 8\pi G_N\rho = \frac{1}{2}G_{ij}\dot{\varphi}^i\dot{\varphi}^j + U, \quad (\text{A.4})$$

and

$$\dot{H} = -4\pi G_N(\rho + P) = -\frac{1}{2}G_{ij}\dot{\varphi}^i\dot{\varphi}^j. \quad (\text{A.5})$$

From these two equations, we obtain the following expression for the acceleration parameter:

$$\begin{aligned} q_a \equiv \frac{\ddot{a}}{H^2 a} &= 1 - \frac{4\pi G_N}{H^2}(\rho + P) = -\frac{8\pi G_N}{6H^2}(\rho + 3P) = \\ &= \frac{1}{6H^2} \left( -4 \times \frac{1}{2}G_{ij}\dot{\varphi}^i\dot{\varphi}^j + 2U \right). \end{aligned} \quad (\text{A.6})$$

It can be easily seen that the equation of state (EoS) parameter  $\omega = P/\rho$  and parameter  $q_a$  are linearly connected:

$$q_a = -\frac{1}{2}(1 + 3\omega). \quad (\text{A.7})$$

From the definition of the acceleration parameter, it follows that  $q_a$  is constant in the case of the power-law and De Sitter-like behavior:

$$q_a = \begin{cases} (s-1)/s; & a \propto t^s, \\ 1; & a \propto e^{Ht}. \end{cases} \quad (\text{A.8})$$

For example,  $q_a = -0.5$  during the matter dominated (MD) stage where  $s = 2/3$ .

Because the minisuperspace metric  $G_{ij}$  is flat, the scalar field equations are:

$$\ddot{\varphi}^i + 3H\dot{\varphi}^i + G^{ij}\frac{\partial U}{\partial \varphi^j} = 0. \quad (\text{A.9})$$

For the action (A.1), the corresponding Hamiltonian is

$$\mathcal{H} = \frac{8\pi G_N}{2a^3}G^{ij}P_iP_j + \frac{a^3}{8\pi G_N}U, \quad (\text{A.10})$$

where

$$P_i = \frac{a^3}{8\pi G_N} G_{ij} \dot{\varphi}^j \quad (\text{A.11})$$

are the canonical momenta and equations of motion have also the canonical form

$$\dot{\varphi}^i = \frac{\partial \mathcal{H}}{\partial P_i}, \quad \dot{P}_i = -\frac{\partial \mathcal{H}}{\partial \varphi^i}. \quad (\text{A.12})$$

It can be easily seen that the latter equation (for  $\dot{P}_i$ ) is equivalent to the Eq. (A.9).

Thus, the Friedmann equations together with the scalar field equations can be replaced by the system of the first order ODEs:

$$\dot{\varphi}^i = \frac{8\pi G_N}{a^3} G^{ij} P_j, \quad (\text{A.13})$$

$$\dot{P}_i = -\frac{a^3}{8\pi G_N} \frac{\partial U}{\partial \varphi^i}, \quad (\text{A.14})$$

$$\dot{a} = aH, \quad (\text{A.15})$$

$$\dot{H} = \frac{\ddot{a}}{a} - H^2 = \frac{1}{6} \left( -4 \times \frac{1}{2} G_{ij} \dot{\varphi}^i \dot{\varphi}^j + 2U \right) - H^2 \quad (\text{A.16})$$

with Eq. (A.4) considered in the form of the initial conditions:

$$H(t=0) = \sqrt{\frac{1}{3} \left( \frac{1}{2} G_{ij} \dot{\varphi}^i \dot{\varphi}^j + U \right)} \Big|_{t=0}. \quad (\text{A.17})$$

We can make these equations dimensionless:

$$\frac{d\varphi^i}{M_{\text{Pl}(4)} dt} = \frac{8\pi}{M_{\text{Pl}(4)} q b a^3} G^{ij} P_j \Rightarrow \frac{d\varphi^i}{dt} = \frac{8\pi}{a^3} G^{ij} P_j, \quad (\text{A.18})$$

$$\frac{dP_i}{M_{\text{Pl}(4)} dt} = -\frac{a^3 M_{\text{Pl}(4)} q b}{8\pi} \frac{\partial(U/M_{\text{Pl}(4)} s q)}{\partial \varphi^i} \Rightarrow \frac{dP_i}{dt} = -\frac{a^3}{8\pi} \frac{\partial U}{\partial \varphi^i}. \quad (\text{A.19})$$

That is to say the time  $t$  is measured in the Planck times  $t_{\text{Pl}}$ , the scale factor  $a$  is measured in the Planck lengths  $L_{\text{Pl}}$  and the potential  $U$  is measured in the  $M_{\text{Pl}(4)}^2$  units.

This system of dimensionless first order ODEs together with the initial condition (A.17) can be used for numerical calculation of the dynamics of considered models with the help of a Mathematica package applied to these equations in [482].

## MATHEMATICAL DETAILS OF THE BRANEWORLD MODEL

### B.1. Variational problem in the presence of the brane

Here, we derive the expression for the first variation of the action for gravity

$$S_g = \int_{\mathcal{B}} \mathcal{R} - 2 \int_{\Sigma} K, \quad (\text{B.1})$$

the notation of which is the same as in (4.7). Equations of this appendix are valid for arbitrary dimension of space-time. In this derivation, we do not assume that the variation of  $g_{ab}$  vanishes at the boundary  $\Sigma$ , which is taken to be time-like.

We start from the standard expression (see, e.g., Appendix E of [508])

$$\delta \left( \int_{\mathcal{B}} \mathcal{R} \right) = \int_{\mathcal{B}} \mathcal{G}_{ab} \delta g^{ab} + \int_{\mathcal{B}} \nabla^a v_a, \quad (\text{B.2})$$

where

$$v_a = \nabla^b (\delta g_{ab}) - g^{cd} \nabla_a (\delta g_{cd}). \quad (\text{B.3})$$

The second integral in (B.2) can be transformed with the use of the Stokes theorem as

$$\int_{\mathcal{B}} \nabla^a v_a = - \int_{\Sigma} v_a n^a, \quad (\text{B.4})$$

where we remember that we are using the *inner* unit normal  $n^a$  to  $\Sigma$ , and

$$\begin{aligned} v_a n^a &= n^a g^{bc} [\nabla_c (\delta g_{ab}) - \nabla_a (\delta g_{bc})] = \\ &= n^a h^{bc} [\nabla_c (\delta g_{ab}) - \nabla_a (\delta g_{bc})]. \end{aligned} \quad (\text{B.5})$$

Then we have

$$\delta K = \delta \left( h^a_b \nabla_a n^b \right) = \delta h^a_b \nabla_a n^b + h^a_b (\delta C)^b_{ac} n^c + h^a_b \nabla_a \delta n^b, \quad (\text{B.6})$$

where

$$(\delta C)^b{}_{ac} = \frac{1}{2} g^{bd} [\nabla_a (\delta g_{cd}) + \nabla_c (\delta g_{ad}) - \nabla_d (\delta g_{ac})]. \quad (\text{B.7})$$

The first term on the right-hand side of (B.6) is identically zero. Indeed, we have  $\delta n_a = -n_a n_b \delta n^b$ , so that

$$\begin{aligned} \delta h^a{}_b \nabla_a n^b &= -(\delta n^a n_b + n^a \delta n_b) \nabla_a n^b = -(\delta n^a - n^a n_c \delta n^c) n_b \nabla_a n^b = \\ &= -\delta n^c h^a{}_c n_b \nabla_a n^b = -\delta n^c n_b K_c{}^b = 0. \end{aligned} \quad (\text{B.8})$$

Thus, variation of the second term of (B.1) is

$$\delta \left( 2 \int_{\Sigma} K \right) = \int_{\Sigma} \left[ n^c h^{ab} \nabla_c (\delta g_{ab}) + 2h^a{}_b \nabla_a \delta n^b - K h_{ab} \delta h^{ab} \right], \quad (\text{B.9})$$

where the last term in the square brackets stems from the variation of the volume element  $\sqrt{-h} d^4x$  in the integral over  $\Sigma$ .

The total boundary term in the variation of action (B.1) is given by the sum of (B.4) and (B.9) with the result

$$(\text{Boundary term}) = - \int_{\Sigma} \left[ n^a h^{bc} \nabla_c (\delta g_{ab}) + 2h^a{}_b \nabla_a \delta n^b - K h_{ab} \delta h^{ab} \right]. \quad (\text{B.10})$$

We transform the first term in the integrand of the last expression:

$$\begin{aligned} n^a h^{bc} \nabla_c (\delta g_{ab}) &= h^{bc} \nabla_c (n^a \delta g_{ab}) - h^{bc} \nabla_c n^a \delta g_{ab} = \\ &= h^{bc} \nabla_c (n^a \delta g_{ab}) + K_{ab} \delta h^{ab}. \end{aligned} \quad (\text{B.11})$$

Then

$$\begin{aligned} (\text{Boundary term}) &= - \int_{\Sigma} \left[ h^{bc} \nabla_c (n^a \delta g_{ab}) + 2h^a{}_b \nabla_a \delta n^b \right] - \\ &\quad - \int_{\Sigma} (K_{ab} - K h_{ab}) \delta h^{ab}. \end{aligned} \quad (\text{B.12})$$

Now we show that the integrand of the first integral in (B.12) is a divergence, so that this integral vanishes for variations of  $g_{ab}$  with compact support in  $\Sigma$ . Indeed,

$$\begin{aligned} h^{bc} \nabla_c (n^a \delta g_{ab}) + 2h^a{}_b \nabla_a \delta n^b &= h^{bc} \nabla_c (\delta n_b - g_{ab} \delta n^a) + 2h^a{}_b \nabla_a \delta n^b = \\ &= h^a{}_b \nabla_a (g^{bc} \delta n_c + \delta n^b) = h^a{}_b \nabla_a (h^b{}_c \delta n^c) = D_b (h^b{}_c \delta n^c), \end{aligned} \quad (\text{B.13})$$



where  $D_a$  is the (unique) derivative on  $\Sigma$  associated with the induced metric  $h_{ab}$ , and the last equality in (B.13) is valid by virtue of Lemma 10.2.1 of [508].

As a final result, we obtain

$$\delta S_g = \int_{\mathcal{B}} G_{ab} \delta g^{ab} - \int_{\Sigma} (K_{ab} - K h_{ab}) \delta h^{ab}. \quad (\text{B.14})$$

### B.2. Graphical representation of the brane evolution

The variables  $\{X, Y\}$ :

$$X \equiv \frac{\rho_{\text{tot}}}{3m^2} - H^2, \quad Y \equiv H^2, \quad \rho_{\text{tot}} = \rho + \sigma, \quad (\text{B.15})$$

allow us to rewrite equation (4.177) in the form

$$X = - \sum_{i=1,2} \frac{\zeta_i}{\ell_i} \sqrt{Y + \lambda_i^{-2}}, \quad (\text{B.16})$$

which has a convenient visual interpretation. Equation (B.16) describes four branches in the physically restricted range  $Y \geq 0$ , with the symmetry of reflection with respect to the  $Y$  axis. If there exists a positive root  $Y_c$  of the right-hand side of (B.16) for  $\zeta_1 \zeta_2 = -1$ , then the two mixed branches intersect each other at the point

$$Y_c = H_c^2 = \frac{\ell_1^2 \lambda_2^{-2} - \ell_2^2 \lambda_1^{-2}}{\ell_2^2 - \ell_1^2}. \quad (\text{B.17})$$

The condition for the existence of this intersection point is that the constant on the right-hand side of (B.17) be positive.

The four branches (with and without intersection) are shown in Figs. B.1 and B.2, respectively.

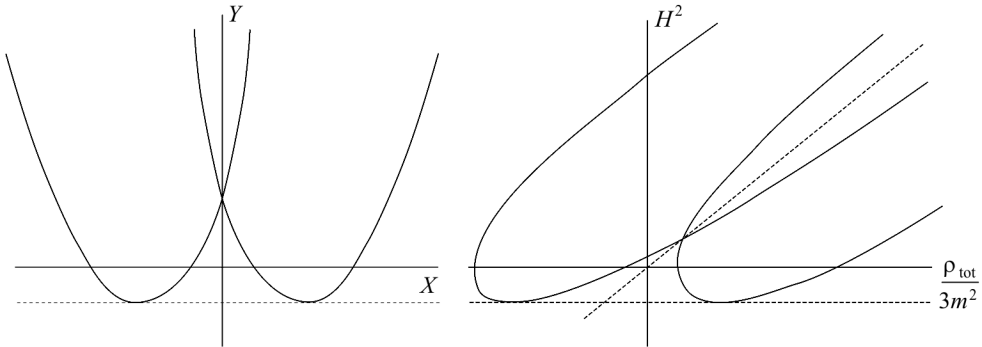


**Fig. B.1.** Four branches described by Eq. (B.16) in the  $(X, Y)$  plane and in the  $(\rho_{\text{tot}}, H^2)$  plane in the case where two of them intersect. The horizontal dotted line indicates the position of the  $H^2 = 0$  axis in the case  $\Lambda_1 \Lambda_2 = 0$ . The region below this axis is nonphysical

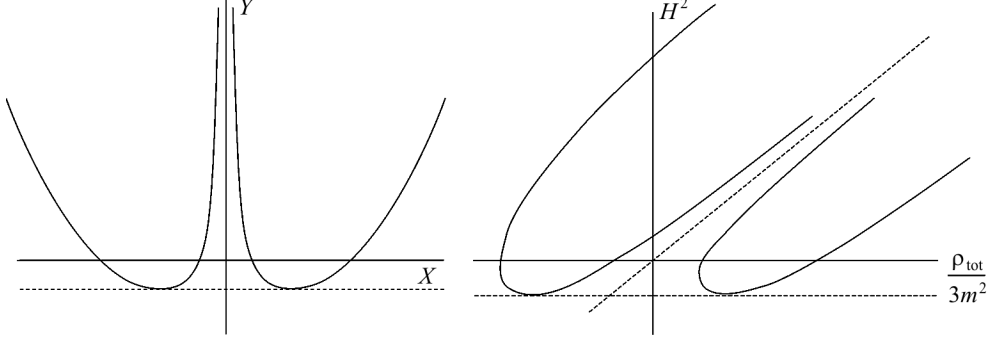


**Fig. B.2.** Four branches described by Eq. (B.16) in the  $(X, Y)$  plane and in the  $(\rho_{\text{tot}}, H^2)$  plane in the case of absence of intersection. The horizontal dotted line indicates the position of the  $H^2 = 0$  axis in the case  $\Lambda_1 \Lambda_2 = 0$ . The region below this axis is nonphysical

The brane evolves along one of the four branches towards decreasing values of  $\rho_{\text{tot}}$  (during expansion). Depending (in particular) on the value of the brane tension  $\sigma$ , three distinct possibilities can arise:

(i) The trajectory may reach the value of  $H = 0$ , after which the universe recollapses and evolves along the same branch in the opposite direction. This happens when the value of  $\rho_{\text{tot}}$  at this point is greater than its minimum value  $\sigma$ .

(ii) The trajectory may asymptotically tend to either De Sitter space or the Minkowski universe with the minimum value  $\rho_{\text{tot}} = \sigma$ . The second possibility occurs when the minimum value of  $\rho_{\text{tot}} = \sigma$  is exactly the point where the corresponding graph crosses the axis  $H^2 = 0$ , which, therefore, requires some amount of fine tuning. This possibility can be realized as *transient acceleration*.

(iii) The trajectory may end in a quiescent singularity at a finite value of  $H$ . This happens when the *critical minimum point* of  $\rho_{\text{tot}}$  on the evolution curve is reached, and if this value of  $\rho_{\text{tot}}$  is greater than its minimum value  $\sigma$ . The reasons for the existence of quiescent singularities can be seen from the right panels in Figs. B.1 and B.2. They occur at the points of infinite derivative  $dH^2/d\rho_{\text{tot}}$ .

### B.3. Background cosmological solution in the bulk

For the background bulk metric (4.12) the following relations are satisfied:

$$\begin{aligned} \mathcal{R}_{abcd} &= R_{abcd}, \\ \mathcal{R}_{aibj} &= -\gamma_{ij} r \nabla_a \nabla_b r, \\ \mathcal{R}_{ijkl} &= r^2 [\kappa - (\nabla_a r)^2] (\gamma_{ik} \gamma_{jl} - \gamma_{il} \gamma_{jk}), \end{aligned} \tag{B.18}$$

where the curvature tensor  $R_{abcd}$  and covariant derivative  $\nabla_a$  correspond to the two-dimensional metric tensor  $\gamma_{ab}$ , defined by

$$ds_{(2)}^2 = \gamma_{ab} dx^a dx^b = -f(r) d\tau^2 + \frac{dr^2}{f(r)}. \quad (\text{B.19})$$

For the case under consideration in this book,  $f(r) = \kappa - \Lambda_b r^2/6$ , the following expressions can be verified:

$$\begin{aligned} R_{abcd} &= \frac{\Lambda_b}{6} (\gamma_{ac}\gamma_{bd} - \gamma_{ad}\gamma_{bc}), \\ \nabla_a \nabla_b r &= -\frac{\Lambda_b r}{6} \gamma_{ab}, \quad (\nabla_a r)^2 = \kappa - \frac{\Lambda_b}{6} r^2. \end{aligned} \quad (\text{B.20})$$

#### B.4. Scalar perturbation of the bulk metric

In the gauge  $h_L = 0$  and  $h_a = 0$ , the general expression for the perturbed bulk metric (4.263), (4.264) can be written in the form

$$ds_{bulk}^2 = \left[ \gamma_{ab} + \sum_k h_{ab} Y \right] dx^a dx^b + \left[ r^2 + \sum_k h_Y Y \right] \gamma_{ij} dx^i dx^j, \quad (\text{B.21})$$

where  $r$ ,  $h_{ab}$  and  $h_Y$  depend on  $x^a$ , while  $Y$  depends on  $x^i$ .

The perturbation of the five-dimensional Riemann curvature tensor  $\mathcal{R}_{ABCD}$  for the metric perturbation (B.21) is found to be

$$\begin{aligned} \delta \mathcal{R}_{abcd} &= \sum_k (h^e{}_{[b} R_{a]ecd} + \nabla_c \nabla_{[b} h_{a]d} - \nabla_d \nabla_{[b} h_{a]c}) Y, \\ \delta \mathcal{R}_{iabc} &= \sum_k \left( \nabla_{[c} h_{b]a} - \frac{1}{r} h_{a[b} \nabla_{c]} r \right) \nabla_i Y, \\ \delta \mathcal{R}_{abij} &= 0, \\ \delta \mathcal{R}_{aibj} &= -\frac{1}{2} \sum_k h_{ab} \nabla_i \nabla_j Y + \\ &+ \frac{1}{2} \gamma_{ij} \sum_k \left[ r (\nabla_e r) (\nabla_a h^e{}_b + \nabla_b h^e{}_a - \nabla^e h_{ab}) - \right. \\ &\quad \left. - \frac{\nabla_a \nabla_b r}{r} h_Y - r \nabla_a \nabla_b \left( \frac{h_Y}{r} \right) \right] Y, \\ \delta \mathcal{R}_{aijk} &= \sum_k \left[ r^2 \nabla_a \left( \frac{h_Y}{r^2} \right) - r (\nabla^b r) h_{ab} \right] \gamma_{i[j} \nabla_{k]} Y, \\ \delta \mathcal{R}_{ijkl} &= \sum_k h_Y (\gamma_{i[l} \nabla_{k]} \nabla_j Y - \gamma_{j[l} \nabla_{k]} \nabla_i Y) + \\ &+ 2 \gamma_{i[k} \gamma_{l]j} \sum_k \left[ r^2 (\nabla_a r) (\nabla_b r) h^{ab} + \kappa h_Y - r (\nabla_a r) (\nabla^a h_Y) \right] Y, \end{aligned} \quad (\text{B.22})$$

where  $R_{abcd}$  is the background curvature tensor, defined in (B.20).

---

■

---

## BIBLIOGRAPHY

---

1. Perlmutter S., Aldering G., della Valle M. et al., Discovery of a supernova explosion at half the age of the universe, *Nature*, **391**, 51 (1998).
2. Perlmutter S., Aldering G., Goldhaber G. et al., Measurements of Omega and Lambda from 42 High-Redshift Supernovae, *Astrophys. J.* **517**, 565 (1999).
3. Riess A.G., Filippenko A.V., Challis P. et al., Observational Evidence from Supernovae for an Accelerating Universe and a Cosmological Constant, *Astron. J.* **116**, 1009 (1998).
4. Schmidt B.P., Suntzeff N.B., Phillips M.M. et al., The High-Z Supernova Search: Measuring Cosmic Deceleration and Global Curvature of the Universe Using Type IA Supernovae, *Astrophys. J.* **507**, 46 (1998).
5. Huterer D. & Turner M.S., Prospects for probing the dark energy via supernova distance measurements, *Phys. Rev. D* **60**, 081301 (1999); astro-ph/9808133.
6. Turner M. Cosmology Solved?, Proceedings of the 49th Yamada Conference: Black Holes and Relativistic Astrophysics (Kyoto, Japan; April 1998), ed. N. Sugiyama (Universal Academy Press, Tokyo, Japan); astro-ph/9811454; Dark Matter and Dark Energy in the Universe, The Third Stromlo Symposium: The Galactic Halo, ASP Conference Series, Vol. 666, 1999, Eds. B.K. Gibson, T.S. Axelrod and M.E. Putman; astro-ph/9811454.
7. ESO Press Release: Distant Supernovae Indicate Ever-Expanding Universe, 12 Dec, 1998.
8. Turner M.S., White M., CDM models with a smooth component, *Phys. Rev. D* **56**, 4439 (1997).
9. Steinhardt P.J., *Critical Dialogues in Cosmology*, edited by N. Turok, World Scientific, Singapore, 1997.
10. Dekel A., Rees M.J., Omega from velocities in voids, *Astrophys. J. Lett.* **422**, L1 (1994).
11. Mould J., Progress in Measuring the Hubble Constant, *Aust. J. Phys.*, **48**, 1093-9 (1994).
12. Jimenez R., Thejll P., Jorgensen U. et al., Ages of globular cluster: a new approach, *Mon. Not. R. Astron. Soc.* **282**, 926 (1996).
13. Bahcall N., Fan X. & Cen R., Constraining Omega with Cluster Evolution, *Astrophys. J. Lett.* **485**, L53 (1997).
14. Smoot G.F., Bennett C.L., Kogut A et al., Structure in the COBE differential microwave radiometer first-year maps, *Astrophys. J. Lett.* **396**, L1 (1992).

15. Bunn E.F., White M., The 4 year COBE normalization and large-scale structure, *Astrophys. J.* **480**, 6 (1997).
16. Peacock J.A., The evolution of galaxy clustering, *Mon. Not. R. Astron. Soc.* **284**, 885 (1997).
17. Henry J.P. & Arnaud K.A., A measurement of the mass fluctuation spectrum from the cluster X-ray temperature function, *Astrophys. J.* **372**, 410 (1991).
18. Dekel A., Dynamics of Cosmic Flows, *Ann. Rev. Astron. Astrophys.* **32**, 371 (1994).
19. Kahniashvili T., Novosyadlyj B., Valdarnini R., Primordial inhomogeneities spectra in mixed dark matter models with non-zero cosmological constant, *Helvetica Physica Acta* **69**, 219 (1996).
20. Valdarnini R., Kihniashvili T., Novosyadlyj B., Large scale structure formation in the mixed dark matter models with a cosmological constant, *Astron. Astrophys.* **336**, 11 (1998).
21. Sandage A., Observational Tests of World Models, *Ann. Rev. Astron. Astrophys.* **26**, 561 (1988).
22. de Bernardis P. et al., A flat Universe from high-resolution maps of the cosmic microwave background, *Nature*, **404**, 955 (2000).
23. Balbi A. et al., Constraints on cosmological parameters from MAXIMA-1, *Astrophys. J.*, **545**, L1 (2000).
24. Copeland E.J., Sami M. and Tsujikawa S., Dynamics of Dark Energy, *Int. J. Mod. Phys. D* **15**, 1753 (2006).
25. Turner M.S., Huterer D., Cosmic Acceleration, Dark Energy, and Fundamental Physics, *J. Phys. Soc. Jap.* **76**, 111015 (2007).
26. Special issue on dark energy, Eds. G. Ellis, H. Nicolai, R. Durrer, R. Maartens, *Gen. Relat. Gravit.*, 40 (2008).
27. Frieman J.A., Turner M.S., Huterer D., Dark Energy and the Accelerating Universe, *Ann. Rev. Astron. Astrophys.* **46**, 385 (2008).
28. Lukash V.N., Rubakov V.A., PHYSICS OF OUR DAYS: Dark energy: myths and reality, *Phys. Uspekhi* **51**, 283 (2008).
29. Caldwell R.R., Kamionkowski M., The Physics of Cosmic Acceleration, *Ann. Rev. Nucl. Part. Sc.*, **59**, 397 (2009).
30. Cai Y.-F., Saridakis E.N., Setare M.R., Xia J.-Q., Quintom cosmology: Theoretical implications and observations, *Phys. Rep.* **493**, 1 (2010).
31. Blanchard A., Evidence for the fifth element. Astrophysical status of dark energy, *Astron. Astroph. Rev.* **18**, 595 (2010).
32. Sapone D., Dark Energy in Practice, *Int. J. Mod. Phys.* **A25**, 5253 (2010).
33. Amendola L. and Tsujikawa S., *Dark Energy: theory and observations*, Cambridge University Press, 507 p. (2010).
34. *Lectures on Cosmology: Accelerated expansion of the Universe. Lect. Notes in Physics 800*, Ed. G. Wolschin, Springer, Berlin–Heidelberg, 188 p. (2010).
35. Ratra B. and Peebles P.J.E., Cosmological consequences of a rolling homogeneous scalar field, *Phys. Rev. D* **37**, 3406 (1988).
36. Wetterich C., Cosmologies with variable Newton’s “constant”, *Nucl. Phys. B* **302**, 645 (1988).
37. Caldwell R.R., Dave R., and Steinhardt P.J., Cosmological Imprint of an Energy Component with General Equation of State, *Phys. Rev. Lett.* **80**, 1582 (1998).

38. Ferreira P.G. and Joyce M., Cosmology with a primordial scaling field, *Phys. Rev. D* **58**, 023503 (1998).
39. Steinhardt P.J., Wang L. and Zlatev I., Cosmological tracking solutions, *Phys. Rev. D* **59**, 123504 (1999).
40. Zlatev I., Wang L. and Steinhardt P.J., Quintessence, Cosmic Coincidence, and the Cosmological Constant, *Phys. Rev. Lett.* **82**, 896 (1999).
41. Brax P. and Martin J., Quintessence and supergravity, *Phys. Lett. B* **468**, 40 (1999).
42. Albrecht A. and Scordis C., Phenomenology of a Realistic Accelerating Universe Using Only Planck-Scale Physics, *Phys. Rev. Lett.* **84**, 2076 (1999).
43. Barreiro T., Copeland E.J. and Nunes N.J., Quintessence arising from exponential potentials, *Phys. Rev. D* **61**, 127301 (2000).
44. Copeland E.J., Nunes N.J. and Rosati F., Quintessence models in supergravity, *Phys. Rev. D* **62**, 123503 (2000).
45. Einstein A., Die Grundlage der allgemeinen Relativitätstheorie, *Ann. Phys.* **49**, 769 (1916).
46. Einstein A., Kosmologische Betrachtungen zur allgemeinen Relativitätstheorie, *Sitz. Preuss. Akad. Wiss. Phys. Math.* 1917. P. 142.
47. Friedmann A., Curvature of the Universe, *Z. Phys.* **10**, 377 (1922).
48. Lemaître G., Un Univers homogène de masse constante et de rayon croissant rendant compte de la vitesse radiale des nébuleuses extra-galactiques, *Ann. Soc. Bruxelles A* **47**, 49 (1927).
49. Robertson H.P., On relativistic cosmology, *Phil. Mag.* **5**, 835 (1928).
50. Walker A.G., Distance in an Expanding Universe, *Mon. Not. R. Astron. Soc.* **94**, 90 (1933).
51. Caldwell R.R., A Phantom Menace? Cosmological consequences of a dark energy component with super-negative equation of state, *Phys. Lett. B* **545**, 23 (2002).
52. Visser M., Jerk, snap and the cosmological equation of state, *Clas. and Quant. Grav.* **21**, 2603 (2004).
53. Weinberg S., *Cosmology*, Oxford University Press, 612 p. (2008).
54. Chiba T., Nakamura T., The Luminosity Distance, the Equation of State, and Geometry of the Universe, *Prog. Theor. Phys.* **100**, 1077 (1998).
55. Weinberg S., *Gravitation and cosmology: Principles and applications of the general theory of relativity*, Wiley, New York, (1972).
56. Phillips M.M., The absolute magnitudes of Type IA supernovae, *Astrophys. J.* **413**, L105 (1993).
57. Kasen D. and Woosley S.E., On the Origin of the Type Ia Supernova Width-Luminosity Relation, *Astrophys. J.* **656**, 661 (2007).
58. Tripp R., A two-parameter luminosity correction for Type IA supernovae, *Astron. Astrophys.* **331**, 815 (1998).
59. Perlmutter S., Gabi S., Goldhaber G. et al., Measurements of the Cosmological Parameters Omega and Lambda from the First Seven Supernovae at  $Z \geq 0.35$ , *Astrophys. J.* **483**, 565 (1997).
60. Goldhaber G., Groom D.E., Kim A. et al., Timescale Stretch Parameterization of Type Ia Supernova B-Band Light Curves, *Astrophys. J.* **558**, 359 (2001).
61. Knop R.A., Aldering G., Amanullah R. et al., New Constraints on  $\Omega_M$ ,  $\Omega_\Lambda$ , and  $w$  from an Independent Set of 11 High-Redshift Supernovae Observed with the Hubble Space Telescope, *Astrophys. J.* **598**, 102 (2003).

62. Wang L., Goldhaber G., Aldering G., Perlmutter S., Multicolor Light Curves of Type Ia Supernovae on the Color-Magnitude Diagram: A Novel Step toward More Precise Distance and Extinction Estimates, *Astrophys. J.* **590**, 944 (2003).
63. Tonry J.L., Schmidt B.P., Barris B. et al., Cosmological Results from High- $z$  Supernovae, *Astrophys. J.* **594**, 1 (2003).
64. Hamuy M., Phillips M.M., Suntzeff N.B. et al., The Morphology of Type IA Supernovae Light Curves, *Astron. J.* **112**, 2438 (1996).
65. Prieto J.L., Rest A., Suntzeff N.B., A New Method to Calibrate the Magnitudes of Type Ia Supernovae at Maximum Light, *Astrophys. J.* **647**, 501 (2006).
66. Guy J., Astier P., Nobili S. et al., SALT: a spectral adaptive light curve template for type Ia supernovae, *Astron. Astrophys.* **443**, 781 (2005).
67. Guy J., Astier P., Baumont S. et al., SALT2: using distant supernovae to improve the use of type Ia supernovae as distance indicators *Astron. Astrophys.* **466**, 11 (2007).
68. Riess A.G., Press W.H., & Kirshner R.P., Is the Dust Obscuring Supernovae in Distant Galaxies the Same as Dust in the Milky Way? *Astrophys. J.* **473**, 88 (1996).
69. Jha S., Riess A. G., Kirshner R.P., Improved Distances to Type Ia Supernovae with Multicolor Light-Curve Shapes: MLCS2k2, *Astrophys. J.* **659**, 122 (2007).
70. Conley A., Sullivan M., Hsiao E.Y. et al., SiFTO: An Empirical Method for Fitting SN Ia Light Curves, *Astrophys. J.* **681**, 482 (2008).
71. Riess A.G., Strolger L.G., Tonry J. et al., Type Ia Supernova discoveries at  $z > 1$  from Hubble Space Telescope: Evidence for past deceleration and constraints on dark energy evolution, *Astrophys. J.* **607**, 665 (2004).
72. Riess A.G., Strolger L.G., Casertano S. et al., New Hubble Space Telescope discoveries of Type Ia Supernovae at  $z > 1$ : Narrowing constraints on the early behavior of dark energy, *Astrophys. J.* **659**, 98 (2007).
73. Astier P., Guy J., Regnault N. et al., The SuperNova Legacy Survey: Measurements of  $\Omega_m$ ,  $\Omega_\Lambda$  and  $w$  from the first year data set, *Astron. Astrophys.* **447**, 31 (2006).
74. Wood-Vasey W.M., Miknaitis G., Stubbs C.W. et al., Observational constraints on the nature of the dark energy: first cosmological results from ESSENCE Supernova Survey, *Astrophys. J.* **666**, 694 (2007).
75. Davis T.M., Mortsell E., Sollerman J. et al., Scrutinizing exotic cosmological models using ESSENCE supernova data combined with other cosmological probes, *Astrophys. J.* **666**, 716 (2007).
76. Sako M., Bassett B., Becker A. et al., The Sloan Digital Sky Survey-II Supernova Survey: Search Algorithm and Follow-Up Observations, *Astron. J.* **135**, 348 (2008).
77. Kessler R., Becker A.C., Cinabro D. et al., First-Year Sloan Digital Sky Survey-II Supernova Results: Hubble Diagram and Cosmological Parameters *Astrophys. J. Suppl.* **185**, 32 (2009).
78. Kowalski M., Rubin D., Aldering G. et al., Improved Cosmological Constraints from New, Old, and Combined Supernova Data Sets, *Astrophys. J.* **686**, 749 (2008).
79. Amanullah R., Lidman C., Rubin D. et al., Spectra and Hubble Space Telescope Light Curves of Six Type Ia Supernovae at  $0.511 < z < 1.12$  and the Union2 Compilation, *Astrophys. J.* **716**, 712 (2010).

80. Press H.W., Teukolsky S.A., Wetterling W.T., Flannery B.P. Numerical recipes in C. The art of scientific computing Second edition, New York, Cambridge University Press, 655 p. (1992).
81. Sullivan M. Type Ia Supernova and cosmology in Lectures on Cosmology: Accelerated expansion of the Universe. Lect. Notes in Physics 800, Ed. G. Woloschin, Springer, Berlin—Heidelberg, p. 59 (2010).
82. Guy J., Sullivan M., Conley A. et al., The SuperNova Legacy Survey 3 years sample: Type Ia Supernovae photometric distances and cosmological constraints, *Astron. Astrophys.*, **523** A7 (2010).
83. Conley A., Guy J., Sullivan M. et al., Supernova constraints and systematic uncertainties from the first 3 years of the SuperNova Legacy Survey, *Astrophys. J. Suppl. Ser.* **192**, id. 1 (2011).
84. Sullivan M., Guy J., Conley A. et al., SNLS3: Constraints on Dark Energy Combining the Supernova Legacy Survey Three-year Data with Other Probes, *Astrophys. J.* **737**, 102 (2011).
85. Tsutsui R., Nakamura T., Yonetoku D. et al., Constraints on  $w_0$  and  $w_a$  of dark energy from high-redshift gamma-ray bursts, *Mon. Not. R. Astron. Soc.* **394**, L 31 (2009).
86. Bennett C.L., Halpern M., Hinshaw G. et al., First-Year Wilkinson Microwave Anisotropy Probe (WMAP) Observations: Preliminary Maps and Basic Results, *Astrophys. J. Suppl. Ser.* **148**, 1 (2003).
87. Spergel D.N., Verde L., Peiris H.V. et al., First-Year Wilkinson Microwave Anisotropy Probe (WMAP) Observations: Determination of Cosmological Parameters, *Astrophys. J. Suppl. Ser.* **148**, 175 (2003).
88. Hinshaw G., Nolte M.R., Bennett C.L. et al., Three-Year Wilkinson Microwave Anisotropy Probe (WMAP) Observations: Temperature Analysis, *Astrophys. J. Suppl. Ser.* **170**, 288 (2007).
89. Spergel D.N., Bean R., Doré O. et al., Three-Year Wilkinson Microwave Anisotropy Probe (WMAP) Observations: Implications for Cosmology, *Astrophys. J. Suppl. Ser.* **170**, 377 (2007).
90. Hinshaw G., Weiland J.L., Hill R.S. et al., Five-Year Wilkinson Microwave Anisotropy Probe Observations: Data Processing, Sky Maps, and Basic Results, *Astrophys. J. Suppl. Ser.* **180**, 225 (2009).
91. Komatsu E., Dunkley J., Nolte M.R. et al., Five-Year Wilkinson Microwave Anisotropy Probe Observations: Cosmological Interpretation, *Astrophys. J. Suppl. Ser.* **180**, 330 (2009).
92. Dunkley J., Komatsu E., Nolte M.R. et al., Five-Year Wilkinson Microwave Anisotropy Probe Observations: Likelihoods and Parameters from the WMAP data, *Astrophys. J. Suppl. Ser.* **180**, 306 (2009).
93. Jarosik N., Bennett C.L., Dunkley J. et al., Seven-Year Wilkinson Microwave Anisotropy Probe (WMAP) Observations: Sky Maps, Systematic Errors, and Basic Results, *Astrophys. J. Suppl. Ser.* **192**, 14 (2011).
94. Komatsu E., Smith K.M., Dunkley J. et al., Seven-Year Wilkinson Microwave Anisotropy Probe (WMAP) Observations: Cosmological Interpretation, *Astrophys. J. Suppl. Ser.* **192**, 18 (2011).
95. Larson D., Dunkley J., Hinshaw G. et al., Seven-year Wilkinson Microwave Anisotropy Probe (WMAP) Observations: Power Spectra and WMAP-derived Parameters, *Astrophys. J. Suppl. Ser.* **192**, 16 (2011).



- 
96. Sachs R.K., Wolfe A.M., Perturbations of a Cosmological Model and Angular Variations of the Microwave Background, *Astrophys. J.* **147**, 73 (1967).
  97. Silk J., Cosmic Black-Body Radiation and Galaxy Formation, *Astrophys. J.* **151**, 459 (1968).
  98. Zel'dovich Ya.B., Kurt V.G. & Sunyaev R.A., Recombination of Hydrogen in the Hot Model of the Universe, *Zh. Eksp. Teoret. Fiz.* **55**, 278 (1968).
  99. Peebles P.J.E., Recombination of the Primeval Plasma, *Astrophys. J.* **153**, 1 (1968).
  100. Matsuda T., Sato H., & Takeda H., Dissipation of Primordial Turbulence and Thermal History of the Universe, *Prog. Theor. Phys.* **46**, 416 (1971).
  101. Zabolotin N.A., Nasel'skii P.D., The Neutrino Background in the Early Universe and Temperature Fluctuations in the Cosmic Microwave Radiation, *Sov. Astron.* **26**, 272 (1982).
  102. Liubarskii Iu.E. & Sunyaev R.A., The spectral features in the microwave background spectrum due to energy release in the early universe, *Astron. Astrophys.* **123**, 171 (1983).
  103. Jones B.J.T. & Wyse R.F.G., The ionisation of the primeval plasma at the time of recombination, *Astron. Astrophys.* **149**, 144 (1985).
  104. Krolik J.H., Further corrections to the theory of cosmological recombination, *Astrophys. J.*, **353**, 21 (1990).
  105. Rubicki G.B. & Dell'Antonio I.P., The time development of a resonance line in the expanding Universe, *Astrophys. J.* **427**, 603 (1993).
  106. Seager S., Sasselov D.D. & Scott D., How Exactly Did the Universe Become Neutral? *Astrophys. J. Suppl. Ser.* **128**, 407 (2000).
  107. Seager S., Sasselov D.D. & Scott D., A New Calculation of the Recombination Epoch, *Astrophys. J.* **523**, L1 (1999).
  108. Kholupenko E.E., Ivanchik A.V. & Varshalovich D.A., CMBR distortion concerned with recombination of the primordial hydrogen plasma, *Grav. & Cosmology (Rus.)* **11**, 161 (2005).
  109. Dubrovich V.K. & Grachev S.I., Recombination Dynamics of Primordial Hydrogen and Helium (He I) in the Universe, *Astron. Lett.* **31**, 359 (2005).
  110. Chluba J. & Sunyaev R.A., Induced two-photon decay of the 2s level and the rate of cosmological hydrogen recombination, *Astron. Astrophys.* **446**, 39 (2006).
  111. Wong W.Y., Seager S. & Scott D., Spectral distortions to the cosmic microwave background from the recombination of hydrogen and helium, *Mon. Not. R. Astron. Soc.* **367**, 1666 (2006).
  112. Novosyadlyj B., Perturbations of ionization fractions at the cosmological recombination epoch, *Mon. Not. R. Astron. Soc.* **370**, 1771 (2006).
  113. Chluba J. & Thomas R.M., Towards a complete treatment of the cosmological recombination problem, *Mon. Not. R. Astron. Soc.* **412**, 748 (2011).
  114. Ali-Haimou Y., Hirata C.M., Christopher M., HyRec: a fast and highly accurate primordial hydrogen and helium recombination code, *Phys. Rev. D* **83**, 043513 (2011).
  115. Bardeen J.M., Gauge-invariant cosmological perturbations, *Phys. Rev. D* **22**, 1882 (1980).
  116. Ma C.-P. & Bertschinger E., Cosmological perturbation theory in the synchronous and conformal newtonian gauges, *Astrophys. J.* **455**, 7 (1995).

117. Seljak U., Zaldarriaga M., A Line-of-Sight Integration Approach to Cosmic Microwave Background Anisotropies, *Astrophys. J.* **469**, 437 (1996).
118. Zaldarriaga M., Seljak U., CMBFAST for Spatially Closed Universes, *Astrophys. J. Suppl. Ser.* **129**, 431 (2000).
119. Doran M., *J. Cosm. Astrop. Phys.*, CMBEASY: an object oriented code for the cosmic microwave background, **10**, 011 (2005).
120. Lewis A., Challinor A. and Lasenby A., Efficient Computation of Cosmic Microwave Background Anisotropies in Closed Friedmann–Robertson–Walker Models, *Astrophys. J.* **538**, 473 (2000).
121. <http://camb.info>
122. Lesgourgues J., The Cosmic Linear Anisotropy Solving System (CLASS) I: Overview, arXiv:1104.2932.
123. Blas D., Lesgourgues J., Tram T., The Cosmic Linear Anisotropy Solving System (CLASS). Part II: Approximation schemes, *J. Cosmol. Astropart. Phys.*, **07**, 034 (2011).
124. <http://lesgourg.web.cern.ch/lesgourg/class.php>
125. Lewis A. and Bridle S., Cosmological parameters from CMB and other data: A Monte Carlo approach, *Phys. Rev. D* **66**, 103511 (2002).
126. <http://cosmologist.info/cosmomc>
127. Naselsky P.D., Novikov D.I., Novikov I.D. The relic radiation of the Universe (in russian), Moscow, Nauka, 2003, 390 p.; The physics of cosmic microwave background, Cambridge University Press, 2006, 252 p.
128. Durrer R., *The Cosmic Microwave Background*, Cambridge University Press, 415 p. (2008).
129. Durrer R., The theory of CMB anisotropies, *J. Phys. Stud.* **5**, 177 (2001).
130. Novosyadlyj B., The large scale structure of the Universe: theory and observations (in ukrainian), *J. Phys. Stud.* **11**, 226 (2007).
131. Novosyadlyj B., Sergijenko O., Apunevych S., Pelykh V., Properties and uncertainties of scalar field models of dark energy with barotropic equation of state, *Phys. Rev. D* **82**, 103008 (2010).
132. Hu W. & Sugiyama N., Anisotropies in the cosmic microwave background: an analytic approach, *Astrophys. J.* **444**, 489 (1995).
133. Hu W. & Sugiyama N., Small-scale cosmological perturbations: an analytic approach, *Astrophys. J.* **471**, 542 (1996).
134. Efstathiou G. & Bond J.R., Cosmic confusion: degeneracies among cosmological parameters derived from measurements of microwave background anisotropies, *Mon. Not. R. Astron. Soc.* **304**, 75 (1999).
135. Hu W., Fukugita M., Zaldarriaga M., Tegmark M., Cosmic microwave background observables and their cosmological implications, *Astrophys. J.* **549**, 669 (2001).
136. Doran M. & Lilley M., The location of cosmic microwave background peaks in a universe with dark energy, *Mon. Not. R. Astron. Soc.* **330**, 965 (2002).
137. Durrer R., Novosyadlyj B., Apunevych S., Acoustic Peaks and Dips in the Cosmic Microwave Background Power Spectrum: Observational Data and Cosmological Constraints, *Astrophys. J.* **549**, 669 (2003).
138. Sakharov A.D. The initial stage of an expanding universe and the appearance of a nonuniform distribution of matter, *Zh. Eksp. Theor. Fiz.*, **49**, 345 (1965); *Sov. Phys. JETP* **22**, 241 (1966).

139. Peebles P.J.E., Primeval adiabatic perturbations: constraints from the mass distribution, *Astrophys. J.* **248**, 885 (1981).
140. Eisenstein D.J., Hu W., Baryonic Features in the Matter Transfer Function, *Astrophys. J.* **496**, 605 (1998).
141. Eisenstein D.J. et al., Detection of the baryon acoustic peak in the large scale correlation function of SDSS luminous red galaxies, *Astrophys. J.* **633**, 560 (2005).
142. Percival W.J., Cole S., Eisenstein D.J. et al., Measuring the Baryon Acoustic Oscillation scale using the Sloan Digital Sky Survey and 2dF Galaxy Redshift Survey, *Mon. Not. R. Astron. Soc.* **381**, 1053 (2007).
143. Percival W.J., Reid B.A., Eisenstein D.J. et al., Baryon acoustic oscillations in the Sloan Digital Sky Survey Data Release 7 galaxy sample, *Mon. Not. R. Astron. Soc.* **401**, 2148 (2010).
144. Sasaki S., A new method to estimate cosmological parameter using the baryon fraction of clusters of galaxies, *Publ. Astron. Soc. Japan*, **48**, L119 (1996).
145. Pen U., The universal deceleration and angular diameter distances to clusters of galaxies, *New Astron.* **2**, 309 (1997).
146. Allen S.W., Schmidt R.W., Fabian A.C., Cosmological constraints from the X-ray gas mass fraction in relaxed lensing clusters observed with Chandra, *Mon. Not. R. Astron. Soc.* **334**, L11 (2002).
147. Allen S.W., Schmidt R.W., Fabian A.C., Ebeling H., Cosmological constraints from the local X-ray luminosity function of the most X-ray-luminous galaxy clusters, *Mon. Not. R. Astron. Soc.* **342**, 287 (2003).
148. Ettori S., Tozzi P., Rosati P., Constraining the cosmological parameters with the gas mass fraction in local and  $z > 0.7$  galaxy clusters, *Astron. Astrophys.* **398**, 879 (2003).
149. Allen S.W., Schmidt R.W., Ebeling H. et al., Constraints on dark energy from Chandra observations of the largest relaxed galaxy clusters, *Mon. Not. R. Astron. Soc.* **353**, 457 (2004).
150. LaRoque S.J., Bonamente M., Carlstrom J.E. et al., X-Ray and Sunyaev-Zel'dovich Effect Measurements of the Gas Mass Fraction in Galaxy Clusters, *Astrophys. J.* **652**, 917 (2006).
151. Allen S.W., Rapetti D.A., Schmidt R.W. et al., Improved constraints on dark energy from Chandra X-ray observations of the largest relaxed galaxy clusters, *Mon. Not. R. Astron. Soc.* **383**, 923 (2008).
152. Samushia L., Ratra B., Constraints on Dark Energy from Galaxy Cluster Gas Mass Fraction versus Redshift Data, *Astrophys. J.* **680**, L1 (2008).
153. Kirkman D., Tytler D., Suzuki N. et al., The Cosmological Baryon Density from the Deuterium-to-Hydrogen Ratio in QSO Absorption Systems: D/H toward Q1243+3047, *Astrophys. J. Suppl. Ser.* **149**, 1 (2003).
154. Freedman W.L., Madore B.F., Gibson B.K. et al., Final Results from the Hubble Space Telescope Key Project to Measure the Hubble Constant, *Astrophys. J.* **553**, 47 (2001).
155. Lifshits E.M., About gravitational stability of expanding worlds, *Zh. Eksp. Teor. Fiz.* **16**, 587, (1946).
156. Linder E.V., Cosmic growth history and expansion history, *Phys. Rev. D* **72**, 043529 (2005).

157. Bond J.R., Szalay A.S., The collisionless damping of density fluctuations in an expanding universe, *Astrophys. J.* **274**, 443 (1983).
158. Novosyadlyj B., Durrer R., Lukash V.N., An analytic approximation of MDM power spectra in four dimensional parameter space, *Astron. Astrophys.* **347**, 799 (1999).
159. Boyarsky A., Lesgourgues J., Ruchayskiy O., Viel M., Lyman- $\alpha$  constraints on warm and on warm-plus-cold dark matter models, *J. Cosmol. Astropart. Phys.* **5**, 12 (2009).
160. Retzlaff J., Borgani S., Gottlober S. et al., Constraining cosmological models with cluster power spectra, *New Astron. Rev.* **3**, 631 (1998).
161. Miller C.J., Batuski D.J., The power spectrum of rich clusters on near-gigaparsec scales, *Astrophys. J.* **551**, 635 (2001).
162. Balaguera-Antolínez A., Sánchez A.G., Böhringer H. et al., The REFLEX II galaxy cluster survey: power spectrum analysis, *Mon. Not. R. Astron. Soc.* **413**, 386 (2011).
163. Reid B.A., Percival W.J., Eisenstein D.J. et al., Cosmological constraints from the clustering of the Sloan Digital Sky Survey DR7 luminous red galaxies, *Mon. Not. R. Astron. Soc.* **404**, 60 (2010).
164. Cole S., Percival W.J., Peacock J.A. et al., The 2dF Galaxy Redshift Survey: power-spectrum analysis of the final data set and cosmological implications, *Mon. Not. R. Astron. Soc.* **362**, 505 (2005).
165. Kolatt T., Dekel A., Large-Scale Power Spectrum from Peculiar Velocities, *Astrophys. J.* **479**, 592 (1997).
166. Freudling W., Zehavi I., da Costa L.N. et al., Large-Scale Power Spectrum and Cosmological Parameters from SFI Peculiar Velocities, *Astrophys. J.* **523**, 1 (1999).
167. Croft R.A.C., Weinberg D.H., Katz N., Hernquist L., The power spectrum of mass fluctuations measured from the Ly $\alpha$  forest at  $z = 2.5$ , *Astrophys. J.* **495**, 44 (1999).
168. Bardeen J.M., Bond J.R., Kaiser N., Szalay A.S., The statistics of peaks of Gaussian random fields, *Astrophys. J.* **304**, 15 (1986).
169. Smith R.E., Peacock J.A., Jenkins A. et al., Stable clustering, the halo model and nonlinear cosmological power spectra, *Mon. Not. R. Astron. Soc.* **341**, 1311 (2003).
170. Tegmark M., Blanton M.,R., Strauss M.A. et al., The Three-Dimensional Power Spectrum of Galaxies from the Sloan Digital Sky Survey, *Astrophys. J.* **606**, 702 (2004).
171. Tytler D., Kirkman D., O'Meara J.M. et al., Cosmological Parameters  $\sigma_8$ , the Baryon Density  $\Omega_b$ , the Vacuum Energy Density  $\Omega_\Lambda$ , the Hubble Constant and the UV Background Intensity from a Calibrated Measurement of H I Ly $\alpha$  Absorption at  $z = 1.9$ , *Astrophys. J.* **617**, 1 (2004).
172. Benjamin J., Heymans C., Semboloni E. et al., *Mon. Not. R. Astron. Soc.* **371**, 702 (2007).
173. Vikhlinin A., Burenin R.A., Ebeling H. et al., Chandra Cluster Cosmology Project. II. Samples and X-Ray Data Reduction, *Astrophys. J.* **692**, 1033 (2009).
174. Reichardt C.L., Ade P.A., Bock J.J. et al., High-Resolution CMB Power Spectrum from the Complete ACBAR Data Set, *Astrophys. J.* **694**, 1200 (2009).

- 
175. Feldman H.A., Cosmic flows on 100  $h^{-1}$  Mpc scales and the non-linear  $\sigma_8$ , Proceedings of the 2009 Snowbird Particle Astrophysics and Cosmology Workshop, ASP Conference Series, **426**, 158 (2010).
  176. Nusser A., Davis M., The cosmological bulk flow: consistency with  $\Lambda$ CDM and  $z \approx 0$  constraints on  $\sigma_8$  and  $\gamma$ , *Astrophys. J.* **736**, id. 93, 9 p. (2011).
  177. Bertschinger E., Dekel A., Faber S.M. et al., Potential, velocity, and density fields from redshift-distance samples: Application — Cosmography within 6000 kilometers per second, *Astrophys. J.* **364**, 370 (1990).
  178. Courteau S., Faber S.M., Dressler A., Willick J.A., Streaming motions in the local universe — Evidence for large-scale, low-amplitude density fluctuations, *Astrophys. J. Lett.* **412**, L51 (1993).
  179. Dekel A., Eldar A., Kolatt T. et al., POTENT Reconstruction from Mark III Velocities, *Astrophys. J.* **522**, 1 (1999).
  180. Sarkar D., Feldman H.A., Watkins R., Bulk flows from velocity field surveys: a consistency check, *Mon. Not. R. Astron. Soc.* **375**, 691 (2007).
  181. Apunevych S., Novosyadlyj B., Large scale structures and integrated Sachs–Wolfe effect in non-zero  $\Lambda$  cosmologies, *J. Phys. Stud.* **4**, 470 (2000).
  182. Rees M.J., Sciama D.W., Large-scale Density Inhomogeneities in the Universe, *Nature* **217**, 511 (1968).
  183. Crittenden R.G., Turok N., Looking for a Cosmological Constant with the Rees–Sciama Effect, *Phys. Rev. Lett.* **76**, 575 (1996).
  184. Peiris H.V., Spergel D.N., Cross-Correlating the Sloan Digital Sky Survey with the Microwave Sky, *Astrophys. J.* **540**, 605 (2000).
  185. Cooray A., Integrated Sachs–Wolfe effect: Large scale structure correlation, *Phys. Rev. D* **65**, 103510 (2002).
  186. Afshordi N., Integrated Sachs–Wolfe effect in cross-correlation: The observer’s manual, *Phys. Rev. D* **69**, 083524 (2004).
  187. Fosalba P., Gaztañaga E., Castander F.J., Detection of the Integrated Sachs–Wolfe and Sunyaev–Zeldovich Effects from the Cosmic Microwave Background–Galaxy Correlation, *Astrophys. J.* **597**, L89 (2003).
  188. Fosalba P. & Gaztañaga E., Measurement of the gravitational potential evolution from the cross-correlation between WMAP and the APM Galaxy Survey, *Mon. Not. R. Astron. Soc.* **350**, L37 (2004).
  189. Boughn S. & Crittenden R., A correlation between the cosmic microwave background and large-scale structure in the Universe, *Nature* **427**, 45 (2004).
  190. Scranton R., Connolly A.J., Nichol R.C. et al., Physical Evidence for Dark Energy, arXiv:astro-ph/0307335.
  191. Padmanabhan N., Hirata C.M., Seljak U. et al., Correlating the CMB with luminous red galaxies: The integrated Sachs–Wolfe effect, *Phys. Rev. D* **72**, 043525 (2005).
  192. Cabré A., Gaztañaga E., Manera M. et al., Cross-correlation of Wilkinson Microwave Anisotropy Probe third-year data and the Sloan Digital Sky Survey DR4 galaxy survey: new evidence for dark energy, *Mon. Not. R. Astron. Soc.* **372**, L23 (2006).
  193. Giannantonio T., Crittenden R.G., Nichol R.C. et al., High redshift detection of the integrated Sachs–Wolfe effect, *Phys. Rev. D* **74**, 063520 (2006).

194. Rassat A., Land K., Lahav O., Abdalla F.B., Cross-correlation of 2MASS and WMAP 3: implications for the integrated Sachs–Wolfe effect, *Mon. Not. R. Astron. Soc.* **377**, 1085 (2007).
195. Corasaniti P.-S., Giannantonio T., Melchiorri A., Constraining dark energy with cross-correlated CMB and large scale structure data, *Phys. Rev. D* **71**, 123521 (2005).
196. Gaztañaga E., Manera M., Multamäki T., New light on dark cosmos, *Mon. Not. R. Astron. Soc.* **365**, 171 (2006).
197. Giannantonio T., Scranton R., Crittenden R.G. et al., Combined analysis of the integrated Sachs–Wolfe effect and cosmological implications, *Phys. Rev. D* **77**, 123520 (2008).
198. Pogosian L., Corasaniti P.S., Stephan-Otto C. et al., Tracking dark energy with the integrated Sachs–Wolfe effect: Short and long-term predictions, *Phys. Rev. D* **72**, 103519 (2005).
199. Bartelmann M. & Schneider P., Weak gravitational lensing, *Phys. Rep.* **340**, 291 (2001).
200. Lewis A., Challinor A., Weak gravitational lensing of the CMB, *Phys. Rep.* **429**, 1 (2006).
201. Hoekstra H., Jain B., Weak Gravitational Lensing and Its Cosmological Applications, *Ann. Rev. Nucl. Part. Syst.* **58**, 99 (2008).
202. Smith K.M., Zahn O. and Doré O., Detection of gravitational lensing in the cosmic microwave background, *Phys. Rev. D* **76**, 043510 (2007).
203. Condon J.J., Cotton W.D., Greisen E.W., Yin Q.F. et al., The NRAO VLA Sky Survey, *Astron. J.* **115**, 1693 (1998).
204. Hirata C.M., Ho S., Padmanabhan N. et al., Correlation of CMB with large-scale structure. II. Weak lensing, *Phys. Rev. D* **78**, 043520 (2008).
205. Das S., Sherwin B.D., Aguirre P. et al., Detection of the Power Spectrum of Cosmic Microwave Background Lensing by the Atacama Cosmology Telescope, *Phys. Rev. Lett.* **107**, 02130 (2011).
206. Sherwin B.D., Dunkley J., Das S. et al., Evidence for Dark Energy from the Cosmic Microwave Background Alone Using the Atacama Cosmology Telescope Lensing Measurements, *Phys. Rev. Lett.* **107**, 021302 (2011).
207. Hollenstein L., Sapone D., Crittenden R., Schafer B.M., Constraints on early dark energy from CMB lensing and weak lensing tomography, *J. Cosmol. Astropart. Phys.*, **04**, 012 (2009).
208. Chaboyer B., The age of the Universe, *Phys. Rep.* **307**, 23 (1998).
209. Chaboyer B., Demarque P., Kernan P.J., Krauss L.M., The age of globular clusters in light of hipparcos: resolving the age problem? *Astrophys. J.* **494**, 96 (1998).
210. Carretta E., Gratton R.C., Clementini G., Fusi P.F., Distances, ages, and epoch of formation of globular clusters, *Astrophys. J.* **533**, 215 (1999).
211. Krauss L.M., Chaboyer B., New globular cluster age estimates and constraints on the cosmic equation of state and matter density of the Universe, *Science* **299**, 65 (2003).
212. Renzini A., Bragaglia A., Ferraro F.R. et al., The white dwarf distance to the globular cluster NGC 6752 (and its age) with the Hubble Space Telescope, *Astrophys. J.* **465**, 23 (1996).

- 
213. Hansen B.M.S. et al., The white dwarf cooling sequence of the globular cluster Messier 4, *Astrophys. J. Lett.*, **574**, 515 (2002).
214. Hill V., Plez B., Cayrel R. et al., First stars. I. The extreme r-element rich, iron-poor halo giant CS 31082-001. Implications for the r-process site(s) and radioactive cosmochronology, *Astron. Astrophys.* **2002**, 560 (2002).
215. Novosyadlyj B., Apunevych S., Durrer R. et al., Best-fit cosmological parameters from observations of the large scale structure of the Universe, *Odessa Astronomical Publications* **12**, 73 (1999).
216. Novosyadlyj B., Durrer R., Gottlöber S. et al., Cosmological parameters from large scale structure observations, *Astron. Astrophys.* **356**, 418 (2000).
217. Novosyadlyj B., Durrer R., Apunevych S., Cosmological parameters from observational data on the large scale structure of the Universe, *Kinematics and Physics of celestial bodies, Suppl. Ser.* **3**, 146 (2000).
218. Novosyadlyj B., Durrer R., Gottlob S. et al., Determination of Cosmological Parameters from Large Scale Structure Observations, *Gravitation and Cosmology. Suppl.*, **6**, 107 (2000).
219. Balbi A., Ade P., Bock J., Boscaleri A. et al., Constraints on cosmological parameters from MAXIMA-1, *Astrophys. J. Lett.* **545**, 1 (2000).
220. Tegmark M., Zaldarriaga M., Current cosmological constraints from a 10 parameter CMB analysis, *Astrophys. J.* **544**, 30 (2000).
221. Tegmark M., Zaldarriaga M., Hamilton A.J., Towards a refined cosmic concordance model: Joint 11-parameter constraints from the cosmic microwave background and large-scale structure, *Phys. Rev. D* **63**, 1 (2000).
222. Durrer R., Novosyadlyj B., Cosmological parameters from complementary observations of the Universe, *Mon. Not. R. Astron. Soc.* **324**, 560 (2001).
223. Jaffe A.H., Ade P.A., Balbi A. et al., Cosmology from MAXIMA-1, BOOMERANG, and COBE DMR Cosmic Microwave Background Observations, *Phys. Rev. Lett.*, **86**, 3475 (2001).
224. Lange A.E., Ade P.A., Bock J.J. et al., Cosmological parameters from the first results of BOOMERANG, *Phys. Rev. D* **63**, 042001 (2001).
225. Novosyadlyj B. & Apunevych S., Cosmological Constraints on the Amplitude of Relic Gravitational Waves, *J. Phys. Stud.* **9**, 198 (2005).
226. Hu W., Scott D., Sugiyama N., White M., Effect of physical assumptions on the calculation of microwave background anisotropies, *Phys. Rev. D* **52**, 5498 (1995).
227. Steigman G., Primordial Nucleosynthesis in the Precision Cosmology Era, *Ann. Rev. Nucl. Part. Phys.* **57**, 463 (2007).
228. Wright E.L, Constraints on Dark Energy from Supernovae, Gamma-Ray Bursts, Acoustic Oscillations, Nucleosynthesis, Large-Scale Structure, and the Hubble Constant, *Astrophys. J.* **664**, 633 (2007)
229. Izotov Y.I., Thuan T.X. Systematic effects and a new determination of the primordial abundance of  $^4\text{He}$  and  $dY/dZ$  from observations of blue compact galaxies, *Astrophys. J.* **602**, 200 (2004).
230. Olive K.A., Skillman E.D., A Realistic Determination of the Error on the Primordial Helium Abundance: Steps toward Nonparametric Nebular Helium Abundances, *Astrophys. J.* **617**, 29 (2004).

231. Riess A.G., Macri L., Casertano S. et al., A Redetermination of the Hubble Constant with the Hubble Space Telescope from a Differential Distance Ladder, *Astrophys. J.* **699**, 539 (2009).
232. Zeldovich Ya.B. Cosmological constant and the theory of elementary particles, *Uspekhi fizicheskikh nauk*, **91**, 209 (1968).
233. Linde A.D., *Particle Physics and Inflationary Cosmology*, New York, 1990.
234. Starobinsky A.A., Beyond the simplest inflationary cosmological models, *Gravit. & Cosmol. Suppl.* **4**, 88 (1998).
235. Antoniadis I., Dimopoulos S., Dvali G., Millimetre-Range Forces in Superstring Theories with Weak-Scale Compactification, *Nucl. Phys. B* **516**, 70 (1998).
236. Sahni V., Starobinsky A., The Case for a Positive Cosmological  $\Lambda$ -Term, *Int. J. Mod. Phys. D* **9**, 373 (2000).
237. Carroll S.M., The Cosmological Constant, *Living Rev. Rel.* **4**, 1 (2001).
238. Peebles P.J.E. and Ratra B., The cosmological constant and dark energy, *Rev. Mod. Phys.* **75**, 559 (2003).
239. Bouso R., The cosmological constant, *Gen. Relativ. Gravit.* **40**, 607 (2008).
240. DeDeo S., Caldwell R.R., Steinhardt P.J., Effects of the sound speed of quintessence on the microwave background and large scale structure, *Phys. Rev. D* **67**, 103509 (2003).
241. Bean R., Doré O., Probing dark energy perturbations: The dark energy equation of state and speed of sound as measured by WMAP, *Phys. Rev. D* **69**, 083503 (2004).
242. Hannestad S., Constraints on the sound speed of dark energy, *Phys. Rev. D* **71**, 103519 (2005).
243. Xia J.-Q., Cai Y.-F., Qiu T.-T. et al., Constraints on the Sound Speed of Dynamical Dark Energy International, *J. Mod. Phys. D* **17**, 1229 (2008).
244. de Putter R., Huterer D., Linder E.V., Measuring the speed of dark: Detecting dark energy perturbations, *Phys. Rev. D* **81**, 103513 (2010).
245. Ballesteros G., Lesgourgues J., Dark energy with non-adiabatic sound speed: initial conditions and detectability, *J. Cosmol. Astropart. Phys.* **10**, 014 (2010).
246. Haq Ansari R.U., Unnikrishnan S., Perturbations in dark energy models with evolving speed of sound. arXiv:1104.4609[astro-ph/CO] (2011).
247. Kodama H., Sasaki M., Cosmological perturbation theory, *Progress of Theor. Phys. Suppl.* **78**, 1 (1984).
248. Hu W., Structure Formation with Generalized Dark Matter, *Astrophys. J.* **506**, 485 (1998).
249. Erickson J.K., Caldwell R.R., Steinhardt P.J. et al., Measuring the Speed of Sound of Quintessence, *Phys. Rev. Lett.* **88**, 121301 (2002).
250. Mota D.F., Kristiansen J.R., Koivisto T., Groeneboom N.E., Constraining dark energy anisotropic stress, *Mon. Not. R. Astron. Soc.* **382**, 793 (2007).
251. Dent J.B., Dutta S. and Weiler T.J., New perspective on the relation between dark energy perturbations and the late-time integrated Sachs–Wolfe effect, *Phys. Rev. D* **79**, 023502 (2009).
252. Grande J., Pelinson A. and Sola J., Dark energy perturbations and cosmic coincidence, *Phys. Rev. D* **79**, 043006 (2009).
253. Christopherson A.J., Malik K.A., The non-adiabatic pressure in general scalar field systems, *Phys. Lett. B* **675**, 159 (2009).



- 
254. Sapone D., Kunz M., Fingerprinting dark energy, *Phys. Rev. D* **80**, 083519 (2009).
255. Novosyadlyj B., Sergijenko O., Evolution of scalar perturbations in cosmology with quintessential dark energy, *J. Phys. Stud.* **13**, 1902 (2009).
256. Sergijenko O., Kulinich Yu., Novosyadlyj B., Pelykh V., Large-scale structure formation in cosmology with classical and tachyonic scalar fields, *Kinematics and Physics of celestial bodies* **25**, 1 (2009).
257. Sergijenko O. and Novosyadlyj B., Perturbed dark energy: Classical scalar field versus tachyon, *Phys. Rev. D* **80**, 083007 (2009).
258. Dave R., Caldwell R.R. and Steinhardt P.J., Sensitivity of the cosmic microwave background anisotropy to initial conditions in quintessence cosmology, *Phys. Rev. D* **66**, 023516 (2002).
259. Watson C.R. and Scherrer R.J., Evolution of inverse power law quintessence at low redshift, *Phys. Rev. D* **68**, 123524 (2003).
260. Liu J., Sensitivity of quintessence perturbations to initial conditions, *Phys. Rev. D* **69**, 083504 (2004).
261. Scherrer R.J., Dark energy models in the w-w' plane, *Phys. Rev. D* **73**, 043502 (2006).
262. Sahlen M., Liddle A.R. and Parkinson D., Quintessence reconstructed: New constraints and tracker viability, *Phys. Rev. D* **75**, 023502 (2007).
263. Dutta S. and Scherrer R.J., Evolution of oscillating scalar fields as dark energy, *Phys. Rev. D* **78**, 083512 (2008).
264. Scherrer R.J. and Sen A.A., Thawing quintessence with a nearly flat potential, *Phys. Rev. D* **77**, 083515 (2008).
265. Unnikrishnan S., Jassal H.K. and Seshadri T.R., Scalar field dark energy perturbations and their scale dependence, *Phys. Rev. D* **78**, 123504 (2008).
266. Copeland E.J., Mizuno S. and Shaeri M., Dynamics of a scalar field in Robertson-Walker spacetimes, *Phys. Rev. D* **79**, 103515 (2009).
267. Chiba T., Slow-roll thawing quintessence, *Phys. Rev. D* **79**, 083517 (2009).
268. Jassal H.K., Comparison of perturbations in fluid and scalar field models of dark energy, *Phys. Rev. D* **79**, 127301 (2009).
269. Gibbons G.W., Cosmological evolution of the rolling tachyon, *Phys. Lett. B* **537**, 1 (2002).
270. Padmanabhan T., Accelerated expansion of the universe driven by tachyonic matter, *Phys. Rev. D* **66**, 021301 (2002).
271. Frolov A., Kofman L. and Starobinsky A., Prospects and problems of tachyon matter cosmology, *Phys. Lett. B* **545**, 8 (2002).
272. Abramo L.R. and Finelli F., Cosmological dynamics of the tachyon with an inverse power-law potential, *Phys. Lett. B* **575**, 165 (2003).
273. Bagla J.S., Jassal H.K. and Padmanabhan T., Cosmology with tachyon field as dark energy, *Phys. Rev. D* **67**, 063504 (2003).
274. Gibbons G.W., Thoughts on tachyon cosmology, *Clas. and Quant. Grav.* **20**, 321 (2003).
275. Abramo L.R., Finelli F. and Pereira T.S., Constraining Born-Infeld models of dark energy with CMB anisotropies, *Phys. Rev. D* **70**, 063517 (2004).
276. Sen A., Remarks on Tachyon Driven Cosmology, *Phys. Scripta T* **117**, 70 (2005).
277. Calcagni G. and Liddle A.R., Tachyon dark energy models: Dynamics and constraints, *Phys. Rev. D* **74**, 043528 (2006).

278. Jain R.K., Chingangbam P. and Sriramkumar L., On the evolution of tachyonic perturbations at super-Hubble scales, *J. Cosmol. Astropart. Phys.* **10**, 03 (2007).
279. Caldwell R.R., Kamionkowski M. and Weinberg N.N., Phantom Energy: Dark Energy with  $w < -1$  Causes a Cosmic Doomsday, *Phys. Rev. Lett.* **91**, 071301 (2003).
280. Fabris J.C. and Goncalves S.V.B., Scalar perturbations and the possible self-destruction of the “phantom menace”, *Phys. Rev. D* **74**, 027301 (2006).
281. Kujat J., Scherrer R.J. and Sen A.A., Phantom dark energy models with negative kinetic term, *Phys. Rev. D* **74**, 083501 (2006).
282. Lima J.A.S. and Pereira S.H., Chemical potential and the nature of dark energy: The case of a phantom field, *Phys. Rev. D* **78**, 083504 (2008).
283. Scherrer R.J. and Sen A.A., Phantom dark energy models with a nearly flat potential, *Phys. Rev. D* **78**, 067303 (2008).
284. Creminelli P., D’Amico G., Norena J. and Vernizzi F., The effective theory of quintessence: the  $w < -1$  side unveiled, *J. Cosmol. Astropart. Phys.* **02**, 018 (2009).
285. Armendariz-Picon C., Mukhanov V. and Steinhardt P.J., Essentials of k-essence, *Phys. Rev. D* **63**, 103510 (2001).
286. Malquarti M., Copeland E.J., Liddle A.R. and Trodden M., A new view of k-essence, *Phys. Rev. D* **67**, 123503 (2003).
287. Malquarti M., Copeland E.J. and Liddle A.R., k-essence and the coincidence problem, *Phys. Rev. D* **68**, 023512 (2003).
288. de Putter R. and Linder E.V., Kinetic k-essence and quintessence, *Astropart. Phys.* **28**, 263 (2007).
289. Aguirregabiria J.M., Chimento L.P. and Lazkoz R., Quintessence as k-essence [rapid communication, *Phys. Lett. B* **631**, 93 (2005).
290. Bilic N., Thermodynamics of k-essence, *Phys. Rev. D* **78**, 105012 (2008).
291. Bilic N, Tupper G. B. and Viollier R.D., Cosmological tachyon condensation, *Phys. Rev. D* **80**, 023515 (2009).
292. Steinhardt P.J., Caldwell R.R., Introduction to Quintessence, ASP Conference Series, ed. Y. I. Byun and K. W. Ng, **151**, 13 (1998).
293. Binetruy P., Models of dynamical supersymmetry breaking and quintessence, *Phys. Rev. D* **60**, 063502 (1999).
294. Masiero A., Pietroni M. and Rosati F., SUSY QCD and quintessence, *Phys. Rev. D* **61**, 023504 (2000).
295. Barreiro T., Copeland E.J. and Nunes N.J., Quintessence arising from exponential potentials, *Phys. Rev. D* **61**, 127301 (2000).
296. Ferreira P.G. and Joyce M., Cosmology with a Primordial Scaling Field, *Phys. Rev. D* **58**, 023503 (1998).
297. Frieman J.A., Hill C.T., Stebbins A. and Waga I., Cosmology with Ultralight Pseudo Nambu-Goldstone Bosons, *Phys. Rev. Lett.* **75**, 2077 (1995).
298. Caldwell R.R. and Linder E.V., The limits of quintessence, *Phys. Rev. Lett.* **95**, 141301 (2005).
299. Chevallier M. and Polarski D., Accelerating Universes with Scaling Dark Matter, *Int. J. Mod. Phys. D* **10**, 213, (2001).
300. Linder E.V., Exploring the Expansion History of the Universe, *Phys. Rev. Lett.* **90**, 091301, (2003).

- 
301. Weller J., Albrecht A., Future supernovae observations as a probe of dark energy, *Phys. Rev. D* **65**, 103512 (2002).
  302. Bassett B.A., Kunz M., Silk J., Ungarelli C., A late-time transition in the cosmic dark energy? *Mon. Not. R. Astron. Soc.* **336**, 1217 (2002).
  303. Parker L., and Raval A., Nonperturbative effects of vacuum energy on the recent expansion of the universe, *Phys. Rev. D* **60**, 063512 (1999).
  304. Parker L., and Raval A., Vacuum effects of an ultralow mass particle account for the recent acceleration of the universe, *Phys. Rev. D* **60**, 123502 (1999).
  305. Parker L., and Raval A., New quantum aspects of a vacuum-dominated univers, *Phys. Rev. D* **62**, 083503 (2000).
  306. Babichev E., Dokuchaev V. and Eroshenko Yu., Dark energy cosmology with generalized linear equation of state, *Class. Quant. Grav.* **22**, 143 (2005).
  307. Holman R., and Naidu S., Dark Energy from Wet Dark Fluid, *arXiv:astro-ph/0408102* (2004).
  308. Sahni V., Shtanov Yu., Braneworld models of dark energy, *J. Cosmol. Astropart. Phys.* **11**, 14 (2003).
  309. Lue A. and Starkman G.D., How a brane cosmological constant can trick us into thinking that  $w < -1$ , *Phys. Rev. D* **70**, 101501 (2004).
  310. Neupane I.P., On compatibility of string effective action with an accelerating universe, *Class. Quan. Grav.* **23**, 7493 (2006).
  311. Aref'eva I.Ya., Volovich I.V., The null energy condition and cosmology, *Theor. Math. Phys.* **155**, 503 (2008).
  312. Elizalde E., Nojiri S., Odintsov S.D., Late-time cosmology in a (phantom) scalar-tensor theory: Dark energy and the cosmic speed-up, *Phys. Rev. D* **70**, 043539 (2004).
  313. Gannouji R., Polarski D., Ranquet A., Starobinsky A., Scalar-tensor models of normal and phantom dark energy, *J. Cosmol. Astropart. Phys.* **09**, 016 (2006).
  314. Onemli V.K., Woodard R.P., Super-acceleration from massless, minimally coupled  $\phi^4$ , *Class. Quant. Grav.* **19**, 4607 (2002).
  315. Onemli V.K., Woodard R.P., Quantum effects can render  $w < -1$  on cosmological scales, *Phys. Rev. D* **70**, 107301 (2004).
  316. McInnes B., The dS/CFT Correspondence and the Big Smash, *J. High Energy Phys.* **0208**, 029 (2002).
  317. Carroll S.M., Hoffman M., Trodden M., Can the dark energy equation-of-state parameter  $w$  be less than -1? *Phys. Rev. D* **68**, 023509 (2003).
  318. Cline J.M., Jeon S., Moore G.D., The phantom menaced: Constraints on low-energy effective ghosts, *Phys. Rev. D* **70**, 043543 (2004).
  319. Arkani-Hamed N., Cheng H.C., Luty M.A. and Mukohyama S., Ghost Condensation and a Consistent IR Modification of Gravity, *J. High Energy Phys.* **05**, 074 (2004).
  320. Piazza F. and Tsujikawa S., Dilatonic ghost condensate as dark energy, *J. Cosmol. Astropart. Phys.* **07**, 004 (2004).
  321. Deffayet C., Pujolas O., Sawicki I., Vikman A., Imperfect dark energy from kinetic gravity braiding, *J. Cosmol. Astropart. Phys.* **10**, 026 (2010).
  322. Sahni V., Saini T. D., Starobinsky A. A. and Alam U., Statefinder — A new geometrical diagnostic of dark energy, *JETP Lett.* **77**, 201 (2003).
  323. Novosyadlyj B., Sergijenko O., Durrer R., Pelykh V. Do the cosmological observational data prefer phantom dark energy? *Phys. Rev. D* **86**, 083008 (2012).

324. Suzuki N., Rubin D., Lidman C. et al., The Hubble Space Telescope Cluster Supernova Survey. V. Improving the Dark-energy Constraints above  $z > 1$  and Building an Early-type-hosted Supernova Sample, *Astrophys. J.* **746**, 85 (2012).
325. Blake C., Kazin E., Beutler F. et al., The WiggleZ Dark Energy Survey: mapping the distance-redshift relation with baryon acoustic oscillations, *Mon. Not. R. Astron. Soc.* **418**, 1707 (2011).
326. Bengochea G.R., Supernova light-curve fitters and dark energy, *Phys. Lett. B* **696**, 5 (2011).
327. Novosyadlyj B., Sergijenko O., Apunevych S., Distinguishability of scalar field models of dark energy with time variable equation of state parameter, *Journal of Physical Studies* **15**, 1901 (2011).
328. Sergijenko O., Durrer R., Novosyadlyj B., Observational constraints on scalar field models of dark energy with barotropic equation of state, *J. Cosmol. Astropart. Phys.* **08**, 004 (2011).
329. Wheeler J.A., *Geometrodynamics*, Academic, New York (1962).
330. Kaluza Th., 1921 Zum Unitätsproblem der Physik, *Sitzungsber. d. Preuss. Akad. d. Wiss.* 966 (1921).
331. Klein O., Quantentheorie and funfdimensionale Relativitätstheorie, *Zeitschrift für Physik* **37**, 895 (1926).
332. Overduin J.M. and Wesson P.S., Kaluza–Klein Gravity, *Phys. Rep.* **283**, 303 (1997).
333. Wesson P.S., *Space-Time-Matter, Modern Kaluza–Klein Theory*, World Scientific, Singapore (1999).
334. Wesson P.S., *Five-Dimensional Physics: Classical and Quantum Consequences of Kaluza–Klein Cosmology*, World Scientific, Singapore (2006).
335. Green M.B., Schwarz J.H. and Witten E, *Superstring Theory*, Cambridge Univ. Press, Cambridge (1987).
336. Polchinski J., *String Theory, Volume 2: Superstring Theory and Beyond*, Cambridge University Press, Cambridge (1998).
337. Strominger A. and Vafa C., Microscopic Origin of the Bekenstein-Hawking Entropy, *Phys. Lett. B.* **379**, 99 (1996).
338. Duff M.J., M-Theory (the Theory Formerly Known as Strings), *Int. Journ. Mod. Phys. A.* **11**, 5623 (1996).
339. Scherk J. and Schwarz J.H., Dual field theory of quarks and gluons, *Phys. Lett. B* **57**, 463 (1975).
340. Freund P.G.O. and Rubin M.A., Dynamics of dimensional reduction, *Phys. Lett. B* **97**, 233 (1980).
341. Salam A. and Strathdee J., On Kaluza–Klein theory, *Ann. Phys.* **141**, 316 (1982).
342. Duff M.J., Nilson B.E.W. and Pope C.N., Kaluza–Klein supergravity, *Phys. Rep.* **130**, 1 (1986).
343. Krippendorff S., Quevedo F. and Schlotterer O., *Cambridge Lectures on Supersymmetry and Extra Dimensions*, arXiv:hep-th/1011.1491.
344. Yano K. and Bochner S., *Curvature and Betti numbers*, Princeton University Press, Princeton (1953).
345. Wolf J.A., *Spaces of Constant Curvature*, McGraw-Hill, New York (1967).
346. A.L.Besse A.L., *Einstein manifolds*, Springer, Berlin (1987).

- 
347. Ellis G.F.R., Topology and cosmology, *Gen. Rel. Grav.* **2**, 7 (1971).
348. Sokolov D.D. and Shvartsman V.F., An estimate of the size of the universe from a topological point of view, *Sov. Phys. JETP* **39**, 196 (1974).
349. Fagundes H.V., Smallest universe of negative curvature, *Phys. Rev. Lett.* **70**, 1579 (1993); Closed spaces in cosmology, *Gen. Rel. Grav.* **24**, 199 (1992).
350. Nikulin V.V. and Shafarevich I.R., *Geometry and Groups*, Nauka, Moscow (1983) (in Russian).
351. Aref'eva I.Ya. and Volovich I.V., Manifolds of constant negative curvature as vacuum solutions in Kaluza–Klein and superstring theories, *Theor. Math. Phys.* **64**, 866 (1985).
352. Bleyer U., Ivashchuk V.D., Melnikov V.N. and Zhuk A., Multidimensional classical and quantum wormholes in models with cosmological constant, *Nucl. Phys. B* **429**, 177 (1994).
353. Bleyer U. and Zhuk A., Multidimensional Integrable Cosmological Models with Positive External Space Curvature, *Gravitation and Cosmology* **1**, 36 (1995).
354. Bleyer U. and Zhuk A., Multidimensional Integrable Cosmological Models with Negative External Space Curvature, *Gravitation and Cosmology* **1**, 106 (1995).
355. Kasper U. and Zhuk A., Integrable Multicomponent Perfect Fluid Multidimensional Cosmology. I, *Gen. Rel. Grav.* **28**, 1269 (1996).
356. Zhuk A., Integrable scalar field multi-dimensional cosmologies, *Class. Quantum Grav.* **13**, 2163 (1996).
357. Kasper U., Rainer M. and Zhuk A., Integrable Multicomponent Perfect Fluid Multidimensional Cosmology II: Scalar Fields, *Gen. Rel. Grav.* **29**, 1123 (1997).
358. Fadeev S.B., Ivashchuk V.D. and Melnikov V.N., On black holes in multidimensional theory with Ricci-flat internal spaces, *Phys. Lett. A* **161**, 98 (1991).
359. Ivashchuk V.D., Multidimensional cosmology and Toda-like systems, *Phys. Lett. A* **170**, 16 (1992).
360. Ivashchuk V.D. and Melnikov V.N., Multidimensional Cosmology with m-component Perfect Fluid, *Int. Journ. Mod. Phys. D* **3**, 795 (1994).
361. Ivashchuk V.D. and Melnikov V.N., Classical and Quantum Multidimensional Cosmology, *Gravitation and Cosmology* **1**, 133 (1995).
362. Ivashchuk V.D. and Melnikov V.N., Billiard representation for multidimensional cosmology with multicomponent perfect fluid near the singularity, *Class. Quantum Grav.* **12**, 809 (1995).
363. Ivashchuk V.D. and Melnikov V.N., Multidimensional Gravity with Einstein Internal Spaces, *Gravitation and Cosmology* **2**, 211 (1996).
364. Ivashchuk V.D. and Melnikov V.N., Topical review: Exact solutions in multidimensional gravity with antisymmetric forms, *Class. Quantum Grav.* **18**, R87 (2001).
365. Bronnikov K.A., Ivashchuk V.D., Melnikov V.N., The Reissner-Nordstrom problem for intersecting electric and magnetic p-branes, *Gravitation and Cosmology* **3**, 203 (1997).
366. Bronnikov K.A., Grebeniuk M.A., Ivashchuk V.D., Melnikov M.N., Integrable multidimensional cosmology for intersecting p-branes, *Gravitation and Cosmology* **3**, 105 (1997).
367. Bronnikov K.A., Block-orthogonal brane systems, black holes and wormholes, *Gravitation and Cosmology* **4**, 49 (1998).

368. Ivashchuk V.D., Melnikov V.N. and Zhuk A.I., On Wheeler-De Witt equation in multidimensional cosmology, *Nuovo Cimento B* **104**, 575 (1989).
369. Günther U. and Zhuk A., Gravitational excitons from extra dimensions, *Phys. Rev. D* **56**, 6391 (1997).
370. Rainer M. and Zhuk A., Tensor-multiscalar theories from multidimensional cosmology, *Phys. Rev. D* **54**, 6186 (1996).
371. York J.W., Role of Conformal Three-Geometry in the Dynamics of Gravitation, *Phys. Rev. Lett.* **28**, 1082 (1972).
372. Gibbons G.W. and Hawking S.W., Action integrals and partition functions in quantum gravity, *Phys. Rev. D* **15**, 2752 (1977).
373. Arkani-Hamed N., Dimopoulos S., Kaloper N. and March-Russell J., Rapid asymmetric inflation and early cosmology in theories with sub-millimeter dimensions, *Nucl. Phys. B* **567**, 189 (2000).
374. Arkani-Hamed N., Dimopoulos S. and March-Russell J., Stabilization of submillimeter dimensions: The new guise of the hierarchy problem, *Phys. Rev. D* **63**, 064020 (2001).
375. Günther U. and Zhuk A., Stable compactification and gravitational excitons from extra dimension, *Hadronic Journal* **21**, 279 (1998).
376. Günther U. and Zhuk A., Stabilization of internal spaces in multidimensional cosmology, *Phys. Rev. D* **61**, 124001 (2000).
377. Günther U., Moniz P. and Zhuk A., Asymptotical AdS space from nonlinear gravitational models with stabilized extra dimensions, *Phys. Rev. D* **66**, 044014 (2002).
378. Günther U., Moniz P. and Zhuk A., Nonlinear multidimensional cosmological models with form fields: Stabilization of extra dimensions and the cosmological constant problem, *Phys. Rev. D* **68**, 044010 (2003).
379. Bleyer U. and Zhuk A., On multidimensional cosmological models with static internal space, *Class. Quantum Grav.* **12**, 89 (1995).
380. Zhuk A., Conventional cosmology from multidimensional models. In Proceedings of the 14th International Seminar on High Energy Physics “QUARKS-2006” in St. Petersburg (May 19-25 2006). **2**, 264. INR press, Moscow (2007).
381. Günther U., Kriskiv S. and Zhuk A., On stable compactification with a Casimir-like potential, *Gravitation and Cosmology* **4**, 1 (1998).
382. Kaya A., Volume stabilization and acceleration in brane gas cosmology, *J. Cosmol. Astropart. Phys.* **0408**, 014 (2004).
383. Rubakov V.A., Large and infinite extra dimensions, *Phys. Usp.* **44**, 871 (2001). (arXiv:hep-ph/0104152).
384. Günther U. and Zhuk A., Multidimensional perfect-fluid cosmology with stable compactified internal dimensions, *Class. Quantum Grav.* **15**, 2025 (1998).
385. Bousso R. and Polchinski J., Quantization of four-form fluxes and dynamical neutralization of the cosmological constant, *J. High Energy Phys.* **0006**, 006 (2000). Susskind L., The anthropic landscape of string theory, hep-th/0302219. Kallosh R. and Linde A., Landscape, the Scale of SUSY Breaking, and Inflation, *J. High Energy Phys.* **0412**, 004 (2004). Schwartz-Perlov A. and Vilenkin A., Probabilities in the Bousso Polchinski multiverse, *J. Cosmol. Astropart. Phys.* **0606**, 010 (2006).

- 
386. Appelquist T., Cheng H.-C. and Dobrescu B.A., Bounds on universal extra dimensions, *Phys. Rev. D* **64**, 035002 (2001). Ponton E. and Poppitz E., Casimir energy and radius stabilization in five and six dimensional orbifolds, *J. High Energy Phys.* **0106**, 019 (2001). Cheng H.-C., Matchev K.T. and Schmaltz M., Radiative corrections to Kaluza–Klein masses, *Phys. Rev. D* **66**, 036005 (2002). Servant G. and Tait T.M.P., Is the lightest Kaluza–Klein particle a viable dark matter candidate? *Nucl. Phys. B* **650**, 391 (2003). Bergstrom L., Bringmann T., Eriksson M. and Gustafsson M., Gamma Rays from Kaluza–Klein Dark Matter, *Phys. Rev. Lett.* **94**, 131301 (2005). De Fazio F., Constraining Universal Extra Dimensions through B decays, hep-ph/0609134.
387. Günther U., Starobinsky A. and Zhuk A., Multidimensional cosmological models: Cosmological and astrophysical implications and constraints, *Phys. Rev. D.* **69**, 044003 (2004).
388. Günther U. and Zhuk A., Massive Scalar Fields in the Early Universe, *Int. Journ. Mod. Phys. D* **13**, 1167 (2004).
389. Townsend P.K., Four lectures on M-theory, hep-th/9612121. Moffat J.W., M-theory on a supermanifold, hep-th/0111225.
390. Morisawa Y., Uzawa K. and Mukohyama S., Excitation of Kaluza–Klein modes of a U(1) field by parametric resonance, *Phys. Rev. D* **62**, 104019 (2000).
391. Scherk J. and Schwarz J.H., Spontaneous breaking of supersymmetry through dimensional reduction, *Phys. Lett. B* **82**, 60 (1979). Salam A. and Strathdee J., On Kaluza–Klein theory, *Ann. Phys.* **141**, 316 (1982). Kolb E. and Slansky R., Dimensional reduction in the early universe: Where have the massive particles gone? *Phys. Lett. B* **135**, 378 (1984).
392. Bleyer U. and Zhuk A., Scalar Field Instability in Multidimensional Cosmology, *Astron. Nachr.* **316**, 197 (1995).
393. Boehm T., Durrer R., and van de Bruck C., Dynamical instabilities of the Randall-Sundrum model, *Phys. Rev. D* **64**, 063504 (2001).
394. Zhuk A., Restrictions on Dilatonic Brane-World Models, *Int. Journ. Mod. Phys. D* **11**, 1399 (2002).
395. Coughlan G. et al, Cosmological problems for the polonyi potential, *Phys. Lett. B* **131**, 59 (1983).
396. Ellis J., Nanopoulos D. and Quiros M., On the axion, dilaton, Polonyi, gravitino and shadow matter problems in supergravity and superstring models, *Phys. Lett. B* **174**, 176 (1986).
397. Starobinsky A.A., A new type of isotropic cosmological models without singularity, *Phys. Lett. B* **91**, 99 (1980).
398. de Carlos B., Casas J., Quevedo F. and Roulet E., Model-independent properties and cosmological implications of the dilaton and moduli sectors of 4D strings, *Phys. Lett. B.* **318**, 447 (1993).
399. Banks T., Kaplan D. and Nelson A., Cosmological implications of dynamical supersymmetry breaking, *Phys. Rev. D.* **49**, 779 (1994).
400. Banks T., Berkooz M. and Steinhardt P., Cosmological moduli problem, supersymmetry breaking, and stability in postinflationary cosmology, *Phys. Rev. D* **52**, 705 (1995).
401. Banks T. et al, Modular cosmology, *Phys. Rev. D* **52**, 3548 (1995).
402. Kolb E.W. and Turner M.S., *The Early Universe*, Addison-Wesley Publishing Company, New York (1994).

403. Kofman L., Linde A. and Starobinsky A.A., Reheating after inflation, *Phys. Rev. Lett.* **73**, 3195 (1994); Towards the theory of reheating after inflation, *Phys. Rev. D* **56**, 3258 (1997).
404. Kolb E.W., Servant G. and Tait T.M.P., The radionactive universe, *J. Cosmol. Astropart. Phys.* **0307**, 008 (2003).
405. Wang L., Caldwell R.R., Ostriker J.P. and Steinhardt P.J., Cosmic Concordance and Quintessence, *Astroph. J.* **530**, 17 (2000).
406. Fischbach E. and Talmadge C.L., *The search for non-Newtonian gravity*, Springer-Verlag, New York (1999). Adelberger E.G., Heckel B.R. and Nelson A.E., Tests of the Gravitational Inverse-Square Law, *Ann. Rev. Nucl. Part. Sci.* **53**, 77 (2003). Kapner D.J. et al, Tests of the Gravitational Inverse-Square Law below the Dark-Energy Length Scale, *Phys. Rev. Lett.* **98**, 021101 (2007).
407. Hannestad S., Possible constraints on the time variation of the fine structure constant from cosmic microwave background data, *Phys. Rev. D* **60**, 023515 (1999). Kaplinghat M., Scherrer R.S. and Turner M.S., Constraining variations in the fine-structure constant with the cosmic microwave background, *Phys. Rev. D* **60**, 023516 (1999).
408. Ivanchik A.V., Potekhin A.Y. and Varshalovich D.A., The fine-structure constant: a new observational limit on its cosmological variation and some theoretical consequences, *Astron. Astrophys.* **343**, 439 (1999).
409. Webb J.K. et al, Further Evidence for Cosmological Evolution of the Fine Structure Constant, *Phys. Rev. Lett.* **87**, 091301 (2001).
410. Melnikov V.N., Gravity as a key problem of the millenium. In *Proc. NASA/JPL Conf. on Fundamental Physics in Microgravity*, NASA (Doc. D-21522, pp. 4.1-4.17) (2001), gr-qc/0007067.
411. Uzan J.-P., The fundamental constants and their variation: observational and theoretical status, *Rev. Mod. Phys.* **75**, 403 (2003).
412. Damour T. and Dyson F., The Oklo bound on the time variation of the fine-structure constant revisited, *Nucl. Phys. B* **480**, 37 (1996). Fujii Y. et al, The nuclear interaction at Oklo 2 billion years ago, *Nucl. Phys. B* **573**, 377 (2000).
413. Kolb E.W., Perry M.J. and Walker T.P., Time variation of fundamental constants, primordial nucleosynthesis, and the size of extra dimensions, *Phys. Rev. D.* **33**, 869 (1986).
414. Martins C.J.A.P. et al., WMAP Constraints on varying  $\alpha$  and the Promise of Reionization, *Phys. Lett. B* **585**, 29 (2004).
415. Baukh V., Zhuk A. and Kahniashvili T., Extra dimensions and Lorenz invariance violation, *Phys. Rev. D* **76** 027502 (2007).
416. Ratra B., Cosmological 'seed' magnetic field from inflation, *Astrophys. J. Lett.* **391**, L1 (1992). Grasso D. and Rubinstein H.R., Magnetic fields in the early Universe, *Phys. Rept.* **348**, 163 (2001).
417. Varshalovich D.A., Moskalev A.N. and Khersonskii V.K., *Quantum Theory of Angular Momentum*, World Scientific, Singapore (1988).
418. Krall N.A. and Trivelpiece A.W., *Principles of Plasma Physics*, McGraw-Hill, New York (1973).
419. Cantcheff M. B., Lorentz Symmetry Breaking and Planar Effects from Non-Linear Electrodynamics, *Eur. Phys. Journ. C* **46**, 247 (2006).



- 
420. Rodríguez Martínez M. and T. Piran T., Constraining Lorentz violations with gamma ray bursts, *J. Cosmol. Astropart. Phys.* **04**, 006 (2006).
421. Birrell N.D. and Davies P.C.W., *Quantum Fields in Curved Space*, Cambridge University Press, Cambridge (1982).
422. Nojiri S. and Odintsov S.D., Where new gravitational physics comes from: M-theory? *Phys. Lett. B* **576**, 5 (2003).
423. Woodard R.P., Avoiding Dark Energy with  $1/R$  Modifications of Gravity, *Lect. Notes Phys.* **720**, 403 (2007).
424. Nojiri S. and Odintsov S.D., Introduction to Modified Gravity and Gravitational Alternative for Dark Energy, *Int. Journ. Geom. Meth. Mod. Phys.* **4**, 115 (2007). Sotiriou T.P. and Faraoni V.,  $f(R)$  Theories Of Gravity, *Rev. Mod. Phys.* **82**, 451 (2010). Nojiri S. and Odintsov S. D., Unified cosmic history in modified gravity: from  $F(R)$  theory to Lorentz non-invariant models, *Phys. Rept.* **505**, 59 (2011).
425. Capozziello S., De Laurentis M. and Faraoni V., A bird's eye view of  $f(R)$ -gravity, arXiv:0909.4672.
426. Witt B., Fourth-order gravity as general relativity plus matter, *Phys. Lett. B* **145**, 176 (1984). Müller V., Schmidt H.-J. and Starobinsky A.A., The stability of the de Sitter space-time in fourth order gravity, *Phys. Lett. B* **202**, 198 (1988). Barrow J.D. and Cotsakis S., Inflation and the conformal structure of higher-order gravity theories, *Phys. Lett. B* **214**, 515 (1988).
427. Maeda K.-I., Towards the Einstein-Hilbert action via conformal transformation, *Phys. Rev. D* **39**, 3159 (1989).
428. Günther U., Zhuk A., Bezerra V.B. and Romero C., AdS and stabilized extra dimensions in multi-dimensional gravitational models with nonlinear scalar curvature terms  $R^{-1}$  and  $R^4$ , *Class. Quantum Grav.* **22**, 3135 (2005).
429. Saidov T. and Zhuk A.,  $1/R$  multidimensional gravity with form-fields: Stabilization of extra dimensions, cosmic acceleration, and domain walls, *Phys. Rev. D* **75**, 084037 (2007).
430. Carroll S.M. et al., Cosmology of generalized modified gravity models, *Phys. Rev. D* **71**, 063513 (2005).
431. Ellis J., Kaloper N., Olive K.A. and Yokoyama J., Topological  $R^4$  inflation, *Phys. Rev. D* **59**, 103503 (1999).
432. Saidov T. and Zhuk A., AdS non-linear multidimensional ( $D = 8$ ) gravitational models with stabilized extra dimensions, *Gravitation and Cosmology* **12**, 253 (2006).
433. Bronnikov K.A. and Rubin S.G., Self-stabilization of extra dimensions, *Phys. Rev. D* **73**, 124019 (2006). Bronnikov K.A., Konoplich R.V. and Rubin S.G., Diversity of universes created by pure gravity, *Class. Quantum Grav.* **24**, 1261 (2007). Bronnikov K.A. and Rubin S.G., Abilities of multidimensional gravity, *Gravitation and Cosmology* **13**, 253 (2007). Bronnikov K.A., Kononogov S.A., Melnikov V.N. and Rubin S.G., Cosmologies from nonlinear multidimensional gravity with acceleration and slowly varying  $G$ , *Gravitation and Cosmology* **14**, 230 (2008). Bronnikov K.A. and Rubin S.G., Svadkovsky I.V., Multidimensional world, inflation and modern acceleration, *Phys. Rev. D* **81** 084010 (2010).
434. Saidov T. and Zhuk A., Problem of inflation in nonlinear multidimensional cosmological models, *Phys. Rev. D* **79**, 024025 (2009).
435. Saidov T. and Zhuk A., Bouncing inflation in a nonlinear  $R^2 + R^4$  gravitational model, *Phys. Rev. D* **81**, 124002 (2010).

- 436. Frolov A.V., A Singularity Problem with  $f(R)$  Dark Energy, *Phys. Rev. Lett.* **101**, 061103 (2008).
- 437. Stelle K.S., Lectures on supergravity  $p$ -branes. In E. Gava et al. (eds.), *High energy physics and cosmology, 1996 Summer School, ICTP, Trieste, Italy 10 June–26 July 1996*, World Scientific, New York (1997).
- 438. Lukas A., Ovrut B.A., and Waldram D., String and M-Theory Cosmological Solutions with Ramond Forms, *Nucl. Phys. B* **495**, 365 (1997); Stabilizing dilaton and moduli vacua in string and M-Theory cosmology, *Nucl. Phys. B* **509**, 169 (1998).
- 439. Freund P.G.O. and Rubin M.A., Dynamics of dimensional reduction, *Phys. Lett. B* **97**, 233 (1980).
- 440. Wiltshire D.L., Global properties of Kaluza–Klein cosmologies, *Phys. Rev. D* **36**, 1634 (1987).
- 441. Gray J. and Copeland E.J., Gravitational instantons, extra dimensions and form fields, *J. High Energy Phys.* **0106**, 046 (2001).
- 442. Frieman J., Turner M. and Huterer D., Dark Energy and the Accelerating Universe, *Ann. Rev. Astron. Astrophys.* **46**, 385 (2008).
- 443. Gutperle M. and Strominger A., Spacelike branes, *J. High Energy Phys.* **0204**, 018 (2002).
- 444. Chen C.-M., Gal'tsov D.V. and Gutperle M., S-brane solutions in supergravity theories, *Phys. Rev. D* **66**, 024043 (2002).
- 445. Ivashchuk V.D., Composite S-brane solutions related to Toda-type systems, *Class. Quantum Grav.* **20**, 261 (2003).
- 446. Ohta N., Intersection rules for S-branes, *Phys. Lett. B* **558**, 213 (2003).
- 447. Burgess C.P. et al., Cosmological Spacetimes from Negative Tension Brane Backgrounds, *J. High Energy Phys.* **0210**, 028 (2002). Burgess C.P. et al., General brane geometries from scalar potentials: gauged supergravities and accelerating universes, *J. High Energy Phys.* **0308**, 056 (2003). Astefanesei D. and Jones G.C., S-branes and (anti-)bubbles in (A)dS space, *J. High Energy Phys.* **0506**, 037 (2005).
- 448. Ohta N., Accelerating Cosmologies from Spacelike Branes, *Phys. Rev. Lett.* **91**, 061303 (2003); A Study of Accelerating Cosmologies from Superstring/M Theories, *Prog. Theor. Phys.* **110**, 269 (2003).
- 449. Townsend P.K. and Wohlfarth M.N.R., Accelerating Cosmologies from Compactification, *Phys. Rev. Lett.* **91**, 061302 (2003).
- 450. Emparan R. and Garriga J., A note on accelerating cosmologies from compactifications and S-branes, *J. High Energy Phys.* **0305**, 028 (2003).
- 451. Roy S., Accelerating cosmologies from M/String theory compactifications, *Phys. Lett. B* **567**, 322 (2003).
- 452. Wohlfarth M.N.R., Accelerating cosmologies and a phase transition in M-theory, *Phys. Lett. B* **563**, 1 (2003).
- 453. Gutperle M., Kallosh R. and Linde A., M/string theory, S-branes and the accelerating universe, *J. Cosmol. Astropart. Phys.* **0307**, 001 (2003).
- 454. Chen C.-M. et al., *J. High Energy Phys.* **0310**, 058 (2003).
- 455. Neupane I.P., Accelerating cosmologies from exponential potentials, *Class. Quantum Grav.* **21**, 4383 (2004).
- 456. Chen C.-M., Ho P.-M., Neupane I.P. and Wang J.E., A note on acceleration from product space compactification, *J. High Energy Phys.* **0307**, 017 (2003).

- 
457. Ivashchuk V.D., Melnikov V.N. and Selivanov A.B., Cosmological solutions in multidimensional model with multiple exponential potential *J. High Energy Phys.* **0309**, 059 (2003).
458. Bleyer U. and Zhuk A., Kasner-like, inflationary and steady-state solutions in multi-dimensional cosmology, *Astron. Nachr.* **317**, 161 (1996).
459. Gavrilov V.R., Ivashchuk V.D. and Melnikov V.N., Multidimensional integrable vacuum cosmology with two curvatures, *Class. Quantum Grav.* **13**, 3039 (1996).
460. Zhuk A., *Gravitation and Cosmology.* **3**, 24 (1997).
461. Zhuk A.I., Multidimensional quantum wormholes, *Phys. Rev. D* **45**, 1192 (1992); Integrable multidimensional quantum cosmology, *Class. Quantum Grav.* **9**, 2029 (1992).
462. Baukh V., Zhuk A., Sp-brane accelerating cosmologies, *Phys. Rev. D* **73**, 104016 (2006).
463. Baukh V., Zhuk A., Dynamical dark energy from extra dimensions, *Kinematics and Physics of Celestial Bodies* **25**, 57 (2009).
464. Hinshaw G. et al., Five-Year Wilkinson Microwave Anisotropy Probe (WMAP) Observations: Data Processing, Sky Maps, and Basic Results, *Astrophys. Journ. Suppl.* **180**, 225 (2009).
465. Landau L.D. and Lifshitz E.M., *The Classical Theory of Fields*, Fourth Edition, Volume 2 (Course of Theoretical Physics Series), Pergamon Press, Oxford (2000).
466. Eingorn E. and Zhuk A., Classical tests of multidimensional gravity: negative result, *Class. Quantum Grav.* **27**, 205014 (2010).
467. Will C.M., *Theory and Experiment in Gravitational Physics*, Cambridge University Press, Cambridge (2000).
468. Straumann N., *General Relativity and Relativistic Astrophysics*, Springer-Verlag, Heidelberg (1984).
469. Bertotti B., Iess L. and Tortora P., A test of general relativity using radio links with the Cassini spacecraft, *Nature* **425**, 374 (2003).
470. Will C.M., Was Einstein Right? Testing Relativity at the Century. In *100 Years of Relativity: Spacetime Structure — Einstein and Beyond*, ed. Abhay Ashtekar. World Scientific, Singapore (2005).
471. Jain Bh. and Khoury J., Cosmological Tests of Gravity, *Ann. Phys.* **325**, 1479 (2010).
472. Eingorn M. and Zhuk A., Multidimensional gravity in non-relativistic limit, *Phys. Rev. D* **80**, 124037 (2009).
473. Eingorn M. and Zhuk A., Non-relativistic limit of multidimensional gravity: exact solutions and applications, *Class. Quantum Grav.* **27**, 055002 (2010).
474. Kramer D., *Acta Phys. Polon. B.* **2**, 807 (1970).
475. Gross D.J. and Perry M.J., Magnetic monopoles in Kaluza—Klein theories, *Nucl. Phys. B.* **226**, 29 (1983).
476. Davidson A. and Owen D., Black holes as windows to extra dimensions, *Phys. Lett. B.* **155**, 247 (1985).
477. Ivashchuk V.D., Spherically-symmetric solutions with a chain of  $n$  internal Ricci-flat spaces, arXiv:gr-qc/1006.4605.
478. De Leon J.P., Effective spacetime from multi-dimensional gravity, *Gravitation and Cosmology* **15**, 345 (2009).

- 479. De Leon J.P., Schwarzschild-like exteriors for stars in Kaluza–Klein gravity, edited by A.D. Wachter and R.J. Propst. Nova Science Publishers, Inc., Hauppauge, New York (2010).
- 480. Eingorn M. and Zhuk A., Kaluza–Klein models: can we construct a viable example? *Phys. Rev. D* **83**, 044005 (2011).
- 481. Eingorn M., de Medeiros O.R., Crispino L.C.B. and Zhuk A., Latent solitons, black strings, black branes, and equations of state in Kaluza–Klein models, *Phys. Rev. D* **84**, 024031 (2011).
- 482. Kallosh R. and Prokushkin S., SuperCosmology, arXiv:hep-th/0403060.
- 483. Eingorn M. and Zhuk A., Remarks on gravitational interaction in Kaluza–Klein models, *Phys. Lett. B* **713**, 154 (2012).
- 484. Chopovsky A., Eingorn M. and Zhuk A., Weak-field limit of Kaluza–Klein models with spherical compactification: experimental constraints, *Phys. Rev. D* **85**, 064028 (2012).
- 485. Chopovsky A., Eingorn M. and Zhuk A., Exact and asymptotic black branes with spherical compactification, *Phys. Rev. D* **86**, 024025 (2012).
- 486. Eingorn M., Fakhri S.H. and Zhuk A., Observational constraints on Kaluza–Klein models with  $d$ -dimensional spherical compactification, arXiv:1207.4339.
- 487. Eingorn M. and Zhuk A., Significance of tension for gravitating masses in Kaluza–Klein models, to appear in *Phys. Lett. B*, arXiv:1202.4773.
- 488. Rubakov V.A., Shaposhnikov M.E., Do we live inside a domain wall? *Phys. Lett. B* **125**, 136 (1983).
- 489. Akama K., An Early Proposal Of ‘Brane World’, *Lect. Notes Phys.* **176**, 267 (1982).
- 490. Barvinsky A.O., Cosmological branes and macroscopic extra dimensions, *Phys. Usp.* **48**, 545 (2005) [*Usp. Fiz. Nauk* **175**, 569 (2005)].
- 491. Gregory R., Rubakov V.A. and Sibiryakov S.M., Brane worlds: the gravity of escaping matter, *Class. Quantum Grav.* **17**, 4437 (2000).
- 492. Dubovsky S.L., Rubakov V.A., Tinyakov P.G., Brane world: Disappearing massive matter, *Phys. Rev. D* **62**, 105011 (2000).
- 493. Dubovsky S.L., Rubakov V.A., Tinyakov P.G., Is the electric charge conserved in brane world?, *J. High Energy Phys.* **0008**, 041 (2000).
- 494. Dvali G.R. and Shifman M.A., Domain walls in strongly coupled theories, *Phys. Lett. B* **396**, 64 (1997) [Erratum-*ibid.* **B 407**, 452 (1997)].
- 495. Polchinski J., TASI Lectures on D-branes, arXiv:hep-th/9611050.
- 496. Kiritsis E., D-branes in standard model building, gravity and cosmology, *Phys. Rep.* **421**, 105 (2005) [Erratum, *ibid.* **429**, 121 (2006)].
- 497. Arkani-Hamed N., Dimopoulos S. and Dvali G., The hierarchy problem and new dimensions at a millimeter, *Phys. Lett. B* **429**, 263 (1998).
- 498. Antoniadis I., Arkani-Hamed N., Dimopoulos S. and Dvali G., New dimensions at a millimeter to a fermi and superstrings at a TeV, *Phys. Lett. B* **436**, 257 (1998).
- 499. Arkani-Hamed N., Dimopoulos S. and Dvali G., Phenomenology, astrophysics, and cosmology of theories with submillimeter dimensions and TeV scale quantum gravity, *Phys. Rev. D* **59**, 086004 (1999).
- 500. Randall L. and Sundrum R., Large mass hierarchy from a small extra dimension *Phys. Rev. Lett.* **83**, 3370 (1999).

- 
501. Randall L. and Sundrum R., An alternative to compactification, *Phys. Rev. Lett.* **83**, 4690 (1999).
502. Hořava P. and Witten E., Heterotic and Type I string dynamics from eleven dimensions, *Nucl. Phys. B* **460**, 506 (1996).
503. Hořava P. and Witten E., Eleven-dimensional supergravity on a manifold with boundary, *Nucl. Phys. B* **475**, 94 (1996).
504. Dvali G., Gabadadze G. and Porrati M., 4D gravity on a brane in 5D Minkowski space, *Phys. Lett. B* **485**, 208 (2000).
505. Collins H. and Holdom B., Brane cosmologies without orbifolds, *Phys. Rev. D* **62**, 105009 (2000).
506. Shtanov Yu.V., On brane-world cosmology, arXiv:hep-th/0005193 (2000).
507. Sakharov A.D., Vacuum quantum fluctuations in curved space and the theory of gravitation, *Sov. Phys. Dokl.* **12**, 1040 (1968) [*Dokl. Akad. Nauk SSSR Ser. Fiz.* **177**, 70 (1967)]; *Sov. Phys. Usp.* **34**, 394 (1991) [*Usp. Fiz. Nauk.* **161**, 64 (1991)]; *Gen. Rel. Grav.* **32**, 365 (2000).
508. Wald R.M., *General Relativity*, The University of Chicago Press, Chicago (1984).
509. Fomin P.I. and Shtanov Yu.V., Towards field theory in spaces with multivolume junctions, *Class. Quant. Grav.* **19**, 3139 (2002).
510. Deffayet C., Cosmology on a brane in Minkowski bulk, *Phys. Lett. B* **502**, 199 (2001).
511. Lukas A., Ovrut B.A. and Waldram D., Boundary inflation, *Phys. Rev. D* **61**, 023506 (2000).
512. Binétruy P., Deffayet C. and Langlois D., Non-conventional cosmology from a brane universe, *Nucl. Phys. B* **565**, 269 (2000).
513. Binétruy P., Deffayet C., Ellwanger U. and Langlois D., Brane cosmological evolution in a bulk with cosmological constant, *Phys. Lett. B* **477**, 285 (2000).
514. Barceló C. and Visser M., Living on the edge: cosmology on the boundary of anti-de Sitter space, *Phys. Lett. B* **482**, 183 (2000).
515. Deffayet C., Dvali G., and Gabadadze G., Accelerated universe from gravity leaking to extra dimensions, *Phys. Rev. D* **65**, 044023 (2002).
516. Deffayet C., Landau S. J., Raux J., Zaldarriaga M. and Astier P., Supernovae, CMB, and gravitational leakage into extra dimensions, *Phys. Rev. D* **66**, 024019 (2002).
517. Gorbunov D., Koyama K. and Sibiryakov S., More on ghosts in the Dvali–Gabadadze–Porrati model, *Phys. Rev. D* **73**, 044016 (2006).
518. Charmousis C., Gregory R., Kaloper N. and Padilla A., DGP spectroscopy, *J. High Energy Phys.* **0610**, 066 (2006).
519. Deffayet C., Gabadadze G. and Iglesias A., Perturbations of the self-accelerated Universe, *J. Cosmol. Astropart. Phys.* **0608**, 012 (2006).
520. Gregory R., Kaloper N., Myers R.C. and Padilla A., A new perspective on DGP gravity, *J. High Energy Phys.* **0710**, 069 (2007).
521. Koyama K., Ghosts in the self-accelerating universe, *Class. Quantum Grav.* **24**, R231 (2007).
522. Shiromizu T., Maeda K. and Sasaki M., The Einstein equations on the 3-brane world, *Phys. Rev. D* **62**, 024012 (2001).
523. Shtanov Yu.V., Closed system of equations on a brane, *Phys. Lett. B* **541**, 177 (2002).

524. Shtanov Yu.V., Flat vacuum branes without fine tuning, *Phys. Lett. B* **543**, 121 (2002).
525. Sahni V. and Kofman L.A., Some self-consistent solutions of the Einstein equations with one-loop quantum gravitational corrections:  $G_{ik} = 8\pi G\langle T_{ik}\rangle_{vac}$ , *Phys. Lett. A* **117**, 275 (1986).
526. Nariai H., On some static solutions of Einstein's gravitational field equations in a spherically symmetric case, *Sci. Rep. Tohoku Univ.* **34** 160 (1950).
527. Nariai H., On a new cosmological solution of Einstein's field equations of gravitation, *Sci. Rep. Tohoku Univ.* **35**, 62 (1951).
528. Kofman L.A., Sahni V. and Starobinsky A.A., An anisotropic cosmological model generated by quantum vacuum polarization, *Sov. Phys. JETP* **58**, 1090 (1983) [*Zh. Eksp. Teor. Fiz.* **85**, 1876 (1983)].
529. Padilla A., Ghost-free braneworld bigravity, *Class. Quantum Grav.* **21**, 2899 (2004).
530. Shtanov Yu. and Viznyuk A., Linearized gravity on the Randall–Sundrum two-brane background with curvature terms in the action for the branes, *Class. Quantum Grav.* **22**, 987 (2005).
531. Maeda K., Mizuno S. and Torii T., Effective gravitational equations on a brane world with induced gravity, *Phys. Rev. D* **68**, 024033 (2003).
532. Smolyakov M.N., Brane-induced gravity in warped backgrounds and the absence of the radion, *Nucl. Phys. B* **695**, 301 (2004).
533. Gruzinov A., On the graviton mass, *New Astronomy* **10**, 311 (2005).
534. Porrati M., Fully covariant van Dam–Veltman–Zakharov discontinuity, and absence thereof, *Phys. Lett. B* **534**, 209 (2002).
535. Dvali G., Gruzinov A. and Zaldarriaga M., The accelerated universe and the Moon, *Phys. Rev. D* **68**, 024012 (2003).
536. Luty M.A., Porrati M. and Rattazzi R., Strong interactions and stability in the DGP model, *J. High Energy Phys.* **0309**, 029 (2003).
537. Rubakov V.A., Strong coupling in brane-induced gravity in five dimensions, [arXiv:hep-th/0303125](https://arxiv.org/abs/hep-th/0303125) (2003).
538. Visser M. and Wiltshire D.L., On-brane data for braneworld stars, *Phys. Rev. D* **67**, 104004 (2003).
539. Kaloper N., Brane-induced-gravity shock waves, *Phys. Rev. Lett.* **94**, 181601 (2005).
540. Kaloper N., Gravitational shock waves and their scattering in brane-induced gravity, *Phys. Rev. D* **71**, 086003 (2005); [Erratum, *ibid.* **71**, 129905(E) (2005)].
541. Lue A. and Starkman G., Gravitational leakage into extra dimensions: Probing dark energy using local gravity, *Phys. Rev. D* **67**, 064002 (2003).
542. Lue A., Scoccimarro R. and Starkman G.D., Probing Newton's constant on vast scales: Dvali–Gabadadze–Porrati gravity, cosmic acceleration, and large scale structure, *Phys. Rev. D* **69**, 124015 (2004).
543. Iorio L., On the effects of Dvali–Gabadadze–Porrati braneworld gravity on the orbital motion of a test particle, *Class. Quantum Grav.* **22**, 5271 (2005).
544. McInnes B., The dS/CFT correspondence and the big smash, *J. High Energy Phys.* **0208**, 029 (2002).
545. Starobinsky A.A., Future and origin of our Universe: Modern view, *Gravit. & Cosmology* **6**, 157 (2000).
546. Alam U. and Sahni V., Confronting braneworld cosmology with supernova data and baryon oscillations, *Phys. Rev. D* **73**, 084024 (2006).

- 
547. Lazkoz R., Maartens R. and Majerotto E., Observational constraints on phantomlike braneworld cosmologies, *Phys. Rev. D* **74**, 083510 (2006).
548. Giannantonio T., Song Y.-S. and Koyama K., Detectability of a phantom-like braneworld model with the integrated Sachs–Wolfe effect, *Phys. Rev. D* **78**, 044017 (2008).
549. Fischler W., Kashani-Poor A., McNees R. and Paban S., The acceleration of the universe, a challenge for string theory, *J. High Energy Phys.* **0107**, 3 (2001).
550. Ellis J., Mavromatos N.E. and Nanopoulos D.V., String theory and an accelerating universe, arXiv:hep-th/0105206 (2001).
551. Cline J.M., Quintessence, cosmological horizons, and self-tuning, *J. High Energy Phys.* **0108**, 35 (2001).
552. Kofinas G., General brane cosmology with  ${}^{(4)}R$  term in  $(A)dS_5$  or Minkowski bulk, *J. High Energy Phys.* **0108**, 034 (2001).
553. Sahni V., Shtanov Yu. and Viznyuk A., Cosmic mimicry: is LCDM a braneworld in disguise?, *J. Cosmol. Astropart. Phys.* **0512**, 005 (2005).
554. Alcock C. and Paczyński B., An evolution free test for non-zero cosmological constant, *Nature* **281**, 358 (1979).
555. Kujat J., Linn A.M., Scherrer R.J. and Weinberg D.H., Prospects for Determining the Equation of State of the Dark Energy: What Can Be Learned from Multiple Observables?, *Astroph. J.* **S72**, 1 (2001).
556. Newman J.A., Marinoni C., Coil A.L. and Davis M., Measuring the cosmic equation of state with galaxy clusters in the DEEP2 redshift survey, *Publ. Astron. Soc. Pacific.* **114**, 29 (2002).
557. Alam U., Sahni V., Saini T.D. and Starobinsky A.A., Exploring the expanding Universe and dark energy using the statefinder diagnostic, *Mon. Not. Roy. Astron. Soc.* **344**, 1057 (2003).
558. Peebles P.J.E., *Principles of Physical Cosmology*, Princeton University Press, Princeton (1993).
559. Dodelson S., *Modern Cosmology*, Academic Press, Boston, Massachusetts (2003).
560. Sahni V. and Shtanov Yu., Did the universe loiter at high redshifts?, *Phys. Rev. D* **71**, 084018 (2005).
561. Richards G.T., Strauss M.A., Pindor B. et al., A snapshot survey for gravitational lenses among  $z \geq 4.0$  quasars. I. The  $z > 5.7$  sample, *Astron. J.* **127**, 1305 (2004).
562. Haiman Z. and Quataert E., The Formation and Evolution of the First Massive Black Holes, in: *Supermassive Black Holes in the Distant Universe*, Ed. by A. J. Barger, Kluwer Academic Publishers, Dordrecht, The Netherlands (2004), Pp. 147-185.
563. Maor I., Brustein R., McMahon J. and Steinhardt P.J., Measuring the equation of state of the universe: Pitfalls and prospects, *Phys. Rev. D* **65**, 123003 (2002).
564. Alam U., Sahni V., Saini T.D. and Starobinsky A.A., Is there supernova evidence for dark energy metamorphosis?, *Mon. Not. Roy. Astron. Soc.* **354**, 275 (2004).
565. Alam U., Sahni V. and Starobinsky A.A., The case for dynamical dark energy revisited, *J. Cosmol. Astropart. Phys.* **0406**, 008 (2004).
566. Bassett B.S., Corasaniti P.S. and Copeland E.J., The essence of quintessence and the cost of compression, *Astrophys. J.* **617**, L1 (2004).
567. Umezū K., Ichiki K. and Yahiro M., Cosmological constraints on Newton’s constant, *Phys. Rev. D* **72**, 044010 (2005).

568. Sahni V., Dark Matter and Dark Energy, arXiv:astro-ph/0403324 (2004).
569. Sahni V., Feldman H. and Stebbins A., Loitering universe, *Astrophys. J.* **385**, 1 (1992).
570. Alexander S., Brandenberger R. and Easson D., Brane gases in the early Universe, *Phys. Rev. D* **62**, 103509 (2000).
571. Brandenberger R., Easson D.A. and Kimberley D., Loitering phase in brane gas cosmology, *Nucl. Phys. B* **623**, 421 (2002).
572. Ichiki K., Yahiro M., Kajino T. et al., Observational constraints on dark radiation in brane cosmology, *Phys. Rev. D* **66**, 043521 (2002).
573. Seljak U., Makarov A., McDonald P. et al., Cosmological parameter analysis including SDSS Ly $\alpha$  forest and galaxy bias: Constraints on the primordial spectrum of fluctuations, neutrino mass, and dark energy, *Phys. Rev. D* **71**, 103515 (2005).
574. Shtanov Yu. and Sahni V., New cosmological singularities in braneworld models, *Class. Quantum Grav.* **19**, L101 (2002).
575. Nojiri S. and Odintsov S.D., Final state and thermodynamics of a dark energy universe, *Phys. Rev. D* **70**, 103522 (2004).
576. Abdalla M.C.B., Nojiri S. and Odintsov S.D., Consistent modified gravity: dark energy, acceleration and the absence of cosmic doomsday, *Class. Quantum Grav* **22**, L35 (2005).
577. Linder E.V., Dark Entropy: Holographic Cosmic Acceleration, arXiv:hep-th/0410017 (2004).
578. Felten J.E. and Isaacman R., Scale factors  $R(t)$  and critical values of the cosmological constant  $\Lambda$  in Friedmann universes, *Rev. Mod. Phys.* **58**, 689 (1986).
579. Liddle A.R. and Lyth D.H., *Cosmological Inflation and Large-Scale Structure*, Cambridge University Press, Cambridge (2000).
580. Piao Y.-S., Feng B. and Zhang X., Suppressing the CMB quadrupole with a bounce from the contracting phase to inflation, *Phys. Rev. D* **69**, 103520 (2004).
581. Contaldi C.R., Peloso M., Kofman L. and Linde A., Suppressing the lower multipoles in the CMB anisotropies, *J. Cosmol. Astropart. Phys.* **0307**, 002 (2003).
582. Bennett C.L., Banday A.J., Górski K.M. et al., Four-year COBE DMR cosmic microwave background observations: Maps and basic results, *Astrophys. J.* **464**, L1 (1996).
583. Lipschutz M.M., *Theory and Problems of Differential Geometry*, Schaum's Outline Series, McGraw Hill (1969).
584. Sahni V., Sathyaprakash B.S. and Shandarin S., The evolution of voids in the adhesion approximation, *Astrophys. J.* **431**, 20 (1994).
585. Sahni V. and Coles P., Approximation methods for non-linear gravitational clustering, *Phys. Rep.* **262**, 1 (1995).
586. Shandarin S., Feldman H.A., Heitmann K. and Habib S., Shapes and sizes of voids in the Lambda cold dark matter universe: excursion set approach, *Mon. Not. Roy. Astron. Soc.* **367**, 1629 (2006).
587. Sheth J.V., Sahni V., Shandarin S.F. and Sathyaprakash B.S., Measuring the geometry and topology of large-scale structure using SURFGEN: methodology and preliminary results, *Mon. Not. Roy. Astron. Soc.* **343**, 22 (2003).
588. Shandarin S., Sheth J.V. and Sahni V., Morphology of the supercluster—void network in  $\Lambda$ CDM cosmology, *Mon. Not. Roy. Astron. Soc.* **353**, 162 (2006).



- 
589. Narayan R., Black holes in astrophysics, *New J. Phys.* **7**, 199 (2005).
590. Tretyakov P., Toporensky A., Shtanov Y. and Sahni V., Quantum effects, soft singularities and the fate of the universe in a braneworld cosmology, *Class. Quantum Grav.* **23**, 3259 (2006).
591. Zeldovich Ya.B. and Starobinsky A.A., Particle creation and vacuum polarization in an anisotropic gravitational field, *Sov. Phys. JETP* **34**, 1159 (1972) [*Zh. Eksp. Teor. Fiz.* **61**, 2161 (1971)].
592. Zeldovich Ya.B. and Starobinsky A.A., On the rate of particle creation in gravitational fields, *JETP Lett.* **26**, 252 (1977) [*Pis'ma v Zh. Eksp. Teor. Fiz.* **26**, 373 (1977)].
593. Grishchuk L.P., Amplification of gravitational waves in an isotropic universe, *Sov. Phys. JETP* **40** 409 (1975) [*Zh. Eksp. Teor. Fiz.* **67** (1974) 825].
594. Grishchuk L.P., Graviton creation in the early universe, *Ann. N.Y. Acad. Sci.* **302**, 439 (1977).
595. Hoyle F., Burbidge G. and Narlikar J.V., A quasi-steady state cosmological model with creation of matter, *Astrophys. J.* **410**, 437 (1993).
596. Hoyle F., Burbidge G. and Narlikar J.V., On the Hubble constant and the cosmological constant, *Mon. Not. Roy. Astron. Soc.* **286**, 173 (1997).
597. Narlikar J.V., *An Introduction to Cosmology*, Cambridge University Press, Cambridge (2002).
598. Kraus P., Dynamics of anti-de Sitter domain walls, *J. High Energy Phys.* **9912**, 011 (1999).
599. Ida D., Brane-world cosmology, *J. High Energy Phys.* **0009**, 014 (2000).
600. Deruelle N. and Doležal T., Brane versus shell cosmologies in Einstein and Einstein–Gauss–Bonnet theories, *Phys. Rev. D* **62**, 103502 (2000).
601. Stoica H., Tye S.-H. H. and Wasserman I., Cosmology in the Randall–Sundrum brane world scenario, *Phys. Lett. B* **482**, 205 (2000).
602. Bowcock P., Charmousis C. and Gregory R., General brane cosmologies and their global spacetime structure, *Class. Quantum Grav.* **17**, 4745 (2000).
603. Davis A.C., Vernon I., Davis S.C. and Perkins W.B., Brane world cosmology without the  $Z_2$  symmetry, *Phys. Lett. B* **504**, 254 (2001).
604. Perkins W.B., Colliding bubble worlds, *Phys. Lett. B* **504**, 28 (2001).
605. Carter B. and Uzan J.-P., Reflection symmetry breaking scenarios with minimal gauge form coupling in brane world cosmology, *Nucl. Phys. B* **406**, 45 (2001).
606. Battye R.A., Carter B., Mennim A. and Uzan J.-P., Einstein equations for an asymmetric brane-world, *Phys. Rev. D* **64**, 124007 (2001).
607. Kofinas G., General brane cosmology with  ${}^{(4)}R$  term in  $(A)dS_5$  or Minkowski bulk, *J. High Energy Phys.* **0108**, 034 (2001).
608. Gergely L. and Maartens R., Asymmetric brane-worlds with induced gravity, *Phys. Rev. D* **71**, 024032 (2005).
609. Liu Y.-X., Zhao Zh.-H., Wei Sh.-W. and Duan Y.-Sh., Bulk matters on symmetric and asymmetric de Sitter thick branes, *J. Cosmol. Astropart. Phys.* **0902**, 003 (2009).
610. Shtanov Yu., Viznyuk A. and Granda L.N., Asymmetric embedding in brane cosmology *Mod. Phys. Lett. A* **23**, 869 (2008).
611. Cordero R. and Vilenkin A., Stealth branes, *Phys. Rev. D* **65**, 083519 (2002).
612. Charmousis C., Gregory R. and Padilla A., Stealth acceleration and modified gravity, *J. Cosmol. Astropart. Phys.* **0710**, 006 (2007).

613. Koyama K., Padilla A. and Silva F.P., Ghosts in asymmetric brane gravity and the decoupled stealth limit, *J. High Energy Phys.* **0903**, 134 (2009).
614. Shtanov Y., Sahni V., Shafieloo A. and Toporensky A., Induced cosmological constant and other features of asymmetric brane embedding, *J. Cosmol. Astropart. Phys.* **0904**, 023 (2009).
615. Sahni V., Shafieloo A. and Starobinsky A.A., Two new diagnostics of dark energy, *Phys. Rev. D* **78**, 103502 (2008).
616. Gorini V., Kamenshchik A., Moschella U. and Pasquier V., Tachyons, scalar fields, and cosmology, *Phys. Rev. D* **69**, 123512 (2004).
617. Barrow J.D., Sudden future singularities, *Class. Quantum Grav.* **21**, L79 (2004).
618. Nojiri S. and Odintsov S.D., Quantum escape of sudden future singularity, *Phys. Lett. B* **595**, 1 (2004).
619. Maartens R., Brane-world cosmological perturbations, *Prog. Theor. Phys. Suppl.* **148**, 213 (2002).
620. Barrow J.D. and Maartens R., Kaluza–Klein anisotropy in the CMB, *Phys. Lett. B* **532**, 153 (2002).
621. Koyama K. and Maartens R., Structure formation in the Dvali–Gabadadze–Porrati cosmological model, *J. Cosmol. Astropart. Phys.* **0601**, 016 (2006).
622. Koyama K., Structure formation in modified gravity models, *J. Cosmol. Astropart. Phys.* **0603**, 017 (2006).
623. Sawicki I., Song Y-S. and Hu W., Near-horizon solution for Dvali–Gabadadze–Porrati perturbations, *Phys. Rev. D* **75**, 064002 (2007).
624. Ishak M., Upadhye A. and Spergel D.N., Probing cosmic acceleration beyond the equation of state: Distinguishing between dark energy and modified gravity models, *Phys. Rev. D* **74**, 043513 (2006).
625. Shtanov Y., Viznyuk A. and Sahni V., Gravitational instability on the brane: the role of boundary conditions, *Class. Quant. Grav.* **24**, 6159 (2007).
626. Mukohyama S., Gauge-invariant gravitational perturbations of maximally symmetric spacetimes, *Phys. Rev. D* **62**, 084015 (2000).
627. Mukohyama S., Integro-differential equation for brane-world cosmological perturbations, *Phys. Rev. D* **64**, 064006 (2001).
628. Wang L. and Steinhardt P., Cluster abundance constraints for cosmological models with a time-varying, spatially inhomogeneous energy component with negative pressure, *Astrophys. J.* **508**, 483 (1998).
629. Benabed K. and Bernardeau F., Testing quintessence models with large-scale structure growth, *Phys. Rev. D* **64**, 083501 (2001).
630. Verde L., Heavens A.F., Percival W.J. et al., The 2dF Galaxy Redshift Survey: the bias of galaxies and the density of the Universe, *Mon. Not. Roy. Astron. Soc.* **335**, 432 (2002).
631. Hawkins E., Maddox S., Cole S. et al., The 2dF Galaxy Redshift Survey: correlation functions, peculiar velocities and the matter density of the Universe, *Mon. Not. Roy. Astron. Soc.* **346**, 78 (2003).
632. Shtanov Yu.V. and Viznyuk A.V. Scalar cosmological perturbations on the brane, *Ukr. J. Phys.* **57**, (2012) [in press].
633. Koyama K., Langlois D., Maartens R. and Wands D., Scalar perturbations from brane-world inflation, *J. Cosmol. Astropart. Phys.* **0411**, 002 (2004).
634. Koyama K. and Mizuno S., Inflaton perturbations in brane-world cosmology with induced gravity, *J. Cosmol. Astropart. Phys.* **0607**, 013 (2006).

- 
635. Gabadadze G. and Iglesias A., Schwarzschild solution in brane induced gravity, *Phys. Rev. D* **72**, 084024 (2005).
636. Sahni V. and Starobinsky A., Reconstructing Dark Energy, *Int. J. Mod. Phys. D* **15**, 2105 (2006).
637. Schoen R., Yau S.-T., On the proof of the positive mass conjecture in general relativity *Commun. Math. Phys.* **65**, No. 1., 47–76 (1979).
638. Witten E., A new proof of the positive energy theorem, *Comm. Math. Phys.* **80**, 381–402 (1981).
639. Tipler F.J., Energy conditions and spacetime singularities, *Phys. Rev. D* **17**, 2521–2529 (1978).
640. Visser M., *Lorentzian wormholes*, AIP Press, New York (1995).
641. Visser M., General relativistic energy conditions: the Hubble expansion in the epoch of galaxy formation, [ArXiv:gr-qc/9705070v1](https://arxiv.org/abs/gr-qc/9705070v1).
642. Visser M., Barcelo N., Energy conditions and their cosmological implications, [ArXiv:gr-qc/0001099](https://arxiv.org/abs/gr-qc/0001099).
643. Shiromizu T., Sugai M., Local energy conditions and asymptotic conditions, *Class. Quant. Grav.* **11** L 103–108 (1994).
644. Parker T., Taubes T., On Wittens proof of the positive energy theorem, *Comm. Math. Phys.* **84**, 223–238, (1982).
645. Reula O., Existence theorem for solutions of Witten’s equation and nonnegativity of total mass, *J. Math. Phys.* **22**, 810–814, (1981).
646. Ashtekar A., Horowitz G.T., Phase space of general relativity revisited: A canonical choice of time and simplification of the Hamiltonian, *J. Math. Phys.* **25**, 1473–1480, (1984).
647. Horowitz G., Strominger W., Witten’s expression for gravitational energy, *Phys. Rev. D* **27**, 2793–2804, (1983).
648. Kijowski J., in Marcel Grossmann meeting of general relativity, Elsevier, 1681–1687, (1986).
649. Nester J., A new general energy expression with a simple positivity proof, *Phys. Lett. A* **83**, 241–244 (1981).
650. Dimakis A., Müller-Hoissen F. Spinor fields and the positive energy theorem, *Class. Quantum. Grav.* **7**, 283–295 (1990).
651. Nester J., Gauge condition for orthonormal three-frames, *J. Math. Phys.* **30**, No. 3, 624–626 (1989).
652. Estabrook F.B., Robinson R.S. and Wahlquist H.D., Hyperbolic equations for vacuum gravity using special orthonormal frames, *Class. Quant. Grav.* **14**, 1237–1255 (1997).
653. Buchman L.T. and Bardeen J.M., Schwarzschild tests of the Wahlquist–Estabrook–Buchman–Bardeen tetrad formulation for numerical relativity *Phys. Rev. D* **72** (2005) 124014, [arXiv:gr-qc/0508111v3](https://arxiv.org/abs/gr-qc/0508111v3).
654. Dimakis A., Müller-Hoissen F., On a gauge condition for orthonormal three-frames, *Phys. Lett. A* **112**, 73–74 (1989).
655. Frauendiener J., Triads and the Witten equations, *Class. Quant. Grav.* **8**, 1881–1887 (1991).
656. Frauendiener J., Nester J.M., Szabados L., Witten spinors on maximal, conformally flat hypersurfaces, [arXiv:gr-qc/1105.5008v2](https://arxiv.org/abs/gr-qc/1105.5008v2).
657. Pelykh V., Equivalence of the spinor and tensor methods in the positive energy problem, *Jour. Math. Phys.* **41**, 5550–5556 (2000).

658. Pelykh V., Knot points of double-covariant system of elliptic equations and preferred frames in general relativity, *J. Phys. A* **35**, 8135–8144 (2002).
659. Pelykh V., Comment on “Self-dual teleparallel formulation of general relativity and the positive energy theorem”, *Phys. Rev. D* **72**, 108502 (2005).
660. Nester J., Special orthonormal frames and energy localization, *Class. Quant. Grav.* **8**, L19–23, (1991).
661. Sommers P., Space spinors, *J. Math. Phys.* **21**, 2567–2571 (1980).
662. Sen A., On the existence of neutrino “zero-modes” in vacuum spacetimes, *J. Math. Phys.* **22**, 1781–1786 (1981).
663. Carleman T., Sur lessystèmes linéaires aux dérivées partielles du premier ordre à deux variables, *Compt. rend. Acad. Sci.* **197**, 471–474 (1933).
664. Morrey C.B., On the solutions of quasilinear elliptic partial differential equations, *Trans. Amer. Math. Soc.* **43**, 126–166 (1938).
665. Müller C., On the behavior of solutions of the differential equations, *Comm. Pure Applied Math.* **7**, 505–515 (1954).
666. Heinz E., Über die Eindeutigkeit bei Cauchyschem Anfangswertproblem einer elliptischen Differentialgleichung zweiter Ordnung, *Nachricht. Akad. Wiss. Göttingen*, **1**, 1–12 (1955).
667. Aronszajn N., An unique continuation theorem for solutions of elliptic partial differential equations or inequalities of second order, *J. Math. pur. et appl.* **36**, 235–249 (1957).
668. Cordes H.O., Über die eindeutige Bestimmtheit der Lösungen elliptischer Differentialgleichungen durch Anfangsvorhaben, *Nachricht. Akad. Wiss. Göttingen. Math.-phys. Klasse* **11**, 239–258 (1956).
669. Agresti J., De Pietri R., Lusanna L., Hamiltonian linearization of the rest-frame instant form of tetrad gravity in a completely fixed 3-orthogonal gauge: a radiation gauge for background-independent gravitational waves in a post-Minkowskian Einstein spacetime, *ArXiv gr-qc/0302084*.
670. Picone M., Una teorema sulle soluzioni delle equazioni lineari ellittiche autoaggiunte alle derivate parziali del secondo ordine, *Rend. Acc. Sci. Lincei* **20**, 331–338 (1911).
671. Picone M., Teorema di unicità nei problemi dei valori al contorno per le equazioni ellittiche e paraboliche, *Rend. Acc. Sci. Lincei* **22**, 275–282 (1913).
672. Bobyk O.I., Bodnarchuk P.I., Ptashnyk B.Y., Skorobohat’ko V.Ya., Elements of qualitative theory of differential equations with partial derivative, *Naukova Dumka, Kyiv, Ukraine*, (in Ukrainian) (1972).
673. Skorobohat’ko V.Ya., Investigations in qualitative theory of differential equations with partial derivative, *Naukova Dumka, Kyiv, Ukraine* (1980) (in Ukrainian).
674. Bartnik R., Remarks on cosmological spacetimes and constant mean curvature surfaces, *Commun. Math. Phys.* **117**, 615–624 (1988).
675. Malec E., O’Murchadha N. Constant mean curvature slices in the extended Schwarzschild solution and collapse of lapse. Part II, *ArXiv gr-qc/0307047v1*.
676. Lopatynsky Ya.B., The dependence of the solutions of the system of differential equations from the coefficients of the system, *Dopovidi AN UkSSR*, **3**, 211–213 (1956) (in Ukrainian); see also: Lopatinskij Ya.B., Theory of general boundary problems, *Naukova Dumka, Kyiv, Ukraine* (1984) (in Russian).

- 
677. Pelykh V.A., Correctness of the formulation of the Cauchy problem for the system of Einstein equations. Coordinate conditions and the theory of reference frames, (English. Russian original) *Sov. Phys., Dokl.* **24**, 566–568 (1979); translation from *Dokl. Akad. Nauk SSSR* **247**, 590–593 (1979).
678. Pelykh V.A., Removable characteristics and physical meaning of the  $x^0$ -hyperbolicity conditions of Einstein's evolution equations, *Sov. Phys. J. (USA)* **27**, 22–25 (1984). Translation of: *Izv. VUZ Eiz (USSR)* **27**, 28–31 (1984).
679. Pelykh V.A., Gauge conditions grounding in general relativity, *Izv. VUZ Fiz (USSR)* **5**, 117–119 (1986) (in Russian).
680. Jackiw R., Rebbi C., Solitons with fermion number 1/2 *Phys. Rev. D* **13**, 3398 (1976).
681. Jackiw R., Quantum meaning of classical field theory, *Rev. Mod. Phys.* **49**, No. 3, 681–706 (1977).
682. Keldysh M.V. and Lavrentiev M.A., On uniqueness of Neumann problem, *Dokl. Akad. Nauk SSSR* **16**, 151–152 (1937).
683. Oleynik O.A., About the properties of the solutions of some boundary values problem for elliptic type equations, *Math. Sbornik* **30**, 695–702 (1952).
684. Penrose R., Quasi-local mass and angular momentum in general relativity, *Proc. R. Soc. London A* **381**, 53–63 (1982).
685. Brown J.D. and York J.W., Quasilocal energy and conserved charges derived from the gravitational action, *Phys. Rev. D* **47**, 1407–1419 (1993), ArXiv gr-qc/9209012.
686. Nester J.M. and Tung R.S., Another positivity proof and gravitational energy localization, *Phys. Rev. D* **49**, 3958–3962 (1994), ArXiv gr-qc/9401002.
687. Chen C.M., Nester J.M. and Tung R.S., Quasilocal energy-momentum for geometric gravity theories, *Phys. Lett. A* **203**, 5–11 (1995), ArXiv gr-qc/9411048.
688. Chen C.M. and Nester J.M., Quasilocal quantities for GR and other gravity theories, *Clas. Quant. Grav.* **16**, 1279–1304 (1999), ArXiv gr-qc/9809020.
689. Chang C.C., Nester J.M. and Chen C.M. Pseudotensors and quasilocal energy-momentum, *Phys. Rev. Lett.*, **83**, 1897–1901 (1999) (ArXiv gr-qc/9809040).
690. Chang C.C., Nester J.M. and Chen C.-M. Energy-momentum (quasi-)localization for gravitating systems, ArXiv gr-qc/9912058.
691. Tung R.S. and Nester J.M., The quadratic spinor Lagrangian is equivalent to the teleparallel theory, *Phys. Rev. D* **60**, 021501 (1999), ArXiv gr-qc/9809030.
692. Christodoulou D. and Yau S.T., in *Mathematics and general relativity*, ed. J. Isenberg (Providence: American Mathematical Society), 9 (1988).
693. Nester J.M., Special orthonormal frames end energy localization, *Class. Quant. Grav.* **8**, L19–23 (1991).
694. Isenberg J. and Nester J.M., in *General Relativity and Gravitation: One Hundred Years After the Birth of Albert Einstein*, Vol. 1, ed. A. Held (New York: Plenum), 23–97 (1980).
695. Regge T. and Teitelboim C., Role of surface integrals in the Hamiltonian formulation of general relativity, *Ann. Phys. (N.Y.)* **88**, 286–318 (1974).
696. Nester J.M., in *Asymptotic behavior of mass and space-time geometry. Lecture Notes in Physics*, **202**, ed. F Flaherty (Berlin: Springer), 155–163 (1984).
697. Nester J.M., Tung R.S. and Zhytnikov V.V., Some spinor-curvature identities, *Class. Quant. Grav.* **11**, 983–987 (1994).

---

■

---

## INDEX

---

- Abelian gauge fields, 152  
Abell-ACO, 51  
accelerated expansion, 13, 21, 74, 150, 178, 183, 192, 205, 303  
acoustic peaks, 15, 30, 35–37, 55, 59, 63–65, 70, 112, 129  
action of spinor field, 307  
ADD model, 207  
age of Universe, 14, 62–64, 157, 159, 164, 170, 230, 239–241, 243, 247, 248, 251  
angular diameter distance, 21, 30, 38, 43–44, 55, 70, 132, 230, 239  
asymmetric branes, 263  
Atacama Cosmology Telescope (ACT), 60  
  
Bardeen potentials, 32, 55  
baryon acoustic oscillations (BAO), 30, 38, 69  
best-fit parameters, 40, 66, 92, 107–110, 123–129, 133  
Big Rip, 118–119, 123–124, 132, 272, 273  
black branes, 199  
black strings, 199  
BOOMERanG, 30  
brane, 184, 210  
braneworld model, 207  
bulk, 210  
bulk flow, 14, 53  
  
CAMB, 33, 67, 80, 107  
canonical Lagrangian, 83, 100, 113  
Chandra, 42  
CLASS, 33, 80  
  
classical Lagrangian, 80, 83, 86  
classical scalar field, 100, 102, 111  
CMB anisotropy, 15, 31, 33, 37, 42–45, 51, 54–57, 64, 66, 80, 82, 105, 112, 128, 255  
CMB power spectrum, 33, 35, 52, 55, 69, 112  
CMB temperature fluctuations, 30–38, 51, 55–60, 65, 97, 107, 112, 128  
CMBEasy, 33  
CMBFAST, 33, 80  
cold dark matter (CDM), 13, 79  
comoving distance, 22  
conformal Newtonian gauge, 33, 77, 81, 120  
conformal time, 16, 32, 167, 190  
conformal time gauge, 143  
conservation law, 17, 76, 82, 119, 261, 275  
correlation function, 30, 38–41, 61  
cosmic coincidence, 72  
cosmic microwave background (CMB), 15, 30–40, 42–44, 51–70, 80, 82, 89, 97, 105, 107, 112–113, 125, 128–130, 184, 236, 239, 243, 244, 254  
cosmic mimicry, 236  
cosmological constant, 13, 15, 16, 19, 33, 38, 72–74, 90, 117, 124, 132, 136, 137, 140–142, 147–152, 160, 177, 183, 184, 209–211, 214, 216, 220, 222, 223, 226, 228, 233, 242, 243, 249, 260, 264–269, 276, 280, 281, 300  
cosmological distance, 43  
cosmological gravexcitons, 170

- cosmological parameters, 33, 37, 44, 80, 110, 225  
cosmological principle, 16  
cosmological recombination, 31, 40, 49  
CosmoMC, 33, 107  
CosmoRec, 31  
cross-correlation function (CCF), 57–59  
curvature-non-linear models, 171
- dark energy dominated (DED) epoch**, 20, 21, 48, 49, 52, 55–56, 120, 126  
**dark energy dominated (DED) model**, 26  
**dark energy in KK models**, 141, 146  
**dark energy in multidimensional models**, 171  
**dark energy parameters**, 64, 66  
**dark matter in KK models**, 141, 156  
**dark radiation**, 214  
**deceleration parameter**, 15, 19, 22, 227, 231  
**deflection of light**, 198  
**density parameter**, 18  
**density perturbations**, 14, 32, 39, 46, 77, 99  
**DGP model**, 279  
**dimensional reduction**, 137  
**Dirac–Born–Infeld Lagrangian**, 103  
**Dirac–Born–Infeld Lagrangian**, 83  
**disappearing dark energy**, 233, 270  
**dominant energy condition (DEC)**, 303
- effective potential**, 141  
**Einstein equations**, 56, 73, 76, 79, 91, 144, 194, 197, 211, 215–216  
**Einstein–Boltzmann equations**, 33, 80  
**Einstein-de Sitter model**, 49  
**elliptic equation**, 315  
**energy-momentum tensor**, 16, 75, 174  
**Einstein equations**, 18  
**EoS parameter**, 17, 21, 22, 26, 37, 42, 50, 64, 69, 71, 75, 76, 81, 85–104, 107–114, 123–126, 131  
**equation of motion**, 75, 83, 157, 172, 179  
**equation of state (EoS)**, 17, 113, 145, 196, 235  
**Equation of State: SupErNovae trace Cosmic Expansion (ESSENCE)**, 25, 27  
**Euler equation**, 54  
**Euler–Lagrange equation**, 75  
**expansion dynamics**, 101  
**extra dimensions**, 184  
**extrinsic curvature**, 257
- fields of forms**, 147, 178  
**fine tuning**, 72, 90, 142, 146, 149  
**fine-structure constant**, 164  
**flat matter dominated (FMD) model**, 26, 27, 32–37, 41–42, 49–52, 56  
**freezing model**, 85  
**Friedmann equations**, 19, 75–77, 236, 334, 335  
**FRW metric**, 16, 30, 75, 134, 144, 157, 166, 212, 226, 294
- galaxy clusters**, 14, 42  
**gamma-ray bursts (GRBs)**, 29, 70, 169–172  
**Gaussian fluctuation**, 54  
**gravitational excitons**, 137, 141, 142, 148, 153, 156–157, 159, 164, 204  
**growth factor**, 14, 49–51, 90, 109, 132  
**growth function**, 53, 58
- HALOFIT**, 52  
**harmonic time**, 189, 191  
**harmonic time gauge**, 186, 188  
**High Energy Astrophysical Observatory (HEAO)**, 58  
**High-Z Supernova Search**, 13, 15  
**Hubble constant**, 13, 33, 44, 45, 63, 64, 68, 108, 157, 214, 281  
**Hubble parameter**, 19, 92, 158, 161, 163, 189–192, 224, 226, 229, 230, 233, 236–239, 243, 247, 248, 251, 253, 254, 258, 260–264, 269, 287, 293, 294, 299–300  
**Hubble Space Telescope (HST)**, 15, 25, 27, 66, 70, 107  
**HyRec**, 31
- Integrated Sachs–Wolfe effect**, 55–61, 70
- jerk**, 23, 126
- Kaluza–Klein models**, 134, 145, 191–205  
**Kaluza–Klein particles**, 135  
**Klein–Gordon equation**, 84

- Lagrangian density, 75  
 LambdaCDM model ( $\Lambda$ CDM), 118, 125, 127  
 LambdaCDM model ( $\Lambda$ CDM), 14, 34, 44, 63, 70, 107, 134, 159  
 large scale structure, 14, 16, 30, 45, 47, 48, 51–53, 55, 57, 60, 64–66, 70, 72, 75, 80, 82, 93, 97, 110, 119, 132  
 latent solitons, 198–205  
 Levi–Civita symbol, 182  
 light-curve fitter, 28  
 light-curve fitting, 25, 27–29, 66, 70, 71, 108  
 light-curve width, 25  
 likelihood function, 28, 37, 65, 112, 124  
 loitering Universe, 240, 243, 246, 248–250, 299  
 Lorentz invariance violation, 166  
 luminosity distance, 22, 24  
 Ly $\alpha$ -clouds, 52, 54  
**M**-theory, 208  
 Markov chain Monte Carlo (MCMC), 33, 44, 65, 68, 107, 108, 123–125, 129, 132  
 matter dominated (MD) epoch, 20, 158  
 matter perturbations, 58, 276, 278, 279, 284, 285, 288  
 MAXIMA, 15, 30  
 metric perturbations, 77, 80–274  
 metric tensor, 16, 340  
 midsuperspace metric, 139  
 Multicolor Light Curve Shape (MLCS), 25, 27–29, 66–71, 108–133  
 multicomponent Universe, 19, 33, 48  
 multidimensional cosmological models, 134  
 Nariai metric, 216  
 no-go theorem, 143  
 NRAO VLA Sky Survey (NVSS), 59  
 open CDM (OCDM) model, 14  
 open matter dominated (OMD) model, 26–31  
 parameter space, 251  
 parametrized post-Newtonian (PPN) parameters, 194, 205  
 perihelion shift, 193, 194, 198, 205  
 perturbation theory, 33, 78  
 phantom dark energy, 18, 68, 113, 225  
 phantom scalar field (PSF), 94, 113–132  
 Planck mission, 62  
 positive energy theorem (PET), 303  
 posterior function, 65–69  
 potential  $U(\phi)$ , 76, 83–100, 181  
 power spectrum, 30, 31, 33, 36–61, 65, 68, 77, 80, 92, 100, 111, 112, 122, 125, 128–129  
 primordial perturbation, 15, 45  
 quantum instability of the vacuum, 119  
 quintessence, 13, 18, 68, 84, 107  
 quintessential scalar field (QSF), 96, 100–113  
 quintessential scalar fields (QSF), 94  
 radiation dominated (RD) epoch, 20, 158, 170  
 Randall–Sundrum model, 213, 246  
 RECFAST, 31  
**S** $p$ -brane, 186  
 S-brane, 185  
 Sachs–Wolfe effect, 32, 55  
 scalar field, 73–133, 136, 140–166, 174, 207  
 scalar perturbations, 56, 81, 109, 174, 255, 274, 276, 280, 281, 283–284  
 scalaron, 157, 176–178, 180–184  
 Sen–Witten equation (SWE), 304, 319  
 Shapiro time-delay effect, 194, 199  
 singularity, 108, 117, 119, 124, 131, 177, 230, 232, 235, 245, 250, 255–263, 269, 272–273, 299, 330  
 Skorobohat’ko theorem, 309  
 Sloan Digital Sky Survey (SDSS), 39, 41, 58  
 snap, 23  
 soliton solutions, 195  
 sound horizon, 40  
 sound speed, 36, 76, 90, 97  
 space-time manifold, 137  
 space-time metric, 17  
 special orthonormal frame (SOF), 303  
 Spectral Adaptive Light curve Template (SALT), 25  
 spinor fields, 311  
 stable compactification, 140  
 standard candles, 24



- standard CDM model (SCDM), 14
- standard rulers, 30
- steady-state model, 263
- Supernova Cosmology Project (SCP), 13, 15, 230
- Supernova Ia, 15, 24
- SuperNova Legacy Survey (SNLS), 25, 28
- SuperNova Sloan Digital Sky Survey (SN SDSS), 25
- synchronous gauge, 33, 46, 80, 109, 120
- synchronous time gauge, 143, 150, 187, 189
  
- tachyonic scalar field, 103–105
- tensor of electromagnetic field, 166
- tensor of extrinsic curvature, 215
- tensor Ricci, 18, 79, 196, 201, 202, 215
- thawing model, 85
  
- transfer function, 50
- two-component Universe, 80
- Two-degree Field Galaxy Redshift survey (2dFGRS), 41
- Two-Micron All-Sky Survey (2MASS), 58
  
- Union sample, 25, 26, 69
- Universal extra dimension model, 151
  
- vacuum brane, 215
- vacuum energy, 73
- variable field, 82
- visibility function, 40
  
- weak gravitational lensing, 60
- Weyl tensor, 292
- WMAP, 30, 34, 37, 57, 88
  
- X-ray gas mass function, 42
- X-ray luminosity, 43



---

## ABOUT THE AUTHORS

---



**Bohdan NOVOSYADLYJ** is a leading researcher of the Astronomical Observatory (AO) and professor of the Astrophysics Department of the Ivan Franko National University of Lviv (LNU). After graduating from the Lviv State University in 1979 he started research activities in the AO LNU. In 1987–1991 he was a post-graduate student at the Astro Space Center of the Lebedev Physical Institute of the Russian Academy of Sciences (Moscow), where he received his PhD degree in 1991. Dr. Novosyadlyj received his Habilitation Doctoral degree in 2007 from the Main Astronomical Observatory of the National Academy of Sciences of Ukraine.

He was a visiting scientist at the Abdus Salam International Center for Theoretical Physics (Trieste, Italy), SISSA (Trieste, Italy), Potsdam Astrophysical Institute (Germany), Department of Theoretical Physics of Geneva University (Switzerland).

His research interests include relativistic astrophysics, cosmology, formation of galaxies and large scale structure of the Universe, the nature of dark matter and dark energy.

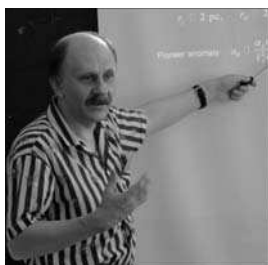
---



**Volodymyr PELYKH** is the head of the Department of Differential Equations at the Pidstryhach Institute for Applied Problems of Mechanics and Mathematics of the National Academy of Sciences of Ukraine in Lviv. After graduating from the Lviv State University in 1971 he started research activities at the Institute for Applied Problems of Mechanics and Mathematics and worked on his PhD thesis under the supervision of V. Skorobohatko. He received his PhD degree in 1980 from the Institute of Physics of the Academy of Sciences of Belorussia. In 2006, he defended his Habilitation Doctoral thesis at the Bogolyubov

Institute for Theoretical Physics of the National Academy of Sciences of Ukraine.

His research interests include mathematical physics, differential equations and general relativity, in particular, the Cauchy problem, dark energy and gravitational energy.



**Yuri SHTANOV** is the head of the Laboratory of Astrophysics and Cosmology of the Department of Astrophysics and Elementary Particles at the Bogolyubov Institute for Theoretical Physics of the National Academy of Sciences of Ukraine. After graduating from the Moscow Institute of Physics and Technology in 1987, he worked on his PhD thesis at the Lebedev Physical Institute in Moscow under the supervision of G.V. Chibisov and V.L. Ginzburg. He received his PhD degree in 1991 from the Moscow Institute of Physics and Technology. Since 1991, he works at the

Bogolyubov Institute for Theoretical Physics of the National Academy of Sciences of Ukraine. In 2012, he defended his Habilitation Doctoral thesis at the same Institute.

Dr. Shtanov was a visiting scientist at Brown University (USA), Inter-University Centre for Astronomy and Astrophysics (Pune, India), Nottingham University (UK), Perimeter Institute (Canada) and other international scientific institutions.

Dr. Shtanov's research interests include the theory of inflationary and post-inflationary universe, the problems of dark matter and dark energy, multidimensional and modified gravity and cosmology. His best known works are devoted to the theory of post-inflationary preheating and to the effects of dark energy in braneworld cosmology.

---



**Alexander ZHUK** is a Principal Scientist at the Research Institute "Astronomical Observatory" of the Mechnikov National University of Odessa. After graduating from the Moscow Engineering Physical Institute in 1977, he received his PhD degree in 1983 from the Lebedev Physical Institute of the Academy of Sciences of USSR in Moscow, and a Habilitation Doctoral degree in 1999 from the Bogolyubov Institute for Theoretical Physics of the National Academy of Sciences of Ukraine. He worked at the Department of Theoretical Physics of the Mechnikov National University of Odessa during 1982–2007. During 1987, he was a

visiting scientist at the Cambridge University where he worked under the supervision of Prof. Steven Hawking. He was also a visiting scientist at several leading international scientific institutions (CERN (Switzerland), Free University (Germany), Albert-Einstein-Institute (Germany), University of Minnesota (USA), Princeton University (USA), Columbia University (USA), Tufts University (USA), Fermi National Accelerator Laboratory (USA), IMFF, CSIC (Spain), etc.). During 2003–2008 and during 2009–2014, he was elected a Senior Associate at the Abdus Salam International Center for Theoretical Physics in Trieste (Italy). His research interests include high energy physics, theories of gravity, multidimensional cosmological and gravitational models, structure of the Universe at large and small scales, dark matter and dark energy. He has published more than 90 peer-reviewed papers in leading international physical journals. He has (co)organized over 10 international conferences and was a (co)editor of several conference Proceedings, including those published by the Cambridge Scientific Publishers and by the American Institute of Physics.

Книга висвітлює сучасний стан проблеми темної енергії та представляє результати досліджень авторів, що працюють в цій галузі. В ній приведені спостережувані аргументи, які вказують на існування темної енергії, методи та оцінки значень і довірчих інтервалів її основних параметрів, моделювання темної енергії скалярними полями, її поява в моделях простору-часу з додатковими просторовими вимірами, зокрема в моделях типу Калуци—Кляйна, в моделях бран з єдиним додатковим виміром, а також аналізуються проблеми, пов'язані з позитивним визначенням гравітаційної енергії в загальній теорії відносності, енергетичні умови та наслідки їх порушення в присутності темної енергії.

Монографія призначена для науковців, викладачів, аспірантів та студентів, які спеціалізуються в загальній теорії відносності, космології та фізиці елементарних частинок і полів.

*Наукове видання*

НАЦІОНАЛЬНА АКАДЕМІЯ НАУК УКРАЇНИ  
ІНСТИТУТ ТЕОРЕТИЧНОЇ ФІЗИКИ ім. М.М. БОГОЛЮБОВА  
ІНСТИТУТ ПРИКЛАДНИХ ПРОБЛЕМ МЕХАНІКИ  
І МАТЕМАТИКИ ім. Я.С. ПІДСТРИГАЧА  
РАДІОАСТРОНОМІЧНИЙ ІНСТИТУТ

ЛЬВІВСЬКИЙ НАЦІОНАЛЬНИЙ УНІВЕРСИТЕТ імені ІВАНА ФРАНКА  
ОДЕСЬКИЙ НАЦІОНАЛЬНИЙ УНІВЕРСИТЕТ імені І.І. МЕЧНИКОВА

## **ТЕМНА ЕНЕРГІЯ І ТЕМНА МАТЕРІЯ У ВСЕСВІТІ**

За редакцією академіка НАН України В. ШУЛЬГИ

У ТРЬОХ ТОМАХ

НОВОСЯДЛИЙ Богдан, ПЕЛИХ Володимир,  
ШТАНОВ Юрій, ЖУК Олександр

### **ТЕМНА ЕНЕРГІЯ: СПОСТЕРЕЖУВАНІ ПІДСТАВИ І ТЕОРЕТИЧНІ МОДЕЛІ**

ТОМ 1

Англійською мовою

Літературний редактор *О. Сергієнко*      Технічний редактор *Т. Шендерович*  
Художнє оформлення *Є. Ільницького*      Комп'ютерна верстка *Л. Шмагайло*  
У оформленні обкладинки використано рисунки *І. Жука*

Підп. до друку 06.12.2013. Формат 70×100/16. Папір офс.  
Гарн. Computer Modern. Друк офс. Ум. друк. арк. 31,04. Обл.-вид. арк. 31,29.  
Тираж 300 прим. Зам. 3764.

---

Видавець і виготовлювач Видавничий дім “Академперіодика” НАН України  
01004, Київ-4, вул. Терещенківська, 4

Свідоцтво суб'єкта видавничої справи ДК № 544 від 27.07.2001 р.